

PHASE 1A STUDY REPORT

VOYAGER SPACECRAFT

VOLUME 5

ALTERNATE DESIGNS

SUBSYSTEMS CONSIDERATIONS

30 July 1965

Prepared for  
California Institute of Technology  
Jet Propulsion Laboratory  
Pasadena, California  
Under Contract Number 951113

*NAS-7-100*

TRW SYSTEMS GROUP

Redondo Beach, California

## CONTENTS

	<u>Page</u>
I. INTRODUCTION . . . . .	1-1
II. SCIENCE PAYLOAD AND PLANET ORIENTED PACKAGE . . . . .	2-1
1. ALTERNATIVE SCIENCE PAYLOADS . . . . .	2-1
1.1 Interplanetary Environment . . . . .	2-1
1.2 Mars Exospheric Environment . . . . .	2-2
1.3 Planetary Observations . . . . .	2-4
1.3.1 Photographic Observations. . . . .	2-4
1.3.2 Spectrometric Experiments . . . . .	2-5
1.3.3 Radiometric Measurements . . . . .	2-6
1.3.4 Photometric - Meteor Flash. . . . .	2-6
1.3.5 Alternative Planet Observation Experiment . . . . .	2-7
1.4 Spacecraft Flexibility . . . . .	2-7
1.4.1 Telemetry and Data Handling . . . . .	2-8
1.4.2 DAE-Spacecraft Sequencer Interface . . . . .	2-9
2. PLANET ORIENTED PACKAGE . . . . .	2-10
2.1 Design Requirements and Objectives . . . . .	2-10
2.2 POP Mechanizations Considered . . . . .	2-11
2.2.1 Body-Fixed POP. . . . .	2-11
2.2.2 Single-Gimballed POP . . . . .	2-12
2.2.3 Double-Gimballed POP . . . . .	2-12
2.2.4 Comparison of POP Gimbal Arrangements. . . . .	2-13
2.3 Boom-Mounted Double-Gimballed POP . . . . .	2-16
2.3.1 POP Drive Mechanization . . . . .	2-16
2.3.2 Operational Considerations . . . . .	2-16
2.4 POP Design Considerations . . . . .	2-17
2.4.1 Fields of View and Coverage . . . . .	2-17
2.4.2 POP-Mounted Instruments . . . . .	2-19
2.4.3 Thermal Control . . . . .	2-19
2.4.4 Gimbal Drive. . . . .	2-19



## CONTENTS (Continued)

	<u>Page</u>
III. TELECOMMUNICATIONS SUBSYSTEM . . . . .	3-1
1. COMMUNICATIONS . . . . .	3-1
1.1 Earth-Spacecraft Communications . . . . .	3-1
1.1.1 Functions . . . . .	3-1
1.1.2 Baseline Antenna Configurations . . . . .	3-2
1.1.3 Selected Configuration . . . . .	3-4
1.1.4 Telemetry Bit Rate Selection . . . . .	3-10
1.1.5 Operations with Multiple Spacecraft . . . . .	3-11
1.1.6 Areas of Future Study . . . . .	3-12
1.2 Capsule-Spacecraft Communications . . . . .	3-13
1.2.1 System Configuration Selection . . . . .	3-14
1.2.2 Dual Spacecraft and Capsule Operation . . . . .	3-14
1.2.3 Parameters and Constraints . . . . .	3-15
1.2.4 Areas of Future Study . . . . .	3-16
1.3 Subsystem Performance Analysis . . . . .	3-17
1.3.1 Range and Range Rate Link Analysis . . . . .	3-18
1.3.2 Telemetry Link Analysis . . . . .	3-21
1.3.3 Command Link Analysis . . . . .	3-31
1.3.4 Capsule-to-Spacecraft Link Analysis . . . . .	3-45
1.4 Spacecraft Antennas . . . . .	3-49
1.4.1 High-Gain Antenna . . . . .	3-51
1.4.2 Medium Gain Antenna . . . . .	3-70
1.4.3 Low Gain Antenna . . . . .	3-72
1.4.4 Capsule Link Antenna . . . . .	3-82
1.5 Equipment and Components . . . . .	3-85
1.5.1 S-Band Modulator Exciter and Low Power Transmitter . . . . .	3-85
1.5.2 Power Amplifiers . . . . .	3-88
1.5.3 Transmitter Selector . . . . .	3-97
1.5.4 S-Band Receivers . . . . .	3-99
1.5.5 Low Noise Preamplifiers . . . . .	3-101
1.5.6 Receiver Selector . . . . .	3-106
1.5.7 Command Detector . . . . .	3-107
1.5.8 VHF Preamplifier for Capsule Link Receiver . . . . .	3-110

## CONTENTS (Continued)

	<u>Page</u>
1.5.9 VHF Capsule Receiver . . . . .	3-112
1.5.10 Capsule Demodulator . . . . .	3-113
1.5.11 RF Switches . . . . .	3-115
1.5.12 Diplexers . . . . .	3-117
1.5.13 Four-Port Coupler . . . . .	3-118
 2. DATA HANDLING SUBSYSTEM . . . . .	 3-121
2.1 Introduction . . . . .	3-121
2.2 Design Considerations and Approaches. . . . .	3-124
2.2.1 General . . . . .	3-124
2.2.2 Data Storage . . . . .	3-125
2.2.3 Mission Profile . . . . .	3-128
2.2.4 Data Formats. . . . .	3-131
2.2.5 Transmission Modes . . . . .	3-139
2.2.6 Interfaces. . . . .	3-143
2.2.7 Bulk Storage Tradeoff. . . . .	3-145
2.2.8 Redundancy Concept . . . . .	3-147
2.2.9 Selected Design . . . . .	3-148
2.3 Design Tradeoff and Implementation . . . . .	3-151
 IV. POWER AND CONTROL SUBSYSTEM DESIGN CONSIDERATIONS . . . . .	 4-1
1. STABILIZATION AND CONTROL SUBSYSTEM . . . . .	4-1
1.1 System Requirements and Gross Tradeoffs . . . . .	4-1
1.1.1 Attitude References . . . . .	4-2
1.1.2 Control Torque Sources . . . . .	4-3
1.1.3 Control Modes . . . . .	4-4
1.2 Functional Modes and Alternate Mechanizations . . . . .	4-4
1.2.1 Cruise Mode . . . . .	4-4
1.2.2 Acquisition Mode . . . . .	4-7
1.2.3 Maneuver Mode . . . . .	4-9
1.2.4 Inertial Attitude Hold Mode . . . . .	4-10
1.2.5 Thrust Vector Control Mode. . . . .	4-10
1.3 Control System Analyses . . . . .	4-12
1.3.1 Pointing Error Analysis . . . . .	4-12
1.3.2 Cruise Mode . . . . .	4-15

## CONTENTS (Continued)

	<u>Page</u>
1.3.3 Sun-Canopus Acquisition Mode . . . .	4-17
1.3.4 Maneuver and Inertial Hold Modes . . . .	4-19
1.3.5 Thrust Vector Control Mode. . . . .	4-21
1.4 Inertial Sensors . . . . .	4-24
1.4.1 Gyro Instruments . . . . .	4-24
1.4.2 Gyro Assembly . . . . .	4-26
1.4.3 Mechanization Tradeoffs . . . . .	4-27
1.5 Sun Sensors and Near Earth Detector. . . . .	4-32
1.5.1 Selected Sun Sensor Design . . . . .	4-32
1.5.2 Design Development . . . . .	4-35
1.5.3 Coarse Sun Sensor Tradeoffs . . . . .	4-35
1.5.4 Fine Sun Sensor . . . . .	4-38
1.5.5 Switching . . . . .	4-41
1.5.6 Near Earth Detector. . . . .	4-44
1.6 Star Sensors . . . . .	4-44
1.6.1 Available Star Sensors . . . . .	4-45
1.6.2 Star Sensor Selection . . . . .	4-48
1.6.3 Conclusions . . . . .	4-51
1.7 Earth Tracker. . . . .	4-53
1.8 Reaction Control System . . . . .	4-55
1.8.1 Summary of Design Tradeoffs . . . . .	4-57
1.8.2 Selection of Working Fluid . . . . .	4-58
1.8.3 Other Types of Reaction Control Systems. . . . .	4-64
1.9 Control System Electronics . . . . .	4-67
1.9.1 Sun Sensor Electronics . . . . .	4-69
1.9.2 Valve Control Electronics . . . . .	4-69
1.9.3 Thrust Vector Control Electronics . . . . .	4-69
1.9.4 Gyro Electronics . . . . .	4-71
1.9.5 Mode Control Electronics . . . . .	4-72
1.10 SCS Reliability Tradeoffs . . . . .	4-73
1.10.1 Control Electronics Reliability . . . . .	4-73
1.10.2 Reaction Control Reliability . . . . .	4-75
1.10.3 Star Sensor Reliability . . . . .	4-76

## CONTENTS (Continued)

	<u>Page</u>
1.11 Other Considerations . . . . .	4-77
1.11.1 Magnetics . . . . .	4-77
1.11.2 Vehicle Interface . . . . .	4-78
2. CENTRAL SEQUENCING AND COMMAND SUBSYSTEM . . . . .	4-81
2.1 Subsystem Command, Sequencing, and Timing Requirements . . . . .	4-81
2.1.1 Science Subsystem . . . . .	4-81
2.1.2 Planet Oriented Package Requirements . . . . .	4-83
2.1.3 Telecommunications Subsystem Requirements . . . . .	4-85
2.1.4 Stabilization and Control Sub- system Requirements . . . . .	4-89
2.1.5 Propulsion Subsystem Requirements	4-92
2.1.6 Power Subsystem Command Requirements . . . . .	4-92
2.1.7 Capsule Requirements . . . . .	4-96
2.1.8 Mission Requirements . . . . .	4-96
2.2 Summary of Requirements . . . . .	4-100
2.3 Command Word Definitions . . . . .	4-103
2.4 Message Failure Protection Requirements	4-106
2.4.1 Error Rejection . . . . .	4-107
2.4.2 Valid Message Rate . . . . .	4-109
2.5 Alternative Processor Configurations . . . .	4-112
2.5.1 Preferred Mechanizations . . . . .	4-113
2.6 Centralized Memory System . . . . .	4-114
2.6.1 Detailed Descriptions of CS and C Subassemblies . . . . .	4-116
2.6.2 CS and C Interfaces . . . . .	4-128
2.6.3 Physical Characteristics . . . . .	4-130
2.7 Distributed, or Decentralized, Memory System . . . . .	4-132

## CONTENTS (Continued)

	<u>Page</u>
2. 7. 1 Description of Distributed Memory System Subassemblies. . . . .	4-138
2. 7. 2 CS and C Interfaces . . . . .	4-143
2. 7. 3 Physical Characteristics . . . . .	4-143
2. 8 Reliability Comparisons . . . . .	4-143
2. 8. 1 Reliability Considerations for the Centralized Memory System . . . .	4-143
2. 8. 2 Reliability Considerations for the Distributed Memory Systems . . . .	4-146
2. 8. 3 Review of Reliability Analysis Assumptions . . . . .	4-149
2. 9 Summary and Conclusions . . . . .	4-150
2. 9. 1 Comparison of Physical Charac- teristics . . . . .	4-151
2. 9. 2 Consideration of Provision for Expanded Science Functions . . . . .	4-153
3. ELECTRICAL POWER SUBSYSTEM . . . . .	4-155
3. 1 Mission Criteria and Load Requirements . . .	4-156
3. 2 Subsystem Design Analysis . . . . .	4-159
3. 2. 1 Approach . . . . .	4-159
3. 2. 2 Candidate Systems . . . . .	4-161
3. 2. 3 Recommended Power Subsystem. . .	4-169
3. 3 Solar Array. . . . .	4-174
3. 3. 1 Solar Cell Selection . . . . .	4-174
3. 3. 2 Module Configuration . . . . .	4-180
3. 3. 3 Array Electrical Design . . . . .	4-192
3. 4 Solar Array Controls . . . . .	4-219
3. 5 Power Conditioning Equipment . . . . .	4-235
3. 6 Battery . . . . .	4-248
3. 7 Battery Charge-Discharge Control . . . . .	4-256

## CONTENTS (Continued)

	<u>Page</u>
V. MECHANICAL SUBSYSTEMS TRADEOFFS . . . . .	5-1
1. STRUCTURE . . . . .	5-1
1.1 Alternate Structural Configurations . . . . .	5-1
1.1.1 Configuration A-1 . . . . .	5-4
1.1.2 Configuration B-1 . . . . .	5-6
1.1.3 Configuration A-2 . . . . .	5-8
1.1.4 Configuration A-3 . . . . .	5-11
1.1.5 Configuration B-2 . . . . .	5-16
1.1.6 Configuration C-2 . . . . .	5-18
1.2 Configuration Evaluation and Conclusions . . .	5-21
1.2.1 Design . . . . .	5-21
1.2.2 Strength Analysis . . . . .	5-22
1.2.3 Dynamic Analyses . . . . .	5-23
1.2.4 Meteoroid Protection Analysis . . .	5-31
1.2.5 Structural Reliability . . . . .	5-34
1.2.6 Manufacturing . . . . .	5-35
1.2.7 Relative Costs . . . . .	5-37
1.3 Selection of Structural Component Design . . .	5-39
1.3.1 Basic Bus Structure . . . . .	5-39
1.3.2 Propellant Tank Support Structure . . .	5-56
1.3.3 Solid Propellant Support Structure . . .	5-59
1.3.4 Solar Panels . . . . .	5-63
2. THERMAL CONTROL SUBSYSTEM . . . . .	5-70
2.1 Over-all Heat Balance . . . . .	5-72
2.1.1 Hot Condition (Near-Earth Cruise Mode). . . . .	5-72
2.1.2 Cold Condition . . . . .	5-73
2.1.3 Over-all Heat Balance with a 40-watt Output TWT . . . . .	5-76
2.1.4 Conclusions . . . . .	5-76
2.2 Spacecraft Thermal Model and Mounting Surface Analysis . . . . .	5-77
2.2.1 Spacecraft Thermal Model . . . . .	5-77
2.2.2 Mounting Surface Analysis . . . . .	5-81
2.3 Louver Design . . . . .	5-90

## CONTENTS (Continued)

	<u>Page</u>
2.3.1 Thermal Performance . . . . .	5-91
2.3.2 Environmental Inputs . . . . .	5-92
2.3.3 Actuation Mechanisms and Louver Construction . . . . .	5-95
2.4 Insulation . . . . .	5-102
2.5 Solar Array. . . . .	5-108
2.6 Rocket Engine Heating . . . . .	5-112
2.6.1 Plume Heating. . . . .	5-112
2.6.2 Heat Transfer Between the Solid Motor and Spacecraft . . . . .	5-118
2.7 External Equipment . . . . .	5-119
2.7.1 Planet Oriented Package (POP) . . .	5-119
2.7.2 External Experiment Packages . . .	5-122
2.7.3 Gimbals . . . . .	5-122
2.7.4 Antennas . . . . .	5-123
2.7.5 Magnetometer . . . . .	5-123
2.8 Summary of the Selected System. . . . .	5-125
2.8.1 Louver System. . . . .	5-125
2.8.2 Insulation . . . . .	5-126
2.8.3 Power Density Constraints . . . . .	5-126
2.8.4 Rocket Engine Heating . . . . .	5-126
2.8.5 Externally-Mounted Components . . . . .	5-126
3. SEPARATION SYSTEMS . . . . .	5-127
3.1 Spacecraft-Booster Separation . . . . .	5-127
3.1.1 Mechanisms Considered . . . . .	5-127
3.1.2 Weight-Reliability Tradeoff . . . . .	5-130
3.2 Capsule Cover Base Jettison System . . . . .	5-130
4. PYROTECHNICS . . . . .	5-133
4.1 Requirements and Design Criteria . . . . .	5-133
4.2 Pyrotechnic Devices . . . . .	5-134
4.2.1 Explosive Bolts . . . . .	5-134
4.2.2 Separation Nuts . . . . .	5-135

## CONTENTS (Continued)

	<u>Page</u>
4.2.3 Collet Release . . . . .	5-136
4.2.4 Pin Pullers (and Reefing Line Cutters) . . . . .	5-136
4.2.5 Flexible Linear Shaped Charge . . .	5-139
4.2.6 Summary and Selection Criteria . .	5-139
4.3 Spacecraft Destruct Systems . . . . .	5-141
4.3.1 Destruct System Concepts . . . . .	5-141
4.3.2 Comparative Evaluation . . . . .	5-142
4.3.3 Brief Description of Destruct System Design . . . . .	5-143
4.4 Safe and Arm Provisions . . . . .	5-144
5. DEPLOYMENT MECHANISMS . . . . .	5-145
5.1 Magnetometer Sensor Deployment . . . . .	5-145
5.1.1 Mechanizations Considered . . . . .	5-145
5.1.2 Configuration Evaluation . . . . .	5-150
5.1.3 Material Considerations for Selected Designs . . . . .	5-150
5.2 Solar Panel Release and Deployment System	5-152
5.2.1 Deployment Configurations Studied	5-153
5.2.2 Configuration Evaluation . . . . .	5-155
VI. ELECTRONICS PACKAGING AND ELECTRICAL DISTRIBUTION . . . . .	6-1
1. ELECTRONICS EQUIPMENT PACKAGING . . . . .	6-1
1.1 Design Objectives and Constraints . . . . .	6-1
1.2 Alternate Approaches and Selection . . . . .	6-4
1.2.1 Cable Routing and Attachment . . . . .	6-4
1.2.2 Equipment Panels and Equipment Mounting . . . . .	6-7
1.2.3 Equipment Size Standardization . . .	6-13
1.2.4 Electronic Packaging Techniques . .	6-14



## CONTENTS (Continued)

	<u>Page</u>
2. ELECTRICAL DISTRIBUTION EQUIPMENT . . . . .	6-24
2.1 Interconnect Cabling . . . . .	6-24
2.2 Power Switching Circuitry . . . . .	6-24
2.3 Circuit Protective Devices . . . . .	6-25
2.4 Pyrotechnic Control . . . . .	6-27
2.4.1 Solid-State Firing Circuits . . . . .	6-27
2.4.2 RF Environment . . . . .	6-28
VII. PROPULSION SUBSYSTEM . . . . .	7-1
1. PROPULSION SUBSYSTEM REQUIREMENTS . . . . .	7-2
1.1 Mandatory Requirements . . . . .	7-3
1.2 Desirable Requirements . . . . .	7-3
1.3 Requirements Resulting From Spacecraft Interaction . . . . .	7-5
2. SOLID PROPELLANT INJECTION MOTOR . . . . .	7-5
2.1 Component Selection . . . . .	7-6
2.1.1 Propellants and Performance . . . . .	7-9
2.1.2 Grain Design . . . . .	7-13
2.1.3 Case . . . . .	7-13
2.1.4 Insulation . . . . .	7-14
2.1.5 Nozzle . . . . .	7-14
2.1.6 Thrust Vector Control . . . . .	7-16
2.2 Weight and Performance . . . . .	7-18
2.3 Problem Areas . . . . .	7-22
2.3.1 Storage in Space Environment . . . . .	7-22
2.3.2 Nozzle Development . . . . .	7-28
2.4 Reliability . . . . .	7-29
2.5 Preliminary Design . . . . .	7-33
2.6 Contractor's Design Solutions . . . . .	7-38

## CONTENTS (Continued)

	<u>Page</u>
2. 6. 1 United Technology Center . . . . .	7-38
2. 6. 2 Lockheed Propulsion Company . . . . .	7-39
2. 6. 3 Aerojet- General Corporation . . . . .	7-41
2. 6. 4 Hercules Powder Company . . . . .	7-43
3. MIDCOURSE PROPULSION SUBSYSTEM . . . . .	7-43
3. 1 Thrust Chamber Design . . . . .	7-44
3. 1. 1 Thrust Level Selection . . . . .	7-48
3. 1. 2 Thrust Chamber Configuration . . . . .	7-48
3. 2 Monopropellant Feed System . . . . .	7-50
3. 2. 1 Operation . . . . .	7-50
3. 2. 2 Pressurization Gas . . . . .	7-51
3. 2. 3 Expulsion Device . . . . .	7-52
3. 2. 4 Selection of System Design Pressure . . . . .	7-52
4. BIPROPELLANT PROPULSION SYSTEM . . . . .	7-52
4. 1 Voyager Bipropellant Engine Design . . . . .	7-52
4. 1. 1 Performance Characteristics . . . . .	7-53
4. 1. 2 Engine Design . . . . .	7-53
4. 2 Bipropellant Feed System . . . . .	7-67
4. 2. 1 Component Selection and Arrangement . . . . .	7-68
4. 2. 2 Gas Pressurant and Storage Tanks . . . . .	7-69
4. 2. 3 Propellant Tanks and Expulsion Devices . . . . .	7-71
5. REFERENCES . . . . .	7-72

## ILLUSTRATIONS

<u>Figure</u>		<u>Page</u>
2-1	Plant Oriented Package . . . . .	2-10
2-2	Conceptual Double-Gimballed POP . . . . .	2-13
2-3	Selected POP Configuration and General Equipment Arrangement . . . . .	2-18
2-4	Wobble Gear Drive . . . . .	2-23
2-5	POP Drive Electronics Block Diagram . . . . .	2-26
3-1	Baseline S-Band Communication Block Diagram for Spacecraft Configurations A and B . . . . .	3-3
3-2	Baseline S-Band Communication Block Diagram for Spacecraft Configuration C . . . . .	3-3
3-3	Selected S-Band Communication Configuration . .	3-5
3-4	Selected VHF Communications Configuration . . . .	3-14
3-5	Signal-to-Noise Density Requirements for Two-Channel Pseudonoise Sync Telemetry . . . .	3-27
3-6	Cone and Clock Angles of Earth Relative to Voyager Spacecraft 1971 and 1973 Launches . . . .	3-50
3-7	Antenna Elliptical Dish (Major Axis 6 ft 6-1/2 in., Minor Axis 5 ft 6 in) . . . . .	3-55
3-8	Basic Gimbal Elements . . . . .	3-59
3-9	Preliminary Layout of High-Gain Antenna Gimbal .	3-62
3-10	Wobble Gear Drive . . . . .	3-63
3-11	Drive Electronics Block Diagram . . . . .	3-64
3-12	Rotary Joint Construction Schematic Diagram . . .	3-66
3-13	Cassegrain and Focal Point Configuration . . . . .	3-68
3-14	Pointing Error of an Antenna with Single Gimbal Movement Whose Axis of Rotation is Oriented at a Clock Angle of 195 Deg and a Cone Angle of 95 Deg	3-71
3-15	Antenna 3-ft Circular Dish . . . . .	3-72

# ILLUSTRATIONS (Continued)

<u>Figure</u>		<u>Page</u>
3-16	Preliminary Layout of Medium Gain Antenna Gimbal	3-73
3-17	Theoretical Pattern Gains . . . . .	3-76
3-18	Theoretical Relative Power Patterns, $P/P_O = \left( \frac{1 + \cos \theta}{2} \right)^k$ . . . . .	3-77
3-19	Rantec Cup-Dipole Antenna . . . . .	3-78
3-20	Theoretical Versus Experimental Relative Voltage Patterns . . . . .	3-79
3-21	Low Gain Antenna System . . . . .	3-80
3-22	Low Gain Antenna . . . . .	3-81
3-23	Helix Configuration . . . . .	3-83
3-24	VHF Antenna . . . . .	3-84
3-25	Modulator-Exciter . . . . .	3-87
3-26	Comparison of Power Amplifiers Input Power Versus Power Output . . . . .	3-96
3-27	20-Watt TWT Power Amplifier Block Diagram . .	3-96
3-28	Exciter Selector State Diagram . . . . .	3-98
3-29	Power Amplifier Selector State Diagram . . . . .	3-98
3-30	Antenna Selector State Diagram . . . . .	3-98
3-31	S-Band Receiver . . . . .	3-100
3-32	Four- and Five-Port Circulator Connections . . .	3-102
3-33	Tunnel Diode I-V Characteristic . . . . .	3-103
3-34	Command Detector . . . . .	3-109
3-35	VHF Preamplifier Block Diagram . . . . .	3-111
3-36	VHF Receiver Block Diagram . . . . .	3-113
3-37	Capsule Demodulator Block Diagram . . . . .	3-114

# ILLUSTRATIONS (Continued)

<u>Figure</u>		<u>Page</u>
3-38	Circulator Switches Function Diagram . . . . .	3-116
3-39	Simplified Block Diagram of Base Line Data Handling Subsystem . . . . .	3-125
3-40	Data Gathering Modes . . . . .	3-133
3-41	Commutation Format . . . . .	3-139
3-42	Transmission Mode Tree . . . . .	3-140
3-43	High Rate Science Data Mix Timing . . . . .	3-142
3-44	Simplified Block Diagram of Selected Data Handling Subsystem . . . . .	3-149
3-45	Simplified Block Diagram of PCM Encoder . . . . .	3-153
3-46	Detail Block Diagram of Digital Telemetry Unit . . . . .	3-155
3-47	Converter . . . . .	3-156
3-48	Simplified Block Diagram of Core Memory . . . . .	3-163
3-49	Timing Diagram . . . . .	3-169
3-50	Read/Write Block Diagram . . . . .	3-169
3-51	Motor Servo System . . . . .	3-170
4-1	Cruise Mode SCS Block Diagram . . . . .	4-15
4-2	Pitch or Yaw Sun Acquisition Mode . . . . .	4-17
4-3	Roll Axis Canopus Acquisition Mode . . . . .	4-17
4-4	Sun Acquisition for 3 deg/sec . . . . .	4-19
4-5	Backup Acquisition at 17 deg/sec . . . . .	4-20
4-6	Incremental Roll Maneuver Block Diagram . . . . .	4-20
4-7	Single Axis Maneuver Mode . . . . .	4-20
4-8	90-degree Reorientation . . . . .	4-21
4-9	Midcourse Correction Mode Block Diagram . . . . .	4-23

# ILLUSTRATIONS (Continued)

<u>Figure</u>		<u>Page</u>
4-10	Deboost TVC Block Diagram . . . . .	4-23
4-11	Gyro Control Loop . . . . .	4-24
4-12	Gyro Reference Assembly Thermal Model . . . .	4-26
4-13	Sun Sensor and Electronics . . . . .	4-33
4-14	Coarse Sun Sensors . . . . .	4-33
4-15	Sun Sensor Output Versus Illumination Angle . . .	4-33
4-16	Fine Sun Sensor . . . . .	4-34
4-17	Sun Sensor Output Signal . . . . .	4-34
4-18	Near Earth Detector Schematic Diagram . . . . .	4-42
4-19	Star Field Near Canopus . . . . .	4-51
4-20	Heated Nitrogen Reaction Control Schematic . . .	4-57
4-21	Reaction Control System Weight for Various Working Fluids . . . . .	4-58
4-22	Heated GN <sub>2</sub> Tri-nozzle Thruster Assembly . . . .	4-61
4-23	Heated GN <sub>2</sub> Tri-nozzle Thruster Assembly . . .	4-61
4-24	Optimum Thrust Regimes for Reaction Control . .	4-62
4-25	Liquid Storage Reaction Control System . . . . .	4-64
4-26	Dissociated Ammonia Reaction Control System . .	4-65
4-27	Control Electronics Assembly . . . . .	4-68
4-28	Sun Sensor Electronics . . . . .	4-69
4-29	Symmetrical Pulse Width Modulator . . . . .	4-71
4-30	Gyro Circuit Block Diagram . . . . .	4-72
4-31	Triple Redundancy Voting Logic . . . . .	4-75
4-32	Midcourse Maneuver Sequence . . . . .	4-91
4-33	Command Formats . . . . .	4-104

# ILLUSTRATIONS (Continued)

<u>Figure</u>		<u>Page</u>
4-34	Probability of a Message Loss versus Message Length for a Bit Error Rate of $1 \times 10^{-5}$ . . . . .	4-110
4-35	Probability of a Message Loss Due to a Sync Error . . . . .	4-110
4-36	Probability of a Message Loss versus Bit Error Rate for Varying Message Lengths . . . . .	4-111
4-37	Probability of Message Loss Due to Bit Error Rate of $1 \times 10^{-5}$ versus the Number of Sync + Parity Bits for Varying Message Lengths . . . . .	4-111
4-38	CS and C Centralized Memory System . . . . .	4-115
4-39	Input Decoder (with redundancy) . . . . .	4-120
4-40	Command Decoder Centralized Memory System . . . . .	4-122
4-41	Sequencer Logic Diagram . . . . .	4-123
4-42	Clock Generator Block Diagram . . . . .	4-124
4-43	Clock and Time Tags . . . . .	4-127
4-44	CS and C Distributed Memory System . . . . .	4-134
4-45	Input Decoder (assuming redundancy) . . . . .	4-138
4-46	Command Decoder (Distributed Memory System) . . . . .	4-139
4-47	Sequencer Block Diagram (Distributed Memory System) . . . . .	4-140
4-48	Storage Cell Distributed Memory System . . . . .	4-142
4-49	Sequencer Timer, Distributed Memory System . . . . .	4-142
4-50	Sequencer Timer, Distributed Memory System . . . . .	4-142

# ILLUSTRATIONS (Continued)

<u>Figure</u>		<u>Page</u>
4-51	Power Converter Block Diagram . . . . .	4-147
4-52	CS and C Subsystem Redundancy . . . . .	4-148
4-53	Comparison of Weight versus Storage Compatibility for the CS and C Subsystem Confirguation . . . . .	4-152
4-54	Power System Block Diagram . . . . .	4-159
4-55	Candidate Power Subsystem Block Diagram . . . . .	4-161
4-56	Comparison of Solar Array Capability with Constant Power Load as Function of Operating Voltage . . . . .	4-162
4-57	Comparison of Solar Array Operating Point and Load Current and Voltage Using Series (Buck) Regulator . . . . .	4-163
4-58	Revised S. A. I-V Characteristics . . . . .	4-166
4-59	Power Subsystem Block Diagram . . . . .	4-171
4-60	Reliability Block Diagram . . . . .	4-173
4-61	Load and Solar Array Current During Voyager Mission . . . . .	4-174
4-62	10-Cell Module Assembly . . . . .	4-181
4-63	10-Cell Module Assembly Exploded View . . . . .	4-182
4-64	Installed Nondegraded Solar Cell Current-Voltage Characteristic . . . . .	4-190
4-65	$I_{sc}$ Versus Angle of Incidence . . . . .	4-192
4-66	Current Degradation Curve AMO Intensity at $T = 27^{\circ}C$ . . . . .	4-197
4-67	Voltage Degradation Curve AMO Intensity at $T = 27^{\circ}C$ . . . . .	4-198



# ILLUSTRATIONS (Continued)

<u>Figure</u>		<u>Page</u>
4-68	Worst Case I-V Curves at Various AU Distances . . . . .	4-207
4-69	Best Case I-V Curves at Various AU Distances . . . . .	4-207
4-70	Effect of Radiation Flux on I-V Curves at 1.67 AU . . . . .	4-207
4-71	Worst Case Relative Power Versus Sun-Spacecraft Distance . . . . .	4-211
4-72	Best Case Relative Power Versus Sun-Spacecraft Distance . . . . .	4-211
4-73	Earth Oriented Worst Case I-V Curves . . . . .	4-212
4-74	Worst Case Relative Power Versus Sun- Spacecraft Distance . . . . .	4-212
4-75	Solar Panel Layout (Sun Side) . . . . .	4-215
4-76	Solar Panel Layout (Dark Side) . . . . .	4-217
4-77	Preliminary Solar Cell Current- Voltage Characteristics . . . . .	4-220
4-78	Full Dissipative Shunt Regulator . . . . .	4-221
4-79	Comparison of Full and Partial Shunts Power Dissipation at 1.0 AU . . . . .	4-222
4-80	Partial Dissipative Shunt Regulator . . . . .	4-223
4-81	Full Shunt Regulator Using Resistive Power Dissipation . . . . .	4-224
4-82	Pulse Width Modulated Switching Partial Shunt Regulator . . . . .	4-225
4-83	Switching Buck-Boost Voltage Regulator . . . . .	4-226
4-84	Buck Boost Regulator Efficiency Versus Input Voltage . . . . .	4-227
4-85	Revised Solar Cell Current-Voltage Characteristics . . . . .	4-228

## ILLUSTRATIONS (Continued)

<u>Figure</u>		<u>Page</u>
4-86	Pulse Width Modulated Series (Buck) Regulator . . . . .	4-229
4-87	Typical PWM Series Regulator Efficiency Versus Input Voltage . . . . .	4-229
4-88	Switched Solar Array Scales Regulator . . . . .	4-230
4-89	Switched Solar Array Shunt Regulator . . . . .	4-230
4-90	Switched Solar Array Limits . . . . .	4-231
4-91	Combined Dissipative Shunt and Switched Solar Array Regulator . . . . .	4-231
4-92	Solar Array Switching Control Decision Points (Combined Shunt and Switched Array . . . . .	4-232
4-93	Tapped Array Sequential Shunt Regulator . . . . .	4-232
4-94	Sequential Shunt Regulator Operating . . . . .	4-234
4-95	Power Conversion System Inverter-Output Regulation . . . . .	4-236
4-96	Power Conversion System, Preregulation Conversion . . . . .	4-237
4-97	Power Conversion System, Combined Inversion and Regulation . . . . .	4-238
4-98	Power Conversion System, AC Distribution . . . . .	4-239
4-99	Transformer-Rectifier Unit Efficiency Versus Output Voltage . . . . .	4-239
4-100	Selected Power Conversion System . . . . .	4-240
4-101	Typical Single Phase Inverter Weight Versus Efficiency . . . . .	4-241
4-102	Inverter Efficiency Versus Voltage . . . . .	4-242
4-103	Relative Weight of Transformers as a Function of Frequency . . . . .	4-243
4-104	Unregulated Inverter Efficiency Versus Power . . . . .	4-243

## ILLUSTRATIONS (Continued)

<u>Figure</u>		<u>Page</u>
4-105	Unregulated Shunt Weight and Volume Versus Output Rating . . . . .	4-244
4-106	Regulated Converter Weight and Volume . . . . .	4-245
4-107	Regulated DC-DC Converter . . . . .	4-245
4-108	Unregulated Inverter Efficiency Versus Load . . . . .	4-246
4-109	Battery Cycle Life Versus Depth of Discharge . . .	4-249
4-110	Battery Weight as a Function of Cycle Life Required . . . . .	4-250
4-111	Silver-Cadmium Cell Typical Charge Voltage Versus Time as a Function of Cell Temperature . . . . .	4-251
4-112	Typical Silver Cadmium Cell Data Peak Charge Voltage Versus Temperature . . . . .	4-251
4-113	Silver Cadmium Voltage Limit-Temperature Relationship, C/10 Charge Rate . . . . .	4-252
4-114	Typical Silver-Cadmium Cell Data Capacity Amp-Hr Versus Temperature as a Function of Current . . . . .	4-253
4-115	Discharge Voltage Versus Time as a Function of Temperature (Constant C Discharge Rate) . . . .	4-253
4-116	Charge Cycling Subsequent to Reaching Upper Voltage Limit . . . . .	4-258
4-117	Battery Charge-Discharge Control . . . . .	4-258
4-118	Standardized Charge Control Concept Logic Diagram . . . . .	4-259
4-119	Battery with Cell-Level-Sensing Charge Control System Schematic . . . . .	4-262
4-120	Boost Regulator DC-DC Converter Type . . . . .	4-264
4-121	Boost Regulator Switching Shunt Type . . . . .	4-264

## ILLUSTRATIONS (Continued)

<u>Figure</u>		<u>Page</u>
4-122	Efficiency Versus Input Voltage for 400-Watt Switching Boost Regulator . . . . .	4-264
4-123	Efficiency Versus Power Level for 50-Volt Switching Boost Regulator . . . . .	4-264
5-1	General Structural Arrangement (Configuration A-1). . . . .	5-3
5-2	General Structural Arrangement (Configuration B-1). . . . .	5-7
5-3	General Structural Arrangement (Configuration A-2). . . . .	5-9
5-4	General Structural Arrangement (Configuration A-3) (Sheet 1). . . . .	5-13
5-4	General Structural Arrangement (Configuration A-3) (Sheet 2 ). . . . .	5-15
5-5	General Structural Arrangement (Configuration B-2). . . . .	5-17
5-6	General Structural Arrangement (Configuration C-2). . . . .	5-19
5-7	Dynamic Model for Free Flight. . . . .	5-30
5-8	Dynamic Model for Launch. . . . .	5-30
5-9	Meteoroid Influx Rate Near Earth . . . . .	5-32
5-10	Meteoroid Influx Rate Cruise . . . . .	5-32
5-11	Meteoroid Influx Rate Circular Orbit . . . . .	5-32
5-12	Sandwich Face Thickness Versus Probability of No Puncture. . . . .	5-33
5-13	Corner Post Design . . . . .	5-39
5-14	Predictable and Allowable Bolt Loading . . . . .	5-42
5-15	Equipment Mounting Panel Design . . . . .	5-44
5-16	Panel Allowable and Applied Stress . . . . .	5-46

# ILLUSTRATIONS (Continued)

<u>Figure</u>		<u>Page</u>
5-17	Material Comparison for Meteoroid Protection. . . . .	5-49
5-18	Meteoroid Shielding Factor . . . . .	5-49
5-19	Optimum Sheet Spacing for Meteoroid Protection . . .	5-49
5-20	Designs for Top and Bottom Panels . . . . .	5-52
5-21	Typical Tank Attachment and Support Structure . . . .	5-56
5-22	Solid Motor Support Structure. . . . .	5-59
5-23	Solar Panel Cross Section Design . . . . .	5-64
5-24	Solar Panel Deflection. . . . .	5-65
5-25	Solar Panel Design Study . . . . .	5-66
5-26	Mode Shapes Used for Dynamic Analysis of Solar Panels . . . . .	5-68
5-27	Schematic of Spacecraft Thermal Model . . . . .	5-77
5-28	Effective Emissivity of a Louvered Panel Radiating to Space . . . . .	5-78
5-29	Configuration I Inboard Profile . . . . .	5-80
5-30	Configuration II Inboard Profile. . . . .	5-80
5-31	Temperature Histories of Equipment Panels at 1 AU with Sun Normal to the Communications Panel. (For conservation all thermal capacities are taken at half actual values.) . . . . .	5-82
5-32	Temperature Histories of Equipment Panels at 1.38 AU with the Sun Normal to the Communications Panel and the Deboost Engine Firing. Half Thermal Thrust. . . . .	5-83
5-33	Temperature Histories of Equipment Panels During Eclipse at 1.67 AU Half Thermal Capacities . . . . .	5-83
5-34	Power Distribution for the Panel Gradient Study. . . .	5-85

# ILLUSTRATIONS (Continued)

<u>Figure</u>		<u>Page</u>
5-35	Louver Configuration. . . . .	5-85
5-36	Power Data . . . . .	5-86
5-37	12-Louver Configuration . . . . .	5-86
5-38	24-Louver Configuration . . . . .	5-86
5-39	Honeycomb Panel Configuration. . . . .	5-87
5-40	Power Input Fabrication. . . . .	5-87
5-41	24 Louvers for 29 x 36 Inch Panel . . . . .	5-87
5-42	Temperature Map for 80-Watt Dissipation. . . . .	5-89
5-43	Louver Performance (fully closed position with diffused or specularly reflecting louver surfaces). . . . .	5-91
5-44	Cold Plate Effective Emissivity as a Function of Cold Plate Emissivity and the Ratio of Louver Length to Louver Width. . . . .	5-93
5-45	Louver Performance (Louvers wide open with specularly reflecting surfaces) . . . . .	5-93
5-46	Reflection of Array Radiation . . . . .	5-94
5-47	Black Body Shape Factor of Array as Viewed by Louvers . . . . .	5-96
5-48	Heat Input to Louver System from Solar Array. . . . .	5-96
5-49	Spiral Bimetal Actuation . . . . .	5-98
5-50	Wax-Filled Thermal Actuator Rack and Pinion. . . . .	5-98
5-51	Augmented Louver Blade Design . . . . .	5-100
5-52	Wax-filled Thermal Actuator Cable and Pulley Drive . . . . .	5-100
5-53	Test Model of Mariner - OGO Type Louver System. . . . .	5-101
5-54	Heat Flux as a Function of Insulation Thickness. . . . . (View 1)	5-103

# ILLUSTRATIONS (Continued)

<u>Figure</u>		<u>Page</u>
5-55	Heat Flux as a Function of Insulation Thickness (View 2) . . . . .	5-103
5-56	Heat Flux as a Function of Insulation Thickness (View 3) . . . . .	5-103
5-57	Heat Flux as a Function of Insulation Thickness (View 4) . . . . .	5-103
5-58	Use of Velcro and Tapes and Ultrasonic Spot Welding for Insulation Attachment on OGO. . . . .	5-105
5-59	Button Insulation Attachment . . . . .	5-106
5-60	Solar Panel Temperatures Including Tolerance $\epsilon_B = 0.85$ . . . . .	5-113
5-61	Solar Panel Temperatures Including Tolerances $\epsilon_B = 0.7$ . . . . .	5-113
5-62	Equilibrium Temperature of Solar Array 1.65 AU . . . . .	5-113
5-63	Solar Panel Equilibrium Temperature . . . . .	5-113
5-64	Solar Panel Temperature During Occultation . . . . .	5-113
5-65	Solar Array Temperature During Eclipse . . . . .	5-113
5-66	Transient Panel Temperatures During Eclipse (View 1) . . . . .	5-113
5-67	Transient Panel Temperatures During Eclipse (View 2) . . . . .	5-113
5-68	Transient Panel Temperatures During Eclipse (View 3) . . . . .	5-115
5-69	Array Power at 1.38 AU . . . . .	5-115
5-70	Solar Panel Temperatures - Transient . . . . .	5-115
5-71	Specific Heat Versus Temperature . . . . .	5-115
5-72	Solar Array Temperature Rise Due to Radiant Heating from the Solid Rocket Particle Plume . . . . .	5-115

## ILLUSTRATIONS (Continued)

<u>Figure</u>		<u>Page</u>
5-73	Solar Panel Temperature - Voyager Earth-Oriented Array . . . . .	5-115
5-74	Refrasil Batt Interval Surface Temperature History Due to Plume Radiation Heating . . . . .	5-116
5-75	Solid Motor Plume Characteristics . . . . .	5-117
5-76	Bipropellant Engine Plume Characteristics . . . . .	5-117
5-77	Solid Motor Insulation Requirement . . . . .	5-118
5-78	Local Temperature of a Cylindrical Volume, 2 Inches High by 2 Inches in Diameter, as a Function of View Area to Space . . . . .	5-120
5-79a	Preliminary POP Configuration . . . . .	5-121
5-79b	Selected POP Configuration . . . . .	5-121
5-80	Antenna Feed Insulation Concept . . . . .	5-123
5-81	POP Gimbal System . . . . .	5-124
5-82	Thermal Control Features of the Selected Voyager Configuration . . . . .	5-125
5-83	Separation Joint Assemblies . . . . .	5-128
5-84	Separation Joint Assembly Showing Cable Connection . . . . .	5-130
5-85	Separation Joint Assembly Showing V-Clamp Connection . . . . .	5-130
5-86	Lander Cover Base Release Mechanism . . . . .	5-131
5-87	Typical Explosive Bolt. . . . .	5-135
5-88	Separation Nut . . . . .	5-137
5-89	Collet Release . . . . .	5-138
5-90	Typical Pin Puller . . . . .	5-140
5-91	Flexible Linear Shaped Charge . . . . .	5-140



## ILLUSTRATIONS (Continued)

<u>Figure</u>		<u>Page</u>
5-92	De Havilland STEM-type Boom . . . . .	5-146
5-93	STEM Boom with Fixed Backup Boom . . . . .	5-147
5-94	Nonretractable Boom . . . . .	5-148
5-95	Retractable Boom . . . . .	5-149
5-96	Nonretractable, Expendable Folding Boom . . . . .	5-150
5-97	Pin Puller and Spring Hinge System . . . . .	5-154
5-98	Spring Actuator and Pin Puller . . . . .	5-154
5-99	Cable Cutter System . . . . .	5-154
5-100	Pin Puller and Swivel Catch . . . . .	5-156
6-1	Electronic Equipment Subsystem Panel Installation Accessibility Concept . . . . .	6-2
6-2	Cable Routing and Attachment Tradeoff Considerations . . . . .	6-5
6-3	Equipment Mounting Tradeoff Considerations . . . . .	6-9
6-4	Typical Arrangement of Equipment Mounted to Panel . . . . .	6-13
6-5	Equipment Size Standardization . . . . .	6-14
6-6	Packaging Technique I Tradeoff Consideration . . . . .	6-16
6-7	Perspective of Generalized Packaging Technique . . . . .	6-18
6-8	Packaging Technique II Tradeoff Considerations . . . . .	6-19
6-9	Packaging Technique . . . . .	6-21
7-1	Solid Propellant Injection Motor . . . . .	7-8
7-2	Parametric Indication of Impulse Requirements . . . . .	7-9
7-3	Comparative Performance Characteristics of Polybutadiene Propellant . . . . .	7-11
7-4	Servoinjector Schematic . . . . .	7-17

# ILLUSTRATIONS (Continued)

<u>Figure</u>		<u>Page</u>
7-5	Velocity Increment Capabilities . . . . .	7-22
7-6	Propellant Burning Rate . . . . .	7-25
7-7	Maximum Tensile Strength Versus Absorbed Radiation. . . . .	7-25
7-8	Per Cent Strain Versus Absorbed Radiation. . . . .	7-25
7-9	Shore "A" Hardness Versus Absorbed Radiation. . . . .	7-26
7-10	Secant Modulus Versus Absorbed Radiation . . . . .	7-26
7-11	Results of Failure Rate Tests . . . . .	7-30
7-12	United Technology Center Design . . . . .	7-39
7-13	Lockheed Propulsion Company Design . . . . .	7-41
7-14	Aerojet-General Design . . . . .	7-42
7-15	Hercules Powder Company Design . . . . .	7-45
7-16	Midcourse Correction System Schematic . . . . .	7-45
7-17	Voyager Midcourse Propulsion System Test Data . . . . .	7-46
7-18	Voyager Midcourse Engine . . . . .	7-47
7-19	Prototype Motor . . . . .	7-49
7-20	Voyager 1000-lb Propellant . . . . .	7-55
7-21	Bipropellant Augmented Configuration . . . . .	7-68
7-22	N <sub>2</sub> O <sub>4</sub> Tank Cross-Section . . . . .	7-72

## TABLES

<u>Table</u>		<u>Page</u>
2-1	Comparison of POP Control and Gimbal Techniques . . . . .	2-14
2-2	Sealed Drive Packaging Tradeoff Summary . . . . .	2-22
2-3	Comparison of Horizon Scanner Flightworthy Characteristics . . . . .	2-28
3-1	Communication Modes for Configurations A and B . . . . .	3-4
3-2	Communication Modes for Configuration C . . . . .	3-4
3-3	Transmission Modes . . . . .	3-8
3-4	Transmitter Selector Logic . . . . .	3-8
3-5	Range Versus Bit Rate . . . . .	3-10
3-6	Capsule-Spacecraft Parameters for Entry Phase . . . . .	3-16
3-7	Synchronization Performance Characteristics (at 128 bits/sec) . . . . .	3-25
3-8	Comparison of Subcarrier Modulation Techniques . . . . .	3-34
3-9	Gimbal Tradeoff Summary . . . . .	3-60
3-10	Elements of the Basic Receiver-Modulator Exciter Equipment . . . . .	3-86
3-11	Comparison of S-Band Power Amplifiers . . . . .	3-95
3-12	Required States for the Power Amplifier Selector . . . . .	3-97
3-13	Electrical Characteristics of the Diplexer . . . . .	3-118
3-14	Summary of Data Rate Requirement . . . . .	3-122
3-15	Data Format as a Function of Mission Profile . . . . .	3-129
3-16	Data Modes . . . . .	3-130
3-17	Video Resolution Versus Storage Requirement . . . . .	3-134
3-18	High Rate Science Data Formatting . . . . .	3-136
3-19	Low Rate Science Data Formatting . . . . .	3-137

# TABLES (Continued)

<u>Table</u>		<u>Page</u>
3-20	Dielectric Video Storage Devices . . . . .	3-146
3-21	Summary of Engineering Data Inputs and the Preferred Sampling Rate . . . . .	3-150
3-22	Comparison of Data Frequencies as a Function of Aperture and Sampling Times . . . . .	3-157
3-23	Truth Table for Successive Approximation Analog-to-Digital Converter . . . . .	3-158
3-24	Analog Gates Comparison . . . . .	3-159
4-1	Gyro Specifications. . . . .	4-25
4-2	Gyro Reference Assembly Specifications . . . . .	4-27
4-3	Characteristics of Mariner C Star Tracker . . . . .	4-49
4-4	Characteristics of Quadrant Photomultiplier Star Sensor . . . . .	4-52
4-5	Comparison of Star Trackers . . . . .	4-53
4-6	Earth Radiance Characteristics . . . . .	4-54
4-7	Stabilization and Control Reliability. . . . .	4-74
4-8	Science Command Sequencing . . . . .	4-84
4-9	Telemetry Command Requirements . . . . .	4-86
4-10	Communications Command Requirements . . . . .	4-87
4-11	Stabilization and Control Command Requirements . . . . .	4-93
4-12	Propulsion System Command Requirements . . . . .	4-94
4-13	Power Subsystem Command Requirements . . . . .	4-95
4-14	Summary of Command Requirements for CS and C . . . . .	4-101
4-15	Telemetry Frequency and Power Supply Synchronization Requirements . . . . .	4-101
4-16	Summary of Sequence Requirements . . . . .	4-102
4-17	Memory Requirements Comparison . . . . .	4-102

# TABLES (Continued)

<u>Table</u>		<u>Page</u>
4-18	Probability of Acceptance of Erroneous Words . . . . .	4-108
4-19	Probability of Acceptance of Shifted Message Versus Number of Sync Bits . . . . .	4-108
4-20	Centralized Memory CS and C Subassembly Functions . . . . .	4-117
4-21	Input Decoder Equations . . . . .	4-119
4-22	Frequencies Associated with Data Rates . . . . .	4-129
4-23	Physical Characteristics of CS and C Centralized Memory System Subassemblies . . . . .	4-130
4-24	CS and C Centralized Memory System Parts Count. .	4-131
4-25	Integrated Circuit Configurations . . . . .	4-132
4-26	Distributed Memory CS and C Subassembly Functions . . . . .	4-136
4-27	Physical Characteristics of CS and C Distributed System with Core Shift Registers . . . . .	4-144
4-28	Physical Characteristics of CS and C Distributed System with Integrated Circuits . . . . .	4-144
4-29	CS and C Distributed Configuration . . . . .	4-145
4-30	Integrated Circuit Configurations . . . . .	4-145
4-31	Characteristics of Over-All Configurations with Redundancy. . . . .	4-152
4-32	Incremental Characteristics for Supplementary Science Requirements . . . . .	4-154
4-33	Estimated Voyager Power Profile . . . . .	4-157
4-34	Comparison of the Properties of Various Tab Materials . . . . .	4-185
4-35	RCA Thermal Cycle Test Results . . . . .	4-188
4-36	Parameters for Worst Case Curve Constructed for Mars Flux Model $E_o = 1.0$ . . . . .	4-208

# TABLES (Continued)

<u>Table</u>		<u>Page</u>
4-37	Parameters for Best Case Curve Construction for Mars Flux Model $E_o = 10^{-1}$ . . . . .	4-208
4-38	Parameters for Worst Case Curve Construction for Mars Flux Model $E_o = 10^1$ . . . . .	4-208
4-39	Typical Data for Earth-oriented Spacecraft . . . . .	4-213
4-40	Comparison of Solar Array Control Schemes . . . . .	4-233
4-41	Comparison of Power Conditioning Approaches . . . . .	4-247
4-42	Normal Depth of Discharge (maximum load) . . . . .	4-255
4-43	Comparison of Cell Level and Battery Level Controls . . . . .	4-260
5-1	Flight Loading Conditions . . . . .	5-22
5-2	Margins of Safety for Configuration A-1 . . . . .	5-24
5-3	Margins of Safety for Configuration A-2 . . . . .	5-25
5-4	Margins of Safety for Configuration A-3 . . . . .	5-26
5-5	Margins of Safety for Configuration B-1 . . . . .	5-27
5-6	Margins of Safety for Configuration B-2 . . . . .	5-27
5-7	Structure Weights for Alternate Configurations (lbs) . . . . .	5-28
5-8	Penetration Equations . . . . .	5-33
5-9	Summary of Relative Costs of Various Configurations . . . . .	5-38
5-10	Material Stress and Weight . . . . .	5-40
5-11	Summary of Relative Costs of Various Materials . . . . .	5-42
5-12	Equipment Panels Weight Breakdowns . . . . .	5-47
5-13	Summary of Dynamic Analysis . . . . .	5-48
5-14	Relative Costs of Various Designs . . . . .	5-51

# TABLES (Continued)

<u>Table</u>		<u>Page</u>
5-15	Bus Top Panel Structure Weight Breakdowns . . . . .	5-54
5-16	Summary of Relative Costs of Top and Bottom Panels . . . . .	5-55
5-17	Tank Support Structure Weight Breakdown . . . . .	5-58
5-18	Solid Motor Support Structure Weight Breakdowns . . . . .	5-61
5-19	Predicted Dynamic Loads for Retrothrust Motors . .	5-62
5-20	Solar Panel Structure Typical Section for an Area of 42 ft <sup>2</sup> Weight Breakdowns . . . . .	5-66
5-21	Solar Panel Frequencies . . . . .	5-67
5-22	Worst Case Cold Conditions Down to 25-Watt Shunt Dissipation . . . . .	5-74
5-23	Worst Case Cold Conditions in Full Sun at 1.67 AU . . . . .	5-75
5-24	Power Profiles of Equipment Panels . . . . .	5-79
5-25	Average Equipment Panel Temperatures . . . . .	5-81
5-26	Average Steady-State Equipment Panel Temperatures . . . . .	5-81
5-27	Heat Flux Out Through 1/4-Mil Aluminized Mylar Insulation for Spacecraft Interior Temperature = 40°F, Heat Flux Rates in Watts/Ft <sup>2</sup> .	5-104
5-28	Heat Flux Out Through 1/4-Mil Aluminized Mylar Insulation for Spacecraft Interior Temperature = 85°F, Heat Flux in Watts/Ft <sup>2</sup> . . . . .	5-104
5-29	Heat Flow Through Heat Shorts . . . . .	5-107
5-30	Evaluation of Selected Pyrotechnic Criteria . . . . .	5-139
5-31	Evaluation of Magnetometer Sensor Deployment Subsystems . . . . .	5-151
5-32	Evaluation of Solar Panel Deployment Subsystems . . . . .	5-157

# TABLES (Continued)

<u>Table</u>		<u>Page</u>
6-1	Cable Routing Approach Tradeoff Considerations . . .	6-6
6-2	Two-Assembly Harness Design Tradeoff Considerations . . . . .	6-8
6-3	Equipment Mounting Tradeoff Considerations. . . . .	6-10
6-4	Mounting Panel Tradeoffs. . . . .	6-12
6-5	Equipment Size Standardization Tradeoff Considerations . . . . .	6-15
6-6	Packaging Technique I Tradeoff Considerations . . . .	6-17
6-7	Packaging Technique II Tradeoff Considerations. . . .	6-20
6-8	Equipment Chassis Design Materials and Pro- cesses Tradeoff Considerations. . . . .	6-22
7-1	Comparison of Vendor Solid Propellant Designs . . . .	7-7
7-2	Performance Parameters of Selected Retromotor Design . . . . .	7-19
7-3	Weight Breakdown and Comparison with Vendor Proposals . . . . .	7-20
7-4	Failure Rate Reduction History for Components . . . .	7-31
7-5	Test Failure Rates after the 20th Test . . . . .	7-31
7-6	Evaluation of Historical Failures . . . . .	7-33
7-7	Engine Performance Parameters. . . . .	7-57
7-8	Component Weight Lists, Bipropellant Supply . . . . .	7-70



## I. INTRODUCTION

Volume 5 presents the design considerations and tradeoffs that resulted in the preferred mechanization of the Voyager spacecraft subsystems. This volume provides the discussion designated as Part B, Section IV of the final report format provided in JPL's statement of work. Possible approaches to mechanization of the subsystems are defined, and design analyses and possible implementation difficulties are described. In general, the selections were based on Mariner approaches and the following criteria:

- 1) That the system or technique performs the required function
- 2) That the most simple and reliable method or approach is utilized
- 3) That the technique is consistent with the 1966 conceptual freeze date
- 4) That the mechanization easily interfaces with other spacecraft functions.

Since Volume 2 contains functional specifications for each area, the selected subsystems are not described in great detail in this volume. The process which resulted in the preferred subsystem approach being selected is described, and performance analyses for the selected subsystems are provided. Detailed analyses and background data are presented in the appendices.

Reliability is of the utmost importance to Voyager, and much effort has been devoted to defining subsystems with this in mind. Since the simultaneous operation of at least portions of the communications, attitude control, and sequencer subsystems are required to maintain ground control of spacecraft functions, the fundamental elements of these subsystems were selected with great care. Each subsystem is described in terms of the approach for attaining increased reliability through the use of alternate modes and redundant components. Strong emphasis was

placed on minimizing switching and control in achieving the alternate functions.

Section II presents the selection criteria and interface requirements of the science payload and planet oriented package (POP). The photographic sequence and its effect on the data handling and data automation equipment (DAE) interfaces are discussed. Considerations relating to the use of a body-fixed POP and one with one and two gimbals are described. A solution of the problem of bearings operating in vacuum, which TRW has used on other spacecraft, is illustrated and applied to the POP gimbal drive mechanization.

Design of the telecommunications subsystem is described in Section III. The main alternates considered were the selection of transmitter power outputs in the range of 10 to 80 watts with telemetry rates between 128 and 8000 bits/sec, the use of single and double gimballed antennas of various sizes, and sizing of bulk storage within the constraints of present capabilities and telemetry capacity. Some of the critical choices related to the attainment of the desired omniantenna coverage and resolution of problems related to the use of a coherent or noncoherent capsule link in the presence of propagation uncertainties.

Section IV describes the design of the stabilization and control (S and C) subsystem, the central sequencer and command (CS and C) subsystem, and the electrical power subsystem. The rationale used in defining the suggested interface between the DAE and the spacecraft sequencer is included in this section.

The processes used to define the structural design, the thermal control system, and separation and deployment mechanisms are described in Section V. Structural considerations that result from use of a liquid bipropellant engine are shown and compared with similar considerations for the solid engine. Also included are the structural designs for the spacecraft using a large fixed-dish antenna (Configuration C) which uses earth-pointing attitude control.

Section VI describes the electrical packaging design and shows integration of the packaging design with spacecraft structural and thermal control considerations.

Finally, in Section VII, the propulsion subsystem design tradeoffs are described. These are based on the three basic vehicle configurations that were selected for design study, considering primarily the liquid bipropellant engine versus the solid engine. Other over-all propulsion/vehicle configuration tradeoffs are described in Volume 4.

Several pages in Section IV (Electrical Power Supply) bear information that is proprietary to TRW. These pages are so identified in the text and should not be reproduced or disclosed to others without the written permission of TRW. The pages to which this pertains are 4-231, 4-232, 4-257, 4-259, 4-260, 4-261, and 4-262.

Analyses and detailed design data to support the considerations discussed in the text are provided in Volume 5 Appendices, A through L.

## II. SCIENCE PAYLOAD AND PLANET ORIENTED PACKAGE

### 1. ALTERNATIVE SCIENCE PAYLOADS

The objective in considering alternative experiments and the resulting science payload changes is to evaluate the flexibility of the spacecraft design concept. It is intended to become involved here neither in the design problems of the experiment equipment nor in the selection of the particular experiments to be included in the final payload. Consequently, some liberties have been taken in combining worst-case conditions without examining fully the likelihood that an experiment embodiment would exhibit all of the features at once.

#### 1.1 Interplanetary Environment

It appears that the next generation of interplanetary experiments will operate on the same principles as those carried today but will be more complex. Additional detectors and signal processing will result in higher data rates. It had been intended to hypothesize a variety of possible sets of instruments to test whether the spacecraft design could accommodate them. However, as the design evolved it became clear that all of the major interplanetary fields and particles experiments could be accommodated. Consequently, a single set of instruments, similar to those for Mariner but with higher data rate, was chosen for evaluation (see VS-4-210).

These instruments are as follows:

- a) A set of four directional meteorite detectors capable of measuring flux, velocity, acoustic energy, and mass
- b) Two solar plasma detectors
- c) Four cosmic detectors
- d) Three solar flare detectors (also suitable for trapped radiation measurements)
- e) Two magnetometers.

A major objective for Voyager is the refinement of magnetic field and plasma data obtained in interplanetary space. Unfortunately, the magnetometers have reached the limit of the state of the art in their detection threshold. The helium magnetometer flown on Mariner, for

example, had a threshold of a few tenths  $\gamma$ . The flux gate magnetometer with a threshold similar to the helium magnetometer, is lower in weight, volume and power consumption. However, it is susceptible to the acquisition of an unknown zero offset ( $<2\gamma$ ) on exposure to large magnetic fields prior to and during launch.

The magnetometer requires that the magnetic field of the over-all flight spacecraft be less than  $1\gamma$  at the sensor. A similar requirement exists for the Pioneer spacecraft which TRW met by selection of non-magnetic components where possible, by careful electronics design, and by cancellation if components (such as the TWT) have a field that exceeds the desired limits. These precautions resulted in a field that was below the threshold of the test instruments ( $<0.2\gamma$ ). Similar precautions will be required for Voyager, including the use of a boom to extend the magnetometer away from the spacecraft.

The state of the art in flight magnetometers has provided sensitivities of the order of  $0.25\gamma$ , therefore, a target field of  $\leq 0.25\gamma$  at the magnetometer sensor is appropriate. In the case of Pioneer the sensor was approximately 7 ft from the control axis of the spacecraft. The electronics on Voyager will be about one order of magnitude more in mass than that on Pioneer. If we assume the magnetic field will be proportional to the mass of electronic components, then using a dipole law, the Voyager sensor should be about 20 ft from the electronics. Since the boom can be mounted at the edge of the solar array, a  $0.25\gamma$  field at the sensor should be obtainable with a 14 ft boom. It appears appropriate, however, to ease the problems of parts selection, ground loop reduction, boom lengths and over-all magnetics control. Accordingly, a boom length of 20 feet was selected for vehicle design purposes.

## 1.2 Mars Exospheric Environment

Basically, the same measurements made in the interplanetary environment are also of interest in Mars orbit.

Prior to Mariner encounter, it was thought that the planetary magnetic field would be several orders of magnitude greater than the interplanetary field. Consequently, the possibility of carrying two magnetometers--one primarily for interplanetary measurements and the other primarily for in-orbit measurements was considered. Use of a flux gate and a helium magnetometer will permit correlation of outputs during cruise. A fixed magnetometer with a precise angular orientation at the edge of the solar array would be prime for the planetary measurements and the boom-mounted instrument would be prime for cruise. The boom-mounted magnetometer would be retractable for the injection acceleration period but would be sized to survive deboost without retraction. This approach still appears desirable because of the backup feature provided. It should be possible to calibrate the spacecraft fields by comparison of sensor outputs and by rotating the spacecraft in Mars orbit such that the fixed sensor can provide an uncertainty less than 1%. Accordingly, two magnetometers are included in the selected design. Further evaluation based on explicit Mariner data compared with estimates of the spacecraft field at the edge of the solar array will be required to ensure the advisability of this approach.

In addition to these instruments, a radio antenna and receiver have been postulated. This experiment involves comparing the phase of VHF or UHF signals with each other or with the telemetry carrier during occultation of the spacecraft by Mars. At other times, the receiver could be used for radio noise measurements. Means for deploying antennas will be required for this experiment.

Several radio noise measurement experiments have been considered such as a VLF plasma wave and EM wave experiment and a LF/MF radio noise experiment. For these experiments, obtaining large unobstructed

fields of view is the most difficult requirement, but a similar requirement exists for the particle and fields experiments, and therefore the RF experiments pose no special problems.

### 1.3 Planetary Observations

Hypothesizing the science payload for planetary observations has largely consisted of collecting a representative list of instruments which approximate the size, weight, and power given in the 1971 Voyager mission guidelines and apportioning the available telemetry capacity among them. The spacecraft design provides more than enough volume for these instruments, permitting larger instruments or some additional instruments as weight and power budgets allow. Specific interface problems are discussed below.

#### 1.3.1 Photographic Observations

As discussed in Appendix A, with the contemplated telemetry rates (up to 4,000 bits/sec) a partial map of Mars at a resolution of 1 km together with nested high resolution pictures can be obtained during the six months in orbit. The coverage will depend on the number of color filter pictures taken. Complete coverage over 120 degrees of latitude could be obtained in three colors for the sample orbit considered.

The most significant interface problems which arise from a photographic experiment are those caused by the data rates into bulk data storage (BDS), the pointing requirements imposed on the planet oriented package, and the complex storage and sequencing required to interleave engineering and other data, amounting to 10 per cent or so of the total, with the almost continuous transmission of pictures. The factors which size the photographic experiment are described in detail in Appendix A.

The fundamental limit on the photographic experiment is the BDS design, assuming existing state of the art tape recorders. The equipment postulated uses a pulsed digital scan of  $1024 \times 1024$  points, obtaining  $6.3 \times 10^6$  bits/picture and a storage vidicon to permit reading into the BDS relatively slowly. The use of a SEC storage vidicon would improve performance somewhat, but such a tube adaptable to pulsed digital scan is felt to be a significant development problem.

Using film is extremely attractive from the standpoint of obtaining high quality pictures with modest optics and open loop image motion compensation (IMC). However, the uncertainty of the radiation environment that will be encountered represents a significant risk in relying on film. Depending on the conclusions reached from the Mariner IV flight it may be desirable to consider film for data storage.

Another storage possibility is dielectric tape. Although the performance of this transducer approaches that of film and its development is proceeding rapidly, some development risk would be involved in selecting such a device.

Although the mission guidelines state that IMC would be the responsibility of the experiment equipment, the preferred design for the POP can provide 5 to 10 per cent IMC for image motion encountered at periapsis. This performance is good enough for obtaining reasonably good resolution for the postulated high resolution camera. Also the high resolution camera is shown as incorporating IMC based on ground command values of predicted motion, which is also expected to be good to 5 per cent or better. To obtain the best resolution possible under lower lighting conditions, the experiment would require active IMC good to 1 per cent or better. This capability was not postulated because of the complexity of such sensors and because EPD 250 indicates a willingness on the part of experimenters to limit the high resolution capability to lighting angles near 180 degrees, for which 5 to 10 percent IMC is adequate.

### 1.3.2 Spectrometric Experiments

The experiments postulated (see Volume 2) for spectrometry generally represent existing state-of-the-art instruments. The fields of view, the wavelength ranges, and the wavelength scanning speed are consistent with instruments of moderate complexity capable of diagnosing the presence of various atomic and molecular constituents with sufficient detail to resolve ambiguity. Quantitative photometric measurements permit estimating scattering cross sections, absorption coefficients, fluorescent lifetime, and the like. Generally, the spectral resolution postulated is not good enough for determining pressure.



If there were no flight capsule, more spectral resolution would probably be desirable. For the 1971 mission, however, it appears better to obtain diversified coverage of the spectrum within the weight and power allocation.

The selected instruments are as follows:

- a) A vacuum UV scanning spectrophotometer covering the range  $0.11$  to  $0.34\mu$  in the first order. This instrument with its 5-inch aperture telescope,  $10\text{\AA}$  spectral resolution, and a  $0.02$  by  $2$  degree field of view is essentially the UV air glow experiment of POGO.
- b) An IR scanning spectroradiometer covering the range of  $0.7$  to  $20\mu$ . This instrument has 6-inch optics, about  $0.02\mu$  wavelength resolution, and an  $0.05$ -radian field of view.

The UV spectrometer could be designed to produce  $1\text{\AA}$  resolution at a sacrifice in sensitivity, although it is possible that the telescope aperture could be designed to retain the sensitivity.

Consideration was given to substituting an interferometric IR spectrometer capable of a resolution of  $5\text{ cm}^{-1}$  over the region  $5$  to  $30\mu$  for the instrument postulated. However, within the weight limits of the mission guidelines it appeared more desirable to obtain coverage of the near IR. Thus, the more conventional scanning instrument was postulated for the tentative science payload.

### 1.3.3 Radiometric Measurements

One thermal-mapping experiment has been postulated. Alternative schemes may eventually be adopted, but requirements for thermal control, clear field of view, and output data rates are representative of a broad range of potential mechanizations. The selected instrument is an IR multichannel scanning radiometer covering the visible and near IR, the water vapor bands, and the far IR. This instrument has a resolution varying between about  $0.5$  and  $3\text{ mr}$  and a scan line length of  $50\text{ mr}$ .

### 1.3.4 Photometric - Meteor Flash

In addition to the complex scanning instruments, it seems appropriate to incorporate a simpler photometric experiment. Such an experiment requires a more continuous pointing at Mars and produces data at a lower

rate over longer periods of time than the others listed above. At the same time, as shown in Appendix B, monitoring the vacuum UV bands appears to offer great potential for obtaining useful statistical data on meteors in the Mars atmosphere. The instrument selected is an UV photometer meteor flash detector. This instrument operates in the 0.25 to 0.3  $\mu$  and 0.3 to 0.45  $\mu$  bands with 30-degree fields of view and 2.3-inch diameter optics.

#### 1.3.5 Alternative Planet Observation Experiment

One alternative which would require relatively major changes in the POP configuration has been suggested by Eastman Kodak Company. A single layer aperture (say 12 inches) reflecting optical system could be used at the central few degrees of the field for obtaining very high resolution photographs (order of 10 meters), with the surrounding segments of the field (say between 5 and 10 degrees) used for spectrometric and radiometric measurements with an order of magnitude improved spectral resolution. The basic telescope would probably weigh about 100 pounds making the the planetary observation sensors weigh 150 instead of 90 pounds. However, some such technique may be the only way to achieve photographs approaching 5 meters' resolution. Since this type of alternate could use up most of the available weight margin and implies the development of all these experiments by one contractor (a significant departure from the experimenter-oriented methods of the past), this alternative has not been considered in our spacecraft design. However, the balanced gimbal POP concept recommended provides a basic design capable of accommodating such a change as this without major redesign.

#### 1.4 Spacecraft Flexibility

The recommended spacecraft design provides a large ( $\approx 60$  ft) circumference. At any point on this disk, sensors can achieve solid angle fields of view of greater than  $2\pi$  steradians with the flight capsule attached and nearly  $4\pi$  steradians after capsule separation. Consequently, within foreseeable growth possibilities, such factors of two or three in weight, the planetary and interplanetary observation experiments of the Voyager 1971 spacecraft science payload are limited only by the degree to which weight reserves are made available for power supply and for the experiments themselves.

The recommended design of the POP provides additional volume, spare leads, and excess heat dissipation capacity to permit adding (about 25 per cent) to these instruments. As mentioned in Section 1.3.5, although significant changes could require redesign of the POP, the spacecraft concept provides the flexibility to accommodate such an increase if the overall weight allocation is available. The limit on weight in the POP will probably be established as much by c.g. control problems as by any other factor. However, sufficient weight allocation to permit the use of counterweights could solve this problem too.

In accordance with the description of the data automation equipment (DAE) given in the mission guidelines, it has been assumed that the DAE has a number of built-in sequences plus the capability to accept new programs from the command and sequencing system. The data sequences contained in Figures 3.5-1, 3.5-2, and 3.5-3 of VS-4-210 (Volume 2) are based on the assumption that the DAE formats the photographs in the BDS so that blanks occur at times at which transmission of other data is planned. An alternative method, that of stopping and starting the tape recorder, has not been postulated for normal (short) interruptions except under failure mode conditions. See section III. For long interruptions in the picture sequence the tape recorders are assumed not to run.

#### 1.4.1 Telemetry and Data Handling

Equipment used for video and IR mapping and imaging imposes the greatest demands on the telemetry and data handling subsystems. Changes in sequencing, scan rates, and resolution can significantly affect the data storage format and write-read requirements in the bulk data storage system and determine the data transmission rate requirements.

The proposed telecommunications and data handling subsystems are sized for a data transmission rate of 4096 bits/sec, corresponding to a total data capability of  $\sim 2 \times 10^8$  bits/orbit. This allows a mapping mission to be performed, using a tricolor television system at a ground resolution of 1 km, and also allows simultaneous thermal mapping at a resolution of a few kilometers. Nesting high resolution ( $\sim 50$  m) TV pictures can also be obtained by time sharing the data storage capability. The system design assumes that images can be stored on the TV sensors for 30 to 40 seconds.

Changes in the selection or operation of other experiments do not significantly affect the telemetry and data storage subsystems, since adequate buffering is provided by a core storage in the data handling subsystem.

#### 1.4.2 DAE-Spacecraft Sequencer Interface

Two definitions of the interface between the DAE and central sequencer and command (CS and C) subsystem are hypothesized and examined in Section III-2 of this volume. One definition is that the spacecraft sequencer simply passes ground commands and data to the DAE and has no further participation in science sequencing. The other definition is that the DAE decodes incoming commands, but virtually all are transmitted at the time of execution and the DAE is not required to have an extensive memory. It is found that the spacecraft sequencer can accommodate the second approach by simply doubling its memory. Since this appears to be the maximum task that is required of the CS and C and since it can easily be performed, the subsystem sizing is based on this requirement. Clearly, any requirements between these extremes can be accommodated by the selected design.

## 2. PLANET ORIENTED PACKAGE

Part of the Voyager science payload will be contained in the planet oriented package (POP) incorporating those experiments that require articulation with respect to the spacecraft body. The instruments and selected POP design are described in Volume 2. The alternate mechanizations and considerations that led to that design are discussed in this section.

### 2.1 Design Requirements and Objectives

The POP provides a minimum of 8 cubic feet for mounting science experiment equipment (SEE) with an area of 6 square feet perpendicular to the nominal line of sight. All equipment requiring Mars visibility will have access to this common face. The structural design of the POP will provide pointing precision for the SEE in both a zero- and one-g environment without realignment or compensation and with an equipment weight of 100 pounds. An objective is to obtain full coverage of Mars from any point in the orbit when the spacecraft is in the normal cruise attitude.

Provisions for mounting the SEE will consist of a single center located equipment-mounting shelf parallel to the viewing direction (Figure 2-1).

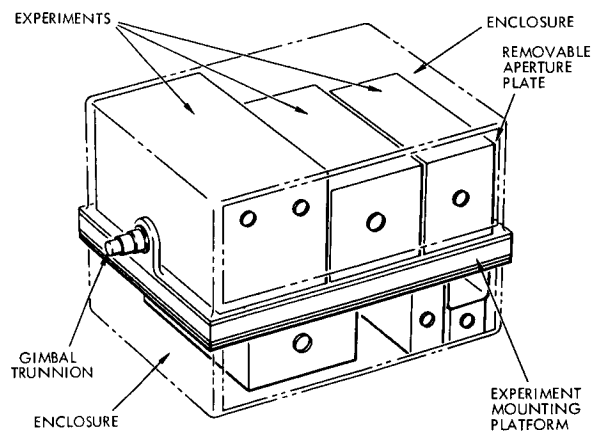


Figure 2-1. Planet Oriented Package

The shelf provides rigidity between instruments, insuring alignment integrity. Mounting provisions are available for equipment installation on both sides of the shelf. This method of mounting will provide a means of attaching numerous SEE with a maximum frontal area for sensors. It also maximizes access room and keeps cable lengths to a minimum.

The accuracy of the POP pointing and spacecraft attitude control system will be such that each axis of the POP will be pointed at the center of Mars or a selected spot on the surface of the planet with an accuracy of 0.5 degree and a maximum rate of  $10^{-4}$  rad/sec. These requirements are based on obtaining no more than 10 per cent overlap on 5 x 5 degree pictures and maintaining image smear rates caused by attitude rates to values commensurate with orbital velocity smear rates (see Appendix A). Exposure of high speed elements of the pointing drive to vacuum is avoided.

## 2.2 POP Mechanizations Considered

POP configurations having no gimbals, one gimbal, and two gimbals have been evaluated in terms of operational utility, vehicle interface, and implementation complexity. In addition, two gimbal sub-systems have received fairly detailed design consideration involving equipment layouts, gimbal and drive design, and evaluation of design difficulty. The tradeoff factors associated with over-all POP design are discussed in the following paragraphs; mechanization techniques are covered in later subsections.

### 2.2.1 Body-Fixed POP

A body-fixed POP is possible if the pointing is accomplished by using the attitude gyros for reference and torquing to the required attitude. The basic reference would be provided by sun-Canopus attitude and the vehicle would be required to return to that attitude every 2 or 3 hours to reset the gyros. This is the simplest system, at least in terms of the POP, but it is also the least accurate for general pointing because of gyro drift and torquing errors. All of the required orientation components are already available in the attitude control system.

However, normal use of this technique introduces considerable complexity in the central sequencing and command (CS and C) subsystem and in the high gain antenna pointing requirements if efficient utilization of communication time is achieved.

Another method of pointing uses body-mounted horizon scanners. A difficulty of this method is that provisions have to be made to enable offset pointing if it is desired to point away from the center of the visible surface. This can be done either by biasing the horizon scanner outputs or by gimbaling the horizon scanner.

### 2.2.2 Single-Gimballed POP

A single gimballed POP was seriously considered for Configuration C, which has a large body fixed antenna pointed along the roll axis toward the Earth. For this configuration, spacecraft roll does not require change in antenna pointing. Hence, the functional replacement of one POP gimbal with spacecraft roll is attractive. The gimbal axis would be parallel to the vehicle yaw axis. A horizon scanner would provide the roll attitude and gimbal angle reference. Pointing in directions other than the center of Mars would be achieved by biasing the horizon scanner output. An alternate (backup) approach would be to use the Canopus sensor or a special star sensor with a wide slit field of view to update the roll attitude based on star recognition (on earth) as they pass the sensor field of view with gimbal angle controlled by command. Because of the variation in orbital rate during the orbit, attitude control gas requirements increase unless a reaction wheel in the roll attitude control channel is included. Configuration C (see Volume 4) shows the system. A single gimballed POP could also be used for a solar pointing spacecraft but has been dropped on the basis of the additional antenna pointing complexity.

### 2.2.3 Double-Gimballed POP

With a double-gimballed POP the vehicle can remain sun-Canopus oriented and a gimbal arrangement devised such that the entire planet can be viewed at any time. Such a gimbal arrangement, indicated in

Figure 2-2, imposes the fewest constraints on the CS and C, the antenna pointing program, and the stabilization and control system.

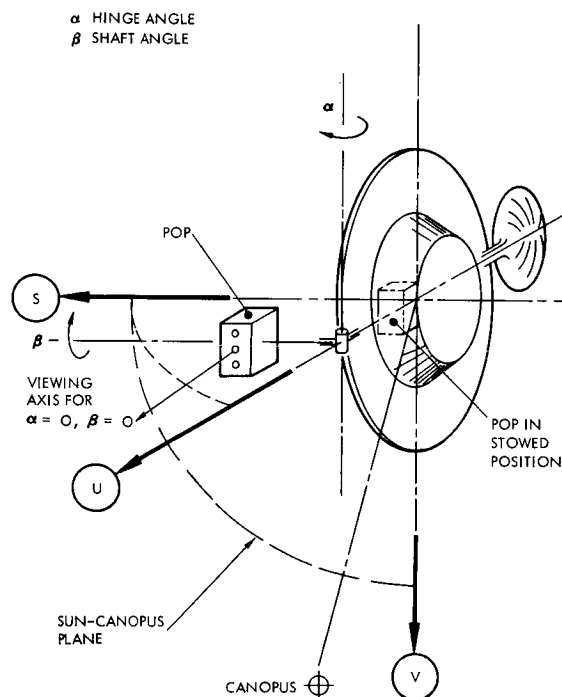


Figure 2-2. Conceptual Double-Gimballed POP

#### 2.2.4 Comparison of POP Gimbal Arrangements

The POP control and gimbal techniques just described are compared in Table 2-1 on the basis of simplicity, accuracy, and the availability of backup or alternate modes of operation. For the accuracy evaluation the following component errors were used in the various system configurations. All errors are assumed to be 3 values.

- Canopus-sensor accuracy, 0.1 degree
- Fixed gyro drift, 0.4 deg/hr
- Gyro torquer (and power supply) scale factor, 0.1 per cent
- Gyro, sun sensor, canopus sensor alignment to TV camera LOS, 0.2 degree
- Sun-sensor accuracy, 0.1 degree



Table 2-1. Comparison of POP Control and Gimbal Techniques

Number of Platform Gimbals	System No.	Pitch	Yaw	Vehicle Attitude Reference	Scan Platform Reference	Estimated Pointing Accuracy, (degrees)	Relative Complexity*	Method of Pointing Platform or Scanning	Programmer Requirements	Possible Backup or Alternate Modes	Comments
None	1	Gyro	Gyro	Gyro	N/A	0.72	1	Gyro torquing	Provide gyro torquing signals to arrive at pointing directions	Sun/canopus attitude	Requires control system reacquisition after picture taking interval
	2	Gyro	Horizon scanner	Horizon scanner	N/A	2.3	3	Bias horizon scanner outputs	Gyro torquing to acquisition Mars; provide offset commands	System No. 1	Roll angle bias uncertainty dominates error
	3	Gyro	Horizon scanner	Horizon scanner	N/A	0.7	5	Gimbal horizon scanner	Same as system 2	System No. 1	
One	4	Earth sensor	Earth sensor	Horizon scanner and bias stars	Gimbal angle pickoff or horizon scanner	1.7	3	Gimbal platform in yaw, bias horizon scanner output for roll	Provide commands for offset pointing	System No. 1	
	5	Earth sensor	Earth sensor	Horizon scanner bias and stars	Roll angle determined by observing stars as they pass Canopus sensor	0.4	4	Same as system 4	Same as system 4	System No. 1 System No. 4	It may be difficult to use star sensor effectively because of variations in the pointing program
Two	6	Sun sensor	Sun sensor	Canopus sensor	Gimbal angle pickoffs	0.46	3	Command the desired gimbal angles	Provide platform gimbal angle commands	System No. 1	Use gyros for attitude reference when sun or canopus is eclipsed. Accuracy $\approx 0.74$ degrees
	7	Sun sensor	Sun sensor	Canopus sensor	Horizon scanners	0.65	5	Bias horizon scanner outputs	Provide scanner acquisition commands and bias commands	System Nos. 1, 2, 4, and 6	Provides capability of reducing orbital position uncertainty
	8	Sun sensor	Sun sensor	Horizon scanner and gyro with star sensor update	Gimbal angle pickoffs	0.43	5	Command desired gimbal angles	Provide platform gimbal angles	System Nos. 1, 2, 4, and 6	Possible that Mars roll orientation will simplify command programming

\*1 least complex, 5 most complex

- Horizon-scanner accuracy, 0.4 degree
- Attitude control system dead zone, 0.25 degree
- Horizon scanner scale factor uncertainty, 8 per cent
- POP gimbal drive error, 0.3 degree (each axis)

These errors are considered typical values that can be obtained by careful design but are not necessarily the best achievable. The accuracy estimates do not include pointing errors because of uncertainty in vehicle orbital position, a significant factor the first few days in orbit.

The complexity factors shown in Table 2-1 refer to the complexity of the instruments required for pointing and do not include complexity introduced in other subsystems. These factors were determined by assigning one point of complexity to each gimbal and drive (POP or horizon scanner) and one point to each ungimballed horizon scanner. If continuous or nearly continuous Mars pointing is required, it is felt that the additional complexity in the sequencer and DAE required for the body fixed or single gimbal system nearly offsets the simplicity of these approaches. Therefore, pointing system complexity alone is not a basis for selection.

As far as accuracy is concerned, all systems are nearly the same except those that use a bias in the horizon scanner output to provide offset pointing. This is brought about by the 8 per cent uncertainty in scanner scale factor.

For the body mounted or single-gimballed platforms, periods of relatively high body or gimbal angle rates may be required for some orbit inclinations. Also, these periods are likely to occur near periapsis, at which time picture-taking operations occur and the best accuracy is required.

System 6 (two gimbals) is capable of performing all of the required operations with a minimum of interaction with other spacecraft subsystems. Its accuracy is compatible with the system requirements and it imposes no restrictions on picture-taking time and does not require

time-consuming sequence to arrive at the required attitude. It also can easily accommodate image motion compensation in the pointing commands. This approach was selected for the baseline design. Although the television experiment will require only brief periods of Mars pointing, some of the instruments will require pointing for long periods. To avoid having to sequence pointing commands continuously for these periods, use of horizon scanners is desirable. For this reason, they are included and the POP will have both closed loop (horizon scanners) and open loop (gimbal angle commands) modes of control. These modes will be selectable by ground command.

### 2.3 Boom-Mounted Double-Gimballed POP

A two-axis boom-mounted system which provides a capability for unlimited fields of view is shown in Figure 2-2. This POP is mounted on a hinged shaft, the hinge located on the outer edge of the solar panel to enable rotation to both sides of the panel. The hinge allows the POP to be swept through  $\pm 90$  degrees. The shaft would then be designed to allow the POP to be rotated through  $\pm 180$  degrees. The shaft is of sufficient length to give full visibility over the equipment section of the spacecraft.

#### 2.3.1 POP Drive Mechanization

Except for the requirement for a cable wrapup instead of an RF joint, the drive mechanization for the boom-mounted double-gimballed POP is identical to that for the high gain antenna (see Section III-1). Both consist of an integral yoke and shaft drive system using sealed wobble gear drives and AC motors. The gimbal angle rotations and general mounting arrangements are as indicated in Figure 2-2. The general vehicle layout shown reflects configuration A-2, which is not the preferred design.

#### 2.3.2 Operational Considerations

The long shaft which enables viewing over the spacecraft equipment compartment requires that the boom-mounted POP be stowed and latched during launch and orbital injection an undesirable feature of this

approach. It may be desirable to use the television cameras or an approach guidance sensor prior to injection; if so, the added requirement to relock the platform prior to injection is a serious deficiency. In addition, design studies showed that it is unreasonable to design the drives to support the POP fully extended in a 1-g field. Therefore special provisions have to be made to test the platform drives at less than 1 g. For these reasons this approach was not selected although its flexibility and ability to handle a variety of orbits is desirable. Instead an approach was devised in which the unbalanced moments restrained by the drives are nominally zero. This system is described in the remainder of this section.

#### 2.4 POP Design Considerations

Figure 2-3 shows the selected POP configuration and general equipment arrangement. Its over-all weight is 125 pounds, including the science instruments. A honeycomb center shelf provides support for all instruments using top and bottom mounting. Access covers are provided in the top, bottom, and rear of the compartment. To avoid feed-through bolts which could interfere with equipment on the opposite face of the shelf, the instruments are mounted to inserts bonded into the honeycomb. TRW has used this mounting approach with success on Pioneer and OGO and has encountered no difficulty with honeycomb panels of this size.

The instruments with the largest fields of view are mounted on the side of the compartment away from the solar array to allow the largest possible gimbal rotation before the solar panel obstructs their view. Conversely, it is desirable to locate the television cameras closest to the array to maximize the shading of their apertures, which is desirable since they are generally not used when the POP is pointing in the general direction of the sun.

##### 2.4.1 Fields of View and Coverage

As shown in Figure 2-3, the instrument package is supported by a fork on the end of a rotatable shaft. The shaft permits  $\pm 180$  degrees of rotation and the fork permits  $\pm 135$  degrees to provide coverage of

somewhat more than a hemisphere, as limited by the spacecraft body or solar panels. The shaft is supported by bearings contained in two housings which are fixed to the spacecraft structure. The shaft angle is set at 22.5 degrees relative to the solar panel, placing the shaft nearly normal to the orbit plane when the spacecraft is in the sun-Canopus attitude. This arrangement permits viewing any point on the visible surface of Mars from any point of the orbit. For most viewing conditions the field of view is perpendicular to the shaft axis, this requiring near zero rotation for the fork angles. To keep the fork angles zero the ideal configuration would be to align the shaft axis perpendicular to the Mars orbit. However, nodal regression can change alignment within a few months by 10 to 20 degrees depending on the orbital characteristics so there is no reason to attempt to obtain exact normality. Fork angle excursions within  $\pm 20$  to 30 degrees would cover the majority of arrival conditions at Mars and orbital inclinations typical for the mission. The large unobstructed field of view for the POP assembly is in the direction of the daylight portion of the planet. A detailed description of the orbital considerations and coverage provided by this system is given in Section III-5 of Volume 4.

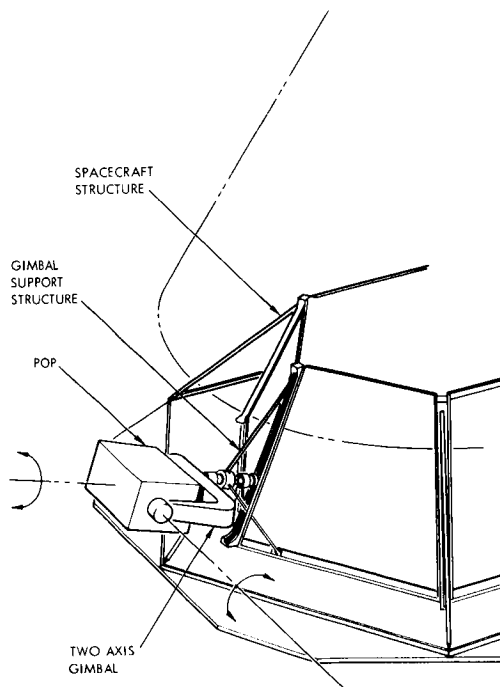


Figure 2-3. Selected POP Configuration and General Equipment Arrangement

#### 2.4.2 POP-Mounted Instruments

Typical POP-mounted science instruments consist of the following:

- Photographic experiment, high resolution television  
low resolution television
- Meteoroid flash
- IR scanning spectrometer
- UV spectrometer
- Scan radiometer

The present design is for 89 pounds of instruments, but heavier weights could be accommodated. In addition to the experiments, the POP will mount the Mars horizon scanner.

#### 2.4.3 Thermal Control

Of the oriented experiments, the television optical systems place the greatest demands upon the thermal design. The high resolution optical systems require a nearly uniform temperature in order to maintain optical resolution. The Mars scanning radiometer requires a fairly uniform temperature since it has an image-forming optical system. The remaining experiments have temperature level but not temperature gradient requirements. Most of the POP will be shaded from the sun by the solar array. Because of this and the rather large heat leaks through the optics, a thermal radiator will not be required. With thermal conductance mounts and multilayer radiation insulation, a 25-watt heater will be required to maintain average package temperature between 0 and 85°F. For a detailed analysis of POP thermal requirements, see Section V-2.

#### 2.4.4 Gimbal Drive

POP gimbal drive design requirements are as follows:

- a) Pointing accuracy relative to spacecraft,  $\pm 0.25$  deg
- b) Angular tracking rate, 3 mr/sec

- c) Slew rate, 10 mr/sec
- d) Angular acceleration,  $0.6 \text{ mr/sec}^2$
- e) Cable wrapup required for 100 wires
- f) Angular freedom:
  - shaft axis,  $\pm 180$  degrees
  - package axis,  $\pm 135$  degrees
- g) Mass imbalance, 8 ft-lb without tumbling
- h) Stall conditions. The drive must withstand stalled conditions without internal damage.
- i) Seals. High speed elements sealed in a pressurized atmosphere.

a. Gimbal Motors

The drive systems considered were: 1) a DC direct drive torque motor, 2) a DC torque motor and gearing, 3) a stepper motor, and, 4) an AC servomotor with gearing. A DC motor coupled directly to the lead gives the theoretical maximum load acceleration. From size and weight considerations, however, a small 400-cps motor with a large gear ratio has a definite advantage, and thus a compromise is indicated. Since high accelerations will not be encountered, a direct-drive DC motor is not a logical choice. In fact, because of the problems associated with brush life, RFI, and magnetic fields the selection of any DC motor is not indicated even when used with appropriate gearing.

Direct-drive using stepper motors cannot be considered because of the prohibitive size and weight of the motors required and the fact that the required system resolution cannot be obtained without gearing. Stepper motors used in conjunction with appropriate gearing, however, offer some desirable characteristics. The size, weight, power, and gear ratio requirements closely approximate those of an AC servo-motor drive system while the response and speed regulation under varying load conditions are superior. In addition, the stepper

motor is particularly adapted to digital control. The undesirable characteristic is the lack of information on which to estimate the possibility of long life, and for this reason a stepper motor is not recommended. In addition, the stepper motor requires relatively complex drive circuitry compared to that required for an AC servomotor.

An AC-servomotor drive system appears to be the logical choice for the following reasons:

- 1) AC servomotors are free from the undesirable features of DC motors, namely brush life, RFI, and high stationary magnetic fields.
- 2) AC servomotors are rugged and reliable and control circuitry is highly developed for either proportional or on-off control.
- 3) The drive mechanism of the AC servomotors can be made into a relatively compact package although the high speed components must be sealed and pressurized to prevent exposure to the space environment.

b. Sealed Drive Selection

Three small, light-weight candidates are available which fall into the category of sealed rotary drives:

- 1) Spur Gear Drive, similar to that developed by Kearfott for JPL.
- 2) Harmonic Drive, developed by United Shoe Machinery Corporation.
- 3) Wobble Gear Drive, developed by TRW Systems Group and used on OGO.

Table 2-2 summarizes the relative tradeoffs for the various candidates. The two most appropriate drives in terms of over-all packaging are the wobble gear and the spur gear drives. Because of its simplicity, sealing provisions, and proven space performance, the wobble gear is preferred. The wobble gears are similar to those developed for the drives for the OGO solar array and experiment package. During the OGO program these drives were subjected to environmental and



Table 2-2. Sealed Drive Packaging Tradeoff Summary

Tradeoffs			
Sealed Drive Candidates	Reliability		Packaging and Gimbal Compatibility
	Number of Gears Based on 100:1 Reduction	Number of Rotating Seals	
Wobble gear (Preferred)	Gears: 2	None Uses bellows and static "O" ring or hermetic seals	Internal design moderately simple, packages extremely well with gimbal
Harmonic drive	Gears: 2	None Uses thin flexible metal tube hermetically sealed	Internal design moderately simple, difficult to package with gimbal, requires additional gears and bearings
Spur gear drive	Gears: 8 (Based on 4:1 reduction per gear mesh)	Two sets of "O" ring seals	Internal design moderately simple, can be designed to package well with gimbal

performance testing and were operated beyond 10,000 hours in vacuum. On OGO I, launched September 5, 1964, and last interrogated on May 27, 1965, the units operated properly upon command.

Figure 2-4 shows a typical OGO sealed drive mechanism. Sealing is accomplished by two bellows installed between the nonmoving parts of the mechanism and the driving gear. The unique feature of the drive mechanism is the use of a pair of specially-cut wobble gears for the output stage. Action of the bearing carrier and a tilted bearing internal to the unit produces a nonrotating conical nutation (or wobble) motion of the driving gear at the end of the main bellows. This motion causes rotation of the output gear and shaft by sequential engagement of a limited number of gear teeth.

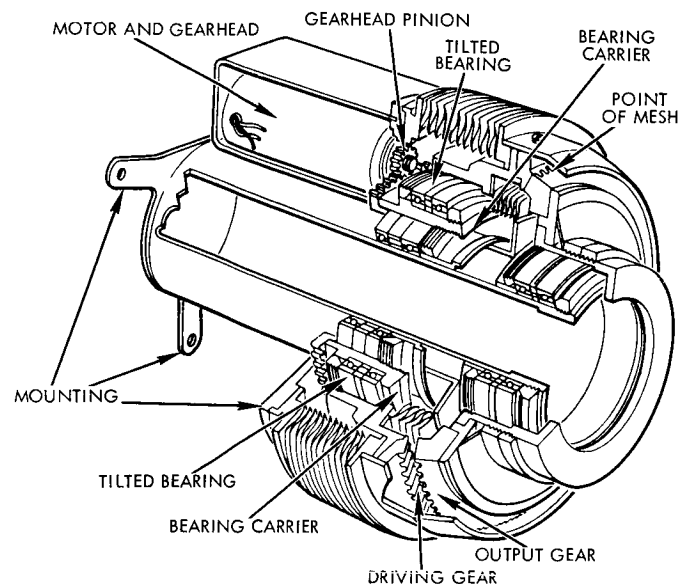


Figure 2-4. Wobble Gear Drive

c. Shaft Position Encoder

Two types of analog devices, the potentiometer and the resolver, were considered for possible use in control of the shaft position. Although potentiometers can be obtained which approach the required resolution and accuracy, they depend on brushes for electrical

contact between the stationary and rotating elements. Brushes are susceptible to shock, vibration, and wear. The requirements for long life, high resolution, and continuous rotation dictate the use of a film type potentiometer. The complete mechanization using potentiometers becomes rather involved. D-to-A converters will be required to convert the command signals to analog form. Also, an A-to-D converter will be required to convert and hold the potentiometer outputs for telemetry. Since the telemetry word length is 7 bits, this information will require two telemetry words. For these reasons and because of the extreme care required to meet the accuracy and linearity requirements, the potentiometer pickoff was rejected.

Resolvers eliminate the need for mechanical contact between the stationary and rotating members by depending instead on magnetic coupling. The resolver produces two outputs which are sine and cosine functions of the shaft angular position. However, both outputs are needed to provide unambiguous position information, and complex electronic circuits are required.

Digital shaft position encoders are basically of four types. These include:

- 1) Brush, in which readout is effected conductively through brushes making contact with a segmented disc
- 2) Magnetic, in which readout is effected magnetically
- 3) Capacitive, in which readout is effected electrostatically
- 4) Optical-photoelectric, in which readout is effected by photoelectric means.

These types can be further divided into devices in which successive increments of position are not identified and therefore must be counted and devices in which successive positions are uniquely coded so that absolute position information can be determined directly.

Since the resolution required is 0.1 degree or better, the direct reading encoders must produce 12 bits of information. These encoders are subject to errors that arise from incorrect relative

positioning of multiple tracks, from optics which use brushes or magnetic or capacitive sensors to read these multiple tracks, and from radial misalignment of an indexing assembly. Brush devices also have multiple brush problems and the photoelectric devices require light sources of questionable long life; the capacitive devices are sensitive to noise, and the magnetic devices produce rotating permanent magnet fields.

The incremental encoder represents the simplest type of encoder, usually consisting of a rotating disk having a single track of equally spaced segments and a suitable sensing member. The data is derived in increments and must be accumulated in external circuitry to represent shaft position. The direction of shaft rotation is obtained by using the output of a second pickoff displaced in phase 90 degrees from the primary output. By operating logically on the outputs of the two pickoffs direction of rotation can be determined. A disadvantage of using incremental encoders for position determination is that errors generated by noise transients, power failure, and other sources are accumulated. However, with the addition of reference points, another pickoff to the encoder, and provision for resetting the reference, these accumulated errors can be eliminated. Because of its simplicity the incremental shaft encoder was selected.

#### d. Drive Electronics

The drive electronics for the POP are dictated by the accuracy requirements and the type of shaft encoder. The electronics for both drive channels is shown in Figure 2-5. Two modes of control for the POP orientation will be selected by command from the spacecraft sequencer. The closed loop mode will point the POP at Mars in response to signals from the Mars horizon scanner, and open loop control will provide for positioning by ground commands programmed by CS and C. In open loop control, a digital signal from the CS and C

corresponding to a shaft position command is loaded serially into an up-down counter register. The logic compares the digital words in the command register with the word in the shaft angle register and generates a signal to drive the motor in the required direction. Preliminary dynamics studies indicated that the drives can provide pointing errors less than 1.5 mr with a steady-state rate variation less than 0.1 mr/sec when subjected to a 3 mr/sec command.

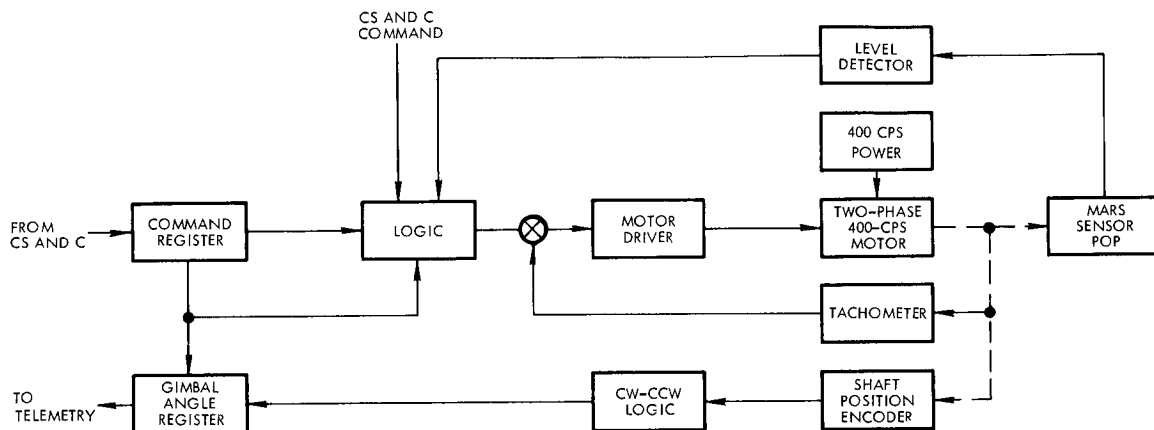


Figure 2-5. POP Drive Electronics Block Diagram

When (in closed loop control) the output signal from the Mars horizon scanner is fed into a level detector, and when the error signal exceeds a predetermined level, the level detector will trigger the motor driver, which will in turn apply two-phase, 400-cps power to the drive motor.

In either mode of operation the output of the shaft position encoder will feed an up-down counter register to accumulate the absolute shaft position angle for telemetering back to earth.

#### e. Mars Horizon Scanner

The initial studies of the radiometric character of Mars and its atmosphere have led to the selection of the planetary disk itself, rather than an atmospheric absorption disk, as the best known and most suitable optical reference to be used for infrared attitude sensing and control for a vehicle orbiting the planet. As discussed in

Appendix L, the wavelength region beyond 20 microns has tentatively been chosen, both because the variation of radiance with temperature difference is smaller in this region and because more energy is available than at shorter wavelengths in the expected temperature range. In addition, it was desired to avoid interference from atmospheric CO<sub>2</sub> radiation. The 20 to 35 micron region will require the use of silicon optics, but both of the principal vendors have manufactured flight hardware using silicon optics.

The possible variation in radiance across the face of the planet is in the order of 4 to 1 for even the most favorable wavelength region. For this reason the accuracy requirements immediately eliminate the simple radiation balance type of sensor, since the total radiation from one half of the planet can greatly outweigh that from the other half. Devices have been breadboarded and tested which eliminate radiance variations to the first order by dividing the detector array and processing the output to compensate for variations. Accuracy of better than 0.5 degree from 4 to 1 radiance variation have been claimed. In addition, the large angular variation makes the radiation balance instrument more difficult to design since a signal range of about 50 to 1 must be accommodated. We are thus restricted to scanners which in one way or another detect the geometrical edge of the planetary image. Five classes of instruments presently exist or are under development which do this.

- Conical scanners
- Rosette scanner
- Edge trackers
- Sector scanners
- Electronically scanned arrays

Table 2-3 presents a comparison of the characteristics of most of the horizon scanners that are flightworthy or in advanced development today. The qualification status of the instruments is indicated in the table.

Edge Trackers. Edge trackers which can accommodate the required angular range have been built and operated successfully in space. The mechanical reliability of such devices will depend strongly upon the specific mechanization used. The ATL device uses a flexure pivot to dither the field of view across the edge of the planet. The dither of about  $\pm 2$  degrees is about a deflection of the flexure pivot necessary

Table 2-3. Comparison of Horizon Scanner Flightworthy Characteristics

Supplier	Number Required	Scanners (2-axis)			Scanning System	Instrument Accuracy (1- $\sigma$ , deg)	Scan Angle (deg)	Instantaneous Look Angle (deg)	Spectral Sensitivity (microns)	Operating altitude (nmi from earth)	Qualified?	Flight tested?
		Volume (cu. inches)	Weight (lbs)	Power (watts)								
ATL (OGO)	2	270	13.2	11 max	Edge track at 4 points (Positor)	$\pm 0.25$ null	>90 for acq 2-4 dither	1 x 1	8.5 - 20	100 to 70,000	Yes	Yes
ATL (Gemini)	1	209	11.0	11 max	Edge scan along a 160 deg sector of horizon	$\pm 0.1$ null	160 deg in azimuth 2-4 dither	1.5 x 1.5	8 - 18	50 to 2000		No
ATL (Advanced Agena)	2	--	25	30	Edge track along a 90 deg sector of horizon	$\pm 0.15$ null		1 x 2		50 to 20,000	Yes	Yes
ATL (LEM)	2	110 (55 ea)	6.4 (3.2 ea)	7 (3.5 ea)	Flexure pivot Rosette scan	$\pm 0.2$	10 x 10 manual acq cone angle > 10°	0.9 x 0.9	14 - 18		Not developed	
BEC Mod 13-132 (Mercury)	2	154	6	7	Conical rotating prism	$\pm 1$ (Mod I3-133 claims 0.5)	70 search + 2 dither	2 x 8	1.8 - 18	50 to 300	Yes	Yes
BEC Mod B-160	3	926	20	4 average 12 peak	Edge - tuning fork dither	$\pm 0.1$		0.5 x 3	1.8 - 20	80 to 22,000		No
Firm edge tracker	3 or 4	Same as B-160, except Firm Cell gives dither of 10° to reduce cloud sensitivity.				$\pm 0.3$			14-16		Engineering model only	
BEC Rosette scanner (Mariner)	2				Rosette - dual rotating prisms, 2.99/1 gear ratio	$\pm 0.1$	70 cone	0.5 x 0.5 flake			Yes	No
BEC Mod 13-194	2	250	14	14	Conical rotating prism	$\pm 0.03$				100 to 200	Yes	Yes
BEC LPHS	4	1100	25	28.5	Electronic commutator	$\pm 1/2$ in error +0.1 with manual interpolation	5 to 170	10 x 90 each head	14 - 50		Engineering model delivered to JPL	
GE (Mark II)	2	2011 *	32.7 *	25 *	Conical scan	$\pm 0.1$	33	1 x 4	14 - 16	50 to 250		Yes
M-H	1	< 200 **	4 **	4 *	Vibrating reed alternates two fields of view on to detector	$\pm 0.36$	11 over each horizon	11 x 11	14 - 25	400 to 600		No
Kodak	4	280 307	25 **	25 **	Scan mirror (nutating)	$\pm 0.03$	3 x 5	3 x 0.5	14 - 16	50 to 500		Partial
TRW (RES)	1	286	7	4 average 5.5 max	--	$\pm 0.5$	64 max	64 max	12 - 20	6000 to 19,000	Yes	No

\* Includes computer to allow linear output of  $\pm 12$  deg; otherwise linear output restricted to  $\pm 1$  deg. This unit adds 3.0 lb., 185 cu. in., and uses 1 watt of power.

\*\* Does not include electronics.

to accommodate the angular span of the planet. The OGO scanner can be deflected to  $\pm 22.5$  degrees (mechanical) on either side of null. An examination of the quoted material properties indicates that for such large deflection angles the flexure pivot is being operated beyond the fatigue endurance limit. However, if null is designed to be at the average angle subtended by the planet, such excessive stress will be avoided and the pivot will operate well below the endurance limit.

Thus, the flexure pivot edge tracker has the advantages of offering adequate instrument accuracy, good potential reliability, and a history of having flown successfully.

Edge trackers in general are sensitive to radiometric anomalies such as cold clouds near the edge. This constitutes a disadvantage, but one which appears less serious for the relatively cloudless climate of Mars than for earth.

Both the edge tracker and the rotating scanners automatically provide a chopped radiation signal which helps to reduce sensitivity to radiation from the surroundings. The presence of chopped radiation also permits the use of thermistor bolometers with their relatively high sensitivity and short time constant. Only a single detector is used, so matching of detectors is not required.

The Barnes Engineering edge tracker uses a tuning fork principle for dithering the scan field across the edge of the planet. This results in a rather small angular shift and makes locking onto the edge of a cold cloud a possibility. Barnes has tested a laboratory model of the same basic scanner configuration which uses the frustrated internal reflection principle rather than the tuning fork dither to provide a field shift of 10 degrees.

Characteristics of Lunar-Planetary Horizon Scanner. An electronically scanned array Lunar-Planetary Horizon Sensor (LPHS) was developed by Barnes Engineering for JPL. Data indicates that analogue interpolation is necessary to meet the accuracy specification. The angular range can readily be met by this scanner. The power and



weight are expected to be reduced very shortly by the use of field effect transistor chopping rather than light modulation chopping. Laboratory tests of FET switching have proved encouraging. The prime advantage of this device is its ability to do the job without the use of moving parts. Disadvantages are the necessity for matching large numbers of thermocouples in the array, the very small signals developed by thermopiles and the necessity for incorporating an offset heater to take care of the problem of negative output signals generated by radiation into space by elements not looking at the planet. As in all devices in which the radiation is not chopped, temperature gradients within the structure are more critical.

Edge Tracker versus LPHS with Respect to Mission Requirements. If a selection of scanners must be made at this time, one would have to choose the OGO-ATL scanner because of its development status. However, both the Barnes edge tracker using the frustrated internal reflection modulator (FIRM) and the Barnes LPHS with analogue interpolation are attractive although further development is necessary. The latter is especially attractive because of its lack of moving parts; it does not presently have the required accuracy but the vendor has indicated that accuracies of  $\pm 0.25$  degree are feasible. The development of these units must be followed carefully during Phase I-B to establish their status in relation to the 1966 development freeze date.

f. Additional Design Considerations

Cable Wrapup. It presently appears that two cable wrapup assemblies will be required to accommodate wires from the POP. Each assembly will consist of approximately 50 wires grouped together in flat ribbons and curled between two discs. A cover will be provided to shield the wires from direct exposure to space environment. This technique is presently being used successfully on OGO.

Lubrication. The gimbal bearing and drive units will employ the same proven lubrication techniques which were developed and used on OGO. All exposed slow-moving elements will be plated with low-shear precious metal and impregnated with molydisulphide.

### III. TELECOMMUNICATIONS SUBSYSTEM

The Voyager spacecraft telecommunications subsystem performs two essential roles. It maintains an adequate two-way link between the spacecraft and the earth for tracking, telemetry, and command and as well keeps contact with the capsule after it separates from the spacecraft and lands on Mars. Data received from the capsule is then relayed to earth over the earth-spacecraft telemetry link. The discussion of the subsystem here first concerns itself with the studies that have led up to selected configurations for both of these roles. Next, the performance analyses that supported the communication subsystem design effort are reviewed. Tradeoff studies covering specific items in the subsystem are finally discussed, first with respect to antennas and then with respect to transmitters, receivers, command detectors, RF switches, and duplexers.

#### 1. COMMUNICATIONS

##### 1.1 Earth-Spacecraft Communications

##### 1.1.1 Functions

The requirements of the earth-spacecraft communication link are as follows:

- a) Telemetry. Transmit the output of the data handling subsystem (engineering and scientific data) from the spacecraft to the Deep Space Network (DSN) stations.
- b) Command. Receive and process commands from the DSN stations and deliver detected command bits to the central sequencer and command (CS and C) subsystem.
- c) Ranging. Receive, demodulate, and retransmit the DSIF ranging code signal.
- d) Range Rate. Receive, coherently translate, and retransmit the RF signal transmitted from the DSIF.

The above functions are required at ranges up to encounter plus 1 month ( $2.3 \times 10^8$  km) and an objective of the design is to provide significant capability at encounter plus 6 months ( $3.8 \times 10^8$  km).

### 1.1.2 Baseline Antenna Configurations

The baseline communication subsystem for spacecraft configurations A and B (see Volume 4) utilizes two antennas, a fixed low-gain antenna and a high-gain, double-gimballed antenna. Configuration C utilizes three antennas, high, medium, and low gain.

A fixed, broad coverage, low-gain antenna is required for early postlaunch coverage and is desirable to permit critical command capability for the entire mission independently of the spacecraft orientation capability. The requirements for a low-gain antenna are essentially identical for the three spacecraft configurations.

In Configurations A and B the nose fairing and spacecraft structure arrangement constrain the size of the high-gain antenna to a maximum of about 6 feet. With two-axis gimbal actuation the antenna can be utilized during cruise and maneuver to keep the beam directed toward the earth. With Configuration C, however, a body-fixed, 16-foot fixed parabolic dish antenna can be incorporated, a capability which, in fact, is the principal advantage of this configuration. With a fixed antenna, earth pointing is accomplished by the vehicle attitude control system.

To communicate while in maneuver attitude, Configuration C requires an additional antenna with  $\pm 90$  degrees of freedom about one axis (assuming the spacecraft can roll to an arbitrary angle). It is desirable to keep the beamwidth of this additional antenna as broad as possible commensurate with adequate communication margin at encounter range to minimize its required pointing accuracy and to enable the antenna to provide backup cruise mode communications if the spacecraft reverts to sun pointing. (See Volume 4, Section III.) A dish of approximately 3-foot diameter appears to be best for this role.

A block diagram of the baseline communication subsystem for spacecraft Configurations A and B are given in Figure 3-1, and operating modes in Table 3-1. The baseline subsystem block diagram for spacecraft Configuration C is given in Figure 3-2, and operating modes in Table 3-2.

In all three configurations, a 20-watt transmitter is used in the spacecraft providing a bit rate capability at encounter plus 1 month of approximately 4000 bits/sec for Configurations A and B and 28,000 bits/sec for Configuration C.

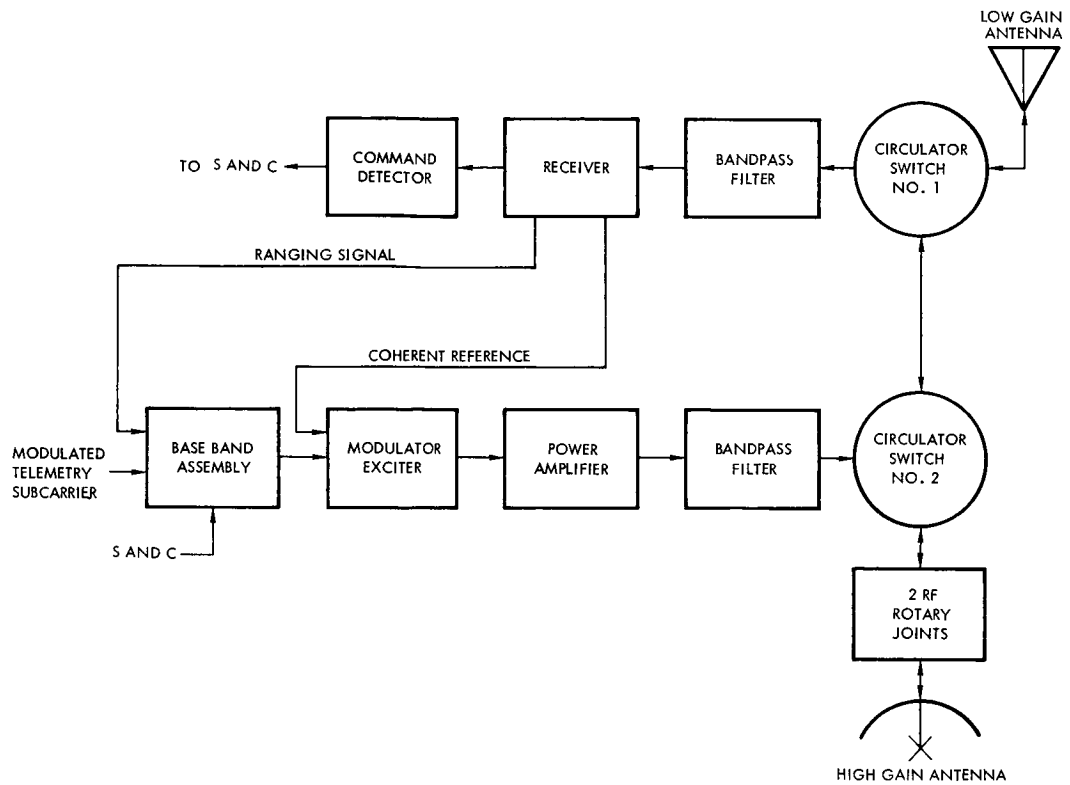


Figure 3-1. Baseline S-Band Communication Block Diagram for Spacecraft Configurations A and B

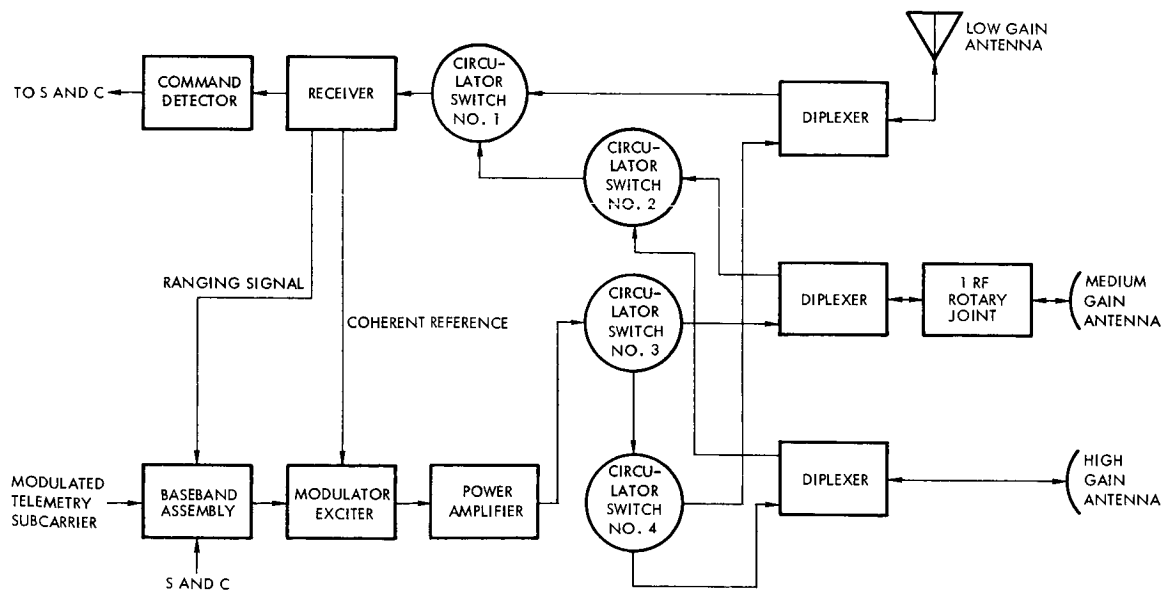


Figure 3-2. Baseline S-Band Communication Block Diagram for Spacecraft Configuration C

Table 3-1. Communication Modes for Configurations A and B

	Receive	Transmit
Early postlaunch	low-gain	low-gain
Cruise	low-gain	high-gain
Maneuver and orbit	high-gain	high-gain

Table 3-2. Communication Modes for Configuration C

	Receive	Transmit
Early postlaunch	low-gain	low-gain
Cruise	low-gain	high-gain
Maneuver	medium-gain	medium-gain
Orbit	high-gain	high-gain

### 1.1.3 Selected Configuration

The basic configuration selected for the spacecraft is Configuration A, as discussed in Volume 4. Consequently, the detailed analysis of the communication subsystem focused on that configuration. Two objectives were dominant in the analysis of the subsystem:

- a) Increase reliability by utilizing redundancy and alternate modes of operation
- b) Minimize switching complexity, particularly in the command link where lock-out failure modes could prevent ground command corrective action.

Six alternate transmitter-receiver antenna configurations were evaluated in the light of the mission requirements, development problems, reliability, and interactions with other subsystems. Weight-reliability tradeoff studies were conducted on a total system basis to assist in over-all choices of configuration. This study is described in Volume 4, Section IV. These studies led finally to the configuration shown in Figure 3-3.

#### a. Antennas

The selected configuration has three S-band antennas, low, medium, and high gain. The medium gain antenna was added to the baseline subsystem since the weight-reliability studies demonstrated that the redundancy thereby provided for operational modes using the high-gain antenna was an efficient means for enhancing total spacecraft reliability.

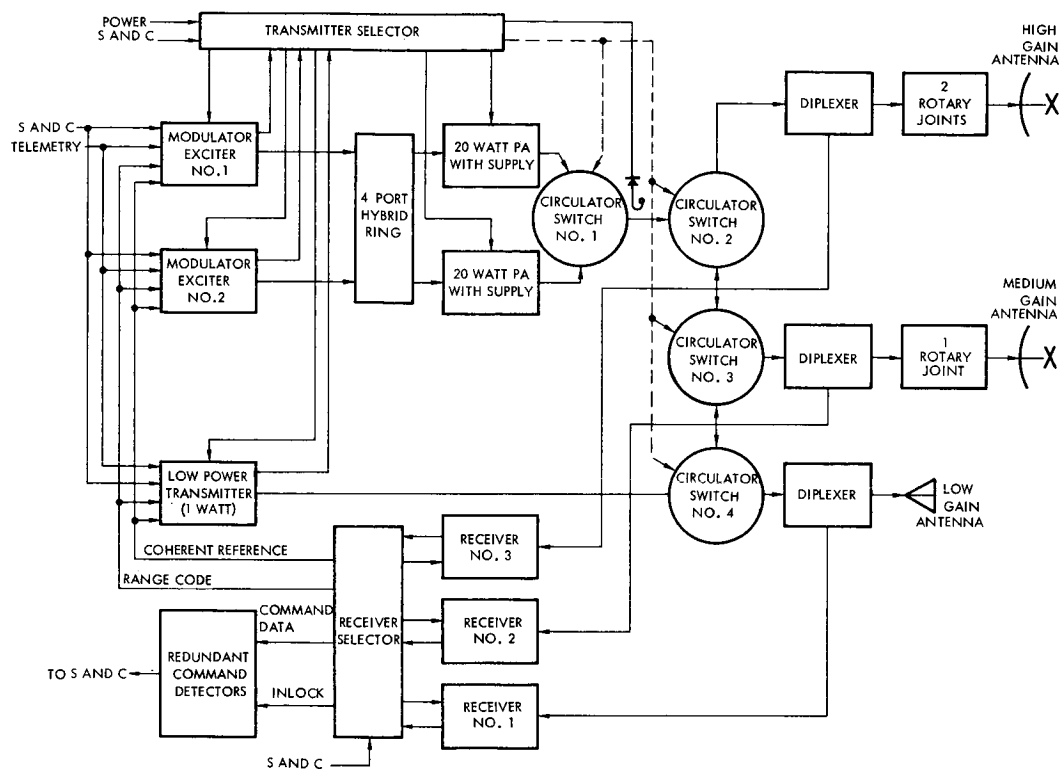


Figure 3-3. Selected S-Band Communication Configuration

Low-Gain Antenna. To meet the performance goals with the low-gain antenna, coverage is required to be as large as possible commensurate with adequate communication margin. In evaluating gain requirements the following criteria were used:

- a) Command capability on low-gain antenna is required to at least encounter plus 1 month when the spacecraft is sun-oriented
- b) The maximum cone angle after launch plus 30 days is 45 degrees (occurs near encounter)
- c) Use of the 100-kw ground transmitter at DSIF Venus site is acceptable, if required, near encounter
- d) Spacecraft receiver noise figure is 10 db
- e) Early cruise will require communication at cone angles up to approximately 110 degrees
- f) The antenna must provide shroud-on communications during boost.

The selected antenna, described in Section 1.4.3 provides approximately hemispherical coverage (-8 db minimum for 90-degree cone angle) for short range, and at least 2 db over a 45-degree cone angle as required for encounter range. (See Link Analysis, Volume 2, Section IV.)

To obtain significantly larger solid angle coverage for command, it would be necessary either to employ a multiplicity of low-gain antennas with associated receivers or receiver-input RF switches, or to increase the effective DSIF transmitter power to reduce the spacecraft antenna gain requirement below 2 db.

High-Gain Antenna. The high-gain antenna is a 5.5 x 6.5 foot elliptical paraboloid providing 30-db gain, the slight ellipticity necessitated by fairing constraints. Since approximately 6 feet is the maximum dimension that can be accommodated for this configuration, an unfurlable antenna is required to obtain higher gain. Until the reliability of unfurling mechanizations is established, it does not appear desirable to incorporate them in a conservative design.

A two-axis actuation on the high-gain antenna is required:

- 1) To prevent a 3-db pointing loss after encounter (see Fig 3-14)
- 2) To provide the capability for a two-maneuver trajectory correction sequence.

Medium-Gain Antenna. A medium-gain antenna (3-foot paraboloid) similar to that used on Configuration C was selected to back up the 6-foot dish. The broader beamwidth of the 3-foot antenna (10 degrees) enables the use of a single gimbal drive without producing excessive pointing loss after the first 30 days of flight. At encounter and in orbit, the maximum pointing error is approximately 2.5 degrees. The single-gimbal, lightweight antenna is a more conservative implementation of redundancy than the provision of an additional 6-foot, double-gimballed dish, but still provides for adequate margins in the redundant mode.

#### b. Transmitters

The selected transmitter configuration provides cross-strap redundancy of modulator-exciter and power amplifiers with operation on

any of the three antennas. The transmitter utilizes power monitor probes to provide on-board switching of the standby exciter and power amplifier in the event of RF power loss because of the long round-trip propagation time needed for ground command switching of redundant transmitter elements. Ground command backup is provided.

Launch mode communication uses a separate low power transmitter (solid-state, 1-watt output) which can operate continuously from liftoff through critical pressure altitude without danger of corona. The separate transmitter was selected for launch communication because the normal transmitter uses power amplifier voltages of 1000 VDC and pressurization would be required to prevent arcing. In addition, 20 watts of RF power would probably produce corona in the RF circuitry. If the exciter were designed to be large enough to use for launch transmission, additional in-line RF switching would be needed and an unnecessary power drain (about 10 watts) would be present during the remainder of the flight.

The normal and backup transmission modes are summarized in Table 3-3. All of these modes can be configured by ground command. In addition, on-board switching is accomplished by the transmitter selector logic summarized in Table 3-4.

As discussed in Section 1.5.2 in more detail, 20-watt TWT amplifiers are proven tubes currently in production for Apollo, and tubes of higher power, 40-watt ESF klystrons or TWT's, would require development for Voyager. Between the two tubes, the TWT development is assessed as the lesser risk for 1969 and 1971 missions, although the klystron will eventually yield superior performance. The spacecraft electrical power profile (see Section IV-3) indicates that a 40-watt transmitter probably cannot be supported at encounter plus 6 months and during the several hours of battery charging at initial sun acquisition, after maneuver and after eclipse. After capsule separation and during the first few months in orbit, however, the available electrical power is adequate to support a 40-watt transmitter. The availability of power suggests that a redundant combination of two tubes, a 20-watt and a 40-watt, is a good arrangement maximizing bit rate capability at encounter (40-watt transmission) and providing reduced power level (20-watt) during cruise and near end of life.



Table 3-3. Transmission Modes

Mode	Power (watts)	Antenna	Circulator Switch Used**			
			1	2	3	4
<u>Normal</u>						
I (launch)	1	low-gain	-	-	-	ccw
II (after sun-Canopus lock)	1	6-ft	-	ccw	cw	cw
III (cruise, maneuver, encounter, orbit)	20	6-ft	cw***	cw	-	-
<u>Backup</u>						
IV	1	3-ft	-	-	ccw	cw
V	20	3-ft	cw***	ccw	cw	-
VI	20	low-gain	cw***	ccw	ccw	cw

\* See Figure 3-3. cw = clockwise, ccw = counterclockwise

\*\* Circulator switch no. 1 selects power amplifier no. 1 or no. 2. Normally, the on-board logic selects the power amplifier, with ground command backup.

\*\*\* Shown for operation with power amplifier no. 1.

Table 3-4. Transmitter Selector Logic

Initial Condition	Malfunction	Backup Condition
Mode I	Loss of power	Mode VI*
Mode II**	Loss of power	Mode III**
Mode II**	Loss of Canopus lock	Mode I***
Mode III**	Loss of power	Switch 20-watt amplifiers****
Mode III**	Loss of Canopus lock	Mode VI

\* Inhibited by interlock for preset time after launch (post spacecraft-Centaur separation).

\*\* If there is a high-gain antenna malfunction, Modes IV and V are substituted for Modes II, III, by ground command.

\*\*\* Inhibited by C and S for fixed time interval during maneuvers.

\*\*\*\* Provided that modulator exciter output is normal; if not, then modulator exciters are switched.

However, risk is incurred in a TWT development, type approval, and life test program within the time scale of the 1971 mission. In view of this risk the selected design utilizes two 20-watt TWT amplifiers. During Phase IB it is proposed to re-assess the scope of a 40-watt TWT development program.

c. Receiver and Command Decoder

The selected receiver configuration (see Figure 3-3) utilizes three on-line receivers, one per antenna and contains no input RF switching. The receiver antenna selection occurs at the receiver output a decision based on the fact that input cross-switching between antennas (i. e., one receiver on each antenna with capability to interchange receivers) is excessively complex. Configurations in which a pair of receivers switch between antennas introduce possible lock-out failure modes if the receivers are on the failed antenna. The three receivers operate continuously on a single frequency. In normal cruise mode, for example, signal acquisition occurs in all three receivers. The choice of the signal fed to the redundant command detectors is made in the receiver selector using the following selection logic:

<u>Mode No.</u>	<u>Logic</u>
1. Maximum Coverage	Select receiver 1 (Figure 3-3) if signal present, if receiver 1 is not present, select receiver 2; if neither 1 nor 2 is present, select receiver 3.*
11. Maximum Gain	Select receiver 3 if signal present; if receiver 3 is not present, select receiver 2; if 3 and 2 are not present, select receiver 1.**

The redundant command detectors utilize mutually orthogonal pseudonoise codes so that detector selection at the DSIF is by selection of the proper code to address the desired command detector. Output switching to the CS and C subsystem is provided by the in-lock function of the command detector.

---

\* If no receiver is in lock, no range code, VCO reference signals, or command subcarriers are sent to either the modulator or the command detector.

\*\* If the spacecraft loses sun-Canopus lock, the CS and C provides signal which automatically switches the receiver selection to Mode 1.

#### 1.1.4 Telemetry Bit Rate Selection

Maximum range capability at the selected bit rates is shown in Table 3-5 for three operating modes: 1) the nominal mode for orbital operation, and 2) and 3) backup modes. A 210-foot DSIF listening station is assumed. (See Volume 2, VS-4-310 for Telecommunications Design Control Tables.)

Table 3-5. Range versus Bit Rate

Mode	Bit Rate			
	128	1024	2048	4096
	( $\times 10^6$ km)	( $\times 10^6$ km)	( $\times 10^6$ km)	( $\times 10^6$ km)
1) 20-watt high-gain antenna	1050	492	336	238
2) 20-watt medium-gain antenna	545	255	174	123
3) 1-watt high-gain antenna	235	110	75	53

Note: Encounter Range      90 to  $185 \times 10^6$  km  
      +1 month                130 to  $230 \times 10^6$  km  
      +6 months              330 to  $380 \times 10^6$  km

The 4096, 1024, and 128 bit rates were selected to obtain 0-db margin operation at the maximum range at encounter plus 1 month for the three operating modes 1), 2) and 3). An intermediate bit rate, 2048, was selected in order to increase the data rate and hence the amount of data received at intermediate ranges.

The bit rates selected also satisfy the objective of communications at encounter plus 6 months for operation in modes 1) and 2).

Additional intermediate bit rate steps could be included with a modest increase of equipment complexity. However, the value of such additional steps has not been established. The 3-db binary step granularity of the three highest bit rates is considered quite adequate. At bit rates below 1024, normal bulk storage tape readout cannot be utilized due to readin/readout ratio limitations. (See Section III-2, Data Handling Subsystem.) Hence, additional steps (e. g., 512, 256) would be utilized normally for non-nominal operation.

The inclusion of a higher bit rate (8192) has considerable justification since a maximum range of about  $168 \times 10^6$  km is possible at this bit rate. At present, however, there appears to be a possible problem on tape recorder readout speed range for speed lock control over greater than a 4/1 range. Hence, with this assumed constraint, inclusion of 8192 bit rate requires deletion of the 1024-bit rate unless separate tape recorders are utilized to cover the 8/1 bit rate range (i. e., one recorder reading out at 8192, 4096, 2048, and the other recorder reading out at 4096, 2048, and 1024). The bulk storage interface will be studied further during Phase IB (and in addition, link parameters further definitized) with a view to including the higher bit rate as discussed above.

#### 1.1.5 Operations with Multiple Spacecraft

The DSIF will be required to communicate with at least two spacecraft and possibly with two capsules for the Voyager mission. To permit this capability, the spacecraft and the capsule should transmit to the DSIF on different downlink frequencies to prevent interference and to facilitate their simultaneous reception. The 85-foot DSIF antennas provide two channel reception (JPL TM No. 33-83) and it is assumed that the 210-foot DSIF antennas will all provide two-channel reception. Hence it appears possible to receive, at a given antenna, from two spacecraft simultaneously or from one spacecraft and one capsule simultaneously. During cruise, and up to nominal encounter range, link calculations show that spacecraft telemetry reception (1024 bits/sec) is possible on the 85-foot antenna as well as on the 210-foot antenna, (see Volume 2, VS-4-310), thus providing four-channel reception capability at sites having both antennas.

There are two methods of obtaining two-way coherent communications with two spacecraft operating on different channels with the same coherency ratio. The simplest is to time-share the uplink, providing doppler data on one spacecraft for a period of hours while receiving from the second spacecraft operating in the noncoherent mode, and then vice versa. A disadvantage of this method is the operational inconvenience of changing transmitter frequency and reacquiring both spacecraft receivers. A second method is to frequency multiplex the uplink, i. e., transmit

simultaneously on both spacecraft receiver frequencies, necessitating duplicate doppler extraction equipment and reducing the effective transmitted power per channel by as much as 6 db as the result of the generation of intermodulation products.

If the transponders of the two spacecraft operate at slightly different coherency ratios so as to obtain downlink frequency separation, it becomes possible to obtain two-way doppler from both spacecraft utilizing a single uplink frequency (simultaneous doppler). However, the practicability of implementing slightly different coherency ratios within transponders has not yet been assessed.

Another alternative is to operate both spacecraft receivers on the same frequency with the same coherency ratio and provide downlink frequency separation by transponding coherently from one spacecraft and noncoherently from the other\* at a different frequency. By ground command, the two spacecraft modes could be interchanged. This method eliminates the need for DSIF transmitter time or frequency multiplexing, but still requires time-sharing for doppler extraction.

In view of the disadvantages and uncertainties of implementation of these alternatives, it is concluded that each spacecraft should be assigned a different frequency channel, both operating at the standard 240/221 coherency ratio, with two-way doppler obtained by time-sharing.

#### 1.1.6 Areas of Future Study

The power amplifier and the low-noise preamplifier are two key areas where component development could increase the capabilities of the communication subsystem.

The selected transmitter configuration uses two 20-watt power amplifiers developed on the Apollo program. Forty-watt TWT amplifiers are currently under development by several manufacturers. These

---

\* A "noncoherent" override transponder mode is provided in the selected design. This mode (activated by ground command) inhibits coherent transmission during receiver lock in order to eliminate turn-around noise degradation of the telemetry link during command transmission at or near threshold.

developments could be expected to meet a mid-1966 date for an engineering model if development were supported on the Voyager program. An attractive possibility for later missions is a 40 to 100 watt ESF klystron (see Section 1.5.2).

At present, the tunnel diode appears to be the best candidate for a low noise preamplifier but further reliability data is required. The tunnel diode is under active development and some life and failure mode data are available. The use of the low-noise preamplifier would reduce the receiver noise figure from 10 to 5 db. A 5-db improvement could be used in several ways. First, for the selected configuration, it would extend the command reception capability on the low-gain antenna to the maximum earth-Mars separation distance when using the 100-kw DSIF Venus site, and to encounter ranges for approximately a 1-month launch window when using the present 10-kw 85-foot antenna DSIF stations. It would similarly reduce the need for the 100-kw Venus site DSIF transmitter for two-way range code at encounter ranges. A second possibility using the device would be to reconfigure the receiver redundancy and provide passive input cross-strapping of receivers.

A third major area requiring further investigation is DSIF operations with multiple spacecraft and capsules. This assumes particular importance for the 1973 mission for which extended postlanding capsule life is anticipated.

## 1.2 Capsule-Spacecraft Communications

The flight capsule mission profile is divided into three phases: separation, entry, and postland. Of these three, the entry phase is the most demanding on the spacecraft communications subsystem, and at the same time the most important, at least for the 1971 mission, since measurement of the Martian atmosphere properties will be of prime importance. A summary of the complete capsule-spacecraft analysis is presented in Section 1.3.4, and the complete analysis is in Section 2 of Appendix F.

The nonredundant baseline configuration selected for study consists of a VHF antenna, VHF receiver, and a demodulator. The receiver and demodulator are switched on at the appropriate time in the mission and the

10 bits/sec asynchronous capsule data are sent to the data handling subsystem for commutation with other telemetry traffic for transmission to earth.

#### 1.2.1 System Configuration Selection

In reaching a configuration, five alternatives were evaluated (see Volume 4, Section IV), in the process of which weight-reliability tradeoffs were conducted on a total system basis to aid in determining the preferred redundancy for the link. A nonswitching configuration was selected primarily because of the short transmission time of the post-blackout entry data and the possibility of signal intermittancy which could create difficulties for on-board signal selection. A common preamplifier for both receiver channels was selected rather than a passive coupling of the receiver inputs in order to avoid a 3 db signal loss.

As a result of these tradeoffs and operational considerations, the configuration shown in Figure 3-4 was selected. This configuration provides two on-line 136-mc receivers for the capsule data; both detected outputs are commutated with other telemetry traffic and transmitted to earth. The antenna on the spacecraft for this link is a fixed, body-mounted turnstile, with reflector, providing a 110-degree beamwidth.

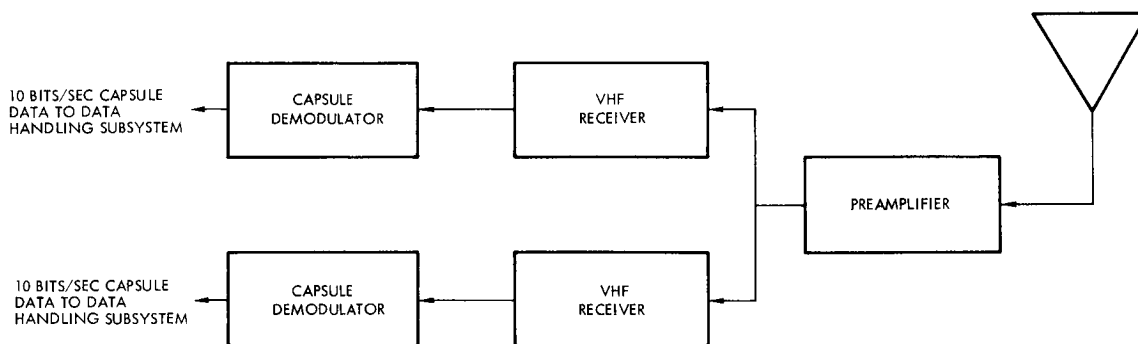


Figure 3-4. Selected VHF Communications Configuration

#### 1.2.2 Dual Spacecraft and Capsule Operation

It is specified for the 1971 mission that spacecraft time separation at arrival will be a minimum of 10 days, whereas post-impact capsule

life is 2 days. Hence, only the first spacecraft can receive from the first capsule; however, the first and second spacecraft might receive from the second capsule. It follows that for the 1971 mission both capsules should be on the same VHF frequency.

In 1973, when capsule life is extended, spacecraft in orbit and two landed capsules may all be operating at once. If spacecraft-to-capsule command is utilized to turn on capsule transmission, both capsules could be on the same frequency and both spacecraft could receive from either capsule. Alternately, both capsules could operate on separate frequencies and two-channel VHF receivers utilized on the spacecraft.

### 1.2.3 Parameters and Constraints

Table 3-6 lists the parameters associated with the spacecraft-capsule link for the entry phase.

The VHF link imposes the following constraints on the spacecraft:

- a) The antenna must have a 4-db gain at 136 Mc and be able to point in the direction of Mars during capsule entry
- b) A control signal is required from the CS and C to turn on and off the power to the VHF receiving and demodulating equipment
- c) The data handling subsystem must be capable of commuting two 10 bits/sec capsule data signals which are asynchronous with respect to the spacecraft timing.

The VHF link imposes the following constraints on the capsule:

- a) The capsule must be preprogrammed or receive commands from its own command system after separation, since no spacecraft-capsule transmitter is provided
- b) For the present mechanization, the capsule VHF antenna must have at least 0-db gain (circularly polarized) over a 90-degree cone angle and a front-to-back ratio of at least 6 db
- c) The capsule VHF transmitter must be capable of providing 20 watts power output with a 22-kc separation between the mark and space channels in the 136 to 138 Mc band.



Table 3-6. Capsule-Spacecraft Parameters for Entry Phase

Frequency	136 Mc
Modulation	FSK
Data rate	10 bits/sec
$P_e^b$	$1 \times 10^{-3}$
Maximum range	$4 \times 10^4$ km
Total system margin <sup>(1)</sup>	12 db
Capsule transmitter power	20 watts
Capsule circuit losses	0.5 db
Capsule antenna gain <sup>(3, 5)</sup>	0 db
Capsule antenna pointing loss	0 db
Spacecraft antenna gain <sup>(2)</sup>	4 db
Spacecraft antenna pointing loss	1 db
Spacecraft circuit loss	1 db
Effective system temperature <sup>(3)</sup>	1020°K
Predetection receiver bandwidth <sup>(4)</sup>	44 kc
Type detection	Matched filter

NOTES:

- (1) Includes 6 db for equipment tolerances and 6 db for fading effects.
- (2) Antenna gains are referenced to perfectly circular isotropic.
- (3) Includes contributions due to cosmic noise and preamplifier noise figure (4 db).
- (4) Total receiver bandwidth is 44 kc; mark and space channel are each 22 kc.
- (5) The capsule antenna should have a front-to-back ratio of 6 db to reduce the effects of multipath.

#### 1.2.4 Areas of Future Study

It is assumed that significantly higher capsule-to-spacecraft data rate is desirable. It is probable that an increase of 10 to 20 db is obtainable by a combination of improvements as discussed below:

- a) Capsule Entry Sequence. For the selected entry sequence (see Volume IV), the spacecraft remains in cruise attitude until after capsule impact. As a consequence, the maximum range at impact is 40,000 km. An alternate sequence

could be employed with the spacecraft in deboost attitude prior to capsule impact. This would effectively add approximately 6 db\* to the power margin.

- b) VHF Spacecraft Antenna. A larger aperture, narrower beam antenna is a possibility, but a careful assessment of look angle history would be required to determine pointing requirements during entry and during orbit.
- c) Capsule Antenna. The present study assumes 0 db capsule antenna gain. Further definition of the capsule design and look angle history may establish the feasibility of a higher antenna gain.
- d) Frequency Uncertainty. The frequency uncertainty establishes receiver predetection bandwidth and directly affects bit rate. Further study can probably establish means of reducing the frequency uncertainty (see Appendix F, Section 2).
- e) Multipath Fading. The present study conservatively allocates 6 db margin for fading. Further study may allow a reduction in margin allocation (see Appendix F, Section 2).

### 1.3 Subsystem Performance Analysis

This section summarizes the tradeoff and performance analyses conducted during the study to support the communication subsystem design effort. Details are given in Appendix F. In brief, four areas are covered:

- 1) The Range and Range Rate Link Analysis (Section 1.3.1) shows that ranging is available at least to encounter +1 month when the 100-kw DSIF transmitter and the spacecraft high-gain antenna are utilized. Range accuracy will be consistent with the DSIF Mark I ranging subsystem specification of +15 meters. Range code acquisition time is about 8 minutes at encounter. The analysis also shows that threshold receiver noise contributions do not limit the given DSIF range rate accuracy of 0.003 m/sec.
- 2) The Telemetry Link Analysis (Section 1.3.2) considers synchronization methods, pseudonoise sync acquisition and retention performance, single- versus two-channel systems, and performance of the selected systems. The communication efficiency for the selected two-channel system is shown to be comparable to the efficiency of a single-channel system. Bandwidth requirements and intermodulation and interference problems do not compromise system performance.

---

\* See Volume 4, Section 3.5.1

- 3) The Command Link Analysis (Section 1.3.3) compares various modulation and multiplexing schemes, concluding that the two-channel configuration of Mariner C will satisfy Voyager constraints. The performance of the selected command system is analyzed for communication efficiency, sync acquisition time, probability of in-lock indication, and the effects of bandwidth restrictions on data and sync channels. The Mariner C system appears adequate in these respects except perhaps for the degradation of the sync loop error function caused by the carrier-tracking loop. This problem requires further study.
- 4) The Capsule Link Analysis (Section 1.3.4) evaluates the effects of propagation (fading), system dynamics, frequency uncertainty, and efficiency on the choice of modulation for the capsule-spacecraft data link. A noncoherent FSK link is recommended because of its more gradual degradation characteristics in a fading environment whereas a coherent PM link has a relatively abrupt threshold characteristics and has potential problems related to frequency search and acquisition. Also considered are the tradeoffs between demodulating the capsule data at the spacecraft and repeater operation where capsule and spacecraft data are transmitted simultaneously in real time. The demodulating mode is chosen as primary with the repeater deserving further consideration in Phase IB.

#### 1.3.1 Range and Range Rate Link Analysis

Range rate information will be available from two-way coherent doppler measurements on the received carrier. One-way doppler can also be obtained but the stability of the spacecraft oscillators is such that the accuracy of the measurement will be no better than 30 m/sec based on a 5-hour minimum tracking period and smoothing times of 1 minute. Considering received noise only this accuracy can be achieved at doppler threshold (0 db in  $2B_{LO}$ ) as shown in Appendix F.

The ranging system will employ the JPL-developed multiple component pseudonoise sequences. After carrier demodulation the range code will simply be turned around, rather than regenerated in the spacecraft. This operation is shown to be feasible out to Mars encounter using the DSIF 100-kw transmitter and the spacecraft high-gain antenna. The thermal noise error at encounter is consistent with the over-all Mark I ranging system accuracy of  $\pm 15$  meters.

The ranging system analysis has assumed the use of the Mark I lunar code which provides unambiguous ranging to 800,000 km. Planetary codes

are available for unambiguous ranging to 100 million miles, although, naturally the acquisition times increase for these longer codes. Acquisition procedures and times are analyzed in Section 1 of Appendix F, which shows an 8-minute acquisition time at encounter for the Mark I lunar code. This is comparable to the 27-minute, two-way transmission time.

Finally, more efficient adaptive codes are being developed\* which offer hope of greater ranging efficiency. An optimum way to choose the code bandwidth (pseudonoise bit rate) is such that more of the downlink power is put into the code and less into the turn-around noise. The relation of the code bandwidth to ranging performance and acquisition time has been derived. Various acquisition schemes have also been considered. The greater efficiency obtainable with these adaptive codes would permit ranging with lower gain spacecraft antennas, lower power ground transmitters, shorter acquisition times, or appropriate combinations of these alternatives.

a. Turn-Around Ranging Analysis

Two effects of the uplink noise in the turn-around system are studied in Section 1 of Appendix F. First, the useful transmitter power is reduced by modulation of the downlink carrier by the uplink noise.

$$\text{Modulation loss caused by uplink noise} = e^{-\sigma_n^2}$$

where

$$\sigma_n = \text{rms phase deviation caused by uplink noise}$$

Second, the uplink noise density adds to the noise density of the ground receiver. However, for the Voyager parameters this effect is shown to be small, adding less than 0.1 db to the downlink noise density.

In addition to these effects, the noise in the IF limiter in the transponder will suppress the pseudonoise signal such that the effective downlink modulation index  $\theta_D'$  will be:

---

\* JPL Space Programs Summary No. 37-30, Volume IV, pp. 253-259.

$$\theta'_D \approx \frac{\pi}{4\beta} \theta_D, \quad \beta > 10$$

where

$\beta = N_1/S_1$  noise-to-signal ratio at input to transponder limiter

$\theta_D =$  downlink phase deviation at strong signal (no uplink noise)

The limiter also serves to control the uplink noise modulation of the downlink carrier. Section 1, Appendix F shows that  $\sigma_n^2$  is determined almost solely by the uplink and downlink deviations at strong signal levels. In particular, the downlink pseudonoise deviation should be minimized and the uplink deviation maximized, both consistent with carrier tracking requirements, to minimize the uplink noise modulation loss as well as its contribution to the over-all noise spectral density at the ground receiver.

Under the nominal conditions of the design control table, the downlink pseudonoise deviation will be 0.355 rads. The mean square phase deviation because of uplink noise is  $0.77 \text{ rad}^2$ .

#### b. Ranging Performance

For a carrier phase-modulated by a turn-around pseudonoise code and uplink noise, the total power  $P_T$  is distributed as follows:

$$\text{Carrier power, } P_C = P_T \cos^2 \theta'_D e^{-\sigma_n^2}$$

$$\text{Ranging power, } P_R = P_T \sin^2 \theta'_D e^{-\sigma_n^2}$$

In principle, the carrier and ranging performance margins can be made equal by the proper choice of  $\theta'_D$ . However, because of the need to restrict the downlink noise modulation ( $\sigma_n$ ), the optimum pseudonoise code deviation cannot be achieved unless the S/N at the transponder is maintained above about 0 db. The telecommunications design control table for ranging (Volume 2, VS-4-310) shows that even with the 100-kw transmitter and the high-gain spacecraft antenna, the S/N is -10 db. Therefore, the optimum deviation is not achieved.

Under the nominal conditions of the design control table, the downlink pseudonoise deviation will be 0.356 rad. The mean square phase

deviation due to uplink noise is  $0.772 \text{ rad}^2$ . The corresponding modulation losses and power requirements are summarized below:

<u>Modulation Losses</u>	<u>Carrier</u>	<u>Ranging</u>
$-10 \log e^{-\sigma_n^2}$	3.35 db	3.35 db
$-10 \log \sin^2 \theta'_D$		9.17
$-10 \log \cos^2 \theta'_D$	0.57	
S/N required in 1 cps	16.8	21.0
Total power S/N in 1 cps	20.7	33.5

More than half the downlink power is wasted in transmitting uplink noise. The total power requirements based on ranging is dominant indicating that the ranging will have the smaller margin. However, the design control table (Volume 2, VS-4-310) shows that the margin (14 db) is adequate to cover the sum of the adverse tolerances.

### 1.3.2 Telemetry Link Analysis

The telemetry link was analyzed (Section 4, Appendix F) for the following:

- Comparison of synchronization methods
- Acquisition and retention performance of pseudonoise synchronization
- Comparison of single- versus two-channel systems
- Performance of the two-channel system.

Methods of acquiring pseudonoise sync, acquisition times, and retention characteristics (mean time to unlock) have been studied. Since the acquisition time for this link is very short, no penalty is paid for utilizing a longer pseudonoise code which provides word as well as bit sync. Furthermore, the longer code minimizes the false-lock probability. The Mariner C sync format is therefore adopted: a 63-bit maximal length sequence with nine pseudonoise bits per information bit and seven data bits per word.

The choice between the single- and two-channel system is considered in the light of the Voyager bit rates. The sync power requirements are shown to vary from less than 1 to about 10 per cent of the data power. This means that two-channel communication efficiency is within less than 1 db of that of the single-channel system except at the lowest bit rate. Consideration of this small performance advantage of the single-channel over the two-channel system weighted against the flight-proven capability of the Mariner C mechanization led to the selection of the two-channel system.

The performance of the selected telemetry system is analyzed in terms of bandwidth requirements, power requirements, and intermodulation and interference effects. No important bandwidth limitations either at low or high frequency are encountered when the Mariner C data and sync formats are adopted. The power requirements considered the effects of receiver thermal noise and timing noise because of carrier, subcarrier, and bit sync jitter. An over-all data threshold S/N is developed which compares favorably with the Mariner C experience. The sync threshold is determined by limiting the data degradation from this cause to 0.5 db.

The intermodulation analysis shows that these products are a large source of wasted power in a two-channel system. An optimization procedure for the phase deviations is developed to minimize the over-all power requirements by minimizing such waste power. However, these products ideally do not appear as interference at baseband. Direct baseband interference between data and sync channels is made small by placing the data subcarrier at the null of the sync spectrum, and by keeping the sync power at least 1 per cent of the data power.

a. Synchronization Methods

Two basic methods of obtaining telemetry bit synchronization, using Voyager parameters have been compared: the pseudonoise synchronization system of Mariner C, and synchronization to a non-return to zero NRZ code as implemented on Pioneer. An integral part of the bit synchronization problem is the choice of bit waveforms to avoid interaction with the carrier loop; hence the problem of demodulation of a subcarrier, where used, is also considered.

The comparison of these systems is restricted to those parameter values most suitable for Voyager. The subcarrier frequency for the two systems is chosen as low as possible, consistent with the maximum bandwidth of the carrier tracking loop in the DSIF receiver. The two systems are chosen to have the same communication efficiency and data degradation caused by jitter on the locally-generated reference.

Other choices which must be made in the comparison are:

- Pseudonoise code length and NRZ subcarrier frequency
- Sync loop bandwidth
- Bandwidth expansion with single level
- Acquisition procedures.

Pseudonoise Code Length and NRZ Subcarrier Frequency. Both synchronization schemes require that the sync (and data) waveforms be such that the carrier tracking loop causes little distortion. The DSIF bandwidth  $2B_{LO}$  is 12 cps at threshold but expands to 120 cps under strong signal conditions. An NRZ subcarrier frequency of four times the data rate yields tolerable distortion at the lowest bit rate (128 bits/sec). Similarly, choosing the pseudonoise code length of 63 bits as in Mariner C, the basic clock rate is  $f_g = 576$  cps at 128 bits/sec and the waveform distortion is comparable to that for the NRZ subcarrier waveform.

Choice of Loop Bandwidths. Based on a 10:1 apportionment of power between data and sync, and a 7-db S/N ratio in the data bandwidth, it is concluded that at 128 bits/sec the pseudonoise sync loop noise bandwidth should be 1.3 cps or less. The required S/N in this bandwidth is 17 to 18 db. The NRZ synchronizer subcarrier demodulator requires a loop bandwidth of 20 cps to achieve the same mean time to unlock (about 200 hours). The bit sync loop following the subcarrier demodulator requires a loop bandwidth of 0.3 cps. At a loop S/N of 12 db in  $2B_{LO}$ , the mean time to unlock is over an hour.

Bandwidth Expansion. Section 4 of Appendix F shows that essentially no expansion of the basic sync loop bandwidths occurs, assuming that the coherent AGC available in the DSIF receiver maintains the signal level



constant into the NRZ demodulator/bit synchronizer. The bandpass limiter in the pseudonoise sync channel accomplishes the same function for that system.

Acquisition Procedures. For acquisition by the frequency offset technique, the acquisition time is about 50 seconds and the oscillator stability must be about 0.05 per cent. For the NRZ synchronizer, the acquisition time depends on the bit transition density but should not exceed 10 or 20 seconds. The subcarrier demodulator oscillator must be stable to 0.1 per cent the bit sync loop VCO to 0.04 per cent. Neither system should suffer from false-lock problems.

The performance of the two systems in terms of mean time to loss of lock, acquisition time, presence of false-lock points, and the required oscillator stabilities to implement these parameters are compared in Table 3-7 at a data rate of 128 bits/sec. As can be seen, the two loops do not differ greatly in performance with the chosen parameters. The pseudonoise synchronizer provides much quieter bit synchronization, while the NRZ synchronizer provides quieter subcarrier demodulation. With frame synchronization available independently, the word synchronization provided by the pseudonoise system is somewhat redundant. However, it may be useful for some real-time data reduction applications. Based on these comparisons, it is concluded that the two-channel pseudonoise synchronization system will best satisfy the over-all Voyager mission requirements. Further justification for the choice of the two-channel versus single-channel pseudonoise sync system is given in 1.3.2c.

b. Pseudonoise Sync Acquisition and Retention

Acquisition Techniques. Two pseudonoise sync acquisition procedures are available:

- 1) Offsetting the frequency of the DSIF sync loop VCO from the predicted spacecraft clock frequency  $f_s$ . The code phases slide by one another until the loop pulls in.
- 2) Automatic acquisition in which the clock is first acquired and then used to step the code bit-by-bit until the correlation peak is reached.

The first procedure is employed on the Mariner C command link and the second is used in acquiring the ranging pseudonoise code. Uncertainties

Table 3-7. Synchronization Performance Characteristics  
(at 128 bits/sec)

	PN	NRZ
Bit waveform		
Sync:	63 pseudonoise bits over 7 information bits	Subcarrier at 1024 cps
Data:	Subcarrier at 1152 bits	
Distance from carrier loop	10 times carrier band- width	20 times carrier band- width
Ratio of synchronization to data power	0.1	0.1
Loop natural frequency	0.2 cps	Demodulator: 3 cps Bit sync: 0.05 cps
Mean-time to loss of lock	> 200 hrs	Demodulator: 140 hrs Bit sync: 10 hrs (worst case)
Acquisition	50 sec max	10 to 20 sec (worst case)
Bandwidth expansion	None	None
Required oscillator stability	Better than 0.05%	0.04%
Jitter in reference generated	Subcarrier: 15 deg Data: 2 deg	Subcarrier: 10 deg Data: 15 deg (worst case)*
Word synchronization provided?	Yes	No
AGC required?	No	Yes

\*Corresponds to no data transitions.

in the spacecraft clock frequency and narrow sync loop bandwidths mitigate against the first technique; however, increased ground equipment complexity is required for the second. Because sync loop bandwidths as narrow as 0.5 cps are contemplated for the Voyager telemetry, it is concluded that automatic acquisition is probably a necessity.

Acquisition Time. Another question of interest is whether pseudonoise sync should be used for bit synchrnoization only or for word sync as well. The advantage of, say, a 7 or 15 bit pseudonoise code giving only bit sync rather than a 63-bit code with word sync is the consequent reduction in acquisition time. On the other hand, the shorter pseudonoise code would have larger false-lock points in its cross-correlation functions as shown in Section 3 of Appendix F. The code acquisition time is calculated in Section 4 of Appendix F with the results shown below:

<u>Code Length in Bits</u>	<u>Acquisition Time (sec)</u>
63	1.77
15	0.35
7	0.15

Since the acquisition times for the 63, 15, and 7 bit maximim length, single component codes are negligible compared to the transmission delay times, the 63-bit code used on the Mariner C is recommended. This code will provide both data bit and word sync, whereas the 15 and 7 bit codes will provide only bit sync. The reduced probability of false-lock is another important advantage of the 63-bit code. In addition, the saving in hardware complexity for the shorter codes is slight.

#### c. Single versus Two-Channel Systems

For a telemetry (or command) system employing pseudonoise synchronization techniques, two basic multiplexing or modulation formats can be devised. In the two-channel scheme, the data and sync channels are linearly summed to form a frequency division multiplexed (FMD) signal. The composite baseband then phase-modulates the carrier. The pseudo-noise sync waveform is essentially two-valued, i. e., square wave, whereas the data is modulated on either a sine wave or square wave subcarrier. In the latter case, since each channel is binary, the composite waveform is four-level. By contrast, in the single-channel system the binary data and sync are summed modulo 2, producing a binary composite waveform.

The modulators and detectors for the two systems are reviewed in Section 4 of Appendix F. The two-channel modulator requires more equipment in the spacecraft but the single-channel detector is more complex than the two-channel detector. Although additional circuits in the

spacecraft are undesirable, the two-channel telemetry system has the important virtue of having been flight-proven on Mariner C.

The communications efficiency comparison favors the single-channel system because no extra power is required for sync. However, at 128 bits/sec rates and above, this advantage is slight. The proportion of power allotted to sync is essentially negligible compared with the required data power. The relative power requirements are shown in Figure 3-5 versus data rate. Sync thresholds for loop bandwidths  $2B_{LO}$  of 0.5 and 2 cps and the carrier threshold appear as constant requirements. The data power increases with data rate. The dashed line below the data requirement indicates the power available for the sync channel if 10 per cent of the sideband power is devoted to sync.

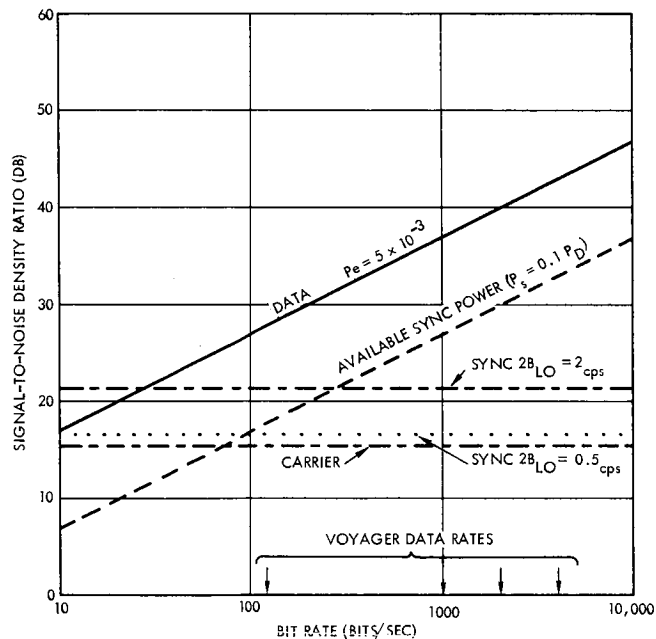


Figure 3-5. Signal-to-Noise Density Requirements for Two-Channel Pseudonoise Sync Telemetry

From Figure 3-5, it is concluded that the sync channel in the two-channel system requires no more than 10 per cent of the power in the data channel. In fact, at 512 bits/sec and above the extra loss to the data over that in a single-channel system is about 0.5 db. For all but the

lowest bit rate (128 bits/sec), the two-channel system is practically equivalent in communication efficiency to the single-channel system. This, coupled with its proven capabilities, makes the two-channel system the choice for the Voyager telemetry link.

d. Performance of Two-Channel System

The performance characteristics of the selected telemetry system studied in Section 4 of Appendix F are: bandwidth, power requirements, and intermodulation and interference. It is concluded that both the low and high frequency limitations of the telemetry channel are acceptable for the Voyager data rates. The power requirements for data and sync are such that the two-channel system will be within 1 db of a single-channel competitor except at the lowest bit rate. Intermodulation and interference are briefly analyzed and shown to be tolerable.

Bandwidth Requirements. The low-frequency limitation results from the high-pass filtering action of the carrier phase-lock loop. Employing an empirical rule given by Springett<sup>\*</sup>, the effect is found not to affect the lock characteristics of the pseudonoise sync loop when the narrowest DSIF carrier loop bandwidth is used.

The high-frequency response of the receiver telemetry channel determines the ability to pass the data subcarrier with small distortion. Following Mariner practice, the data subcarrier is placed at  $4f_g$  in the null of the sync spectrum. The available DSIF telemetry bandwidths are sufficiently wide to pass not only the square-wave subcarrier fundamental, but up to the fifth harmonic at the highest data rate.

Power Requirements. Consideration of the degrading effects of timing noise caused by the carrier, subcarrier, and bit sync reference cycle yields the following:

Carrier degradation	> 1.0 db
Subcarrier degradation	> 0.5
Bit sync degradation	> 0.1
Total	> 1.6 db

---

\* J. C. Springett, "Telemetry and Command Techniques for Planetary Spacecraft," Technical Report No. 32-495, JPL, 15 January 1965.

In addition, data is degraded by the finite telemetry bandwidths. If the fifth harmonic of the square-wave subcarrier is passed, the degradation should be about 0.5 db. The total required S/N ratio in a bandwidth  $1/T$  equal to the bit rate is:

$$\frac{ST}{N/B} = 7.3 \text{ db}$$

for a theoretical S/N of 5.2 db for an error probability of  $5 \times 10^{-3}$ .

The corresponding sync channel threshold has been developed following Springett. The data degradation by the  $4 f_s$  subcarrier was set at 0.5 db. This implies an 18.4 db S/N in the noise bandwidth of the sync phase-lock loop which operates at frequency  $f_s$ .

The data and sync channel power requirements can be satisfied by noting that the total signal power will divide as follows:

$$P_D = P_T \sin^2 \theta_D \cos^2 \theta_S \text{ (data)}$$

$$P_S = P_T \sin^2 \theta_S \cos^2 \theta_D \text{ (sync)}$$

$$P_C = P_T \cos^2 \theta_D \cos^2 \theta_S \text{ (carrier)}$$

where  $\theta$  = phase deviation. It is found that only at the lowest bit rate (128 bits/sec) can the power division be optimized in the sense that the three components reach threshold simultaneously. The data power requirements at the higher data rates are so much greater than those of the sync and carrier that the deviation  $\theta_D$  approaches  $\pi/2$  radians. A deviation for the data above 1.25 radians is undesirable because of the danger of reaching a carrier null due to modulation index calibration drift. Therefore, for 1024 bits/sec and above the deviations are:

$$\theta_D = 1.25 \text{ rads}$$

$$\theta_S = 0.32 \text{ rad}$$

At 128 bits/sec:

$$\theta_D = 1.12 \text{ rads}$$

$$\theta_S = 0.45 \text{ rad}$$

Intermodulation and Interference. The intermodulation between data and sync channels is analyzed in Section 4 of Appendix F. For ideal square-wave data and sync signals, the intermodulation noise does not appear at baseband and therefore does not cause mutual interference. For a sine-wave data subcarrier, intermodulation products will create interference at baseband. In either case, signal power is wasted in these products.

The intermodulation power for square waves is:

$$P_{IM} = P_T \sin^2 \theta_D \sin^2 \theta_S$$

and the sum of this power with the three useful components gives the total signal power. The superior communication efficiency of the single-channel system is due basically to freedom from wasted IM power. However, as indicated above, at Voyager data rates this two-channel penalty is small.

Under certain conditions an optimum set of deviations can be found which minimizes the power wasted in IM products (and excess carrier power), or, more fundamentally, minimizes the total power required. The optimum deviations are given by:

$$\tan^4 \theta_D = \frac{P_D}{P_S}$$

and

$$\theta_S = \frac{\pi}{2} - \theta_D$$

These relations were used to set the indices for the lowest bit rate whereas the high rate deviations were governed by the carrier suppression limitation discussed above.

Direct interference between the data and sync channels results from colocation of the spectra. Sync interference with the data is minimized by placing the data subcarrier at  $4 f_s$ , the null of the sync spectrum. The sync channel is protected from data interference by the cross-correlation of the sync with the local pseudonoise code. A matched-filter argument shows that if the sync power is constrained to be no greater than 20 db below the data power, no important interference with the sync functions should occur.

### 1.3.3 Command Link Analysis

In the command link, as in other portions of the Voyager design, the general approach has been to seek a conservative design, taking advantage, wherever possible, of the equipment and techniques developed and experience gained in the Ranger, Mariner-R, and Mariner-C designs. Moreover, in the command link the Voyager design must be compatible with the DSIF and the command verification equipment (CVE). The command link at threshold is to operate at a bit error probability less than  $P_e^b = 10^{-5}$ . The command equipment is to employ pseudonoise synchronization techniques. The use of narrowband phase modulation of the carrier and a modulation-restrictive phase-locked loop demodulator which tracks the carrier component is also considered a requirement. Bit-by-bit detection and reconstruction of the noisy data stream in the spacecraft receiver is presumed to be a practical requirement.

The Voyager command link has a carrier tracking loop bandwidth and carrier power requirement of the same order of magnitude as the data channel bandwidth and data power requirement. Since total required received power (translatable to spacecraft capability in terms of range) is the primary concern, the carrier power requirements are of paramount importance in assessing the relative performance of various modulation and multiplexing techniques. From an assessment of the signal dynamics for the Voyager mission and based upon the similarities with the Mariner-C requirements, the carrier loop bandwidth  $2B_L = 32$  cps and a loop S/N ratio of 6 db in  $2B_L$  has been chosen as a design requirement for the purpose of the comparisons to be made here.

A 1-bit/sec data rate is considered the desired command capability. This rate is sufficient to transmit the quantitative and discrete commands envisioned for the Voyager mission. Lower data rates might be considered if justifiable, but because of the carrier power requirements and the difficulties in mechanization of the lower rates, the transmitter power requirements do not decrease enough to make such a choice advantageous. Also, the Mariner-C system has effectively implemented and utilized the 1-bit/sec data rate.



The rationale for choosing the dual channel PSK system of the Mariner-C type for the Voyager command link is presented. The performance in terms of total power required for this system comes within 1.8 db of the theoretical performance of PSK for the same carrier power requirements. A single-channel PSK/pseudonoise sync system is expected to have only 0.8 db advantage over the recommended dual channel system. The pseudonoise clock frequency has been chosen to be  $2 f_s = 511$  cps, based upon a tradeoff between carrier loop effects and pseudonoise acquisition time. Since the carrier loop bandwidth will expand at high signal levels to  $2B_L = 200$  cps, there may be a problem in regard to high-pass filtering effects on the pseudonoise correlation properties. At threshold S/N the time required to achieve a 90 per cent probability of acquisition appears to be as high as 34 minutes. As in the Mariner-C system, a sync loop in-lock indicator is provided which essentially computes the autocorrelation of pseudonoise  $\oplus 2 f_s$ . The data signal is biphase-modulated onto a sinusoidal subcarrier of frequency  $2 f_s$ . The coherent reference for demodulation is provided by the sync loop. It is shown that the direct interference between the sync signal and the data is negligible. At the phase deviations to be used for this link, the intermodulation effects are of no consequence.

a. Synchronization

To obtain reasonable efficiencies in the demodulation of PCM, it is generally advantageous to have synchronization information available at the receiver. For bit-by-bit detection, this entails only bit synchronization for the demodulation. For Voyager, it is specified that bit sync is to be transmitted through the use of a pseudonoise sequence which becomes a part of the command signal. This technique provides good sync with reasonable acquisition time and probably works as well as any alternate methods at a data rate of 1 bit/sec.

b. Modulation and Multiplexing Tradeoffs

The various modulation techniques which seem most reasonable and straightforward within the constraints set forth above have been compared on the basis of efficiency. For the specified error probability and carrier loop bandwidth, the most meaningful criteria for comparison is the

required total receiver input power divided by the receiver noise density,  $P_T/\Phi$ , to provide the desired performance. With properly chosen phase deviations, the total power at this threshold level divides into the carrier power, data power, and sync power to maintain each of these component signals at their respective thresholds. The six cases of modulation and multiplexing described below and compared in Table 3-8 were chosen to bound the command link possibilities. Table 3-8 provides a quantitative comparison of the efficiencies which can be obtained for these schemes. It shows that these techniques do not differ greatly in terms of total power required. The merging of the various efficiencies is a direct result of the required carrier loop bandwidth  $2B_L = 32$  cps and a loop S/N of 6 db in  $2B_L$ , which is considered to be a constraint. The fact that the data rate for this link is 1 bit/sec is a major factor in determining the stated efficiencies.

Theoretical PSK is considered to provide the lower bound on the achievable efficiency for this link. It assumes that the bit sync and subcarrier reference are present in the receiver without costing anything in terms of transmitter power. The theoretical efficiency for PSK under these ideal conditions is  $P_D/\Phi = 9.6$  db for a bit error probability  $P_e^b = 10^{-5}$ .

Mariner-C Dual Channel PSK. The efficiencies of the data channel and sync channel are quoted as  $P_D/\Phi = 13.7$  db/cps and  $P_S/\Phi = 16.7$  db/cps in the Mariner-C specification. Thus the sync channel requires twice as much power as the data channel. The power required by the sync loop, which has a noise bandwidth  $2B_{LO} = 2$  cps, is to provide the desired acquisition and tracking behavior of the loop and to provide a subcarrier reference for data demodulation. It is with the quality of reference provided by the  $P_S/\Phi = 16.7$  db/cps that the data efficiency of  $P_D/\Phi = 13.7$  db/cps for  $P_e^b = 10^{-5}$  is achieved. The major degradation from theoretical for the dual channel is associated with constructing a subcarrier reference and the desired bit synchronization information for coherent data demodulation with a data rate of 1 bit/sec. Even at the sync channel level of  $P_S/\Phi = 16.7$  db/cps the reference is not exceptionally good and the data demodulation process is degraded at least 2 db because

Table 3-8. Comparison of Subcarrier Modulation Techniques

Residual Carrier Phase Modulation		$2B_L = 32 \text{ cps}$
Carrier Loop Noise Bandwidth		$P_e^b = 10^{-5}$
Bit Error Probability		
Total Input S/N Ratio in a 1 cps Bandwidth		
$P_T/\Phi$		
$P_T$ = Total Receiver Input Power		
$\Phi$ = Receiver Noise Spectral Density		

1. <u>Theoretical PSK</u>			
Data	$\frac{P_D}{\Phi} = 9.6 \text{ db/cps} = 2 J_1^2 (0.375) \frac{P_T}{\Phi}$		21.3 db/cps
Carrier	$\frac{P_C}{\Phi} = 21.0 \text{ db/cps} = J_0^2 (0.375) \frac{P_T}{\Phi}$		
2. <u>Mariner-C Dual Channel</u>			
Data	$\frac{P_D}{\Phi} = 13.7 \text{ db/cps} = 2 J_1^2 (0.58) \cos^2 (0.55) \frac{P_T}{\Phi}$		23.1 db/cps
Sync ( $2B_{LO} = 2 \text{ cps}$ )	$\frac{P_S}{\Phi} = 16.7 \text{ db/cps} = \sin^2 (0.55) J_0^2 (0.58) \frac{P_T}{\Phi}$		
Carrier	$\frac{P_C}{\Phi} = 21.0 \text{ db/cps} = \cos^2 (0.55) J_0^2 (0.58) \frac{P_T}{\Phi}$		
3. <u>Dual Channel With Narrow Sync Loop</u>			
Data	$\frac{P_D}{\Phi} = 13.7 \text{ db/cps} = 2 J_1^2 (0.58) \cos^2 (0.36) \frac{P_T}{\Phi}$		22.3 db/cps
Sync ( $2B_{LO} = 2 \text{ cps}$ )	$\frac{P_S}{\Phi} = 12.4 \text{ db/cps} = \sin^2 (0.36) J_0^2 (0.58) \frac{P_T}{\Phi}$		
Carrier	$\frac{P_C}{\Phi} = 21.0 \text{ db/cps} = \cos^2 (0.36) J_0^2 (0.58) \frac{P_T}{\Phi}$		
4. <u>Single-Channel With Wide Sync Loop</u>			
Data and Sync ( $2B_{LO} = 2 \text{ cps}$ )	$\frac{P_{DS}}{\Phi} = 16.3 \text{ db/cps} = \sin^2 (0.76) \frac{P_T}{\Phi}$		22.3 db/cps
Carrier	$\frac{P_C}{\Phi} = 21.0 \text{ db/cps} = \cos^2 (0.76) \frac{P_T}{\Phi}$		
5. <u>Single-Channel With Narrow Sync Loop</u>			
Data and Sync ( $2B_{LO} = 0.75 \text{ cps}$ )	$\frac{P_{DS}}{\Phi} = 12.0 \text{ db/cps} = \sin^2 (0.34) \frac{P_T}{\Phi}$		21.5 db/cps
Carrier	$\frac{P_C}{\Phi} = 21.0 \text{ db/cps} = \cos^2 (0.34) \frac{P_T}{\Phi}$		
6. <u>Noncoherent FSK</u>			
Data	$\frac{P_D}{\Phi} = 19.4 \text{ db/cps} = 2 J_1^2 (1.02) \frac{P_T}{\Phi}$		23.4 db/cps
	$\frac{P_C}{\Phi} = 21.0 \text{ db/cps} = J_0^2 (1.02) \frac{P_T}{\Phi}$		

of the noisy reference. Constructing a subcarrier reference for a data rate of 1 bit/sec is difficult. Any other subcarrier reference reconstruction process, such as a squarer or an I-Q loop, will encounter difficulties similar to the Mariner-C dual channel system and will suffer degradations of the same order of magnitude. It appears difficult to construct a coherent PSK system that will achieve a better efficiency at 1 bit/sec.

Dual Channel PSK With Narrow Sync Loop Bandwidth. In an attempt to obtain better efficiency than the Mariner-C dual channel system, the use of a lower sync loop bandwidth such as  $2B_{LO} = 0.75$  cps has been investigated. This has the disadvantage of increasing the acquisition time for the sync loop. In the case shown in Table 2-8(3), the quality of the subcarrier reference provided by the loop was maintained so that the sync channel power requirements decrease proportionally as the loop bandwidth is decreased.

Single-Channel PSK Systems. To avoid the inherent inefficiency of the power split associated with the dual channel frequency division multiplex, a single-channel PSK system with pseudonoise synchronization is described by Springett. The estimated efficiency for such a system is given in Table 3-8(4 and 5) for the same loop bandwidths as the dual channel system of Table 3-8(2 and 3). This represents about as good efficiency as one can expect to achieve within the constraints provided.

Noncoherent FSK. Because the total efficiencies of the modulation techniques mentioned above are not a strong function of the data subcarrier efficiencies, one might consider utilizing FSK rather than PSK for the Voyager command link. The efficiency quoted in Table 3-8(6) for noncoherent FSK represents an estimate of the performance of the Pioneer command equipment built by TRW. It uses nonsynchronous sampling rather than sending or constructing bit sync. The efficiency,  $P_D/\Phi = 19.4$  db may be somewhat optimistic since the bit error rate of the system has not been directly measured.

Within the carrier loop constraints set forth above, the Mariner-C dual channel PSK system comes within 1.8 db of the theoretical performance of PSK in terms of total power required. The single-channel system, discussed more fully in the telemetry section, is only 0.8 db more efficient

than the comparable dual channel system. Therefore, the Mariner-C configuration is a reasonable compromise among efficiency, ease of implementation, and reliability. Since this system has been mechanized and proven, it represents the conservative design approach for the Voyager mission.

c. Performance of Command Link

Given that a dual channel system similar to Mariner-C has been chosen, the specific modulation parameters for and the expected performance of the Voyager command link were then determined. A coherent PSK system is to be mechanized operating at a bit rate of 1 bit/sec, a bit error probability of  $P_e^b = 10^{-5}$ , utilizing a pseudonoise sequence for synchronization.

The dual channel Mariner-C command system has the following characteristics, all of which will be translated to the Voyager design:

- a) Pseudonoise sequence for synchronization, Sync signal is  $PN \oplus 2 f_s$ , which is a pseudonoise code split-phase encoded
- b) Coherent PSK modulation of a sinusoidal subcarrier
- c) The use of pseudonoise code generator which is locked to input code through sync loop to provide subcarrier reference for coherent demodulation. This necessarily means the data subcarrier is coherent with clock of pseudonoise code generator
- d) The employment of a quadrature phase detector, an integrate and dump circuit, and a threshold device to provide an indication of detector lock, i. e., sync loop acquisition.

The use of  $PN \oplus 2 f_s$  as the sync signal allows the ready formulation of  $PN \oplus 2 f_s \oplus PN(\tau)$  in two steps, which provides a suitable error signal for the sync loop. A square-wave as an alternative to the sine-wave for the data subcarrier offers an advantage at high phase deviations of the carrier provided that the higher order sidebands are utilized in the demodulator. At high deviations, even if the higher order square-wave sidebands are not utilized, the square-wave which achieves a fractional sideband power of  $\frac{8}{\pi^2} \sin^2 \beta$  has about the same efficiency as a sine wave which achieves a fractional sideband power of  $2 J_1^2(\beta)$ . However, at low deviations of the

data subcarrier, which must be used for the Voyager dual channel command system because of the carrier and sync power requirements, the sine-wave subcarrier provides better performance than the square-wave since it allows predetection bandpass filtering (and limiting) and utilizes essentially all of the power  $\left[ J_0^2(\beta) + 2 J_1^2(\beta) \approx 1 \right]$ .

Even though the pseudonoise code is utilized for synchronization, it need not be used to derive the data subcarrier reference. There are other methods such as squaring and dividing by two, or the equivalent I-Q loop, which reconstruct a reference from the data subcarrier itself. However, at a data rate of 1 bit/sec, these techniques are generally quite inefficient and difficult to mechanize. Therefore, the use of the sync signal to derive the subcarrier reference is probably as good as any other method and involves the minimum of circuitry.

The use of a quadrature phase detector to indicate the detector lock condition is typical for phase-locked loops. For this pseudonoise sync system when an integrate and dump circuit is used at the quadrature detector output, this operation essentially consists of computing the autocorrelation of  $PN \oplus 2 f_s$  and sampling at its peaks. Since this detector operates independently of the actual loop, it is the setting of the detector threshold which determines the probabilities of incorrect indications.

The major parameters of interest for the Voyager command link are the pseudonoise code clock frequency  $2 f_s$ , which for 1 bit/sec data rate is the length of the maximal-length shift register sequence which constitutes the pseudonoise code, and the frequency of the sinusoidal subcarrier. Another parameter of lesser importance is the receiver bandwidth. The major considerations in making these choices are the interactions in the carrier loop, sync channel, and data channel. The design considerations and performance of these three channels will be discussed below.

The communication efficiency has been quoted in Section 1.3.3b, in terms of total power divided by noise density as  $P_T/\Phi = 23.1$  db/cps for the Mariner-C dual channel system operating with the prescribed Voyager carrier loop bandwidth. This is based on the Mariner-C specifications of  $P_D/\Phi = 16.7$  db/cps for the data and  $P_S/\Phi = 13.7$  db/cps for the sync. For the purposes of power budgeting, these same efficiencies are used for

Voyager. The phase deviations of 0.55 rad for the sync and 0.58 rad for the data balance out the three channels and maintain the same performance margin for all. At this low deviation level only 4 per cent of the power is lost in higher order nonrecoverable sidebands in the modulation process. Thus, there should be no appreciable degradation of the link performance due to intermodulation effects.

Carrier Loop. The carrier loop design bandwidth of  $2B_L = 32$  cps at a loop S/N ratio  $P_C/\Phi 2B_L = 6$  db expands at higher signal levels since the loop gain is directly proportional to the input signal amplitude. This assumes, of course, that a predetection limiter is employed to control the dynamic range of the signal input to the carrier phase detector. A coherent AGC or a combination limiter and coherent AGC can be utilized for this same purpose. A properly designed AGC can maintain a near constant signal input to the demodulator and thereby maintain the carrier loop bandwidth at a desired width. However, for proper functioning of the command link over the extent of the spacecraft range or receiver input levels, it is desirable that the loop be allowed to expand a controlled amount in bandwidth since the shorter ranges or higher input levels generally correspond to the more severe vehicle dynamics where a wider loop may be needed. However, since the carrier loop bandwidth represents the low frequency constraints on the pseudonoise clock frequency  $2f_s$  and the data subcarrier frequency, too much expansion in bandwidth can be detrimental.

For the purposes of this analysis, a limiter only is assumed. It is also assumed that the damping ratio is set at  $\zeta = 0.707$  at the loop threshold design point of  $2B_L = 32$  cps and  $S/N = 6$  db. With a predetection bandwidth of 4.5 kc the limiter suppression factor at the design loop bandwidth of 32 cps is:

$$\alpha_d = \sqrt{\frac{1}{1 + \frac{4}{\pi} \left(\frac{N}{S}\right)_i}}$$

where

$$\begin{aligned} \left(\frac{S}{N}\right)_i &= S/N \text{ power ratio at limiter input} \\ &= \frac{P_T}{\Phi(4500)} = \frac{P_C}{\Phi(32)} = \frac{32}{4500} = M \end{aligned}$$

$$\begin{aligned}
 &= 6 \text{ db} - 2.4 \text{ db} - 21.5 \text{ db} \\
 &= -17.9 \text{ db}
 \end{aligned}$$

where

$$\begin{aligned}
 P_T &= \text{Total power at limiter input} \\
 P_C &= \text{Carrier power at limiter input} \\
 \Phi &= \text{Noise density at limiter input} \\
 M &= \text{Carrier modulation loss} = -2.4 \text{ db}
 \end{aligned}$$

Therefore,

$\alpha_d = 0.112$  and the maximum loop bandwidth is given by:

$$\begin{aligned}
 2B_{Lm} &= \left( \frac{2B_{Ld}}{3} \frac{2}{\alpha_d} + 1 \right) \\
 &= 32 \left( \frac{18.84}{3} \right) = 200 \text{ cps}
 \end{aligned}$$

The amount of interference introduced by the presence of the command signal is also considered in the carrier-loop operation. The data subcarrier itself can be prevented from interfering to any pronounced degree by simply making its frequency large enough. The pseudonoise code for synchronization will have sidebands which are within the carrier tracking loop. However, by making the clock rate  $2 f_s$  of the code large, the percentage of its energy within the loop can be made quite small. Both the pseudonoise code and the data subcarrier will introduce modulation phase error in the carrier tracking loop, which will affect its threshold, acquisition, and tracking behavior. However, the effect of the modulation on the loop will be considerably less important than the effect of the loop on the modulation. Therefore, the important consideration in regard to the carrier tracking loop is the degradation of performance which it introduces into the command PSK signal, particularly the sync signal. The carrier loop will operate in approximately the same manner (regarding acquisition and tracking) with the command signal modulation present as without it. Therefore, no alteration in the loop threshold S/N of 6 db has been made to account for the degrading effect of the data and sync modulation.



Sync Channel. When the sync signal is  $PN \oplus 2 f_s$ , and the pseudonoise code split phase encoded, the spacecraft code generator can be locked in time synchronism with the input pseudonoise code through the use of a phase-locked loop. The error signal to drive the loop VCO is developed by multiplying the input  $PN \oplus 2 f_s$  plus noise first by  $PN(\tau) \oplus f_s(\tau)$  and then by  $f_s(\tau)$  to develop essentially the cross-correlation  $PN \oplus f_s \times PN(\tau)$ . The use of the two-step correlation allows for the use of a bandpass filter and limiter before the final correlation. This filter and limiter does distort the error function and introduces possible false-lock points.

To keep the power requirements of the sync channel within reasonable limits, it is desirable to minimize the sync loop bandwidth. However, the lower bound on this loop bandwidth is set by the allowable acquisition time. To allow the received and locally generated codes to slide past one another and eventually lock up, an offset of the transmitter clock is provided for. With an offset in  $2 f_s$  of  $\Delta f$  there is a time difference between the codes of  $\frac{\Delta f}{2 f_s} t$ . For this time difference to equal a multiple of the bit time,  $kT_b$ , where the loop error function has the proper lock-in properties, a maximum time  $T_C = \frac{2 f_s T_b}{\Delta f}$  is required.

This is the time for one complete code correlation. For a given  $2 f_s$ ,  $T_C$  decreases with increasing  $\Delta f$ . But, for a given loop bandwidth, there is a limit on  $\Delta f$  which will provide a reasonable probability of lock-up on a single code correlation. Therefore, to minimize acquisition time, the clock offset frequency  $\Delta f$  must be chosen carefully. For a loop with  $2B_{LO} = 2$  cps, the Mariner-C specification states that an offset of 1.5 cps will achieve a probability of lock-up on a single correlation of 1/3 at the loop S/N ratio of 14.7 db. It seems that this acquisition probability is smaller than one might expect and that a smaller offset may be advantageous.

In choosing the pseudonoise code clock frequency,  $2 f_s$ , the following two constraints are determining:

- 1) Upper limit – acquisition time for sync loop
- 2) Lower limit – carrier tracking loop high pass filtering effect on sync signal cross-correlation and autocorrelation functions.

The upper limit due to acquisition time has already been discussed. An estimate on the lower limit is provided by Springett and is represented by the following equation:

$$\begin{aligned} 2 f_s &\geq 10.08 B_o \sqrt{\frac{\alpha}{\alpha_o}} \\ &\approx 10(2B_{Ld}) \sqrt{\frac{\alpha}{\alpha_d}} \\ &= 10(32) \sqrt{\frac{1}{112}} = 956 \end{aligned}$$

According to this criterion, the most reasonable possibility for  $2 f_s$  is 1023 cps. However, the above equation cannot be considered a strict requirement since it is arbitrary and has not been shown to be directly related to any such quantity as the probability of unlock or the probability of false-lock for a given S/N ratio. Therefore, the frequency  $2 f_s = 511$  cps is also a possibility. As is shown later, acquisition time for the sync loop is very critical. This leads to the recommendation that 511 cps be utilized for the pseudonoise clock frequency. There may indeed be a problem with carrier loop high-pass filtering effects on the sync signal correlation properties at high carrier S/N ratio or wide loop bandwidth. It is possible to alleviate this problem through loop input signal control, either by transmitter power attenuation or coherent receiver AGC, or perhaps through premodulation amplification of low frequency code components.

Assuming a sync loop bandwidth  $2B_{LO} = 2$  cps, and a code clock frequency  $2 f_s = 511$ , the maximum time for a single code correlation becomes 5.7 minutes for a 1.5 cps clock offset and 8.5 minutes for a 1 cps offset. As is mentioned above, the probability of lock-up in a single correlation of 1/3 for the 1.5 cps offset at design level loop S/N ratio is not good. To achieve a 90 per cent probability of acquisition requires 6-code correlations, corresponding to 34 minutes for the 1.5 cps offset. The only way the acquisition can be improved and maintain the efficiency is to reduce the pseudonoise clock frequency  $2 f_s$ . This involves reducing the expansion of the carrier loop bandwidth.

Since the sync signal and the data subcarrier overlap in frequency, it is natural to consider the degradation of the sync channel resulting from interference from the data channel. The effect of correlating the data subcarrier against the local pseudonoise code is to spread its energy over a wide spectral range so that the degradation in the operation of the sync detection system is negligible. Therefore, the possibility of interference with the pseudonoise sync signal places no constraint on placement of the data subcarrier.

The RF bandwidth required of the command system, determined by the pseudonoise code, is a minimum of  $8 f_s \approx 2 \text{ kc}$ . However, system performance is not a strong function of this predetection bandwidth so a value of 4.5 kc has been chosen, commensurate with the Mariner-C bandwidth.

In-Lock Detector. The sync loop in-lock detector essentially computes the autocorrelation of the sync signal  $PN \oplus 2 f_s$ , neglecting the effect of the bandpass filter and limiter at the input to the sync loop. The decision device at the output of the integrate and dump provides an in-lock or out-of-lock indication for each bit time by comparing the output signal to a predetermined threshold. The important performance parameters for this detector, all of which depend solely upon the threshold level, for a given S/N ratio, are the probability of detection, the probability of no detection, and the probability of false alarm. The most important parameter to set is the probability of no detection, which is the determining factor in the probability of the in-lock detector allowing the processing of a command, given by:

$$1 - MP_{ND}$$

where  $M$  = number of bits in command and  $P_{ND}$  is the probability of no detection or the probability of the detector giving an out-of-lock indication for any single bit time when the loop is actually in lock. If  $P_{ND}$  is set at  $2 \times 10^{-5}$ , the probability of the detector indicating in-lock for the entire word and allowing execution of the command is 0.9997 for a 16-bit discrete command and 0.9993 for a 35-bit quantitative command.

Assuming that the input noise is not changed in form or in level by the code correlation operation and the multiplication by the quadrature reference, the S/N ratio at the decision time at the output of the integrate and dump filter is given by

$$\frac{S_o}{N_o} = \frac{2(2B_{LO}) k^2}{H} (S/N \text{ ratio})_{loop}$$

where

$$(S/N \text{ ratio})_{loop} = \text{sync loop S/N ratio in } 2 B_{LO}$$

$$2B_{LO} = \text{sync loop noise bandwidth}$$

$$H = \text{bit rate}$$

$$k = \text{fraction of perfect correlation that is achieved.}$$

The threshold of the decision circuit and the probability of no detection are related by

$$P_{ND} = \frac{1}{\sqrt{2\pi}} \int_{\sqrt{\frac{S_o}{N_o}} - \sqrt{\left(\frac{S_o}{N_o}\right)_t}}^{\infty} \exp(-Z^2/2) dZ$$

where

$$\left(\frac{S_o}{N_o}\right)_t = \text{threshold value of S/N ratio}$$

The probability of a false alarm indication of detector in-lock because of noise alone is then

$$P_{FA} = \frac{1}{\sqrt{2\pi}} \int_{\sqrt{\left(\frac{S_o}{N_o}\right)_t}}^{\infty} \exp(-Z^2/2) dZ$$

Since the detector must indicate in-lock for a large number of successive bits and the data format must check out for the processing of a false command to take place, the probability of such an occurrence is extremely small.

Data Channel: The data channel is a biphas modulated subcarrier which is coherently demodulated using a reference derived from the pseudonoise code generator. For the clock frequency  $2 f_s$  of 511 cps, the accuracy in the bit sync is better than 0.1 per cent of a bit time when the sync loop is locked up and the data is to be processed. This sync accuracy is sufficient to be considered perfect. The coherent reference at the data subcarrier frequency, though derived from the same loop, will have nowhere near this relative accuracy. The quality of the subcarrier reference is determined by the frequency of data subcarrier, the rms phase jitter being directly proportional to this frequency. Although the degradation of the data performance because of the subcarrier reference decreases with decreasing frequency, the interaction between the data and the carrier loop becomes more severe. A data subcarrier frequency of  $2 f_s$  is used in Mariner-C and appears reasonable for Voyager. The use of  $f_s$  would provide for a better reference and might be acceptable in regard to carrier loop effects. The conservative approach dictates a recommendation to use  $2 f_s$ , with perhaps future investigation into the possibility of moving to  $f_s$ .

In the above discussion, no mention is made of the possible interference of the sync signal with the data channel. It is readily recognized that the sync signal interferences does not appreciably affect the data channel error probabilities no matter where in the sync spectrum the data subcarrier is placed as long as the powers in the signals are of the same order of magnitude. This is because the data channel with the integrate and dump filter has a characteristic  $\frac{\sin \pi f T_B}{\pi f T_B}$  centered at the data subcarrier frequency, where  $T_B$  is the bit time. Since the sync signal is periodic with a period of  $T_B$ , all frequency components except that directly at the data subcarrier are at nulls in the data channel response. With the data subcarrier at  $2 f_s$ , which is near the peak of the sync signal, the fraction of the sync power which gets into the data channel is

$$\left. \frac{2}{2f_s T_B} \frac{\sin^4(\pi f/4f_s)}{(\pi f/4f_s)^2} \right|_{f=2f_s} = \frac{8}{\pi^2} \frac{1}{2f_s T_B} = 0.00159$$

Therefore, in regard to interference from the sync channel, there are no constraints on placement of the data subcarrier.

#### 1.3.4 Capsule-to-Spacecraft Link Analysis

In Section 2 of Appendix F, a detailed analysis of the capsule-to-spacecraft link is presented. This section summarizes the assumptions, rationale, and the conclusions reached in the appendix.

##### a. Mission Profile

The communication mission profile for the capsule-to-spacecraft link is divided into three phases; separation, entry, and postlanding. Of these, the entry phase is given the highest emphasis. The traffic requirement for this link is 10 bits/sec, with an assumed error rate of  $1 \times 10^{-3}$ .

A number of parameters influence the design of this link, the maximum range of 40,000 km (see Volume 4, Section III-5.1), the specified minimum capsule entry angle of 45 degrees, the high acceleration associated with the parachute deployment (14 g), and the short period of time available for transmission of the post blackout entry data (4 to 19 minutes depending upon the atmospheric model and the entry angle assumed).

##### b. Multipath Propagation

An analysis of the multipath effect considered the vector relationship of the direct and indirect signals at the receiving antenna. The path of each reflected signal at the receiver antenna is likely to be random, and the spacing between the capsule and spacecraft will change with time. The problem is complex; a rigorous analysis has not yet been done. However, a simple two-signal model was analyzed to provide an understanding of the multipath effects.

The results of the analysis indicated that:

- a) Modulation. Interference between the direct and reflected signal might produce amplitude modulation of the order of 30 per cent.
- b) Fading Rate. For the assumed entry profile parameters, rates would vary between a maximum of about 1420 cps (between blackout and before parachute opening) and 11 cps minimum (nearly equal to the data rate) after parachute opening.

c. Frequency Uncertainty

The total frequency uncertainty between receiver and capsule transmitter (see Section 2, Appendix F) because of doppler shift and oscillator instabilities is estimated to be 21 kc, which is large compared to data rate and is an important parameter affecting system design. Four design approaches were considered:

- 1) Utilize a noncoherent (nontracking) receiver with a pre-detection bandwidth large enough to encompass the total frequency uncertainty
- 2) Partially compensated nontracking system in which ground command is utilized to adjust frequency thus reducing the required predetection bandwidth.
- 3) A coherent phase-lock tracking receiver.
- 4) A nondemodulating repeater in which demodulation and data detection are accomplished at the DSN receiver terminal.

Technique 1) represents the most conservative approach and is the recommended system (see Section 1.3.4d). Technique 2) is a growth possibility to improve the signal margin of 1). Technique 3) is not recommended for the 1971 mission for the reasons outlined in Section 1.3.4d. Technique 4) offers substantial promise at higher spacecraft power levels and might provide additional data (multipath amplitude, fading rate, etc.) which is lost by on-board demodulation and detection. This will be studied further in Phase IB.

d. Modulation and Demodulation

The two predominant requirements of the capsule line are:

- 1) The link must operate in the presence of multipath echos. The magnitude of the multipath problem is uncertain; however, preliminary estimates indicate it is moderately severe.

- 2) The link will suffer a blackout when the capsule enters the Martian atmosphere. It is imperative that data be received after the time of blackout and before impact.

The multipath echoes will cause amplitude and phase modulation of the received signal due to the presence of the delayed signals. Therefore any system of amplitude, phase or frequency modulation will be degraded by the multipath, including any system using subcarrier modulation. The principal alternatives are a noncoherent direct FSK system and a coherent PM system with the modulation on a subcarrier. These two possibilities normally provide the best performance for the noncoherent and coherent systems, respectively. It is shown in Section 2 of Appendix F, that both the noncoherent and coherent systems will operate satisfactorily with a 20-watt transmitter power, assuming that a 6-db fading margin and a 6-db system margin are required.

The coherent system involves a modulation restrictive phase-locked loop which tracks the carrier component. This necessarily involves an acquisition process in which the frequency uncertainty range must be searched for the signal whenever loss of lock occurs or the signal is interrupted, such as after the capsule link blackout. It is possible, at any time that the loop attempting to acquire, to have a lock-up on the higher order sidebands of the received signal. Such a false-lock, unless detected and corrected, will result in loss of data for the duration of the lock. This problem can be alleviated by an I-Q loop at the expense of added equipment complexity. The presence of the multipath echoes can cause a phase error for the phase-locked loop and increase the loss of lock probabilities significantly.

It is because of the above drawbacks that noncoherent FSK has been recommended for the capsule link. It has been shown to provide the desired data performance. No signal acquisition is involved for the FSK receiver since it is designed to operate properly whenever the signal lies within the known uncertainty range. In addition, the noncoherent FSK degrades more gracefully in the presence of severe multipath and will simply provide data with a higher error rate instead of dropping out of lock at high echo levels. In Phase IB, the possibility of programming the



transmitter and receiver frequencies to reduce the range of frequency uncertainty will be studied.

e. Frequency Choice

Six factors were considered in choosing the frequency of this link:

- 1) The frequency uncertainty problem
- 2) Propagation efficiency
- 3) Receiving system noise temperature
- 4) Efficiency of solid-state transmitters
- 5) Spacecraft and capsule antenna design problems
- 6) Blackout duration.

The general frequency band over which these factors are considered is 100 to 400 Mc. It is recognized that at microwave frequencies the blackout duration might be significantly less, but this possible advantage is offset by the implementation difficulties of a microwave capsule transmitter, low-noise temperature spacecraft receiver, and the fact that a spacecraft antenna with sufficient effective aperture would have a narrow beamwidth, creating a pointing problem.

Items 1) and 2) strongly indicate the use of as low a frequency as possible because the magnitude of the total frequency uncertainty  $\Delta F_F$  is directly proportional to the frequency and because propagation takes place between an isotropic antenna and a fixed-beamwidth antenna. Items 3) and 4) vary rather slowly and are not of major significance in the VHF region. The design problems associated with the design of the capsule and spacecraft antennas favor the higher frequencies. The most difficult problem is the capsule antenna because:

- Certain capsule dimensions limit the permissible size of the antenna
- Obtaining a high front-to-back ratio is easier at the higher frequencies.

It appears that a VHF range of 136 to 138 Mc offers the best compromise among these factors.

f. Link Performance

The telecommunications design control table for the capsule limits is given in Volume 2, VS-4-310. This table shows that for a maximum range of 40,000 km and a 20-watt lander transmitter, the 10 bit/sec data can be received with a  $1 \times 10^{-3}$  bit error rate. The table allows 6 db for fading and propagation effects and approximately 6 db for equipment tolerances. The assumed spacecraft capsule antenna gains are 4 and 0 db, respectively. A 4-db noise figure for the spacecraft receiver is assumed.

1.4 Spacecraft Antennas

The spacecraft trajectory to Mars establishes the cone and clock angles of earth with respect to the spacecraft, shown in Figure 3-6. These curves show that for the majority of the trajectories the clock angle remains in the vicinity of 90 degrees up to 40 days after launch. The cone angles generally travel from 90 to 15 degrees during this time. Thus, the high-gain antenna beam will remain at a nearly constant clock angle of 90 degrees, while traversing cone angles from approximately 90 to 10 or 15 degrees.

Once this attitude is established, the period from 40 to 70 days after launch involves, primarily, a clock angle change with very small cone angle variations. The clock angles during this time may travel either between 90 (through 180) and 230 degrees, or, depending upon the particular trajectory, between 90 (through 0) and 320 degrees.

From approximately 70 days after launch to encounter, approximately 140 to 200 days after launch, the angular changes will involve both clock and cone angles. The cone angles will change from approximately 15 to 40 degrees, while the clock angle will change from either 230 to 280 degrees, or from 320 to 280 degrees, again depending upon the particular trajectory.

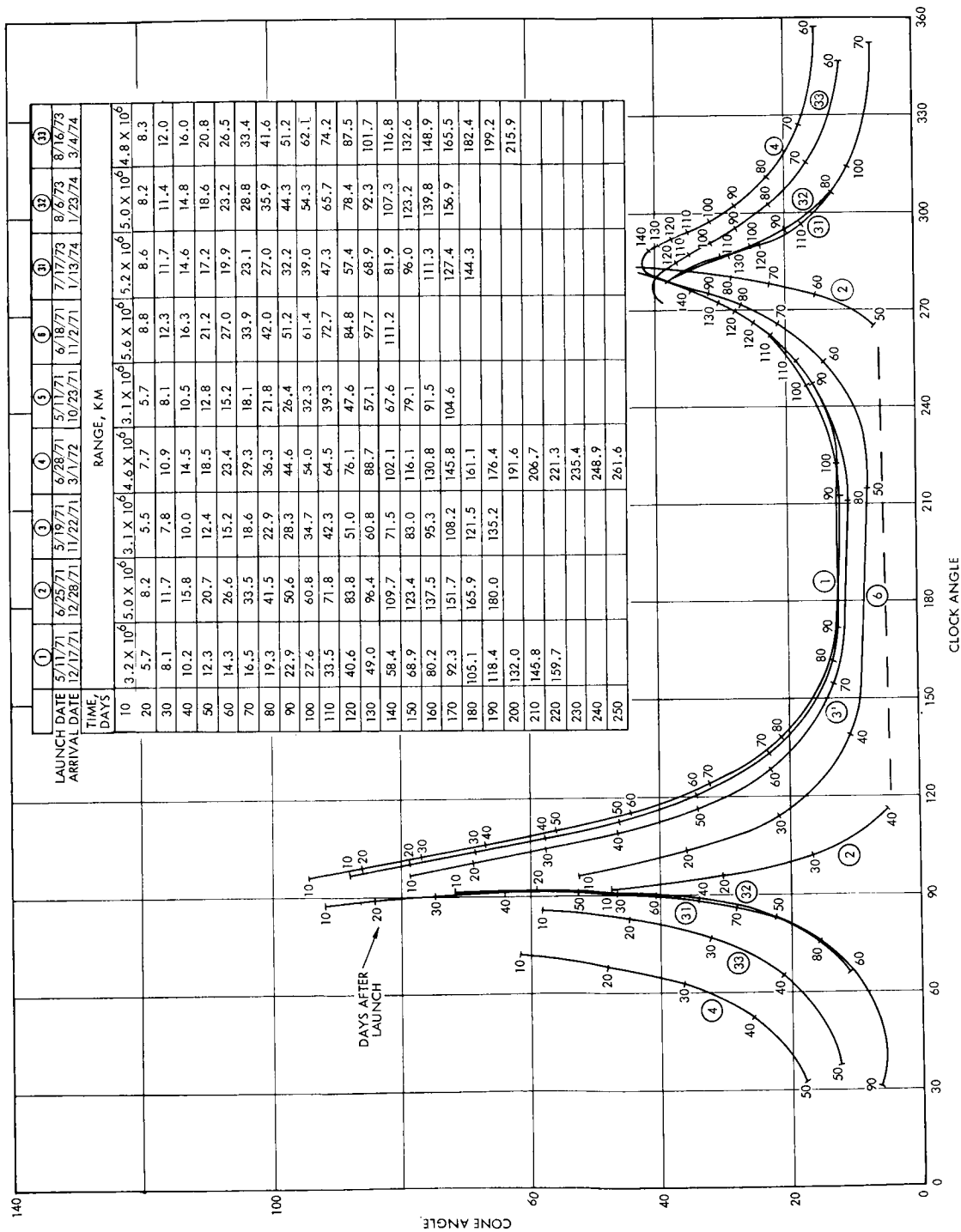


Figure 3-6. Cone and Clock Angles of Earth Relative to Voyager Spacecraft 1971 and 1973 Launches

#### 1.4.1 High-Gain Antenna

These variations in look angles, together with the requirement to provide communication during midcourse correction, at which time the required angles are arbitrary, indicate that for a beamwidth less than 8 to 10 degrees, a double-gimballed antenna is required. The nose fairing and the structural arrangement of Configuration A limits the maximum dimension of the high-gain antenna to approximately 6 feet for a circular or near circular aperture. A gain of approximately 30 db is thus selected as a design requirement.

##### a. Arrays Versus Continuous Apertures

The required 30 db gain implies large-aperture antennas. General requirements can be established regarding beamwidth, sidelobe levels, VSWR, efficiencies, weight, size, power handling capabilities, and other parameters to determine the type of antenna best suited to the particular application, keeping in mind that proven techniques with high reliability, moderate cost, and ease of manufacturability and maintenance are favored. Accordingly the field of large-aperture antennas was reviewed to determine the type of antenna most suitable for the Voyager mission. The two most likely candidates appeared to be the planar array and the paraboloid.

The uniformly illuminated planar array will produce the highest directivity for a given area of any of the large-aperture antennas. The maximum available directivity from an aperture radiator is given by:

$$D = 4\pi A / \lambda^2$$

where A is area of the aperture and  $\lambda$  is wavelength. The minimum possible aperture area for a lossless antenna having a directivity of 30 db (power gain of 1000) is

$$A = D \lambda^2 / 4\pi = \frac{1000}{4\pi} \lambda^2 = 79.6 \text{ square wavelengths.}$$

Typical efficiencies of planar arrays which have been reported in the literature\* are in the region of 70 per cent; thus the actual aperture required to obtain the desired gain becomes 1138 square wavelengths.

The typical planar array consists of slots, cut in the wall of a waveguide, which must be placed with great precision. Good control of the relative amplitude coupled into each radiating aperture requires an aperture-coupling structure at each slot opening. These generally take the form of iris or probe structures. The entire slot array is generally fed by a series of parallel waveguides branching off of a main feed waveguide, and at times the entire transmission path is formed of a corrugated structure to maintain proper phase and amplitude control within the feed lines. The costs of such a structure, and the reliability and manufacturability are relatively unknown factors at this time.

The uniformly illuminated paraboloid provides the same theoretical directivity as that of the planar array and thus the same requirement for aperture area for a directivity of 30 db, i. e., 79.6 square wavelengths. Since uniform illumination of a paraboloid is impractical, requiring a keyhole feed pattern with infinite taper at the edge of the paraboloid, common practice is to provide a compromise taper at the edge of the paraboloid, generally in the region of 10 db below the peak of the main lobe of the feed. Typical values of gain ratio for various sidelobe ratios are as follows:

Sidelobe Ratio (db)	$G/G_0$
20	0.90
22	0.84
23	0.81

where  $G/G_0$  is the ratio of the equivalent directivity to that of a uniform line source. The effective aperture, for an equivalent sidelobe level of

---

\* 1963 IEEE International Convention Report, Part I, pp. 2-9.

23 db, is 0.81 of the actual aperture. The actual aperture, therefore, must be increased to maintain the gain level, to 97.3 square wavelengths. Since the highest feed efficiency which can be expected is also approximately 70 per cent, an aperture size of 140 square wavelengths is implied.

The manufacturability of a paraboloid has been thoroughly explored, and a great deal of background has been accumulated in this field. Such apertures can be fabricated from sheet metal by spinning, stretch forming, or explosive forming. The surface tolerance can be maintained extremely close by relatively inexpensive methods. The rigidity of such a surface can be maintained by known methods. The costs are extremely low, and the reliability extremely high. The feed system can be a simple low-gain radiator. It thus appears that in view of its high reliability, ease of fabrication, and use of standard design and construction techniques, the paraboloid is the logical choice of antenna type for the high-gain antenna.

#### b. Antenna Design

Because of the limited space between the flight capsule and the spacecraft solar array, a circular 6-foot diameter paraboloid cannot be used; a sectoral elliptical paraboloid is necessary to obtain the desired gain within the available storage volume. Since gain is directly proportional to the area of the aperture, an elliptical reflector having a minor axis of 66 inches and a major axis of 78.5 inches, with a 28.8-inch focal length, will produce the same gain as a 6-foot circular reflector. Such an unsymmetrical shape requires a shaped beam from the primary feed to produce equal edge illumination of the reflector.

The reflector is perforated to remove 50 per cent of the material (and thereby weight) but the perforations are sufficiently small to maintain the RF transmissivity below -20 db. The surface tolerance is  $\pm 0.10$  inch or less, equivalent to  $\pm 0.02 \lambda$ , maintaining the sidelobe level degradations from random surface irregularities below -27 db.

The selected configuration for the high gain antenna is shown in Figure 3-7. The concept illustrated is a straightforward approach using state-of-the-art techniques. The paraboloidal surface is formed from 30-mil 2024 aluminum sheet. A 3-foot diameter yoke ring is utilized fabricated from 2-inch diameter, 0.050 wall, 6061 T6 aluminum tubing attached with blind rivets spaced approximately every two inches. By attaching the paraboloid at this diameter, the need for a rolled edge to provide stiffness is eliminated. The yoke ring also provides a four-point attachment structure for the yoke. The yoke is a simple structure of bent and welded 0.050 wall, 2-inch diameter, 6061 T6 tubing with appropriate stiffeners. The base shaft of the yoke provides for a pinned attachment to the actuator output shaft. The coaxial transmission line from an actuator assembly is routed through this junction to the base of the feed. At the center of gravity of the paraboloid yoke structure, a stowing arrangement is provided which fastens the antenna to the spacecraft structure by two fixed pin hard points and a squib actuated clevis with redundant squibs. The pins control lateral stability and the clevis provides axial stability in unison with the actuator as a third hard point. Hard stowing of the antenna is required by the calculated 40-g, 60-cycle damped wave input imparted to the antenna during shroud separation.

The antenna feed, a focal point horn-type radiator, obtains its primary support from a structural member attached to the vertex of the paraboloid extending directly to the horn, where a dielectric support carries the load directly to the back wall of the horn assembly. This structural member is also the coaxial feed line to the horn, feeding through the vertex of the paraboloid, to which it is attached by an integral flange.

The 3-foot diameter of the paraboloid to which the feed base attaches may be stiffened with radial ribs terminating at the yoke attachment ring, if required, to suppress diaphragm modes of vibration in the paraboloid resulting from the feed mass and wire tension loads. The

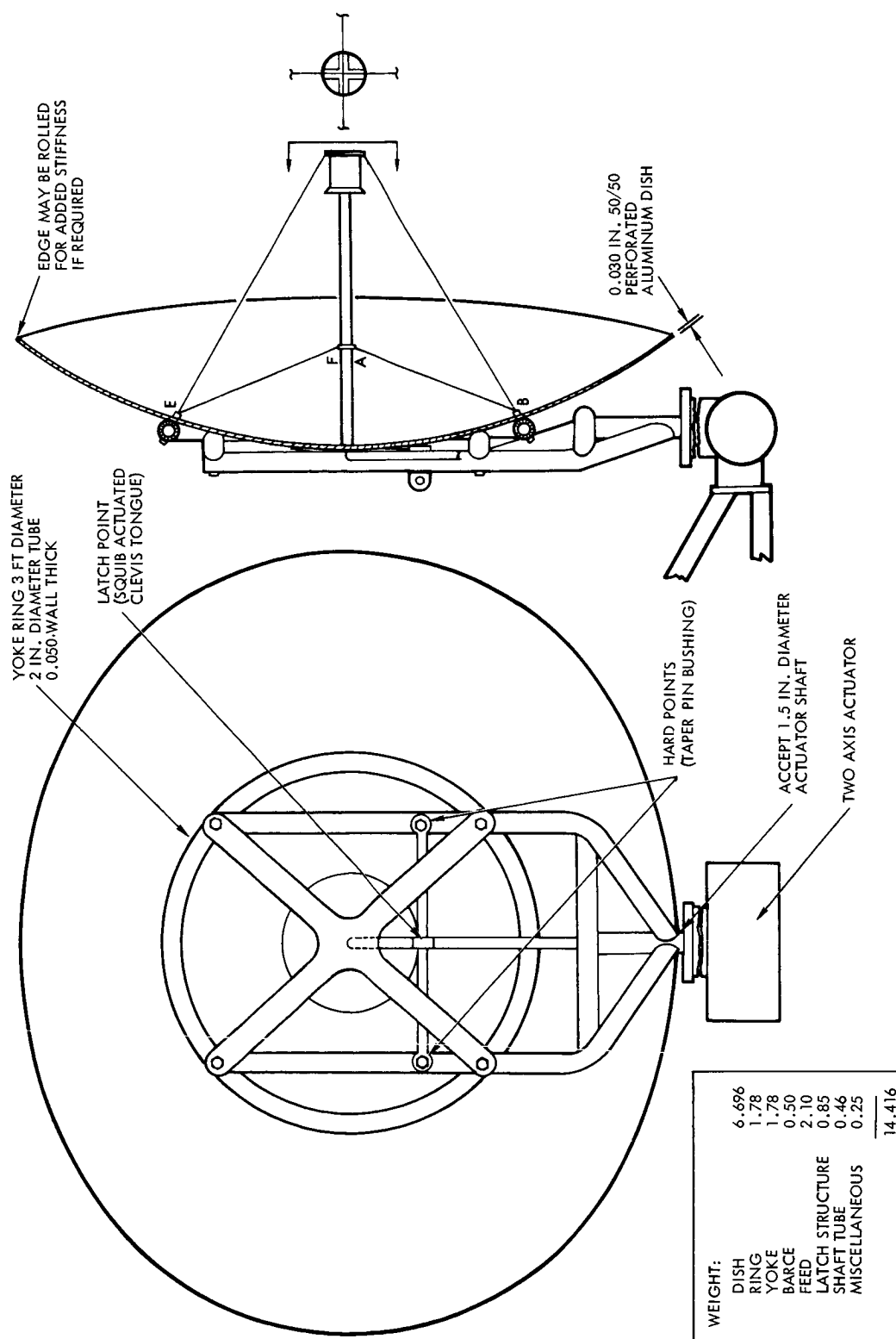


Figure 3-7. Antenna Elliptical Dish (Major Axis 6 ft 6-1/2 in.,  
Minor Axis 5 ft 6 in.)



feedline and the horn are aluminum. The horn is mechanically stabilized by four woven aluminum wire tension elements. Stranded aluminum wire provides reliability in the form of multiple strand redundancy, together with some temperature compensation since the same material will be used in the related antenna assembly. Differential thermal expansion and contraction resulting from nonuniform heat gradients will be further compensated by the use of a cross spring tension limiter and compensator.

The coaxial feed line in the paraboloid and the remainder of the antenna system are of the low loss variety utilizing foamed polyethylene dielectric and aluminum outer conductor. All antenna surfaces are painted with thermally and optically black paint which, with the transmission provided by the perforations of the paraboloidal surface, will limit the temperature to a calculated range of  $152^{\circ}\text{F}$  maximum to  $-300^{\circ}\text{F}$  minimum, worst case. The dielectric and other materials used in this assembly can retain both structural and electrical integrity over this range.

The following surfaces were considered with the tradeoff factors noted.

Furled, deployable. Two furled, deployable surfaces were considered, the Sunflower hinged rigid segment type and the rib and flexible aluminized Mylar umbrella type. There is no saving in weight for either type, when balanced against the fixed solid aluminum paraboloid. The number of stiffeners, ribs, and overlaps required to provide a satisfactory surface contour, and the stowing and deployment mechanisms, result in total structure weights comparable to the rigid paraboloid, even though the basic surfaces are lighter. Deployable surfaces, in adding an additional failure mode, i. e., failure to deploy, reduce the over-all reliability of the communication subsystem.

Honeycomb. Neither honeycomb aluminum or honeycomb plastic structures offer any weight advantage over a solid aluminum paraboloid when all considerations, such as structural supports and attachment inserts, are considered. From a thermal standpoint, the aluminum

honeycomb is superior, since the plastic honeycomb materials have poor thermal conductivity. Degradation of the plastic because of long-term exposure to ultraviolet and IR radiation is predictable. Metallizing the plastic honeycomb surface would reduce the exposure effects and would be desirable, for this reason, over the use of a bonded mesh surface, but with external surfaces metallized thermal gradients across the poorly-conducting core would be greater, resulting in internal stress reversals that could, in time, break internal bonds and cause delamination and surface degradation. Outgassing is also likely to be a problem.

Sheet Metal. Fabrication of sheet metal paraboloid reflectors generally uses methods such as spinning, explosive forming, or stretch forming. The resulting structure is a grain oriented self-supporting structure of simple, one-piece construction with inherent strength and stability. As a homogeneous structure, its thermal conductivity provides optimum characteristics for distribution of thermal gradients, both face-to-face and laterally. Attachments to provide supplemental structure can easily be made by a variety of standard techniques. Minor damage is easily repaired. Over-all weight, using 50 per cent perforated sheet stock, is comparable to other approaches configured to meet Voyager design criteria. The material used would probably be 2024 aluminum, either annealed or in a T4 state in the forming stage, with aging at 350°F to a T6 state for maximum strength.

Support Structure. The support structure attaches the paraboloid to the actuator mechanism. It must provide sufficient structural integrity to insure the survival of the over-all antenna assembly through boost, the shroud separation shock, and the variation in temperature to be expected. It must also provide a means of stowing the assembly in a secured position until deployment is initiated. The same considerations that resulted in selection of aluminum sheet metal as the paraboloid material yield the same conclusion for the support structure material.

c. Gimbal Drive

Requirements and criteria for the antenna gimbal drive studies were as follows:

- A rotary output is required.
- All high speed elements must be sealed in a pressurized inert atmosphere.
- Minimum number of parts and minimum number of rotating seals for maintaining internal pressure are desired.
- A straightforward method of attaching to the gimbal is preferred.
- Use of magnetic materials and fields generated by the drives minimized.
- The coaxial cable must not be subject to flexure as the antenna is rotated.
- Slew rate of 5.3 milliradians per second maximum about either axis.
- Angular acceleration of 0.5 milliradian per sec<sup>2</sup>.
- Hinge axis of  $\pm 90$  degrees and shaft axis of  $\pm 180$  degrees.
- Pointing accuracy of  $\pm 4$  milliradians relative to the flight spacecraft.
- Acceleration loading of 3 g steady-state acceleration with antenna deployed.
- The drive must withstand stalled conditions at the output without internal damage.

Tradeoff studies were conducted to define gimbal arrangements, the type of sealed drives, and associated electronic components which can satisfy the pointing requirements of the high-gain antenna. For the tradeoffs, consideration was given to performance, reliability, size, weight, and packaging.

Stowage requirements and the desire for maximum coverage dictate the mounting of the antenna at the edge of the solar array and a configuration in which the dish is mounted at the end of a 3-foot shaft with the drive unit at the base of the shaft.

Two gimbal schemes were compared on the basis of reliability and complexity. Scheme A consists of a standard two-axis gimbal assembly in which each axis is operated by a separate drive. This scheme is attractive because of its simplicity and high reliability. Scheme B makes use of a unique feature of the differential gear. For this scheme two drives supply simultaneous inputs to the differential gear. If the drives operate in the same direction, an output about the hinge axis is produced; if they operate in opposite directions, the output is about the shaft axis. The advantage of using this scheme is that the drives would be working together in overcoming large antenna hinge moments produced during retrorocket firing. Table 3-9 summarizes the main tradeoffs for each gimbal candidate. Based on the tradeoff considerations, it was concluded that Scheme A was the better.

The basic gimbal minus drives, pickoffs, etc., is made up of three primary parts, a yoke, a gimbal, and a trunnion shaft. When assembled with ball bearings, these parts form the basis for a two-axis gimbal as shown in Figure 3-8. The yoke is a fixed member which

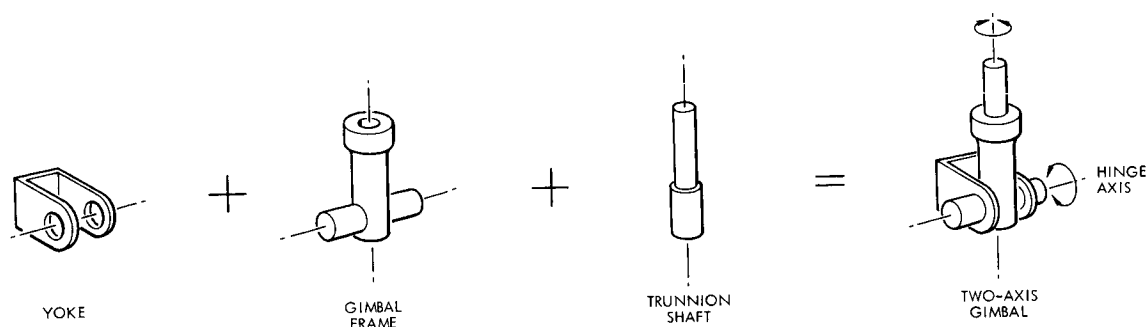
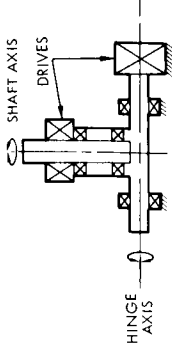
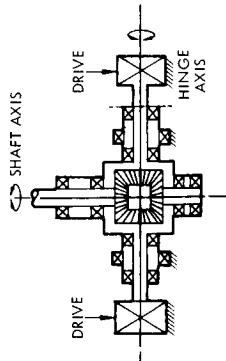


Figure 3-8. Basic Gimbal Elements

Table 3-9. Gimbal Tradeoff Summary

Gimbal Arrangements	RELIABILITY			Complexity
	Number of Critical Parts	Operating Characteristics		
Standard Cross Gimbal (Preferred) 	Bearings: 4 Gears: 0 Structural: 3	Movement about any one axis requires input from one drive only. Failure of one critical part causes failure of one axis only.	Minimum complexity. Simple to package, manufacture, and assemble. Minimum manufacturing cost.	
Differential Gimbal 	Bearings: 10 Gears: 4 Structural: 3	Movement about any one axis requires that both drives operate simultaneously Failure of one critical part causes failure of both axes.	Highly complex. Difficult to package, manufacture, and assemble. High manufacturing cost.	

attaches to the spacecraft and supports all other gimbal elements. The gimbal frame when mounted to the yoke forms the hinge axis of the gimbal. The trunnion shaft mounted in the gimbal frame forms the gimbal shaft axis and acts as a mount for the high-gain antenna. The elements are preloaded for rigidity and accuracy and employ solid lubricant coatings.

Detailed tradeoff studies were conducted to select the proper sealed drive unit, motor, position pickoff, and drive electronics mechanization for the antenna drive. These studies were conducted in parallel with the similar studies for the POP drives. The considerations and basic conclusions are the same and are thus not repeated here (see Section II-2).

The preferred drive consists of a simple two-axis gimbal operated by sealed wobble gear drives. It incorporates digital pickoffs for sensing gimbal positions and RF rotary joints for maintaining the RF path through gimbal members. Figure 3-9 shows a preliminary design layout of the preferred antenna drive. One hinge axis drive and one shaft axis drive are required. The drives are similar to those developed for the OGO solar array and OPEP drives. During the OGO program these drives were subjected to environmental and performance testing and operated for more than 10,000 hours in vacuum. They have performed satisfactorily in space since launched in September 1964. In preparing the final design in Phase IB, efforts will be directed toward optimizing size, weight, and reliability and standardizing as many parts as possible for use on other articulated Voyager subsystems.

Sealing is accomplished by two bellows (Figures 3-9 and 3-10) installed between the rigid parts of the mechanism and the driving gear. Action of the bearing carrier and a tilted bearing internal to the unit produces a non-rotating conical nutation (or wobble) motion of the driving gear at the end of the main bellows. This motion causes rotation of the output gear and shaft by sequential engagement of a limited number of

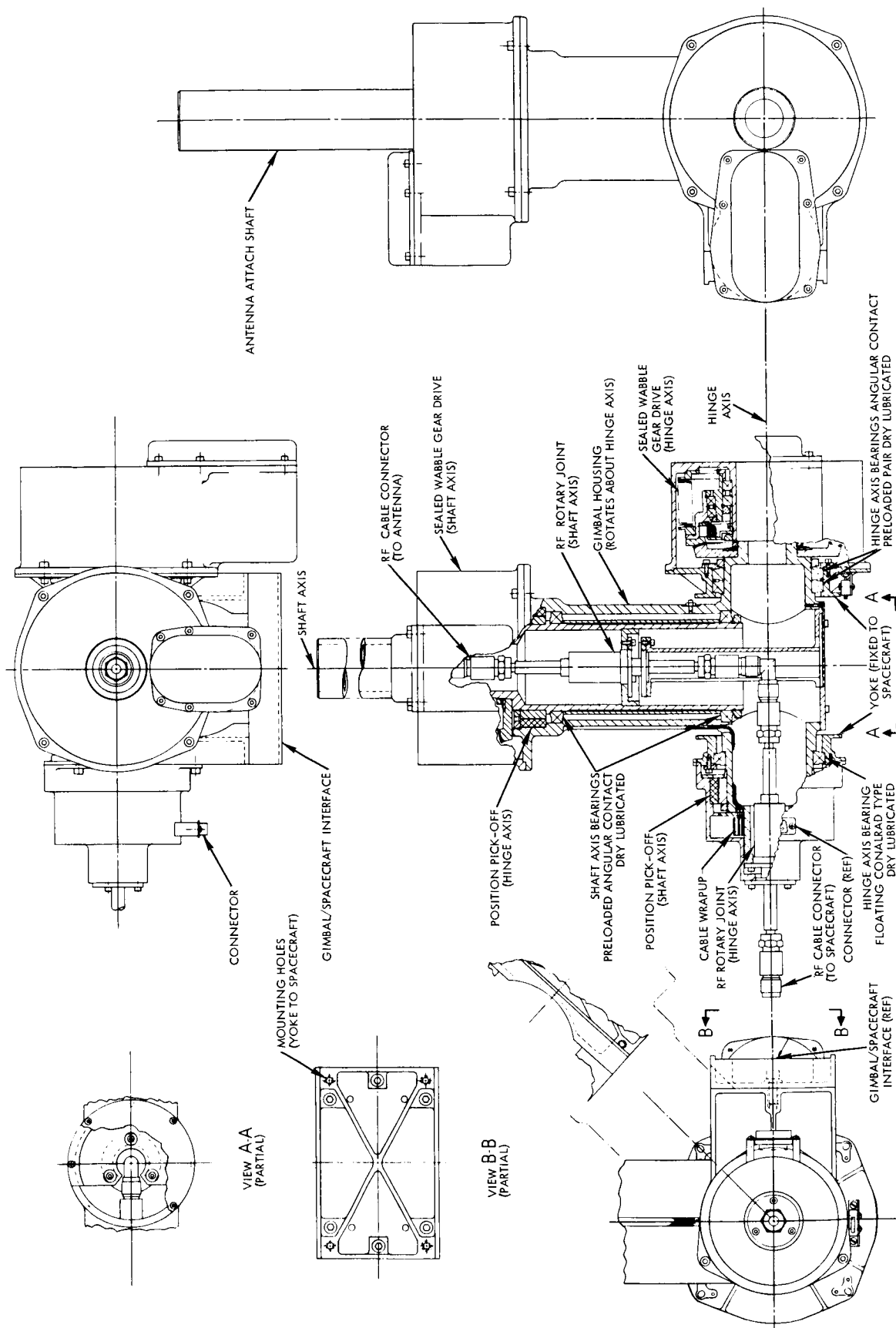


Figure 3-9. Preliminary Layout of High-Gain Antenna Gimbal

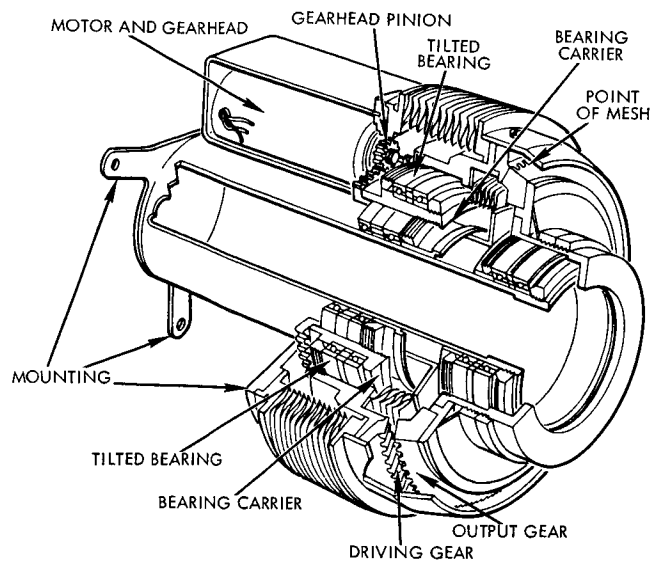


Figure 3-10. Wobble Gear Drive

gear teeth. The gimbal bearing and drive units employ the same lubrication techniques developed and used on OGO. All exposed slow-moving elements are plated with low-shear precious metal and impregnated with molydisulphide.

The prime movers for the drive mechanism will be two-phase, 400 cps, induction servomotors.

The drive electronics (Figure 3-11) for both the hinge axis and shaft axis drives will be identical in concept. The main difference will be in the power delivered to the drive motor. A digital signal from the CS and C corresponding to an incremental shaft position is loaded serially into an up-down counter register. The register output triggers the motor driver which applies two-phase, 400 cps power to the drive motor. The pulses fed back to the register from the shaft position encoder decrement the input register back toward zero as the drive shaft approaches the desired position. An additional up-down counter register accumulates the absolute shaft position angle for telemetering back to earth.



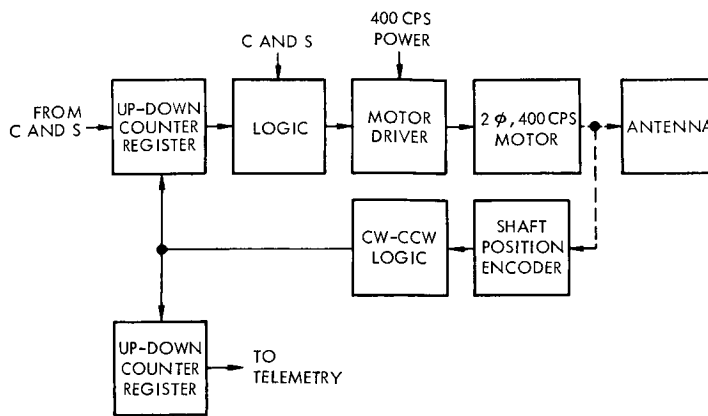


Figure 3-11. Drive Electronics Block Diagram

Two gimbal position pickoffs are required for determining the position of the antenna about each axis. Antenna position is measured by a magnetic, noncontract incremental shaft encoder using a variable reluctance transducing technique.

A small cable wrapup assembly is required on the hinge axis to accommodate wires from the shaft axis drive and position pickoff.

This assembly consists of wires grouped together in a flat ribbon which is wound around the hinge axis trunnion and shielded from direct exposure to space.

Motion about the hinge axis is limited by a set of limit switches to interrupt the drive motor circuit at appropriate hinge axis positions. Motion about the shaft axis is controlled by logic circuitry to prevent damage during deployment or stowage of the antenna. The shaft axis is inoperative until the antenna is deployed; the antenna is not capable of entering the stowage position until it is first properly oriented about the shaft axis.

The RF transmission path is required to traverse two axes of rotation in the high-gain antenna assembly. Three methods of providing the required relative motion across the axes were studied, cable wrap-up, contacting rotary joints, and noncontacting rotary joints. The cable wrap-

up was considered the least desirable because of the bulk and weight resulting from the number of turns required. Spring tension exerted on the actuator mechanism and fatigue of the coaxial cable were also considered as detracting from reliability. Flexible cable would be used for this case, but the fact that it becomes a rigid element if the cable heater fails necessitated a layout on the basis of its behavior as a rigid coil structure. Such a case would require a bobbin and minimum of six turns per axis on approximately a 6-inch diameter with additional radial clearance for growth during rotary motions, causing unwinding of the coil. Such an arrangement would weigh approximately three times that of the non-contacting rotary joint arrangement and would have the additional negative factors of noise during flexure, increased electrical losses due to the additional cable lengths involved, and restriction of angular rotation in one axis.

The contacting type rotary joint was eliminated because of problems associated with providing reliable electrical continuity without contact welding in a space environment. The non-contacting type is proposed as the simplest, most reliable, and the lightest in weight. By utilizing the bearing structure integral with the actuator geometry, and so arranging the actuator shafting to accommodate the required hardware, it was possible to design the rotary joints into the actuator assembly so that they are an integral part of that assembly and utilize its bearing system. To keep insertion loss as small as possible and to provide rotation capability at the extreme temperatures of space environment, air dielectric, noncontacting, choke-coupled rotary joints are used. The insertion loss is less than 0.1 db over the operating frequency band of 2000 to 2500 Mc. The rotary joint is an integral part of the gimbal axis structure (see Figure 3-9); relying on the gimbal structure for alignment as well as the rotating mechanism.

The construction of the rotary joint is shown schematically in Figure 3-12.

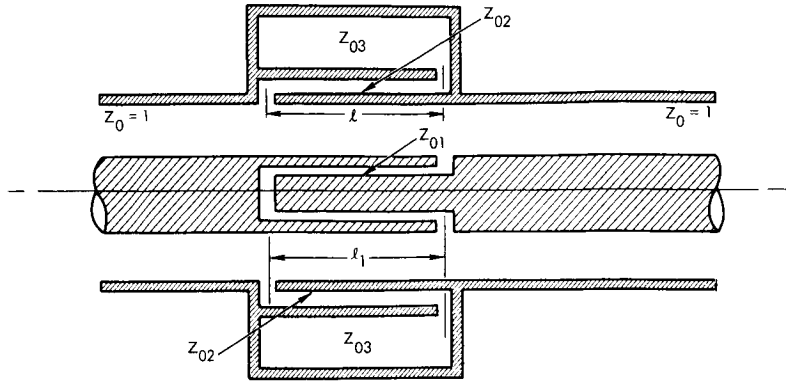


Figure 3-12. Rotary Joint Construction Schematic Diagram

All the choke sections, denoted by 1, are one quarter-wave long at the center frequency. To prevent leakage an external choke of impedance  $Z_{o3}$  is added to the outer conductor choke section.

For simplicity  $Z_{o3}$  is assumed infinite, and  $Z_{o1}$  equal to  $Z_{o2}$ . The Characteristics impedance  $Z_o$  is normalized to one. The ABCD matrix of the two chokes displaced by the length 1 along a lossless transmission line is

$$\begin{array}{cc} \cos \beta l + Z_{o1} \cot \beta l_1 \sin \beta l & -j Z_{o1} \cot \beta l_1 - j Z_{o1}^2 \cot^2 \beta l_1 \sin \beta l + j \sin \beta l \\ j \sin \beta l & \cos \beta l + Z_{o1} \cot \beta l_1 \sin \beta l \end{array}$$

where  $\beta l$  is the electrical length of the choke sections and  $\beta l_1$  is the electrical spacing between the two chokes. The insertion is then given by

$$L = 10 \log_{10} \left\{ 1 + \frac{1}{4} \left[ (A-D)^2 - (B-C)^2 \right] \right\} \quad (3.1)$$

If

$$|K|^2 = \left| (A-D)^2 - (B-C)^2 \right| \text{ and } \beta l_1 = \left( \frac{\pi}{2} + \phi \right)$$

where  $\phi$  is the difference in electrical length from the center frequency choke length of  $\frac{\pi}{2}$ , then

$$\beta_1 = \beta_{1_1} = \left( \frac{\pi}{2} + \phi \right) \text{ and } |K| = \frac{2Z_{01} \tan \phi \cos \left( \frac{\pi}{2} + \phi \right)}{Z_{01}^2 \tan^2 \phi \sin \left( \frac{\pi}{2} + \phi \right)} \quad (3.2)$$

The relation of  $|K|$  to the coaxial transmission line VSWR is

$$|K| = \frac{\text{VSWR} - 1}{\sqrt{\text{VSWR}}} \quad (3.3)$$

For the case of 0.1 db insertion loss, Equation (3.1) yields

$$|K|^2 \leq 0.08$$

This is the maximum  $|K|^2$  possible for the specified amount of loss.

Using Equation (3.2) with a band center of 2250 Mc, band edges of 2000 and 2500 Mc and assuming  $Z_{01} \approx Z_{02} = 0.40$ , normalized to one,

$$|K| = 0.062$$

This corresponds to a VSWR of 1.065:1 attained from Equation (3.3).

#### d. Feed System

Two possible types of feed for the high-gain antenna were considered, Cassegrain and focal point.

Figure 3-13a illustrates a simple Cassegrain configuration, consisting of a paraboloid main dish, hyperboloid subdish, and a feed horn at or near the vertex of the paraboloid. The hyperboloid subreflector enables the placement of the primary feed at a more convenient point in the system. Figure 3-13b illustrates a conventional feed at the focal point of the paraboloid. The requirement of 5-degree half-power beamwidth is easily supplied with the focal point feed. The Cassegrain feed is generally used for half-power beamwidths of 2 degrees or less.

The Cassegrain feed allows the use of shortened transmission lines from equipment compartments to the feed assembly; focal-point

feed must utilize a longer length of transmission line with its associated insertion loss. However, the increased mechanical complexity in the fabrication and suspension of two continuous reflectors for a Cassegrain outweighs the advantage of the lower cable loss.

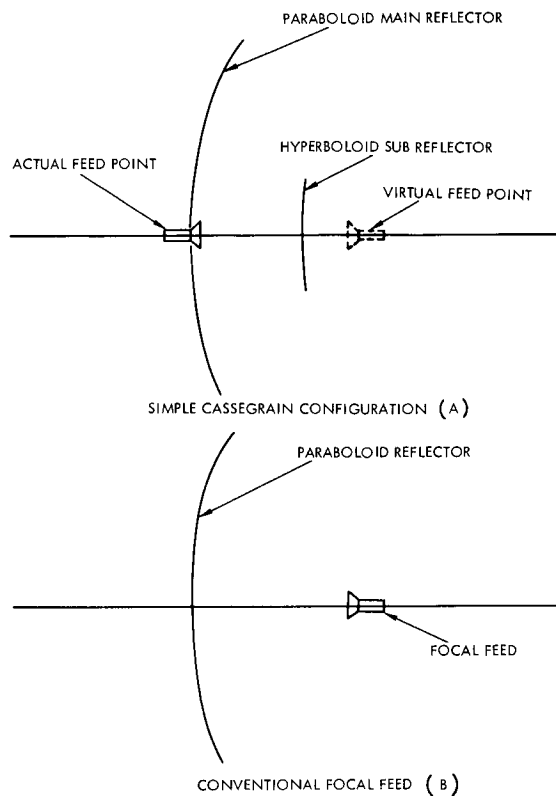


Figure 3-13. Cassegrain and Focal Point Configuration

The required aperture of the focal feed assembly to illuminate the 6-foot diameter paraboloid reflector leads to a first side-lobe level on the order of 23 db down from the main beam. If a similar feed is used, and the restriction of minimum aperture blockage is imposed on the simple Cassegrain, the side-lobe level increases to 18 db below the main beam. The effect arises from increased aperture blockage.

Advances in present coaxial techniques, such as low loss semi-rigid cable, make it feasible to use the cable itself as the supporting structure for a focal feed.

Based on simplicity of design, coupled with the above mentioned electrical advantages, a focal feed was selected.

A major development consideration in a paraboloid reflector antenna is the primary feed and its supporting structure. Preliminary investigation has shown that it is possible to excite a two-arm Archimedian spiral within a circular waveguide. By launching a wave that is already circularly polarized, rather than creating one using phase delay techniques, many components required to produce a circularly polarized wave are eliminated, thus increasing the reliability of the primary feed. The diameter of the flared aperture will be approximately 4 inches, which gives a calculated side lobe of -23 db due to aperture blockage. A balun transformer, as described by J. W. Duncan and V. P. Minerva, is incorporated in the transmission line to match the spiral element.

The length of the circular waveguide feed is approximately 3 inches. Investigation will be conducted on the aperture shape to obtain the required beam taper. In the narrow plane of the elliptical paraboloid reflector, the subtended angle from the focal point to the edges is 119 degrees, while the broad plane subtends an angle of 130 degrees. The radiation pattern of the primary feed will be so shaped that the edge illumination is constant at -10 db from the beam peak.

The feed horn is a simple aluminum dip-brazed shell composed of the flare, straight tubular section, and the back wall. Incorporated in the assembly is a bonded phenolic structure to clamp the double spiral launcher in place and provide a column load reaction path from the coaxial line feed/balun extending from the vertex of the paraboloid to the back wall of the dip brazed assembly. Integral with the top of the feed is a crossed spring tensioner/compensator working in conjunction with the stabilizing wires.

A portion of the transmission line acts as a feed support strutt as well as a transmission line. The remainder of the transmission line serves only as an RF path. The transmission line between the feed and the diplexer contains two rotary joints and a short section of line internal to the actuator which completes the rf path. All of the line utilizes safety wired aluminum type "N" connectors for joint continuity, and is routed adjacent to structure where appropriately spaced tie down points support it during ground handling and dynamic environmental conditions. The line

uses aluminum tubing for the outer conductor with a dielectric foamed polyethelene. The center conductor is copper. This material was chosen over an air dielectric, bead supported line since there is little difference in the electrical performance of the two and the foamed type provides a considerably more reliable structure. Although the cells are closed in the foamed type of dielectric structure, Pioneer and OGO have demonstrated that the outgassing is gradual and causes no significant problems. The possibilities of connected cell foamed dielectric structures and other dielectric materials need to be investigated further. Teflon was considered inapplicable because of its expansion and contraction characteristics over the temperature ranges which, in the case of the coaxial line, can range between 160 and 320<sup>o</sup>F.

#### 1. 4. 2 Medium Gain Antenna

As a backup to the high gain antenna and to provide additional flexibility for communications during attitude maneuvers, a single gimbal medium gain antenna is used. The power budget indicates that communications can be maintained out to a rainge of  $2.3 \times 10^8$  kilometers at a rate of 1024 bits/sec with a 24 db gain antenna. Naturally, at shorter ranges, higher bit rates are possible.

The angular coverage requirements for the 24 db antenna are similar to those of the high gain antenna. However, it has been determined (see Volume 4) that a single gimbal properly oriented can provide acceptable earth coverage if the beamwidth is at least 10 degrees.

Figure 3-14 plots the error of the single gimbal medium gain antenna look angles as functions of time. As shown, the error decreases with time, such that the earth becomes centered on the beam of the antenna as the range increases, providing a nearly constant gain level toward the earth throughout the flight of the spacecraft. Greater than 3 db pointing loss will be experienced during a portion of the trajectory, but this condition occurs close to earth, at which time the loss can be tolerated.

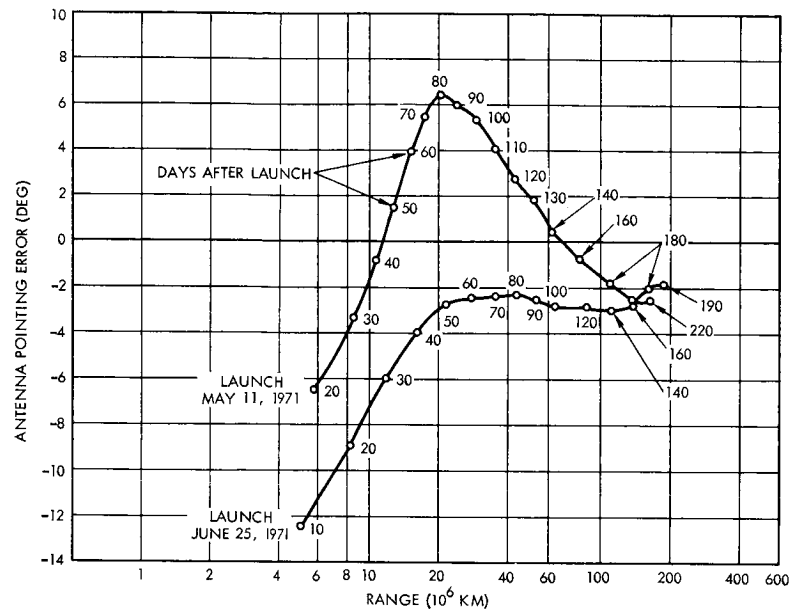


Figure 3-14. Pointing Error of an Antenna with Single Gimbal Movement Whose Axis of Rotation is Oriented at a Clock Angle of 195 Deg and a Cone Angle of 95 Deg

Except for the difference in size between the 3-foot paraboloid (Figure 3-15) and the high gain sectoral elliptical antenna, the construction and geometry are generally the same. The materials are also identical except for gauge which, in the case of the 3-foot paraboloid is reduced to 0.020 inch, and the yoke and yoke ring to 0.030 inch. Stowing is accomplished in the same manner.

A major difference, however, is that for the medium gain antenna only one axis of motion is required, which will provide both deployment and look angle positioning. Because of the lower mass of the 3-foot antenna structure, the shorter moment arm, and the elimination of one axis of rotation, the actuator is considerably smaller. Functionally it is a scaled version of the dual axis actuator on the high gain paraboloid, incorporating a single integral rotary joint.



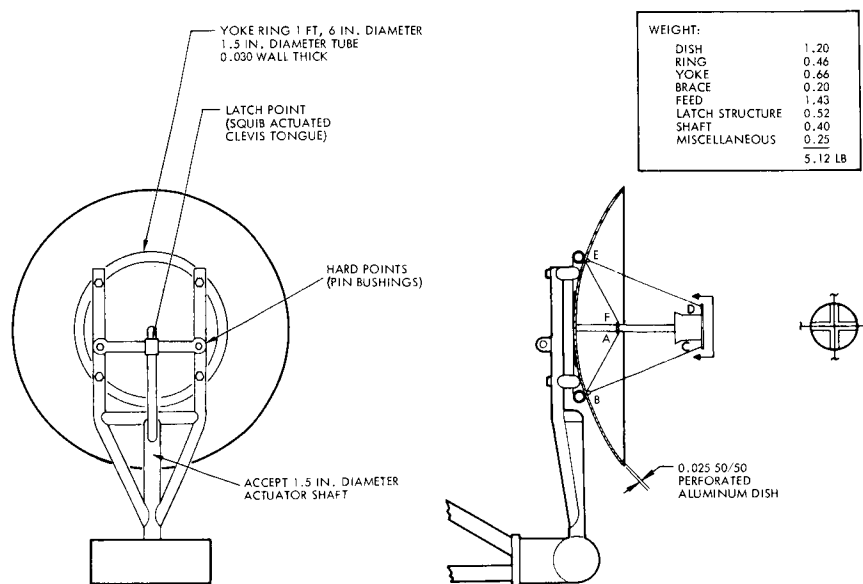


Figure 3-15. Antenna 3-ft Circular Dish

The basic drive mechanism, rotary joint, and mounting arrangements are similar to the design for the high gain antenna. Gimbal freedom of the medium gain dish is  $\pm 90$  degrees relative to the plane of the solar array. Figure 3-16 shows the drive mechanization.

The medium gain antenna is a circular paraboloid utilizing a circular feed horn with a conical flare. The  $f/D$  ratio is 0.4, providing an angle of 128 degrees from the focal point over which the feed must provide illumination. The proper aperture to provide illumination at the center of the paraboloid is in the region of 4 inches, requiring only a small flare from the 3.6-inch diameter of the circular waveguide. The same method of excitation as in the case of the high gain antenna is utilized, and the same method of support to maintain the feed horn at the focal point.

#### 1.4.3 Low Gain Antenna

The low gain antenna coverage provides telemetry coverage during boost through a coupling aperture in the vehicle fairing. Its gain requirement is 2 db at cone angles of 45 degrees to enable command reception at encounter plus one month; and a primary design objective is to attain the largest possible coverage within this constraint.

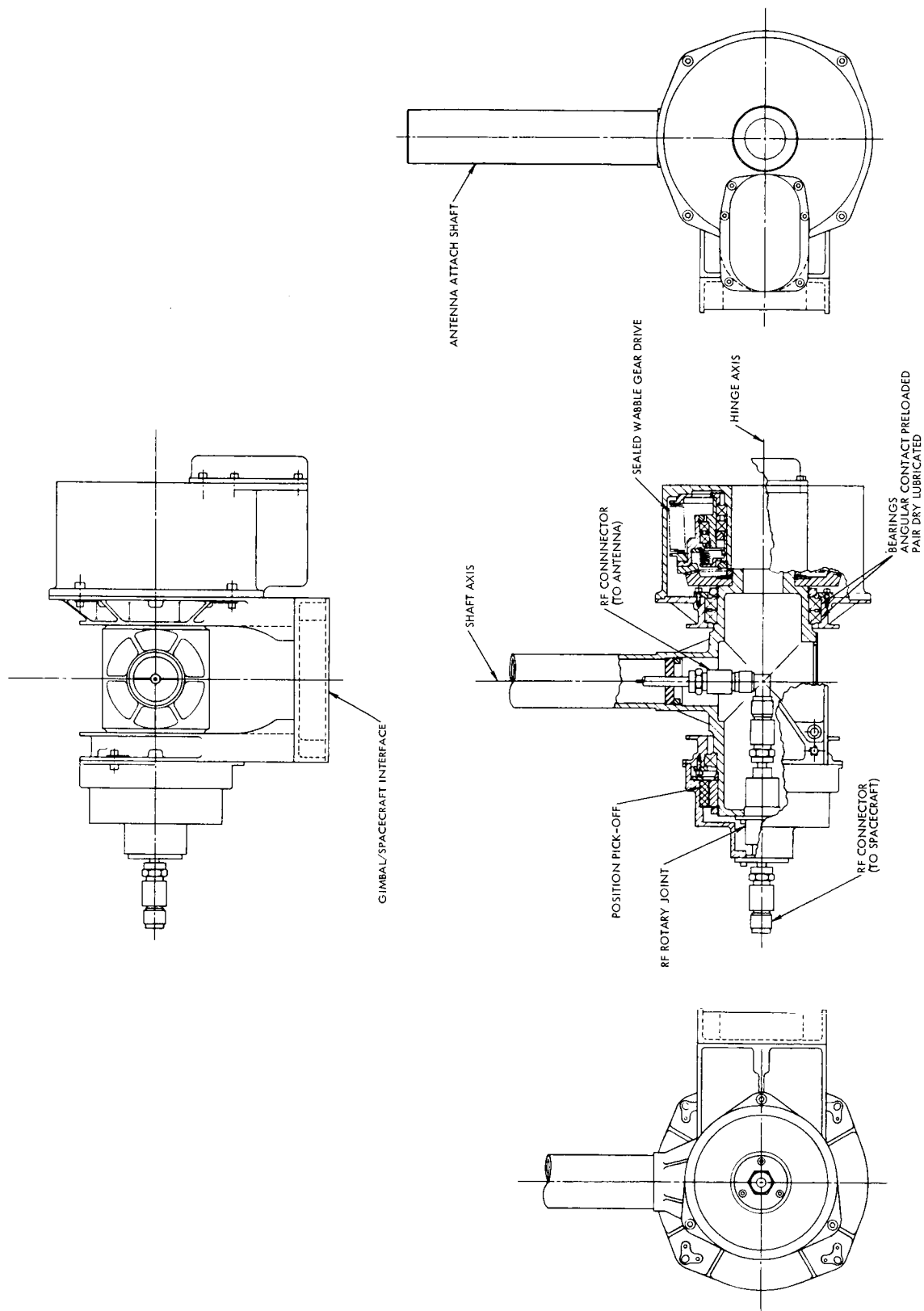


Figure 3-16. Preliminary Layout of Medium Gain Antenna Gimbal

a. Coverage Requirements

The configuration of the low gain antenna is governed primarily by its coverage requirements. These, in turn, are determined by the look angle history from the spacecraft to earth as a function of the spacecraft trajectory.

Before and during launch, the downrange direction will be located at the 45-degree spacecraft clock angle relative to the Canopus Sensor. Thus the low gain antenna must be capable of covering the appropriate cone angles at this 45-degree clock angle during these phases. A window must be provided in the shroud to allow communication with the ground station.

After the shroud has been removed, and until the sun has been acquired, the time history of cone and clock angles of the spacecraft relative to earth have not been defined. This is not considered critical, however, since sun acquisition is an automatic function.

After sun acquisition, and until Canopus acquisition, it is desirable to provide antenna coverage to a cone angle of 110 degrees at clock angles from 0 to 360 degrees since, in case of false Canopus acquisition, it is desirable to be able to command the spacecraft to repeat the Canopus acquisition maneuver. These maneuvers, however, will occur relatively early in flight at relatively short ranges. Consequently, communication can successfully be accomplished with antenna gain on the order of -30 db.

After Canopus acquisition, the angles to be covered by the antenna pattern are defined in Figure 3-6. It can be seen that a cone angle of 110 degrees is still required for some of the flights but at a specific clock angle of 90 degrees. At this range antenna gain levels as low as -22 dbi are allowable (command and 128 bits per second telemetry) since, for these angles, the spacecraft is still relatively close to earth. The antenna, tentatively selected, is located at 45-degree clock angle, with its primary lobe centered at 0 degree cone angle with a free space radiation pattern having a signal level no less than -8 dbi at 90-degree cone angle. However, there will be an effect on the antenna pattern for certain look angles at cone angles greater than 90 degrees. This effect will be seen as a shadowing and diffraction of the pattern by the spacecraft, resulting in reduced gain

and some lobing as the direction of coverage goes below the line-of-sight to the spacecraft. Complete loss of signal will occur over an unpredictably small angular portion of the volume about the antenna. This loss is caused by masking by the spacecraft. Coverage in this region is important early in flight, where a gain of -30 to -22 dbi is required, but is less important after Canopus acquisition, in which case the line of sight from the earth is not in the shadowed region of clock angles. After 20 days, the cone angle for all trajectories considered is less than 90 degrees; hence, full clock angle coverage is obtained. As the spacecraft approaches encounter, radiation pattern coverage is required within a cone angle no greater than 45 degrees. The gain required near encounter is 2 dbi minimum. The primary antenna has a gain of 2 dbi minimum at the 45 degree cone angle for all clock angles.

A possible solution to the coverage requirement for the low gain antenna is in the use of a deployable boom. To improve the coverage, it would be necessary to place the antenna such that the line-of-sight angle from the antenna to the spacecraft is equal to or greater than 110 degrees at all spacecraft clock angles. This, of course, adds complexities with accompanying loss in reliability to the antenna system. However, detailed look angle pattern studies are required and consideration of various approaches including the use of booms will be conducted in Phase IB.

To obtain the pattern coverage required for the earth-spacecraft link, consider the idealized radiation power pattern

$$P = P_o \left( \frac{1 + \cos \theta}{2} \right)^k \quad (3.4)$$

The boresight directivity gain relative to an isotropic radiator of matched polarization is obtained from

$$g = \frac{4\pi P_o}{\int_{\phi=\phi_o}^{2\pi} \int_{\theta=\theta_o}^{\pi} P \sin \theta d\theta d\phi} = \frac{2}{\int_{\theta=\theta_o}^{\pi} \left( \frac{1 + \cos \theta}{2} \right)^k \sin \theta d\theta} = k + 1$$

The gain at a cone angle,  $\theta$ , off the antenna boresight is then

$$g = k + 1 \left( \frac{1 + \cos \theta}{2} \right)^k \quad (3.5)$$

Figure 3-18 shows plots of Equation (3.4) for various values of  $k$ .

Figure 3-17 gives plots of Equation (3.5) for various cone angles. Just after launch the high cone angles will be of importance. The plots indicate low signal levels for these angles. However, the spacecraft is initially relatively close to earth. As the spacecraft moves closer to Mars, the cone angles of consideration lie between 0 and 45 degrees.

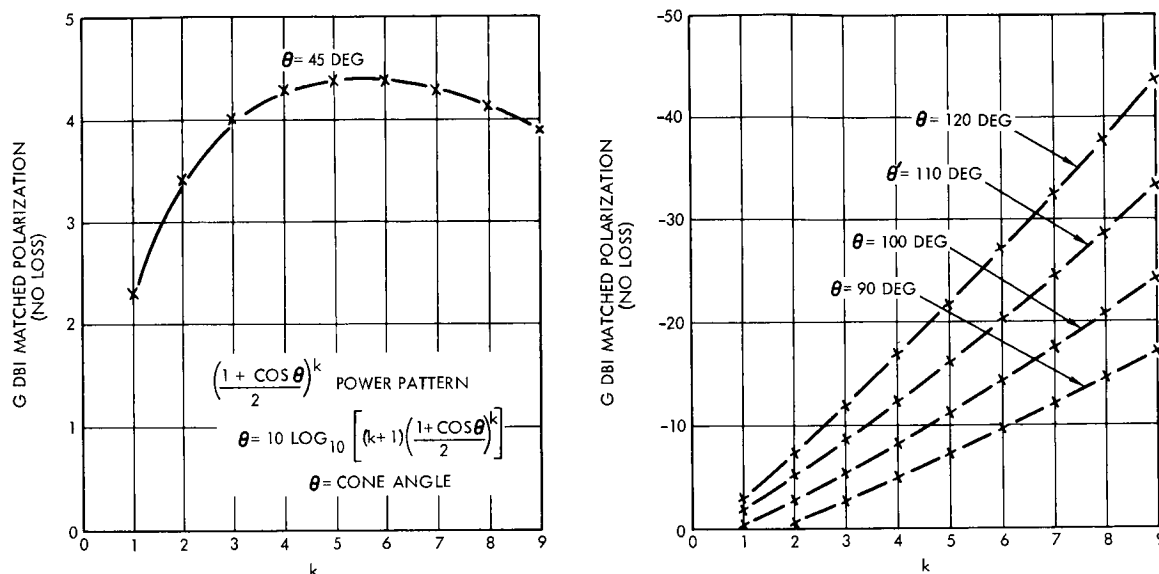


Figure 3-17. Theoretical Pattern Gains

Figure 3-17 indicates that the maximum pattern gain obtainable at 45 degrees is 4.4 dbi for an antenna with a matched polarization ellipse. However, the maximum is fairly broad, so that from the point of view of high angle radiation, it is better to design around as small a value of  $k$  as is compatible with the over-all gain requirements at 45 degrees. The reason for the maximum at 45 degrees is that as the gain on boresight gets larger, the radiation pattern becomes narrower faster than the gain increases, and finally becomes so narrow that at 45 degrees the gain decreases. It may of course be possible to obtain more gain at a given angle by appropriately shaping the radiation pattern so that the functional relationship is different from that of Equation (3.1). However, from a practical point of view, such shaping is generally difficult, can be frequency sensitive, and may require more space and additional weight. Since circular polarization is required, the combined problem of maintaining the beamshape and the axial ratio can become prohibitively difficult.

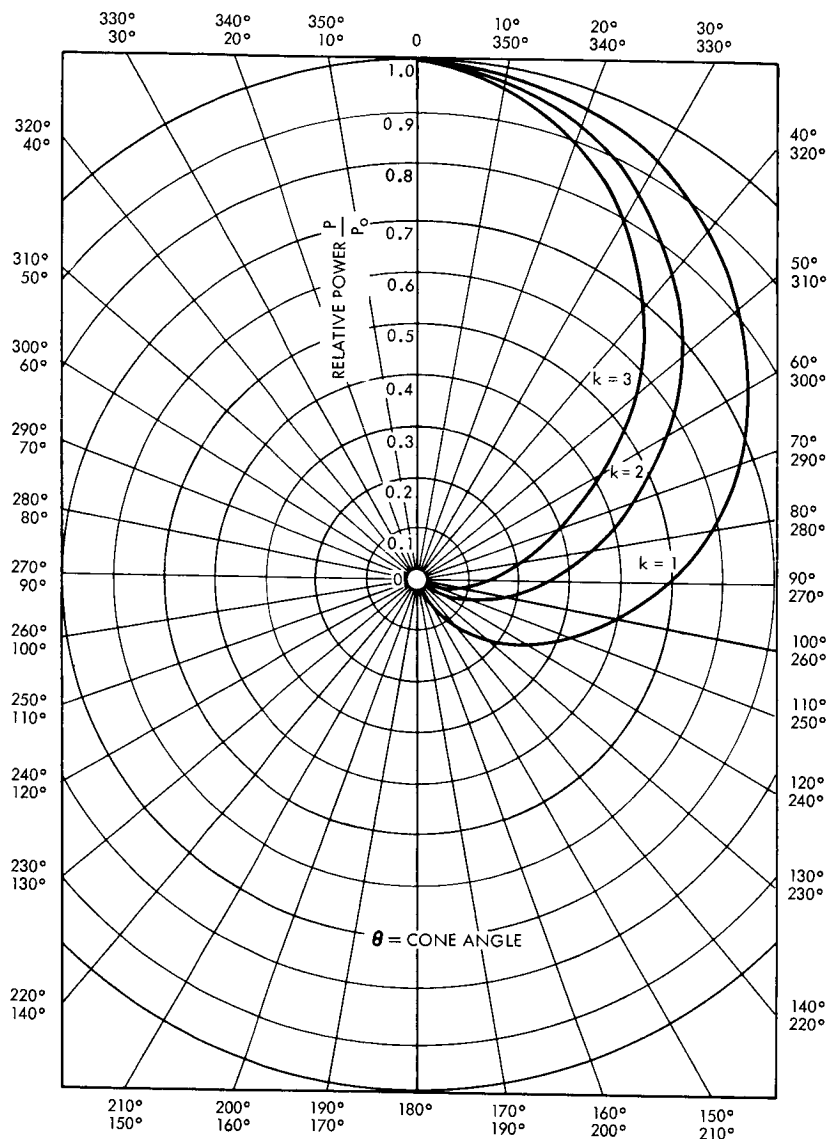


Figure 3-18. Theoretical Relative Power Patterns,  $P/P_o = \left( \frac{1 + \cos \theta}{2} \right)^k$

b. Selected Antenna

Figure 3-19 shows the antenna selected, pending further study, which closely approximates the pattern of Figure 3-17. This antenna utilizes a cup-dipole configuration to obtain equal E- and H- plane radiation characteristics throughout one hemisphere. The following performance characteristics are provided on Rantec Corporation.

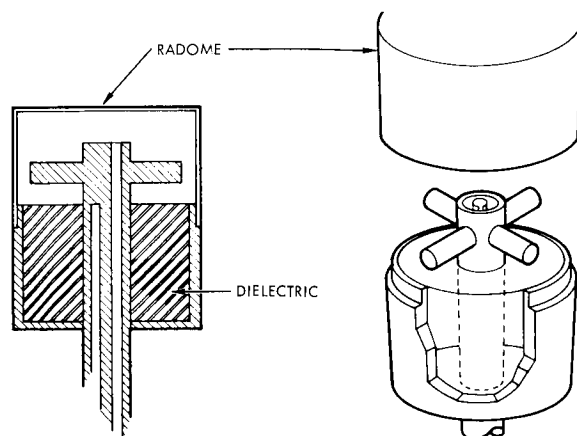


Figure 3-19. Rantec Cup-Dipole Antenna

Functional characteristics of the antenna are as follows:

Frequency	5.4 to 5.9 Gc
Impedance	50 ohm nominal
VSWR	1.5:1 max
Radiation Pattern	Hemispherical, circular polarization
Axial ratio	1.5 db max at 5.7 Gc 6 db max at 5.4 to 5.9 Gc (at any look angle within the hemisphere)
10 db beamwidth	180 degree min

Physical characteristics are as follows:

Diameter	1.25 in.
Height	1.25 in. (less connector) 2.35 in. (over-all)
Weight	3.5 oz
Connector	Type "N" Male

It will of course, be necessary to scale the antenna to the frequency band 2110 to 2300 Mc. It is found that the factor 2.57 almost exactly scales the extremes of the 5.4 to 5.9 Gc band to the required frequencies. Figure 3-20 shows the experimental radiation pattern obtained from the Ranted antenna at 5650 Mc. A theoretical pattern is also shown for Equation (3.4) with  $k = 3$ . The measured gain on the antenna boresight is 5.8 dbi at 5650 Mc. The theoretical gain is obtained from Equation (3.5) at 6 dbi on the antenna boresight relative to a matched polarization antenna.

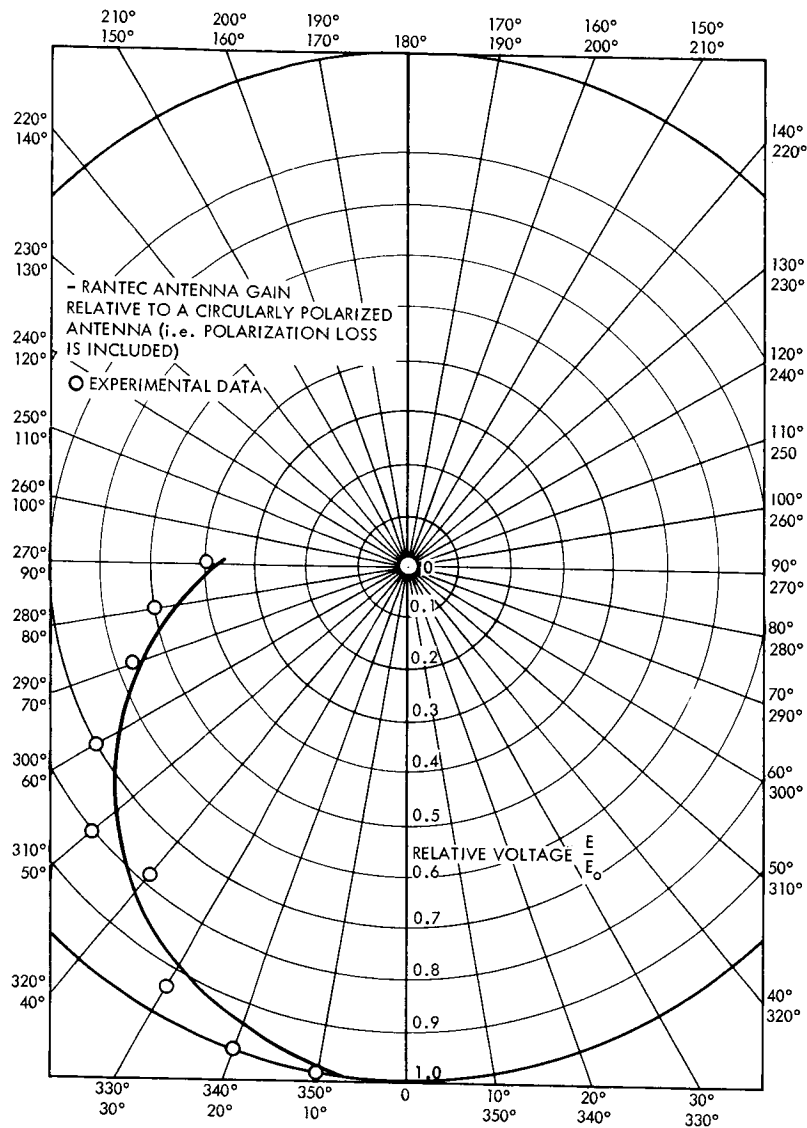


Figure 3-20. Theoretical Versus Experimental Relative Voltage Patterns

### c. Antenna Spacecraft Configuration

The proper pattern coverage is realizable assuming no spacecraft perturbation. However, to provide pattern coverage at cone angles greater than 90 degrees for the launch and preorbital phase of the mission, a second antenna is mounted with the primary antenna as shown in Figure 3-21, such that the primary antenna is boresighted along 0 degrees cone angle and the secondary antenna is boresighted along a cone angle of 135 degrees and a clock angle of 70 degrees. This second antenna is decoupled from the first, using an antenna coupler, rather than an RF switch,



for increased reliability. The two antennas are mounted as close together as possible to reduce the ripple voltage in the array pattern in the neighborhood of a cone angle of 90 degrees. The maximum allowable coupling to the side-looking antenna is determined as follows:

Gain of Rantec antenna (pointed at  $\theta = 0$  degrees)  
at the 45 degree points in the pattern (relative to  
a circularly polarized antenna) = 3.8 dbi

Required gain at 45 degree points = 2.0 dbi

Maximum allowable loss due to coupled  
side looking antenna = 1.8 db

Therefore,  $10 \log \left[ \frac{1}{1 - X} \right] = 1.8 \text{ db}$

Where  $X$  = ratio of decoupled power to input power

Therefore,  $10 \log X = -4.7 \text{ db} = \text{minimum}$   
allowable decoupling

The effects of the spacecraft on the radiation patterns of either antenna must be determined by suitable pattern measurements.

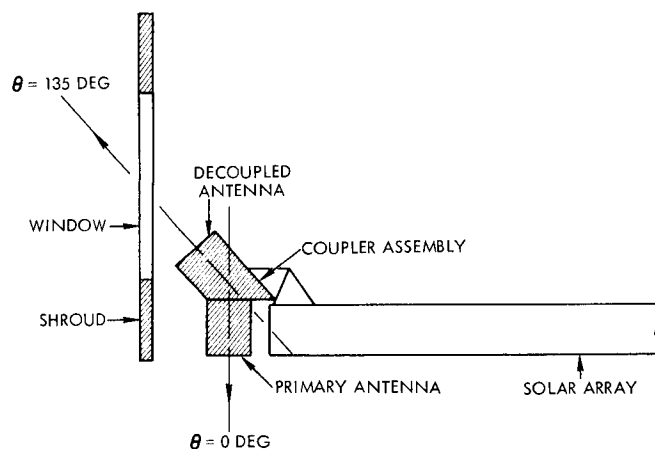


Figure 3-21. Low-Gain Antenna System

Figure 3-22 shows the geometry of the low gain antenna, which as just described is actually two antennas in one package. The structure is basically three tubes configured to form a "Y" shaped housing with one leg providing the mounting strut and the other two legs containing the turn-stile radiating elements. 6061 Aluminum 0.030 wall tubing is used, and fabrication is by flux-bath dip-brazing. The mounting strut is terminated in an attachment flange and houses a coupler which provides for unequal

power splitting between the antennas. This strut also contains the transmission line which connects to the coupler, the two antennas, and the spacecraft electronic equipment. A rib is brazed integrally with this structure to provide additional structural integrity in the direction of boost and deboost dynamic loading. The aperture of each turnstile tube is closed with an epoxy-fiberglass radome for protection during ground handling and storage, and is vented internally for pressure release during launch. Total loss of or major damage to this radome should not affect the operation of the antenna. The structure is sufficiently compact so that elements are resonant substantially above any dynamic inputs from the spacecraft structure.

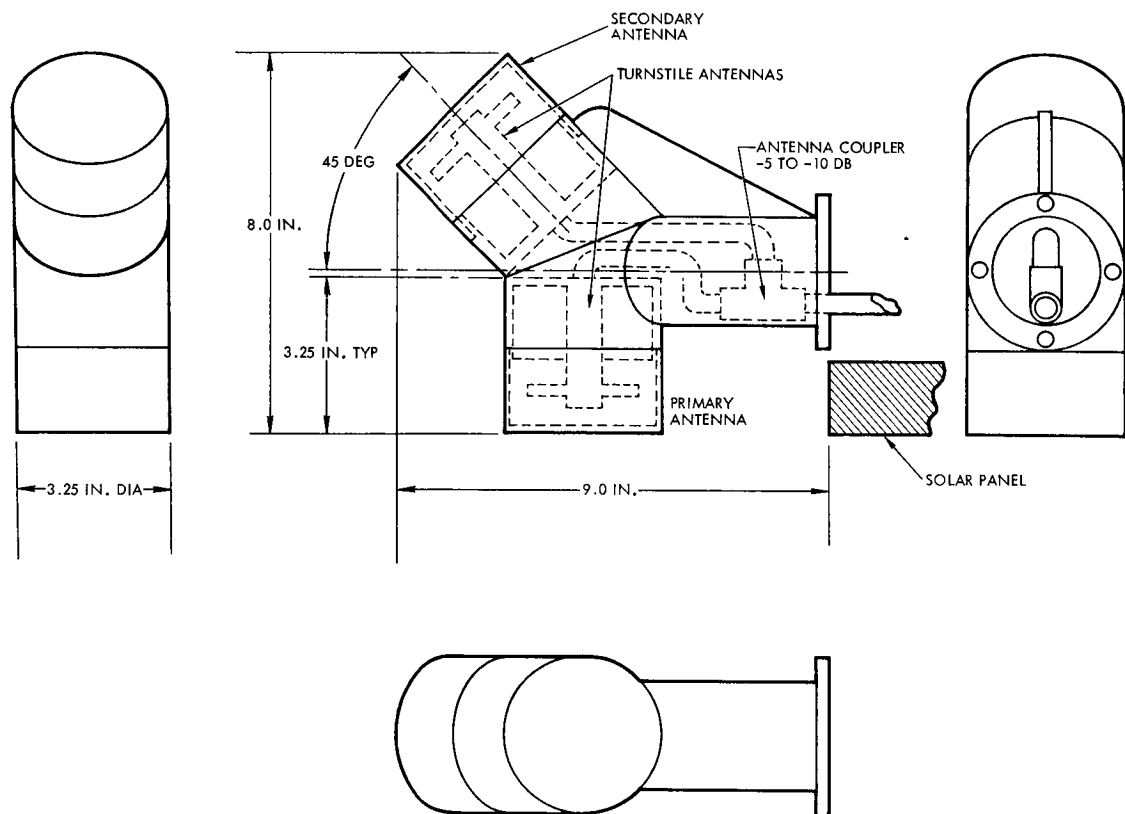


Figure 3-22. Low-Gain Antenna

#### 1.4.4 Capsule Link Antenna

The VHF antenna system, to enable the spacecraft to receive telemetry signals from the capsule, at 136 Mc, consists of a right-hand circularly polarized turnstile, with reflector, whose pattern is a cardioid figure of revolution with the maximum radiation along the axis of the array or normal to the plane of the turnstile. The assembly is mounted on the back of the solar cell panel such that its axis is 50-140 degrees above the plane of the solar cells, or at a cone angle of 50-140 degrees, and at a clock angle of 105 degrees. The turnstile elements are symmetrically oriented with respect to the spacecraft axis, each element forming a 45 degree angle with the solar cell array. The antenna is located at the out-board edge of the solar cell array to provide as close to a free space environment as possible, i. e., there will be essentially no reflections from the spacecraft to cause perturbation in the basic cardioid pattern.

The gain of the VHF antenna is 4 db on the antenna axis with a beamwidth of approximately 120 degrees at the -3 db points. Circular polarization is obtained by feeding the two dipoles from the balanced end of a balun and phasing the alternate elements capacitively and inductively to achieve phase quadrature.

The gain and beamwidth of the VHF antenna is such that the coverage is sufficient for any encounter date. The angles for the extremes of encounter dates vary from approximately 80 to 170 degrees cone angle from 100 to 155 degree clock angle. The choice of 140 degree cone angle and 105 degree clock angle represent an average of the most probable angles of the various arrival dates.

A possible alternate configuration for the VHF antenna is a low gain helix. For the electrical characteristics as outlined for the turnstile, a helix would have the configuration shown in Figure 3-23. Although this antenna would have a gain of 4 db, and a beamwidth of 112 degrees, the radiation characteristics are somewhat unstable. Since each of the parameters, circumference, spacing, and number of turns, is at the lower limit

for the axial radiation mode. In addition, because of the axial length of the helix it would be difficult to mount it to prevent interference from the spacecraft structure. Mounting of the helix on the back side of the solar cell array would provide no mechanical problem, but since the helix structure is more complex, than that of a turnstile, it would be somewhat more difficult to maintain its structural integrity.

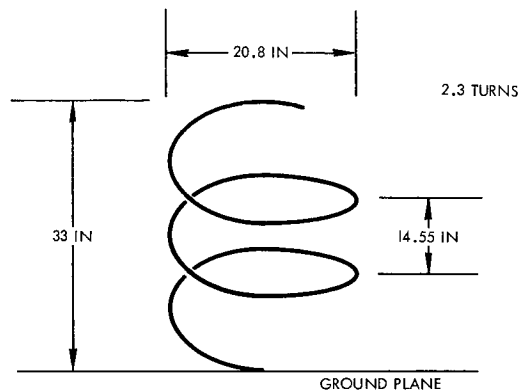


Figure 3-23. Helix Configuration

Figure 3-24 shows the geometry of the turnstile antenna. The radiating elements are oriented at 90 degrees and are fed at their centers by a stripline balun. The housing for the balun and the coaxial transmission line form the central support structure for the turnstile and are mounted to a ground plane which constitutes the reflecting element of the turnstile array. To obtain maximum structural integrity with minimum weight, an epoxy laminate shear web, 0.030 inch thick, is bonded between the radiating elements and the reflector. The radiating elements are 0.375-diameter aluminum tubing with 0.020-wall thickness, while the reflector will be 0.030-aluminum sheet. To provide stiffness in modes perpendicular to the shear web an epoxy laminate is used for lateral webs at three points along each of the four legs of the turnstile.

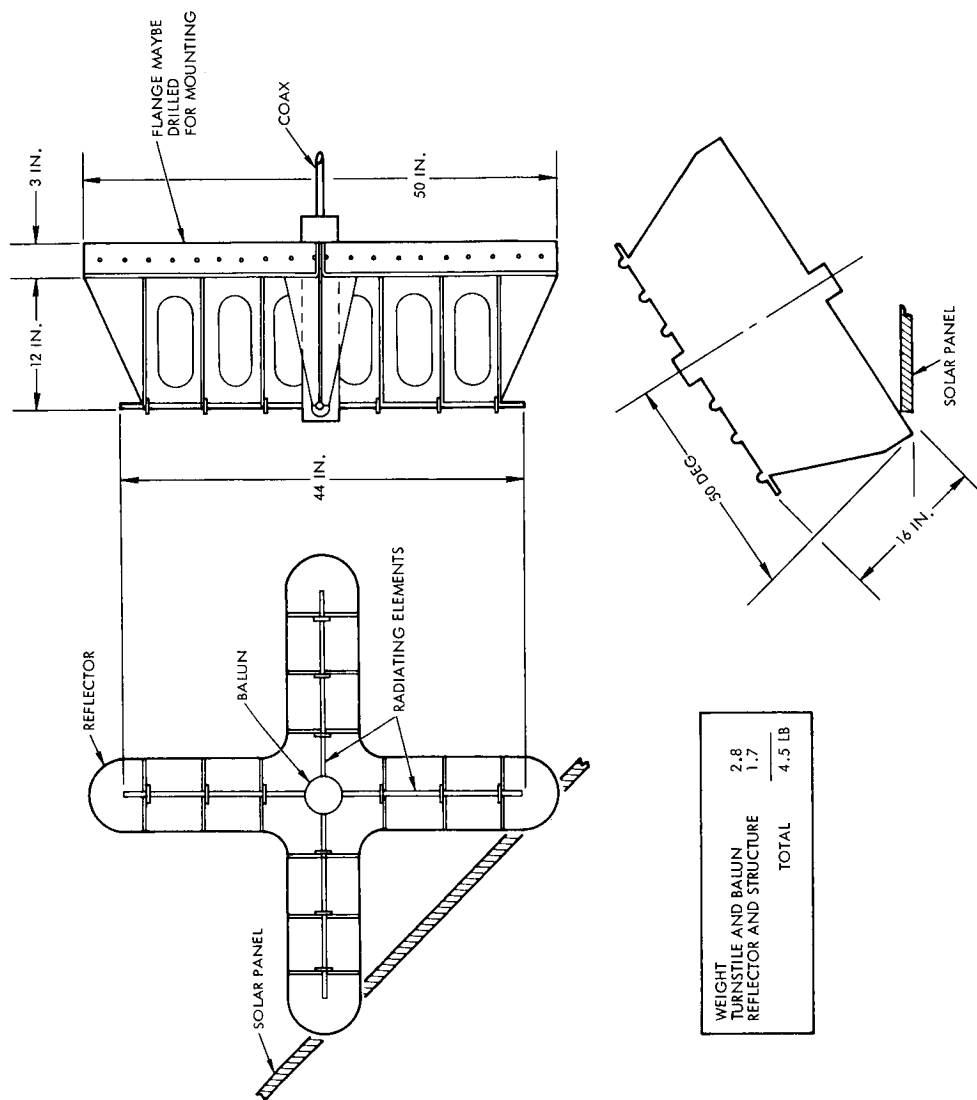


Figure 3-24. VHF Antenna

## 1.5 Equipment and Components

### 1.5.1 S-Band Modulator Exciter and Low Power Transmitter

Several programs make use of S-band equipment similar to that required for Voyager. Mariner C, Lunar Orbiter, Lunar Excursion Module, Apollo Command and Service Module, Pioneer, Saturn, and the Air Force Space Ground Link Subsystem (SGLS) each use phase-lock receivers and coherent exciters. These programs, however, have different performance, environmental, and packaging requirements. In fact, no two programs use identical equipment, although each is compatible with either the S-band DSIF or Apollo ground network (SGLS is only partially compatible).

The receiver parameters are strongly mission dependent, these being determined by the doppler profile, received signal power, command modulation, ranging modulation, and acquisition characteristics. The type of telemetry modulation, the gain of the power amplifier, and the available input power determine the modulator-exciter parameters. Table 3-10 shows the range of parameters, input power required, and other functional elements used with the basic receiver-modulator exciter equipment in existing projects.

Each of the modulators considered are basically the same. They make use of varactor diodes to phase modulate the RF signal at a low submultiple of the output frequency. For example, given the output frequency  $240 f_1$  and a submultiple  $8f_1$ , at the modulated stage, the phase deviation is  $\theta = m/30$  for an output deviation of  $m$ .

The  $8f_1$  signals are appropriately frequency multiplied by transistors and varactor diode stages to the final output frequency and output power. Since all of the exciters use varactor multipliers each must consider the stability problems caused by input dynamic range, temperature, and load VSWR. Some designs require operating the multiplier chains into bandpass filters.

The Mariner C exciter does not use a built-in bandpass filter or isolator; these were external to the equipment. The Lunar Orbiter and LEM exciters have isolators and filters built into the transceiver assembly. The Pioneer exciter required neither. The power output of

Table 3-10. Elements of the Basic Receiver-Modulator Exciter Equipment

Program	Weight (lb)	Size (in)	Input Power (watts)	Output Power (m watts)	S-Band Receivers - Transmitters			Duplexer	Auxiliary Oscillator	Magnetics Requirement	Mounting Construction
					Modulation	2BLO/2BLO (cps)	Predef Ranging BW (kc)				
Mariner C	14.5	16 x 6 x 6	22	500	PM, $\pm 4$ rad	20/233	4.5	Yes	No	Yes	Tray/Tee Frame
Lunar Orbiter	12.5	17 x 9 x 4-1/2	17	400/30	PM, $\pm 4$ rad	100/540	4.5	Yes	Yes	None	Plate/Tee Frame
LEM-Apollo	20	15 x 8 x 7	36	750	PM, $\pm 2$ rad, FM	155/1500	10	Yes	No	None	Rail/Flat Mod
CSM-Apollo		20 x 9 x 17		250	PM, FM	155/1500	10	Yes	No	None	Fail/Tee Frame
Pioneer	4.5	8 x 5 x 5	27	50	PM, $\pm 1.3$ rad	20/88	3	No	No	3 y at 1 ft	Plate/Flat Mod
SGLS	14.3	12 x 7 x 5	44	2500/500	PM, FM	200/760	20	Yes	Yes	None	Plate/Flat Mod

each of the equipment ranges from 50 milliwatts to 2.5 watts with efficiencies ranging from 8 to 15 per cent. The thermal problems associated with these exciters are relatively minor.

The one design factor not required in most of the designs is magnetic cleanliness. Only the Pioneer unit is magnetically clean; its maximum permissible field is 3  $\gamma$  at 1 foot. Unless the design is made with prior thought to magnetic properties, it is unlikely that the equipment will be within an order of magnitude of the required value.

The exciter-modulator chosen for Voyager operates in either a coherent or noncoherent mode. A diode switch selects the output of the auxiliary crystal oscillator or the coherent reference (VCO) from the S-band receiver. The presence of the in-lock signal from the receiver selector operates the switch and turns off the power to the crystal-controlled local oscillator. The oscillator output is multiplied to  $4f$  and phase modulated by either of two inputs, the telemetry and PN subcarriers or the ranging code. The modulated carrier is then amplified and frequency multiplied by varactor stages to  $240f$ . An isolator and bandpass filter provide the spurious rejection required and provide added stability against load variations (see Figure 3-25).

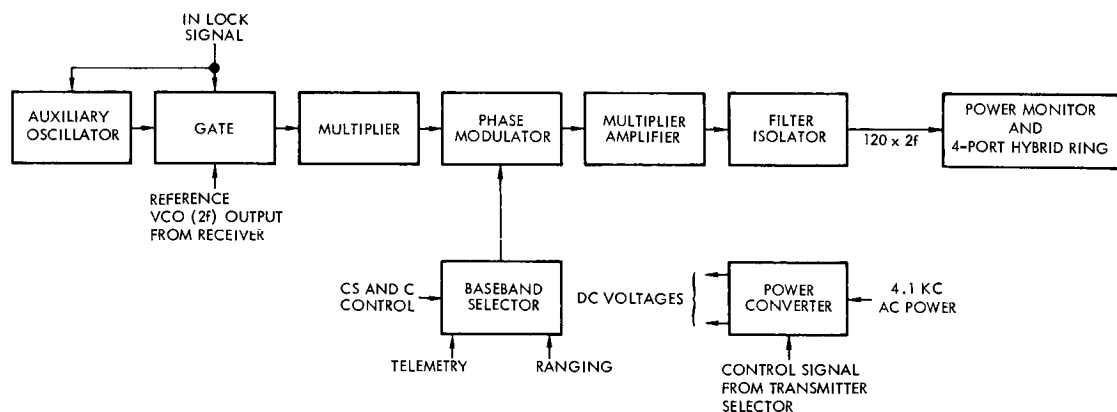


Figure 3-25. Modulator-Exciter

The transmitter requires that only one modulator-exciter be energized at a time. The unit operates from the 4800 cycle power source and uses a transformer-rectifier AC to DC converter. A control signal switches the prime power on or off.



The following are the basic parameters of the modulator-exciter:

Modulation	PM, 0 to $\pm 4$ radians
Modulation bandwidth	1.8 Mc
Reference frequency	2f; 19.1 Mc
Multiplier ratio	120
Output frequency	2295 Mc
Power output	100 milliwatts

The low power transmitter is identical to the modulator-exciter except for the power output. The primary function of this transmitter is for telemetry transmission during boost and the early part of the mission. The power output required is 1 watt.

#### 1.5.2 Power Amplifiers

The recommendations included in this section are based upon the information obtained in an S-band equipment survey. This survey was completed in June 1965 and was centered around devices capable of producing from 20 to 40 watts, CW, at 2.295 Gc. The lower bound of 20 watts is considered to be the current state of the art and the upper bound is set by the worst case primary power limitations of the spacecraft at encounter plus 1 month.

The S-band power levels under consideration dictate the use of microwave tubes as opposed to solid-state devices. Present day projections for transistors are that reproducible devices capable of 15 watts at Gc will be available in 1968. Varactor chains achieve efficiencies near 10 per cent, and although improvements can be anticipated, solid-state gains are expected to be offset by gains in tube efficiencies. Therefore, it appears that S-band solid-state power amplifiers need not be considered at least for the first several Voyager missions.

The microwave tubes that were considered for Voyager are as follows:

- Amplitrons
- Electrostatically focused klystrons (ESFK)
- TWT's
- Triode cavity amplifiers

As a result of this survey and subsystem comparisons, amplitrons and triode cavity amplifiers were eliminated. It was determined that ESFK's possess the greatest potential when used as a power amplifier at power levels equal to or exceeding 40 watts, but fundamental development effort is required. Traveling wave tubes have emerged as the best choice for both the 20-watt and 40-watt power amplifier because of their availability and proven history.

An accurate comparison between the various devices cannot be completed from a tube consideration only. The peripheral equipment required by each tube is markedly different in some instances; therefore, an amplifier package containing the tube power supply, regulator, and RF equipment must form the basis of comparison.

Amplitrons. Although 20-watt amplitrons are being successfully integrated into the LEM, many of the desirable features of this tube are lost in achieving a reliable package. Anticipated tube life poses a question of such magnitude that there is justification for employing a tandem connection of two tubes in series, each with its own power supply. This configuration is particularly well suited for the amplitron because the unattenuated slow wave structure permits selective operation of a single tube through the low loss path (0.6-0.7 db) of the inactive tube. This scheme enhances reliability but the package parameters decrease so that, typically, a worst case RF gain of only 14 db is realized at a worst case package efficiency (including power converter) of near

23 per cent. Thus, the advantages which appear to be offered by a 55 per cent basic tube efficiency are degraded to a point where the amplatron package efficiency fails to equal that achieved by other devices. Furthermore, the question of amplatron package life is not completely satisfied by the added redundancy presented because the life expectancy of the amplatron has not been demonstrated or adequately predicted. Since the amplatron is a crossed-field device similar to the magnetron, it is reasonable to expect amplatron tube life similar to that experienced in a magnetron. Magnetron lifetimes near 5000 hours are frequently experienced, insufficient for the Voyager mission.

The broadband noise and spurious content of the output spectrum of the amplatron impose additional requirements on output RF filtering. Measurements on the LEM package have revealed the presence of coherent spurious signals as great as 20 dbm in amplitude less than 80 Mc away from the desired output signal. Noise figures are anticipated to be as high as 50 or 60 db. These measurements indicate the need for filtering beyond that required for other tubes.

Triode Cavity Amplifiers. Triode cavity amplifiers are available from Resdel Engineering, at both 20- and 40-watt levels. Over-all tube efficiencies greater than 23 per cent at 20 watts and 24 per cent at 40 watts cannot be anticipated. An 88 per cent power supply efficiency decreases the power amplifier to an over-all efficiency near 20 and 21 per cent for 20- and 40-watt levels. The greatest disadvantage, however, is that only 10 db RF gain is provided by the triode cavity amplifier, requiring a much greater power output from the modulator-exciter than does the ESFK or TWT.

Electrostatically Focused Klystron. At the 20-watt power level, a prototype design exists for an ESFK. The total package efficiency is only 17 per cent at this level. At the 40-watt power level, the ESFK is expected to be competitive with the TWT after completion of development and establishment of reliability data. The ESFK offers potential advantages over the TWT as follows:

- a) Efficiency. Predicted tube efficiency of 35 to 40 per cent at frequency band center.
- b) Power Supply Requirements
  - 1) The regulation required of the power supply would be considerably lessened due to the relationship between RF power out and variation of beam voltage. The TWT requires approximately four times more regulation than the ESFK for the same deviation in power output.
  - 2) The ripple requirements on the power supply would be approximately one-fourth those required with a TWT inasmuch as the phase sensitivity of the klystron is less than 1 deg/volt.
  - 3) Only two voltages are required for tube operation plus the filament as opposed to the three voltages plus filament required in a traveling wave tube.
  - 4) With a klystron, the power supply need not be tailored to each individual tube and can be cross-strapped for redundancy in the power amplifier section.
  - 5) The power supply should inherently weigh less because of the above considerations and the added efficiency.
- c) Filter Characteristics. The electrostatically focused klystron utilizes cavities coupled to the beam for its amplification characteristics. Therefore it inherently provides bandpass characteristics in the order of 2 to 10 Mc.
- d) Multiple Power Operation. The output power of the klystron is directly proportional to the beam power, which varies proportional to  $V^{5/2}$ . Thus, a 1 per cent change in beam voltage will yield approximately 1.25 per cent change in RF output power, as opposed to a 5 per cent change in the traveling wave tube. This difference is brought about because of the beam synchronism requirements inherent within the traveling wave tube. Directly resulting from this independence of synchronism, the collector and beam voltage scale proportionately as RF power output is changed, thus yielding the capability of multiple power operation or failure mode operation.

c) Reliability

- 1) Ion Trapping. The focusing anodes distributed through the tube will be at cathode potential, therefore producing a higher voltage gradient than the cathode to any ions produced beyond the first focusing anode.
- 2) Interaction Structure. The beam length is approximately one-fourth that of a traveling wave tube, therefore requiring much less precision in alignment. Furthermore, because of electrostatic focusing rather than magnetic focusing, the defocusing of the beam caused by temperature is almost nonexistent.
- 3) Partial Power Supply Failure. In the case of a major primary power deviation, the chances of damage to the tube are much less than for a traveling wave tube because of the proportionality of beam and collector voltages.
- 4) Failure Modes. It is predicted that the failure modes would be similar to those of normal klystrons such as cathode emission, heater failure, vacuum leak, and arcing.

The main shortcomings of the ESFK are

- Its inherent efficiency degradation at the frequency band edges, and
- The lack of actual life data.

Traveling Wave Tubes. TWT's are the most desirable approach in fulfilling the S-band power amplifier requirements for Voyager because they have been successfully used in many different space programs, Telstar, Relay, Syncom, Early Bird, and Mariner. Thus more data is currently available on the characteristics of a TWT in the space environment than any other contemplated power amplifier.

A 20-watt TWT, qualified for the Apollo program and currently in production by Hughes Aircraft, Microwave Tube Division, has the following characteristics:

Frequency	2.2 - 2.4 Gc
Power output	20 watts (min)
RF gain	30 db
Efficiency	30 per cent (min)
Phase sensitivity	3 deg/volt
Weight	22 oz

Five of these tubes have been placed on life test and have accumulated over 10,000 hours of successful operation. In conjunction with an 85 per cent efficient power supply, the power amplifier package exhibits a worst case efficiency (including output filter) of 22 per cent. The attributes of availability, efficiency, and demonstrated reliability cannot be matched by any other device in its output power range.

Several TWT's have been operated at higher power levels. Although these experiments required cathode current densities inconsistent with long life, they did illustrate the 40-watt capability of spaceborne TWT's. A flight qualified 40-watt tube would incorporate a larger gun, helix, and magnet stack to accommodate the larger currents. All manufacturers are in general agreement that this development can be accomplished in 9 months.

Although tube manufacturers are claiming tube efficiencies in excess of 40 per cent at the 40-watt level, the constraints of variable RF drive, environmental excursions, aging, and long term power regulation are expected to yield a worst case tube efficiency of near 33 per cent. When matched to an 85 per cent efficient power supply, the power amplifier package worst case efficiency would be 28 per cent. This figure will be degraded further if the insertion loss of the required output bandpass filter is included. This filtering will be in excess of that required by the ESFK since the second harmonic output of the TWT is expected to be 10 db below the fundamental. This added filtering could decrease the

package efficiency to as low as 26 per cent. Since RF gains of both the 20- and 40-watt tubes are equal to or in excess of all other devices considered, driver power levels are minimal.

A possible disadvantage of the TWT when compared with the ESFK is the external magnetic field produced by the magnetic focusing assembly. Experience on Pioneer, however, has shown that stray field effects can be controlled.

The preceding comparison of amplitrons, triode cavity amplifiers, ESFK's and TWT's is summarized in Table 3-11 and Figure 3-26. Based upon availability, proven reliability and life history, the 20-watt TWT has been selected for the 1971 Voyager spacecraft, operating in a redundant configuration. An increase in RF power output to 40 watts, using either a TWT or ESFK can be supported by the spacecraft power system at encounter plus 1 month, but involves some power amplifier development risks.

The salient electrical and mechanical parameters and constraints for the 20-watt TWT amplifier are as follows:

Maximum DC input power	90 watts, which accommodates a 22.5-watt TWT to overcome estimated RF filter losses.
Minimum filtered power output	20 watts
Minimum power gain	28.5 db, accommodating a 50 mw $\pm$ 2 db driver and filter losses.
Maximum weight (including power supply)	6 lb
maximum base plate temperature	100°C

Table 3-11. Comparison of S-Band Power Amplifiers

Tube Manufacturer	Tube Development Status	Tube Prototype Feasibility After Start	Weight, Including Power Supply (lb)	Estimated Tube Life (hr)	Tube Worst Case Efficiencies	Power Gain (db)	External Magnetic Fields Present	Relative Power Supply Complexity	Noise Characteristics (db)	Bandwidth (Mc)	Phase Sensitivity	RF Filtering Requirements
<u>Amplifrons</u> 20 watts 40 watts	Prototype	Present	10-12	Relatively uncertain	45-50	14	Yes	High	50-60	20 (3 db)	1 deg/ma change in anode current	High
	Pre-prototype	6-9 months	12	5,000-10,000	50-55	16	Yes	High	50-60	20 (3 db)		High
<u>Triode Cavity Amplifiers</u> 20 watts 40 watts	Prototype	Present	6	10,000	23	10	No	Low	Not Available	20 (3 db)		Low
	Prototype	Present	7 (driver not included)	10,000	24	10	No	Low	Not Available	20 (3 db)		Low
<u>ESFK's</u> 20 watts 40 watts	Prototype	Present	7	>40,000	19	30	No	Least	< 30	3.5 (1 db)	< 1 deg/volt	Low
	Pre-prototype	9 months	8	>40,000 (depressed collector)	35	30	No	Least	< 30	3.5	< 1 deg/volt	Low
<u>TWT's</u> 20 watts 40 watts	Qualified	Present	6	>40,000	30	30	Yes	Moderate	< 30	>20 (1 db)	2-3 deg/volt	High
	Pre-prototype	6-9 months	8	>40,000	33	34	Yes	Moderate	35	>20 (1 db)	2-3 deg/volt	High



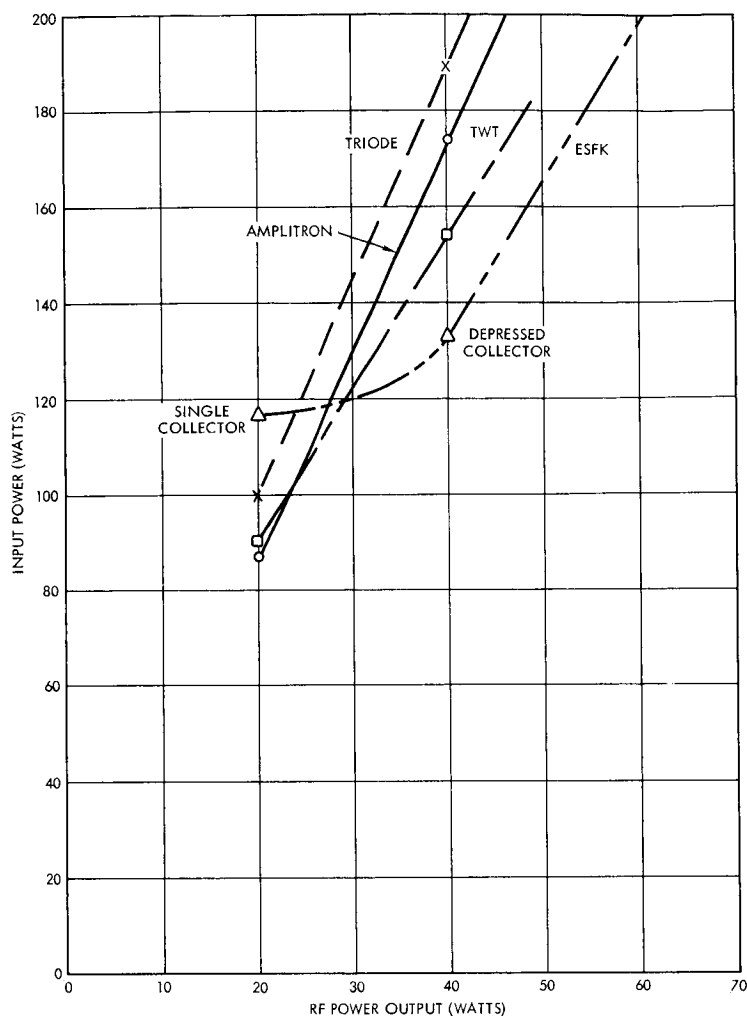


Figure 3-26  
Comparison of Power  
Amplifiers Input Power  
Versus Power Output

A block diagram of the power amplifier package is given in Figure 3-27. All microwave components are sized to handle at least 40-watt power level. It is proposed to investigate during Phase IB development risk of a 40-watt TWT for the 1969 and 1971 missions together with the possibility of an ESKF klystron development for the power range of 40 to 100 watts for use on later missions.

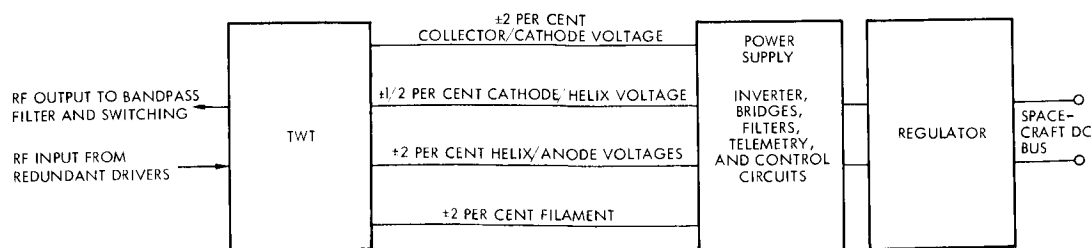


Figure 3-27. 20-Watt TWT Power Amplifier Block Diagram

### 1.5.3 Transmitter Selector

The transmitter selector consists of four logic devices: the exciter selector, power amplifier selector, the antenna selector, and the mode selector. The transmitter selector operates in six modes (as shown in Section 1.1).

Figure 3-28 is the state diagram of the exciter selector. If both transmitter output power and exciter output power drop off, the redundant exciter is switched in, providing that the exciter power is on. The exciter selector is an autonomous unit which operates independently of external commands except for ground checkout commands. It requires two flip-flops and four dual gates.

Figure 3-29 is the state diagram of the power amplifier selector. It operates upon loss of output power and upon CS and C command to provide the maximum possible output power, subject to CS and C command, at all times. Two flip-flops and four dual gates are required.

Figure 3-30 is the state diagram of the antenna selector, which operates on ground command or on loss of Canopus lock. If loss of lock occurs, the maximum-coverage antenna is selected automatically. The antenna selector requires two flip-flops and four dual gates.

Table 3-12 shows the required states for the power amplifier selector and the antenna selector for each of the six modes discussed in Section 1.1. This table defines the operation of the mode selector, which requires 14 dual gates to drive the circulator switches and transmitter DC power switches.

Table 3-12. Required States for the Power Amplifier Selector and Antenna Selector

Mode	Power Amplifier Selector State	Antenna Selector State
I (launch)	1	1
II (after sun-Canopus lock)	1	2
III (cruise, maneuver, encounter orbit)	2, 4	2
IV (backup)	3	2
V (backup)	1	3
VI (backup)	2, 4	3

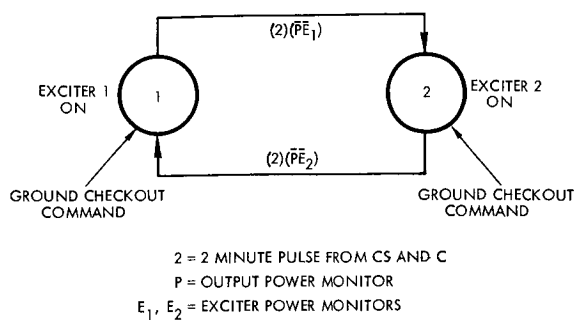


Figure 3-28. Exciter Selector State Diagram

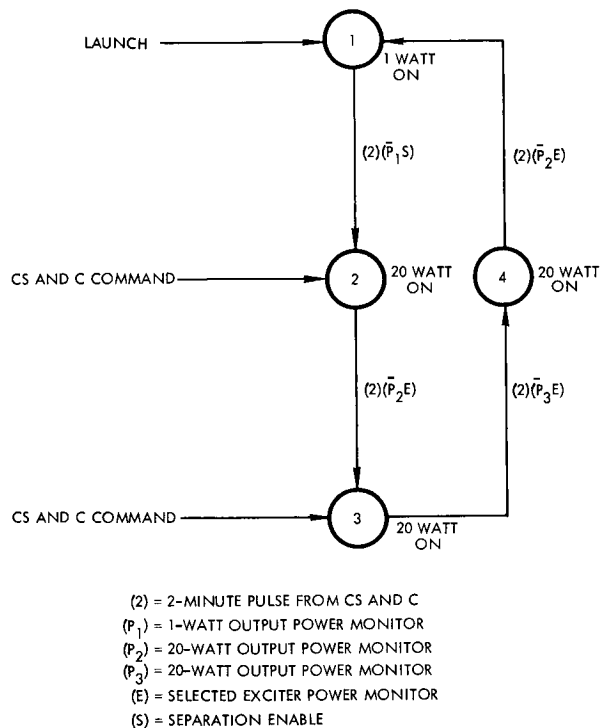


Figure 3-29. Power Amplifier Selector State Diagram

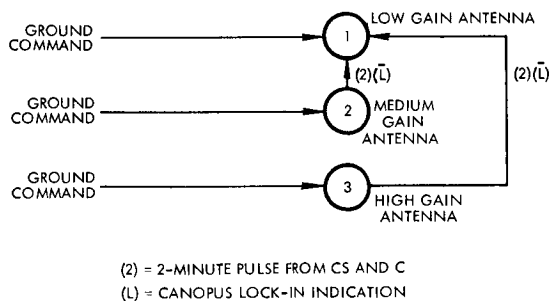


Figure 3-30. Antenna Selector State Diagram

#### 1.5.4 S-Band Receivers

The Voyager S-band receiver requirements are similar to those of Mariner C and several other space programs. The receivers considered correspond to the transponders investigated (see Section 1.5.1 and Table 3-10). The receiver must accept and process the following signals from the DSIF.

- Locked VCO reference signal for two-way doppler tracking
- Detected pseudo-random range code
- Detected composite command subcarrier.

An analysis of phase lock loop bandwidth requirements based on threshold performance and worst case dynamic tracking error in orbit has established a threshold criteria of  $2 B_{10} = 22.5$  cps and 8 db S/N in  $2 B_{10}$  as carrier performance threshold with commands present. This corresponds to  $2 B_1 = 32$  cps at 6 db SNR (see Section 6 of Appendix D).

The receivers listed as part of Table 3-10 use similar design techniques for the mechanization of the phase-lock loops. However, one difference is worthy of note, the use of an offset frequency reference oscillator. A separate offset frequency reference oscillator is used in the Pioneer and SGLS receivers; the SGLS receiver has a ranging detector, but the Pioneer receiver does not. However, it should not be inferred that other mechanizations will not work; the Lunar Orbiter has no separate offset frequency references oscillator, but has been redesigned slightly to eliminate some of the difficulties noted during some of the Mariner C tests. A thorough re-evaluation of this problem should be made in Phase IB.

The implementation of the ranging detectors used in Mariner C and the LEM, CSM, and SGLS receivers differs somewhat. Mariner C makes use of automatic gain control prior to the range code synchronous detector, followed by a high-gain video amplifier. The other receivers use hard limiting (as in the phase-lock loop) prior to synchronous detection. These designs also make use of higher IF levels and thus small video gain after detection. The hard limiter design has been adapted

when there has been a possibility of an interfering signal in the receiver, as is the case in the Apollo program.\*

The magnetic properties of the receivers were not considered in any of the programs except Pioneer. The parts and materials used for the Pioneer equipment were chosen with the total magnetics problem considered. The residual magnetic fields were measured at about 3  $\gamma$  at 1 foot, approximately an order of magnitude better than could be expected from the other existing designs.

The basic selected receiver configuration is shown in Figure 3-31. The RF selectivity is provided by the diplexer apart from the receiver. The mixer uses conventional diodes in a balanced mixer configuration, followed by wideband IF and a second conversion. The output is split for the ranging demodulator and the narrowband phase-lock loop. A crystal filter precedes the hard limiter, which feeds the carrier phase detector, loop filter, and VCO. The command output is taken off prior to the loop filter. An inphase synchronous detector is used to derive the in-lock signal, which is used by the receiver selector. The wideband IF output goes to the ranging detector, where it is hard limited and synchronously detected with the coherent reference from the carrier phase-lock loop. The ranging detector must be commanded on and off as required so as not to interfere with telemetry function in the modulator-exciter. The output of the ranging detector is sent to the modulator-exciter. The detailed receiver implementation to be finally selected will depend upon a careful review of reliability and performance, but the survey of present programs makes clear that several acceptable receivers exist.

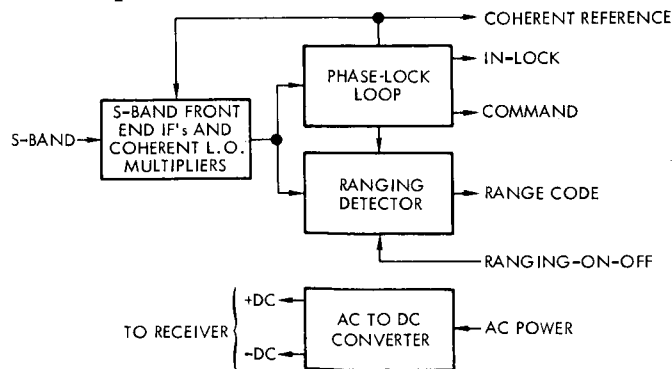


Figure 3-31. S-Band Receiver

\*"Final Report: Apollo Unified S-Band System Tests, Phase I," Volume I, Contract NAS 9-2563, of August 1964, presented to NASA/MSC by Motorola.

The receivers are always powered. The outputs of each receiver (command subcarrier, coherent reference, range code, and in-lock signal) are sent to the receiver selector, where the choice of receivers is made.

The following are the major receiver parameters:

Noise figure	10 db
Carrier tracking bandwidth	$2B_{\ell} = 32$ cps (operating threshold, $\alpha = 0.1$ ) $2B_{\ell} = 20$ cps (strong signal, $\alpha = 1.0$ )
Frequency	$2115 \pm 5$ Mc
Predetection bandwidth	4.5 Kc
Ranging channel RF bandwidth	3.3 Mc
Dynamic range	-142 to -50 dbm

#### Outputs

- Reference signal 19 Mc
- In-lock signal
- Composite command subcarrier
- PN range code

#### Inputs

- Power
- RF signal
- Ranging on-off

### 1.5.5 Low Noise Preamplifiers

This section discusses alternate methods of improving the noise figure of the S-band receiver. Devices considered include tunnel diode RF amplifiers, transistorized RF amplifiers, and improved mixer-IF amplifier combination.

Tunnel diode amplifiers (TDA) are clearly the most promising of the various techniques possible for receiver noise figure improvement.

Many TDA's are currently marketed providing typically a 4 to 5 db system noise figure and a power gain of 14 to 17 db, in the 2200 to 2300-Mc band. The TDA's which result in system noise figures close to 4.0 db employ gallium antimonide (GaSb) tunnel diodes. For the following reasons it is recommended, however, that germanium (Ge) tunnel diodes be used in any TDA considered for the Voyager program:

- 1) Germanium diodes can be constructed with fewer undesired impurities than gallium antimonide.
- 2) TDA's made with germanium diodes do not require temperature compensation to assure gain stability.

A TDA constructed with the Ge tunnel diode would provide 15 to 17 db gain and result in a system noise figure of less than 5 db. Absolute stability of the tunnel diode amplifier is assured through the use of four or five port circulators connected in the manner shown in Figure 3-32.

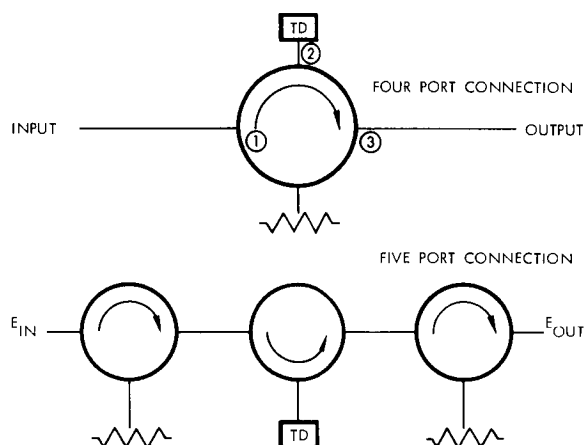


Figure 3-32  
Four- and Five-Port  
Circulator Connections

Assuming a 17-db amplifier gain, the four-port circulator requires approximately 30 db isolation between the tunnel diode port and the input port to ensure a return loss of 13 db. The five-port circulator amplifier, on the other hand, ensures a greater return loss with less critical specification of the port-to-port isolation of the circulators. A typical return

\*R. P. Nanavanti, "Some Physical Mechanisms Contributing to Tunnel Diode Failures," Proc., Symposium on the Physics of Failures in Electronics.

loss at the TDA input port of the five-port circulator coupled amplifier would be on the order of 23 db. The price paid for this greater return loss is the size and weight of the tunnel diode amplifier. The return loss can be considered as a first approximation to the relative stability against oscillations. Despite the size and weight penalty, it is recommended that a five-port circulator coupled amplifier be used because of its higher return loss. Reliability is perhaps the greatest question concerning TDA's since little meaningful life test data is available. If a TDA is used in the Voyager spacecraft, a great deal more information must be obtained by more meaningful life tests than have been run previously. The most significant reliability feature associated with tunnel diode amplifiers is that the predominate failure modes (open or short) are not catastrophic. An open circuit failure will result in the loss of gain and add approximately 1 db insertion loss to the receiver input. A short circuit failure is slightly worse, the result being loss of amplifier gain and a 3 to 5 db insertion loss.

Power supply requirements are quite rigorous at the diode, since gain is derived by biasing the diode in the negative resistance region of the diode I-V characteristic. (Figure 3-33.)

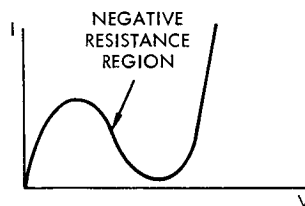


Figure 3-33. Tunnel Diode I-V Characteristic

Usually  $\pm 0.5$  per cent is required for close regulation at the diode. Such a regulated voltage is ordinarily derived from a temperature compensated Zener diode voltage regulator. This approach is recommended for any TDA considered for the Voyager program.

A brief summary of typical tunnel diode amplifier characteristics follows:



Frequency range	2150 to 2250 Mc
Dynamic range of RF input levels	-150 to -40 dbm
Noise figure	4.7 db
Gain	17 db
Resulting system noise figure*	4.96 db
Operating temperature range	-20 to +60°C
Storage temperature range	-50 to +100°C
Power supply characteristics	12 Ma at 15 volts $\pm$ 5 per cent
Maximum ripple on power supply	0.75 volts peak-to-peak

Transistor technology has developed rapidly in the microwave frequency area and transistor amplifier noise figures in the 2 Gc region have been measured as low as 4.8 db. Texas Instruments is currently marketing an experimental transistor, the TIX 3024, whose guaranteed maximum noise figure at 1 Gc is 5 db. While this is still a long way from 2.1 Gc, the state of the art is advancing so rapidly that 2.1 Gc units with noise figures of better than 5 db should be marketed in less than a year.

Unfortunately it is not expected that the gain of these units at 2.1 Gc will be consistently high enough to provide a system noise figure comparable to the tunnel diode amplifier. Additionally, it would take several years to obtain sufficient reliability data on these units to qualify them for the Voyager program.

The advent of the hot carrier diode has led to re-evaluation of the noise figure possible in mixer-IF preamplifier front ends. These diodes are majority carrier devices which are essentially void of shot noise and thus provide extremely low excess noise ratios. The specifications for the HPA 2150 mixing diode provide the following parameters:

$$NR = 1.0 \text{ maximum}$$

$$L_c = 6.0 \text{ db maximum}$$

$$*F_{\text{system}} = F_{\text{TDA}} + \frac{F_{\text{mixer}} - 1}{G_{\text{TDA}}}$$

Assuming selection of diodes for conversion loss less than 5 db, and assuming operation of the mixer into an IF preamplifier whose noise figure is 2 db, the over-all noise figure is

$$\begin{aligned}
 (F_o)_{\text{db}} &= L_c \text{ db} + 10 \log_{10} (F_{\text{IF}} + \text{NR} - 1) \\
 &= L_c \text{ db} + 10 \log_{10} \log_{10} (F_{\text{IF}} + 1.0 - 1) \\
 &= L_c \text{ db} + F_{\text{IF}} \text{ db} \\
 &= 5 \text{ db} + 2 \text{ db} = 7 \text{ db}
 \end{aligned}$$

This is felt to be the limit of noise figure performance available on a consistent basis using hot carrier diode mixer IF preamplifier combinations. This has the technical merits of offering a 3-db noise figure advantage over the baseline system without the addition of any new circuits, i. e., RF preamplifiers.

From a reliability viewpoint while the hot carrier diode promises to be a highly manufacturable device due to the epitaxial process of manufacture and the large junction area, little information is available about the reliability of the device. A second drawback from a reliability viewpoint is that Hewlett Packard Associates is at present the only manufacturer of these diodes. In addition, poor aging effects on the 2150 diode has recently forced a change in the manufacturing process to produce a more reliable unit. Because of the uncertainties associated with the reliability and supply of hot carrier diodes, this approach to noise figure improvement could be taken only on a high risk basis.

Of the three techniques considered, tunnel diodes amplifiers are recommended as the best choice based on availability and performance. However, because of the lack of life data they are not recommended for the selected configuration. A life test reliability program should be started so that these devices could be included at a later date. If used, the tunnel diode amplifier could provide over-all increased receiver reliability, decreased need for the 100-kw DSIF transmitter, and increased command reception capability with the low-gain antenna.

### 1.5.6 Receiver Selector

The receiver selector receives output signals and lock indication from three receivers and on the basis of present logic selects the receiver for each of two modes. The mode is selected in accordance with a signal from the CS and C. In the selected configuration these modes are:

Mode I        Select for maximum antenna coverage

Mode II       Select for maximum antenna gain

The receivers are ordered as follows:

R1            Maximum coverage, minimum gain

R2            Intermediate coverage and gain

R3            Minimum coverage, maximum gain

Variations in modal operation or receiver characteristics will not have a major effect on the receiver selector design or reliability.

The selector uses a priority system rather than a search procedure for acquisition to reduce the time required to find the best selection in the event of signal loss and to permit a better selection when reception improves (in the event of reorientation of the spacecraft, for example, or a change to a higher-power ground transmitter). The priority scheme is as follows:

a)    Mode I    Use R1 if R1 in-lock indication is present.

                 Use R2 if R1 is not in-lock and R2 in-lock signal is present.

                 Use R3 if R1 and R2 are not in-lock and R3 in-lock signal is present.

b)    Mode II   Use R3 if R3 in-lock signal is present.

                 Use R2 if R3 is not in-lock and R2 in-lock signal is present.

                 Use R1 if R2 and R3 are not in-lock and R1 in-lock signal is present.

The control signals from the receiver selector logic are used to route three signals. First, the control signal enables power to command channel baseband amplifier in the selected receiver. Second, the control signal is added to commands from the CS and C to power the selected

range code baseband amplifier. Third, the control signal enables a solid state switch in the selected receiver which permits the VCO output to be sent to the modulator exciters. In addition, a signal is sent to the modulator exciter to turn off the local oscillator signal and switch in the VCO reference signal.

The control signals are generated by means of integrated logic gates. A total of 16 gates in 8 micro packages are required.

#### 1.5.7 Command Detector

Section 1.3.3 discusses the relative performance characteristics of the two-channel command system and a one-channel system, both analyzed within the constraints of the Voyager mission. It is concluded that the relative simplicity and proven technology of the two-channel Mariner design outweigh the slight improvement in efficiency offered by the one-channel system at a 1 bps data rate.

The selected receiver system described in Section 1.1.3c utilizes redundant command detectors to provide the requisite reliability. On-board automatic switching of detectors based on failure malfunction detection is not practicable, and ground command switching cannot be invoked through the failed unit. Therefore an addressing technique is necessary.

Two methods of command detector addressing were considered: separating the VCO rest frequencies sufficiently so that subcarrier frequency address could be utilized, and use of mutually orthogonal PN codes in each of the command detectors.

Several maximal length PN sequences having maximum cross correlation of about seven per cent have been examined. This amount of cross correlation appears to be sufficiently small to enable reliable command detector operation without false lockup of the unaddressed detector. If it is found that false lockup can occur (most likely at high signal to noise ratios) then this can be eliminated by separating the two VCO rest frequencies by the order of 10 per cent in addition to using the orthogonal PN codes.

The determining constraints in choosing the clock frequencies are:

- a) Lower limit-signal energy in carrier tracking loop bandwidth, causing distortion of the synchronizing signal.
- b) Upper limit-acquisition time.

Existing Mariner equipment uses a subcarrier around 500 cps and a PN sync code of approximately 500 bits, which is considered to be a reasonable compromise value for the frequency (see Section 1.3.3c).

The command detector is similar to the Mariner C detector described in JPL EPD 277 "Mariner Spacecraft Functional Description." The PN generator is modified to permit selective addressing of each of two redundant detectors through the use of different orthogonal PN codes for each. The data output of the detector is inhibited unless the sync channel exhibits an in-lock condition. Figure 3-34 is a block diagram of the detector.

Conditions imposed on the detector are as follows:

- a) The S-band link is required to provide a composite command subcarrier channel for the baseband signal.
- b) The CS and C subsystem is required to accept NRZ data at 1 bps whenever the command detector provides an in-lock signal.
- c) The modulation method, subcarrier frequency, and data rate must be compatible with the DSIF command-generating and transmitting equipment.
- d) Command data bits to the CS and C will be inhibited whenever the command detector is not in lock.
- e) Both the command word information subcarrier and the sync information signal must be contained in the composite command signal.
- f) At high input-signal-to-noise ratios, lock-up on the first correlation of the transmitted and locally-generated PN codes must be highly probable with a maximum 1.5 cps frequency offset between the command signal and local  $2f_s$  frequencies. At a 19.5 db/cps command signal-to-noise spectral density ratio, the probability of lock-up at the first opportunity with a 1.5 cps offset is approximately 1/3.

g) Detector acquisition will occur in one of two ways, depending on the availability of telemetry data:

- 1) If telemetry data are available indicating the detector  $2f_s$  frequency and the lock condition of the detector, the transmitted  $2f_s$  will be adjusted to a 1 cps offset from the detector  $2f_s$  frequency and dummy command data (all zeros) transmitted until a lock condition is received.
- 2) If telemetry is not available, the transmitted  $2f_s$  frequency will be swept through the range of possible detector  $2f_s$  frequencies at a slow enough rate to insure detector lock-up some time during the scan.

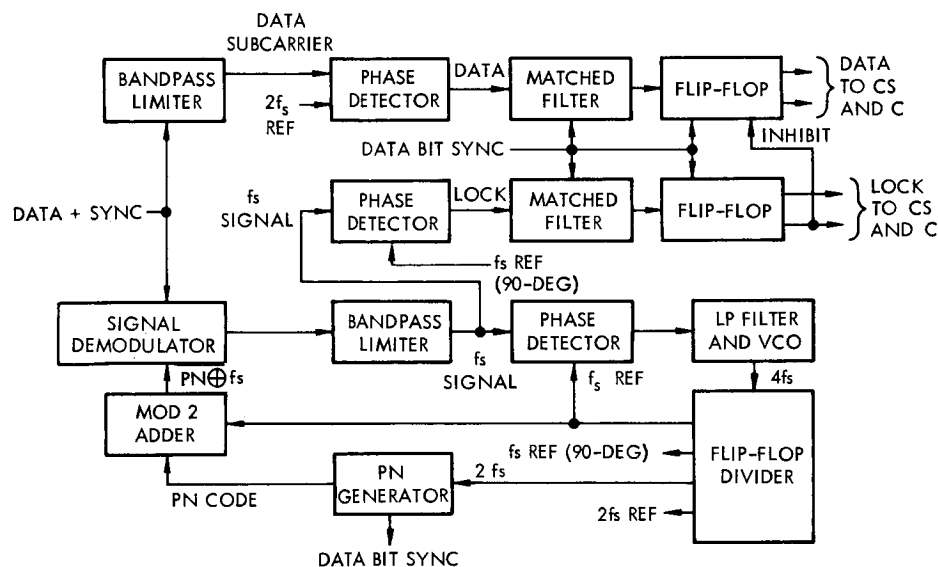


Figure 3-34. Command Detector

The functional characteristics of the selected detector are as follows:

- Subcarrier frequency 511 cps
- Sync code bit rate 511 bps
- Sync bandwidth approx. 1500 cps

- Sync code length 511 bits
- Data bit rate 1 bit/sec
- Sync channel loop bandwidth ( $2B_{LO}$ ) 2 cps
- Data detection Phase demodulation and matched filter
- Threshold  $P_e^b$   $1 \times 10^{-5}$
- Input S/N at threshold:
  - 1) Data signal 13.7 db/cps
  - 2) Sync signal 16.7 db/cps
  - 3) Composite signal 18.5 db/cps
- Outputs
  - 1) Data bit train - NRZ
  - 2) Data bit sync
  - 3) In-lock signal

#### 1.5.8 VHF Preamplifier for Capsule Link Receiver

Mechanization of the VHF preamplifier is based on the capsule link analysis (Section 1.3.4) and the VHF configuration (Section 1.2). This unit receives a signal from the VHF antenna and provides two outputs, one to each receiver.

The preamplifier provides sufficient gain with a low noise figure to realize an over-all system noise figure  $\leq 4$  db. The unit consists of a single stage RF amplifier driving two buffer amplifiers, one for each channel. DC power is derived from both VHF receivers through a diode "or" gate. Thus either receiver can power the preamp. A block diagram of the preamplifier is shown in Figure 3-35.

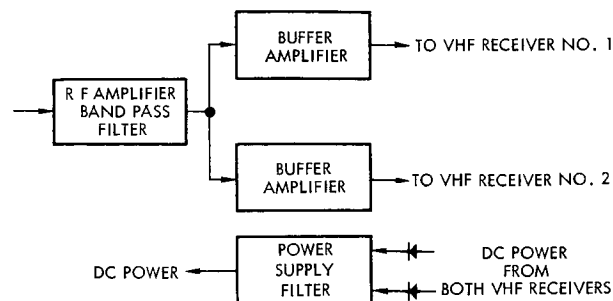


Figure 3-35  
VHF Preamplifier  
Block Diagram

The over-all system noise figure is dependent upon preamplifier noise figure, preamplifier gain, and receiver noise figure. An allocation of 3.5 db preamplifier noise figure, 10 db single-channel preamplifier gain, and a 4 db receiver noise figure has been made. All these parameters are within the current state of the art. For these parameters the over-all VHF receiver noise figure is given by:

$$NF_t \text{ (db)} = 10 \log_{10} \left( NF_{Pre} + \frac{NF_{RX}^{-1}}{G_{Pre}} \right)$$

where

$NF_t \text{ (db)}$  = over-all VHF receiver noise figure

$NF_{Pre}$  = preamplifier noise figure = 3.5 db or 2.24

$NF_{RX}$  = receiver noise figure = 4 db or 2.5

$G_{Pre}$  = preamplifier single-channel power gain  
= 10 db

Thus:

$$\begin{aligned} NF_{(t)} \text{ (db)} &= 10 \log_{10} \left( 2.24 + \frac{2.5-1}{10} \right) \\ &= 3.8 \text{ db.} \end{aligned}$$

Characteristics of the preamplifier are as follows:

- Single-channel gain                      10 db min
- Preamplifier noise figure                3.5 db max
- Frequency                                    136 Mc
- Bandwidth (1 db)                          50 Mc





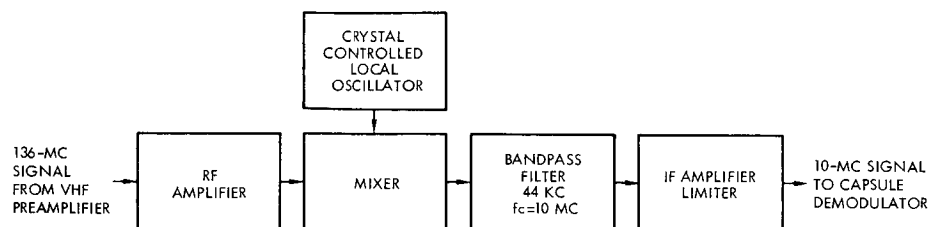


Figure 3-36. VHF Receiver Block Diagram

The following table gives the parameters of the VHF receiver:

Frequency (set to nominal $\pm 0.001$ per cent)	136 to 138 Mc
L. O. stability	$\pm 0.002$ per cent
Noise figure	4 db
Maximum signal input (20 db below saturation)	-45 dbm
Input impedance	50 ohms, nominal
Minimum input level for hard limiting	Noise
Output impedance	50 ohms
Output level (constant)	0 dbm
IF frequency (output frequency)	10 Mc
IF bandwidth (3 db)	44 kc

#### 1.5.10 Capsule Demodulator

The capsule demodulator, which processes the 10-bit/sec data received on the VHF link, accepts the 10-Mc FSK signal from the capsule receiver. The output of the demodulator is a 10-bit/sec (NRZ) signal which is coupled to the data handling subsystem.

The selected scheme for demodulation is required to work at low and negative signal-to-noise ratios. For this reason, the first step of the demodulation process is the separation of the mark and space channels with narrow band filters. These will be crystal filters since the mark and space frequency separation is 22 Kc centered about the 10 Mc IF of the

receiver. The bandwidth of each of these filters must be 22 Kc to accommodate the total frequency uncertainty in the data channel at the IF output frequency.

The mark and space filters are followed with envelope detectors connected with a summing circuit to provide positive and negative outputs corresponding to the mark and space. The NRZ output from this summing network is coupled to a matched filter detector and to a synchronizing circuit. The reconstructed data bits and a bit sync signal are sent to the data handling subsystem. The synchronizing signal is required for interrogation of the matched filter and the clocking out of the data bits to the data handling subsystem. A primary constraint on the synchronizer is the short acquisition time required and the multipath signal conditions.

A block diagram of the demodulator is shown in Figure 3-37. Mark and space crystal filters with the characteristics shown are readily available. The envelope detectors and summing circuit are straightforward. The 10 bit/sec data demodulator consists of a bit sync detector and a data bit detector of the matched filter variety. The matched filter is an integrate and dump circuit keyed by the bit sync information.

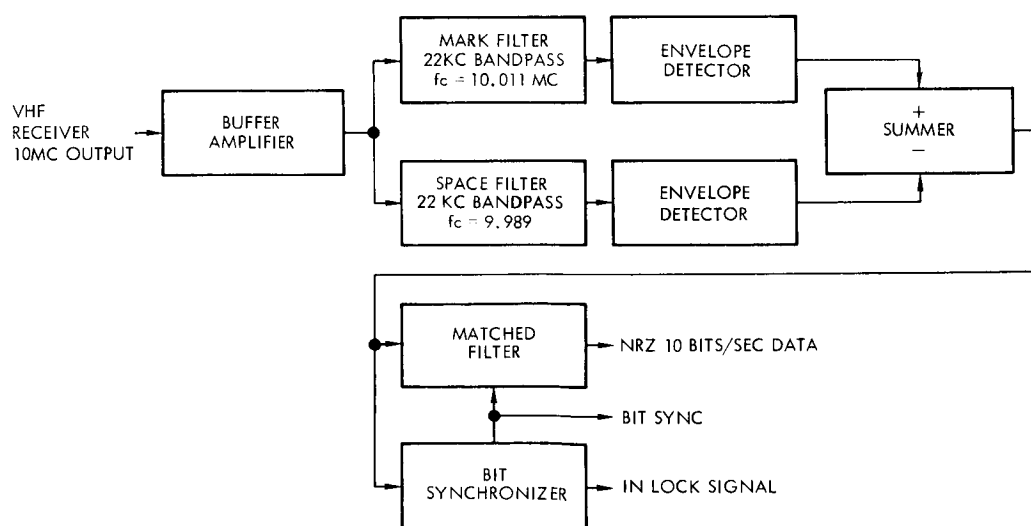


Figure 3-37. Capsule Demodulator Block Diagram

The following summarizes the parameters of the capsule demodulator:

Input Frequency	10 Mc
Modulation	FSK
Mark Filter, $f_c$	10.011 Mc
Space Filter, $f_c$	9.989 Mc
Mark and Space Filter Bandwidths	22 kc
Input Power Level	0 dbm
Input impedance	50 ohms
Output Signal Rate	10 bit/sec NRZ (asynchronous with the data handling rates)

Input Signals

- A. Power Supply Inputs
- B. 10 Mc Noncoherent FSK Signal from the Capsule Receiver

Output Signals

- A. 10 bit/sec NRZ signal to data handling subsystem
- B. 10 pulse/sec bit sync signal to data handling subsystem
- C. Digital in-lock signal indicator to data handling subsystem

1.5.11 RF Switches

The telecommunication subsystem provides the capability of utilizing any one of the three transmitters with any one of the three antennas. Additionally, a probe in the high-power transmitter system provides information to the transmitter selector on the status of the operating transmitter. The transmitter selector selects one of the transmitters and provides a signal to allow that unit to utilize one of the three antenna systems.

Two four-port circulator switches are used to connect the selected transmitter to the desired antenna systems. The functional diagram is

shown in Figure 3-38. Each circulator section of the two section switch can be switched independently. Switching is done by reversing the DC magnetic field through the ferrite, which is an integral portion of the strip transmission line inside the circulator. This magnetic field will not exceed 7.5  $\gamma$  at 1 foot. Total insertion loss from transmitter input port to either output port is 0.7 db maximum. The isolation between transmitters is 20 db minimum. The maximum VSWR over the frequency range does not exceed 1.36:1 with respect to 50 ohms impedance at all ports.

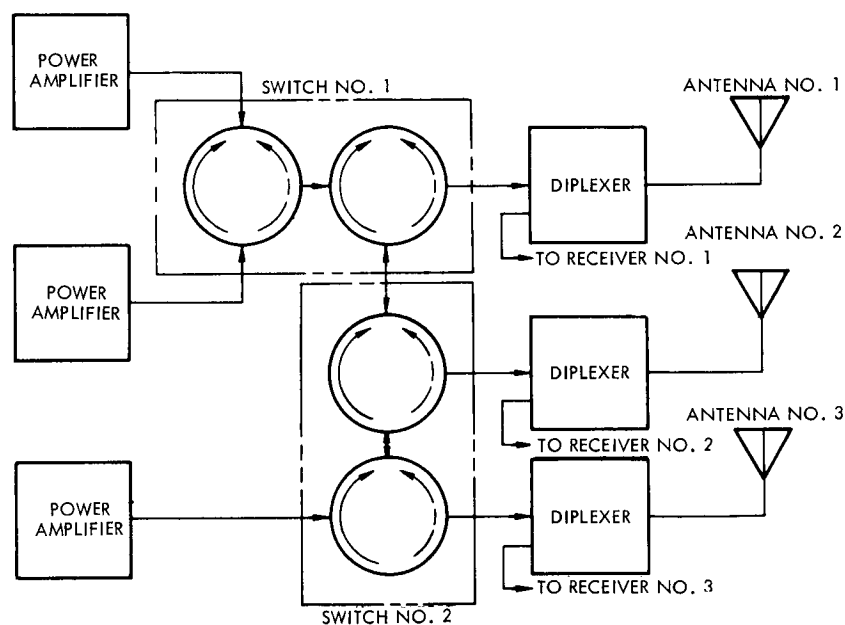


Figure 3-38. Circulator Switches Function Diagram

Two other devices have been studied for use in the same switching function, solid-state semiconductor switches and mechanical latching switches. The drawbacks in using semiconductor switches include high inherent mismatch, high insertion loss of unit, high drive power necessary for operation, and inability to handle high average power levels. The advantage of using switches of this type is the fast switching time. However, for Voyager fast switching time is not required.

Drawbacks of mechanical latching switches include high drive power necessary for operation, inherent ringing of the latching mechanism

causing some FM of the carrier, long switching time between output ports, low reliability as experienced in previous systems. Mechanical switches have electrical characteristics comparable to the circulator type.

#### 1.5.12 Diplexers

The simultaneous operation of a receiver and transmitter with a common antenna requires diplexing circuitry. Since the transmitter and receiver operate at different frequencies it is possible to connect them to a common antenna through frequency selective devices, consisting of bandpass filters tuned to the proper frequencies. The filters provide isolation between channels and reject spurious signals outside the pass-bands.

The electrical characteristics of the diplexer are summarized in Table 3-13. These characteristics will be maintained over the temperature range of  $-40$  to  $+90^{\circ}\text{C}$ .

The receiver pass-band, nominally 10 Mc centered about some frequency between 2110 and 2120 Mc, and the transmitter pass-band, nominally 10 Mc centered about some frequency between 2290 and 2300 Mc, have an insertion loss of 0.5 db maximum from their respective ports to the antenna port. Amplitude ripple within these pass-bands does not exceed 0.1 db peak to valley. The VSWR at any port does not exceed 1.36:1 with all unused ports terminated in a 50-ohm load.

Isolation between the receiver and transmitter terminals is 70 db minimum throughout the frequency range of 1500 to 4584 Mc.

The transmitter terminal of the diplexer exhibits a DC open circuit from center conductor to ground to minimize the magnetic loop characteristics from the TWT power amplifier.

The diplexer consists of a five-element bandpass filter in both the receiver and transmitter arms whose feed is a common antenna terminal. This device is employed in the Pioneer spacecraft in a similar configuration and identical manner. The physical envelope is approximately 2.0 x 3.5 x 6.8 inches exclusive of connectors. The total weight of the unit will not exceed 13 ounces.

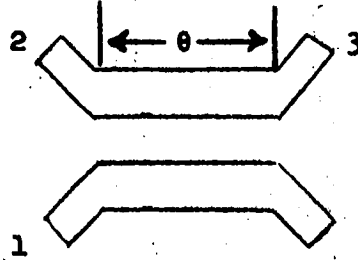
Table 3-13. Electrical Characteristics of the Diplexer

Frequency (Mc)	Insertion Loss		Isolation Receiver to Transmitter (db)	VSWR WRT to 50-Ohm Line
	Antenna to Receiver (db)	Antenna to Transmitter (db)		
1500	70	70	70	Amount to Transmitter Amount to Receiver
1700				
1900				
2014	70	70		
2060				
2105	0.50	70		
2110	0.50	70		
2115	0.50	70		
2157				
2252				
2287	70	0.50		
2292	70	0.50		
2297	70	0.50		
2338				
2550	70	70		
4584	70	70	70	
6876	70	70	40	

#### 1.5.13 Four-Port Coupler

A four-port coupler is used between the exciter stages and power amplifiers (TWT) of the transmitting system to provide the necessary isolation between the two exciter inputs and the two power outputs to the TWT power amplifiers. This alleviates the use of a switching mechanism between these devices and, further, permits power to be continually

supplied to both of the power amplifiers regardless of which exciter is being utilized. Any mismatch as seen by the coupler will cause a minimum of disturbance to the rest of the system. The unit consists of a four-terminal pair capacitively coupled quadrature hybrid.



As sketched above, when all the ports are terminated in their characteristic impedance  $Z_o$ , the coupled voltage,  $V_2$ , at port 2 produced by an applied voltage,  $V_1$ , at port 1 is equal to

$$\frac{V_2}{V_1} = \frac{jk \sin \theta}{\sqrt{1 - k^2} \cos \theta + j \sin \theta} \quad (3.3)$$

while the voltage at port 4,  $V_4$ , at the end of the straight-through arm is

$$\frac{V_4}{V_1} = \frac{\sqrt{1 - k^2}}{\sqrt{1 - k^2} \cos \theta + j \sin \theta} \quad (3.4)$$

The voltage,  $V_3$ , at port 3 is zero for all frequencies. Here  $\theta$  is the electrical length of the coupled-line region. The midband amplitude coupling factor,  $k$ , is given in terms of the even and odd characteristic impedances,  $Z_{oe}$  and  $Z_{oo}$ ,

$$k = \frac{Z_{oe} - Z_{oo}}{Z_{oe} + Z_{oo}}$$

while the characteristic impedance  $Z_o$  is expressed as

$$Z_o = \sqrt{Z_{oo} Z_{oe}}$$

Upon imposing the restriction of equal power split at ports 2 and 4, and  $\theta$  equal to a quarter wavelength at the center frequency of 2250 Mc,



the power split over the entire range of 2000 to 2500 Mc is obtained. Since this is normally an octave device the power split in ports 2 and 4 will be  $-3 \pm 0.25$  db over the frequency range given above.

The isolation of port 3 from port 1, or port 2 from port 4 is 28 db minimum, and the maximum VSWR for all ports with respect to 50 ohm resistive impedance is 1.15:1.

The coupler occupies less than 3" x 3" x 1" and weighs 11 ounces maximum.

## 2. DATA HANDLING SUBSYSTEM

### 2.1 Introduction

The Voyager spacecraft data handling subsystem is required to perform the following functions:

- a) Sample and encode spacecraft engineering and science data into a time-multiplexed PCM signal.
- b) Record high rate science data and enable playback under control of the data automation equipment (DAE).
- c) Accept capsule telemetry data in a serial bit stream from either the capsule-spacecraft umbilical or the capsule telemetry receivers.
- d) Mix (or interleave) formatted capsule data, scientific data (video, scan, and low rate) and engineering data into a serial PCM bit stream. Both real-time and stored data may be interleaved.

The output of the data handling subsystem is composed of two linearly mixed subcarriers, one modulated with the time multiplexed PCM data as described above and the second modulated with a PN code.

Transmission rate tradeoffs as a function of communication system design and measurement requirements have resulted in a maximum transmission bit rate of 4096 bits/sec.\* Based upon the measurements required, a range of bit rate requirements is presented in Table 3-14. As can be seen, the sum of the maximum bit rate in each data category exceeds the maximum transmission rate capability. However, it is not necessary to provide all peak rates simultaneously. For example, a low duty cycle sampling rate is used for engineering data during the video transmission. Also until the spacecraft orbits Mars video transmission is not employed.

---

\*The transmission bit rates selected are 4096, 2048, 1024, and 128 bits per second. See Section III, Paragraph 1.1.5.

Table 3-14. Summary of Data Rate Requirement

Data Form	Bit Rate (bits/sec)	Duty Cycle	Average Bit Rate (bits/sec)
Engineering	350-1200	Continuous	350-1200
		Low Duty Cycle Basis	50
Science (Scan or Mapping)	--	260 Scan per hour	195
Science (Ambient, Flare and Calibration)	40-140	Continuous	40-140
Science (Video)	163,000	12 picture pairs per 14.4 hour orbit	2920
Synchronization and Identifica- tion	--	--	100-400
Total (max) 4855 bits/sec (min) 1995 bits/sec			

Based upon transmission rate limitations, it is desirable to provide flexibility for different operating modes and formats as a function of mission profile and thereby achieve an efficient match of data transmission. For example, some of the data (e.g., video) is best processed in a data block form both from the standpoint of vehicle and ground data processing. Additionally, it is pertinent to consider longer transmission distances and failure modes in the RF link which would limit the transmission rate to lower values such as 128 bit/sec. Consequently, design considerations and tradeoffs are required to achieve a system organization which is adaptive to changing mission requirements as well as possible failure modes. An additional factor favoring a degree of flexibility is the long mission duration (approximately one year).

Other constraints which lead to design tradeoffs relate to the interfaces of the telemetry subsystem. For example, compatibility is necessary with the spacecraft DAE, CS and C, power supply, receiver demodulators and transmitter.

Since the data handling subsystem is required to interleave different data streams, it is therefore necessary to exchange synchronization between the DAE and the data handling subsystem. Special interface considerations are necessary during special activity conditions such as a solar flare.

A ground rule for the design of the data handling subsystem is that implementation be based upon the present state of the art (1966). Based upon over-all spacecraft system considerations, a reasonable allotment for data handling weight and power appears to be approximately 45 pounds and 30 watts, respectively. As will be shown, these bounds do not present difficult design constraints. Therefore, prime consideration during this study is oriented toward system organization, implementation and maximization of reliability.

Other considerations concern such factors as the design of the format and synchronization such that a ground data processor can reliably detect, synchronize and process received data regardless of the format or mode in use. For example, these considerations lead to use of standard frame and word sizes, as well as common synchronization coding.

Redundancy has been investigated in terms of:

- Basic need
- Level of application
- Compatibility with interfaces

The design approach during the study has been oriented to the use of black box functional redundancy as well as backup modes which provide a measure of redundancy.

## 2.2 Design Considerations and Approaches

### 2.2.1 General

Figure 3-39 is a simplified block diagram of the data handling subsystem which illustrates the basic functions and general interfaces required. The signal conditioner, PCM encoder, bulk storage, and low capacity buffer store provide a functional capability for the requirements as discussed in Section 2.1. (This figure does not show equipment redundancies which are included to improve reliability. The system is shown in the form of Figure 3-39 to clarify the functional description.)

The signal conditioner provides linearization and voltage normalization for various sensors such as temperature transducers.

The PCM encoder functions to:

- a) Sample and encode approximately 380 engineering analog and digital inputs into a time multiplexed output signal.
- b) Interleave combinations of the capsule, low rate science, high rate science, and engineering data into a serial PCM output.
- c) Provide a PCM modulated data subcarrier and PN modulated sync subcarrier to the transmitter.

The bulk storage operates to store up to twelve picture pairs per orbit, as well as high rate science, the actual number of pictures depending upon the specific orbit. Command control via the CS and C selects the program for this picture processing according to the following possibilities:

<u>Orbit</u>	<u>Video Storage</u>	<u>Readout Time (at 4096 bits/sec)</u>
Nominal (14.4 hr)	6 pictures pairs/orbit	1/2 orbit
Nominal (14.4 hr)	12 pictures pairs/orbit	1 orbit
Non-nominal (>14.4 hr)	Store to complete "Fill"	Depend upon orbit



rate scan data which results in a total storage requirement of approximately  $2 \times 10^8$  bits. For the resolution indicated, video data is read into the storage unit at a rate of 163,800 bits/sec. The principal consideration in the choice of bulk storage is reliability. Power, weight, and speed control with regard to interfacing with synchronous formats are important parameters.

Based on the above write-in rate, a significant technical problem for this data storage is the high write-read ratio (greater than 1280:1) required at the lowest rate of 128 bits/sec. At the present state of the art, tape recorders cannot practically achieve this ratio. On the other hand, tape recorders provide one of the most reliable approaches to bulk storage and are proven in spacecraft environments. It is possible to employ a tape recorder, and circumvent the ratio limitation by the use of a small magnetic core storage, which acts as a temporary buffer before final readout when using the lower bit rate. Present day tape recorder write-read ratios are approximately 100:1 and investigation indicates a 2:1 improvement by 1966. Therefore it is reasonable to assume that tape readout directly into telemetry can be used down to 1024 bits/sec. In this way, the core buffer need only be used during adverse conditions or failure modes, i.e., at 128 bits/sec. The buffer is implemented using square loop 20-mil magnetic cores in the form of a matrix. This type of memory, for moderate size, has all the well known advantages of a static storage. Many magnetic storage units of this type have operated in space for periods over two years.

At the present state of the art,  $10^8$  bits storage (6 picture pairs) can be satisfied with one tape recorder. In order to provide redundancy, two units are provided. These two recorders can also be used in series to obtain twice the number of pictures per orbit. While three to four tape recorders could be used, sufficient reliability is obtained by use of two.

The use of the magnetic core buffer to achieve the step-down in speed ratio does require some consideration. Basically, a "two beat"

cycle is involved. That is, the tape storage output is written into core storage until it is filled and then the tape recorder is stopped for the period required to read out the core buffer. This cycle can repeat continuously for this mode. A loss of some tape recorder data is incurred during start and stop cycles. The scope of this loss is a function of the transient start and stop time intervals relative to the magnetic core buffer size. Based on this factor as well as weight, size and complexity for this type of memory, a magnetic core buffer capacity of approximately 115,000 bits is chosen. The loss, with this size memory, represents 1 part in 160. However, the 128 bits/sec rate is a backup mode and normally this special step-down technique is not required. One approach to eliminate this small loss involves programming the stored data on the tape (with appropriate start-stop synchronization). Block storage on the tape recorder is required whose capacity is less than or equal that of the core memory. However, the extra complexity in programming and logic is not believed to be warranted for the gain achieved.

There are several approaches which have been evaluated in regard to the transmission mode for video:

- a) The video may be regularly interlaced (within the interval of one picture) with RT scientific and engineering data. However, it is preferable to read out one complete picture without any interruption. In case of synchronization problems or other failure modes, the regular interlaced case could result in confused or lost picture data.
- b) A mode having video and scan data exclusively could be used. However, there would be excessively long periods during which low rate scientific and engineering data would be absent. Sensing of scientific environment and consolidation with spacecraft performance is considered necessary and therefore this approach is rejected.
- c) A mode which interlaces one continuous picture ( $7 \times 10^6$  bits) and scan data with sequential frames of low rate science accumulated in a buffer storage followed by frames of engineering is considered the most reliable approach. This provides a low but sufficient sampling rate for the engineering and scientific data.



Synchronization of the tape recorder output data with the interlaced low rate scientific and engineering data (and PN synchronous) involves several design considerations. A basic need is that the tape recorder output be phase synchronous with the real time clock for the PCM encoder. This will insure that the ground bit synchronizer and signal conditioner will maintain lock and is achieved by providing word rate clock to the tape recorder. Advantages of using word rate (rather than bit rate) is that the absolute rate is more compatible with the tape recorder speed control loop and additionally the tape recorder output is forced to be phase synchronous with the PN sync. Also, the bit rate clock at 163 kc is more difficult to record on a single track.

### 2.2.3 Mission Profile

The design of the data handling subsystem is based on providing formats and modes of operation which adapt to the various portions of the mission. The flexibility for format, mode, and bit rate changes are required to permit efficient use of the available sampling rates under both normal and degraded conditions. Table 3-15 shows the data formats as a function of the mission profile. Since the capsule format requires such a low bit rate (i.e., = 10 bits/sec), it is included within the engineering format. Additionally, the scientific ambient, flare and calibration data are mutually exclusive. Six different formats are provided for the transmission of data. These are:

- Format A - High Rate Scientific
- Format B<sub>1</sub> - Low Rate Scientific (Ambient)
- Format B<sub>2</sub> - Low Rate Scientific (Flare)
- Format B<sub>3</sub> - Science Calibration Data
- Format C - Engineering
- Format D - Capsule

Table 3-15. Data Format as a Function of Mission Profile

Mission Profile	Engineering	RT Scientific Ambient	RT Scientific Flare	High Rate Scientific (Video & Scan)	Scientific Data Calibration	Capsule
Preflight	X	X	X	X	X	X
Launch (Low gain antenna)	X					X
Post-separation (Low gain antenna)	X					X
Interplanetary Cruise	X	X	X		X	X
Trajectory Corrections	X					X
Capsule Separation to Capsule Impact	X	X				X
Orbital Insertion	X					
Orbital Operation	X	X	X	X	X	

All possible permutations (modes) of the formats are not necessary because very small gain in information transmission is achieved. Table 3-16 shows the seven possible modes which result as a function of the following:

- a) The calibration mode is for a short time and need only be correlated with science engineering data.
- b) Video and other high rate science data will also be accompanied by a small fraction of engineering and low rate scientific data to provide correlation and general status information.
- c) The seventh mode is added to provide a slow readout video when the transmission bit rate is 128 bits/sec. Although the sequence of this mode is identical to that of Mode 4, the absolute amount of picture or scan data in each sequence is only 256 data frames ( $\approx 115,000$  bits rather than  $7 \times 10^6$  bits).

Table 3-16. Data Modes

Data Mode	Capsule	Engineering	Science (Low Rate)	Video and Scan	Calibration Science
I	X (RT)	X (RT)			
II			X (RT)		
III	X (RT)	X (RT)	X (RT)		
IV	X (RT)	X (RT)	X (B)	X (S)	
V					X (RT)
VI	X (B)				
VII (Failure Mode)	X (RT)	X (RT)	X (RT)	X (S and B)	

RT = Real-time data

S = Stored data in bulk storage ( $2 \times 10^8$  bit tape recorder)

B = Stored data in buffer storage ( $1.15 \times 10^5$  bit core storage)

The operational modes just described are summarized below in relation to the formats:

- |                  |  |
|------------------|--|
| a) Data Mode I   | 97 per cent engineering and 3 per cent capsule data. Transmission of Format C, including 2 words of Format D in each frame.  |
| b) Data Mode II  | 100 per cent real time scientific data. Transmission of either Format B <sub>1</sub> or B <sub>2</sub> as selected by DAE.   |
| c) Data Mode III | 1/5 engineering (1 frame) and 4/5 science format (4 frames). B <sub>1</sub> or B <sub>2</sub> with C. As selected by DAE.  |
| d) Data Mode IV  | 98 per cent bulk storage playback, 2 per cent real time engineering and buffer stored scientific. Transmission of Formats A, B, and C in sequence.   |
| e) Data Mode V   | 100 per cent transmission of science payload calibration data, Format B <sub>3</sub> .   |
| f) Data Mode VI  | 100 per cent transmission of playback of buffer stored capsule data, 256 frames, Format D.   |
| g) Data Mode VII | Playback of bulk stored data through the buffer. 256 frames of high rate science data from the DAE followed by 5 frames of real time engineering data. Transmission of Formats A, B and C in sequence. |

#### 2.2.4 Data Formats

##### a. Basic Format Sizing

Six different formats are used for processing various types of data inputs. Usual considerations in the design of a single format include such factors as frame synchronization (if used), frame, and word sizes, etc. Additionally, for Voyager, it is desirable to provide commonality of format design among all formats, since they will be used in different combinations to provide seven data transmission modes.

The reason for this is not only to simplify ground data processing, but is to provide the means for synchronously meshing these formats, not only in bit synchronism but also phase locked in frame groups. These formats are shown in relation to the data modes in Figure 3-40.

Since the frame size is related to a multiple number of words, it is practical to consider word size prior to the choice of frame size.

The following is the approximate accuracy (in bits) required from various data sources:

- |                |             |
|----------------|-------------|
| 1) Science     | 7 to 8 bits |
| 2) Video       | 6 bits      |
| 3) Engineering | 6 to 7 bits |

A 7-bit word size appears compatible with nominal accuracy requirements and additionally is compatible with the approach for using a 63-bit PN code (9 times the bit rate) to derive word synchronization. Choice of frame size is primarily based on efficiency, that is, it should be reasonable long so that fixed words such as group synchronization and format (or mode) identification result in a low percentage of total bit rate capacity. Based on allowing 10 per cent for these items, and simplicity of implementation, a 64-word frame is chosen for all formats (448 bits).

Within this main frame structure, certain words are used for synchronization and identification, namely:

- a) three words for frame synchronization
- b) one word for format and bit rate identification
- c) one word for subcommutator identification (engineering)
- d) four words for subcommutator channels (engineering)
- e) 7 to 12 bits for video and scan identification (high rate science only)

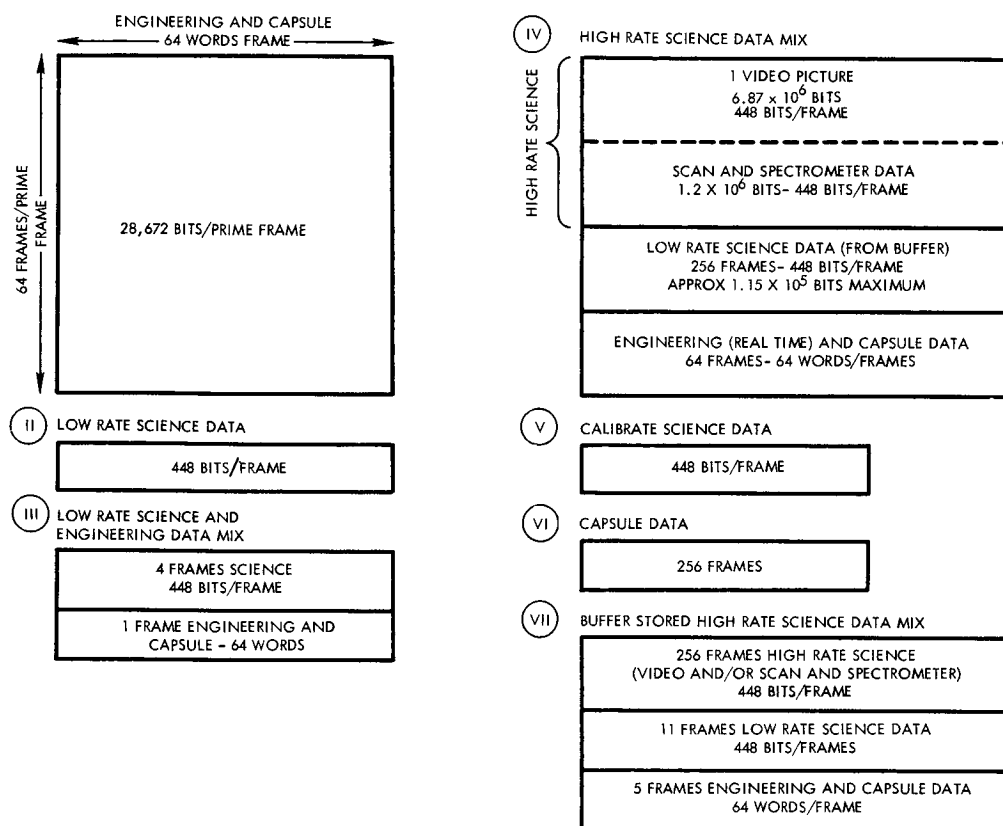


Figure 3-40. Data Gathering Modes

The choice of frame synchronization code is primarily based on the ability for the ground data processor to optimally detect and recognize the code. Based on the analysis performed in Section 5 of Appendix F, the code pattern chosen is 21 bits in length consisting of a 7-bit Barker code followed by two complement Barker codes.

b. High Rate Science Data

This category of science data consists of the following outputs:

- 1) Video (photographic)
- 2) Scan

The video requires 80 to 90 per cent of the data capability during the orbital phase. All of these inputs must use pretransmission

buffering to match the real time transmission rate. Consequently, it is logical to time share one output from the DAE which is applied to the tape recorder.

The magnitude of the bulk storage is primarily a function of the picture resolution. Table 3-17 shows a tradeoff of storage requirements versus resolution. Based on the objective of providing Ranger resolution, and since the corresponding storage capacity is feasible, this resolution was selected.

Table 3-17. Video Resolution versus Storage Requirement

	Resolution Similar to Ranger	Intermediate Resolution	Resolution Similar to Mariner C
Raster Bits/Picture	1020 x 1024 x 6	500 x 500 x 6	200 x 200 x 6
Total Bits/Raster	$6.3 \times 10^6$	$1.5 \times 10^6$	$2.4 \times 10^5$
Write-In (bits/sec)	$1.64 \times 10^5$	$3.5 \times 10^4$	$5.5 \times 10^3$
Readout (bits/sec)	4096/2048/1024	4096/2048/1024	4096/2048/1024
Write-In/Readout Ratio	40/80/160	8.8/17.5/35	1.4/2.7/5.5
Total Store	$1 \times 10^8$ bits	$2.5 \times 10^7$	$2.5 \times 10^7$
Recording Tracks*	9	3	3
Picture Pairs	6	6	36
Density	1000 bits/in.	2000	2000
Viewing Resolution	1 km	2 km	5 km

\*Includes clock track and data gap track.

Six-bit quantization of the intensity level of each point provides an intensity resolution equal or in excess of the capability of the human eye to distinguish. While this does not match the 7-bit word size of the engineering data, the tape recorder capacity and transmission requirements are reduced by 14 per cent. The main consideration in terms of commonality between formats is to provide a standard frame size and an integral number of words per frame.

The number of 6-bit video words that can be formatted within the 448-bit frame selected (as the standard vehicle main frame) is now considered. Within each frame, a number of bits are allocated to identify the location within the raster. In addition, frame synchronization, format and bit rate identification are required. Consideration of these items shows that 408 of the 448 total bits (68 elements) can be accommodated for video within each frame. Fifteen of these frames then provide 1020-element resolution for a video line. This is in excess of 1.4 times the resolution of existing vidicons and therefore does not become a limiting factor in the quality of the transmitted picture. Vertical resolution is satisfied by 1024 lines per picture. This information, and how it affects the total bit transmission, is summarized in Table 3-18. One frame of engineering data within the DAE has been added to allow inclusion of elapsed time, pointing, temperature and voltage measurements to permit correlation with the TV picture. The sync and identification bit total of 40 was arrived at by summing the 21 bits for frame sync, 7 bits for format and bit rate identification and 12 bits required to locate a frame within the video raster to within one quarter of a video line.

The scan data was then considered for the period of time of one video picture. To compare these on a practical basis, the scans have been formatted similarly and the resultant data appears in the previously mentioned Table 3-18. The sum of the scan data is almost one-fifth as large as the video raster. To store this quantity ( $1.2 \times 10^6$  bits) in a core memory storage or on a separate tape recorder would



Table 3-18. High Rate Science Data Formatting

Experiment	No. Scans Over a Period of One Picture Readout	Data Bits per Measurement	Sync and Identification Bits/Frame	Frames per Measurement	Frames Accumulated Over a Period of One Picture Readout	Bits( $10^6$ ) Accumulated Over a Period of One Picture Readout
1. Television Camera	1	$6.3 \times 10^6$	40	15,361	15,361	6.87
2. Scan Radiometer	10 - TV Area 150 - Others	$3.3 \times 10^3$	36	8	1,360	0.61
3. IR Reflection Spectrometer	4 - TV Area 15 - Others	$2.4 \times 10^3$	35	6	114	0.05
4. UV Spectrometer	5 - TV Area 75 - Others	$2.5 \times 10^3$	35	6	496	0.22
5. Meteoroid Flash	--	70 bits/sec	36		365	0.16
6. Other Instruments	--	70 bits/sec	36		<u>365</u>	<u>0.16</u>
Total					18,061	8.07

be considerably less efficient than to store this data immediately following the video raster on the tape storage unit. Therefore, the scan data is made a part of the high rate data format.

Consequently, the high rate science data format is composed of a sequence of frames equal in length to the engineering data frame. The over-all sequence of frames consists of one video picture followed by many scans of radiometer, infrared, and ultraviolet data plus other high rate data such as meteor flash. The data is digitally encoded and formatted within the DAE of the science payload and provided on a single output line. The format will contain elapsed time data, data location identification and any engineering measurements relative to the science measurements (e.g., the pointing angles of a camera at the time a video picture is taken).

#### c. Low Rate Science Data

This section discusses three categories of low rate science data. These three categories, the ambient, flare and calibration, are transmitted through one interface line to the data handling subsystem.

Ambient. The ambient low rate science data is composed of science measurements from several particle and field experiments, such as particle counters, magnetometers, and meteor impact measurements. A summary of a hypothetical group of such experiments is shown in Table 3-19. The low rate science data measurements can be format arranged, as long as standard frame size and synchronization are included.

Table 3-19. Low Rate Science Data Formatting

Experiment	Number Sensors	Average Bit Rate (bits/sec)	Data Bits During Readout of Complete High Science Format (at 4096 bits/sec)	Frames (at 4096 bits/sec)
1. Meteoroid Impact	4	1.0	2,070	
2. Magnetometer	1	5.0	10,350	
3. Plasma Probe	2	2.0	4,140	
4. Cosmic Ray	4	0.16	330	
5. Trapped Radiation	3	3.5	7,245	
6. Ionosphere	1	0.25	520	
Engineering Measurements	35	4 measurements per raster	980	
Synchronization and Identification at 10 per cent			<u>2,565</u>	
Total			28,200	63

Summarizing, the low rate science data is digitally encoded and formatted within the DAE into a sequence of frames equal in length to the engineering data frame. Each data frame will contain synchro-

nization signals and data format identification. Any necessary channel location identification will be contained within the data, in addition to elapsed time and any engineering measurements within the science payload.

Solar Flare. The DAE will sense the presence of a solar flare and control the operation of the data handling subsystem during its occurrence, taking precedence over any other data format. The solar flare format is supplied on the low rate science data interface line. The DAE will provide any necessary integration or data sampling required to reduce its content to the current telemetry bit rate.

Calibration. The DAE will provide a format for calibrating science experiments at programmed intervals, or on command. This mode will provide calibration signals matched to the experiments. The resulting output signals will be formatted into standard frames with synchronization, identification, and elapsed time signals.

Engineering. The engineering data is composed of spacecraft and subsystem performance measurement (including command verification). A representative set of measurement requirements are listed in Section 7, Appendix F. The capsule data format is also interleaved within this format. To handle the 330 analog, binary, and discrete channels required within the basic 64 word standard format, subcommutation is used. Table 3, Section 7, Appendix F summarizes sampling rate requirements. Two sampling rates (main frame and subframe) satisfy all requirements. The resultant format is shown in Figure 3-41. Using four subcommutators, a growth factor of 16 per cent remains on a per channel basis. However, since only 43 channels of the main frame have been assigned, a sampling rate growth factor of 39 per cent remains. This is considered a reasonable factor recognizing the historical growth patterns of measurement requirements of previous flight programs. The channel allocations have included

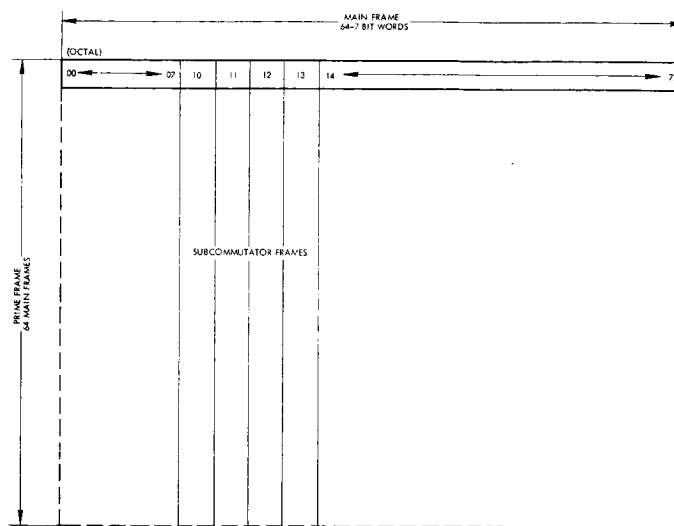


Figure 3-41  
Commutation Format

provisions for synchronization signals, data format and bit rate identification, subcommutator location, identification, and an elapsed time indication.

Capsule Data. Capsule data is formatted in the standard spacecraft frame size of 448 bits. Fixed words provide frame synchronization, format identification, and other identification, as required. The capsule data is hardwired to the PCM encoders prior to separation and forms a portion of the engineering data format. After separation, the capsule data is available to the PCM encoders as dual outputs of the demodulators. With the capsule data supplied at 10 bits/sec, approximately 3 per cent of the engineering data format is required for this data, using dual channels for redundancy. The capsule data is buffered within the PCM encoder to permit bit phase synchronization. In addition, three hours of capsule data can be stored in the buffer storage for playback upon command.

## 2.2.5 Transmission Modes

### a. General

The operating modes for data transmission were briefly outlined in Section 2.2.3 as they pertain to the mission profile. Now

that the formats have been described in some detail, this section will examine the seven data modes in more detail. Figure 3-42 shows the different transmission modes and Figure 3-40 illustrates the format content of the seven data modes. The following paragraphs describe these modes:

b. Engineering Data (Mode I)

During the launch and maneuvering phases, maximum interest is directed toward acquiring spacecraft and subsystem performance data as well as command verification. Minimal interest is expected in science data during these times and most of the available sampling rate is required for engineering data. Therefore, an operational mode has been provided which gathers only the engineering data format (which also includes capsule data).

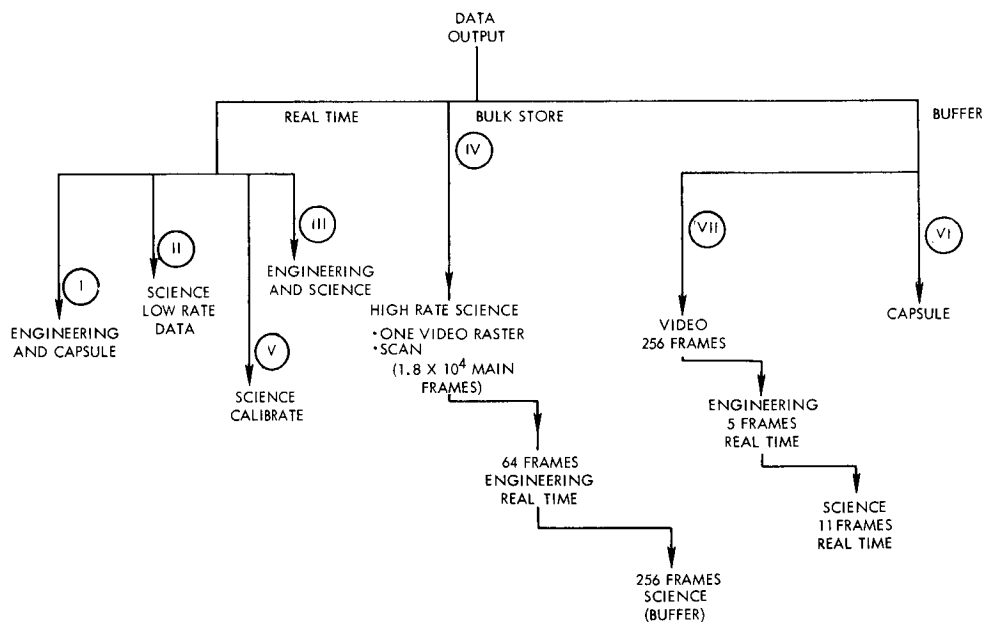


Figure 3-42. Transmission Mode Tree

c. Low Rate Science Data (Mode II)

During the long interplanetary cruise phase, there may be periods when maximum interest will be in science data (e.g., solar flares). Consequently, this mode provides an exclusive transmission of science data.

d. Low Rate Science and Engineering Data (Mode III)

During the major portion of the cruise phase, it is desirable to provide a large capability for the gathering of science data, while still monitoring the engineering data. During this phase the minimum engineering sampling requirement (300 bits/sec) is considered adequate. Therefore, a science-engineering data mix corresponding to four frames of science for each frame of engineering is selected.

e. High Rate Science Data (Mode IV)

During orbital operations, the transmission of video data becomes the major mode of the data handling subsystem. To provide a complete cross section of data, the video is interlaced with science and engineering data. Design considerations are oriented to provide the following features, that

- 1) Video be recorded and read out for transmission as a block of frames (equivalent to one picture) without interruption.
- 2) Scan data follows video (synchronously).
- 3) Method of recording is continuous (no start-stop) during this mode.

To interleave the low rate science accumulated in the buffer with the high rate science output of the recorder, the DAE programs a "no" data gap on a separate track so that these two separately derived data can be synchronously interleaved. Figure 3-43 illustrates this case.

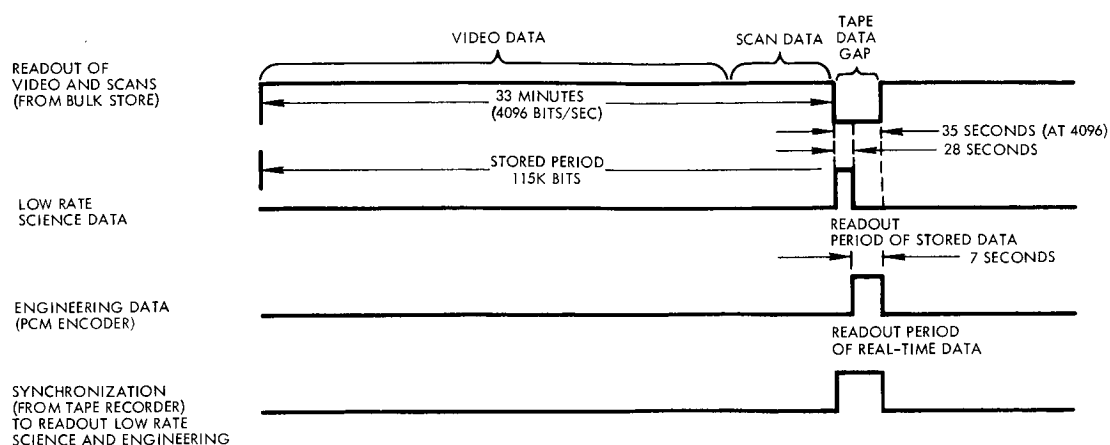


Figure 3-43. High Rate Science Data Mix Timing

Based on the objective of maximum video and science transmission, the engineering sampling rate is chosen to be approximately 2 per cent of the total link capacity. If engineering data is required at a higher rate (because of some anomalies), an exclusive engineering format can be commanded.

f. Calibration Science Data (Mode V)

A data calibrate mode is an exclusive mode within the low rate science output.

g. Capsule Data (Mode VI)

Capsule entry, descent, and landing is a critical period for data retrieval. Consequently, to provide backup to the real-time relay link transmission, the capsule data will be stored within the buffer storage. Approximately three hours of 100 per cent capsule data storage is provided. Playback, upon command, will require approximately 1/2 minute at the 4096 bit rate.

h. High Rate Science (Low Bit Rate Transmission) (Mode VII)

As previously discussed, the tape recorder write-read ratio is too high at 128 bits/sec to permit direct readout. Instead, a magnetic

core buffer is used as an auxilliary speed step-down device. Sizing the buffer at 256 frames, or approximately  $1.15 \times 10^5$  bits, permits the readout of 17 video lines at one time. Reading data into the buffer from the tape at 2048 bits/sec requires 56 seconds. During these 56 seconds, 11 low rate science data frames and 5 engineering data frames can be transmitted. It then requires 896 seconds to read the data out of the core buffer. The time period required for the transmission of a complete high rate science data format, allowing time for loading the buffer and starting and stopping the tape recorder, is approximately 68,000 seconds. This permits the transmission of a video picture each 1-1/3 nominal orbits. A small amount of high rate science data, approximately equal to one and one-half frames, will be lost during each stop and start of the tape recorder. However, this 1/10 of a raster line will be barely distinguishable to the eye in the video data, and a very minor item in the highly redundant scan data.

#### 2.2.6 Interfaces

The data handling interfaces and corresponding signal/control exchanges are as follows:

<u>Data Handling (DH)/DAE</u>		
<u>Lines</u>		<u>To</u>
2	Scientific data	DH
1	Bit rate	DAE
2	Bit rate status	DAE
3	Mode status	DAE
1	Frame rate	DAE
1	Word rate	DAE
1	Tape "no" data gap	DH
1	Flare format status	DH
1	Word rate for tape recorder	DH
1	Start signal for tape recorder	DH
1	Stop signal for tape recorder	DH
1	End of tape signal	DAE



The first item provides the science data for telemetry, the remainder are synchronization and controls.

Data Handling/CS and C

1	Bit rate signal	DH
2	Bit rate status	DH
3	Mode control status	DH
2	Redundancy control (PCM encoder and tape recorder)	DH
1	Elapse time 21 bits/each	DH
2	Command memory 21 bits/each	DH
2	Word gates	CS and C
1	Bulk storage on/off	DH
1	Store capsule data	DH

Data Handling/Power

1	50 volts, 4800 cps single phase square wave	DH
---	---	----

Data Handling/Transmitter

<u>Lines</u>		<u>To</u>
1	Output (data subcarrier mixed with sync subcarrier)	Transmitter

Data Handling/Engr. Measurements

230	Analog
82	Discretes
2	Capsule data
3	Binary data

Data Handling/Receiver Demodulator

2	Capsule data (hardwired or receiver demodulator)	DH
2	Bit rate line	DH

### Data Handling/Test Connector

1	Modulation output
4	Data serial output
1	Word synchronization
1	Frame synchronization

### 2.2.7 Bulk Storage Tradeoff

#### a. General

Storage of video data requires an order of magnitude more capacity in the bulk data store than the storage capacity required by other instruments. The design of the bulk data storage unit could be simplified by the use of visual sensors capable of long term image retention with slow speed readout. Such devices include the photographic film camera, the vidicon TV camera, and the dielectric tape camera.

#### b. Photographic Film Camera

Although satisfying the storage requirements, it is unlikely that photographic film cameras will be used for early Voyager orbiting missions because of excessive weight, power consumption and film fogging problems due to radiation.

#### c. Large Area Storage Vidicon

Photoconductive target surfaces employing a dielectric storage layer are capable of storing the charge pattern formed by visual imaging for several days with no detectable deterioration of the image quality. The use of such a camera, having an effective area several times that of the conventional 1-inch vidicon (format size 11.2 mm square), offers an attractive means of storing large quantities of video data for one or more orbital periods.

Assuming a conservative value for the limiting resolution of 30 line pairs (60 TV lines) per mm, and 6-bit grey scale quantization, the equivalent data storage per square centimeter of picture area is  $\sim 2 \times 10^6$  bits.

An active format area of 7 x 7 cm (2.75 x 2.75 inches), would give a total storage capability of  $1.37 \times 10^8$  bits, using a 4-1/2 inch vidicon recently developed for high resolution close circuit television. Further development of such a camera for space applications, together with a suitable optical system for multiple imaging or large area coverage offers a possible long term solution to the video data storage problem, particularly in multiple camera installations.

d. Dielectric Film Camera

In the dielectric film or tape camera image retention is achieved, as in the storage vidicon, through the use of a photoconductive layer on a dielectric film. A panoramic strip camera using 100 feet of 35 mm dielectric film is being qualified for use in NASA spacecraft.

With a resolution of 30 line pairs/mm (18 line pairs/mm at 50 per cent response) and assuming 6-bit grey scale quantization, the equivalent bit storage capacity is  $10^{10}$  bits.

Recent developments in electron optics and tape manufacturing techniques may result in this figure being increased to  $> 10^{11}$  bits.

The parameters of these devices are summarized in Table 3-20.

Table 3-20. Dielectric Video Storage Devices

<u>Device</u>	<u>Minimum Resolution (Optical line pairs/mm)</u>	<u>Equivalent Bit Storage</u>
4-1/2 inch storage vidicon	30	$1.27 \times 10^8$
35 mm dielectric tape camera (100 ft of tape)	30	$1 \times 10^{10}$
Advanced 70 mm dielectric tape camera (100 ft of tape)	70	$1.83 \times 10^{11}$

e. Conclusion

While these advanced techniques of imaging and data storage offer a significant improvement and simplification in video data storage, it is assumed that the most conservative approach in the design of the video experiment will employ a vidicon camera and magnetic-tape recorder.

2.2.8 Redundancy Concept

Redundancy has been considered on two levels. Within each unit, redundancy has been considered for key serial elements which have high part counts. Additionally, redundancy has been supplied for each of the two units which are in series with the major portion of the data flow (see Volume 4).

Redundancy will be supplied within the PCM encoder for the buffering of capsule data. In addition, a redundant PCM encoder will be supplied. Selection of the PCM encoder will be accomplished by switching input power.

Two tape recorders have been selected to provide unit redundancy. The addition of a second recorder also added flexibility to the high rate science data mix mode, permitting the recording of 6 through 12 picture pairs in a single time sequence and providing sufficient storage for the nominal orbit at the maximum bit rate.

The two capsule data trains are fed into separate buffers within the PCM encoder. This data is fed out on main commutator channels so that the loss of one channel or buffer will not prevent transmission of capsule data.

During the design and development phase, the internal redundancy decisions will be re-examined based upon actual implementation techniques and complexities. For example, it may be found desirable to provide redundancies in major elements in series with all data, such as the data and PN modulator and mixer, or in major series elements for engineering data, such as the analog-to-digital converter.

### 2.2.9 Selected Design

Figure 3-44 is a simplified block diagram of the selected data handling subsystem. This subsystem consists of two engineering telemetry units, two bulk storage tape recorders, a buffer core memory, and a signal conditioner. Redundant units have not been provided for the buffer core memory and the signal conditioner since these units are not in line to the flow of the major portions of the data in normal operating modes. Although the buffer is used to store low rate science data during video and scan transmission, in the event of buffer failure, low rate data can be transmitted directly out of the DAE in smaller samples.

The redundant PCM encoder is used upon receipt of a ground command for switching.

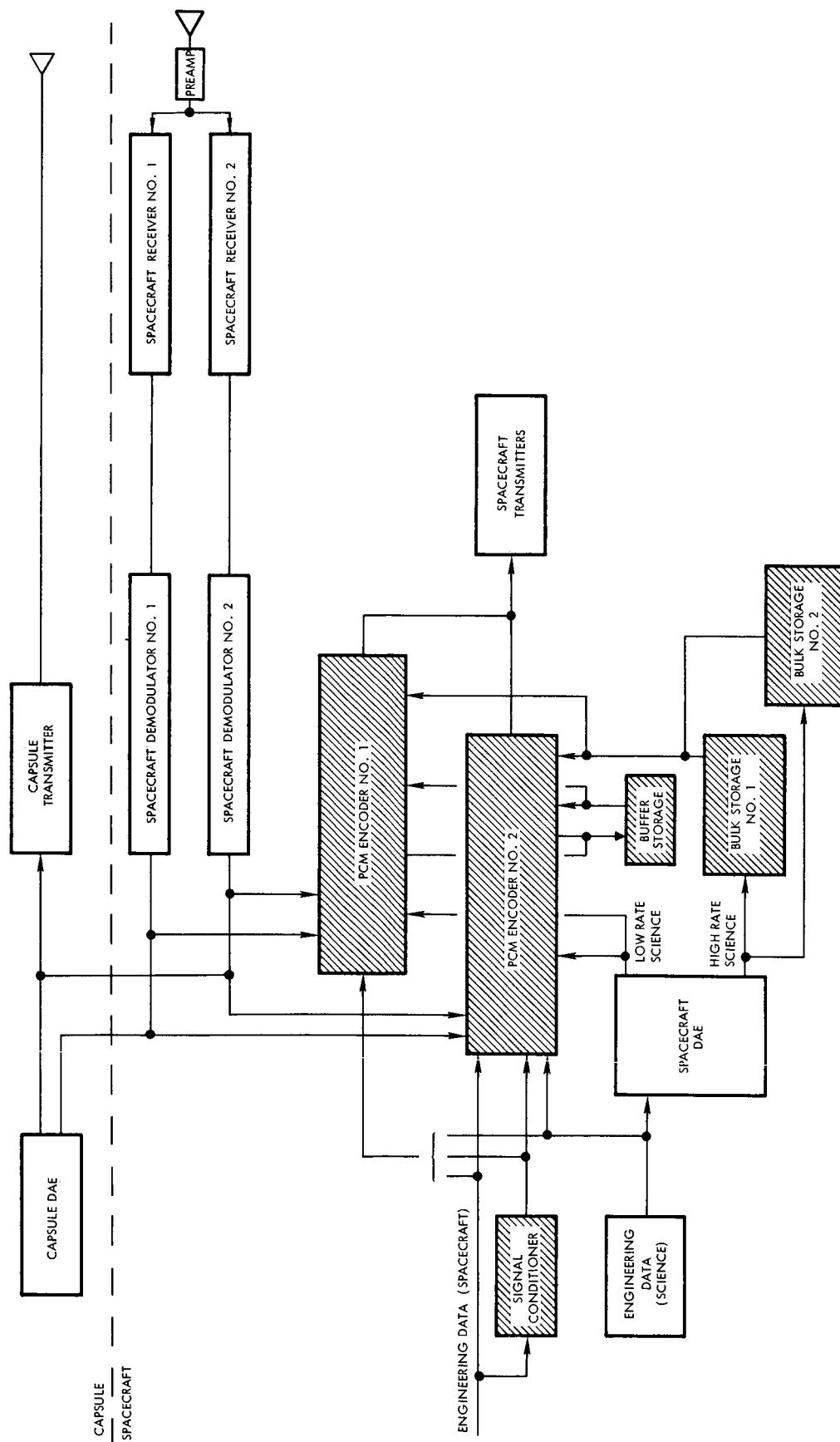
This subsystem operates in seven separate data gathering modes each of which is a unique combination of the six data formats to be transmitted. The combinations of formats and operating modes were shown in Figure 3-40. In addition, there are pretransmission storage phases involved in three of the data modes described.

Upon command from the CS and C, the PCM encoder selects the various data formats and interlaces them as required. The composite signal modulates a square wave subcarrier, and the data modulated subcarrier is linearly added to a PN code modulated subcarrier. The subcarrier mix is supplied to the communications subsystem for transmission to earth.

The operational characteristics peculiar to a specific data format or data mode were described in Sections 2.2.4 and 2.2.5.

In summary, the operation of the subsystem is as follows:

- a) All analog engineering data will be time shared and converted from analog voltages to 7-bit binary data words.



NOTE:

SHADED ITEMS COMPRISE DATA HANDLING SUBSYSTEM

Figure 3-44. Simplified Block Diagram of Selected Data Handling Subsystem

a. Requirements

The design concept of the PCM encoder is primarily based on:

- 1) Sampling and encoding approximately 230 analog and 82 discrete engineering measurements and capsule data into a PCM time multiplexed output. Table 3-21 is a summary of the measurement requirements listed in Section 7 of Appendix F.
- 2) Programming of the science and engineering data mix for transmission to earth both from real-time and storage sources.
- 3) Providing control signals for synchronization of data flow.
- 4) Modulating the serial data wave train on a data subcarrier and linearly mixing it with the PN coded synchronization subcarrier.

Table 3-21. Summary of Engineering Data Inputs and the Preferred Sampling Rate

	Supercom- munication No. 1, 73.2 samples/sec	Supercom- munication No. 2, 36 samples/sec	Main Com- munication 9.1 sam- ples/sec	Subcom- munication, 8.5 sam- ples/min	Total
Engineering Analog	--	1	12	217	230
Engineering Discretes	4	--	26	52	82
Capsule Data (Channel alloca- tion)			2		2
Binary Data (elapse time CS and C memory)				3 (21 bits/ each)	3

\* Sampling rate based on bit rate of 4096 bits/sec

- b) All digital engineering data and capsule data will be time shared with the analog engineering data.
- c) During the launch phase, initial acquisition and maneuvers, only engineering data will be transmitted.
- d) During the cruise, blocks of science data 1792 bits long are alternated with blocks of engineering data 448 bits for real time transmission.
- e) During a solar flare encounter, or at any other desired time during cruise, only scientific data will be transmitted. The above mix of science and engineering data may be transmitted during the latter portion of a solar flare.
- f) During capsule entry, capsule data will be transmitted in real time and simultaneously stored in the buffer and held for command read-out.
- g) During planetary encounters, a large portion of the high rate science data will be stored in the on-board magnetic tape recorder. While in this store mode the low rate science data mixed with engineering will be transmitted in real time.
- h) The stored high rate science data will be transmitted after planetary encounters during a specified portion of an orbit or orbits (while low rate science is being stored). During the gaps in the high rate science data, both real time engineering and stored low rate science will be transmitted.
- i) Transmission of science instrument calibration data on command during cruise and orbital operation phases.

## 2.3 Design Tradeoff and Implementation

### 2.3.1 PCM Encoder

This section discusses various PCM encoder design tradeoffs relating to efficient analog multiplexing, analog-to-digital conversion, and programming of data mix.



Figure 3-45 is simplified block diagram of the proposed PCM encoder which is sized to match the engineering data format requirements. Although this design specifically is sized for these formats, the basic concepts and logic are easily expanded or contracted to meet additional format requirements. The functional blocks which are shaded (cross hatch) do not form part of the PCM encoder.

As shown in the diagram, the main functional blocks are:

- Programmer
- Multiplexer
- Analog-to-digital converter
- Combiner
- Capsule buffer
- Data programmer
- Data/PN modulator and mixer
- Command control unit

The programmer provides the necessary control signals to the multiplexers for main frame and subframe selection of analog and bi-level gates. Additionally the programmer supplies timing pulses to the analog-to-digital converter to derive frame synch and subcommutator identification. Also, as shown, the programmer supplies timing signals to the DAE, bulk storage and buffer store. The programmer derives the bit rate clock from the CS and C unit. Consequently, bit rate selection is performed by the CS and C.

The multiplexer provides isolation and selection of analog and bi-level inputs at the main and subframe rates.

The analog-to-digital converter encodes each analog input to a seven bit word. The combiner serves to interleave the encoder analog, bi-level and capsule data with identification signals in a serial time multiplexed wavetrain.

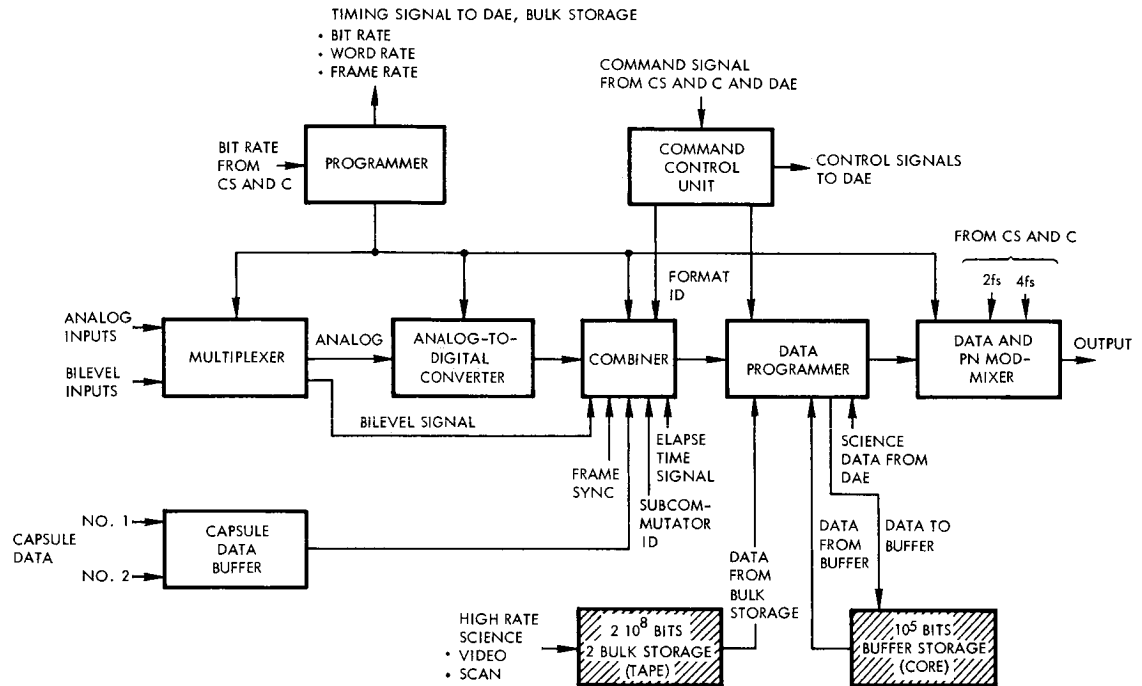


Figure 3-45. Simplified Block Diagram of PCM Encoder

The data programmer provides the function for a single data selection or mixing a combination of data sources as shown:

- Engineering data
- Data from bulk storage
- Data from buffer storage
- Low rate science data from DAE

Also this logic provides the necessary modes and data format interleaving described in section 2.2.5.

The output binary data from the data programmer modulates a  $4f_s$  subcarrier. The output of the data subcarrier is linearly mixed with the output of the PN synch subcarrier.

The capsule buffer provides the means of buffering capsule data. Two capsule data trains are fed and stored separately.

The command control unit provides control signals to the DAE data programmer and data storage in order to alter the operating modes of the data handling subsystem. Additionally the command control receives inputs from the CS and C and DAE.

Figure 3-46 is a more detailed block diagram which shows a functional breakdown of each basic portion of the simplified block diagram of Figure 3-45 (such as programmer, multiplexer and data/PN modulator and mixer).

The design of the PCM encoder will make maximum use of proven reliable integrated circuits wherever feasible in order to reduce weight and volume.

b. Analog-to-Digital Converter Design Approach

The technique of analog-to-digital conversion and sampling of the analog inputs strongly influences the implementation design of the programmer analog multiplexer and in general the efficiency of the complete system.

The effects relate to speed of operation, encoding error and complexity of logic. Various techniques could be used to make an analog conversion to 1 part in 128 and having the necessary speed. A ramp encoding technique could be used but requires a high speed clock and counter (74 Kb/sec). Successive approximation provides a reduction in speed since an "n" bit conversion can be made in "n" bit times. This is the technique proposed here which provides an effective logic rate of 4096 bits/sec. Additional advantages of successive approximation technique are the stability of the digital to analog decoding which only depends upon the semi-conductor switches and stable resistors. This is in contrast to the uncertainty of stability for a capacitor and current source which might be used for ramp encoding.



Also pertinent to the design of any analog-to-digital converter is the aperture error which arises from noninstantaneous sampling and conversion to digital form. Previously, the computation of this error has been undertaken on a pessimistic peak error basis or by an optimistic analogy to aperture errors in PAM systems. However, a more exact analysis of the aperture error is based on calculating the average error instead of the peak error. It can be shown that in order to maintain the average aperture error less than  $1/2$  of a quantization level, for 7 bit quantization, the aperture conversion time  $T$  must be no more than 5.3 degrees of a full scale sine wave.

Table 3-22 shows the maximum data frequencies possible for the case where aperture error (based on  $1/2$  quantum error) limits the upper frequency or sampling rate is the limiting factor.

Based upon the premise that data frequency requirements will never exceed that allotted for the aperture error, the use of sample and hold or compressed analog-to-digital conversion techniques are not required.

Figure 3-47 is a simplified diagram of the analog-to-digital converter technique which consists of analog-to-digital logic gates, a 7 bit

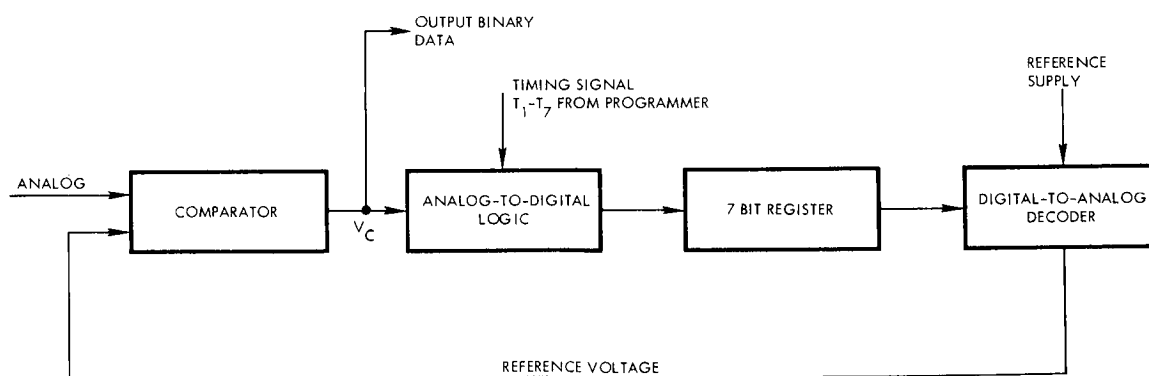


Figure 3-47. Converter

register (flip-flops  $a_1$  through  $a_7$  not shown) a digital-to-analog converter (switch and ladder adder) and reference supply.

The timing signals ( $T_1$  through  $T_7$ ) from the programmer provide sequential sampling pulses to the analog-to-digital converter. The digital-to-analog logic consists of the logic and binary elements whose states are decoded by the digital-to-analog switches and resistive ladder adder. The adder output is the trial reference analog voltage which covers a 0 to 3 volt range in quantized steps of 3/128 volt.

The truth table, as shown in Table 3-23 describes the logic necessary to achieve successive approximation. As shown by the truth table, pulse  $T_1$  clears old states of the analog-to-digital register except the most significant weight. Therefore the output of this binary weight as decoded by the ladder adder causes a trial voltage of half the full scale value, or 1.5 volt. For subsequent times the decision is made whether the analog input is greater or less than half scale value of the last reference voltage.

Table 3-22. Comparison of Data Frequencies as a Function of Aperture and Sampling Times

Bit Rate (bits/sec)	Aperture Time (in sec)	Frequency as a Function of Aperture Time (cps)	Main Frame Data Sampling Rate Samples/sec	Frequency as a Function of Sampling Rate (cps)
4096	$1.71 \times 10^{-3}$	8.30	9.12	3.65
2048	$3.42 \times 10^{-3}$	4.25	4.52	1.82
1024	$6.84 \times 10^{-3}$	2.12	2.26	0.92
128	$54.72 \times 10^{-3}$	0.26	0.28	0.12

Note:

1. Frequency of the sine wave signal with average aperture error less than 1/2 of quantization error (7 bits)
2. In order to reconstruct the sine wave signal the sampling rate must be greater than 2.0 times that of the highest signal frequency; 2.5 is assumed above

Table 3-23. Truth Table for Successive Approximation  
Analog-to-Digital Converter

Flip-Flop	State	Logic Timing						
		$T_1$	$T_2$	$T_3$	$T_4$	$T_5$	$T_6$	$T_7$
$a_1$	1	$T_1$						
	0		$T_2 V_c$					
$a_2$	1		$T_2$					
	0	$T_1$		$T_3 V_c$				
$a_3$	1			$T_3$				
	0	$T_1$			$T_4 V_c$			
$a_4$	1				$T_4$			
	0	$T_1$				$T_5 V_c$		
$a_5$	1					$T_5$		
	0	$T_1$					$T_6 V_c$	
$a_6$	1						$T_6$	
	0	$T_1$						$T_7 V_c$
$a_7$	1							$T_7$
	0	$T_1$						

c. Analog Multiplexer Design Approach

The function of analog multiplexing is to electrically connect each signal source in turn to the analog-to-digital connector while disconnecting all other signal sources. The multiplexer should be capable of performing the connections and disconnections as rapidly and accurately as possible in accordance with the required word rate and system accuracy. In general the analog multiplexer must fulfill the following requirements:

- 1) Accept input voltages from 0 to 3 volts
- 2) Withstand reasonable fault voltages
- 3) Cause minimum offset
- 4) Have a gate off and power off impedance greater than 10 megohms
- 5) Have minimum leakage currents to and from analog source
- 6) Cause minimum cross talk
- 7) Minimum power requirements
- 8) Simplicity of hardware
- 9) Maximum reliability
- 10) Reasonable failure modes

Several types of analog gates were analyzed and the results shown in Table 3-24.

Table 3-24. Analog Gates Comparison

	Fault Isolation	Offset Voltage	Input Impedance (power off and gate off)	Leakage Current	Cross Talk Error	Type of Gate Drive	Weight	Speed
1. Gated comparator for each input	high	none	high	low	none	DC	light	high
2. Gated differential amplifier	poor	small	high	low	small	DC	light	medium
3. Diode	high	high	poor	high	medium	DC	light	medium
4. Bright switches								
a) transformer coupled	high	low	high	low	small	AC	high	medium
b) capacitor coupled	poor	low	high	low	small	AC	medium	medium
c) isolated power supply for multiplexer	high	low	high	low	small	DC	medium	medium
5. Field effect transistors switcher								
a) metal oxide silicon (enhancement type)	high	none	high	low	small	DC	light	medium
b) standard type	poor	none	poor	low	small	DC	light	medium



Based on the information listed in this table the metal oxide silicon type is favored over the others listed. The metal oxide silicon provides very high fault mode protection and low DC drive requirements.

d. Capsule Data Buffer Memory Design Approach

The capsule data is a non-return-to-zero serial train of coded data at a rate of 10 bits per second. Since the data rate is not compatible with the telemetry bit rate, the buffer storage is required in order to intermix capsule data with engineering data (Format C). Two - 448 bit storages are used for each capsule data line. While one buffer is accepting data from the capsule, the other will be read out at the commanded telemetry bit rate. If the read out rate is faster than the storing rate (10 bits/sec) zero's will be read out. At the lowest telemetry bit rate (128 bits/sec) the capsule data will be sampled on a duty cycle basis. The proposed buffer consists of coincident current memory (16 x 28) and its associated drivers. The advantage of this approach is low weight and power consumption because of its low duty cycle. The use of shift registers is precluded for this size storage capacity since the equipment complexity increases linearly with the number of bits as compared to the square root increase using a matrix memory.

e. PN Code Generator Design Approach

The PN code generator consists of a six-bit shift register and exclusive-or circuit whose output is shifted into the first bit register. By this technique  $2^n - 1$  selection states (63) will be obtained.

By selecting (and'ing) the output of the six register (flip-flop), the word and bit sync signals are generated. The use of core-shift register is precluded because of its high average power consumption at the high bit rate. Integrated flip-flop circuits appear to provide the simplest configuration with the requirements of low power.

f. Programmer and Logic Design Approach

A general design consideration for logic operation is the

merits of synchronous or clocked logic versus nonsynchronous or "ripple" type. In the asynchronous method of counting, pulses to each flip-flop are provided by differentiating the change of state. This method has disadvantages in that deterioration of rise and fall times or amplitude of any flip-flop output in the count down chain can prevent the next stage from being properly triggered.

Additionally the propagation delays in the count down chain may in some instances be critical. Synchronous logic is based upon using the flip-flop states to control logic gates which are sampled by a clock. Consequently the change of state characteristics are less critical, therefore this latter approach is favored.

### 2.3.2 Buffer Storage Unit

#### a. Requirements

The buffer memory provides storage of 115 K bits of data. This data is written into and read out in a serial fashion at bit rates ranging from 128 to 4096 bits/sec.

#### b. Memory Organization

Several methods of organizing the memory have been considered in attempting to optimize the design relative to the requirements of low weight and power and high reliability for the Voyager program. While it is possible to operate a random access memory in a sequential mode by using a counting address register, this results in a considerably higher semiconductor count than if magnetic counting address circuits are used. Therefore, such magnetic ring counters have been chosen for accessing the memory plane.

This method of operation has been used in the past several years by TRW Systems in such programs as Vela and Pioneer with success.

Although the requirements for the memory are for bit-serial input and output, it would be highly inefficient to operate the magnetics in that manner. Such an organization, accessing one bit at a time, would

involve a very extensive drive system, and operating power considerably higher than if a number of bits were accessed in parallel. Since it is impractical to link all the cores of a  $10^5$  bit capacity memory with a single sense winding or digit winding, multiple circuits for those functions are required in any case. In the proposed design, 12 matrices are used, with slightly over 10,000 cores within each. Using a time-staggered drive, excellent signal to noise ratio is obtainable with this size matrix, and the DC resistance and inductance of the digit winding is not excessive.

Serial to parallel conversion of input data is obtained by applying the incoming data to a 13 stage flip-flop register which operates as a shift register. The extra stage is used as a "flag" bit. Initially, the first of these flip-flops is forced to the binary "ONE" state, while all other stages are forced to the binary "ZERO" condition. Each clock pulse then shifts the data, and on the 12th clock pulse, the flag bit reaches the 13th stage. This activates the memory, storing all 12 data bits in parallel, after which the input register is again cleared as before.

In the read/restore mode, each of the 12 matrices provides one bit of data in parallel, and after the restore action, clock pulses shift the data through the output register to provide bit-serial interface format.

The diagram of Figure 3-48 shows the organization of a sequential core memory driven by transistor switch ring drivers. The storage consists of 12 identical matrices, each having 104 columns and 99 rows of driven cores. Thus 115,000 bits of storage are provided.

During the read phase operations the two half select currents in the X and Y axes of the drive select one core in each of the ten matrix planes and the resulting sense signal is amplified by sense amplifiers and transferred to a 12 place flip-flop output register.

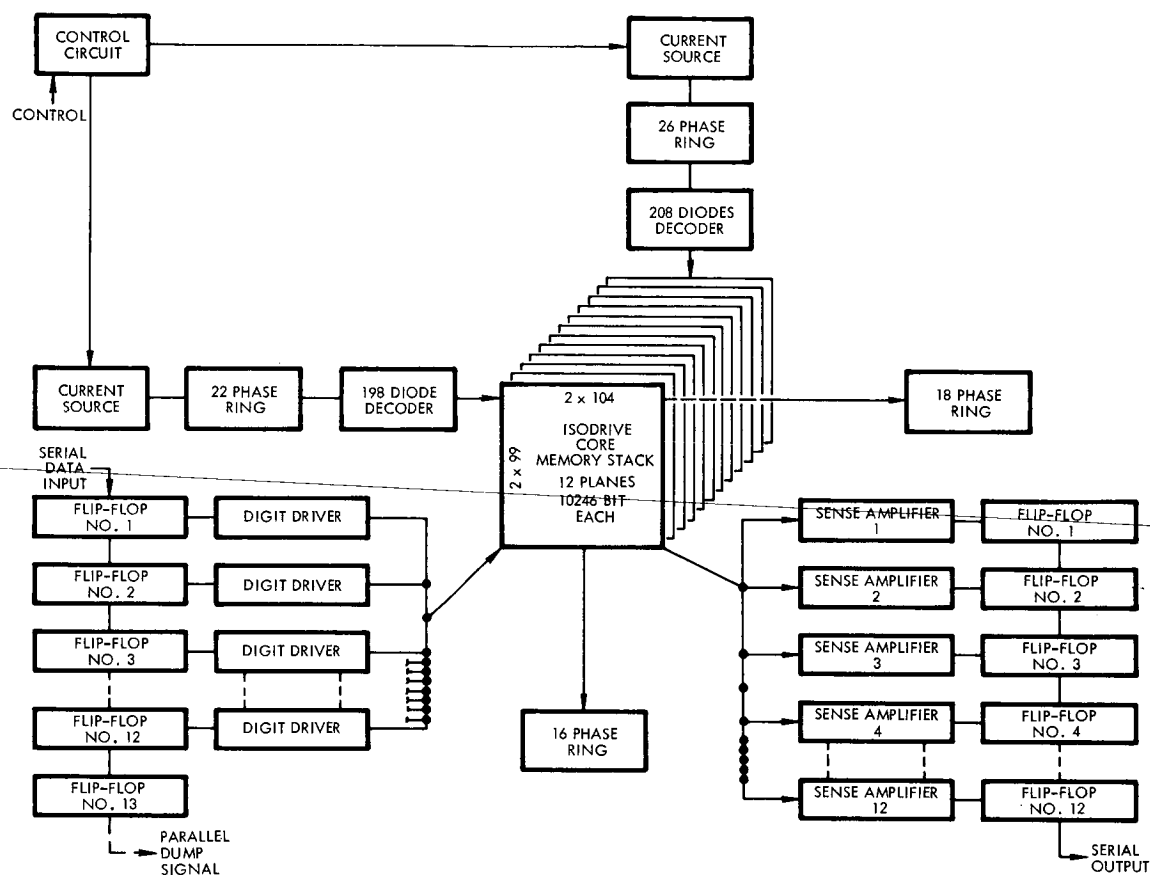


Figure 3-48. Simplified Block Diagram of Core Memory

During the write phase of operation the transistors are connected to provide a current in the opposite direction through the stack by means of a second set of current stabilizers, thus providing the required conditions for writing new data into the accessed bit. During this write beat, the data input lines to the memory control a set of digit drivers which operate individually on those matrices where the data to be written is a binary zero.

The core storage matrix contains four wires through each core: X, Y, sense, and digit. For optimum reliability a continuous wiring technique is used in stringing the X and Y drive lines. As a result, more than 7,000 soldered joints are eliminated. This method has been used extensively and experience has shown that higher reliability and greater tolerance to high level shock and vibration results.

The use of a coincident current organization of the memory permits a minimum number of semiconductors with resulting high reliability. To provide substantial design margin for the Voyager environment, the isodrive type memory core is used. This core is superior to any other ferrite storage core presently available. It has a lower temperature coefficient than lithium types, and far greater temperature tolerance than conventional magnesium manganese cores. Even more important for the memory the isodrive core has a considerably better squareness ratio over the entire temperature range from -55 to 100°C than any other core exhibits at midrange temperature. This increased squareness ratio provides greater operating margins for the system since considerably greater degradation of other component parameters such as drifts in semiconductors, resistors, etc., can be tolerated without memory error.

### 2.3.3 Tape Recorder

#### a. General

The following is a sample implementation of a tape recorder based on preliminary investigations to show feasibility of meeting the bulk storage requirements and not as a final decision on implementation.

The basic input/output requirements and storage capacity dictate how the tape recorder system must be implemented. The input/output serial data requirements are:

Input data rate:	163,812 bits/sec
Output data rate:	1) 4096 bits/sec 2) 2048 bits/sec 3) 1024 bits/sec
Word format:	*7/bits word
Bit storage:	1 x 10 <sup>8</sup> bits

The output data must be synchronized to the spacecraft stable clock.

b. Record/Playback Configuration

Based on these requirements, a review of the parameters of satellite recorders which are available today, and discussions with tape recorder manufacturers (Ampex, Consolidated Electrodynamics, Kinellogic, R. M. Parsons, Lockheed Electric, Raymond Engineering, and RCA-AED), the following basic guide rules for developing a representative tape recorder unit were chosen. This data does not represent absolute limits but rather levels which are conservative, proven, and available in off-the-shelf units.

Tape length	1000 feet
Tape speed	Low limit: 0.1 in. /sec High limit: 30 in. /sec
Packing density	Multiple tracks: 1000 bits/sec Single track: 2000 bits/sec
Write/read ratio	100:1
Speed change for a single motor	4:1

---

\*The video word is 6 bits, but since the tape recorder is not concerned with the word length and word sync for 7-bit words is available for both the write and read modes, it was decided that a 7-bit word would be most convenient.

After carefully reviewing several configurations it was finally decided that a reasonable set of compromise parameters for a sample implementation would be:

Data tracks	7
Clock track	1
Data gap track	1
Packing density per track	1200 bits/in.
Tape length	1200 ft
Tape speed	
Write Mode:	19.5 in. /sec
Read Mode:	1) 0.4876 in. /sec
	2) 0.2438 in. /sec
	3) 0.1219 in. /sec
Write/read ratio	
Read Mode:	1) 40:1
	2) 80:1
	3) 160:1

A comparison of these parameters with the previous list of idealized parameters will show the only major deviation to be in the write/read ratio. This number cannot be reduced without changing the system requirements, since, in a serial input/output system of the type being discussed, the system design parameters dictate the ratio, not the machine design. The numbers chosen reflect the best compromise of design parameters as they exist today for state-of-the-art design. Considering that these parameters are acceptable, certain approximations can be made concerning the size, weight, and power requirements based on machines presently being built either for satellite use or in connection with design studies of satellite recorders. The approximations are:

Size: 350 in<sup>3</sup>  
(roughly 9 x 9 x 4.25)

Weight: 12-15 pounds

Power: Write Mode: 10-15 watts  
Read Mode: 5 watts

The use of integrated circuits wherever possible will help reduce the volume and weight. Integrated circuits can be used for flip-flops, gates, and read amplifiers.

Write Mode. The serial non-return-to-zero input data is shifted into a 7-bit flip-flop register for parallel transfer to the write amplifiers. The data is transferred to the tape via the write amplifiers under the control of the word clock. This requires three inputs from the spacecraft system, a data bit signal, a word clock, and a bit clock. Recording the write clock on tape provides a synchronizing signal during the playback mode.

One consideration during the write mode would be to use phase shifted clock for writing data so that a clock which occurs in the center of a data bit is stored instead of a clock in phase synchronization with the data. This will allow easy implementation of a strobe pulse for reading data out of the read amplifiers during the read function.

Read Mode (Synchronization Technique). To meet the data output synchronization between tape recorder data and the spacecraft clock requirements, a servo loop must be used in the read mode to control the rotor speed, hence the tape speed. Units have been designed using hysteresis synchronous motors (without servo control) which demonstrated  $\pm 0.1$  per cent tape speed control. On this basis, considering the use of a phase lock servo system, a tape speed control better than this, which will limit the accumulation of speed variation to a period of a few seconds, appears feasible. Therefore, a system which will allow a time displacement of approximately  $\pm 7$  bits on a bit-



to-bit basis between the tape recorder and the system clock, assuming the servo uses the spacecraft clock as a reference for error generation, should be more than feasible.

Examining Figure 3-49, it can be seen that a plus and minus one word or plus and minus 7-bit variation is provided in the sample implementation. Data is "read" into one of the three buffer registers under the control of a read-in pulse. The pulse is generated from the tape recorder clock, which was recorded at the same time as the data. The leading edge of the tape recorder clock is used, with a delay technique, to produce a read-in pulse which strobes the data out of the read amplifiers during the center of the read bit period. This reduces the problem of noise as well as limiting the read-in time to the minimum possible for reliable operation. A divide-by-three counter is used to read-in the data to the correct buffer in a count sequence.

The readout of the data is accomplished by use of the spacecraft clock and a divide-by-three counter. A spacecraft word clock and bit clock are combined to produce seven shift pulses via the divide-by-three counter to read-out the correct buffers in a count sequence.

An output gate (and/or) is used to combine the buffer outputs in the correct sequence to produce the reassembled serial data.

Note that no effort is made to synchronize the read-in/read-out logic. This is accomplished by the servo system and will be discussed in the next section.

Speed Control. The operational description of the read/write block diagram (Figure 3-50) shows that under ideal operating conditions synchronization should be between the start of the first bit of a word being read out, to the parallel read-in pulse for the information being read-off of the tape. In considering this condition, it can be seen that one of the reference points discussed can vary plus and minus 7 bits before improper operation occurs. Figure 3-49 is a timing diagram showing the idealized conditions.

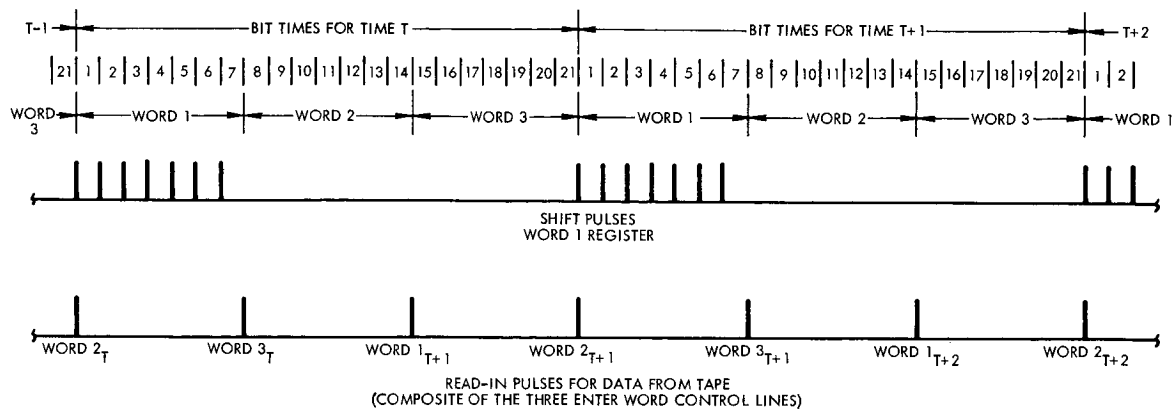


Figure 3-49. Timing Diagram

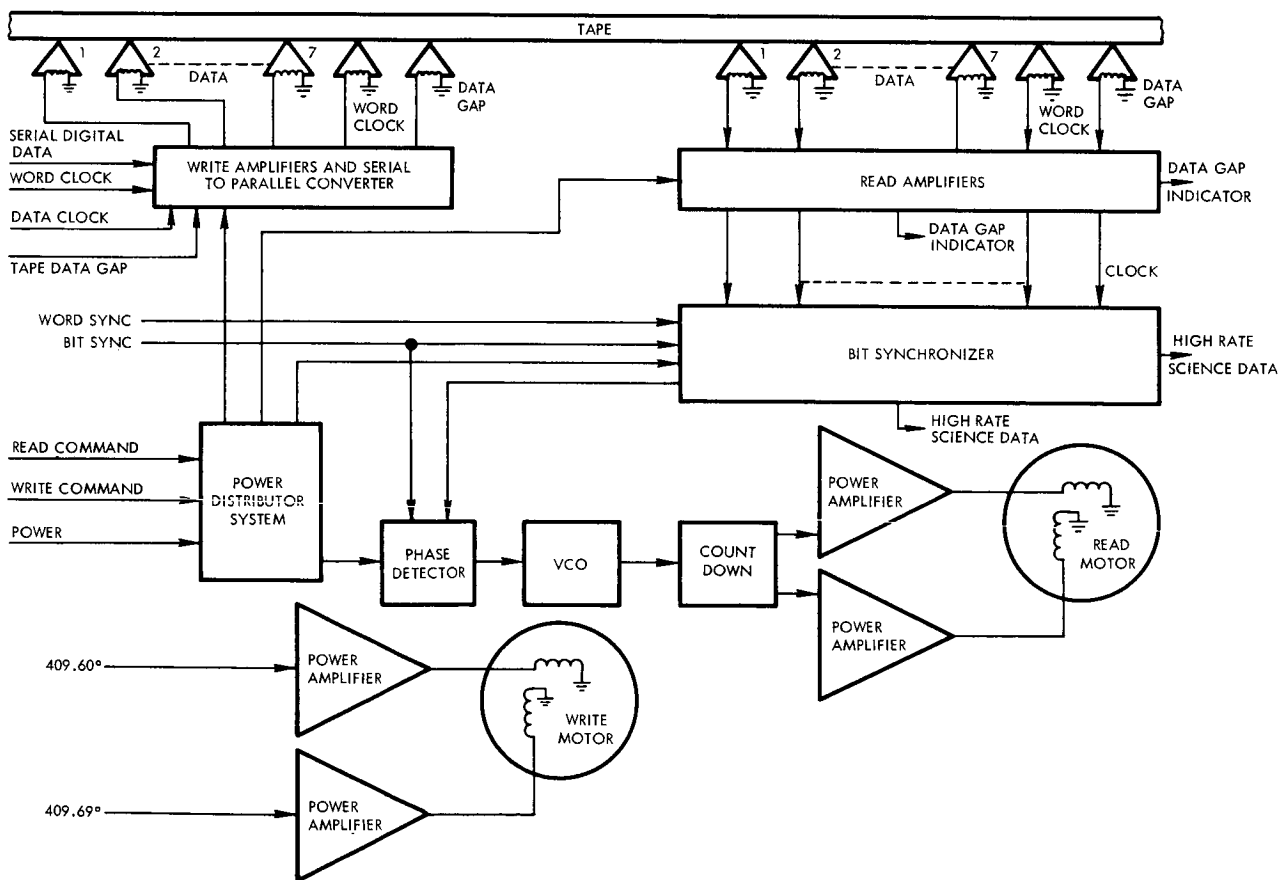


Figure 3-50. Read/Write Block Diagram

If the word 1 bit 1 shift pulse is used as a toggle input to one flip-flop and the read-in word 2 pulse is used as a toggle input to a second flip-flop, the outputs of these two flip-flops could be used as inputs to a phase detector to generate a DC-error signal which would represent the time positional error of the tape. This DC error could then be used as an input to a variable controlled oscillator (VCO) to develop a frequency change. The VCO output is shaped into a square wave and counted down so as to produce two 400 cps square waves which are time displaced by 90 electrical degrees. These signals via power amplifiers are applied to the two windings of a hysteresis motor. As phase variations which deviate from 180 electrical degrees develop between the output of the toggle flip-flops, the motor speed will be altered to bring the phase shift back into the correction 180-degree relationship. Figure 3-51 is a block diagram of the technique described.

At start up a continuous change will be in the error signal as the system approaches the phase lock condition. The design will be implemented so that the DC error voltage will be narrow enough, representing about  $400 \pm 1$  cps, so that the motor will approach the designed speed. As the motor approaches the phase lock condition, the servo control loop will come out of saturation, taking over control of the motor speed.

Once the servo loop is in control, the correct time relationship will exist between the spacecraft read-out clock and the tape

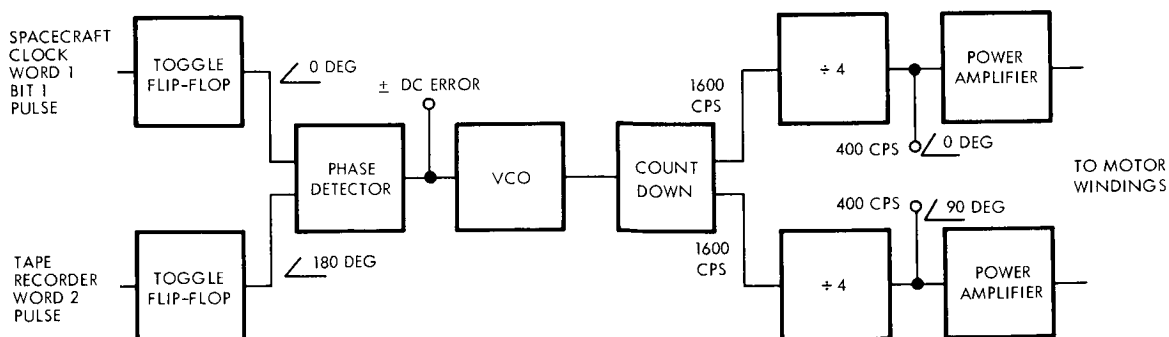


Figure 3-51. Motor Servo System

recorder read-in clock. Therefore, no special start logic in the data buffering logic is needed.

The system examination has been based on the 4096 bits/sec data output rate. At the other output rates the word jitter created by erratic tape movement will increase. However, the servo loop recovery time requirements will decrease because of the lower output data rates. No particular problem is anticipated due to the reduced data rates.

Speed Change. Speed change as presently envisioned will be accomplished by logically changing the motor input synchronizing frequency and the spacecraft data clock inputs during the read mode. This will be accomplished under the control of the spacecraft command system. The three speed read-back requirement will necessitate a development effort to determine whether it will be more optimum to use a single motor that operates at three speeds, or a single motor that operates at a single speed with a mechanical switching arrangement to obtain the 3 speeds, or possibly the need for multiple motors.

Erase Technique. Several erase techniques are possible. The use of a permanent magnet or an AC erase head are under study. Also being studied is erasing by simply writing over previously recorded data. The latter approach appears the most desirable since it does not need any erase circuitry. This technique is preferred but will be investigated to assure an adequate signal-to-noise ratio.

Command System. With the planned use of redundancy a simple command system which utilizes the tape recorder status information to automatically sequence the tape recorders is being considered. The command arrangement will also allow individual control of either tape recorder unit.

Data Gap Indicator. The purpose of the data gap indicator is to detect the absence of data during the playback mode to allow insertion of other data in the output. The technique planned is to utilize a separate "trash" or "narrative" track to indicate when data is present

and when data is absent. The circuit used will be designed to ignore a momentary dropout. The signal output will be a discrete where a low level indicates the presence of data and a high level the absence of data.

Further study is required to devise a simpler method requiring less hardware.

b. Transport

Reel Configuration. Several reel configurations are available. After considering the advantages and disadvantages, a reel-to-reel inline technique is considered the best choice.

Reel-to-Reel Inline Configuration. This is the simplest system, is the best-known and the easiest to implement. It, however, does not produce minimum induced angular momentum. It also does not provide the simplest technique for negator spring tape tensioning. It is the simplest technique for isoelastic drive technique. A simple mounting base provides rigid support.

Reel-to-Reel, Coaxial, Counter Rotating. This method inherently produces the minimum induced angular momentum without compensation. It is not simple from a tape guiding standpoint. It lends itself to a negator spring tensioning technique but is not simple for an isoelastic drive system.

Mounting is complex since a single support results in a weighty cantilevered system. The technique around this problem involves the use of two mounting plates with the reels mounted between the plates. This is a more complex technique involving more sophisticated machining and assembly techniques.

Endless Loop and Loop Bin Type. Because of the large storage capacity the amount of tape required exceeds the amount which is normally considered to be within the design guideline of an endless loop or a loop bin machine.

c. Tensioning System

Negator Springs. Generally in a reel-to-reel tape recorder where power is a premium, negator springs are used to maintain tension. Thus, energy is conserved. This approach is used because during half of a tape cycle the tensioning system acts as a source of energy and during the other half cycle the tensioning system acts as a load (when the negators are storing energy). In actual practice there is very little saving in power during the portion of a cycle where the negator spring is acting as an energy source. This is because the motor must be designed to handle the worst case load and operating the motor below its designed load level does not reduce the input power to a noticeable degree.

The tape tension characteristic produced by a negator spring system is not constant as ultimately desired. Normally the tension varies in the order of 30 per cent over a complete cycle of operation.

Endless Loop. The endless loop system produces a tape tension which varies in an irregular fashion because of reflected load variations as individual loops in the endless loop pack are shortened. Lubrication is used to minimize the friction in the tape pack and thus to reduce the peak load variations as well as the average load requirements. This, however, creates the problem of lubricant build-up at the heads. In addition, differential variations of tape tension across the tape width causes a skew problem which must also be isolated from the head area during record and playback of the unit.

Endless loop systems, however, have an advantage of producing very low components of momentum into the spacecraft. Small data handling units have been successfully used in spacecraft systems where tape lengths of 300 feet or less were required.

This technique is not recommended for Voyager.

Isoelastic Drive. This technique has several advantages over those previously mentioned and is recommended as a result of the preliminary review for the following reasons:

- 1) It is a simple technique. A belt is passed over both reels and the belt driven by differential pulleys. A spring-loaded idler is used to maintain correct belt tension.
- 2) The tape tension across the read and write heads, over a complete cycle of operation, can be controlled to within approximately 10 per cent of the desired value.
- 3) It is best suited to an in-line reel-to-reel configuration which enhances the over-all simplicity of the transport.

It is found that there is excessive jitter problems with the basic tape handling technique chosen, a differential capstan drive technique over the read and write head region can be used to reduce the jitter to a lower level. At this time use of differential capstans is not anticipated.

Incremental Drive. One method which cannot be considered conservative or proven for satellite recorders is the incremental drive technique. This method will be investigated in detail to determine its relative merits. At the moment, it appears to have at least one questionable area, angular momentum disturbances.

Guide Technique. There are several tape guiding techniques. At this time, no particular method has been chosen. The life requirements in terms of tape wear can be met by use of either rolling or stationary guides. Crown rollers have been used successfully and do reduce edge wear to a minimum. Fixed guides with various techniques of containing the tape have been considered but further study is required before a final decision is made.

Speed Change. Speed variation between the read and write modes is so wide as to dictate a two motor system. The coupling of the two motors to the drive system will be accomplished via a Mylar belt transmission system. Whether this will be a belt differential or a clutch operated linkage has not yet been decided.

In addition to the read/write speed change is the three-speed readout requirement. The method of accomplishing this requirement is presently being investigated. The tradeoff of an AC servo motor versus a hysteresis synchronous motor in the read mode is being studied. The selected approach, consistent with the conservative design, is to use a single motor to obtain the 4:1 speed range required, using a servo loop in conjunction with a hysteresis synchronous motor.

Package Arrangement. In review of transports developed to date for satellite use, a rectangular package has been chosen as most desirable although the strength, hence weight, of a rectangular package which is pressurized must be slightly higher than the dome shaped enclosure. Better utilization of internal space is feasible in the rectangular configuration as well as the space within the spacecraft surrounding the package. This configuration is also well-suited for the in-line reel-to-reel transport configuration presently being considered.



## IV. POWER AND CONTROL SUBSYSTEM DESIGN CONSIDERATIONS

### 1. STABILIZATION AND CONTROL SUBSYSTEM

The stabilization and control subsystem (SCS) described in Volume 2 represents the result of a series of tradeoff studies which considered a variety of system design concepts and mechanization alternatives. The conceptual studies were directed toward defining the simplest and most reliable system to accomplish the required stabilization tasks considering the development status of components, the performance requirements, availability of alternate modes of operation, and possible developmental difficulties. These studies resulted in the definition of a subsystem very similar to the Mariner C implementation.

The following sections discuss these tradeoff studies as follows:

1) system requirements and gross tradeoffs, 2) functional descriptions of alternate mechanizations, 3) the analytical studies which contributed to the configuration selection, and 4) the implementation tradeoffs which take into account the various approaches available for celestial sensing, inertial sensing, control torque generation, and electronic circuit design.

#### 1.1 System Requirements and Gross Tradeoffs

Many of the Voyager mission requirements are similar to those for Mariner C. The cruise and reorientation requirements, for example, are very similar although other requirements, such as capsule separation, orbit injection, and planet-oriented instrument pointing, are peculiar to Voyager. The orbit injection requirement, although not unlike a mid-course maneuver, imposes the necessity for attitude control during either a long thrusting period if a bipropellant engine is used, or the necessity to accommodate large thrust if a solid engine is used. It is desired to point the planet-oriented package to an accuracy of 0.5 deg relative to Mars, and this imposes the most severe accuracy requirement on the stabilization and control subsystem. The requirement for POP pointing introduces consideration of the use of Mars sensors and of SCS modes to minimize POP gimbal travel or the number of gimbals required.

### 1.1.1 Attitude References

In over-all system definition the establishment of easily acquired attitude references that are useful throughout the mission is a prime objective. This permits communications antenna and POP orientation commands to be body-referenced with minimum complexity. During the study, consideration was given to the use of earth-canopus and sun-Mars as well as sun-canopus references, and the latter were selected because of the overall simplicity they provide. This simplicity reflects into reduced requirements on the spacecraft sequencer as well as the stabilization and control subsystem. Spacecraft configuration C, as discussed in Volume 4, features a large body-fixed communications antenna and an earth-canopus reference is most suitable for this configuration.

Attitude reference requirements imposed by reorientation for velocity corrections and capsule separation can be met by using gyroscopes or aspect sun sensors. Gyros offer both flexibility and a straightforward design using well known techniques and components. In addition, gyroscopic reference for reorientation offers backup modes of inertial control. The use of aspect sun sensors, although possibly simpler, is not as well established and the devices themselves have not, as yet, been used for this application. The gyroscopic reference can be implemented with one single degree of freedom rate integrating gyro on each control axis. Each instrument can be used as a rate or an attitude error sensor by incorporating a caging loop. By maneuvering one axis at a time, satisfactory reorientation accuracy can be achieved with a very simple system mechanization.

The mission specification includes a requirement to verify the spacecraft attitude before capsule separation or midcourse propulsion is initiated. The verification can make use of the gyros in a rate mode during turns and integrating their outputs to measure the angles traversed for ground verification. Another method, which is not as accurate, is to preposition the high-gain antenna so that the beam will intersect earth when the spacecraft is in the desired orientation. If communication is established the attitude will be verified to an accuracy of twice the 3-db beamwidth, or about  $\pm 5$  deg. The latter approach was tentatively selected because it allows

the verification function to be realized without additional components and because, in general, the attitude error will be large (and therefore detectable by the antenna) if a malfunction occurs.

#### 1.1.2 Control Torque Sources

Control torques for periods other than velocity corrections can be generated by reaction control devices, reaction wheels, or solar vanes. Reaction control devices, such as gas thrusters, have received extensive application and are well understood. Their use for the Voyager mission presents no problems. Reaction wheels offer no special advantages since they are most advantageous for applications where there are significant cyclical disturbances; and the principal disturbances for the Voyager mission appear to be of a secular nature. Solar vane systems appear to be best suited as trim mechanisms because of their low response bandwidth. As trim devices, the solar vanes might be used in parallel with the reaction control system, as on Mariner C. They were not selected for Voyager because the saving in control fuel that they might provide can be effected more reliably with a heated-gas reaction control system.

Control torques during periods of engine thrusting can be generated by various control schemes which rotate or translate the thrust vector. Thrust vector rotation can be accomplished for liquid fuelled motors by gimbaling the thrust chamber or deflecting the exhaust stream by jet vanes and for solid fuelled motors by gimbaling the exhaust nozzle or by liquid injection thrust vector control. Thrust vector translation can be realized by a linkage which is moved by linear actuators. The preferred spacecraft configuration employs a monopropellant liquid fuel midcourse correction motor and a solid fuel motor for retropropulsion. Jet vanes were chosen for the monopropellant engine as in Mariner C since the selected motor for Voyager is similar. Liquid injection selected for the solid motor thrust control because it is a proven technique and minimizes development risks for the motor. Details of the thrust vector control tradeoffs are presented in Section VII.

### 1.1.3 Control Modes

The Voyager mission requires that the SCS provide several distinct modes of operation. These control modes make use of various combinations of sensors and actuators, together with some more subtle variations of implementation. For example, the short term stability requirements imposed on the SCS by the photographic payload during the orbit phase must be integrated with over-all requirements to provide minimum complexity. These considerations influence the selection of control thrust level and control modulation technique. The following sections examine these modes in the light of the tradeoffs which comprise the configuration selection process. Performance and reliability for the various alternatives are compared.

## 1.2 Functional Modes and Alternate Mechanizations

### 1.2.1 Cruise Mode

Since the greatest percentage of the Voyager mission time for both the transit and orbital phases is spent in the cruise mode (>98 percent), it is essential that this mode combine the maximum possible reliability with the minimum control fuel consumption. Detailed analyses were conducted to ensure that the thrust levels and firing times provide satisfactory limit cycle characteristics under disturbance free cruise conditions and in the presence of worse case disturbances. These analyses are discussed in detail in Sections 1 and 2 of Appendix E.

The design conditions selected for the cruise mode were based on Mariner C characteristics and reflect the pointing accuracy requirements and control fuel consumption considerations. A nominal limit cycle amplitude of  $\pm 0.5$  degree and a limit cycle rate (for the transit configuration prior to capsule separation) of 1 deg/hr are consistent with accuracy and weight requirements and were chosen as design objectives. The SCS parameters which provide the transit limit cycle rate result in a limit cycle rate of about 5 deg/hr in orbit. This in-orbit value is compatible with the stability requirements imposed by image motion considerations during photographic operations. Error analyses showed the need to use

a limit cycle amplitude of  $\pm 0.25$  degree for flight capsule separation and during photographic operation, as dictated by photographic coverage requirements.

Several configurations were studied for the cruise mode mechanization. Primary consideration was given to passive stabilization schemes. The configurations included:

- a) An on-off controller driven by lead compensated signals from the celestial reference sensors.
- b) A fixed-pulse controller driven by the signals from the celestial sensors.
- c) A pulse-modulated controller driven by signals from the celestial sensors.

Efficient limit cycle operation with an on-off controller requires large lead-lag ratios and thus entails large gain reduction. Because of the relative complexity and potential noise problem thus imposed, this approach is not used for the cruise mode.

Fixed-pulse controllers can provide acceptable limit cycle performance in the absence of disturbances. When disturbances are present, however, the control logic required to reacquire and maintain the nominal limit cycle becomes relatively complex. For this reason, fixed pulse controllers were eliminated from detailed consideration.

a. Pulse Modulation Techniques

Three control thrust pulse modulation techniques were considered:

- Pulse-width modulation (PWM)
- Pulse frequency modulation (PFM)
- Pulse-width, pulse frequency modulation (PWPFM)

PWM is well suited for digital computation but if used only with attitude feedback, it does not damp the double integration vehicle dynamics, and thus requires compensation in the control law. In many applications this may be easy to obtain (e. g. attitude differencing in a digital computer),

and performance requirements may be simple enough that pulse width modulation is adequate. Since PWM is not compatible with the desire to use passive stabilization techniques for cruise, however, it was not considered further.

PFM offers an advantage over PWM in that the modulator mechanisms can be realized by relatively simple analog circuitry. PFM techniques have been shown to result in efficient limit cycle operation. As with PWM, lead compensation is required in the control law to stabilize the spacecraft. This compensation can be obtained by using lead networks operating on the output of the attitude reference sensor. Noise amplification by a lead network can be reduced by the use of integral pulse frequency modulation which introduces an additional integration into the signal path. Integral pulse frequency modulation control has an additional advantage in that analytical procedures have been developed for design.

The additional degree of control freedom inherent in PWPFM systems promises greater control capacity than is available with either PWM or PFM. For example, it may allow optimum control (in some sense) to be approached more readily. A significant advantage of PWPFM is that it can stabilize the open-loop-unstable, double integration dynamics without additional compensation. This is readily observed from the derived rate increment stabilization scheme in which a low pass filter feedback loop around a bang-bang controller functionally constitutes a PWPF modulator and, combined with sensed attitude feedback, results in a stable system. The derived rate increment implementation of PWPFM has been successfully applied to the Ranger and Mariner spacecraft. Because of the simple mechanization and previous successful experience with derived rate increment control, it has been selected for Voyager.

b. Cruise Mode Backup

Providing some form of backup for at least the cruise mode of operation is mandatory. It is also desired to maintain attitude reference in orbit during solar eclipse and in the event that reflected light from Mars causes the Canopus sensor shutter to close temporarily. A straightforward solution to this problem can be implemented by using attitude gyros in place

of the celestial reference sensors. The gyros will provide an inertial attitude hold mode which can also be used at other times in the mission, as discussed later. This backup cruise mode can be initiated automatically by the sun acquisition gate sensor during solar eclipse. Backup roll axis control can be initiated automatically by the star acquisition gate. Similar operation could be provided for the alternate earth-Canopus oriented configuration.

#### 1.2.2 Acquisition Mode

Constraints and objectives of the acquisition mode were to size the system such that:

- 1) Minimum fuel is consumed in nulling the initial spacecraft angular momentum.
- 2) Acquisition times are compatible with the power subsystem and thermal control requirements.
- 3) Hardware requirements and special switching are minimized.
- 4) An acceptable terminal state is established for transition to the cruise mode.
- 5) Alternative but degraded acquisition performance can be realized with gyros inoperative.

The mechanizations which were considered for the normal operation acquisition mode include:

- 1) Sun-Canopus position feedback with rate gyros.
- 2) Lead-lag compensation of the sun-Canopus sensors.
- 3) Sun-Canopus position reference with derived rate feedback for stabilization.

The primary factor which determined the selection of an acquisition configuration was the requirement to null large tip-off rates about each axis following the initial boost and capsule separation phases of the Mars trajectory. Although the magnitude of these rates is largely dependent on

the separation mechanism employed, typical maximum values are up to 3 deg/sec. This value was assumed for the Voyager acquisition studies. In addition, calibration of the magnetometer may require accurate control of rates about one or more control axes.

Lead-lag compensation of the sun and Canopus sensor outputs was not selected for the normal operation acquisition mode because of the difficulty in accurately controlling the spacecraft angular rate. Because of the narrow field of view of the Canopus sensor ( $\pm 2$  degrees), roll rate sensing is required to properly control the roll axis rates. Since the coarse sun sensors exhibit a sinusoidal variation of output as error is increased (zero output in the proper orientation), the rate information obtained from lead-lag compensation of the coarse sun sensor would indicate the wrong sign for pointing errors in excess of 90 degrees. This problem could be corrected by proper shaping of the sun sensor output; however, the added complexity of the shaping network and lead-lag compensation render this mechanization undesirable.

The normal acquisition mechanization which was selected uses three miniature rate-integrating gyros, coarse sun sensors, and the pneumatics system. The electronic switching amplifiers and derived rate feedback are employed during acquisition. The advantage of maintaining the derived rate feedback during acquisition is that a backup sun acquisition mode is automatically provided in case of gyro failure. Although preliminary analog computer studies of single-axis effects indicate a slight degradation in acquisition performance with derived rate feedback, the feasibility of this objective was established. Detailed three axis simulations must be conducted to ensure satisfactory performance and optimize system parameters (e.g., derived rate limit, time constant, etc.).

Because of the narrow field of view of the Canopus sensor and the possible tip-off rates (3 deg/sec), use of the roll gyro is included in normal Canopus acquisition. Provision has been made, however, for a ground-controlled incremental roll maneuver mode, such as is employed on Mariner C. This mode is identical to the roll axis reorientation mode



with the exception that the precision torquing current is controlled by fixed timers which results in a fixed incremental roll attitude change. In addition, provision can be made for direct control of the roll axis jets by ground initiated, timed commands. These modes provide backup control for Canopus acquisition and for the high gain antenna pointing.

The acquisition mode for the earth-Canopus oriented spacecraft would contain the features described above plus those necessary to acquire earth-pointing. Initial acquisition to the sun and Canopus is desirable since it is so readily mechanized. Earth acquisition would be mechanized by augmenting the maneuver sequence to provide a gyro-controlled turn to acquire earth.

### 1.2.3 Maneuver Mode

For the midcourse velocity correction, capsule separation, and de-boost phases, the desired spacecraft orientation is determined by ground computation, transmitted to the spacecraft, and stored in the CS and C before the maneuver. Gyro torquing current generators produce a precision current that will command the desired reorientation attitude. In the maneuver sequence a roll turn is made, followed by a pitch turn. In some cases a second roll turn may be required to enable the high-gain antenna to point to the earth. Following the reorientation maneuver, the desired attitude is maintained by the inertial attitude hold mode.

Consideration was given to the following control techniques for the reorientation mode:

- 1) Position gyro reference with derived rate feedback
- 2) Position plus rate gyro control
- 3) Lead-lag compensation of the position gyro.

System simplification was the primary factor leading to the selection of the technique for accomplishing the maneuver. Since the inertial attitude hold mode follows reorientation, the switching logic is simplified by using the derived rate feedback for the cruise, reorientation, and inertial attitude hold modes. Consequently, position gyro reference with derived rate feedback was selected for the normal operation reorientation mode.

#### 1.2.4 Inertial Attitude Hold Mode

The inertial attitude hold mode is required to maintain a desired attitude reference prior to midcourse and deboost thrusting and during capsule separation. In addition, roll attitude stabilization during midcourse velocity correction thrusting is achieved by the roll axis inertial hold mode. Failure of the cruise mode because of solar eclipse or loss of Canopus lock will also result in switching to the inertial attitude hold mode.

The maneuver and attitude hold mechanizations are identical with the exception that the torquing current generators are disconnected during the attitude hold operation. Position feedback is derived from the position gyros with stabilization obtained from derived rate feedback. This mechanization combines high reliability and performance due to the simplicity of the switching logic and the desirable limit cycle characteristics.

#### 1.2.5 Thrust Vector Control Mode

To satisfy the Voyager mission accuracy requirements for the midcourse velocity correction and deboost phases of the Mars trajectory, some form of thrust vector control is required. Studies of thrust vector control for the liquid propellant engines have considered the following system configurations:

- Use of cold gas
- Gimballed engine
- Lateral translation of the thrust nozzle  
(vehicle Configuration B only)
- Spin stabilization
- Jet vanes.

Some factors which led to the selection of the TVC configuration were disturbance torques caused by thrust misalignment and lateral center of gravity offsets which cause thrust offset angles.

Since the midcourse velocity correction employs a low thrust engine (50 pounds), attitude stabilization by the inertial attitude hold mode was considered. The disturbance torques resulting from  $3\sigma$  values of thrust

misalignment and center of gravity offsets, however, render this control scheme marginal for the pitch and yaw axes unless special high thrust jets are used. Roll attitude stabilization can be maintained by the roll axis inertial attitude hold mode (using the cold gas jets) and was selected as the normal midcourse TVC mode.

Because of its proven ability, simplicity, and reliability, jet vane TVC, similar to that employed on Mariner C, was selected for the pitch and yaw axes midcourse correction mode. Stabilization of the pitch and yaw axes is achieved by lead-lag compensation of the gyro attitude signals.

For the solid rocket TVC, consideration was given to the following configurations:

- 1) Spin stabilization about the spacecraft roll axis
- 2) Gimballed nozzle
- 3) Gimbal entire engine
- 4) Liquid injection
- 5) Gimballed monopropellant engines.

The tradeoff analysis of these approaches is described in Section VII.

Based on disturbance torque estimates and pointing accuracy requirements, the required spin rate for 1 above is 2.6 rad/sec. Since the resulting centrifugal acceleration (2.1 g) increases the required lateral structural loading and imposes additional requirements on appendages, it is considered undesirable to spin stabilize the spacecraft for control.

A liquid injection thrust vector control mechanization was selected for the pitch and yaw axis control during the deboost thrusting because of the proven performance (Minuteman, Polaris) and ease of checkout (see Section VII). Two liquid injectors are utilized for each control axis. Stabilization is achieved by lead-lag compensation of the position gyro signal.

Because of high engine thrust levels, center of mass uncertainties during deboost, and null errors in the TVC the roll disturbance torque level may exceed the normal inertial attitude hold control torque. As a result, a requirement may exist to increase the roll axis jet thrust level (e. g. by a separate jet pair operating from the cold gas system) during the deboost maneuver. This requirement will be re-evaluated later when the spacecraft geometry center of mass offsets and rocket motor characteristics are better defined. Worst-case analyses which have been conducted indicate that the thrust sizing for this operation are probably not unreasonable for cold gas. The derived rate feedback and on-off electronic switching amplifier used with the normal roll axis inertial hold mode are probably adequate for use with the high level gas jet system. As indicated in Section VII, the use of a hot gas bleed-off from the LITVC gas pressurization system was also considered for roll control. If required, this approach can provide high thrusts with small additional weight, but the cold gas approach appears more desirable at present.

### 1.3 Control System Analyses

This section summarizes the factors leading to the selection of the subsystem configuration and components. Detailed analyses of SCS operation are given in Section 2 of Appendix E.

#### 1.3.1 Pointing Error Analysis

Pointing requirements for the Voyager mission involve interaction between the SCS, the high-gain antenna, the POP, velocity corrections, and the flight capsule. The sources of error include the attitude reference errors, the articulated component drive errors, alignment errors, and SCS pointing errors. Several error analyses were made to define an acceptable attitude control limit cycle amplitude.

The high gain antenna must be pointed to within  $\pm 1.4$  degrees,  $3\sigma$ , to keep the earth within the 1 db points of the beam. The pointing requirement, reflected into a single-axis error, results in an allowable error of one degree.

The primary error sources are:

Attitude reference accuracy	$\pm 0.1$ deg, $3\sigma$
Limit cycle error	$\pm 0.499$ deg
Antenna drive program quantization	$\pm 0.5$ deg
Antenna drive dynamic error	$\pm 0.2$ deg, $3\sigma$
Antenna drive pickoff error	$\pm 0.15$ deg, $3\sigma$
Antenna boresight error	$\pm 0.2$ deg, $3\sigma$
Alignment (antenna to S/C reference)	$\pm 0.25$ deg, $3\sigma$

The RSS total of  $\pm 0.822$  degree, assuming that the limit cycle and program step contributions are  $3\sigma$  values, is well within the  $\pm 1$  degree requirement.

The Voyager mission guidelines states that the pointing accuracy required during velocity corrections is  $\pm 0.5$  deg,  $1\sigma$ . This requirement has been interpreted to apply to each of the two components of the total pointing error. Because of the short moment arm available for control of the solid motor, the errors produced by center of mass offsets are greater for this engine than for the monopropellant engine.

The primary sources of error during velocity corrections are:

Gyro torquing error	$\pm 0.2$ deg, $3\sigma$
Gyro alignment error	$\pm 0.1$ deg, $3\sigma$
Gyro drift error	$\pm 0.4$ deg, $3\sigma$
Limit cycle error	$\pm 0.34$ deg, $1\sigma$
TVC limit cycle error	$\pm 0.2$ deg, $3\sigma$
Control error from thrust misalignment	$\pm 0.5$ deg, $3\sigma$
Control error from c.m. offset	$\pm 1.1$ deg, $3\sigma$

The RSS total for the midcourse correction is  $\pm 0.55$  deg,  $1\sigma$  ; stemming largely from control error from c.m. offset. If the control deadband is reduced to  $\pm 0.25$  degree, the  $1\sigma$  error is 0.465 degree. A fine control deadband is therefore required to meet the velocity pointing requirements. Tight control over lateral c.m. offset must be exercised to assure the required 0.5 degree accuracy.

For the reorientation maneuver prior to capsule separation, the error sources are as shown below:

Gyro torquing error	$\pm 0.2$ deg, $3\sigma$
Gyro alignment error	$\pm 0.1$ deg, $3\sigma$
Gyro drift error	$\pm 0.4$ deg, $3\sigma$
Limit cycle error ( $\pm 0.5$ deg)	$\pm 0.499$ deg, $3\sigma$
Capsule to spacecraft alignment	$\pm 0.4$ deg, $3\sigma$

For a  $\pm 0.5$  degree limit cycle, the  $3\sigma$  error is 0.79 degree. If the control deadband is reduced to  $\pm 0.25$  degree, the  $3\sigma$  error is 0.66 degree. It is therefore necessary to switch to a fine control deadband to meet the capsule separation pointing accuracy requirement.

The POP pointing requirement of  $\pm 0.5$  degree,  $3\sigma$ , imposes the most stringent constraint on the SCS. For this case, the primary error sources are assumed to be:

1) Attitude reference accuracy	$\pm 0.1$ deg, $3\sigma$
2) Spacecraft limit cycle error	$\pm 0.249$ deg, $3\sigma$
3) Drive accuracy	$\pm 0.25$ deg, $3\sigma$
4) POP pointing sensor errors	$\pm 0.2$ deg, $3\sigma$
5) Camera boresight error	$\pm 0.05$ deg, $3\sigma$
6) Alignment of POP to spacecraft reference	$\pm 0.25$ deg, $3\sigma$

The RSS error of  $\pm 0.490$  degree,  $3\sigma$ , is within the requirement. As indicated above, the limit cycle error must be reduced to  $\pm 0.25$  degree during imaging operations to meet the POP pointing requirements.

For high gain antenna pointing and midcourse velocity corrections, a  $\pm 0.5$  degree limit cycle amplitude is probably acceptable. The POP, retropropulsion, and capsule separation pointing requirements can be met by decreasing the control deadband from 0.5 to 0.25 degree by command from the CS and C a short time before the maneuver or picture sequences begins. To minimize reaction control fuel consumption, it is desirable to provide two control deadbands, a wide range for normal cruise and a smaller range for precise pointing.

### 1.3.2 Cruise Mode

The normal cruise configuration employs sun-Canopus position reference with derived rate feedback around an on-off electronic switching amplifier. A block diagram of a single axis (pitch, roll, or yaw) cruise mode configuration is shown in Figure 4-1.

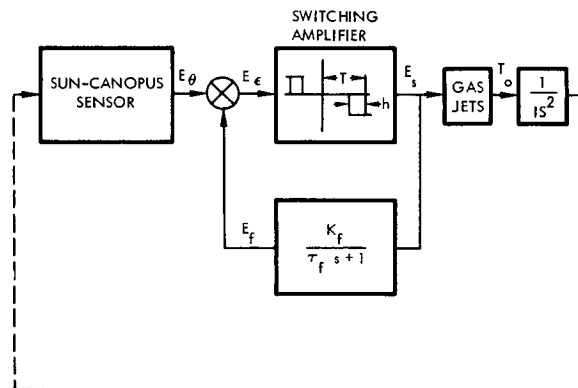


Figure 4-1. Cruise Mode Attitude Control System Block Diagram

in Figure 4-1,

- $E_s$  = Switching amplifier output voltage
- $E_f$  = High gain filter output
- $E_\theta$  = Sun-Canopus sensor output
- $E_\epsilon$  = Switching amplifier error input
- $T$  = Switching amplifier threshold
- $K_f$  = Filter gain

- $\tau_f$  = Filter time constant  
 $T_o$  = Gas jet torque output  
 $\theta$  = Spacecraft attitude  
 $h$  = Switching amplifier hysteresis.

Based on a 1 deg/hr limit cycle rate before capsule separation, the maximum limit cycle rate during Mars orbit is 5.2 deg/hr, well below the POP imaging limit of 20.6 deg/hr. In addition, the limit cycle rates chosen yield acceptable fuel consumption characteristics even in the presence of worst case disturbance torques. Based on these design criteria, the jet thrust and torque level were computed as 0.044 lb/nozzle and 0.83 ft-lb, respectively, using two jets to provide couples in normal operation. In the absence of disturbance torques, the maximum limit cycle fuel consumption for a 177-day transit period and an orbit lifetime of 6 months is approximately 6 pounds.

During the mission, the Voyager spacecraft experiences disturbances from external as well as internal sources. The major external sources of disturbance include torques resulting from solar radiation pressure and, when in Mars orbit, gravity gradient. Internal sources of disturbance are the result of reaction torques from rotating devices such as tape recorders and the POP. To maintain three-axis stabilization, the cruise mode attitude control system will remove the momentum imparted to the body by expending fuel. Based on a 6-month transit and a 6-month orbit life, the maximum fuel expenditure because of disturbance torques is estimated as

<u>Fuel (lb)</u>	<u>Disturbance Source</u>
1.5	Solar radiation pressure
1.21	Gravity gradient torques in Mars orbit
0.72	Reaction forces



The net result of the disturbance torques is to increase the maximum cruise mode fuel consumption from 6 to approximately 9.5 pounds. The maximum amplitude of disturbance torque was found to be approximately  $5 \times 10^{-4}$  ft-lb resulting from gravity gradient torques in orbit. A detailed analysis of the major disturbances expected on the Voyager spacecraft is given in Section 1, Appendix E.

### 1.3.3 Sun-Canopus Acquisition Mode

As discussed in Section 1.2.2, several mechanizations were considered for the sun and Canopus acquisition modes. The primary factors which determined the selection of an acquisition configuration were 1) nulling large initial rates about each axis following the boost and capsule separation phases of the Mars trajectory, 2) minimizing acquisition time and fuel consumption and 3) providing acceptable pointing errors and error rates for transition to the cruise mode.

The acquisition mechanizations shown in Figures 4-2 and 4-3 use three rate gyros, coarse sun sensors with a  $4\pi$  steradian field of view, cruise sun sensors with a  $\pm 10$ -degree conical field of view about the pitch and yaw axes, and a Canopus sensor with a  $\pm 2$ -degree field of view about the roll axis. Control is achieved through gas jets with derived rate feedback maintained around the electronic switching amplifiers. During the roll search maneuver, jet firing times are electrically integrated to prevent excessive roll rates in case of a roll rate gyro failure, as is done on Mariner C.

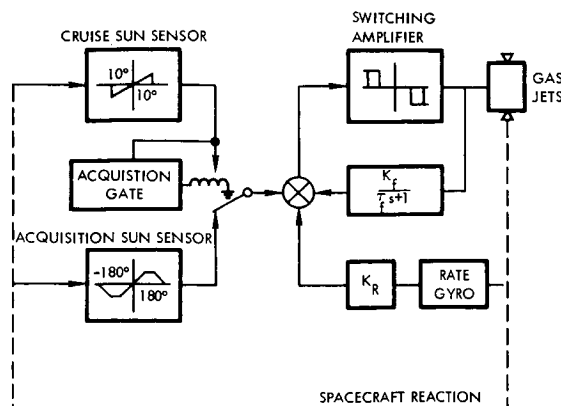


Figure 4-2. Pitch or Yaw Axis Sun Acquisition Mode

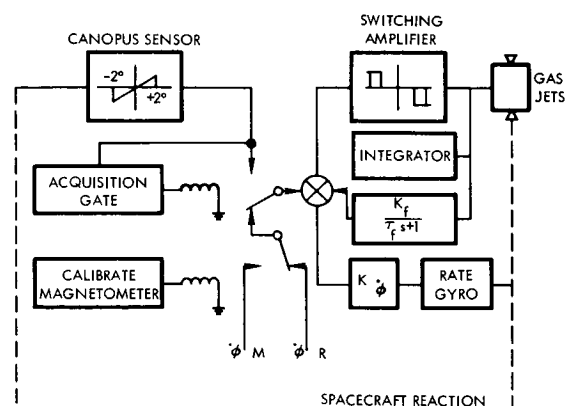


Figure 4-3. Roll Axis Canopus Acquisition Mode

Based on worst case initial rates (3 deg/sec) and position errors ( $\pm 180$  degrees) sun acquisition may take up to 20 minutes. Since the Canopus sensor field of view is  $\pm 2$  degrees, Canopus acquisition (based on a 0.1 deg/sec search rate) could take up to 60 minutes. The total fuel consumed for an initial acquisition, four midcourse correction acquisitions, acquisition after flight capsule separation and deboost is less than 1.4 pounds.

Preliminary studies have shown that there may be an advantage in having a coarse sun sensor whose output saturates for large error signals. The spacecraft would accelerate or decelerate to the rate corresponding to the error saturation value and coast into the control deadzone. Operation in this manner appears to offer economy in control fuel expenditure and response time for the proper control parameter values. As discussed in Section 2, Appendix E, it is also possible to obtain approximate deadbeat response by selection of appropriate sun sensor output characteristics.

A disadvantage of using a saturating coarse sun sensor characteristic is that operation of the backup acquisition mode is degraded in the saturated region since no rate information is available. Detailed studies are needed to examine the tradeoffs involved in 1) increased fuel consumption required for a non-saturating coarse sun sensor during normal sun acquisition and 2) degraded backup sun acquisition performance using a saturated coarse sun sensor.

Figure 4-4 shows a phase plane trajectory of a single-axis sun acquisition without derived rate feedback for an initial rate of 3 deg/sec zero initial pointing error, and a coarse sun sensor output saturation level corresponding to approximately 0.2 deg/sec. As discussed in Section 2, Appendix E, inclusion of the derived rate feedback increases the rate damping but may reduce the duty cycle and result in longer acquisition times.

In addition to providing calibration of the magnetometer and reduction of initial tip-off rates, accurate control of the sun-Canopus search rate may also allow the use of a switching logic which gives a deadbeat response

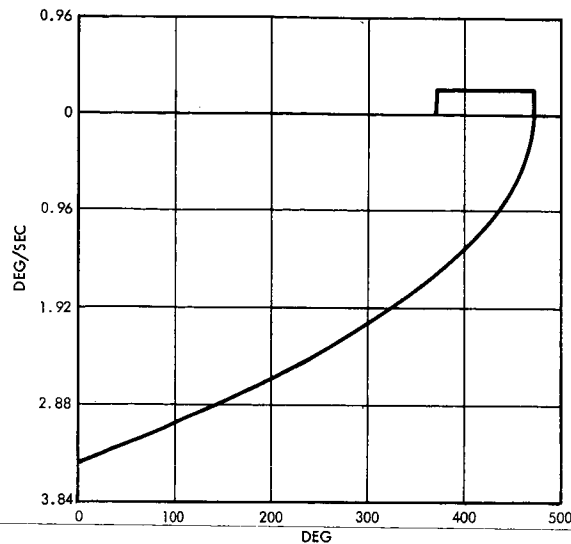


Figure 4-4. Sun Acquisition for 3 deg/sec

with the pointing error and error rate approaching zero at the same time. Since control of the spacecraft is transferred to the cruise mode after acquisition, minimization of the spacecraft position error and rate are desirable to reduce the mode switching transient. Since the acquisition gyro gains determine the initial cruise mode rates (which may be as high as 0.2 deg/sec), several pulses may be required to acquire the cruise mode limit cycle. The magnetometer calibration considered here assumes a single axis rotation as is used on Mariner C. If sequential rotation about all three axes is required for Voyager, it can easily be provided.

Backup sun acquisition in case of gyro failure can be provided automatically by the derived rate feedback. Figure 4-5 shows a phase plane trajectory for a single axis sun acquisition with an initial rate of 1.7 deg/sec and an initial pointing error of 20 degrees. Since rates this large are extremely unlikely after the initial acquisition, the reacquisition even after gyro failure should be much faster than that indicated in Figure 4-5.

Backup Canopus acquisition or high gain earth pointing antenna positioning can be obtained by the incremental roll maneuver mode. Figure 4-6 shows a block diagram of this mechanization.

#### 1.3.4 Maneuver and Inertial Attitude Hold Modes

The selected configuration for the maneuver and inertial attitude hold/rate-integrating mode employs gyros and derived rate feedback.

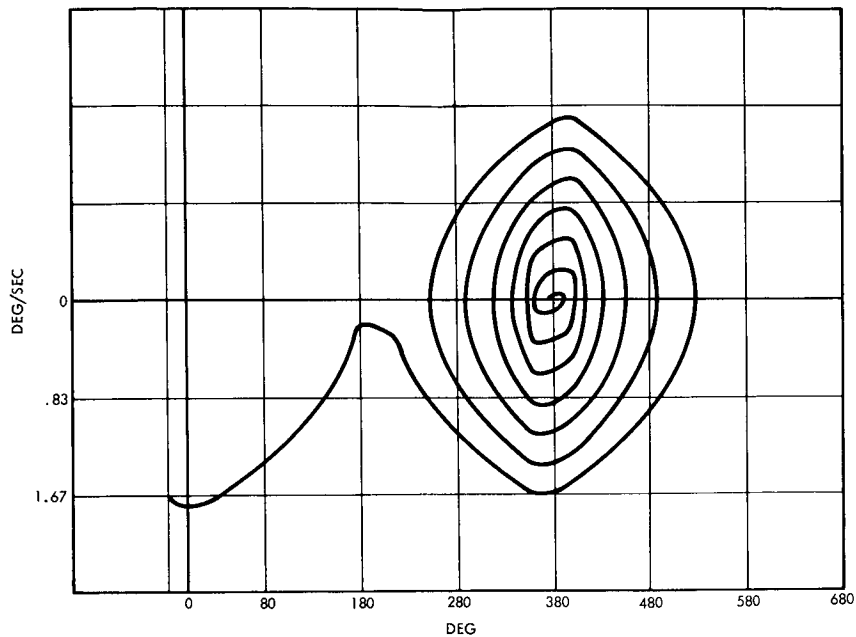


Figure 4-5. Backup Acquisition at 1.7 deg/sec

Figure 4-7 shows a block diagram of a single axis (pitch, roll or yaw) maneuver or attitude hold mode.

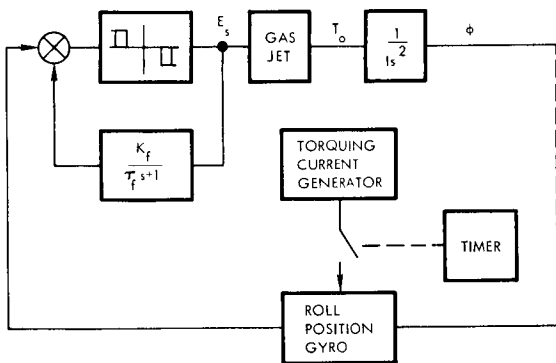


Figure 4-6. Incremental Roll Maneuver Mode Block Diagram

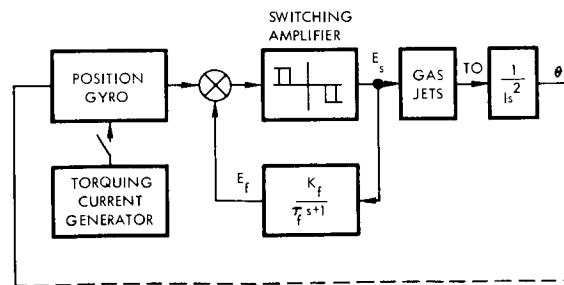


Figure 4-7. Single Axis Maneuver Mode

Based on a 90-degree maneuver angle, the maximum time and fuel consumed during a single axis reorientation were determined by analog computer simulation to be 35 minutes and 0.08 pound, respectively. Assuming four midcourse velocity corrections, capsule separation and

the deboost reorientation, the maximum fuel consumed was found to be 0.96 pound. Figure 4-8 shows a phase plane trajectory of a 90-degree single axis reorientation maneuver.

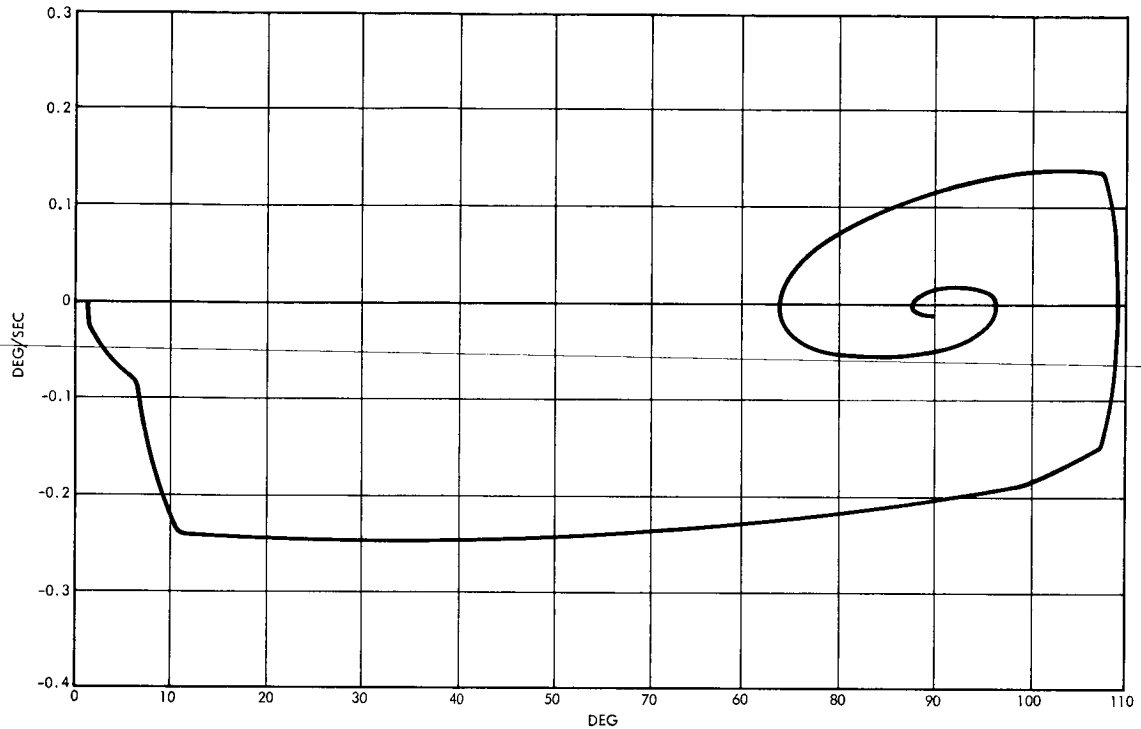


Figure 4-8. 90-Degree Reorientation

#### 1.3.5 Thrust Vector Control Mode

##### a. Monopropellant Engine TVC

Jet vane thrust vector control was selected to provide control torques for the pitch and yaw axes during midcourse velocity corrections. A block diagram of the TVC mechanization is shown in Figure 4-9.

Where

- $\delta_j$  = Jet vane position
- $\delta_{tv}$  = Thrust vector deflection
- $T$  = Engine thrust
- $l_c$  = Control moment arm
- $I_\epsilon$  = Principal axis moment of inertia
- $\theta$  = Attitude error

$K_j$  = Lead-lag compensation gain

$\alpha_j \tau_j$  = Lead time constant.

As shown in Figure 4-9, two jet vanes are utilized for each control axis. The maximum jet vane deflection and the ratio of jet vane deflection to thrust vector deflection are nominally 25 degrees and 5 degrees, respectively. Based on a criterion of one-half the maximum jet vane deflection for a 1/2-degree pointing error, the attitude error gain ( $K_j$ ) was chosen to be 25. A lead time constant ( $\tau_j$ ) of 0.2 second and a lead ratio of 10 were selected. The lead-lag compensation parameter values mentioned above were selected on the basis of providing satisfactory closed loop response characteristics with reliable hardware components. Roll attitude stabilization during the midcourse velocity correction maneuver is maintained by the roll axis inertial attitude hold mode.

Because of the center of mass and the lateral c.m. uncertainties, large thrust vector offset angles are generated. Based on a lateral c.m. uncertainty of 0.2 inch, the  $3\sigma$  thrust offset angle is approximately 0.4 degree. The resulting sensed attitude error is 0.08 degree. The net result is, however, an effective thrust offset angle of 0.48 degree since the attitude error and thrust offset angle are additive. This analysis indicates that stringent control will have to be exercised over lateral center of mass uncertainties.

b. Solid Engine TVC

The selected TVC mechanization for the solid rocket engine employs liquid injection thrust vector control. A block diagram of the deboost TVC configuration is shown in Figure 4-10,

where

$K_\ell$  = Lead-lag compensation gain

$\tau_\ell$  = Time constant

$\alpha_\ell$  = Lead-lag time constant ratio

As shown in Figure 4-10 two liquid injectors are used for each control axis. The maximum thrust vector deflection obtainable from the liquid injection is approximately  $\pm 4$  degrees.

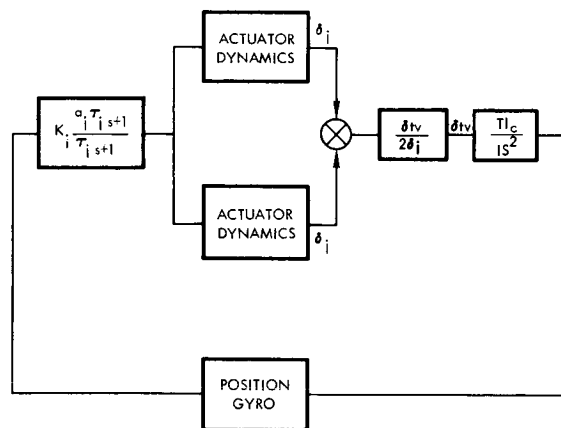


Figure 4-9. Midcourse Velocity Correction Mode Block Diagram

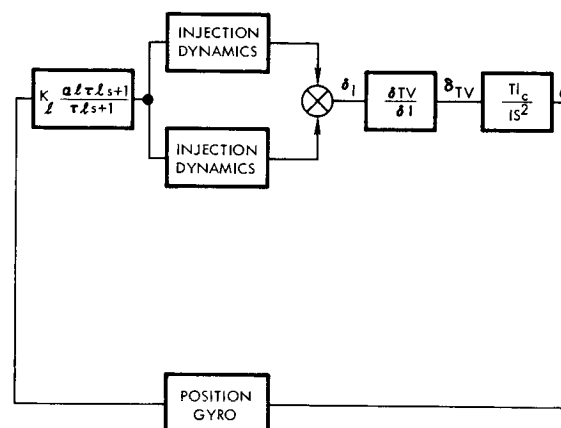


Figure 4-10. Deboost TVC Block Diagram

Because of the relatively high thrust levels at deboost compared to midcourse values, the loop gain parameter  $\frac{Tl_c}{I}$  is correspondingly higher, permitting a lower electronic forward loop gain ( $K_1$ ). Based on a gain ( $K_1$ ) of 2, lag-time constant ( $\tau_1$ ) of 0.05 second, and lead ratio ( $\alpha_1$ ) of 10, satisfactory closed-loop response characteristics are achieved with reliable hardware components.

Because of the proximity of the effective gimbal point to the vehicle c.m., and the lateral c.m. offset, large thrust vector errors will be generated. Based on an assumed 0.2 inch lateral c.m. uncertainty, the  $3\sigma$  thrust vector offset angle is 0.75 degree. The resulting attitude error is 0.38 degree, which results in an effective 1.1-degree thrust error angle. Due to the injection liquid weight required to accommodate the thrust vector offset, tight control of the lateral c.m. offset is indicated. Estimates of the lateral c.m. control achievable by proper appendage location and standard balancing techniques indicate a 0.1 inch lateral c.m. uncertainty is possible.

Present roll axis disturbance torque estimates show that an increased roll axis jet thrust level will probably be required during the deboost maneuver. Based on the deboost thrust level, present lateral c.m. uncertainties, and maximum thrust vector deflection, a roll disturbance torque upper limit of 3 lb-ft may exist during retrofire. Jets

with a thrust level of 0.5 pound, mounted in separate pairs about the roll axis, are sufficient to counteract the effects of this disturbance. Although the resulting undisturbed limit cycle rate is increased to approximately 0.01 deg/sec, the use of the auxiliary roll jets during 100-second deboost maneuver does not result in significantly increased fuel consumption.

#### 1.4 Inertial Sensors

##### 1.4.1 Gyro Instruments

The selected approach utilizes three single-degree-of-freedom, rate integrating gyros, one for each spacecraft axis. The physical parameters of the gyro are specified in Table 4-1.

Since the equipment for each axis is essentially identical describing one axis (roll), a typical axis will in effect describe all three axes as shown in Figure 4-11. In the acquisition mode Switch No. 1 is closed and the gyro is caged with an analog torquing signal. The electrical output is the voltage across the gyro torquer and is proportional to the input roll rate experienced by the spacecraft.

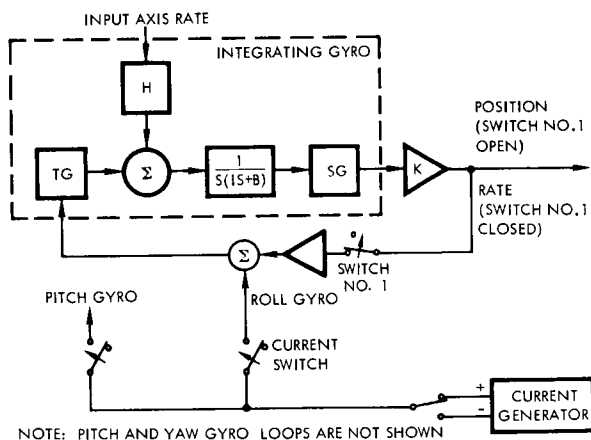


Figure 4-11. Gyro Control Loop

Reorientation of the spacecraft is achieved by opening Switch No. 1 in the roll gyro loop and closing the roll gyro current switch. The precise torquing current of the desired polarity is applied to the gyro torquer. These operations are accomplished by commands from the CS&C. The current is applied by command for a predetermined length of time and then the current switch is opened. The gyro is then the inertial reference during the reorientation of the other axis and the velocity correction maneuver. The same turning procedure is then followed using the pitch gyro loop.



Table 4-1. Gyro Specifications

Weight	1.0 pound (maximum)
Size	2.0 inches diameter x 3 inches long
Gimbal Gain	$0.6 = \frac{\text{Output Angle}}{\text{Input Angle}}$ at 140°F
Input Axis Angular Freedom	±5 degrees (minimum)
Gimbal Freedom	±3 degrees (output axis)
Gimbal Bearing	Pivot and jewel or flexure
<hr/>	
Motor	
Type	Synchronous hysteresis, 4 pole
Excitation	Two phase square wave 800 cps
Starting power	10.0 watts peak for less than 45 seconds
Running power	2.0 watts (maximum)
Signal Generator Power	4100 cps, 0.5 watts (maximum)
Spin Bearing	Hydrodynamic with notches added to the journal portion
Long Term Drift	
G-Insensitive	Initial value ±0.3 deg/hr (maximum) Stability 0.4 deg/hr, 3σ, 1 year
G-Sensitive	Initial value ±1.0 deg/hr-g (maximum) Stability 0.7 deg/hr-g, 3σ, 1 year
MTBF	10 <sup>6</sup> hours

The switching sequence is designed in such a manner that the gyros are always caged by means of the rate loop (Switch No. 1 closed) prior to operating open loop (Switch No. 1 open), ensuring that the gyro floats will be at pickoff null prior to being utilized as an inertial reference in the attitude hold and maneuver modes.

During the attitude hold mode Switch No. 1 is opened and position signals are obtained in the same manner as during the maneuver. The position signal is proportional to the angle through which the gyro input axis has turned and this signal is servoed to null by utilizing the gas jets to torque the spacecraft about the three axes.

#### 1.4.2 Gyro Assembly

The three gyros and their associated electronics are mounted in a temperature controlled block, the temperature maintained by a proportional servo which applies DC power to an appropriate combination of gyro and block heaters. The gyro temperature sensors are used as the temperature reference for the control electronics. Present spacecraft temperature design indicates a heat sink temperature range of 30 to 90°F; in the worst case (30°F) approximately 9.6 watts of heater power will be required. These considerations are outlined in Figure 4-12. Gyro and heater power are not required when the instruments are not being utilized. The gyro reference assembly specifications are given in Table 4-2.

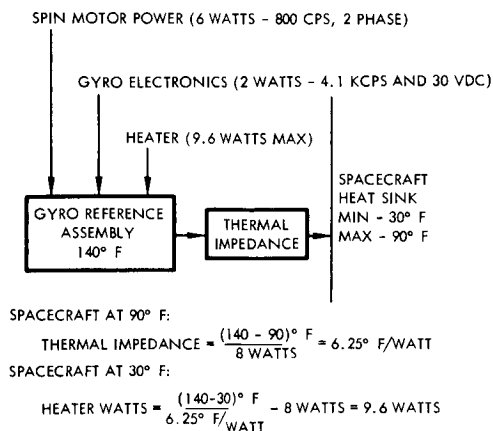


Figure 4-12. Gyro Reference Assembly Thermal Model

Table 4-2. Gyro Reference Assembly Specifications

Size	180 cubic inches (6 x 6 x 5 inches)
Weight	10.0 pounds
Operating temperature	140°F (required only during gyro operation)
Power required	800 cps, 2 phase, 6 watts 4100 cps, 1.5 watts (maximum) 30 VDC, 10 watts (maximum)

#### 1.4.3 Mechanization Tradeoffs

Various tradeoffs were considered before arriving at the configuration just defined. The system of least complexity and highest reliability capable of performing the required functions with the spacecraft limitations was selected. Details of the gyro tradeoff studies are given in Section 3 of Appendix E and summarized here.

##### a. Sensor Heaters

Utilizing unheated gyros is attractive because of the savings in heater power. However, the 60°F variation in heat sink temperature would result in a 2.8:1 change in gyro gain. In addition, the fixed drift coefficient would be subject to change as the temperature varied and this approach was described. Compensation for both of these effects might be included in the circuit electronics; however, at this time little information exists on the performance of inertial guidance quality gyros when operated in this manner. Since excess electrical power is available during most of the mission and the gyros are on for such short times, the more conservative approach was chosen. Should spacecraft power requirements increase in the future, this area can be reinvestigated.

Note that the heater power requirement in the worst case (30°F) is directly related to the amount of power dissipated in the reference assembly. The largest power sources are the gyro spin motors which are currently undergoing considerable improvement. Manufacturers are

quoting power requirements of 2 watts, which is considered conservative. Should the actual gyros selected for Voyager dissipate less power than this, the required heater power would also be reduced. Loss of heater power would result in degraded SCS performance but would not be catastrophic. The gyros would continue to operate at reduced gain which would result in a larger SCS deadzone. The fixed drift coefficient would also be different from its value at normal operating temperatures.

b. Signal Processing

Pulse torquing the gyros was considered and discarded because it was found unnecessarily complex relative to the SCS requirements. Possibly three advantages are associated with a bang-bang pulsed torquing scheme. This approach would:

- 1) Improve the effective torquer linearity of the instrument
- 2) Maintain constant power dissipation in the gyro
- 3) Provide for a digital integration of angular rate.

The first item is not necessary since only one precise slew rate is required (0.2 deg/sec). The second item is useful in those applications where the torquer power at times is considerable and it is desired to improve gyro drift performance by minimizing internal temperature fluctuations. Here, however, the utility is not applicable since the torquer power dissipated at 0.2 deg/sec is approximately 5 milliwatts, negligible relative to the other instrument power input. The third item might be desirable, but does not appear to be needed since the high gain antenna is used for attitude verification.

Caging the gyro with an analog torquing loop and integrating the torquing signal to obtain spacecraft position was also considered. Capacitors such as utilized on Mariner C and voltage-to-frequency converters operating on the indicated rate signal were considered and were discarded because of the increased complexity they introduce.

Gyro torquing scale factor accuracy and linearity of 0.01 and 0.01 percent, have been obtained with a high degree of stability by existing permanent magnet torquer designs. Torquing current generation with an accuracy of 0.5 percent is readily achieved today with simple, straightforward circuitry. Both of these factors contributed to the decision that analog signal processing is able to satisfy the Voyager maneuver accuracy requirements.

c. Spin Motor Bearings

A hydrodynamic gas spin bearing was selected for the Voyager gyros for two reasons:

- 1) The dominant gyro failure mode in a ball bearing gyro is considered a wheel bearing failure.
- 2) The mission operating life is longer than conservative estimates of the expected ball bearing lifetime.

A properly designed gas spin bearing should thus substantially increase the gyro reliability. The tradeoff associated with this selection is a slight increase in spin motor power, which is outweighed by the improvement in reliability.

A consideration associated with gas journal bearings is the argument that they may resonate at half motor frequency (half speed whirl) when unloaded during the zero g portion of the flight. Although this is not considered likely, the possibility does exist and there is little data available to prove or disprove the argument. Tentatively it has been decided to incorporate supplementary notches in the journal portion of the bearing to provide positive centering at zero load. Minuteman platforms have been observed to operate satisfactorily for periods up to 30 seconds after thrust termination, indicating that the gyros do not fail in a zero g environment. In this case, the observation time was determined by other flight constraints, and gyro bearing failure would have produced torques which would have resulted in the platform running abruptly to its gimbal stops (dumping). The Minuteman platform carries two degree of freedom

gas bearing gyros (G6-B4) and one single degree of freedom gas bearing gyro (GI-T1-B). Both types of instruments exhibit half speed whirl, and because of the high resonant frequencies (75 and 200 cps, respectively) it is considered likely that a resonance type bearing failure would have occurred in the 30-second observation period, if this phenomenon does in fact exist. In any event, there will be ample opportunity to test for this effect and obtain assurance for this approach before Voyager specifications are firm.

d. Spin Motor Excitation

Two-phase spin motor excitation is chosen because it is as efficient as three phase and requires one less inverter to generate. Single phase, split with capacitors, is not being used because the start and run capacitors should be of different values and switching from one to the other is more complex and, hence, potentially less reliable. Square wave excitation is being used because the increase in power is slight and it is simpler to generate than a sinusoidal or quasi-sinusoidal wave. A four-pole motor is selected over a two-pole design because better radial centering is achieved, optimizing starting of a gas spin bearing, and lower end turn losses result in a more efficient motor, and the leakage flux from the motor is lower. The motor drive frequency selected is 800 cps because it is considered undesirable to operate the wheel at 400 cps which, with the four-pole motor, would result in a half normal spin speed and double drift coefficients.

e. One Degree of Freedom versus Two Degrees of Freedom

Single-degree of freedom gyros (as opposed to two degrees of freedom gyros) were selected for this application because:

- 1) They have been used previously in many similar applications (Ranger, Mariner, etc.)
- 2) More is known about the performance of single degree of freedom instruments.
- 3) More vendors are producing single degree of freedom instruments.

The use of single-degree of freedom gyros in this application is certainly the more conventional design approach and thus has the advantage that the instrument characteristics are generally well known and predictable. Another consideration is that any of the two-degree of freedom instruments presently available would require caging and some form of rate integration to be used in the SCS. Thus, more circuit complexity may be required.

However, one two-degree of freedom gyro may merit further study before a final configuration is selected. The Autonetics G10 and G40 are small two-degree of freedom gyros which appear to have many desirable characteristics. They do not require heating, utilize gas spin bearings are not floated, and have no flex leads or gimbal bearings. They are a miniaturization of the Autonetics G6 gyro which has demonstrated an extremely low failure rate in the Minuteman guidance system. The spin motor power required in space would be less than 1 watt per gyro. A configuration based on these gyros would presumably have the desirable characteristics of high reliability, low power, and small size. However, not enough is known about the instruments to verify that they would meet the other design constraints required of the SCS. Further investigation in this area is intended. Note that two-degree of freedom instruments have a potential reliability advantage in that only two instruments are required instead of three. Therefore, if the reliability of the two-degree of freedom gyro is approximately the same as the single-degree of freedom unit, an improvement in inertial reference system reliability might be realized. Failure of the gyro on any SCS axis could be catastrophic to the mission so that failure of the two axes associated with a two-degree of freedom gyro is no worse than failure of a single-degree of freedom gyro associated with a single axis.

f. Other Design Details

The more complex suspension systems, such as magnetic or electrostatic suspension, and hydrostatic bearings were considered because of reliability and power characteristics.

The flotation fluid type does not freeze over the temperature range of interest in both storage and flight. Magnetic cleanliness will be considered in future detailed designs, but, at present, the gyro could not be selected on the basis of producing less than 1  $\gamma$  at a specified distance since this type of information is not presently available from gyro manufacturers. A requirement of part of the gyro reference assembly design is to apply suitable shielding to the gyros and entire assembly in order to obtain the desired magnetic cleanliness.

### 1.5 Sun Sensors and Near Earth Detector

The recommended design approaches for the sun sensor and the near-earth detector were selected on the basis of reliability, performance, size, weight, and power requirements as they were met by alternate techniques and devices. The rationale for the designs is presented in the following sections. Additional design details are presented in Sections 4 and 5 of Appendix E.

#### 1.5.1 Selected Sun Sensor Design

The recommended sun sensor consists of three separate assemblies:

- a) A coarse pitch sun sensor
- b) A coarse yaw sun sensor
- c) A two-axis fine sun sensor.

The logical interconnections of the sun sensors are indicated in Figure 4-13. The electronic circuits are shown on a functional basis only. Redundant signal processing circuitry is used in all channels, consistent with the SCS electronics design concept discussed more fully in Section 1.10.

Each of the two coarse sun sensors consists of a pair of solar cells back-to-back, with plano-convex lenses in optical contact with the cell surfaces as shown in Figure 4-14. The two solar cells are connected with opposing polarities across a low resistance. The output signal will have a characteristic similar to that shown in Figure 4-15. The coarse sun sensors are mounted on the spacecraft periphery at locations which



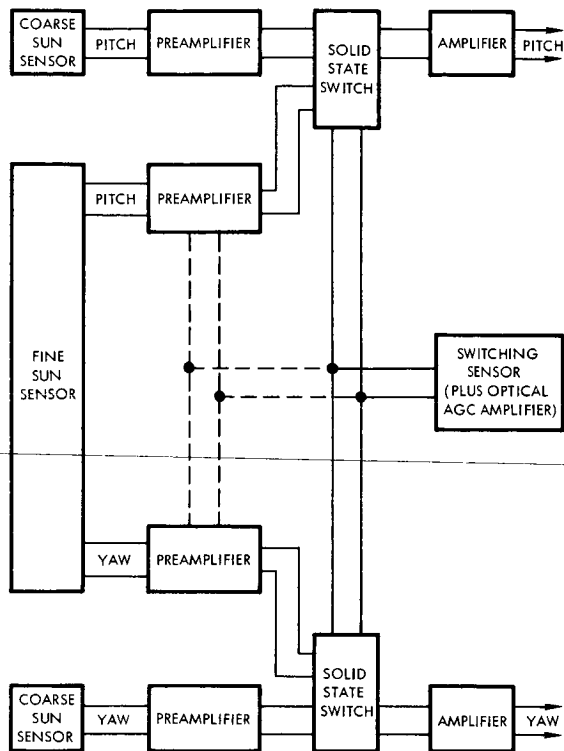


Figure 4-13. Sun Sensors and Electronics

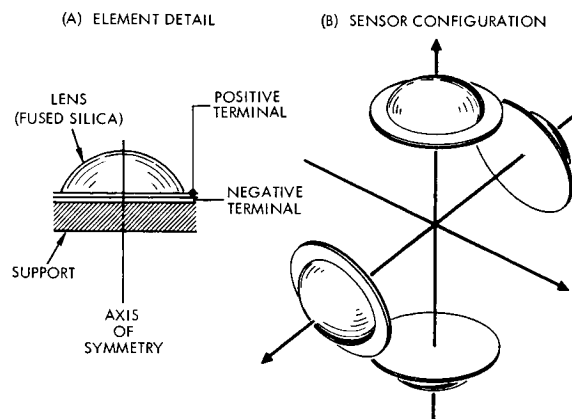


Figure 4-14. Coarse Sun Sensors

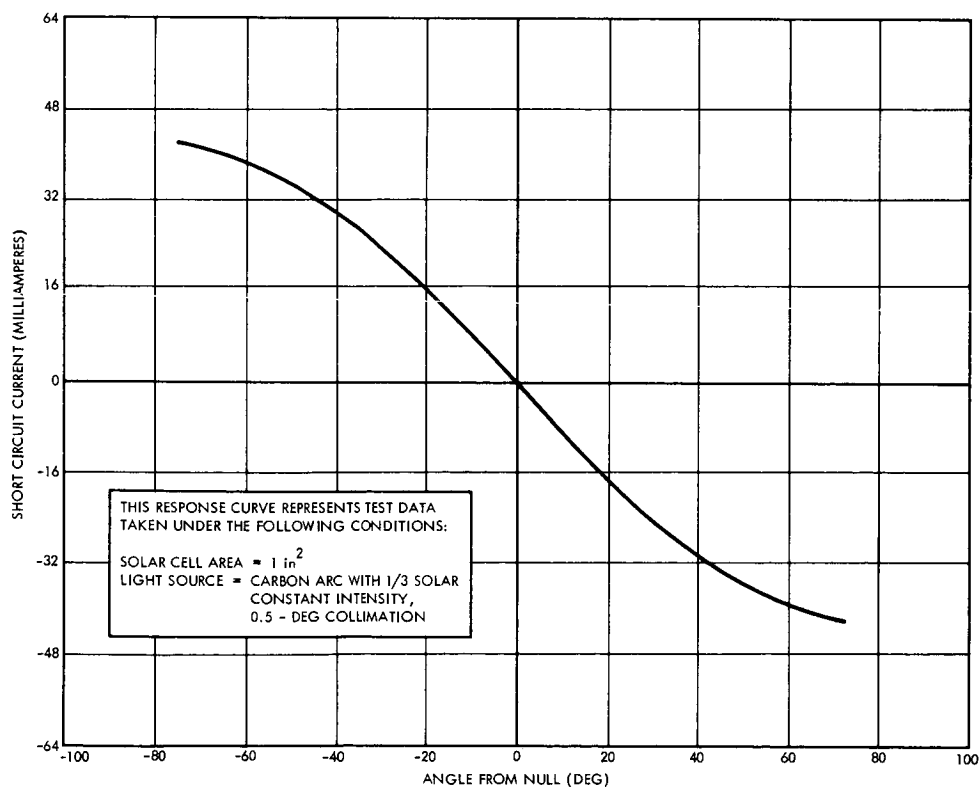


Figure 4-15. Coarse Sun Sensor Output Versus Illumination Angle

provide maximum unobstructed viewing angles. The null stability of the coarse sun sensors is between 0.5 and 1 degree (as determined by the geometrical and thermal characteristics of the mounting structure) so that with suitable mounting surfaces and with proper initial alignment the coarse sun sensors can provide a good backup system in the event of a failure of the fine sun sensor.

The fine sun sensor consists of a silicon photovoltaic quad cell mounted behind a mask which acts as a shadowing structure (see Figure 4-16). The sensor is designed to have nearly linear output in two orthogonal axes when the sun angle is within 10 degrees of the sun sensor axis. The output signal will have a characteristic similar to that shown in Figure 4-17.

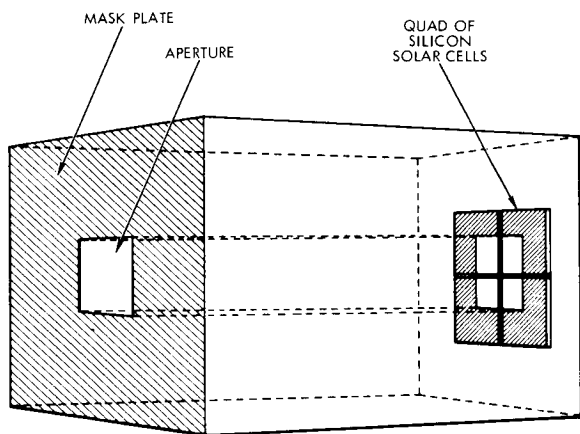


Figure 4-16. Fine Sun Sensor

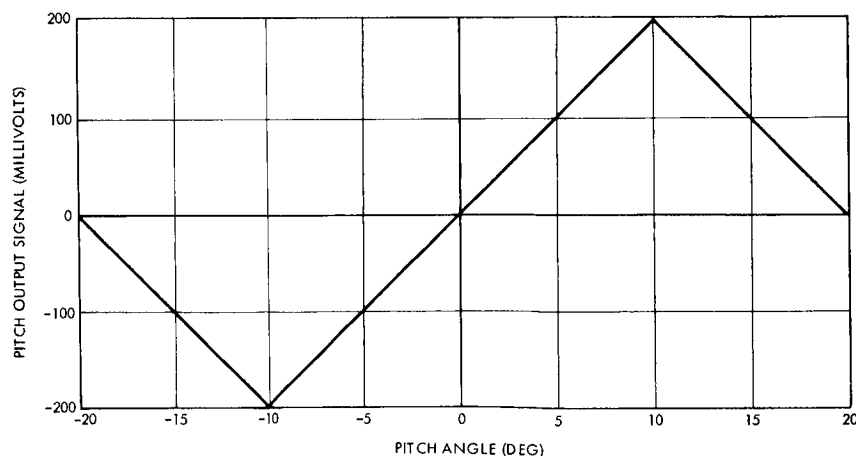


Figure 4-17. Sun Sensor Output Signal

The scale factors for the coarse and fine sun sensors are designed to be nearly equal between 8 and 10 degrees from the fine sun sensor axis. The attitude control system is switched from the coarse sun sensor to the fine sun sensor within the 8 to 10-degree band so that the transition will not produce a discontinuity in the signal. The switching is initiated by a miniature silicon solar cell behind a plate having a pinhole aperture. Switching from coarse sun sensors to a fine sun sensor makes it possible to have a  $4\pi$  steradian acquisition field of view without susceptibility to null errors caused by light reflected from the surface of Mars during the orbital phase of the mission.

#### 1.5.2 Design Development

The sun sensors for the Voyager spacecraft are required to sense the sun over a  $4\pi$  steradian field of view to facilitate acquisition of the desired attitude. In addition, the sun sensors are required to provide relatively high accuracy about the null point which occurs when the spacecraft is properly oriented with respect to the sun. To obtain the comprehensive field of view, sensors must be mounted at outboard locations where the temperature and structural rigidity are likely to be unfavorable for a sensor of high accuracy. This consideration led to the adoption of coarse sun sensors mounted on the spacecraft exterior and a fine sun sensor mounted inside the spacecraft where the environment is more carefully controlled and greater protection can be provided against micro-meteorite damage.

It is possible, in theory, to obtain the required field of view by many small sensors having small acceptance angles with the output signals combined in some fashion, allowing all of the sensors to be located inside the spacecraft if suitable mounting spots could be found. The relative complexity and high parts count for this approach, however, more than offset any advantages it may have.

#### 1.5.3 Coarse Sun Sensor Tradeoffs

##### a. Requirements

The chief requirements for the coarse sun sensors are listed below:

- 1)  $4\pi$  steradian field of view for the sensor combination.
- 2) Output signals must be suitable for acquisition of the sun.
- 3) Sensors must operate over a relatively wide temperature range.
- 4) Sensors must operate over the range of spacecraft-sun distances associated with the Voyager mission.
- 5) A reasonably high signal level is desirable to minimize the requirements for amplification.
- 6) The output signal should be compatible with that of the fine sun sensor such that a smooth transition from coarse to fine can be made.

It will be shown that all of the requirements can be met using an analog null-seeking sensor. This type of sensor is considerably less complex (and requires fewer parts) than a digital sensor or a solar aspect sensor, i.e., a sensor which provides a quantitative measurement of the sun's position at all points within its field of view. Since the analog null-seeking sensor was found to be the most reliable type adequate to meet the requirements, various techniques for implementing such a sun sensor were evaluated. The most significant of these techniques are discussed next.

b. Evaluation of Specific Devices and Designs

The detectors most suitable for use in a visible light sensor, neglecting image tubes and devices especially designed to detect faint sources, are listed below:

- 1) Photovoltaic devices
  - Silicon solar cells
  - Radiation tracking transducers
  - Other photovoltaic cells

## 2) Photoconductive devices

- CdS and CdSe photocells
- Photo diodes
- Photo SCR's and light activated switches
- Photo transistors

To cover the required  $4\pi$  steradian field of view with a minimum number of detectors, each detector should be adaptable to sense light over a wide solid angle. One technique for accomplishing a wide angle is to immerse the detector by placing a lens in optical contact with the photosensitive surface. Another approach is to use a detector having a surface with convex curvature (CdS and CdSe photoconductive grids have been deposited on flexible substrates). If the detector has an acceptance angle of  $2\pi$  steradians or more, two detectors facing opposite directions can provide a suitable signal for one-axis sun angle information.

Among the available photovoltaic detectors, the silicon solar cell is the logical choice for the coarse sun sensor application. The radiation tracking transducer, a lateral photocell which indicates the position of a spot focused onto its surface, cannot be readily adapted to cover the large viewing angles required. The other types of photovoltaic cells do not have the proven reliability and performance which the silicon solar cells have demonstrated in space applications. In addition, sun sensors using immersed silicon solar cells have been built and tested extensively for use on other spacecraft such as OGO and Vela V. The design will be flight tested well before the completion of the Voyager spacecraft design.

For photoconductors, the CdS and CdSe photocells appear the best choice for the application. Photo diodes, photo SCR's, and light activated switches do not have the analog type of signal needed to meet requirements 2 and 6 of Section 1.5.3. Photo transistors have a lower assessed reliability than the CdS or CdSe photocells, and they do not lend themselves to wide viewing angle applications. The only notable point in which CdSe cells excel over CdS cells is in the speed of response. Since fast response is not needed, the CdS cells are preferred because they have greater stability with temperature change and have had more use in space applications.

Choosing between the photoconductive CdS cell and the photovoltaic silicon solar cell is difficult. Both devices have adequate response, temperature stability, and flight-proven reliability. The solar cell sun sensor would require only one load resistor (per axis) and no power consumption; the CdS cell sun sensor would require one active CdS cell and one dummy CdS cell per axis and two resistors for both axes to complete the resistance bridge and would require external excitation. However, the signal level from the CdS cell bridge could possibly be higher than that of the silicon solar cell, providing savings in amplification. The final choice in favor of the silicon solar cell was made because of the following arguments:

- 1) The immersed solar cell sensor has already been designed, built, and tested and will have been flown before the Voyager mission.
- 2) CdS cells in conventional packages could not be used for this wide angle application without using more than two cells per axis.
- 3) The intensity of incoming sunlight would probably have to be reduced by filters to prevent hard limiting of the detector bridge at angles only a few degrees away from the null plane.
- 4) The solar cell design has exhibited fairly good linearity for about  $\pm 30$  degrees from the null plane (Figure 4-15). This linearity might be difficult to achieve with the CdS photocells.

Preliminary analyses show that it may be desirable to limit the sun sensor output to provide improved acquisition performance for the nominal configuration with rate gyro feedback and for backup operation without rate gyros. A complete assessment of this technique, involving interactions among the sun sensor parameters and the derived rate modulator characteristics, is beyond the scope of the present study. It is planned to examine important design consideration in detail in the Phase IB studies.

#### 1.5.4 Fine Sun Sensor

##### a. Requirements

The following list tabulates the requirements for the fine sun sensor:

- 1) Accuracy of 0.1 degree at null
- 2) Two-axis output
- 3) Field of view approximating a cone of 10 degrees half angle.
- 4) Good linearity within the field of view.

As in the case of the coarse sun sensors, an analog null-seeking sensor is the simplest and most reliable type of sensor for this application. The various techniques available for implementing such a sensor are compared below.

b. Comparison of Specific Devices and Designs

Most of the general discussion of detectors applicable to coarse sun sensing applies directly to the detectors for the fine sun sensor. Only two of the devices which were considered for the coarse sensor, the radiation tracking transducer (RTT) and the photo transistor, were dismissed in that context because they did not readily suit the wide angle viewing requirement of the coarse sun sensor. The photo transistor, as before, appears to be neither sufficiently reliable nor sufficiently adaptable to the fine sun sensor task to be a good choice. The RTT, however, is almost tailor-made for this type of application, and therefore qualified as a candidate for consideration. Thus the eligible devices for use in the fine sun sensor are the silicon solar cell and the RTT, from among the photovoltaic devices, and the CdS photocell from among the photoconductive devices.

For the RTT, a lens would be used to focus an image of the sun onto the photosensitive surface. The differential voltages appearing at two pairs of contacts on the back of the cell would provide the pitch axis and yaw axis signals. Five resistors would be required, and a dual-channel amplifier would be required. The signal level at the amplifier input would be approximately 5 millivolts per degree, assuming a 10-degree half-angle field of view. Only one RTT would be required. The assessed failure rate of the RTT is four times that of a silicon solar cell.

The techniques for applying the solar cell or the CdS photocell in the fine sun sensor are the same for either device. One technique is to use exactly the same scheme as for the coarse sun sensors. The superior structural and thermal environment in the fine sun sensor mounting location would permit the coarse sun sensor design to maintain the required accuracy. Another technique which could be used is a quad cell design (Figure 4-16). For this design, four detectors are fitted close together in a square pattern. An aperture plate in front of the detectors admits a spot of sunlight onto the detector plane. The diagonal cells provide equal response when the spot is centered between their centers; as the spot moves away from the center point, a two-axis error signal is produced.

For the quad cell design or for the back-to-back cell design, four detectors are required, whether silicon solar cells are used or CdS cells are used. Silicon solar cells are preferred over the CdS cells in either design for the same set of reasons given previously for the coarse sun sensor design selection, with the exception that a wide acceptance angle is not required in this case.

The choice between the back-to-back cell design and the quad cell design was made in favor of the quad cell approach, chiefly because of the greater simplicity and ease of fabrication. Also, the cells can be more easily matched in the quad cell design since a single wafer can be divided into the quad pattern by means of electron beam slicing.

The assessed reliability of the quad cell design using silicon solar cells is almost exactly the same as that of the RTT design. Both designs have exhibited excellent performance in laboratory tests. The quad cell design is favored, however chiefly because:

- 1) The signal output level with the quad cell design can be made higher than that of the RTT. This will result in a simplification of the amplifier required to obtain a given stability.
- 2) Ease of detector procurement.
- 3) The RTT design would require a lens, which the quad cell design does not use, and the RTT sun sensor would probably be larger than the quad cell sun sensor.



- 4) The solar cell detectors exhibit lower variation in scale factor with temperature change.

#### 1.5.5 Switching

It is desirable to switch from the coarse sun sensors to the fine sun sensors when the sun is within about 10 degrees from the fine sun sensor axis. This switching could be initiated by the signal from the fine sun sensor except for that the signal does not have a unique level at the 10 degree point (see Figure 4-17). The same problem would exist if the coarse sun sensor signal were used to perform the switching. The most straightforward solution is to use a separate sensor to indicate when the sun is within the linear region of the fine sun sensor field of view. This sensor would be quite small, using pinhole optics. The detector would be a silicon solar cell masked to dimensions which define the desired field of view. The solar cell is preferable to the photoresistive detectors because its photosensitive surface is homogeneous, allowing the field of view to be sharply defined. The solar cell also has the advantage of maintaining uniformity among the detectors used in the sun sensors.

#### 1.5.6 Near Earth Detector

Initial acquisition of the star Canopus was found to be a fairly tricky operation on Mariner C because of the wide acceptance range of the Canopus sensor. Should the star tracker for Voyager have a wide acceptance range, it may also lock on to celestial objects other than Canopus. It is therefore desirable to provide means for verification of star acquisition. One technique is to monitor signals from the high gain antenna which is prepositioned on the spacecraft so that the beam intersects the earth when the proper orientation is attained. This is a particularly useful method for verification of reacquisition at large distances from earth. Early in transit, a technique which was employed on Mariner C may prove useful. A simple optical device, geometrically positioned on the spacecraft relative to the star tracker, will be illuminated by sunlight reflected from earth when the star tracker is locked on Canopus. This device need not be in line in the reliability sense, but rather serves as a sensing instrument for data to be telemetered to earth to assist verification of Canopus acquisition.

This section discusses such a simple optical sensor and the tradeoffs that went into the design selection.

a. Selected Design

The near-earth detector senses the earth by means of a cadmium sulfide cell mounted near the focal plane of a light-collecting lens. The detector, which senses visible light reflected from the earth, provides a signal which indicates the presence or absence of the earth within the detector field of view. The field of view, typically a conical sector of 10 degrees half-angle, is determined by the dimensions of the photoconductive grid of the photocell and the distance between the photocell and the objective lens. The photocell is connected in a bridge circuit which is excited with an ac voltage to facilitate signal detection. To minimize the temperature dependence of the detector a dummy photocell, shielded from light, is used in the bridge to balance the active photocell. The detector is capable of detecting the earth under the conditions expected during the first 10 days of the Voyager mission, with conservative allowances for the earth's phase and albedo. A diagram of the near earth detector is shown in Figure 4-18. Design details are given in Section 5 of Appendix E.

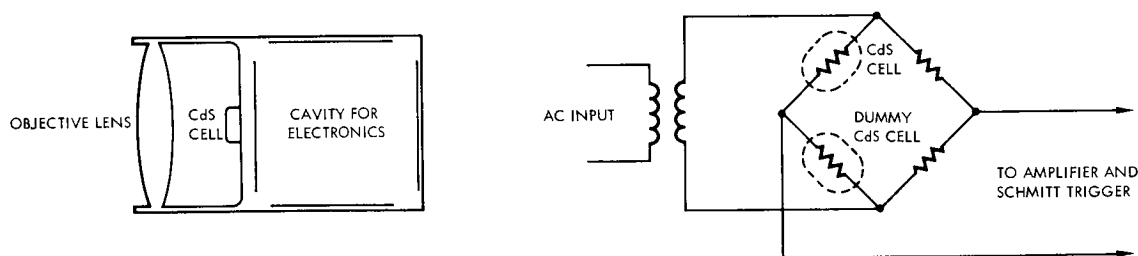


Figure 4-18. Near Earth Detector Schematic Diagram

b. Design Tradeoffs

The near earth detector is required to sense relatively low levels of illumination, since it is designed to detect the earth from distances of approximately 2 million kilometers. A number of devices were considered for use as detectors before the CdS photocell was selected. The best of the alternate devices, and the reasons for their rejection, are enumerated below:

- 1) Silicon Solar Cells. Silicon solar cells were found to produce a lower signal level than the CdS photocell bridge. The amount of dc amplification needed would require more parts and complexity than the photocell design. The greater need for light gathering capacity would probably result in a unit of greater size and weight than the photocell design.
- 2) Electronically Scanned Detectors. Electronically scanned detectors, such as image dissector tubes, possess adequate sensitivity but have the disadvantages of complexity, lower reliability, and high voltage supply requirement.
- 3) Photo Transistors. Several photo transistors, including photo field-effect transistors, were considered for use in the near-earth detector. The device with the best ratio of signal current to leakage current found was the GS-600 photo transistor. With 2-inch diameter optics, the calculated output voltage at the time of minimum illumination would be approximately 8.5 millivolts DC, which is satisfactory. This signal, however, depends upon focusing the earthshine onto a small spot in the detector plane; the size of this spot would limit the field of view of the near-earth detector to a conical sector with a half-angle of only 3 degrees. In addition, photo transistors have not yet established the flight-proven reliability of the photoconductive CdS cells.
- 4) Cadmium Selenide Cells. Cadmium selenide cells were rejected in favor of cadmium sulfide cells because of their greater temperature dependence, especially at low levels of illumination, and because CdS has a better spectral response for detecting light of the solar spectrum.

The CdS photocell which was finally selected as the light detecting element of the near-earth detector has the advantages of high light sensitivity and a good spectral response fit for sunlight. It can be used in a bridge that is excited with an AC voltage (already available on the spacecraft) so that AC amplifiers can be used to amplify the signal. With the CdS cell design, the field of view of the detector can be set at any desired size in the range of interest simply by choosing the proper focal length

for the objective lens. The high sensitivity of the photocell permits the use of relatively small optics. The CdS cell, due to the simplicity of its construction, is a very reliable device; no special development or modification of existing photocells is required for this application.

## 1.6 Star Sensors

On such flights as Mariner 3 and 4, attitude control is provided by directing the roll axis of the spacecraft toward the sun by a sun sensor, and then rolling the entire spacecraft to acquire the star Canopus with a star tracker. It is also possible to point the spacecraft roll axis toward the earth, using an earth sensor. This, again, provides two-axis localization, and a Canopus sensor provides the third axis information. Both of these methods have been investigated for Voyager.

Several problem areas exist in the two-sensor system:

- a) It is necessary to accommodate a wide range of trajectories and geometrical properties because of variation in the apparent position of Mars with regard to the position of the sun and Canopus, which will change several degrees during the last few weeks of the midcourse flight.
- b) It is necessary to find an optimum location on the spacecraft for a single, two-sensor package which permits optimum field of view. Mounting all sensors in a single guidance package increases the field-of-view problems and geometrical problems.
- c) Close thermal control is required for the package so that image quality will not be degraded by thermally induced misalignments.

The star Canopus has been chosen as one of the two celestial reference points because of its intensity and its location, some considerable angular distance from the plane of the ecliptic. The visual magnitude of Canopus outside of the earth's atmosphere is  $M_V = -0.92$ , which makes it second only to Sirius in stellar apparent brightness\*, although Venus, Mars, and Jupiter also exceed the visual magnitude of Canopus. Through the

---

\*"The Absolute Spectral Energy Distribution of Canopus," JPL Technical Report 32-641

visual portion of the spectrum, it appears to be reasonably represented by a Plankian radiator of surface temperature  $\sim 7000^{\circ}\text{K}$ , with a spectral peak at  $\gamma = 0.415\mu$  and a radiance flux at the peak of  $1.22 \times 10^{-11}$  watts  $\text{cm}^{-2} \mu^{-1}$ .

To lock onto a particular star, various means for rejecting the myriad of other stellar sources must be incorporated into the system. The spectral characteristics of Canopus permit the use of matching color filters which will reduce the intensity of stars of any temperature other than  $7000^{\circ}\text{K}$ . Canopus possesses an F-O type spectrum. Stars in this class represent 10 percent of the 20 bright stars ( $M_V < + 1.50$ ) and 10 percent of the 40 bright stars ( $M_V < + 2.00$ ), 9 percent of the 100 bright visual stars ( $M_V < + 2.65$ ) and 18 percent of the average stellar distribution ( $M_V < + 8.5$ ). Thus, some useful filtering can be achieved by this means. Of considerably greater value, though, is the intensity thresholding of the sensor to remove radiation sources equivalent to flux densities from stars outside of a particular magnitude.

At this time, however, the lack of confidence in tracker calibration and the absolute intensity of Canopus prevents an extremely narrow setting of the gates about the intensity of Canopus to obtain automatic acquisition. Therefore, proper acquisition of Canopus will probably be a ground decision based on telemetered intensity data and an earth gate signal (see Section 1.5), with the number of possible targets being limited to at most about 4 by intensity thresholding and proper choice of sensor field-of-view. Canopus intensity data from the Mariner C mission should, however, increase the confidence in the absolute value of the intensity and thus permit a simpler and more reliable means of Canopus acquisition.

#### 1.6.1 Available Star Sensors

Several star tracking devices have been built, tested, and evaluated on a number of space missions, and all have been considered for the present application. Because the various designs have been directed toward the solution of specific problems or have been required to supply specific information pertaining to the mission requirements, not all were deemed suitable for the Voyager Canopus tracker requirement. These sensors are:

- a) Gimballed Sensors. Various star sensor configurations exist, which utilize mechanical gimbaling in one or two axes. Large acquisition field coverage is provided but, in general, these devices are unsuitable because they require heavy DC torque motors, lubricant reservoirs, and carefully designed seals plus extra weight and power for the drive mechanism, and, of course, have relatively low reliability.
- b) Reticle Devices have the advantage of very high precision pointing, are light in weight and size, and require moderate power, by utilizing a photomultiplier tube as detector. To sweep the star field across the telescope field of view and the reticle pattern, either a mechanical movement must be imparted to the reticle, a mirror or wedge, or the entire craft must roll to operate without moving parts.
- c) Mosaics. Devices have been implemented using mosaics of small solid-state photosensitive elements. Although the reliability of a single element, or small number of elements is high as compared with electronic tubes, the large number of elements required to provide adequate field of view with good resolution, creates problems in electronic complexity. The advantage of having no moving parts is offset by this circuitry complexity.
- d) Bilinear Photomosaic Detector is essentially the same as the preceding except that two linear rows of cells are used, one for azimuth and one for elevation information. Thus, the cell number is reduced from  $n^2$  to  $2n$ , and 720 elements can provide 129,600 bits of information. The number of elements is still large and the circuitry unwieldy, however.
- e) Solid-State Tracker utilizes a single silicon photocell, but requires mechanical gimbaling with torque motor drive which must respond to both telescope derived error signals and command signals.
- f) Solar Referenced Star Tracker is a device which utilizes the photomultiplier tube plus reticle design discussed above with the requirement for mechanical scanning. It is listed separately

because of its unique star identification technique. Since the roll axis of the craft is always pointed at the sun, the star sensor takes, through a separate optical path, a small amount of the sunlight. Since the solar flux is well known, and the proportion of it directed to the photomultiplier tube known exactly, the brightness of any star can be photometrically compared with this value. Thus, Canopus can be specifically identified by the ratio of its image brightness to the solar flux.

- g) Reticle Pattern with Vidicon. Imaging tubes such as a 1-inch, electrostatically-focused and deflected vidicon tube have been employed with reticle patterns to achieve digital readout. Although scanning is all electronic, the power and weight requirements of such a device are considerably greater than found in many of the previously discussed sensors.
- h) Electronic Scanning Trackers. In addition to TV pick-up tubes, several star trackers have been constructed using other types of electronic tubes which permit all electronic gimbaling, switching, or scanning. The image dissector tube, in particular, has been adapted as a detector in a number of star trackers either in conjunction with mechanically rotated mirrors to provide large acquisition fields of view or with carefully designed optics to provide moderately large acquisition fields without the need for moving parts. One or two axis scanning can be effected depending on the operation of the deflection mechanism and the image dissecting aperture. The deflection mechanism as well as the focusing mechanism can be all magnetic or all electrostatic or combinations of the two.
- i) Electronically Switched Fields. A standard type of tracking device utilizes four photomultiplier tubes covering four quadrants, and a point lying between them serves as null center. Four quadrants in a single photomultiplier tube have been manufactured; because the deadtime between quadrants is about  $10^{-3}$  inch, highly accurate tracking of point sources is possible. The quadrants are rapidly, sequentially scanned and appropriate circuitry reads out the error signal.

### 1.6.2 Star Sensor Selection

After evaluating all of these existing types of sensors, and taking into account the Voyager mission requirements and the need for high reliability, two star sensors remainder for consideration: the image dissector type and the quadrant photomultiplier type. Both require no moving parts, and have low power, size, and weight requirements. Of the several sensors which employ the image dissector tube, the chosen configuration is the one now operating as the Canopus tracker on the Mariner C. Both sensors are discussed below.

#### a. Mariner C Canopus Tracker

The star tracker utilized on board the Mariner C appears to be performing satisfactorily, and has demonstrated an acceptable level of reliability. This tracker has a total electronically scanned field of view of 4 degrees in the roll axis and 30 degrees in the pitch axis. The instantaneous field of view of the tracker is  $0.86 \times 11.0$  degrees. Electronic scanning to  $\pm 2$  degrees in the roll axis is necessary to provide sufficient field to prevent spacecraft roll corrections from causing the excursion of Canopus out of the field once it has been acquired. The 11 degree pitch field can be extended to 30 degrees by electronic stepping of the cone angle axis, by command. A total of 30 degrees in pitch will encompass all trajectory geometries for the acquisition of Canopus.

A more detailed description of this sensor\*, its configuration, operation and performance are discussed in Section 6 of Appendix E and summarized in Table 4-3.

#### b. Star Tracker Utilizing a Quadrant Photomultiplier Tube

Another type of electronically scanned phototube for use in a star tracker was given considerable attention for two reasons. First, it demonstrates the same advantages provided by the Canopus sensor

---

\*"System Description and Performance of a Canopus Star Tracker," Barnes Engineering Co., Stanford, Conn.



Table 4-3. Characteristics of Mariner C Star Tracker

Total Field of View	4 (roll) x 30 deg (pitch)
Instantaneous Field of View	0.86 (roll) x 11 deg (pitch)
Gimballing	All electronic
Roll	Continuous sinusoidal sweep
Pitch	Six positions - 4.6 deg/position
Sensitivity (threshold settings)	+ 0.6M to -2.4M
Null Offset	< $\pm 0.1$ deg
Error Gradient (at null)	8 volts/deg
Equivalent Noise	+ 0.013 deg peak-to-peak
Time Constant (roll axis)	0.5 sec
Optics	0.8" f/1.0 semisolid Cassegrain Schmidt
Size	4 x 5 x 11 in.
Weight	6 lb
Power	1.8 watts (average)

configuration employed in Mariner C, that is, coverage of the necessary field of view with high resolution capability, required sensitivity and spectral characteristics, coupled with the ability to scan the field of view without moving parts. Second, it appears possible that the electronic scan mechanism is of such a simple nature as to provide increased reliability. The power requirements are increased, however, and several other problem areas concerning multiple targets in the field of view must be given more detailed consideration.

The photomultiplier tube contains four independent quadrants of photocathode. Since, in the Voyager application, only single axis information is required, the quadrants can be biased in pairs to provide,

essentially, two detection surfaces in bridge circuitry. A more complete treatment of the tube, its configuration and operational characteristics, is given in Section 6 of Appendix E. Here, it is sufficient to point out that the Canopus image is deliberately blurred by the optics to produce an image of finite size. Depending on the switching speed, the degree of null centered noise, and the S/N ratio, an optimum image size can be defined.

Optics to be employed should provide not only the desired image size, but a field of view comparable with that utilized in the Mariner C type of Canopus tracker, that is, 30 x 4 degrees total. This can be provided by lenses and a slit diaphragm. Since the photocathode active face is 10 mm in diameter, and the desired field of view is 30 degrees, the focal length of the collector lens is given by:

$$f1 = \frac{d/2}{\tan \frac{\theta}{2}} = 19.2 \text{ mm}$$

where

$$d/2 = \text{Radius of photocathode} = 5.0 \text{ mm}$$

$$\theta/2 = \text{Half angle FOV} = 15^\circ$$

Assuming fast, f/1 optics, the collecting lens has a diameter of 19.2 mm. The image would be intentionally defocused to a diameter of 0.25 mm.

Since only single axis information is required, a slit diaphragm is employed to narrow the field of view at right angles to the 30 degrees. A roll axis dimension of  $\pm 2$  degrees was chosen in a tradeoff analysis. As the field in the roll dimension increases, it becomes easier to stop the spacecraft roll during acquisition maneuvers, and keep the acquired star in the field. Thus broadening the field also increases the probability of acquiring false targets, and  $\pm 2$  degrees is considered the minimum dimension to stop the spacecraft during acquisition.

Figure 4-19 is a star map of the sky in the region of Canopus. Utilizing a 30 x 4-degree slit, it is found that the worst case includes

3-1

either three stars of 4th magnitude, or two stars of fourth and one of third magnitude. No other first or second magnitude stars can be included within this field of view regardless of orientation or location of Canopus within the field. Thus, during tracking operation, the total flux from these sources plus general integrated radiance from all other stellar sources, appears to be insufficient to introduce significant errors in the null stability of the tracker.

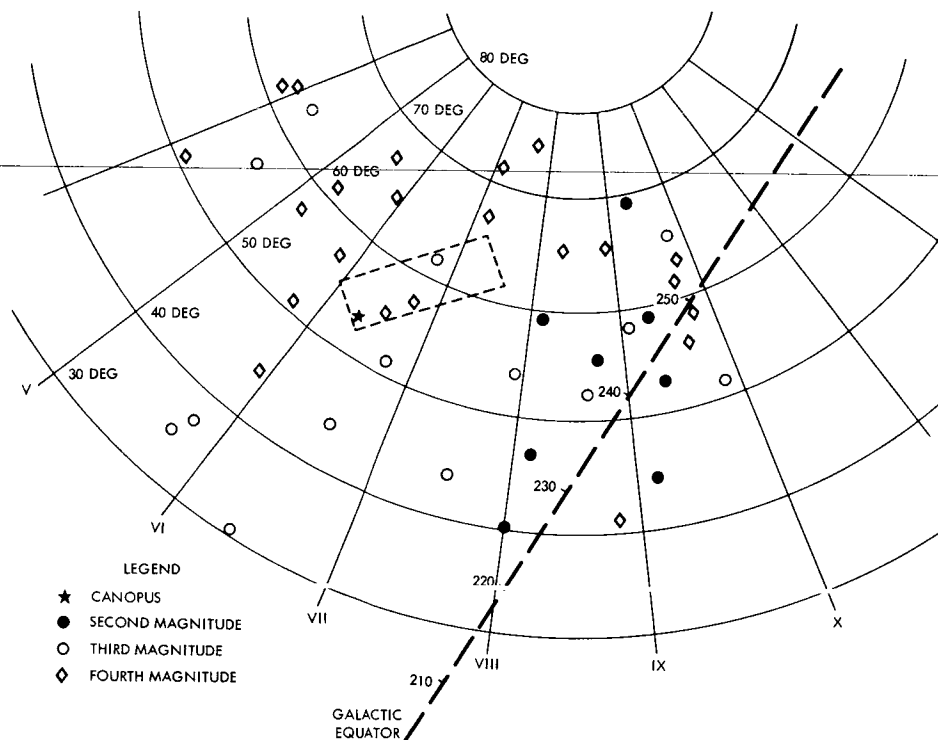


Figure 4-19. Star Field Near Canopus

The operation and design of the quadrant photomultiplier Canopus star tracker is described in detail in Section 6 of Appendix E and summarized in Table 4-4. The operation of the quadrant photomultiplier tube itself is also discussed in the Appendix.

### 1.6.3 Conclusions

Two different configurations of Canopus star tracker have been considered in detail to provide single axis localization to the Voyager spacecraft attitude control system. Both have the advantage of providing

Table 4-4. Characteristics of Quadrant Photomultiplier Star Sensor

Lens system	corrected refractor f/1.0
Focal length	19.2 mm
Detector	quadrant photomultiplier tube - ASCOP 568A
Instantaneous field of view	4 x 30 deg rectangular
Scan and rate	all electronic switching, 1600 cps
Power	5.35 watts (28 VDC)
Weight	6.00 lb
Size	204 in <sup>3</sup>

sufficient field of view for acquisition without requiring any mechanical scan, and tracking is performed by electronic means. The first, utilizing an image dissector tube as sensor, is essentially the Canopus tracker carried on the Mariner C. The second utilizes a quadrant photomultiplier tube, whose electronic signal processing is made to provide one axis information only.

While the first sensor has proven its reliability on previous missions, the second has received considerable attention because the electronic switching is of such a simple nature that reliability may be considerably enhanced. It may also, through careful optical design, provide a sufficient field of view (30 x 4 degrees) without requiring the commanded step function which is needed with the Mariner C star tracker to encompass all anticipated geometry and trajectory situations.

Both star trackers are compared in Table 4-5. If a recommendation must be made at this time, then the Mariner C type Canopus tracker must be given the preference, for despite the attractive features of the quadrant photomultiplier type sensor, it does not have the flight tested performance reliability already well proven with the former type of sensor. For whatever sensor is chosen, attention must be given to spacecraft cleanliness to minimize the possibility of dust particles reflecting sunlight in the sensor optics.

Table 4-5. Comparison of Star Trackers

Sensor	Canopus Tracker 1	Canopus Tracker 2
Detector	image dissector tube, CBS - Type CL 1147	quadrant photomultiplier, ASCOP Type 568A
Photocathode	S - 11	S - 11
Instantaneous field of view	0.86 x 11 deg	4 x 30 deg
Optics Diameter	0.8 in.	0.76 in.
F/no	F/1.0	F/1.0
Output time constant	0.5 sec	0.5 sec
Null noise	0.013 deg	0.002 deg
Gimballing and scan	all electronic	all electronic
Power	1.75 watts (50 volts)	5.35 watts (28 volts)
Size	220 in <sup>3</sup>	204 in <sup>3</sup>

### 1.7 Earth Tracker

It is possible to provide three-axis stabilization for the Voyager spacecraft by aligning the roll axis of the craft along the spacecraft-earth line, thus providing two-axis stabilization, and rolling about the craft roll axis to acquire some well-known star, i. e., Canopus, to provide the three-axis information. The constant pointing toward earth through the use of an earth tracker permits optimum alignment of the high-gain antenna with the DSIF on earth. If fixed solar panels are considered, a loss is taken on optimum solar radiation absorption for power, but this is more than compensated by the larger antenna possible (16 ft). This mechanization was considered for vehicle configuration C described in Volume 4.

Table 4-6 indicates, for various periods before and after insertion into Mars orbit, the range from the spacecraft to the earth, and the angular subtense of the planet, plus its radiance, having considered the appropriate phase of the earth.

Table 4-6. Earth Radiance Characteristics

Time (reference to Mars orbit insertion)	R (km)	$\theta$ (rad)	I (watts - $\text{cm}^{-2}$ )
-10 days	$1.05 \times 10^8$	$1.36 \times 10^{-4}$	$7.4 \times 10^{-12}$
0	$1.22 \times 10^8$	$1.18 \times 10^{-4}$	$1.2 \times 10^{-11}$
+ 1 month	$1.58 \times 10^8$	$0.915 \times 10^{-4}$	$1.25 \times 10^{-11}$
+ 2 months	$1.95 \times 10^8$	$7.4 \times 10^{-5}$	$1.00 \times 10^{-11}$
+ 3 months	$2.32 \times 10^8$	$7.4 \times 10^{-5}$	$8.0 \times 10^{-12}$
+ 4 months	$2.70 \times 10^8$	$5.35 \times 10^{-5}$	$6.5 \times 10^{-12}$
+ 5 months	$0.308 \times 10^8$	$4.67 \times 10^{-5}$	$5.3 \times 10^{-12}$

Assuming that the radiance in the visual portion of the spectrum from the earthlight is similar in proportion to that from reflected sunlight ( $6000^\circ\text{K}$  black body with peak wavelength at  $\lambda = 0.5\mu$ ) and that the earth's albedo through this octave ( $0.36\mu$  to  $0.72\mu$ ) is panchromatic, then visual radiance levels vary from  $8.5 \times 10^{-13}$  to  $4.3 \times 10^{-13}$  watt/ $\text{cm}^2$  or visual magnitudes from approximately 0 to -0.7. Thus the apparent brightness is roughly equivalent to that of Canopus.

The image subtended by the target is on the order of 0.1 milliradian or less as seen on Table 4-6, and therefore, regardless of the sensor type selected, the planet image will be equal to or greater than the resolution of sensor. Thus the earth image is not essentially different from a bright star image, and earth phase will not affect accuracy.

Because the earth is starlike at the ranges under consideration, an appropriate earth tracker can utilize the design of any number of star trackers already in existence. A review of various star tracker designs has been performed, as it had been when Canopus tracker considerations were being studied. These included the following general categories:

- a) Mechanically gimbaled sensor
- b) Reticle and photomultiplier tube
- c) Mosaic detector arrays
- d) Bilinear photomosaic detector
- e) Solid-state tracker, mechanical scan
- f) Radiation transducing tracker
- g) Vidicon plus reticle detector
- h) Electronically switched track fields
- i) Electronically scanned trackers.

The advantages and disadvantages of these sensors are discussed in Section 1.6.3. The conclusion reached in that section is applicable to the present problem, that is, the two most attractive sensors are those that utilize the quadrant photomultiplier tube, and the reconotron image dissecting tube. The general application of these tubes in Canopus tracking is discussed in Section 1.6 and Section 6 of Appendix E.

The image dissector tube sensor (reconotron) was selected as the recommended Canopus tracker because of its proven performance and reliability on the Mariner C flight to Mars. This conclusion makes its selection as the earth sensor detector preferable to other sensors.

The earth sensor should be able to operate without excessive error when pointing as close as 10 to 15 degrees from the sun. Thus stray light baffling becomes a serious requirement. Preliminary calculations indicate that a tube, with light baffles, extending nearly the full depth of the spacecraft is needed to insure adequate multiple reflections off the baffles before the stray sunlight could reach the sensor.

## 1.8 Reaction Control System

The reaction control selection and design for the Voyager SCS lends itself to mass expulsion rather than momentum exchange techniques, as discussed in Section II-1.1. Consequently, effort on the reaction control problem has been concentrated on tradeoff studies aimed at selection of a particular mass expulsion reaction control system configuration.

In the process of selection, various requirements of the SCS operation were considered as they affect the reaction control system: 1) type of control modulation, 2) dynamic response requirement, 3) mission total impulse requirement, and 4) allowable limits on pulse width and amplitude variation. Other considerations entering into the trade-off study include the total expected amount of (solar) energy available for conversion to energy for reaction control. This factor is influential in establishing the practicality of a heated gas system or liquid storage system. In addition, the possibility of affecting experiments, contaminating Mars, and the effects of reaction control gas in the neighborhood of the spacecraft must be contended with. For example, atomic and diatomic gas molecules are less likely to adhere to spacecraft components than those of heavy molecular gases (continuous long-term deposition on sensors and optical devices might pose a problem).

The reaction control system configuration selected for the Voyager spacecraft is a stored, gaseous nitrogen system with resistance heating of the gas immediately upstream of the nozzles, and incorporating redundant tankage and feed systems. This system, illustrated schematically in Figure 4-20 consists of two storage tanks, 12 normal thrust nozzles, 4 high thrust roll nozzles, 16 on-off solenoid valves, 2 pressure regulators, relief valves and charging valves, and 4 pressure transducers. The nitrogen is heated only during periods in which an excess of electrical power is available. In this manner, its use will provide an increase in potential life by approximately a factor of two when compared with a cold nitrogen system of the same weight. A similar heated gaseous nitrogen system has already been flight qualified for reaction control on the Vela satellite. The system on Voyager is sized to provide at least twice the required impulse, not considering the effect of the heaters, and the heaters therefore have no reliability implications for the required mission life.

As illustrated in Figure 4-20, the high-thrust nozzles used for roll control during solid engine operations are fed by the same pressure regulators as the low thrust nozzles. However, detailed design studies



involving regulator flow requirements may show advantages for independent regulators supplying these thrusters. Design of the higher (0.5 lb) thrusters will be based on cold gas operation, since it is not expected that they will require a significant amount of impulse on a percentage basis.

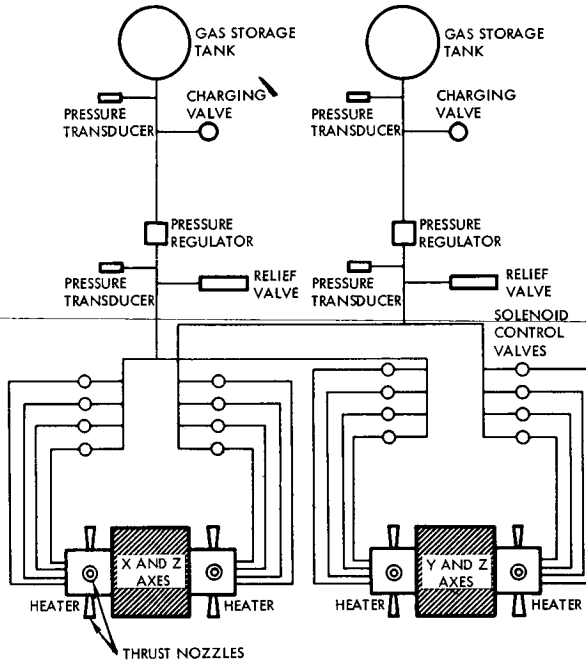


Figure 4-20. Heated Gaseous Nitrogen Reaction Control System Schematic

### 1.8.1 Summary of Tradeoffs

Liquid storage systems employing cold gas expulsion were studied and found to offer no weight or any other advantages over a heated  $\text{GN}_2$  system. Conversely, they represent greater complexity and less reliability.

A resistively heated ammonia decomposition system offers a weight advantage over the heated  $\text{GN}_2$  system by a factor of two, but is not considered to be state of the art. Even if it were as fully developed, it would represent greater complexity, as do all liquid storage systems.

Hot gas reaction control systems were eliminated on the basis of their incapacity for reliable performance at the low thrust levels required. Performance here refers to combustion or decomposition stability, repeatability, and efficiency (loss of specific impulse).

Subliming solids are generally inapplicable at this thrust level, and are not capable of coping with continuous demand, as in the acquisition mode of the mission, at the thrust level required.

Solid propellants, of course, are of such a nature that combustion requires continuous burning since multiple starts have not yet been made practical. Thus, they are incompatible with pulse type operation.

### 1.8.2 Selection of Working Fluid and System Configuration

Stored gas systems for spacecraft attitude control are generally accredited with offering maximum reliability, based on system simplicity and proven flight performance. Because of the relatively low mission impulse requirement, i. e., 1200 lb/sec, stored gas systems are competitive with liquid storage and hot gas systems on a weight basis as well as reliability. This is illustrated by the results of system weight studies, presented in Figure 4-21, which plots reaction control system weight for various working fluids as a function of mission total impulse. This figure does not consider redundant gas supplies. As shown, of the several inert gases, nitrogen represents nearly the lightest weight for a stored cold gas system, 63 pounds of system weight for 1200 lb/sec. For a heated nitrogen system of the same weight, the total impulse available is nearly doubled. Therefore, as part of the effort in subsequent phases of this program, tradeoff studies will be refined to arrive at an optimum system weight in light of the reliability of the added feature, resistance heaters, the probability of loss of gas due to leakage and valve failure, and the probability of disturbances requiring the amount of gas estimated.

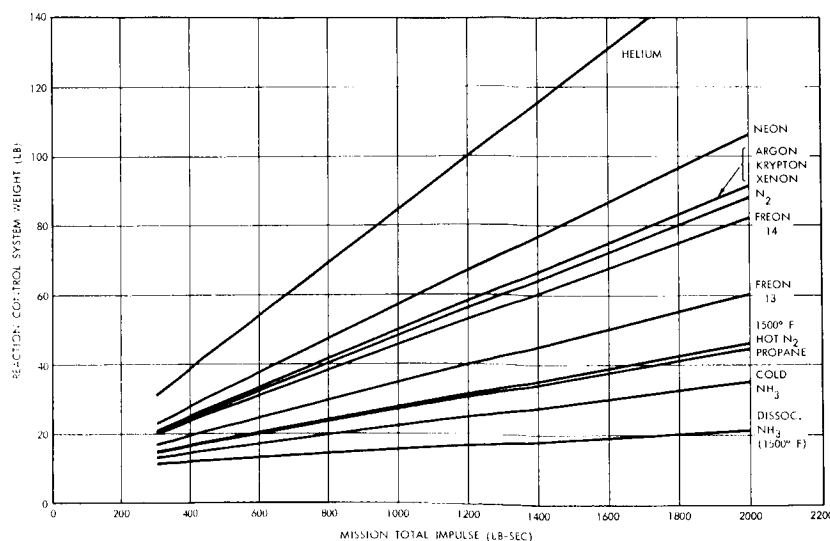


Figure 4-21. Reaction Control System Weight for Various Working Fluids as a Function of Mission Total Impulse

The gain in available impulse by approximately a factor of two using heated gas results entirely from an increase in  $I_{sp}$ . The higher gas temperature results in an increase in gas characteristic exhaust velocity which is proportional to the square root of absolute gas temperature. The cost of this performance gain is the addition of four resistance heating coils coupled with the four thrust nozzle assemblies. Only one heating coil per nozzle assembly appears necessary in view of the low probability that more than one nozzle will fire at any given time. In the event that more than one nozzle fires simultaneously, the loss in specific impulse is easily tolerated.

The philosophy of exploiting the advantages of a heated gaseous nitrogen system would be essentially that reaction control system design would be based on heated gas system operation with a cold gas system serving as backup in event of power cut-off or heater failure. Inclusion and operation of gas heaters, directly upstream of the nozzles, during most of the mission should add considerable life expectancy to that available with a cold gas system. At this stage in the program it is expected that excess power will be available during most of the cruise mode and during the early Mars orbit phase. The gas heaters would be operated on an as-available basis with respect to electrical power thereby maintaining maximum flexibility in favor of other more critical power requirements. This approach does not impose any new requirements on the design or implementation of the electrical power supply.

Power consumption of the four heaters is estimated at 10 watts per heater or a total of 40 watts when the heaters are on. This estimate is based on heater operation at constant temperature, i. e., continuous power to the heaters as opposed to switching on and off in keeping with the SCS limit cycle. Supplying continuous power to the heaters avoids the thermal transient response associated with cyclic heater operation. The 40-watt power consumption results from thermal radiation to space from a heating coil designed to heat a 50-millisecond pulse of ambient temperature nitrogen gas to 1500°F. As the heaters are turned on and off the gas specific impulse changes, but the thrust level is nearly constant.

This, of course, is desirable to avoid the necessity of changing pulse width to maintain a constant attitude control limit cycle and to benefit from the higher gas specific impulse. Therefore, added complexity to the SCS electronics will not be necessary.

An additional consideration in studying a heated  $\text{GN}_2$  system for application to the Voyager SCS is the effect on dynamic response due essentially to the additional line length of heat exchanger coil. The dominant factor in determining system response is the equivalent pneumatic pressure divider formed by a solenoid control valve, line capacitance, and nozzle. If this circuit is linearized and treated as a lumped parameter system, its transfer function is simply a first order lag with a time constant proportional to pneumatic capacitance and resistance and inversely proportional to gas temperature. Assuming no change in resistance (line flow area  $\gg$  inlet and exit restrictions) or gas temperature, the increase in time constant will proportionate to the increase in line length due to the heater coil. It is expected that the developed length of the heater coil will be no greater than 12 inches. The increase in time constant should be acceptable in terms of SCS dynamics.

A similar gaseous nitrogen heater has been designed, developed, and incorporated into the velocity correction thruster for the Vela 3 satellite and has been flight qualified\*. The thruster for this application produces 0.042 pound of thrust as compared to the requirement of 0.044 pound for the Voyager thrusters. Test data indicates a constant nozzle thrust level over a  $1000^\circ\text{F}$  variation in temperature.

In addition to development of heated  $\text{GN}_2$  thrusters for the Vela 3 satellite, development efforts are also being conducted in connection

---

\* Jackson, Kruger, Stansel, Starr, "Vela Launch 3 Thruster Development Program Final Report," Vol. I, TRW Report No. 2409-6023-RU000, June 1965.

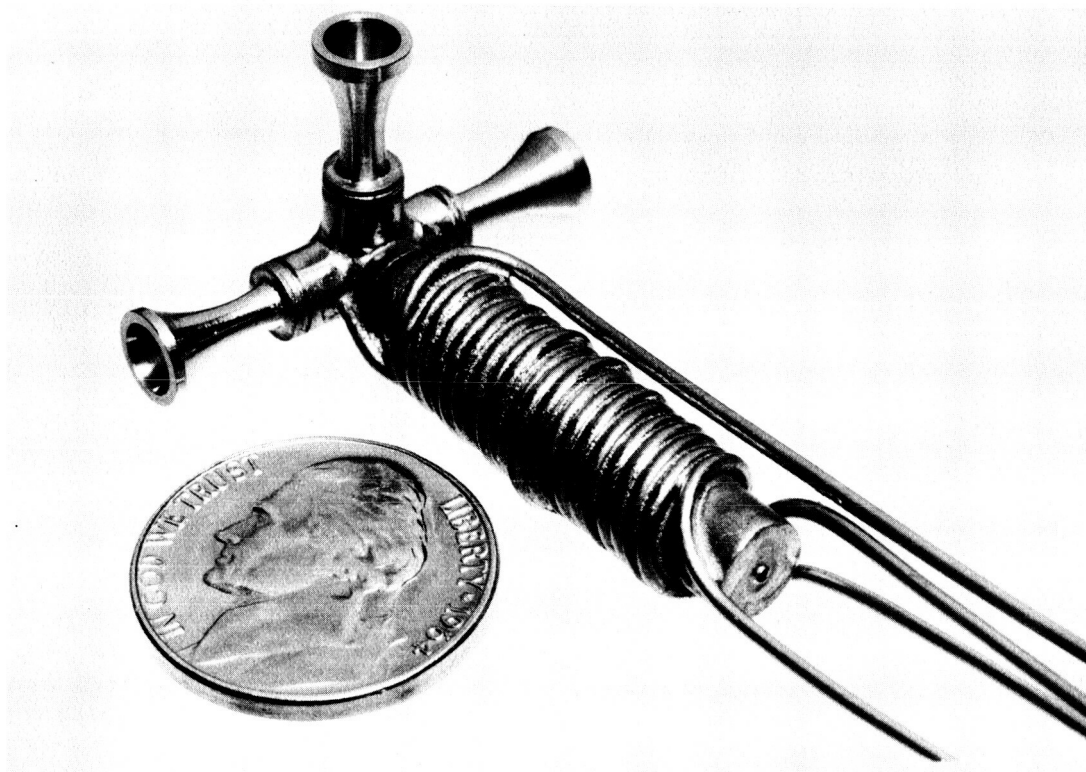


Figure 4-22. Heated  $\text{GN}_2$  Tri-Nozzle Thruster Assembly

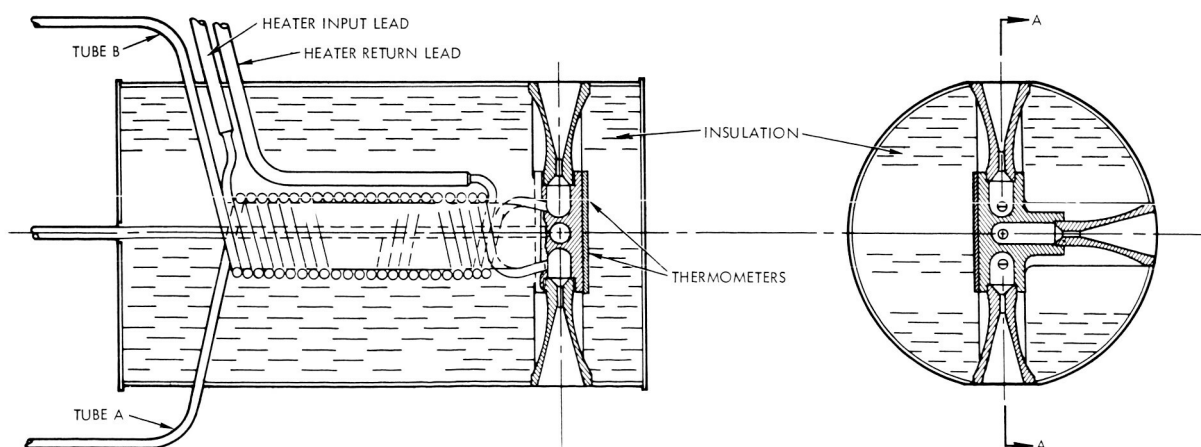


Figure 4-23. Sectional Schematic Illustration, Tri-Nozzle Thruster Assembly

with the Vela 5 program. A photograph of a development model of a tri-nozzle thruster assembly for this program is presented in Figure 4-22. A sectional drawing of the same assembly is presented in Figure 4-23. Optimum regimes for the various types of reaction control systems are presented in Figure 4-24\* in terms of thrust level and total mission impulse requirements. The boundaries between the different types of reaction control systems are not defined by weight alone; reliability, performance, state of the art, cost, and lead time also influenced these boundary definitions. The Voyager SCS requirements for reaction control appear to be represented by a point well within the region for stored gaseous system, i. e., 0.044-pound thrust and 1200 lb/sec total impulse.

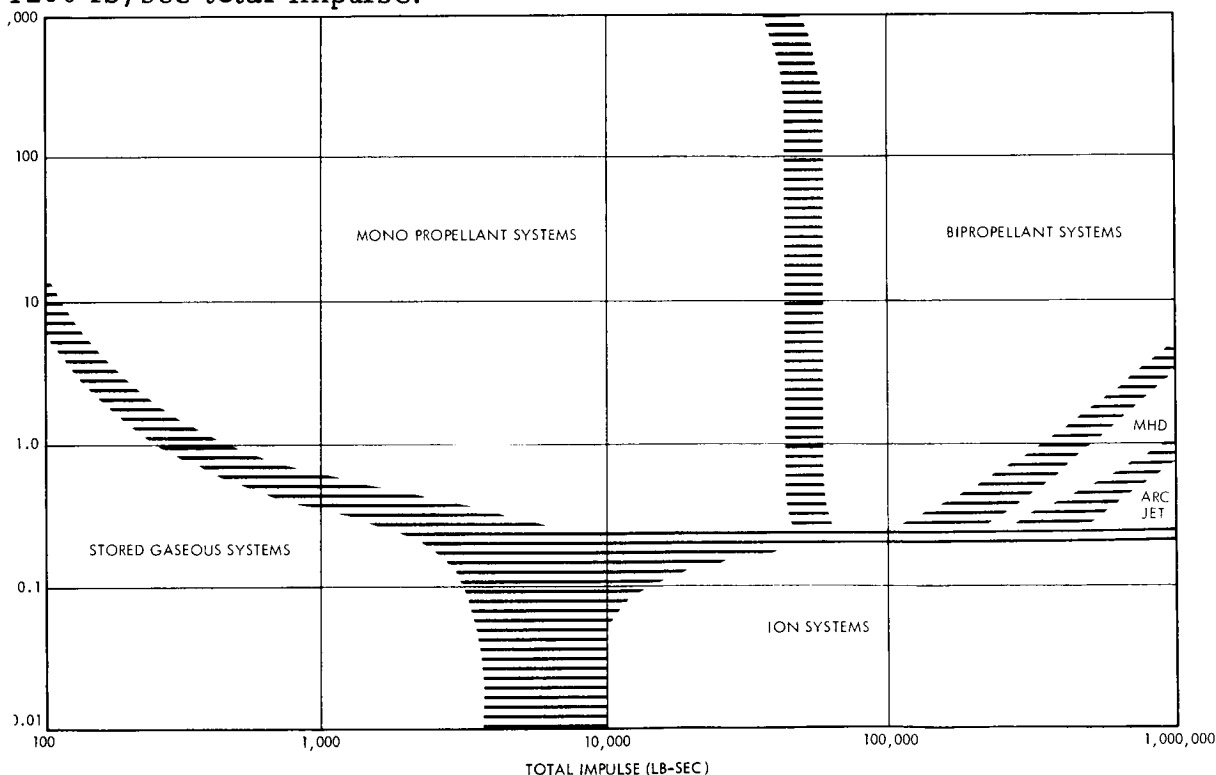


Figure 4-24. Optimum Thrust Impulse Regimes for Reaction Control System

#### b. System Mechanization Employing Redundancy

The baseline configuration assumed here employs a total of eight nozzles together with one solenoid control valve for each nozzle. The eight nozzles include six normal-thrust nozzles for pitch, yaw,

\* Adapted from Walter Kidde Company data.

and roll control torques and two high-thrust nozzles for roll control during retrofire. The nozzles provide unbalanced control torques. During limit cycle operation, the unbalanced forces alternate in sign and therefore the linear impulse imparted to the spacecraft tends to have zero average value. The net linear velocity imparted to the spacecraft during reorientation is negligible because of the low thrust levels.

To improve system reliability, redundant tankage, gas feed systems, and valves are used to supply coupled pairs of nozzles. As indicated in Figure 4-20, coupled pairs of gas jets supplied from completely independent feed systems will assure attitude control operation in the presence of any single failure.

If a valve fails to open, the acceleration constant will be halved and pure couples will no longer be applied to the vehicle. The linear momentum imparted to the spacecraft under such conditions will be negligible as discussed above. If a valve fails to close, the disturbance torque it applies to the spacecraft will be countered by the opposing coupled pair. The SCS will operate in a stable, one-sided limit cycle until the gas supply feeding the failed valve is exhausted.

The system also protects against regulator failures in the ways it protects against valve failures. The effects of a completely open regulator failure will be minimized by proper placement of the relief valve vent so that the disturbance torque is within the capability of the remaining half of the system.

Mechanical design of the solenoid control valves and pressure regulators employs redundant seating techniques. Redundant seating has been shown to reduce leakage to negligible amounts. It contributes little to component weight and is presently incorporated in valves and regulators being designed by aerospace fluid power control manufacturers.

Additional discussion of reaction control system redundancy is given in Section 1.10.

### 1.8.3 Other Types of Reaction Control Systems

#### a. Liquid Storage Systems

Liquid storage systems are typified by Figure 4-25 (for redundant gas supplies). Liquid storage systems, which rely on heat input to vaporize the propellant to yield a cold gas, are somewhat lighter than the stored cold gas systems, as shown in Figure 4-21. However, they depend on a source of thermal energy for operation, and are much less reliable than the heated nitrogen system. Although environmental heat transfer to the liquid would probably suffice to vaporize it at an acceptable rate for the mission cruise mode, initial acquisition demands would undoubtedly require active heat input. In addition, there is the problem of ascertaining that vapor only and not two-phase fluid is fed to the control valves.

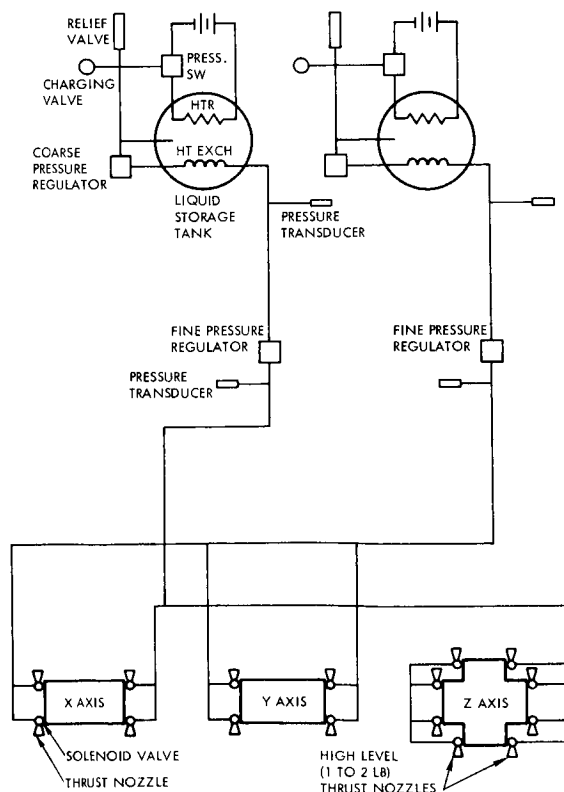


Figure 4-25. Liquid Storage Reaction Control System - Typical Mecronization



The system weight comparison in Figure 4-21 indicates that the heated  $\text{GN}_2$  system is competitive with regard to weight with liquid storage systems. For this mission, its weight exceeds that on an ammonia liquid storage system by 6 pounds, hardly enough to warrant the added complexity of the ammonia system.

b. Dissociated Ammonia Systems

A resistively heated ammonia decomposition system is similar in mechanization to the liquid storage system just described. It differs in that resistance heaters are coupled to the thrusters in a manner similar to that for the heated  $\text{N}_2$  system, in order to achieve decomposition. A typical configuration for this type of system, with redundant gas supplies, is presented in Figure 4-26.

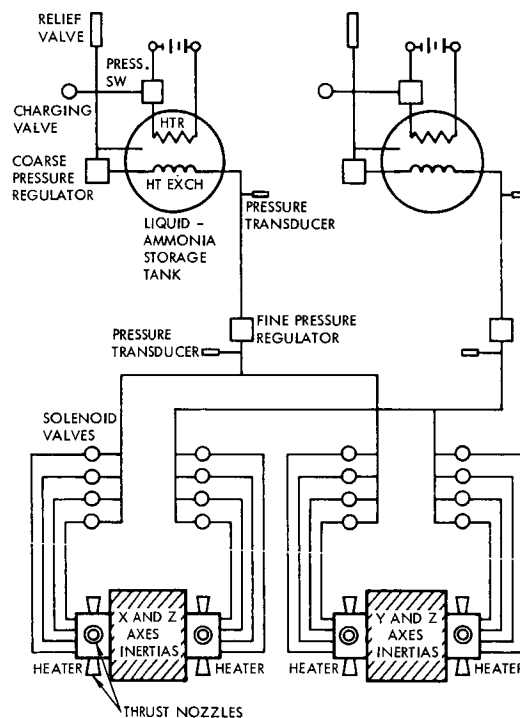


Figure 4-26. Dissociated Ammonia Reactive Control System Schematic

The baseline nonredundant system weight comparison shows an advantage for a dissociated ammonia system over a heated  $\text{N}_2$  system: 16.5 as compared to 31.5 pounds for the nitrogen system. However, as mentioned previously, a reaction control employing heated  $\text{N}_2$

has been fully flight qualified, which places it considerably further along in the state of the art than this low-weight contender. The corresponding projections of development time and cost are the primary factors contributing to preference of a heated  $N_2$  system over a dissociated ammonia system. It is expected that power requirements and dynamic response of these two types of systems would be comparable.

c. Hot Gas Systems

Hot gas systems include both the monopropellant and bipropellant classes of systems as well as modifications thereof. Primary objections to these systems have to do with state of the art, and the same comments that were made with respect to a dissociated ammonia system apply. The comments are qualified in that they apply to a low thrust, low impulse application in which the duty cycle is low and a great number of repetitive starts are required in conjunction with short pulse durations. For the low thrust level required, combustion stability is a problem even for continuous firing. In addition, good repeatability is difficult to obtain, i. e., pulse amplitudes can be expected to vary significantly. For monopropellant systems employing hydrogen peroxide or hydrazine decomposition, poor thruster efficiency can be expected for the pulse-type operation required.

In an attempt to overcome the shortcomings of these monopropellant thrusters, TRW Systems has developed a nuclear isotope monopropellant hydrazine engine (NIMPHE). This engine design is based on the use of a radioisotope capsule to heat the catalyst bed, thereby maintaining high specific impulse for a great number of start-ups. Because of its early stage of development, and its present incapacity for good repeatability at this thrust level, it is not considered a candidate for application to this mission.

All the comments made for monopropellant systems are also applicable to bipropellant systems. Repeatability is even more difficult to obtain because of the short time available for mixing and reaction of the two constituents. This view of hot gas system applicability at this thrust level (0.044 lb) is collaborated by the information presented in Figure 4-23.

d. Subliming Solids

The subliming solid rocket is generally applicable to systems operating at the micropound thrust level. Although it is conceivable that this type of system could be developed for operation at the thrust level required, it would not be capable of adequate performance during the acquisition mode, when all of the available energy contained in the products of sublimation at that time would be quickly consumed. It is doubtful that the sublimation process could be sufficiently accelerated to keep up with the demand of continuous firing in that mode. Even if it could, the process does not lend itself to regulation, and this implies the need for spillage of sublimation products to regulate chamber pressure.

1.9 Control System Electronics

The control system electronics assembly supplies power to the reaction control jet solenoids and to the thrust vector control (TVC) actuators in response to signals from the pitch and yaw sun sensors, the Canopus sensor, the pitch, roll, and yaw gyros, and the control, sequence, and command subsystem.

A functional block diagram of the control system electronics is shown in Figure 4-27. The electronics process all sensor error signals to provide control of the gas jets and TVC systems for all modes of operation and include mode switching logic controlled by inputs from the sensors and the CS and C. The switching shown is for functional illustration only. All switching will actually be performed using transistor switches to minimize magnetic interference. The lead networks shown are used to compensate the TVC drive signals during the midcourse correction and retropropulsion modes.

The control system electronics use redundancy in several functions to increase reliability. Not all of the redundancy is indicated in the block diagram. The redundancy to be used and the considerations which lead to its use are explained in Section 1.10.

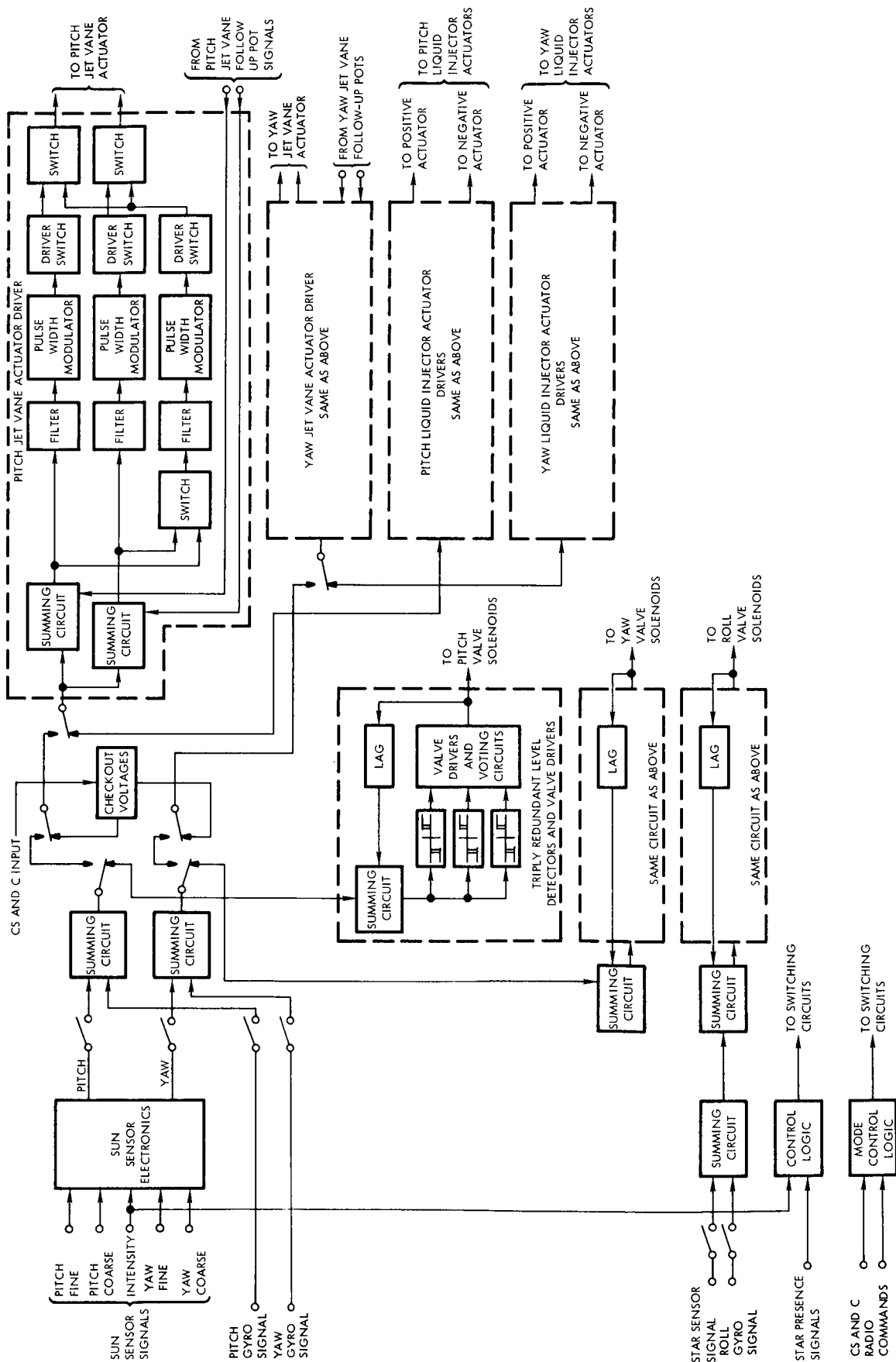


Figure 4-27. Control Electronics Assembly Function Block Diagram

### 1.9.1 Sun Sensor Electronics

The sun sensor electronics is shown in the block diagram of Figure 4-28. As indicated, the assembly consists of preamplifiers, signal amplifiers, a level detector, and automatic gain control. The level-detected intensity signal is used to switch between the fine sun sensor signals and the coarse sun sensor signals. The switching is performed by the use of dual emitter chopper transistors. The AGC is used to compensate for changes in sun sensor gain resulting from changes in sun intensity, which changes as a result of the increase in distance to the sun during the Voyager mission. The AGC increases the scale factor of the fine sun sensor signal in proportion to decreases in the sun intensity signal. While the need for AGC has not been firmly established at this time, it is included for the purpose of sizing the electronics.

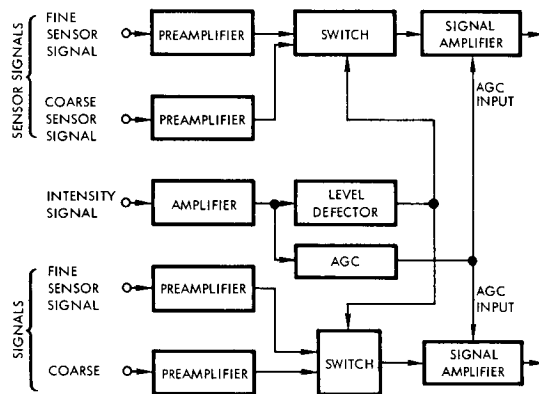


Figure 4-28. Sun Sensor Electronics

### 1.9.2 Valve Control Electronics

The valve control electronics consists of a double-ended level detector (detects both positive and negative levels) driving transistor valve driver switches. Each level detector has a lag network with a time constant of 100 seconds around it to provide pseudo-rate signals.

### 1.9.3 Thrust Vector Control Electronics

The TVC electronics supplies power to either the jet vane actuators on the liquid monopropellant engine or to the liquid injector actuators on the solid propellant engine in response to position signals from the pitch and yaw gyros operating in the position mode. The block diagram of Figure 4-27 indicates a separate channel for each of the TVC actuators. Functionally, the channels are the same, each channel consists of a lead compensation network, a pulsewidth modulator, and an output switching

amplifier. The parameters for the jet vane actuators are not the same as those for the liquid injector actuators.

A backup TVC electronics channel is provided such that it can be switched into use if one of the primary TVC channels is determined to have a malfunction. By ground command, tests will be made before all thrusting periods to provide assurance of the operability of the electronics.

It may be possible to simplify the design of the servo amplifier section by combining the drives to the jet vane actuators and LITVC servo valves. A single electronic signal channel would thereby drive both types of actuators. The differences in gain and filter characteristics would be accommodated by switching of the appropriate components. A detailed study is needed to examine the tradeoff factors to determine whether this mechanization results in an over-all improvement of subsystem performance.

The main advantage of pulse-width modulation for the TVC control is that it can be used to supply varying amounts of power while operating amplifier transistors in the switching mode where they dissipate minimum power and have greater certainty of operation. Figure 4-29 is a schematic diagram of the pulse-width modulator. It consists of two integrated circuit differential amplifiers and other discrete passive components. A sawtooth wave is applied to the input of each differential amplifier. The differential amplifier gain is so high that its output is saturated either positively or negatively corresponding to the positive and negative portions of the sawtooth ramp. The DC signal input to the entire pulsewidth modulator varies the DC level of the sawtooth waves and thus varies the time that the sawtooth ramp passes through zero. Varying the time that the sawtooth ramp passes through zero varies the time of transition of the output from positive to negative transition, thus varying the width of the positive pulse out of the differential amplifier. Actually, there are two pulsewidth modulators in Figure 4-29; one generates variable positive pulses and the other generates variable negative pulses. With a zero DC signal input, the positive and negative pulse widths are equal and cancel each other out so that there is no pulse.

Varying signals lengthen the width of one of the pulses and shorten the width of the other pulse. This provides a total pulse either positive or negative as determined by the polarity of the input signal. This pulse can be used to turn on driver transistor switches.

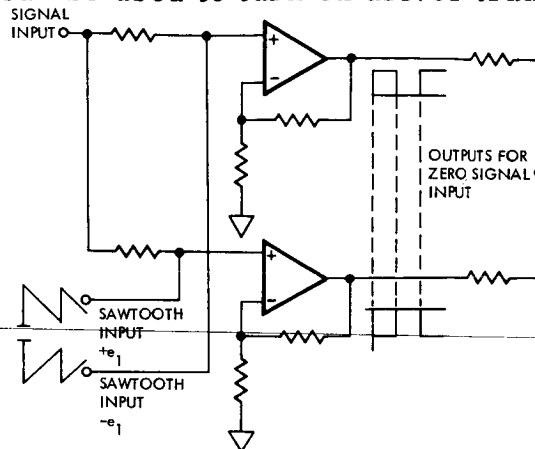


Figure 4-29

Symmetrical Pulse Width Modulator

Another technique for pulse-width modulation consists of using a triggered voltage controlled one-shot multivibrator in which the time the one-shot output is on is proportional to the input voltage. Two such one-shot multivibrators are necessary, one for positive signals and one for negative signals, the output of each inhibiting the other in a manner similar to the above pulse-width modulator. The disadvantage of this second technique for pulse-width modulation is that it requires the use of more components since a voltage controlled one-shot multivibrator is not presently available as an integrated circuit. Hence the technique has not been considered further.

#### 1.9.4 Gyro Electronics

The gyro electronics is shown functionally in Figure 4-30. The electronics consists of an amplifier, demodulator, and precision torquer. The circuits provide for operation in the rate mode by electrically caging the gimbal. Open loop operation is in the conventional, rate integrating mode. A precision current generator provides means for commanding turning rates to the spacecraft by torquing the gyro. The gyro electronics also provides temperature control to the attitude reference assembly by controlling the current to the gyro heaters.

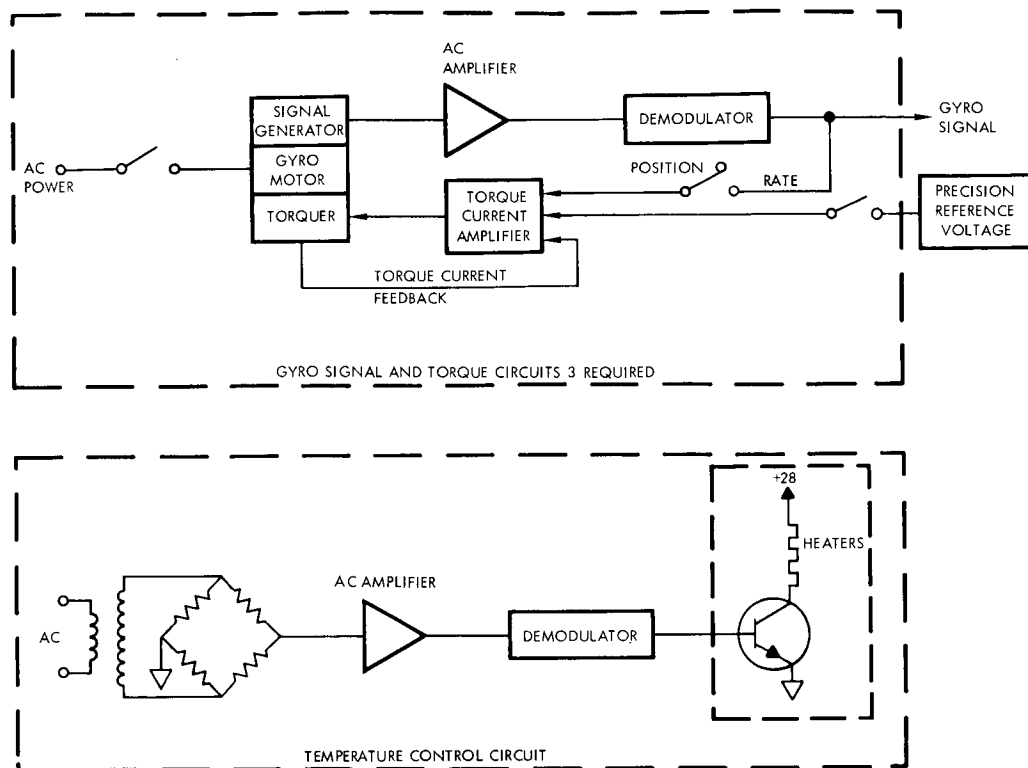


Figure 4-30. Gyro Circuit Block Diagram

#### 1.9.5 Mode Control Electronics

The mode control electronics controls the switching necessary to couple the sensors with the torque sources for all modes of operation. This switching control is provided in response to signals from the CS and C, the sun sensors, and the star tracker. The mode control electronics consists of logic circuits and switching transistors.



## 1.10 SCS Reliability Tradeoffs

Considerable emphasis was placed on reliability tradeoffs during this study. This effort, discussed in detail in Volume 4, involved the definition of several degrees of system redundancy and compared the reliability increment as a function of additional weight.

A baseline configuration was defined which consisted of a direct nonredundant mechanization of the system functional requirements. The reliability of this configuration was assessed for six periods: 1) boost into the transfer trajectory, 2) cruise through capsule separation, 3) ~~cruise following capsule separation and spacecraft retropropulsion~~ into orbit, 4) 1 month in orbit, 5) 5 additional months in orbit, and 6) the entire mission. Augmented configurations were then defined which included varying degrees of redundancy. These configurations were assessed for reliability for the five mission phases.

The resultant assessments are summarized in Table 4-7. These assessments provide a guide for the judicious use of weight to obtain redundancy so that the overall SCS reliability was compatible with the Voyager mission goals. The selected SCS configuration showed that a significant improvement over the baseline configuration was achievable within the overall spacecraft weight margin allowance.

Some of the design factors which were included to enhance over-all reliability are discussed in the following sections.

### 1.10.1 Control Electronics Reliability

#### a. Integrated Circuits

Although not much reliability data is available on integrated circuits in analog applications, it is felt that one circuit, the Fairchild  $\mu$ A702 circuit, will have received sufficient development to enable its use for Voyager. This circuit probably has more known about its operating characteristics than any other type of DC amplifier. It is presently being used on more space programs than any other DC amplifier design.

Table 4-7. Stabilization and Control Reliability Assessment

Option	Weight (lb)	Mission Phase					Mission	Weight in-crease from Baseline (0)	Reliability in-crease from Baseline (0)
		1	2	3	4	5			
0	59	0.985143	0.864623	0.996742	0.973782	0.877540	0.725668	0	0
1	96	0.987118	0.926530	0.998212	0.987939	0.939218	0.847126	37	0.1214
2	68.5	0.991289	0.936092	0.998112	0.987831	0.938105	0.858286	9.5	0.1326
3	94.5	0.990184	0.959412	0.998838	0.985188	0.967548	0.904498	35.5	0.1788
4	90.5	0.985966	0.911255	0.997932	0.984726	0.926331	0.817870	31.5	0.0922
5	64.5	0.987065	0.889107	0.997208	0.977903	0.898144	0.768648	5.5	0.0429
6	63	0.991132	0.920662	0.997834	0.985068	0.925236	0.829868	4	0.1042
7*	100	0.991342	0.975492	0.999117	0.997969	0.981007	0.945916	41	0.2202

\* Selected configuration.

Option

- 0 Baseline
- 1 Redundant Canopus sensor with override + redundant reaction control
- 2 Redundant Canopus sensor with override + redundant signal electronics
- 3 Redundant signal electronics + redundant reaction control + Canopus override
- 4 Redundant reaction control + Canopus override
- 5 Redundant Canopus sensor with Canopus override
- 6 Redundant signal electronics with Canopus override
- 7\* Redundant Canopus sensor with override, redundant reaction control, redundant signal electronics

Note: Redundant signal electronics refers to several selected redundancies in the electronics package and therefore does not mean complete redundancy.

### b. Redundancy

The probability of failure of the control electronics can be decreased significantly by the use of redundancy. The redundancy planned for the control electronics is as follows:

- 1) Triple redundancy and voting logic are used in the level detector and valve drive circuits, as shown in Figure 4-31. Any two of the channels working properly will give proper operating. The probability of failure with this type of redundancy is approximately.

$$Q_r = 3Q_{nr}^2,$$

where  $Q_r$  is the probability of failure with redundancy, and  $Q_{nr}$  is the probability of failure without redundancy.

- 2) This same triple redundancy and voting logic is planned for the mode control logic circuits.
- 3) Each pair of TVC channels has one extra channel which can be substituted for either one of the primary channels if either should fail. Since the TVC is used only when the engine is fired, many convenient times will be available when the primary TVC channels can be tested to verify that they are functioning properly.

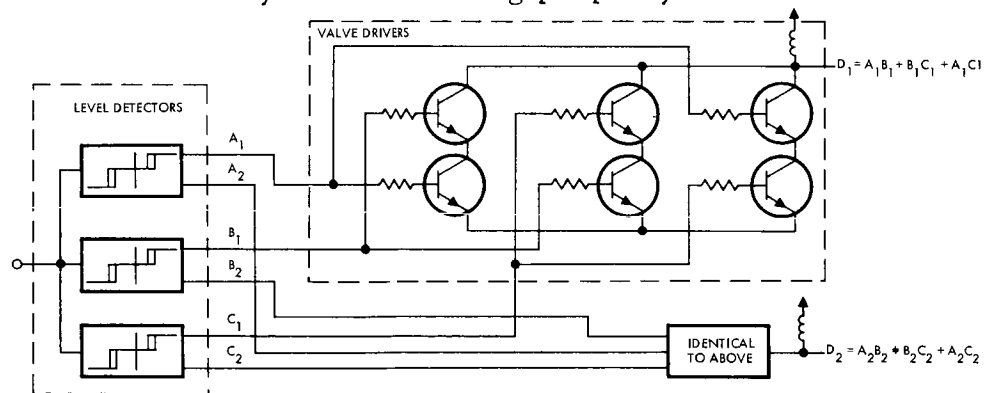


Figure 4-31. Schematic to Show Triple Redundancy and Voting Logic Used on the Level Detectors, Drivers and Voting Logic

#### 1.10.2 Reaction Control Reliability

Reliability factors were of considerable significance in the selection of the reaction control system implementation. The valves and regulators selected are designs which have leakage redundant seals.

These components are used on programs such as Vela V which also have very stringent reliability goals. They will have received adequate flight experience prior to Voyager design freeze dates.

The use of independent, parallel reaction control systems provides a high degree of redundancy and protection against control fuel leakage. This technique was used on Mariner C and is applicable to Voyager. Mariner C carried three times the maximum calculable amount of control fuel to protect against an open valve failure. In such an event, the tank feeding the failed valve would be completely depleted and the other tank would use one third of its fuel supply. In the event of a valve closed failure, the control authority would be halved and unbalanced torques would be imparted about one axis.

The use of a heated gas system for Voyager allows the same functional reliability with double lifetime expectancy for a given system weight. The selected reaction control system is sized for twice the maximum calculable requirements, based on cold gas. The use of heaters provides an effective supply of four times the maximum requirement. The system is, therefore, adequately protected against an open valve failure. An alternate implementation of reaction control system which is protected against both open and closed failure of valves utilizes four valves in series-parallel for each nozzle. All four valves are driven by the same valve driver. This approach is not competitive in regard to weight, power and volume with parallel independent gas supplies.

#### 1.10.3 Star Sensor Reliability

Although the assessment has shown the star tracker to be reliable, it was decided to employ redundant sensors to augment the over-all reliability. The additional weight necessary for this is small relative to the system reliability gain. In addition, several alternative methods of roll control are available, as discussed previously, which provide for backup of the Canopus sensor, should this prove necessary.

## 1.11 Other Considerations

### 1.11.1 Magnetics

Many of the components to be used on this subsystem will be selected from parts with known low field levels and already used on other programs such as OGO, Pioneer, and 2029. Examples of these parts are:

<u>Component</u>	<u>After Magnetization</u>
Solenoid valve	9 $\gamma$ at 12 in
Pressure switch	<25 $\gamma$ at 12 in
Pressure transducer	1 $\gamma$ at 6 in
Pressure regulator	11 $\gamma$ at 6 in
Pressure vessel	Nonmagnetic
Plumbing	Nonmagnetic

#### a. Canopus Sensor

Using an electrostatic deflection type poses no problem other than the usual selection of preferred nonmagnetic components. If, on the other hand, a magnetic deflection type is used, because of the fields generated by the deflecting coils, particular attention to the uniformity of the windings to prevent stray fields due to leakage must be made, along with the use of shielding materials enclosing the coil assembly.

#### b. Inertial Sensors

The gyros, powered by 800 cps, are not expected to be a problem since the frequency of the power to drive these gyros will probably fall outside the pass-band of the magnetometer. The use of magnetic pick-offs from the gyros will require compensation and shielding to bring them within the required limits.

#### c. Electronic Packages

No problems are anticipated in the control electronics when the components are selected from the approved parts lists already

established on the OGO, Pioneer, and 2029 programs. The switching will be performed by solid state techniques, so that magnetic shielding will not be necessary.

#### 1.11.2 Vehicle Interface

The SCS interface with the vehicle, for other than functional requirements, is primarily in the areas of view angles and alignment accuracies.

##### a. View Angles

The view angle requirements have been discussed previously in the descriptions of the various optical sensing elements. The  $4\pi$  steradian field of view required of the coarse sun sensor is provided by mounting pairs of sensors in diametrical opposition on the periphery of the solar array. The fine sun sensor field of view is provided by mounting it in the bus looking in a direction normal to the plane of the solar array.

The Canopus sensor view angle requirements are established primarily by the need to maintain an unobstructed field of view. These requirements must be integrated with those established by the articulated components such as the high-gain antenna, the planet oriented package, and the deployable scientific instruments.

Another item which falls under the category of view angles for control concerns the positioning of the reaction control jets. It is desirable to place the jets so that the exhaust streams do not impinge on portions of the spacecraft. The impingement degrades reaction control performance because it partially offsets the effect of the jet force. The need for a clear field of action for the reaction control jets has resulting in the jets being skewed relative to the principal inertial axes of the spacecraft.

The spacecraft layout which minimizes the exhaust stream impingement has another effect on the SCS. If it were required that the control axes and principal inertial axes coincide, a mixing network would

be required to transform the applied torques from reaction jet axes to principal axes. However, the differences between the two axes are not great and the cross-coupling that arises when the control torques are not transformed is a minor effect which does not degrade either pointing accuracy or the stability of the SCS.

b. Alignment Accuracies

The alignment accuracies of the primary optical sensing elements reflect the pointing accuracy requirements. Pointing accuracies for midcourse velocity corrections, capsule separation, and retropropulsion ~~require that the celestial sensors and the inertial sensors be~~ precisely referenced to each other. Pointing accuracy requirements for the planet oriented package require that the celestial sensors and the POP drive mechanism be precisely referenced to each other. Incorporation of these requirements into the over-all design has resulted in the mounting of the Canopus sensors and gyros on a special mounting structure located near the POP support structure. The precise sun sensor is mounted nearby on the spacecraft structure.

## 2. CENTRAL SEQUENCING AND COMMAND SUBSYSTEM

A sequencing and command system for a mission such as Voyager can range considerably in complexity depending on the functions it is called upon to perform. It can be as simple as a temporary data holding device or as complex as a full scale general purpose computer with pattern recognition capabilities, adaptive control, or decision-making features. It may or may not have to store data more than momentarily, perform simple or complex arithmetic or logic, handle large amounts of information, or make decisions based on real-time occurrences. Thus, it may or may not have a memory, an arithmetic unit, decoding capability, timers, or logic. Consequently, when the requirements are established so that essential characteristics of the processor can be identified, a large design step has been taken.

A requirement analysis must identify the decoding and timing requirements, the need for special registers and counters, memory requirements, and the need for arithmetic capability or decision logic. From the requirements analysis, basic approaches and component sizing studies can be conducted to identify word sizes, formats, voltage, power levels, etc.

In regard to Voyager design two areas of over-all systems tradeoff studies strongly affect the selection of the central sequencing and command system (CS and C) configuration. These are 1) choices pertaining to the distribution of onboard functions between the CS and C and the various subsystems, and 2) choices relating to the ground versus onboard distribution of control. The selection of onboard commands must consider the resulting spacecraft mechanization, and the selection of ground commands must provide adequate real-time ground control with backup as required for onboard control. In general, the selection is strongly influenced by reliability and over-all mission requirements.

It is necessary to determine the need of all of the spacecraft subsystems in making the final selection. Tradeoffs must be made to determine requirements imposed by guidance, occultation, mission phases,



propulsion increments, the desirability and use of backup commands, science sequencing, attitude control, data handling, fault detection, and antenna pointing. These requirements are reviewed in the system and mission requirements sections which follow, and the design tradeoffs which were conducted are described. These result in the selection of a sequencer with a centralized function-oriented core memory. The memory will have a storage capability of 256 words and the command decoder will have the capability of decoding 128 distinct commands.

## 2.1 Subsystem Command, Sequencing, and Timing Requirements

It is evident that the following requirements are basic to the mission. The CS and C subsystem must:

- Accept and decode ground commands
- Store commands for execution at designated times
- Store data to be issued at designated times
- Decode and distribute stored commands to the various spacecraft subsystems
- Provide clock pulses for frequency control of electrical power and data handling operations.

The precise extent of these requirements must be determined and special functions involved in the sequencing and command processing must be identified.

The requirements imposed on the CS and C subsystem are, of course, the aggregate of the requirements imposed by the various spacecraft subsystems. In the paragraphs which follow, the requirements of each subsystem are reviewed and factors leading to specification of on-board versus ground commands are described.

### 2.1.1 Science Subsystem

As a general principle, the control and sequencing of onboard scientific operations is accomplished by the data automation equipment (DAE) rather than by the CS and C. However, the CS and C can provide considerable support in this function. As a minimum capability it can

perform a handover function, merely transferring ground commands to the data automation equipment (DAE). However, it may be required to interact intimately with the DAE by performing over-all timing functions in coordination with the DAE.

For most of the scientific instruments involving direct commands the best division of responsibility between the DAE and the spacecraft sequencer appears to be one in which the CS and C simply identifies the commands as science-oriented and transmits them to the DAE. This applies to the power on/off functions of the various instruments and to over-all mode control. For the scan instruments, coordination between the CS and C and the DAE is needed, with each controlling portions of the total spacecraft operations.

There are three approaches to the division of responsibility between the two sequencers. In one approach, based on ground inputs, the CS and C selects the desired data handling mode and transmits the POP angles, television shutter operation times, image velocity rates, filter settings and lens sequencing necessary to carry out the picture taking and readout. It formats the video and other high scan rate data and controls the tape recorder during storage. This approach results in the simplest CS and C subsystem and the most complicated DAE.

In the second approach, the CS and C selects the desired data handling mode and controls the POP angles. The remaining data is transferred to the DAE prior to the start of the picture taking sequence. The DAE then performs all of the necessary sequencing. If the image velocity compensation is accomplished by varying the POP angles, or if different angles are required during a photographic sequence, the DAE must then either apply the changes just before the shutter operation times or so inform the CS and C that it can perform this function at the proper times.

In the third approach, the CS and C is more intimately involved in the photographic operations. In this case, the camera settings are stored in the CS and C memory. The sequencer controls POP angles and issues quantitative and discrete commands to the DAE at the appropriate times to provide coarse control of the photographic operations. The DAE then

performs minor sequencing in fixed formats based on these commands and controls the bulk storage and data formatting operations. The implementation of the DAE is therefore greatly simplified as it is not required to have as extensive a memory or sequencing capability.

To obtain an understanding of the tradeoffs in CS and C and DAE implications for these approaches, the first one was selected for CS and C sizing studies. The first part of this section of the report will deal with design requirements for such a system. In the final part, the implications of having the CS and C perform the larger tasks are evaluated.

Science operations in Mars orbit are assumed to be programmed in fixed formats which are keyed to the orbital period and selectable by ground command. In the TV operations mode, pictures are taken near periapsis, recorded on bulk storage, and read out during the remainder of the orbit. The operation and control of the Mars scanning and spectroscopic instruments are phased into this sequence by the DAE. The required CS and C operations are programmed in a fixed format which is time-referenced to the nominal orbit. After completion of a sequence, the program is updated by the orbital period (time) to provide for the next sequence. As the orbit becomes better known, the initiate times of the sequences are corrected by ground command. For periods devoted entirely to the non-television experiments, the mode is selected through the CS and C, and the DAE again controls instruments and data operations.

The command and sequencing requirements of the science payload are summarized in Table 4-8. The minimum requirements category indicated in the table refer to the first approach described above, and the supplementary requirements are those that are added by using the third approach.

#### 2.1.2 Planet Oriented Package Requirements

Most of the command and control requirements of the POP relate to its pointing and control. Quantitative pointing commands of 12-bit length are required for each gimbal drive. These are transmitted from earth along with their effect times and are stored in memory. At the proper times they are issued as a serial train of pulses to load the

Table 4-8. Science Command Sequencing

Function	Number of Direct Commands	Minimum Requirements			Remarks
		Number of Quantitative Commands	Ground or CS and C	Data Requirements (bits)	
DAE Mode Control	4		ground		
Elapsed Time Update		1	ground	14	
Orbit Period		1	ground	14	
Science Instrument Discrete Commands	70 to 100		ground and DAE		Includes calibration commands

Function	Number of Direct Commands	Supplementary Requirements			Remarks
		Number of Quantitative Commands	Ground or Onboard	Data Requirements (bits)	
POP Angles Nos. 1 and 2		8	both	12	4 groups of 3 picture pairs
Camera Shutter Actuation		12	both	14	
Magnification	2		both		
Filter Selection	4		both		4 positions assumed
Image Motion Compensation		8	both	7	
Exposure Duration	4		both		
Camera Selection	2		both		

command angle registers in the POP subsystem. If image motion compensation is to be added to the commands, these values are added to the register just before each picture is taken and removed after the picture-taking interval. Other command requirements include discretes for horizon scanner on/off and open loop/closed loop pointing.

### 2.1.3 Telecommunications Subsystem Requirements

Command and control requirements for the telecommunications subsystem are summarized in Tables 4-9 and 4-10. These tables include all commands and data required by this subsystem, irrespective of the mission phases. The units of this subsystem and the states into which they can be switched are also included.

#### a. Data Handling Subsystem

The six telemetry data modes must be adapted to the sequencing of spacecraft operations. Some planning is therefore required and pre-programming is needed to time the consecutive events. These operations are readily handled by a sequencer. Consequently, the primary source for telemetry mode control signals is the sequencer. In the event of a failure, or to enable a special mode to be used, a ground command override is provided for each mode. If the normally sequenced mode is overridden by ground command, the system stays in the commanded mode until another ground command is executed. A similar argument applies to the selection of the data rates for telemetry. The desired rate is a function of the distance of the spacecraft from earth and the information to be transmitted, so the nominal times for commanding bit rates prior to encounter can be determined in advance and stored on board. Operations after encounter depend on transmitter power output and antenna availability and require DSN decisions for full utilization of the telemetry link. For this reason ground command capability is necessary for all bit rates.

#### b. Transmitter/Antenna Selection

Commands to the transmitter selector are required to select

Table 4-9. Telemetry Command Requirements

Function Telemetry Modes	Number of Separate Commands	Ground Commands	Onboard Commands	Logic for Onboard Command
Maneuver Mode	1	X	X	Spacecraft in maneuver mode
Low Rate Science	1	X	(X)	(X) From DAE only
Science Calibrate Mode	1	X		
Cruise Mode	1	X	X	Spacecraft in cruise mode
Orbit Mode	1	X	X	Spacecraft in orbit mode
Orbit; Video Buffered	1		X	No special commands needed automatic if data rate = 128 and spacecraft in orbit mode
Capsule Only Mode (Read Out Capsule Data)	1	X		
Data Rate Select				
4096	1	X		
2048	1	X		Based on time after separation from booster
1024	1	X	X	
128	1	X	X	
PCM Encoder Select	2	X		Preliminary unit selected at launch
Select Bulk Storage	2	X	(X)	Preliminary unit selected at launch. DAE controlled
Bulk Storage on/off	2	X	(X)	Onboard sequencing under joint control of the DAE and data handling subsystem.
Store Capsule Data	1	X		

Table 4-10. Communications Command Requirements

<u>Unit/Function</u>	<u>Number of Separate Commands Required</u>	<u>Primary Source of Commands</u>	<u>Backup</u>	<u>Quantitative or Discrete Output</u>	<u>Logic for Onboard Commands</u>
Transmitter/Antenna Selection	10	ground	2-CS and C	discrete	
Range Code on/off	2	ground	none	discrete	
High and Medium Gain Antenna Angles	3	(CS and C)	ground	quantitative (12 bits)	CS and C Increments command register as required.
Antenna Angle Generator		CS and C		internal	
Antenna Deploy or Unlock (3 Antennas)	2	CS and C	ground	discrete (pyrotechnic)	Time after space- craft separation
Receiver Mode Select	8	ground, onboard special	CS and C (2)	discrete	Special mode select in event of loss of attitude control
Capsule Data	2	ground	CS and C (2)	discrete	

the desired antenna and power level to be utilized. This requires 10 separate discrete commands. Three are required for normal operation; the rest are involved in selecting back-up modes or redundant equipment.

c. Antenna Pointing Commands

Several methods have been considered to provide high gain antenna pointing commands. The angles may be updated by supplying increments to a counter which then counts down to zero as the antenna is being driven to the correct position, or the command angles themselves may be stored in a register and the antenna driven until its gimbal angles match the command angles. The first method requires a decrementing counter, while the second needs a comparator and is therefore more complicated. No difference exists in the number of commands or data words in either case. The word size would of course be smaller in the decrementer so, from the point of view of the CS and C, is favored. However, it is required that the actual antenna angles be available for verification by telemetry, so the use of separate command and actual angle registers is indicated.

The total number of times that the antenna pointing angle has to be updated depends on the length of time that it is deployed, the amount of the accumulated change of the sun-spacecraft-earth angle, and the allowable variation of pointing angle before transmission is lost. Since the pointing angle can change by a total angle of up to 130 degrees for the trajectories under consideration, at least one gimbal angle must be changed frequently and the use of a ground command for each increment is undesirable. The angles change most rapidly during the first three months of flight but the accuracy requirements are less severe during that period. Over-all accuracy of  $\pm 2.1$  degrees (including attitude control errors) is allowable and the allowable quantization of the antenna program can be 1.5 degrees. Later in flight the angular rate of change is less, but the pointing accuracy is more critical. Since the antenna must be pointed to an accuracy of 1.4 degrees,  $\pm 0.5$  command



granularity is required.

The following methods of updating the pointing angles were considered. At one extreme, the onboard processor generates all the gimbal quantities from a stored function one pair at a time. At the other extreme all of the quantities are computed at the SFOF and transmitted one pair at a time to the spacecraft. The first technique requires an onboard function generator and imposes no requirement other than backup on the ground station, while the second needs only a pair of registers onboard but involves the DSIF on a continuous basis.

An unjustifiably large number of memory cells would be required to store all of the pointing commands required for the whole mission. Even if enough commands for 1 month are stored and updated at 2-week intervals by loading in another set by ground transmission, the number of memory cells required is excessive. Since the number of command angles is several hundred, a function generator approach appears most suitable. In this approach the antenna angle versus time graph for 1 month or more is approximated by a series of straight line segments, and data representing the slopes and start times for each slope are stored in the sequencer. Six slopes appear sufficient to provide pointing commands with the required granularity during the first month or for 6 months after encounter.

The foregoing remarks apply to a single gimbal of the high gain antenna. Since the other gimbal axis during cruise will be nearly normal to the ecliptic, it needs to be updated only infrequently. The commands which are generated for the high gain antenna gimbal which undergoes large angular change also apply to the medium gain antenna. This is possible because the gimbal angles of the two antenna are nearly parallel during cruise and commands of sufficient accuracy for the high gain antenna will be more than accurate enough for the medium gain one.

#### 2.1.4 Stabilization and Control Subsystem Requirements

The Voyager stabilization and control system is very similar to

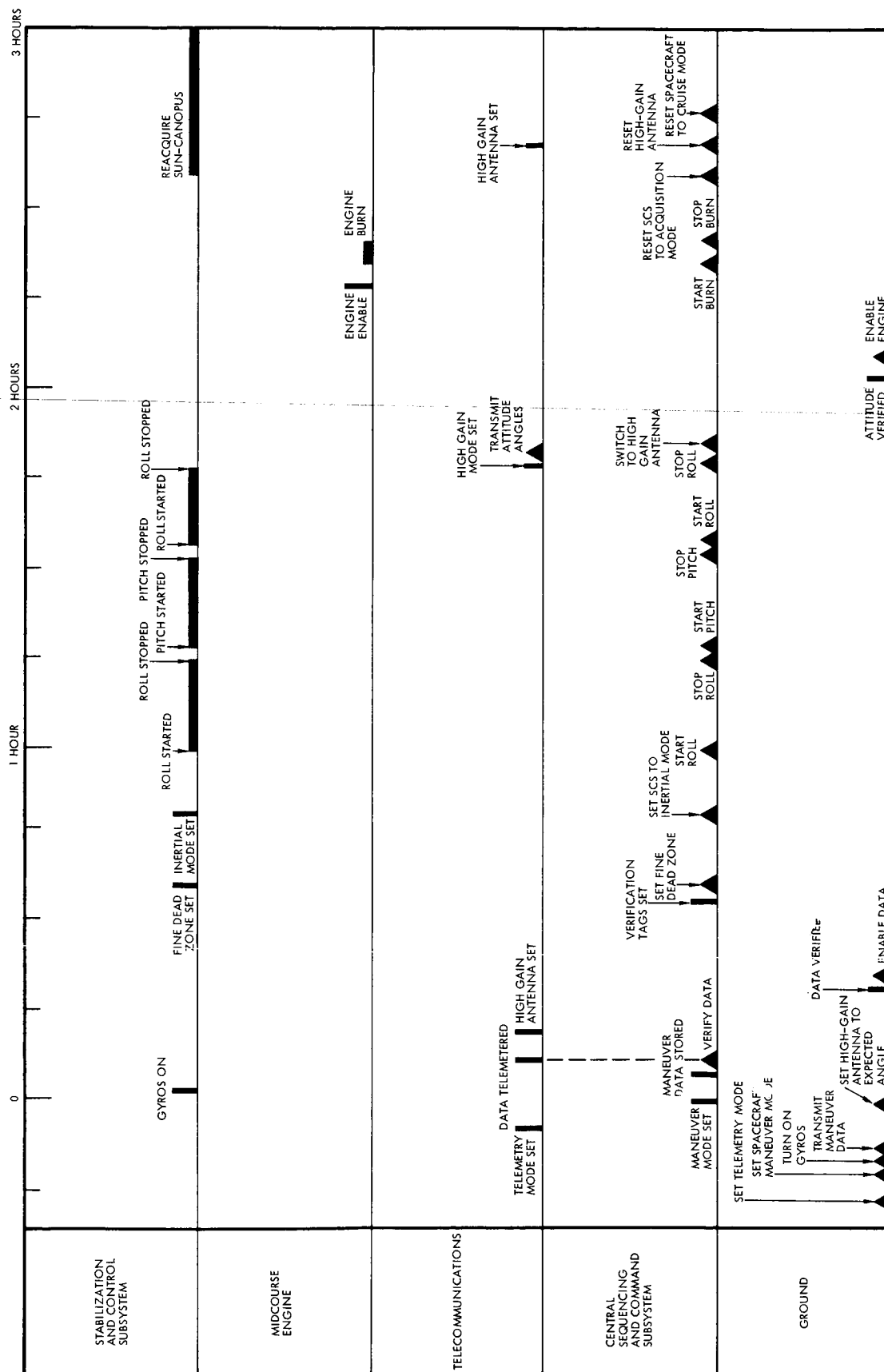
the Mariner system, and its command requirements for maneuver control are also much the same. However, there are several additional requirements that must be accommodated. One of these is the desire to verify attitude commands before maneuver initiation (see Section 2.1.8). In addition to providing adequate time for this in the maneuver sequence, the primary effect of this operation on the CS and C subsystem is to require a special internal telemetry sequence for rapid readout of the required data. The switching for this sequence is accomplished as part of the maneuver mode.

Another requirement is brought about by the need to enable engine firing by ground command. If the vehicle is in the attitude to fire the engine and the enable command is not received prior to the commanded time of engine fire, the CS and C must switch the attitude control system to the acquisition mode and inhibit engine fire.

The stabilization and control subsystem includes provisions to test the thrust vector control electronics prior to use. This is done early in the maneuver sequence and is accomplished by applying an input step function by ground command. The resulting response is observed via telemetry. The CS and C has only to supply the discrete test signal.

The maneuver mode imposes one of the most exacting timing requirements on the CS and C. The turning rate for maneuvers is 0.22 deg/sec and it is desired to limit the quantization error to about 0.11 deg/sec. Thus, a minimum timing interval of 1 second is required.

This maneuver is employed during the midcourse corrections, capsule separation, injection into Mars orbit, and orbit trim. The detailed sequence is therefore of special interest, so an illustrative case is presented in Figure 4-32. This time-flow diagram shows the interactions of the S and C subsystem with propulsion, telemetry and communications as well as the CS and C and ground control centers. Originating sources are shown as dark arrow heads. The effects on the receiving systems are shown as pulses and are appropriately labeled.



Summary command requirements for this maneuver are presented in Table 4-11. Initial and backup command sources are identified in the table, and the number of different kinds of commands and data are presented. Onboard logic requirements are also summarized.

#### 2.1.5 Propulsion Subsystem Requirements

For the midcourse engine three pairs of start and stop squib activated valves, with solenoid backup, are used to permit the corrections. Each valve requires a separate command signal, and the commands must be inhibited prior to the receipt of an enable signal after spacecraft orientation is verified. In addition, it is desirable to provide logic such that failure to fire a given valve actuates the next squib in the sequence. This logic must, of course, be accomplished on board the spacecraft.

For the retromotor a start command is needed to ignite the liquid injection thrust vector control pressurant grain and a second start command (delayed by 100 milliseconds) is required to ignite the main motor. Again, the ground command enable signal must be present.

The capsule separation approach requires that the spacecraft be accelerated laterally after separation to allow the capsule to pass after its engine has fired. After separation a cold gas blowdown system is activated to provide the clearance. The fire signal for this system is timed by a special sequence which is started by the separation event. The command requirements for the propulsion subsystem are summarized in Table 4-12.

#### 2.1.6 Power Subsystem Command Requirements

A summary of the power subsystem command requirements are given in Table 4-13. No stored commands are required by this subsystem and all commands are discrete. The switching functions are accomplished by logic contained in the power control unit. Therefore, only override commands are needed.

Table 4-11. Stabilization and Control Command Requirements

Function	Number of Separate Commands Required	Initial Source of Commands	Onboard Command Source	Quantitative or Discrete Output	Logic for Onboard Commands
Pitch Start and Stop Time	2	ground	CS and C	discrete	CS and C control gyro torquing
Pitch Turn Polarity	1	ground	CS and C	discrete	
Roll Start and Stop Times	4	ground	CS and C	discrete	CS and C controls gyro torquing
Roll Turn Polarity	2	ground	CS and C	discrete	
Canopus Sensor Select	1	ground and onboard	SCS	discrete	SCS delects sensor based on star AC with ground over- ride
Command Acquisition Mode	1	onboard	CS and C	discrete	
TVC Test Signal	1	ground		discrete	see text
TVC Electronics Select	4	ground		discrete	
Gyros on/off	2	ground	SCS	discrete	
Roll Incremental Maneuver	2	ground	CS and C	discrete	
Mode Control and Override	4	ground	SCS	discrete	
Dead-zone Select (1/2 and 1/4 deg)	2	ground	CS and C	discrete	
Heater Control for Reaction Control Gas on/off	2	ground		discrete	

Table 4-12. Propulsion System Command Requirements

<u>Function</u>	<u>Number of Separate Commands Required</u>	<u>Initial Source of Commands</u>	<u>Onboard Command Source</u>	<u>Quantitative or Discrete Output</u>	<u>Logic for Onboard Commands</u>
Monopropellant Squibs and Solenoids	8	ground	CS and C	discrete	see text
Solid Engine TVC	1	ground	CS and C	discrete	
Solid Engine Igniter	1	onboard	CS and C	discrete	keyed to TVC signal
Lateral Thrust	1	onboard	CS and C	discrete	initiated by capsule separation

Table 4-13. Power Subsystem Command Requirements

<u>Unit</u>	<u>States</u>	<u>No. of Ground Commands</u>
Battery No. 1, Charge Control Override	On/Off	2
Battery No. 2, Charge Control Override	On/Off	2
Battery No. 1, Disconnect	Open/Close	2
Battery No. 2, Disconnect	Open/Close	2
4.1 Kc Inverter Transfer	Main Inverter on/ Standby Inverter on	2
820 Cycle Inverter Transfer	Main Inverter on/ Standby Inverter on	2
410 Cycle Inverter Transfer	Main Inverter on/ Standby Inverter on	2
Charge Rate Select	Charge Rate 1 Regulator No. 1	4
	Charge Rate 2 Regulator No. 1	
	Charge Rate 1 Regulator No. 2	
	Charge Rate 2 Regulator No. 2	

### 2.1.7 Capsule Requirements

Commands required by the capsule consist of the five commands indicated in the mission specification and the capsule separation events. The separation events consist of capsule cover removal, capsule separation, and cover base separation. All are ground initiated or can be stored in the spacecraft for execution at the required times. The capsule separation events are also backed up by ground command discretes at the designated times.

### 2.1.8 Mission Requirements

In the preceding section the detailed command requirements for the subsystems of the spacecraft system were examined from a word structure point of view. Commands were identified to perform specific functions for each of the subsystems, and arguments were given in support of onboard and/or ground initiation of those functions. Specific logical conditions which must be reasonably fulfilled were also discussed. In consequence, a command list was obtained for each subsystem.

Other requirements are imposed by the timing accuracy required by the various mission phases, the requirement to verify some commands prior to execution, and possible requirements for diagnosis or analysis of spacecraft functions. These functions are discussed in the paragraphs which follow.

#### a. Mission Timing Requirements

A detailed flow of mission events was prepared and analyzed to determine the timing requirements, timing intervals, and resolution of commands. The mission is, of course, characterized by long periods during which the vehicle states or modes remain fixed and no commands are required of the CS and C. During other periods, functions are required every few seconds with timing resolution requirements of the order of tenths of a second.

It is assumed that internal timing of the order of milliseconds



or tenths of seconds will be accomplished by special time delay circuits and that such requirements are not imposed on the basic CS and C design. The timing resolution required during midcourse maneuvers is determined by the required accuracy of the velocity increment and the attitude maneuvers. An allowable attitude error caused by timing granularity is of the order of 0.1 degree which leads to a minimum allowable timing interval of 1 second. This value is commensurate with the propulsion requirements. Since the acceleration prior to capsule separation is no less than  $0.07 \text{ m/sec}^2$ , the maximum quantization error is  $0.035 \text{ m/sec}$ , which is well within the allowable value. For the velocity trim maneuvers in Mars' orbit the acceleration is about  $0.22 \text{ m/sec}^2$  and the minimum commandable velocity or quantization error is  $0.11 \text{ m/sec}$ . The complete maneuver sequence will last about 3 hours.

Another period of significant timing resolution is the first two or three hours after separation from the booster. During this period the various antennas and booms are deployed, the sun-Canopus references are acquired, and the cruise configuration is established. Timing granularity of the order of 30 seconds appears adequate for this period.

For orbital operations the maximum duration of a sequence is the orbital period which has been nominally set at 14.3 hours. The maximum timing resolution is established by the picture-taking sequence. The pictures will normally be taken with time spacing between 40 and 100 seconds. The spacing may vary within a single picture-taking sequence. In the worst case, a 4-second timing granularity leads to a 5-per cent picture overlap, which appears commensurate with other errors.

During cruise the requirement is to establish an absolute time base from which to establish fine-grain timing. It appears that two-hour steps are adequate for this period.

b. Command Verification

A review of the Voyager command requirements was conducted to define those commands which require ground verification prior

to execution. One criterion that was used in this evaluation is the effect of a direct command being transmitted to the incorrect spacecraft function. This, of course, could seriously affect spacecraft operation, but its probability can be reduced by using error rejecting codes in the command word. This is being done (see Section 2.3). Even with these provisions, as a general ground rule, the system must be so arranged that an incorrectly decoded direct command cannot result in catastrophic consequences. This can be handled by using delayed direct commands for all functions of this nature or by using enable or two-command capability. Since delayed direct commands can be transmitted in time to permit verification, assurance of correct reception via telemetry can be obtained, and this type of format will be used for commands to be verified.

The following commands require verification and are placed in the CS and C memory and read out on telemetry prior to execution:

- Pitch turn time and sign
- Roll turn times and sign
- Propulsion start and stop times
- Function select (monopropellant or solid engine or capsule separation)
- Antenna gimbal angles
- Capsule cover separation
- Capsule separation
- Capsule base separation.

c. Spacecraft Diagnostics and Correction Requirements

From the foregoing analysis of requirements for the central processor it is clear that the computing capability of a general purpose computer is not needed. At most, only special purpose equipment for function generation is necessary. However, no requirements were

specified in the previous sections to provide onboard fault detection, diagnosis, and correction for the spacecraft. Extensive diagnostic and repair capability cannot be obtained onboard without a computer, so the question of this being part of the central processor requirements is a serious one.

The central issue is whether the incorporation of onboard correction techniques enhances spacecraft reliability and mission success and, if so, how extensive the capability must be to enhance it. The problem is an extremely difficult one because the number of possible failures is very large and the decision logic to cover the alternatives is very complex.

The problem is compounded by the fact that the instrumentation needed to detect the faults is itself subject to failure. The inline reliability of the spacecraft is reduced with each equipment addition, so, as the detection, diagnosis and correction mechanization increases, the reliability of the system tends to decrease. To be useful, the sensing devices have to be coupled with the subsystems, units or components being sensed, so the reliability of the equipment set is decreased. Thus, it is entirely possible that the survival probability can be reduced in the effort to increase performance reliability.

Special conditions, may, however, permit some capability in this direction. Two alternative concepts present themselves. The condition assumed for both is that the communication link fails and the spacecraft control is left entirely to onboard devices. In this event, it is possibly desirable to perform sufficient diagnosis and correction on board to regain control. However, the diagnosis of the possible failures in the communications, stabilization and control, or power subsystems is very complex. Also, the provision of adequate redundancy, alternate modes, and/or failure sensing and switching within the subsystems is not difficult and is provided in the selected design. This approach is favored over the use of a fairly complicated computer. However, there are some specific cases in which the CS and C can

assist in checkout and mode switching without introducing significant additional complexity. Examples of this are capsule checkout, thrust vector control electronics checkout, switching of alternate units based on time, and function switching based on elapsed time since a valid command has been received. These operations are being employed in several spacecraft subsystems.

A similar example is the use of decision logic for detection of the closing of the normally open thrust termination valves when a command signal has been issued to cut off the engine. If the valve has not been actuated, a signal should be sent immediately to the next valve in line to attempt to terminate thrust.

## 2.2 Summary of Requirements

Summary requirements for commands, data quantities, timing frequencies, clocks, and memory are presented in Tables 4-14 through 4-17. The command requirements table calls for a decoder capability of 125 different commands, just short of a natural binary division of 128 so this number was selected.

### a. Timing Requirements

Timing requirements are shown for the telemetry clock and for the power supply. In support of this, the clock generator frequency summary requirements are given in Table 4-15. Internal frequency requirements (e.g., 1 cps) are also derived from this clock system.

A summary of the timing requirements of various mission phases is given in Table 4-16. From this summary it is evident that five different sequences are needed with the resolutions and durations indicated.

### b. Memory Requirements

The number of memory cells needed in the CS and C subsystem is determined by the peak load experienced by the processor during the entire flight if a general purpose memory is used, or by the total number

Table 4-14. Summary of Command Requirements for CS and C

<u>Subsystem</u>	<u>Ground Commands</u>	<u>CS and C Commands</u>	<u>Decoder Lines</u>
Science	6	4	6
Telemetry	17	6	18
Communications	27	11	29
Stabilization and Control	28	14	28
Propulsion	9	11	11
Power	18	0	18
Capsule	5	5	5
Jettison System	2	2	2
Central Sequencing and Command	<u>10</u>	<u>8</u>	<u>8</u>
Totals	122	61	125

Table 4-15. Telemetry Frequency and Power Supply Synchronization Requirements

<u>Telemetry Frequency Requirements</u>			
<u>TBR</u>	<u>PN Bit Rate</u>	<u>PN Synchronization Subcarrier Oscil- lator Frequency</u>	<u>Data Subcarrier Oscillator Frequency</u>
4096	36,864	73,728	147,456
2048	18,432	36,864	73,728
1024	9,216	18,432	36,864
128	1,152	2,304	4,608

Power Supply Synchronization Requirements

(4096, 409, 819) cps

Table 4-16. Summary of Sequence Requirements

<u>Mission Phase</u>	<u>Required Resolution</u>	<u>Time Range</u>	<u>Required Number of Bits</u>
Over-all Mission	2 Hours	400 Days	13
Postlaunch Sequence	30 Seconds	3 Hours	9
Attitude Maneuvers (Midcourse, capsule separation, and injection)	1 Second	3 Hours	14
Pre-encounter	4 Seconds	8 Hours	13
Orbit	4 Seconds	17 Hours	14

Table 4-17. Memory Requirements Comparison

<u>Spacecraft System</u>	<u>Number of Storage Cells</u>	
	<u>(a)</u> G. P. Memory Worst-Case Analysis	<u>(b)</u> Function Oriented Memory
Science	6	6
Telemetry	3	6
Communications	29	29
Stabilization and Control	14	28
Propulsion	6	11
Central Sequencing and Command	8	10
Capsule Jettison System	0	2
Miscellaneous Growth Items	<u>6</u>	<u>10</u>
Totals	72	102

of distinct types of stored commands and data if a function-oriented memory is used. In the first case, just enough storage is needed to satisfy the worst-case condition. A review of the command and timing requirements developed above is therefore necessary to identify this condition. These memory requirements are summarized in Column a of Table 4-17.

A total of 72 words of memory is indicated. A natural binary break point of 128 words of memory is therefore indicated for this approach.

In the second case, where specific functions are identified by the memory location, the number of such locations is determined by the total number of distinct commands and data required. The summary data for the above requirements is presented in column b of Table 4-17. A total of 102 locations is needed, so the natural set of 128 words of memory is again called for. In these summaries it is assumed that the DAE controls the science operations. The effect of increased requirements on the CS and C when it provides assistance in science functions is considered in Section 2.8 of this volume.

### 2.3 Command Word Definitions

There are four types of messages which must be processed by the CS and C.

#### a) Direct Commands

This command provides a designated spacecraft subsystem with a discrete pulse. The discrete pulse is issued by the CS and C or by the DAE as soon as the incoming command is decoded.

#### b) Delayed Direct Command

This command provides a designated spacecraft subsystem with a discrete pulse at some time after the receipt of the command. The time of execution is dependent on the time tag value accompanying the command. The command is stored in memory until its execution time,

at which point a discrete pulse is issued to the designated subsystem. The memory location identifies the designated subsystem.

c) Verified-Enable Command

This command accesses the memory and changes the verification bit in the memory location indicated by the command address. The same format as delayed direct commands is used with a zero time tag. The zero time tag identifies that the command is a verification command rather than one to be stored.

d) Quantitative Data

This provides a designated spacecraft subsystem with serial data. Before the data is transmitted to the subsystem it is placed in the CS and C memory with an associated delayed direct command which determines when this data is to be provided to the designated subsystem. The same format is used for quantitative data as for delayed direct commands. However, the memory cell to which it is addressed insures that the data cannot be interpreted as a command.

2.3.1 Word Format

Figure 4-33 illustrates the two message formats that accommodate the four message types identified above. The following description identifies the constituent parts:

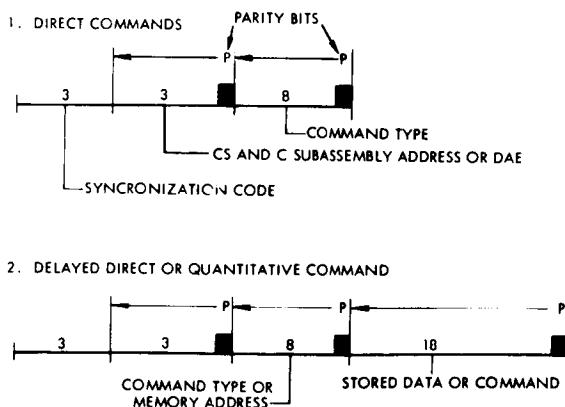


Figure 4-33  
Command Formats



a. Synchronization Code (3 bits)

A synchronization code is examined by the CS and C to determine the validity (format bit position) of the incoming message. A 3-bit code is used to check the sync between successive messages in a continuous bit stream; however, a longer unique pattern is required to initially establish sync after a detection of sync loss. This can easily be handled by requiring ground to send a constant pattern (e.g., 12 or more zeros) followed by the normal 3-bit sync code at the beginning of message transmission, even when a loss of sync is detected (e.g., via telemetry).

b. DAE Decoder and CS and C Subassembly Address (3 bits)

This address code provides the ground station with a code capable of selecting the particular CS and C subassembly to be used. It distinguishes among direct commands to redundant CS and C decoders, direct commands to DAE decoders, and quantitatives to the sequencers.

c. Command Type (8 bits)

These 8 bits are used directly in the command decoders to determine which subsystem or experiment (which output line) is to be picked for execution of direct commands. For the other message types these bits determine the memory address where the command, data or verification bit is to be stored. In the case of stored commands the memory address (the same 8 bits) identify the subsystem (output line) which is to be pulsed at the appropriate time.

d. Stored Data or Command (18 bits)

These 18 bits are stored in the memory for stored quantitative data and stored command messages. For the stored commands the

18 bits consist of 1 verify bit, 3 CS and C mode bits and 14 time tag bits. The exact format of the stored quantitative data is not critical since it will not require all 18 bits.

e. Parity bits

Up to a total of three parity bits are checked by the CS and C during receipt of a quantitative command. The parity bits are distributed as shown in Figure 4-33. The distribution has been selected on the basis of the number of message bits being decoded at any given time in the decoding process.

## 2.4 Message Failure Protection Requirements

In previous sections the command and timing requirements for the central processor were discussed. Arguments were presented for the selection of the commands and for the decision whether the commands should be ground initiated or programmer initiated. Care was taken to insure that backup signals were provided for critical commands and that verification procedures were adopted. As another step in this cross checking against failures, message transmission errors must be guarded against.

Basically two types of errors can be made in the message even though the sources for the errors may be quite diverse. The message can either be out of sync or have individual bits in error. In the first case the command is difficult to distinguish from random noise and in consequence is likely not to be executed.

In the second case an error in the message prevents the intended command from being activated, but the probability is quite high that a false command would be issued, unless some measures were taken to detect errors. These measures are considered in the following paragraphs.

As a general procedure, both parity and sync bits are used to detect errors. The parity bits are also used as sync bits. Since the essence of the synchronizing process is to detect patterns in the

message or to incorporate well defined patterns in the code, there is no reason why the bits should not be judiciously distributed over the whole message or isolated parity bits used as additional protection against asynchronous messages. If a message is only partly out of sync, say if a bit is lost in transmission, then the parity bit helps to establish that fact.

#### 2.4.1 Error Rejection

Analysis of planned system parameters indicates that a satisfactory error rejection probability can be obtained using simple parity checks and a synchronizing code. More sophisticated error detection is conceivable, but requires additional complexity. If it is assumed that each group of 7 bits, above, is augmented by one (even or odd) parity bit or is given a two bit distance from any other valid member of the group, then for each group two errors are required for that group to be improperly accepted. Table 4-18 indicates the probabilities of this occurrence for each group in the presence of transmission errors. No allowance has been made for the additional distance created by not fully utilizing the field within each group.

The total probability given in Table 4-18 assumes that all portions of a message would be rejected if any of its constituents is in error.

An additional source of errors results from decoding commands which are shifted some number of bits from the reference position at the decoder. The synchronizing code shown in the message format is included to limit errors from this source. This is independent of error rate since the shifted message is assumed to be a random bit configuration. Table 4-19 lists the number of bits checked versus the probability of accepting a shifted (or random) sequence.

The number of bits to be used to protect against acceptance of a shifted message may be selected from Table 4-19 to give the desired protection. Those bits assigned to parity check information and any fixed bits such as spacecraft address may be subtracted from the

Table 4-18. Probability of Acceptance of Erroneous Words

Bit Error Rate	Address	Command Type	Quantitative Data	Total
$10^{-1}$	$1.6 \cdot 10^{-1}$	$3.6 \cdot 10^{-1}$	$4 \times 8.4 \cdot 10^{-1}$	$5.36 \cdot 10^0$
$10^{-2}$	$1.6 \cdot 10^{-3}$	$3.6 \cdot 10^{-3}$	$4 \times 8.4 \cdot 10^{-3}$	$5.36 \cdot 10^{-2}$
$10^{-3}$	$1.6 \cdot 10^{-5}$	$3.6 \cdot 10^{-5}$	$4 \times 8.4 \cdot 10^{-5}$	$5.36 \cdot 10^{-4}$
$10^{-4}$	$1.6 \cdot 10^{-7}$	$3.6 \cdot 10^{-7}$	$4 \times 8.4 \cdot 10^{-7}$	$5.36 \cdot 10^{-6}$
$10^{-5}$	$1.6 \cdot 10^{-9}$	$3.6 \cdot 10^{-9}$	$4 \times 8.4 \cdot 10^{-9}$	$5.36 \cdot 10^{-8}$
$10^{-6}$	$1.6 \cdot 10^{-11}$	$3.6 \cdot 10^{-11}$	$4 \times 8.4 \cdot 10^{-11}$	$5.36 \cdot 10^{-10}$
$10^{-7}$	$1.6 \cdot 10^{-13}$	$3.6 \cdot 10^{-13}$	$4 \times 8.4 \cdot 10^{-13}$	$5.36 \cdot 10^{-12}$

Table 4-19. Probability of Acceptance of Shifted Message  
Versus Number of Sync Bits

Bits	Probability of Single Sequence
6	$1.56 \cdot 10^{-2}$
7	$0.780 \cdot 10^{-2}$
8	$0.390 \cdot 10^{-2}$
9	$0.195 \cdot 10^{-2}$
10	$0.975 \cdot 10^{-3}$
11	$0.488 \cdot 10^{-3}$
12	$0.244 \cdot 10^{-3}$
13	$0.122 \cdot 10^{-3}$
14	$0.610 \cdot 10^{-4}$
15	$0.305 \cdot 10^{-4}$
16	$0.152 \cdot 10^{-4}$
17	$0.764 \cdot 10^{-5}$
18	$0.382 \cdot 10^{-5}$

required number since they will already contribute to protection against a shifted message. The remainder are the sync code shown in the message format which might be any convenient code which the decoder would recognize, the only precaution being that it can be selected to guard against decoder failure.

#### 2.4.2 Valid Message Rate

The preceding section has dealt with the acceptance of invalid messages by a vehicle. Of some importance in determining the message structure is the probability that the intended message is accepted.

Messages will be rejected for two causes: bit errors and false sync recognition. The resultant message failure rate is the resultant of these two probabilities. Figures 4-34 through 4-37 show the message errors because of each cause and plot the resultant curve for selected numbers of synchronizing bits. These curves are based upon the following equations:

- a) Probability of messages lost because of sync error  $P_S$

$$P_S = 2^{-R_S}$$

where  $R_S$  = number of synchronizing and parity bits

- b) Probability of messages lost because of bit errors  $P_B$

$$P_B = R_T P_E$$

where  $R_T$  = total number of transmitted bits

- c) Probability of messages lost because of  $P_S$ ,  $P_B$  and  $P_M$

$$P_M = P_S + (1 - P_S) P_B$$

It is important to note the comparison of the probability of command failure (as contrasted with total message loss) of the scheme used in this analysis with the coding scheme used in Mariner C.

Mariner C uses a Hamming separation scheme whereas a single

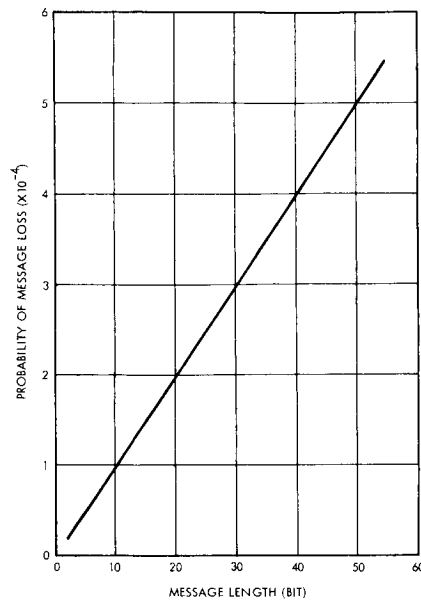


Figure 4-34. Probability of a Message Loss versus Message Length for a Bit Error Rate of  $1 \times 10^{-5}$

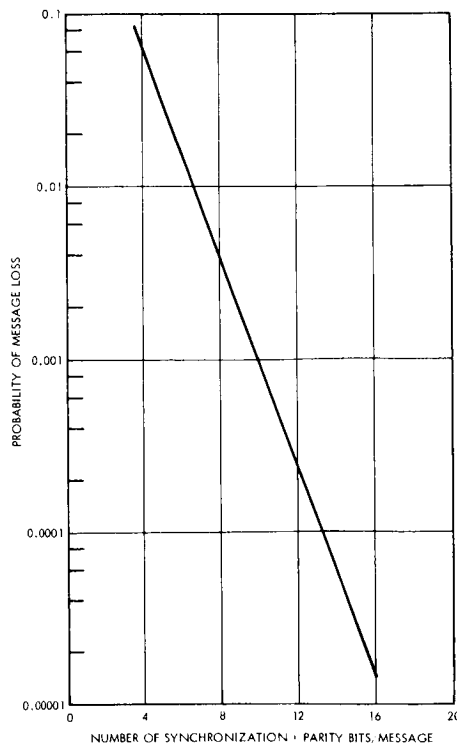


Figure 4-35. Probability of a Message Loss Due to a Sync Error

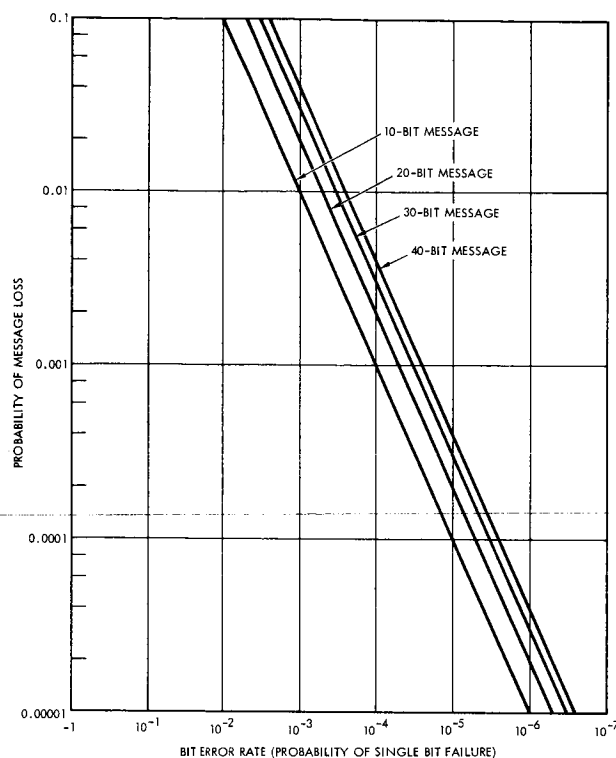


Figure 4-36. Probability of Message Loss versus Bit Error Rate for Varying Message Lengths

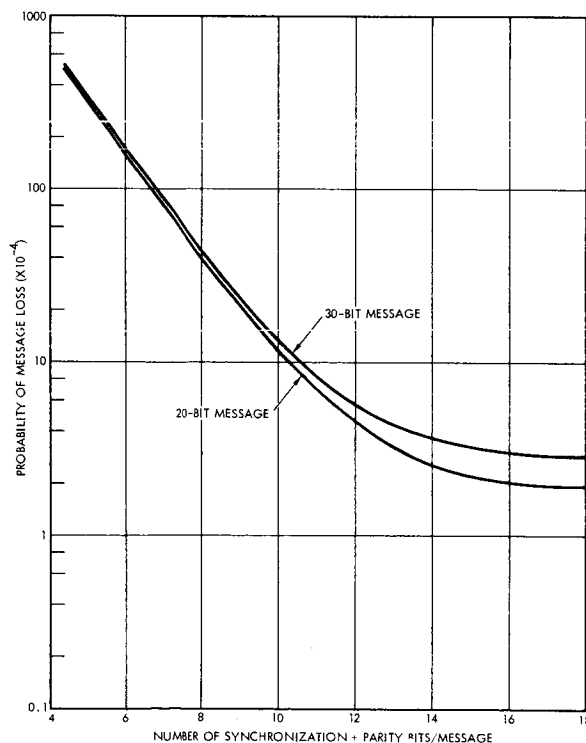


Figure 4-37. Probability of Message Loss Due to Bit Error Rate of  $1 \times 10^{-5}$  versus the Number of Sync + Parity Bits for Varying Message Lengths

bit parity technique has been employed here. For a Hamming number equal to two, there is no difference in probability of incorrect command execution between the two methods. If higher Hamming spacing is used, the loss probability is improved. To do an equally good job with parity bits, two bits would have to be used, but the mechanization is difficult. Since Mariner C uses a spacing of two, it is deemed sufficient to use a single parity bit for the command.

## 2.5 Alternative Processor Configurations

As the requirements for the CS and C began to take shape, many alternative mechanizations were considered. The numerous possibilities quickly reduced to two basic configurations which were studied in more detail to arrive at the recommended CS and C approach. The following is a brief discussion of alternative mechanizations of the command and control requirements which were discarded without detailed study.

A general purpose computer was only briefly considered because there was no requirement for onboard computation. Specific areas which were reviewed for possible computational requirements were: attitude control, navigation, spacecraft subsystem failure analysis and correction, data compacting, and experiment sequencing. While a small general purpose computer could do the required spacecraft sequencing with a maximum of flexibility, the reliability, weight, power, and cost, are unjustifiably high without a firm onboard computation requirement.

A physically distributed (or dispersed) approach to the command and control problem where each major subsystem would have its own separately packaged command storage and sequencing capability was also briefly considered. However, because time sharing of circuits was virtually eliminated in this approach it did not appear desirable from a weight, power, and reliability point of view.

The spacecraft and mission requirements were also briefly re-examined to determine the feasibility of eliminating most or all of the onboard storage and sequencing requirements to try to solve the command and control problem with a simple command distribution unit (CDU)



which could only decode real-time ground commands. The feasible uplink bit rates, the long transmission times and the bit error rates combine to make this approach unworkable for the number of precise sequences required by the mission.

The two configurations which were studied in some detail are described below. This is followed by the tradeoff criteria which led to the selection of the first of the two approaches as the recommended one.

#### 2.5.1 Preferred Mechanizations

It is evident from the previous remarks that the central processor must be configured to handle all timing and sequencing control functions, from on board the spacecraft as well as from the ground. The mechanization is therefore of the order of complexity of a programmer or sequencer.

A clock of some sort is needed to issue timing pulses, and a decoding tree or matrix is necessary to interpret commands and issue discretes. Since some of the commands and data are to be stored on-board the spacecraft, a memory device is needed to hold the information. The memory can be a collection of separate shift registers or it can be a centralized stack. As a separate consideration the memory might be special purpose, in which case each location (memory cell) is uniquely associated with a particular function (a unique discrete or group of data bits). The memory might also be a general purpose, randomly accessed system, in which certain extra bits stored in each location determine the current function of that location.

Since commands have to be issued directly to various subsystems during the flight or stored onboard in advance for execution at specified times during the flight, access must be provided via the telecommunications subsystem up-link. Messages must be checked, verified, and decoded in a preliminary way before being executed. Some simple command processing equipment is therefore needed.

It becomes clear immediately that the combination of memory and onboard sequencing requires substantially more hardware to implement

than a simple CDU. Therefore, it is desirable to implement the Voyager CS and C in such a way that failure of the memory/sequencer portion of the system does not cause loss of ground command capabilities via the CDU portion of the system. Further, because of the hardware complexity of all parts of the CS and C, consideration must be given in preliminary design of the system to methods of enhancing its reliability. The result of these considerations is a functionally modular CS and C in which the memory/sequencer is not in line for ground command execution; reliability may be improved by simply adding additional modules redundantly.

Therefore, the two configurations for the CS and C described below have nearly identical CDU portions (input decoder and command decoder) and differ mostly in the type of memory/sequencer employed.

## 2.6 Centralized Memory System

This configuration is one of two systems considered to fit the above requirements in a satisfactory manner. It has a centralized, random access memory whose word locations are function-oriented. A command decoder is used to interpret all commands, whether they issue from the sequencer memory or come directly from the ground. An input decoder is also used to preprocess command messages and route the information to the appropriate units. A block diagram of this approach is given in Figure 4-38.

Basic timing for spacecraft operations is provided by issuing serial data and discrete commands at specified times to the appropriate spacecraft subsystems. This is done either by ground command or by the sequencer. A clock within the sequencer provides the necessary timing signals for onboard control and distributes various clock frequencies to other spacecraft subsystems. The input decoder routes messages to either the programmer or the command decoder. The command decoder distributes discrete pulse outputs to the spacecraft subsystems based on direct ground commands or delayed programmer commands.

The input decoder inspects the incoming command for a valid

synchronization code and spacecraft address and directs the information to the appropriate location. (In the final configuration equipment redundancy is employed to enhance the reliability of the system and selection of the redundant subassemblies is made by a code in the incoming message.) The input decoder also checks on the correct parity of the spacecraft address, CS and C subassembly address, and memory cell address or direct command address.

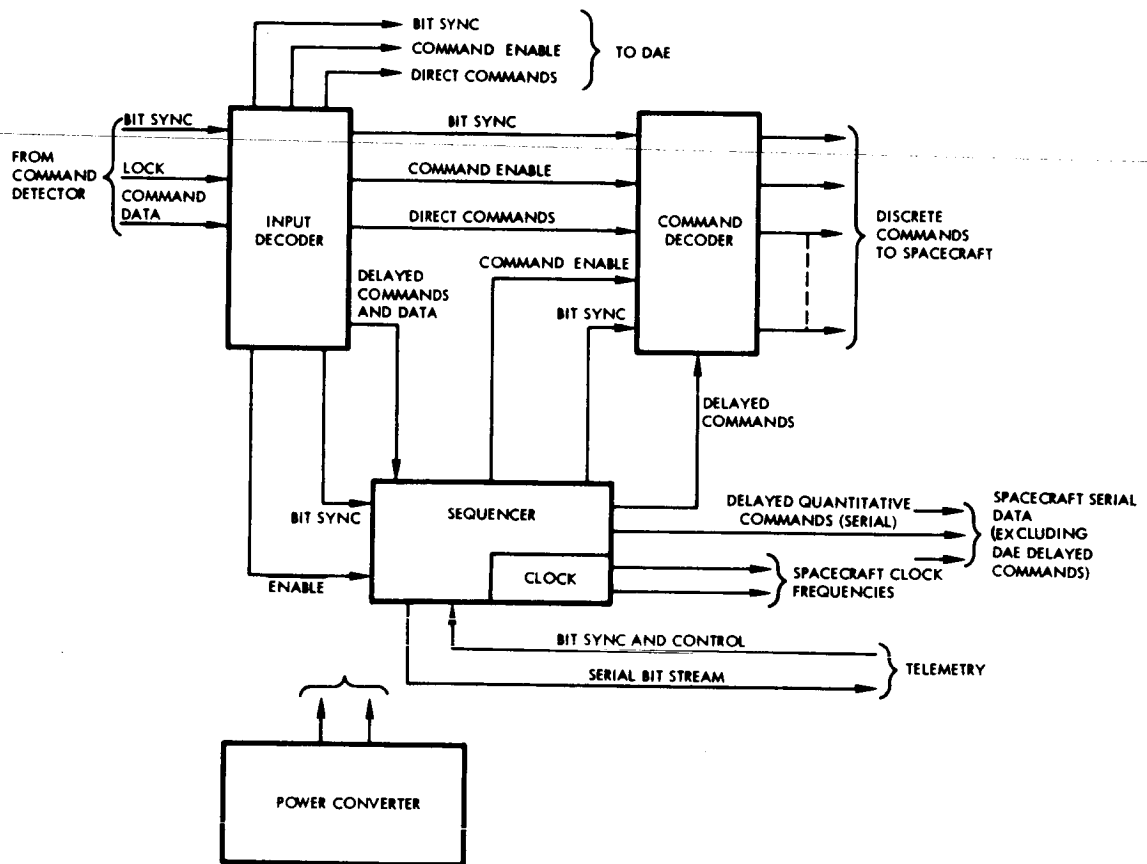


Figure 4-38. CS and C Centralized Memory System

The command decoder decodes incoming direct commands into one of 128 discrete pulses issued to a particular spacecraft subsystem. The command decoder also accepts discrete pulses from the sequencer to be issued through its output circuits. These signals represent delayed discretes, the commands for which were issued prior to the issuance of the discrete pulse.

The sequencer consists of a random-access core memory, a clock, parity checking logic, and the logic necessary to address and

store information in the memory. Further, the sequencer has the necessary logic to maintain an updated time and mode word and to compare this with the time and mode tags stored in the memory. The core elements in the memory are grouped into storage cells which can contain either commands or numerical information. Commands are identified through particular cell locations in the memory. The data in the cells contain the time of execution, a spacecraft mode tag and a verification bit. If the command is to be verified prior to execution, it is not executed until a verification is transmitted. If spacecraft conditions are satisfactory the verification tag is transmitted in a "do" execute mode which enables the command. The command may, of course, be inhibited by ground at any time by a "do not" execute signal.

The sequencer continuously scans that portion of each storage cell containing the time tag and mode code. Whenever a match occurs between the flight elapsed time register and mode code within the sequencer and a particular storage cell the address of that storage cell is interpreted as the spacecraft subsystem address to which a discrete must be issued or as the spacecraft subsystem to which serial data must be issued. Before the command or data is issued the verification bits are interrogated. If no match occurs between the elapsed time register and mode code and the particular cell being inspected, the next memory cell is inspected. This sequential scan is continued throughout the mission.

A summary of the CS and C functions is presented in Table 4-20.

#### 2.6.1 Detailed Descriptions of CS and C Subassemblies

##### a. Input Decoder

The input decoder provides the routing function to the DAE or within the CS and C by enabling the various subassemblies to be responsive to the command information transmitted by the command detector. The input decoder samples the command information to determine the validity of the message establishes the appropriate subassembly that will respond to the data, and checks some of the parity bits.

Table 4-20. Centralized Memory CS and C Subassembly Functions

Input Decoder

- 1) Determines the presence of an incoming message. The input decoder expects the first bit after the 3 sync bits to begin with a one bit.
- 2) Checks the message bit stream for a correct synchronization code. This code insures against a message shift or a random sequence of bits that may resemble a valid message.
- 3) Determines which input decoder, command decoder, DAE, or which sequencer is to process this incoming message. (Redundancy assumed)
- 4) Examine the parity bit covering item 3.
- 5) Resets input decoder for incorrect parity in item 4.
- 6) Enables the command decoder, DAE, or sequencer depending on item 3.
- 7) Examines the parity bit covering the command type portion of a direct command or the cell address portion of any command to be stored in memory.
- 8) Resets input decoder for incorrect parity in item 7.
- 9) Resets input decoder after issuing the enable to command decoders, DAE, or sequencers. (Redundancy assumed)

Command Decoder

- 1) Decodes command type portion of direct ground commands from command detector via the input decoder to be issued as discretes.
- 2) Decodes memory cell addresses from sequencer to be issued as discretes.
- 3) Issues drive signals on appropriate lines to spacecraft subsystems upon receipt of enable from either input decoder or sequencer.

Sequencer

- 1) Accepts storage cell address from command detector via the input decoder and conditions memory addressing logic.

Table 4-20. Centralized Memory CS and C Sub-assembly Functions (Continued)

- 2) Accepts time tag or data (the latter in the case of a quantitative command) from the command detector via the input decoder.
- 3) Accepts enable from the input decoder indicating receipt of complete time tag or data.
- 4) Examines parity of input message (time tag or data).
- 5) Resets memory cell for incorrect parity in item 4.
- 6) Distinguishes between delayed commands and verified execute command.
- 7) Stores information in appropriate memory cell.
- 8) Maintains updated elapsed time register and mode code.
- 9) Scans time tags in storage cells for a match with elapsed time.
- 10) Transmits storage cell address to command decoder in the event of a match in item 8.
- 11) Enables command decoder if item 9 has been verified.
- 12) Transmits serial data to spacecraft subsystem if item 9 is a quantitative type command (associated with data in adjacent memory cell).
- 13) Distributes clock frequencies to spacecraft subsystems.
- 14) Provides serial outputs from the elapsed time register and special output register to the telemetry subsystem. (Special output register contains the contents of memory sampled one cell at a time.)

#### Power Converter

- 1) Converts its own power as needed from the regulated, primary 50 VAC power available.
- 2) Supplies the working voltages to the remaining subassemblies in the CS and C.
- 3) Assuming redundancy the power converter also provides power switching to the redundant sequencer in the event of a sequencer failure.

Table 4-20. Centralized Memory CS and C Sub-assembly Functions (Continued)

- 4) Provides continuous power to redundant input decoder and command decoder.
- 5) Provides self-switching to redundant power converter in the event of a power converter failure.

---

An address register is shifted and loaded by the command detector's command data line and bit sync line. The bit sync pulses also pulse a bit counter which is used to establish the times at which specific portions of the message are in the address register. The address register is 8 bits long. At specified bit counts, e.g., at spacecraft address time, synchronization code time, etc., the outputs of the address register are sampled to establish the validity or presence of the message portion in question. Table 4-21 lists the logical conditions that must be met for various phases of the input message. Figure 4-39 is a block diagram of the input decoder.

---

Table 4-21. Input Decoder Equations

The decoded outputs of the address register are:

Sync Code	SYNC
Spacecraft Address	S/C
Command Decoder Address	CD1, CD2
Sequencer Address	S1, S2
DAE Address	DAE
Parity	PAR
Failure Reset	FR
Normal Reset	NR

Associated with each of these decoded outputs is a bit time which is defined as t1 through t4 for the purpose of these equations.

Command Decoder No. 1 Enable =  $(\text{SYNC} \cdot t1)(\text{S/C} \cdot \text{CD1} \cdot t2)(t3)(\overline{\text{FR}}) = \text{CDE1}$

Table 4-21. Input Decoder Equations (Continued)

Sequencer No. 1 Enable =  $(\text{SYNC} \cdot t1)(\text{S/C} \cdot \text{S1} \cdot t2) \overline{\text{FR}} (t4) = \text{SE1}$   
(for discrete data)

Input Decoder Failure Reset =  $\overline{\text{LOCK}} + (\overline{\text{PAR}} \cdot t2) + (\overline{\text{PAR}} \cdot t3) + (\overline{\text{SYNC}} \cdot t1) = \text{FR}$

Input Decoder Normal Reset =  $\text{CDE1} + \text{CDE2} + \text{SE1} + \text{SE2} + \text{DAE} = \text{NR}$

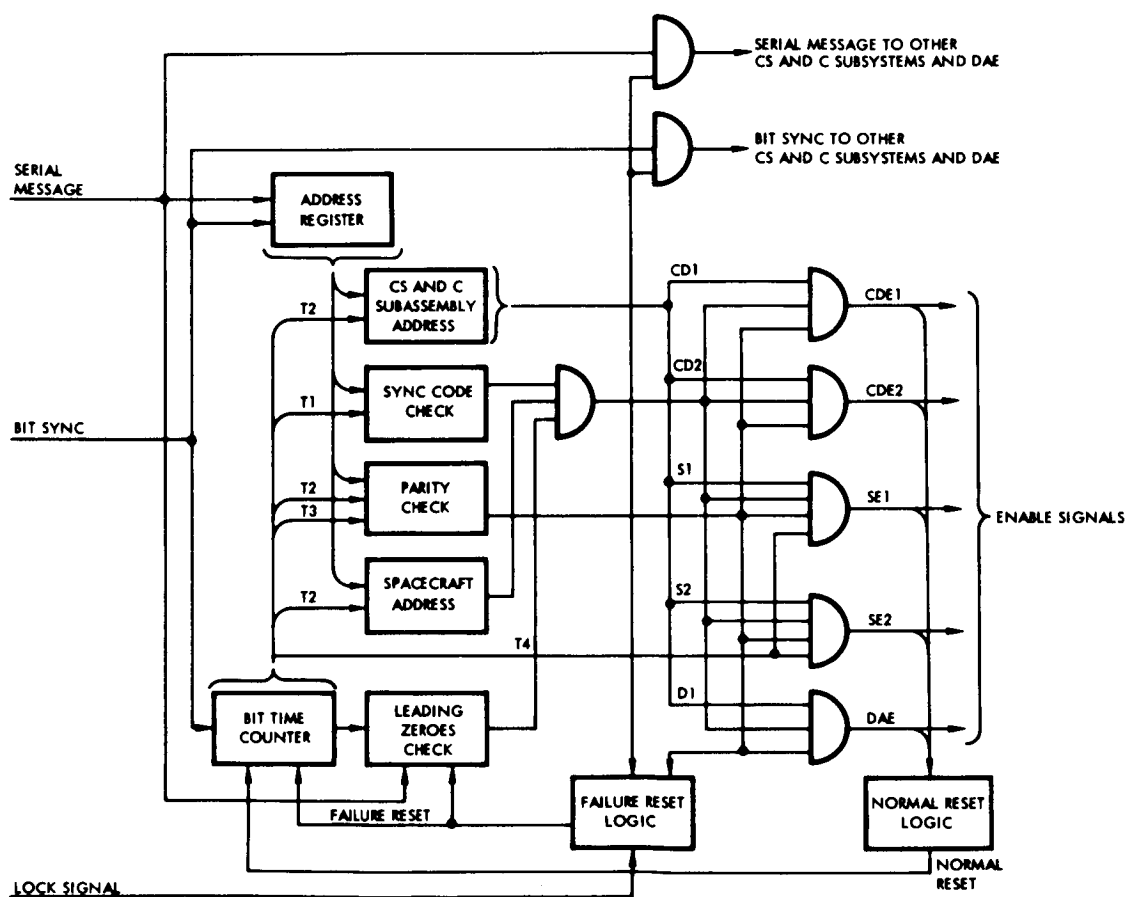


Figure 4-39. Input Decoder (with redundancy)

In the event that a test condition fails, such as parity, the input decoder is reset. The reset immediately places the input decoder in a condition ready to accept the next command. Loss of receiver lock at the command detector, as signified by the lock line, also resets the input decoder.



A normal reset of the input decoder occurs when the message is complete. Since there are only 2 message lengths, the input decoder interrogates the address register at specified times to determine the type of command. This information is necessary to reset the input decoder as well as to provide the command decoders or sequencer with an enable signal signifying that the subassembly in question has received the complete message and can now act on its contents. The command decoder and sequencer each receive a separate enable signal.

Logic is provided at the bit sync input to the address register to sense a "one" bit as the lead bit in a message. No bits are shifted into the address register following a normal reset or a reset because of a failure condition until a "one" bit has been detected. However, the bit counter counts the number of successive "zeros" after a failure condition, thus effectively increasing the sync code requirements (e.g., 12 extra bits) prior to acceptance of new messages.

b. Command Decoder

The incoming command data and bit sync pulses from the command detector (via the input decoder) or from the sequencer load and shift the address register. Since the command decoder is continuously sampling these lines, the register is in constant action and the decoding matrix associated with the register is constantly decoding. However, discrete pulse outputs are inhibited until an enable signal is received from either the input decoder or sequencer.

The outputs of the output buffers are 150 ma + 28 volt pulses. A block diagram of the command decoder is shown in Figure 4-40.

c. Sequencer

Figure 4-41 illustrates the functional block diagram of the sequencer. The four major functions are:

- 1) Clock generation

- 2) Memory storage
- 3) Elapsed Time Updating
- 4) Time Comparison.

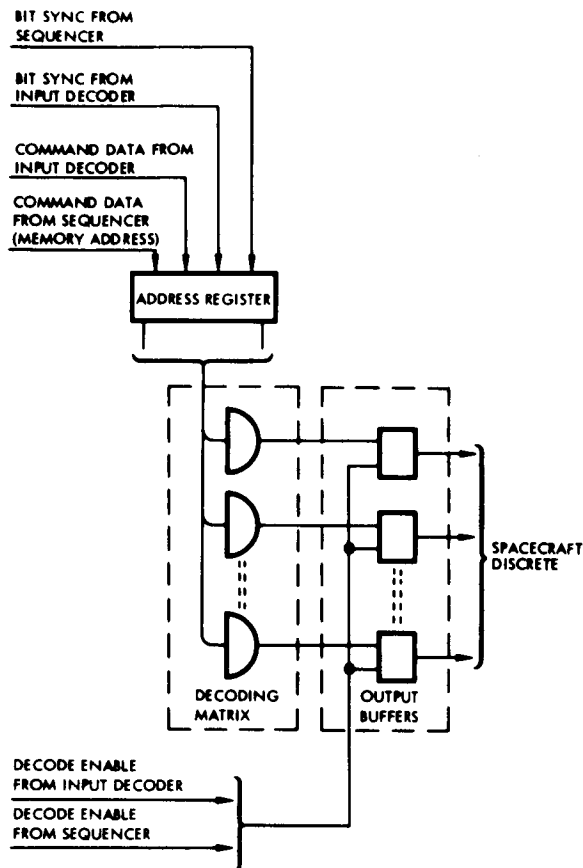


Figure 4-40  
Command Decoder Centralized  
Memory System

The sequencer accepts commands from the command detector (via the input decoder) and acts on these commands only upon receipt of an enable signal from the input decoder. The command inputs in the form of delayed direct commands and quantitative commands (time tagged data) are stored in a 128 word coincident-current core memory. The sequencer sequentially scans the contents of memory, matching the execution time tag and mode code associated with each storage cell with the mission elapsed time indication. A valid match indicates that the command specified by the particular location is to be executed. The sequencer provides the ground with telemetry data reflecting the contents of memory and the elapsed time register.



The clock generation portion of the sequencer provides the frequencies necessary to operate the sequencer's memory as well as the remaining spacecraft subsystems. The interface description in Section 2.6.2 identifies these clock frequencies and their destination. The clock generation process starts with a 1.032 Mc crystal controlled oscillator which provides an input to 6 counters. The clock logic consists of the following counters:

Modulo 5

Modulo 7

Modulo 9

Modulo 64

Modulo 128

Modulo 256

These counters divide the oscillator frequency down to the 18 required output frequencies. This is shown in Figure 4-42.

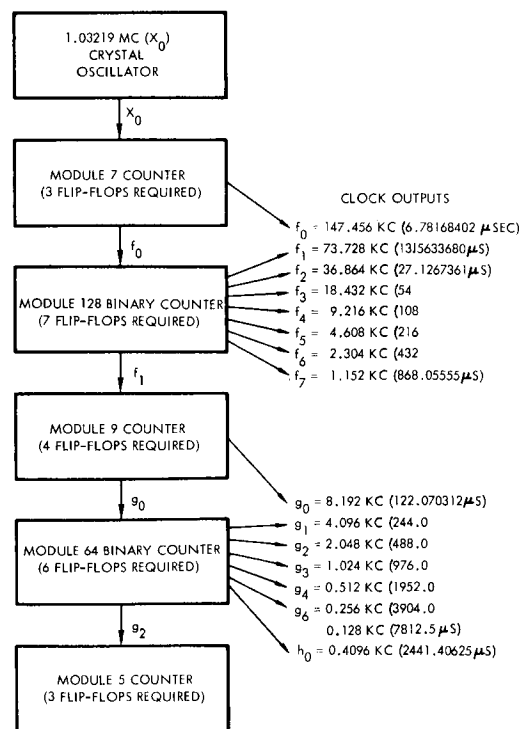


Figure 4-42. Clock Generator Block Diagram

The input addressing register decodes the 8-bit address portion of the command and energizes the appropriate drivers to store the input data. The input data is stored in an input data register prior to being stored in the core memory. The command and data line and bit sync line from the command detector/input decoder fill the address register and input data register. Upon receipt of an enable from the input decoder the address register performs the memory storage cell selecting process and the input data register is checked for correct parity. The correct parity indication along with the received enable permit storage of the input register contents in the specified storage cell.

The memory bit and memory address decoding blocks provide the bit timer and word location times necessary to address the memory.

In the case of a quantitative command the memory address decoding logic initiates a transfer of data from the adjacent storage cell to the data output register. From the output register this data is transferred to the designated subsystem in a serial stream. The data is clocked out of the output register at a 73-Kc rate. This clock rate is provided to the recipient subsystem to maintain synchronization in the data transfer.

For the case of command verification the sequencer is expected to alter the verification bit in any delayed direct command storage cell. Specific commands are transmitted to the sequencer with the function of inhibiting or enabling the execution of an existing command in memory. This inhibit function is accomplished without altering the time tag associated with the command.

A general purpose random access memory sequencer was considered in place of the functionally oriented memory. One major advantage of a general purpose memory with no fixed association between memory cells and subsystem functions is the flexibility of reassigning memory locations to any spacecraft functions. Any subsystem may be addressed by any particular cell in memory depending on that cell's current command content. Therefore, reassignment can be made by ground commands while the spacecraft is in flight, thus affording a

saving in total number of cells required. The disadvantage of such a completely flexible memory lies in the additional storage bits (command bits) necessary to specify which subsystem is being addressed by the contents of a particular memory cell. An additional 8 bits is required to address a subsystem. These 8 bits do not reflect an appreciable weight and power requirement for the sequencer, but they do reflect an additional burden on command message length. The command message must be augmented by the subsystem address as well as the additional protection bits necessary for the increased message.

d. Clock Mechanization

In the summary of clock requirements above (Figure 4-42) range and resolution estimates were provided for various segments of the mission, including the cruise condition. The maximum range requirement is one second, so a 26-bit counter register can be used to provide the basic clock for the mission.

Resolution requirements range from 1 second for the various maneuvers to two hours for the cruise condition. A convenient break point for the specific requirements divides the timing into two classes, one which uses the lower order bits of the basic clock (elapsed time register) and another which uses the higher order bits. With the indicated set of requirements, four secondary clocks are defined on the lower order bits and one on the higher order.

However, a mechanization simplification can be realized by providing greater resolution capability for the cruise modes and the postlaunch sequence clocks. Increasing the postlaunch sequence resolution to 1 second increases the number of bits from 8 to 14 required for its clock. This is the number needed for the mid-course maneuver and capsule separation timing, so, one clock can be used for all three sequences. The 14 lower order bits of the basic clock can therefore be used as the reference.

An increase in the cruise mode resolution also simplifies the

mechanization since the 14 higher order bits can now be used as the reference and the same number of memory bits can be used as before.

Since the orbit time granularity is 4 seconds and the 14 bits provide adequate range, it is necessary only to use bits 3 through 16 of the basic clock for this reference. The same time tag length as that for the other clocks can therefore be used.

Since the same memory bits are used for three different clock time tags, some additional bits are needed for identification. These additional bits can readily be combined into a mode reference to fully define the time at which events occur. The modes are conveniently tied to the 5 major sequences and the over-all cruise condition, so a 3-bit mode tag is sufficient. One configuration of bits in the mode tag identifies the cruise mode and indicates that the time tag bits in this memory location are to be compared to coarse clock time. A second configuration identifies the orbit time (least bit 4 sec.), and the remaining tags identify the fine clock time (least bit 1 sec). A 3-bit mode indication register in the sequencer is required to hold the current mode.

Commands for diverse sequences may be stored in memory at the same time, so mode change commands must precede each non-cruise sequence group to enable commands in that group to be executed. These mode enabling commands set the 3-bit mode register to agree with the mode tags associated with the particular commands in the sequence. Thus, both a time and a mode agreement is needed to issue a discrete or data word from memory. The memory word and clock system are shown in Figure 4-43.

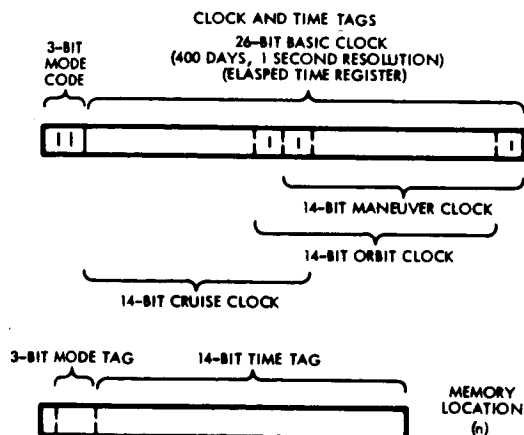


Figure 4-43. Clock and Time Tags

## 2.6.2 CS and C Interfaces

### a. Command Detector

The input decoder accepts the serial bit stream from the command detector. Along with the serial data the command detector provides a bit synchronization and a separate enable signal which assures the input decoder that the message is in LOCK at the command detector. The moment that LOCK is lost the command detector removes this enable signal, thereby informing the input decoder that the incoming message is no longer locked with the receiver in frequency, phase, and PN code.

The frequency and logic levels of the three input lines from the command detector unit are:

- |                        |                                      |
|------------------------|--------------------------------------|
| 1) Command Line        | 1 pulse/sec, 0, + 3 volts            |
| 2) Bit synchronization | 1 pulse/sec, 0, + 3 volts            |
| 3) LOCK                | DC                      0, + 3 volts |

### b. Telemetry

For the purpose of verifying specific stored commands prior to their execution or for a general check on the contents of the sequencer's memory, an output is provided to telemetry. An 18 bit register holds a memory word until it is sampled by telemetry and an end-of-sample message is given to the CS and C. At this time the next word in line is transferred to that register. Each 18 bit group contains one entire storage cell content comprised of a time tag plus verification bits and mode tag, or data. Each cycle through memory starts or ends with a sampling of the elapsed time register, which resynchronizes the bookkeeping process of tracking the cell location with the cell contents.

The elapsed time register is available to the telemetry subsystem at all times.



The telemetry subsystem is also provided with a discrete signal indicating one of four data rates. These discrettes exhibit a logic level swing between  $0 \pm 1$  volt, a rise time less than  $\mu\text{sec}$ , and a 10 ma drive capability at the 0 state. Along with the discrete, the CS and C supplies the appropriate group of frequencies for the particular data rate. Table 4-22 illustrates the four groups of frequencies associated with the data rates.

Table 4-22. Frequencies Associated With Data Rates

Data Rate Group	1	2	3	4
Frequency (Kc)	4.096	2.048	1.024	0.128
	147.456	73.728	36.864	4.608
	73.728	36.864	18.432	2.304
	36.864	18.432	9.216	1.152

These frequencies are provided to the telemetry subsystem with a 0.005 per cent long term accuracy.

c. Spacecraft Subsystem Discrettes

The command decoder provides one discrete pulse to a particular spacecraft subsystem on the basis of the command address. One hundred twenty-eight discrettes can be decoded from the command address. Each of these decoded discrettes provides the spacecraft subsystem interface with a 120 ma, + 28 volts capability. The discrete pulse is enabled for a minimum of 1 second in the case of direct ground commands or for a minimum of 8 milliseconds in the case of sequencer issued commands.

d. Data Automation Equipment

Direct command data which initiate discrettes to the science subsystems are routed by the CS and C input decoder to the DAE decoder. This requires bit sync, command enable and the direct command data to the DAE.

### 2.6.3 Physical Characteristics

Table 4-23 summarizes the weight, volume, and power dissipation for this system. Both the individual subassemblies and total CS and C system values are indicated. A relatively small size, low weight and power system is indicated.

Components and parts count for the various subassemblies and the total CS and C subsystem are shown in Table 4-24. Detailed information is given for the various integrated circuit classes that are used, the inductors, transformers, crystals, cores, diodes, etc.

Table 4-23. Physical Characteristics of CS and C Centralized Memory System Subassemblies

CS and C Subsystem	Physical Characteristics		
	Weight (lb)	Volume (in <sup>3</sup> )	Power (watts)
Input Decoder	1.0	20	1.8
Command Decoder	1.0	20	0.5
Sequencer Including Clock	6.5	160	9.1
Power Converter	3.8	90	2.9
Total	12.3	290	14.3

Table 4-24. CS and C Centralized Memory System Parts Count

CS and C Subassembly	IC(A)	IC(B)	IC(C)	IC(D)	Transistor	Transistor	Resistor	Capacitor	Inductors	Trans-	Capacitor	Crystal	Cores	Diodes	Diodes
					Digital	Analog		Metal		Glass					
Input Decoder	40	25			12		12	4							8
Command Decoder	16	10			384		512								
Sequencer including Clock	130	150	32	24	210		400	20	1			1	4148		16
Power Converter						40	120	55	6	16	29			10	50
Total	186	185	32	24	606	40	1044	79	7	16	29	1	4148	10	74

Finally, the discrete component counterpart to the integrated circuits used in this configuration is given in Table 4-25. The discrete components are shown for each of two integrated circuit gates, a flip-flop and memory isolation diodes.

Table 4-25. Integrated Circuit Configurations

- |    |        |                            |
|----|--------|----------------------------|
| 1. | IC (A) | Dual Nand Gate             |
|    |        | 6 film resistors           |
|    |        | 2 digital transistors      |
|    |        | 9 digital diodes           |
| 2. | IC (B) | Flip-Flop                  |
|    |        | 11 film resistors          |
|    |        | 5 digital diodes           |
|    |        | 4 digital transistors      |
|    |        | 4 mica or glass capacitors |
| 3. | IC (C) | Diode Gate                 |
|    |        | 1 film resistor            |
|    |        | 6 digital diodes           |
| 4. | IC (D) | Memory Isolation Diodes    |
|    |        | 16 digital diodes          |

## 2.7 Distributed, or Decentralized, Memory System

This is the second of the two configurations considered as reasonable mechanizations of the requirements developed in Section 2.2 above. It has a decentralized-memory system with special purpose registers and associated timers rather than a random access-memory system. In this respect, it is quite different from the centralized memory system but it is also similar in that it has a command decoder and an input decoder. However, commands from the special purpose timers are decoded directly and do not pass through the command decoder.

The command decoder interprets requests on all direct commands, i. e., all ground commands, and a sequencer interprets all indirect commands, i. e., sequences or delayed commands. An input decoder unit accepts the serial bit stream from the detector subsystem of the telecommunications system and routes acceptable messages either to the command decoder or to the sequencer.

The command decoder and the sequencer deliver signals to other spacecraft subsystems. Both provide logic level outputs, and the power distribution unit supplies the balance to attain the proper power level at the spacecraft subsystems.

In this configuration the sequencer is a hard-wired unit in the sense that special circuits are provided for each function. It is in principle the Mariner C, CS and C<sub>2</sub> adapted to the requirements of the Voyager mission. It contains an additional pair of subassemblies over that of the CS and C. These are the orbit subassembly which provides the pointing and sequencing operations for the science packages during Mars orbit and the antenna command generation subassembly.

The memory unit uses core shift registers or integrated circuits, but, as mentioned above, the memory cells are not general purpose. Each cell is associated with one and only one function, provided by one of the subassemblies. No special decoding is required. The core and integrated circuit tradeoffs are illustrated in the weight versus reliability figures presented in this and later sections.

A general block diagram shown in Figure 4-44 describes the subassemblies included within this subsystem. Specific storage cells and sequence event counters are assigned to specific spacecraft functions, so no programming alterations can be made in this assignment. Only the numerical values (time value or data) may be altered within the storage cells or sequence event timers. The time values or data may be prestored on the ground or transmitted to the CS and C via ground commands.

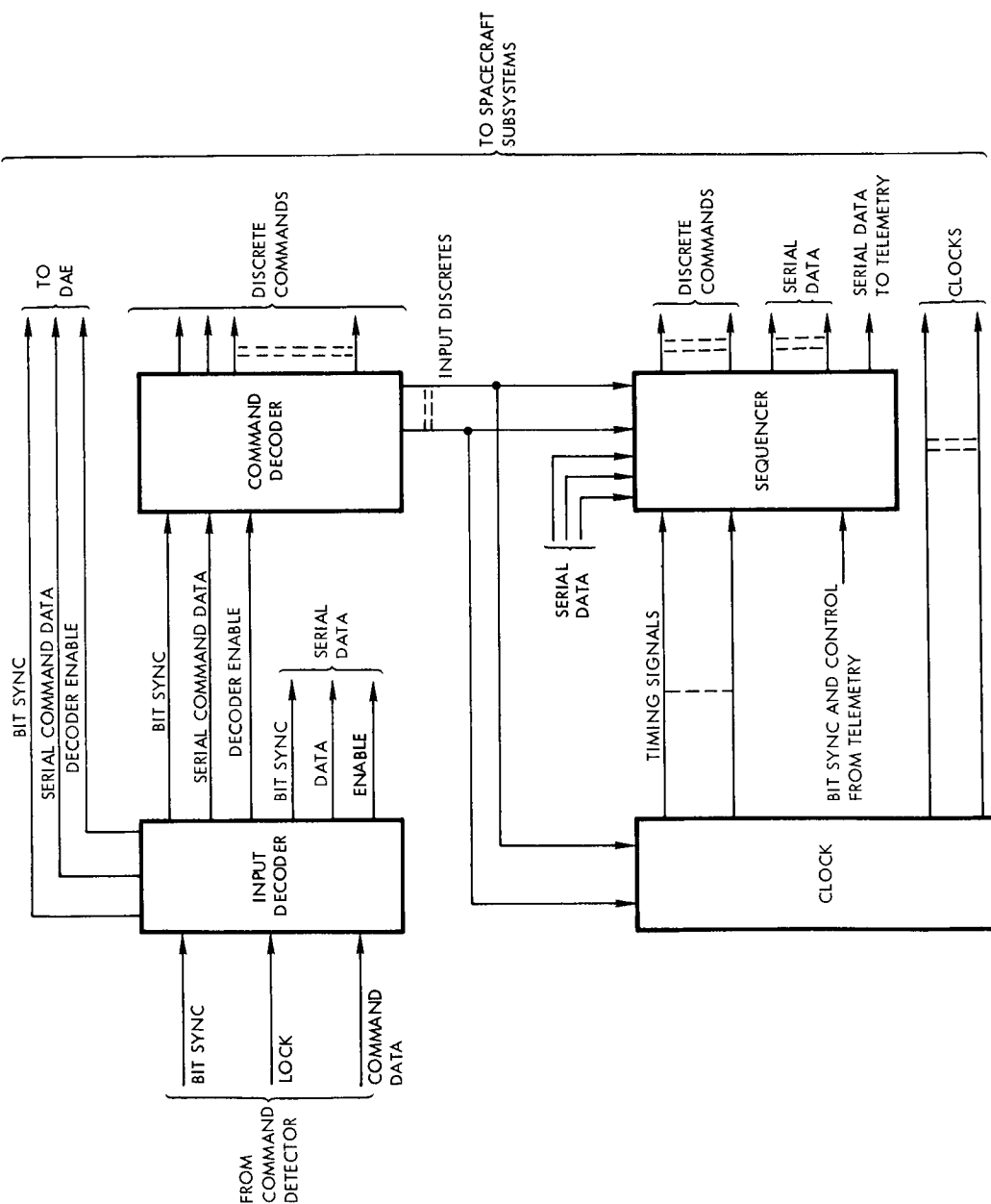


Figure 4-44. CS and C Distributed Memory System

The input decoder accepts ground communication data from the command detector. This data is examined for correct synchronization code and subsystem address. Included within the address code are enough bits to specify the data automation equipment or redundant subassemblies within a particular spacecraft's CS and C subsystem. The input decoder also determines whether the command message is a direct discrete command, in which case it is transmitted to the command decoder, or a delayed command or data to be stored in a CS and C storage cell.

The command decoder accepts information from the input decoder in the form of an address specifying a particular discrete. The command decoder decodes this address into the various discrettes issued to other spacecraft subsystems or within the CS and C subsystem. Some portion of the original spacecraft address portion of the message will provide enabling signals to one or more command decoders in the event of a redundant subsystem. These enable signals assure that only one command decoder responds to the message.

The sequencer issues discrettes to other spacecraft subsystems as well as within the CS and C subsystem through a series of sequence timers. The sequence decoder also contains a group of storage cells which either provide serial data to other spacecraft subsystems or time tag data to sequence timers.

The clock provides various timing signals to other spacecraft subsystems and within the CS and C subsystem. Ground command discrettes or discrettes issued by the sequence decoder may turn-on, turn-off, or enable various clock outputs.

A summary list of functions for the decentralized memory CS and C is presented in Table 4-26.

Table 4-26. Distributed Memory CS and C Subassembly Functions

#### Input Decoder

- 1) Determines the presence of an incoming message. The input decoder expects the first bit of a valid message to begin with a one bit.
- 2) Checks the message bit stream for a correct synchronization code. This code insures against a message shift or a random sequence of bits that may resemble a valid message.
- 3) Determines which input decoder, DAE, command decoder or sequencer is to process this message. (redundancy assumed).
- 4) Examines the parity bit covering item 3).
- 5) Resets input decoder for incorrect parity in item 4).
- 6) Enables the command decoder or sequencer depending on item 3).
- 7) Examines the parity bit covering the address portion of a direct command or the cell address portion of any command to be stored in memory.
- 8) Resets input decoder for incorrect parity in item 7).
- 9) Resets input decoder after issuing the enable to command decoders or sequencer (redundancy assumed).

#### Command Decoder

- 1) Decodes address portion of direct ground commands from command detector via the input decoder to be issued as discretes.
- 2) Issues drive signals on appropriate lines to spacecraft subsystems upon receipt of enable from either input decoder or timer.

#### Sequencer

- 1) Accepts enable signal from input decoder and checks parity of incoming messages
- 2) Routes delayed commands to proper registers



- 3) Issues delayed discretes to spacecraft subsystems at designated times
- 4) Stores numerical data in holding registers
- 5) Shifts data to spacecraft registers at designated times
- 6) Provides serial outputs from sequencer memory cells to telemetry subsystem

#### Power Converter

- 1) Converts its own power as needed from the regulated, primary 50VAC power available
- 2) Supplies the working voltages to the remaining subassemblies in the CS and C.
- 3) Assuming redundancy the power converter also provides power switching to the redundant sequencer and clock in the event of failure.
- 4) Provides continuous power to redundant input decoder and command decoder.
- 5) Provides self-switching to redundant power converter in the event of a power converter failure.

#### Clock

- 1) Provides required frequency and timing signals to spacecraft subsystems and to sequencer.



b. Command Decoder

Figure 4-46 illustrates the command decoder. The purpose of this decoder is to route direct discrete commands to the appropriate spacecraft subsystem or within the CS and C subsystem. An input register accepts data from the input decoder. This register issues a particular discrete output pulse by means of a decoding matrix. Buffers or level shifting devices are shown on the output of each decoding gate prior to the command decoder interface. These are provided to increase the voltage and current capabilities of the decoding gates.

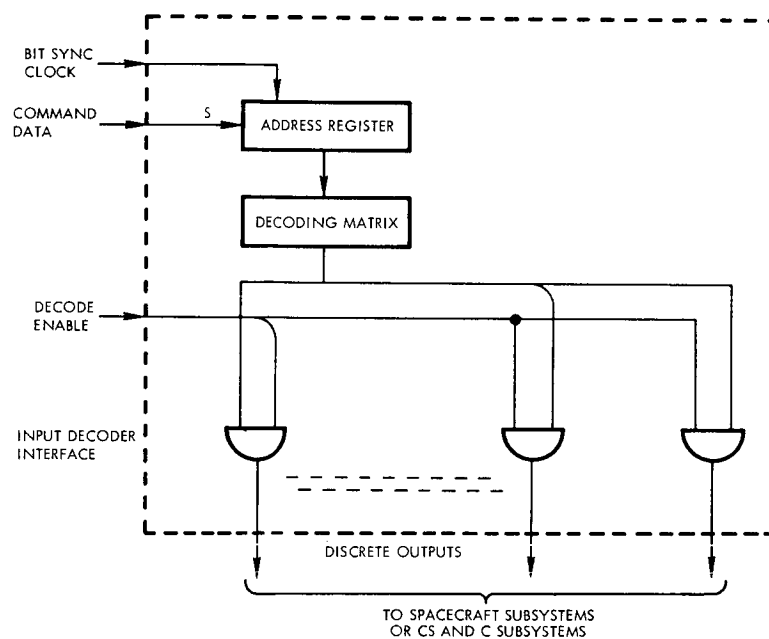


Figure 4-46. Command Decoder (Distributed Memory System)

The decoder enable signal from the input decoder is required to enable pulses to be output from the CS and C command decoder. Note that this subassembly is similar to the decoder described above in Section 2.5.3

c. Sequencer

The sequencer for the distributed memory CS and C is a collection of storage cells and sequence timers. Figure 4-47 illustrates a number of storage cells and sequence timers and some possible

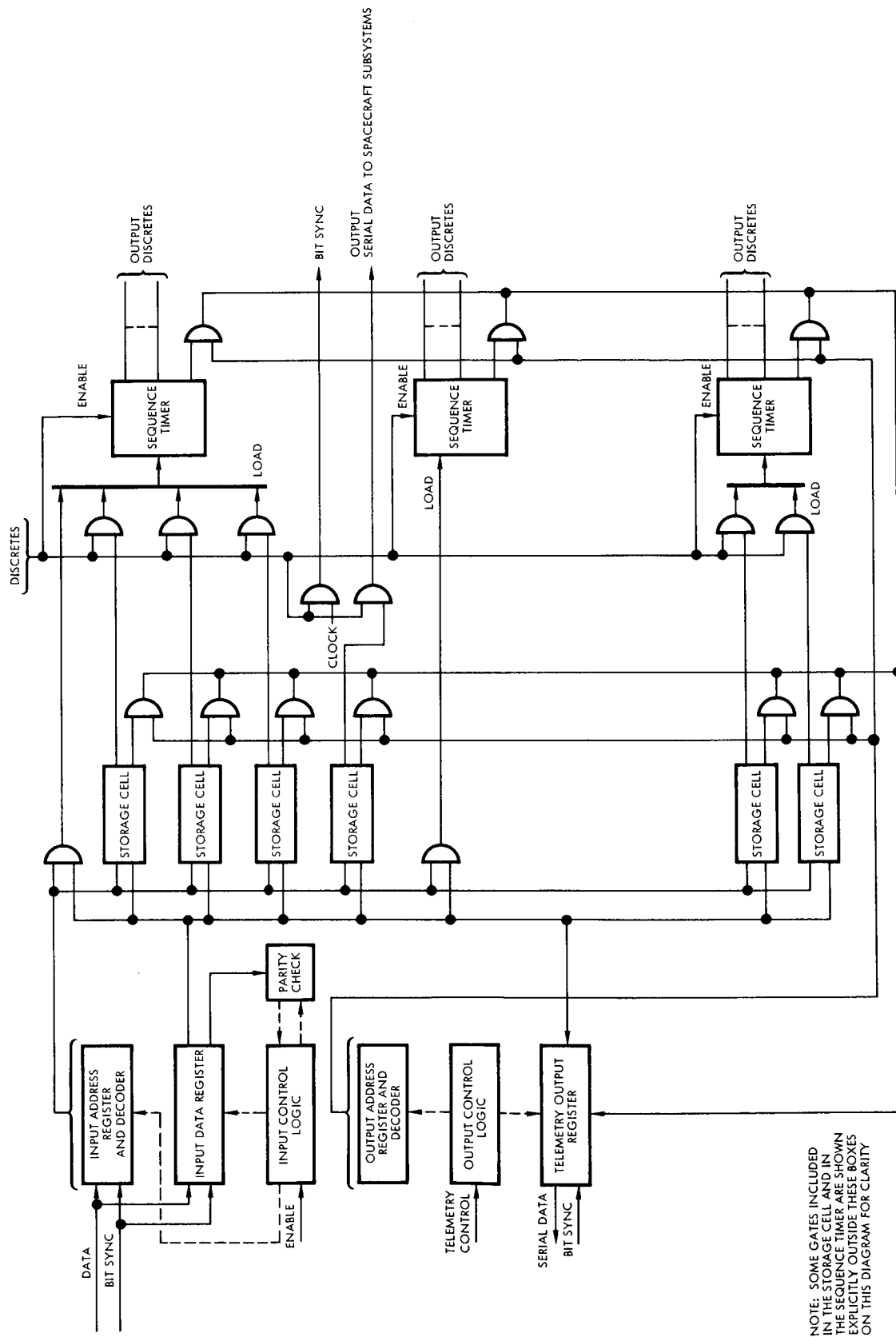


Figure 4-47. Sequencer Block Diagram (Distributed Memory System)

interconnections between them. Figure 4-48 illustrates additional storage cells which are used only in the delayed transmission of serial data to other spacecraft subsystems. Figures 4-49 and 4-50 illustrate in detail a typical storage cell and sequence timer.

All storage cells in the sequence decoder are loaded via a ground command through the input decoder. This may be accomplished either on the ground or during flight. Each of these storage cells is connected to a particular sequence timer or, as in Figure 4-48, to a particular spacecraft subsystem. More than one storage cell may be connected to a sequence timer. Discretes are used to determine which cell inputs data to the sequence timer at which time. For this purpose the discretes may be ground commanded discretes or discrete outputs from other sequence timers.

A sequence timer may also be loaded through a direct quantitative ground command or a combination of ground commands and storage cell combinations as determined by discretes. These options are shown in Figure 4-47. The flexibility implied by this figure is only a design flexibility. Once the cells and timers are physically interconnected, the sequencer becomes rigid and no alteration in the storage cell or sequence timers assignment can be made other than by major rewiring.

The details of the storage cell in Figure 4-49 show a data register which can be loaded via a ground command and unloaded to a specific location via a discrete. This discrete may be issued by a ground command or sequence timer. The storage cell may also be circulated and its contents read out to telemetry.

The sequence timer illustrated in Figure 4-50 contains a data register which may be loaded through a storage cell, a ground command, or any combination of these under the control of discretes. A discrete input initiates the timer operation which circulates the data register and decrements the contents of this register. Decoding gates connected to the decoding register issue discretes to other spacecraft subsystems or within the CS and C subsystem. The data register may also be circulated and its contents read out to telemetry.

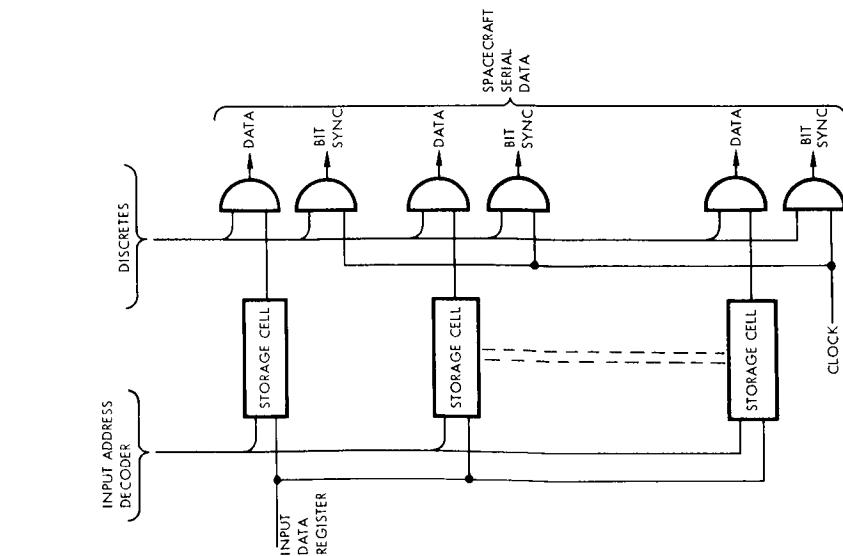


Figure 4-48. Storage Cell Distributed Memory System

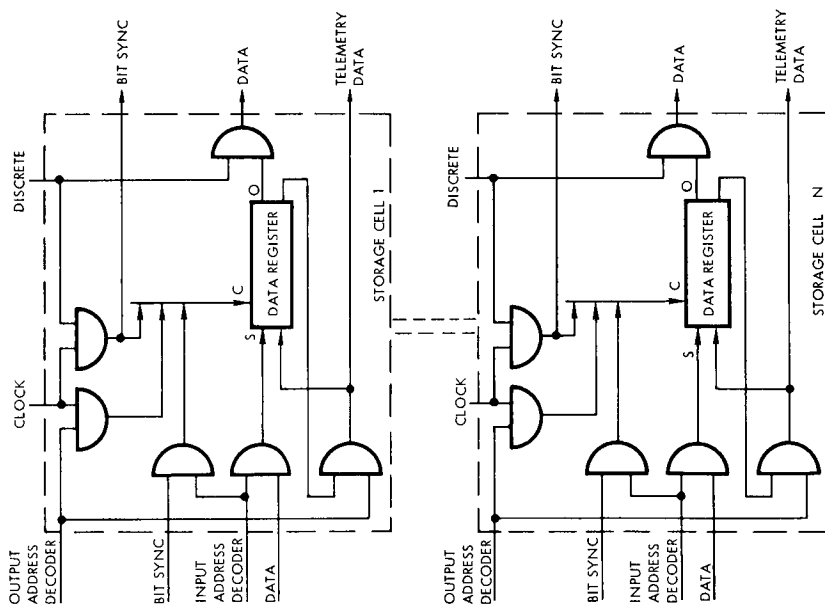


Figure 4-49. Sequencer Storage Cell Distributed Memory System

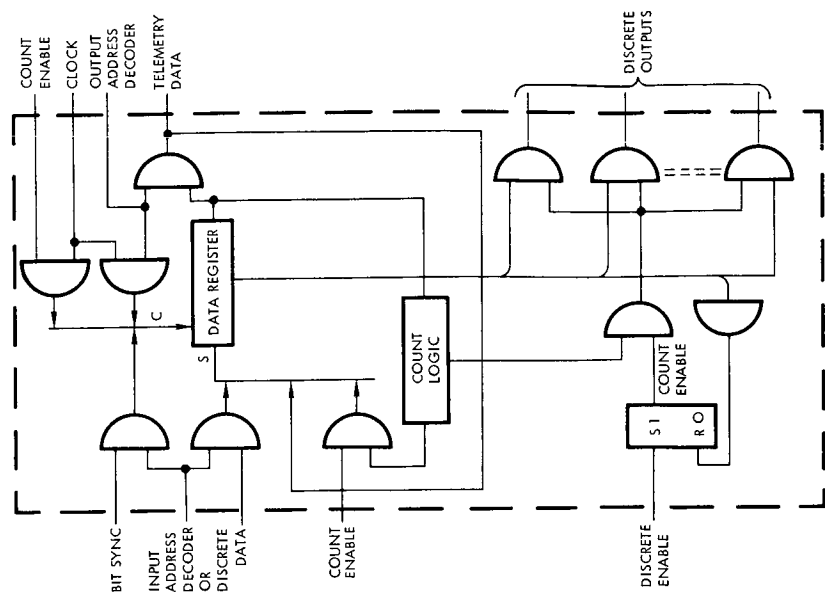


Figure 4-50. Sequencer Timer, Distributed Memory System

### 2.7.2 CS and C Interfaces

The CS and C interfaces are the same for the decentralized memory system as for the centralized memory system and are described in Section 2.5.4.

### 2.7.3 Physical Characteristics

Weight, volume, and power dissipation for this configuration are summarized in Tables 4-27 and 4-28. In the first table the physical characteristics are given for the system using core shift registers packaged like the Mariner C CC and S. The data from the second table assumes that integrated circuits are used. Both the individual sub-assemblies and the total CS and C subsystem values are indicated. Note that a 25 per cent reduction in weight and a 35 per cent reduction in volume is obtained in converting from core registers to integrated circuits but the power consumption is increased by more than a factor of 2.

Table 4-29 contains detailed parts counts for the various sub-assemblies and for the whole system. Counts for both the integrated circuits version and the discrete system are included. Only the sequencer is affected by this alternative.

## 2.8 Reliability Comparisons

### 2.8.1 Reliability Considerations for the Centralized Memory System

In this configuration failure can occur in each of four sub-assemblies.

#### a. Input Decoder

A failure in this unit inhibits all messages entering the spacecraft from ground. Direct commands and updated numerical data are then not available to the spacecraft, and control of spacecraft operations is possible only via the sequencer, which uses previously stored command and numerical information. The likelihood of this failure is relatively low, but the associated risk is very high.

#### b. Command Decoder

In this configuration a failure in the command decoder is disastrous since it interprets all commands and sequencing. Neither ground nor onboard control would be possible.

Table 4-27. Physical Characteristics of CS and C Distributed System with Core Shift Registers

Subassembly	Weight (lb)	Volume (in <sup>3</sup> )	Power (watts)
Input Decoder	1.0	20	1.8
Power Converter	5.2	130	3.7
Clock	0.7	14	1.5
Sequencer (core registers)	15.0	360	11.0
Command Decoder	1.0	20	0.5
Total	22.9	544	18.5

Table 4-28. Physical Characteristics of CS and C Distributed System with Integrated Circuits

CS and C Subassembly	Weight (lb)	Volume (in <sup>3</sup> )	Power (watts)
Input Decoder	1.0	20	1.8
Power Converter	6.5	145	8.6
Command Decoder	1.0	20	0.5
Clock	0.7	14	1.5
Sequencer (Integrated circuits)	7.7	170	30.4
Total	16.9	369	42.8



Table 4-29. CS and C Distributed Configuration

CS and C Subassembly	IC(A)	IC(B)	Transistor Digital	Transistor Analog	Resistor Metal	Capacitor Glass	Inductor	Trans-former	Capacitor Tantalum	Crystal	Resistor Wire Wound	Diodes Digital	Diodes Zener	Cores
Input Decoder	40	25	12		12	4						8		
Command Decoder	16	10	384		512									
Clock	20	40	10		20	4				1		10		
Power Converter				25	80	40	4	10	20			30	6	
Sequence Decoder (integrated circuit)	440	870	96		128									
Total 1	516	945	502	25	752	48	4	10	20	1		48	6	
Sequence Decoder (Cores)	62	70	360		1250	170		4	80		50	900	60	700
Total 2	136	145	766	25	1874	218	4	14	100	1	50	948	66	700

Table 4-30. Integrated Circuit Configurations

1. IC (A) Dual Nand Gate  
6 metal resistors  
2 digital transistors  
9 digital diodes
2. IC (B) Flip-Flop  
11 metal film resistors  
5 digital diodes  
4 digital transistors  
4 mica or glass capacitors

c. Sequencer (Including Clock)

A failure in the sequencer results in a complete loss of onboard control of spacecraft operations. This loss is not as serious as either a loss in the input unit or in the decoder, since ground command capability is not jeopardized, but spacecraft performance would be severely limited because of the low bit-rate up-link and the long transmission time to the spacecraft. Also clock outputs to the telemetry and spacecraft power supply may be lost. Note that clocks to the spacecraft power supply are not needed to maintain primary AC power.

d. Power Converter

A failure in the power converter results in a complete loss of onboard and ground control of the spacecraft.

Use of Redundancy

In order to reduce the risk of these failures, a simple redundancy scheme was considered in the form shown in Figure 4-51 (see Volume 4 for more details). An additional unit has been added for each of the four subassemblies in the system. Switching is accomplished in the decoders and sequencer by addressing the desired unit via bits in the command message. The redundant units in each subassembly receive the commands, so the designated command decoder or sequencer must receive an enable signal after the command has been accepted by the designated input decoder. The outputs of the pairs of subassemblies are logically OR'd so that either unit can accomplish all of the functions. In the case of sequencer outputs to the command decoders, selection is done via a previously executed discrete which is remembered by a flip-flop in each sequencer.

2.8.2 Reliability Considerations for the Distributed Memory Systems

In this configuration failures can occur in each of five subassemblies, only catastrophic failures which would render a subassembly inoperative are considered.

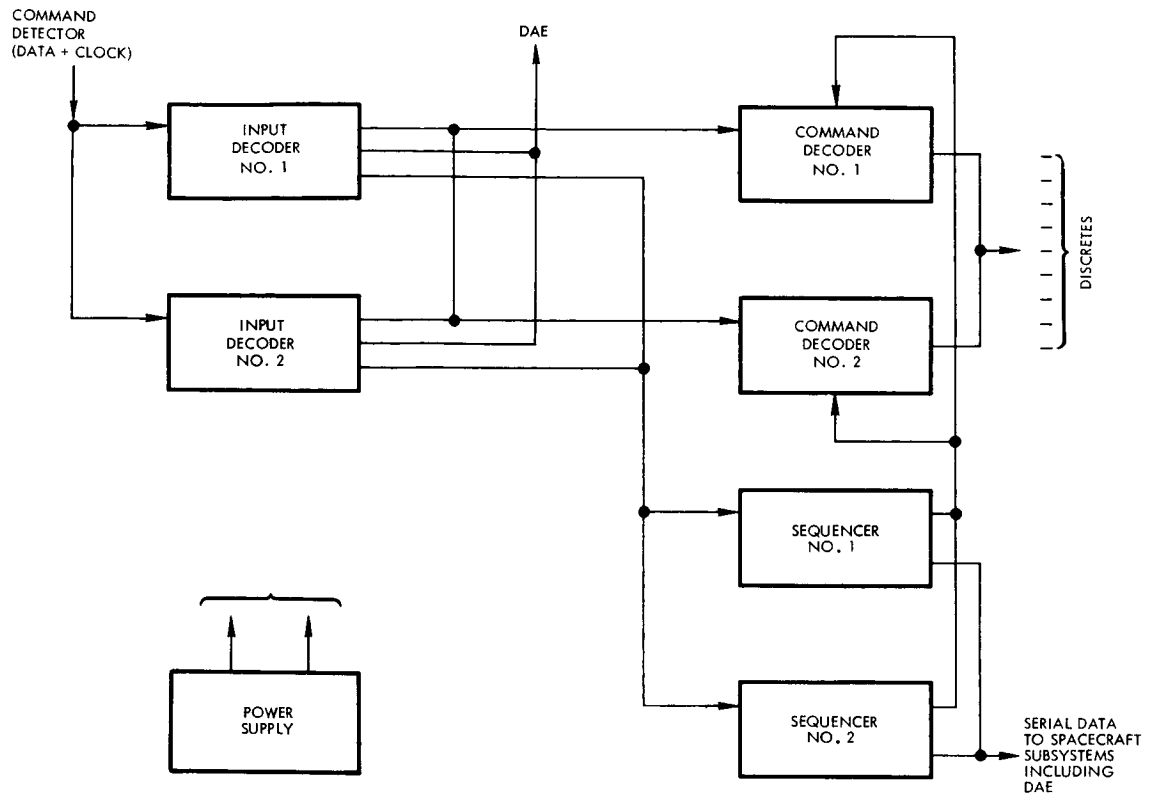


Figure 4-51. Power Converter Block Diagram

a. Input Decoder

A failure in this unit inhibits all messages to the spacecraft. Direct commands or delayed commands are then not available to the spacecraft subsystems. Control of spacecraft operation is therefore possible only through the prestored commands in the sequencer storage cells.

b. Command Decoder

A failure in the command decoder prevents direct control of the spacecraft subsystems via ground commands, (because the sequencer issues discrete commands on its own) but it does not hamper control of the spacecraft through any sequencer functions.

c. Sequencer

A failure in the sequencer prevents control of the spacecraft through prestored data. However, direct control of the spacecraft can still be exercised through ground commands. Since the sequencer is constructed of modular storage and timing functions, total loss of the sequencer is unlikely.

d. Clock

A failure in the clock subassembly prevents timing signals from being issued to the power supply and telemetry subsystems, as well as the sequencer. (Note that clocks to the spacecraft power supply are not needed for it to maintain primary AC power.)

e. Power Converter

A failure in the power converter results in a complete loss of onboard and ground control of the spacecraft.

To guard against such failures the redundancy configuration shown in Figure 4-52 is considered. This is the best of several alternatives which were considered (see Volume 4). The reliability data for both the integrated circuits version and the core register system show that the core system is the best from a reliability point of view.

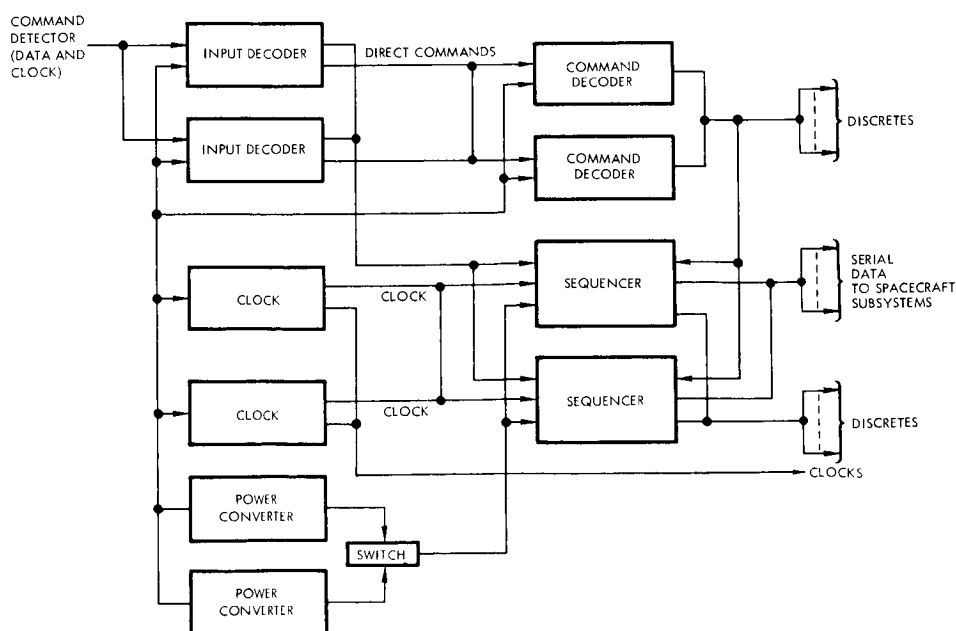


Figure 4-52. CS and C Subsystem Redundancy

To address the appropriate command decoder in the redundant system, incoming messages to the spacecraft contain the necessary bits as a part of the subsystem address. The outputs of the two input decoders are wire OR'd, thereby providing two input decoder functions at all times. Selection via ground command to select the input decoder for each command is also done by bits in the subsystem address portion of the message. The redundant clock outputs are selected by a discrete from the command decoder as a result of a ground command.

In the sequencer, redundancy is implemented by the use of additional storage cells and sequence timers for those functions that are critical to mission success (i. e., perhaps redundant sequencer does not implement all functions of the primary sequencer). Ground commands which store information in the sequencer permit ground control of the selected redundant portions in the sequencer. If the sequencers are implemented with integrated circuits, power must be provided to both of the redundant units. However, if cores are used, power can be switched to the redundant portions of the sequencer via ground commands, since cores normally retain their information even when power is off.

Complete power converter redundancy is provided, and self-testing circuits and/or command decoder discretes may be used to switch power sources to the CS and C.

### 2.8.3 Review of Reliability Analysis Assumptions

The following assumptions were made in the implementation of the CS and C centralized and distributed memory systems:

- a) The integrated circuits used in both configurations are of the type shown in Table 4-25.
- b) The storage cells and sequence timers within the sequencer in the distributed system can be constructed with either integrated circuits or cores. Both implementations were studied to size the configurations and to establish their reliability.

- c) In the redundant subsystem designs, Figures 4-51 and 4-52 power converter switching is only necessary for the sequencers in both systems. The input decoders, command decoders, and clocks in both configurations are connected to both converters simultaneously. The additional load to one converter because of a failure in the other is a small percentage of the total load and can be compensated for by regulation.
- d) The output discretes of both direct ground commands, and delayed commands issued by either the sequencer for the distributed memory system or the sequencer through the command decoder for the centralized memory system are capable of delivering 150 ma at +28 volts.
- e) The redundancy schemes for the two configurations (developed in detail in Appendix B, Volume 4) consider only block redundancy. Component redundancy within a functional block has been ruled out as ineffective in this application. In the case of the clock in the decentralized system the redundancy may be limited to the oscillators rather than the entire clock distribution function. But in this event, the additional oscillators can still be considered as a functional block redundancy rather than component redundancy.
- f) Power switching is indicated in the redundancy schemes shown in Figures 4-51 and 4-52. This switching applies only to the sequencers in the configuration. Core memory elements such as those in the core shift registers in the decentralized version and the core memory plane in the centralized version retain their information content in the event of a power failure. Should power be switched to a sequencer that was not previously in use, no information prestored in it would have been altered during the inoperative period. This is not the case for the integrated circuit sequencer.

## 2.9 Summary and Conclusions

For the reasons described in the preceeding pages and summarized below, the centralized memory sequencer is the selected approach. The major difference between the centralized memory CS and C and the distributed (or decentralized) system, as the names indicate, lies in the way in which the memory is mechanized. In the centralized approach a single random-access core array is used, while in the decentralized version the memory cells are isolated. Thus, a common clocking system is used in the former case, whereas separate counters and timers are used in the latter system.

4-1

In the two systems, the command decoder subassemblies are very much the same. Functionally they are identical, although the sequencer in the distributed system issues its own discretes. In both cases the full decoding compatibility is provided, but additional logic is required in the centralized system to coordinate the two sources of command inputs to the decoder.

The input decoders, like the command decoders, are basically the same in the two systems. Both must test for sync, examine the subassembly address, and route the commands and data to the appropriate locations.

#### 2.9.1 Comparison of Physical Characteristics

Summary data on the physical characteristics of the two systems are given in Figure 4-53 and in Table 4-31. In Figure 4-53 the weights of the CS and C mechanizations are shown as functions of the number of bits of storage. At the lower bit levels the weight for the centralized system is greater than that for the decentralized scheme. This is reasonable in view of the fact that basically the same logic and drive circuitry is used for the random-access memory for a wide variation in the number of memory locations, while the weight is reduced proportionately with the reduction in the special purpose counters and timers in the decentralized system. At the higher bit levels the reverse is true, for an increase in memory can be made at a relatively small additional cost in drive circuitry on the centralized memory system. To enable a realistic comparison of weight, the CS and C power requirements for each configuration shown in Figure 4-53 have been converted to equivalent weight.

In Table 4-31 the characteristics of the over-all configurations with redundancy are summarized. Weight, power volume, and reliability are considered for each system, including the two forms of the distributed memory system. The data indicates that the centralized memory CS and C has lower weight and volume and uses less power than each of the other configurations. Comparison in reliability

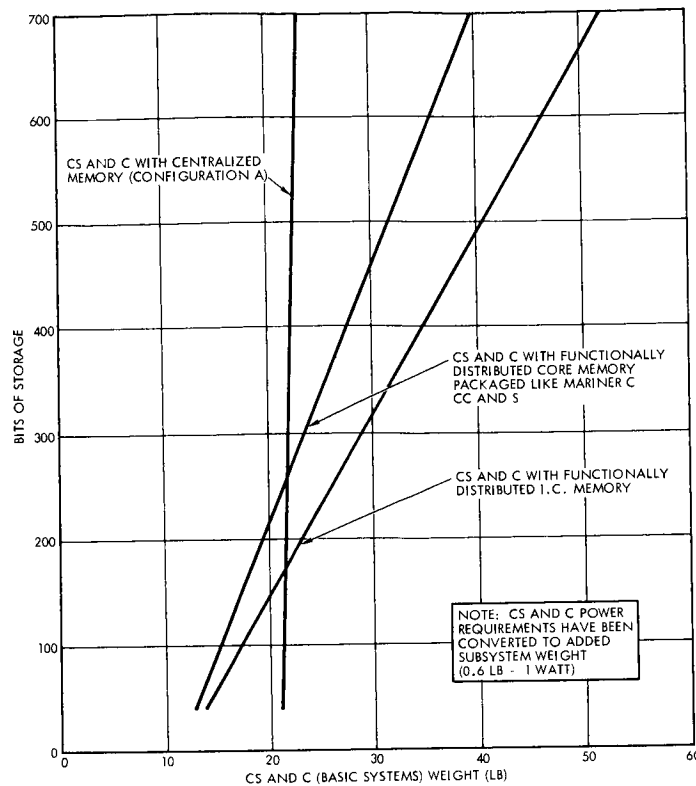


Figure 4-53. Comparison of Weight versus Storage Capability for the CS and C Subsystem Configuration

Table 4-31. Characteristics of Over-all Configurations with Redundancy

CS and C Subsystem	Weight (lb)	Power* Watts	Volume (in <sup>3</sup> )	Reliability	Memory Retention Through Power Failure	Additional Storage Capability
Decentralized system with integrated circuit sequencer	33.8	65.1	738	0.98250	No	No
Decentralized memory system with core sequencer	45.8	30.9	1088	0.97600	Yes	No
Centralized memory system with core memory	24.6	17.4	580	0.99343	Yes	Yes

\*Systems are made up of two modules of each type. However, power is applied to only one sequencer.



is made in terms of the additional weight required over the baseline or nonredundant system. The data shows that the centralized memory CS and C has a higher reliability and lower added weight than either of the other systems for the several redundancy options that were considered. For these reasons, the centralized memory system was selected.

#### 2.9.2 Consideration of Provision For Expanded Science Functions

Finally the effects of incorporating the supplementary science requirements indicated in Table 4-8 are evaluated. In this case, the CS and C is required to store camera settings and exposure times and transmit data to the DAE at the proper times. Additional memory is needed for control of the POP angles and for the camera shutter actuation, filter selection, and magnification commands.

The numerical data and timing commands are stored in the CS and C memory from ground using quantitative commands. The data and commands have time tags associated with them and are issued as serial data to the DAE command decoder and data register one word at a time at the designated times. Hence, two CS and C memory words are required for each DAE command or each DAE command or data. The total storage requirement (see Table 4-17) thus changes from 102 words to 170 words, as reflected in the special purpose memory systems which characterize the two alternatives being considered here. For the centralized system this requirement means that a second plane of 128 core elements is needed, whereas for the distributed system a comparable addition of shift registers is needed.

The weight, size and power of the two systems are thus increased as shown in Table 4-32 so the reasonableness of the function-oriented centralized memory increases. Some of the cores in the plane could also be left out, if necessary, thereby decreasing the weight slightly, but due to the nature of the core plane construction there is no real advantage in doing so. Nor is there a disadvantage in retaining the extra cores.

Table 4-32. Incremental Characteristics for  
Supplementary Science Requirements

<u>Incremented Properties</u>	<u>Centralized Memory System</u>	<u>Distributed Memory System Core Registers</u>
Weight	2	20.0
Volume	40	400
Power	0.2	12.0

The advantages of using a general purpose centralized-memory seem to increase for the augmented requirements because a 128-word core plane remains sufficient to handle the memory requirements, as Table 4-17 shows. However, this advantage is illusory in that the memory word size has to be increased by 50 per cent to encode the commands and data that have to be stored. Furthermore, by adding the 8-bit command identification tag to the memory word, the uplink command message is increased correspondingly, so the addition is not desirable. The function-oriented memory system is therefore still to be preferred.

Considering the ease with which the additional functions can be provided by the centralized, function-oriented memory system, and in view of the simplification in DAE implementation, the centralized memory CS and C is still recommended if the augmented capability is required.

### 3. ELECTRICAL POWER SUBSYSTEM

Four approaches to the design of the Voyager spacecraft power subsystem have been evaluated and individual elements of the subsystem have been studied to define preferences. In addition to the goals prescribed by the power loads and environments of the mission, the evaluation sought an optimized subsystem applicable particularly to the preferred spacecraft configurations as determined in Volume 4. A fifth approach, making use of a radioisotope thermoelectric generator has been studied in some depth not, however, because it was conceived as a candidate approach but because its evaluation permitted quantitative data against which the solar-cell alternatives could be compared and because it could emerge as a candidate subsystem for Voyager should certain constraints, such as those on radiation levels, be changed. The RTG approach is discussed in detail in Appendix H.

Mission criteria and power requirements for the Voyager power subsystem are defined in Section 3.1.

Section 3.2 describes the approach used in the subsystem design analysis and compares the four candidate subsystem designs in terms of reliability, power utilization, and compatibility with the spacecraft. The recommended design is selected and discussed, and the estimated reliability and performance of the selected design are presented.

Section 3.3 covers solar cell selection, module configuration, and electrical design of the solar array. Mechanical and thermal design considerations of the solar array are given in Appendix G, as is a solar cell tradeoff study.

Section 3.4 presents the results of studies on solar array controls, and Section 3.5 analyzes the alternatives available in power conditioning.

Battery selection and design, as well as battery charge control requirements, are given in Section 3.6. Implementation of the battery controls is discussed in Section 3.7.

Factors relative to the mechanical and thermal design of the solar

array substrate are discussed in Appendix G, with stress calculations provided in Appendix C.

### 3.1 Mission Criteria and Load Requirements

The study of the Voyager power supply was founded on the mission criteria and power requirements established in the system studies discussed in Volume 4. The analysis was thus based on the following nominal mission criteria:

- Illumination of solar array 90 minutes after launch.
- Spacecraft maneuver at 1 AU of 1 hour duration with solar array not illuminated.
- Additional midcourse maneuver of 2 hours duration.
- Retro maneuver at 1.4 AU of 2 hours duration.
- Orbital operation for 3 months before eclipse season begins.
- Maximum eclipse of 2.3 hours in 14.5-hour elliptical orbit.
- Minimum 6 month orbital life at Mars.
- Approximately 25 minutes between command from earth and verification of response at maximum range.

Estimated load power requirements as a function of mission phase are listed in Table 4-33. On the basis of the Mariner C power system, as well as those of many other spacecraft, it appears that the majority of these loads require well regulated (2 to 4 per cent) DC or AC voltages at a variety of voltage levels. The power levels shown include power regulation, control, and conditioning losses. A power requirement for reaction control gas heaters to improve the impulse characteristics of the stabilization and control system is included in Table 4-33, but the heaters are not essential to success of the mission and are utilized to improve performance only when the power system capability exceeds the essential load requirement by a suitable margin.

Estimated minimum, average and peak power requirements for the spacecraft equipment are included in Table 4-33. For purposes of this power system analysis, minimum and average values have been assumed to be representative steady state limits. Estimated load peaks

SUBSYSTEM IDENTIFICATION	LOADS	FORM	PRE-LAUNCH	LAUNCH	ACQUIRE	CRUISE
COMMUNICATIONS	DATA HANDLING	4.1 KC ↑	5	5	5	
	ELECTRONICS		23	23	23	
	BULK STORAGE		0/4/12	0	0	0/4
	ANTENNA DRIVE ELECTRONICS		0	0	0	0/1
SCS	CONTROL ELECTRONICS ASSEMBLY	↑	9/9/45	9/9/45	9/9/45	9/9
	SENSORS		4	4	4	4
	GYRO ELECTRONICS		0	0	0	0
SCIENCE	EXPERIMENTS	↑	0/5/55	0/5/35	0/35/55	0/55
	PLANET ORIENT. PKG		0	0	0	0
CS AND C	ELECTRONICS	4.1 KC	18	18	18	18
TOTALS	MINIMUM	4.1 KC	59	59	59	49
	AVERAGE		68	64	94	109
	MAXIMUM		182	130	150	156
4KC INVERTER INPUT	MINIMUM	50V DC	78	78	78	65
	AVERAGE		84	79	113	130
	MAXIMUM		211	152	176	183
SCS	GYROS	2φ 820 CPS	0	0	0	0
820 CPS INV INPUT	GYRO INVERTER	50 VDC	0	0	0	0
SCIENCE	POP DRIVE	1φ 410 CPS	0	0	0	0
COMMUNICATIONS	ANTENNA DRIVES	1φ 410 CPS	0	0	0/1/7	0/1/7
410 CPS INVERTER INPUT	DRIVE MOTOR INVERTER	50 VDC	1	1	1/2/10	1/2/10
CAPSULE	NOT SPECIFIED	50 VDC	0	0	0	0/200/200
THERMAL CONT	HEATERS	↑	0	0	0	0/27/54
COMMUNICATIONS	TWTA		0/90/90	0/90/90	0/90/90	90
SCS	VALVES		0	0	0/0/48	0/0/48
	LITVC INJ	50 VDC ↓	0	0	0	0
	JET VANE ACT		0	0	0	0
	GYRO HEATERS		0	0	0	0
	GAS HEATERS		0	0	0/40/40	0/40/40
PROPULSION	VALVES	29 - 47 VDC	0	0	0	0
INTEGRATION	ORDNANCE	4.1 KC	←			
TOTALS (LOAD + INVERTERS)	MINIMUM	50 VDC	79	79	79	156
	AVERAGE		175	170	245	489
	MAXIMUM		302	243	364	623
POWER	BATTERY + CHARGE REGULATOR	50 VDC	0	0	125	0/0/125
	BOOST REG (AVE)		45	45	6	6
	POWER CONTROL UNIT	50 VDC	10	10	10	10
AVERAGE SOLAR ARRAY OUTPUT		50 VDC	—	—	386	505
AVERAGE BATTERY OUTPUT		30-40 VDC	230	225	—	—

①

Table 4-33. Estimated Voyager Power Profile

CRUISE CALIBRATE	MANEUVER	SEPARATION	LANDER TRACK	INJEC MANEU- VER	ENCOUNTER	ORBITAL		NOTES
						SUNLIGHT	ECLIPSE	
5	5	5	5	5	5	5	5	MIN/AVE/MAX VALUES
13	13	13	13	13	13	13	13	
0/4/12	0	0	0	0	0/4/12	0/4/12	0/4/12	
0/1/4	0/2/4	0	0	0	0	0/2/4	0/2/4	
9/9/45	9/9/45	9/9/45	9/9/45	9/9/45	9/9/45	9/9/45	9/9/45	
4	4	4	4	4	4	4	4	
0	2	0	0	2	0	0	2	
0/55/55	0/55/55	0/55/55	0/55/55	0/55/55	0/55/55	0/63/110	0/63/110	3 PERCENT DUTY CYCLE IN ORBIT
0	0	0	0	0	0	0/0/2	0/0/2	
18	18	18	18	18	18	18	18	
49	51	49	49	51	49	49	51	
109	108	104	104	106	108	118	120	
156	146	140	140	142	152	213	215	
65	67	65	65	67	65	65	67	
130	129	124	124	127	129	140	142	EFF = 76 PERCENT
183	171	164	164	166	178	248	250	EFF = 79 TO 85 PERCENT
0	6	0	0	6	0	0	6	EFF = 84 TO 86 PERCENT
0	8	0	0	8	0	0	8	27 WATT START UP PEAK
0	0	0	0	0	0	0/1/14	0/1/14	ASSUMES INV INPUT SWITCHED
0/1/7	0/1/33	0/0/33	0/0/33	0/1/33	0/0/33	0/1/33	0/1/33	
1/2/10	1/2/38	1/1/38	1/1/38	1/2/38	1/1/38	1/3/53	1/3/53	ASSUMES INV OUTPUT SWITCHED
0/200/200	0	—	—	—	—	—	—	
0/27/54	0/27/54	0/27/54	0/27/54	0/27/54	0/27/54	0/25/49	0/25/49	
90	90	90	90	90	90	90	90	5 WATT AVERAGE FOR FIRST 40 DAYS OF CRUISE
0/0/48	0/0/48	0/0/48	0/0/48	0/0/48	0/0/48	0/0/48	0/0/48	NONESSENTIAL LOAD
0	0	0	0	1	0	0	0	
0	0/6/12	0	0	0	0	0	0	
0	10	0	0	10	0	0	10	
0/40/40	0/40/40	0/40/40	0/40/40	0/40/40	0/40/40	0/40/40	0/40/40	
0	① 0/0/45	0	0	② SEE NOTE	0	0	0	① NORMAL 30 WATT SEC SQUIBS, 45W PK FOR SOLENOID BACKUP ② SQUIBS ONLY
		SQUIBS						NEGLIGIBLE POWER DEMAND
156	176	156	156	177	156	156	176	AVE INCLUDES NONESSENTIAL LOADS
489	312	282	282	305	287	298	318	
625	471	434	434	455	448	528	548	
0/0/125	0	0/0/125	0/0/125	0	0/0/125	③ 0/125/125	0	③ MAX ECLIPSE ORBIT (CONTINUOUS BATTERY CHARGING IN SUN) ← ASSUMED 80% EFFICIENCY DURING AVERAGE BATTERY DISCHARGE AND 6 WATT NO LOAD LOSS
6	80	6	6	78	6	6	80	
10	10	10	10	10	10	10	10	
505	—	298	298	—	303	③ 439	—	INCLUDES NONESSENTIAL LOADS
—	402	—	—	393	—	—	408	

constitute low energy requirements supplied by the spacecraft batteries in those cases where the instantaneous power demand exceeds the solar array capability.

### 3.2 Subsystem Design Analysis

#### 3.2.1 Approach

Any photovoltaic power system with provisions for energy storage can be represented by the functional block diagram of Figure 4-54. The major system elements are the solar array and its controls, the battery and its controls and the power conditioning equipment which provides the output power characteristics required by the loads from the basic DC output of the system. The governing criteria in evaluation of the various approaches to each of these functions are to maximize reliability and to make maximum utilization of available power when the load demand approaches the power source capability. The approach taken toward maximizing reliability has centered on minimizing the complexity of the units which make up the subsystem. In addition to maximizing unit efficiency, alternative system configurations have been evaluated with respect to minimizing the number of series power handling units between the solar array and loads.

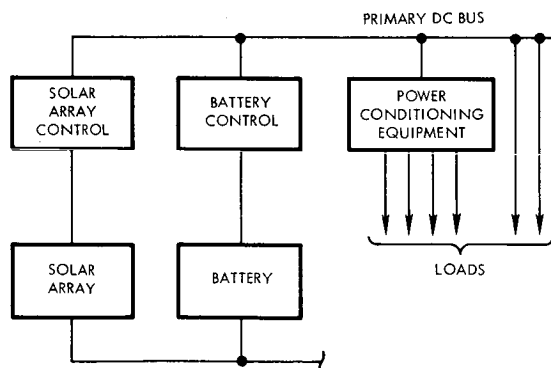


Figure 4-54. Power System Block Diagram

The selected design point for the system is at 1.67 AU after 6 months in orbit and conservatively assumes a coincident maximum-duration eclipse orbit, although as discussed in Volume 4, the actual eclipse duration is expected to be approximately 65 per cent of maximum, or 1.5 hours at this point. Although the solar array design is based on providing at least a 5 per cent margin at the end-of-life under worst case conditions, the uncertainties in predicting solar array degradation make it clear that the subsystem will need to be designed to make maximum use of all available solar array power to support the loads at Mars. Thus, all systems considered are based on supplying load power preferentially over battery charging. Finally, because of the elapsed time from command to verification, automatic operation of the power system to include fault isolation and redundant unit energization are essential design requirements. Command over-ride capability for these automatic functions is considered desirable although not essential to achieving a suitably high reliability in the system design.

The study of candidate power system concepts for the Voyager mission has consisted of the following major tasks:

- a) Define system requirements to include best estimates of magnitudes and characteristics of loads.
- b) Evaluate power conditioning approaches on the basis of reliability, efficiency, and flexibility with respect to probable changes in load requirements.
- c) Select battery and configure system controls compatible with power conditioning equipment, battery and solar array characteristics, and spacecraft thermal control.
- d) Assess system reliability and determine weight penalties associated with adding redundancy to improve reliability.
- e) Determine redundancy control logic requirements and concepts for implementation.
- f) Re-evaluate system reliability in light of redundant units and associated switching control logic.



### 3.2.2 Candidate Systems

On the basis of the analyses of the power conditioning equipment, solar array, battery, and controls, discussed in Sections 3.3 through 3.7 four baseline system configurations, were established as shown in Figure 4-55. In each case, a regulated 50 VDC output is assumed based on the power conditioning analysis (Section 3.5).

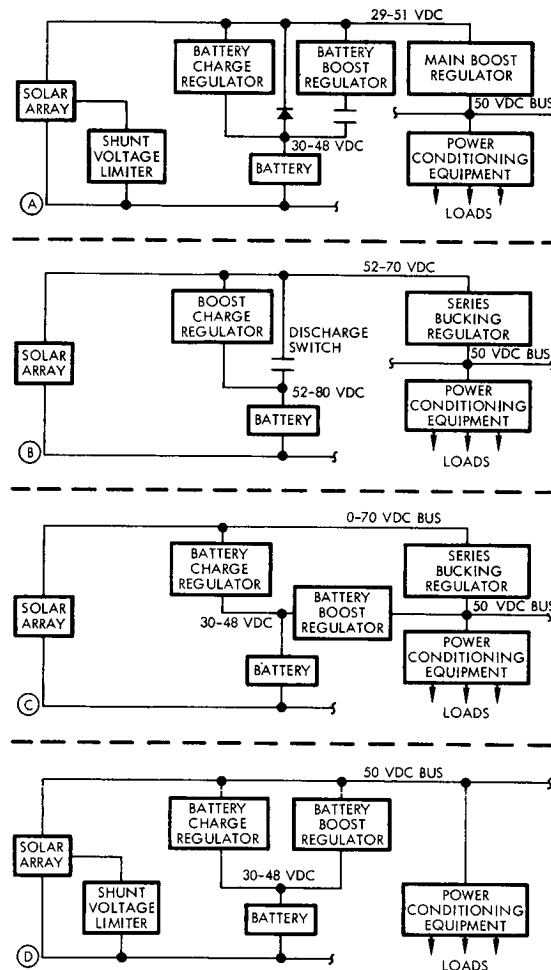


Figure 4-55. Candidate Power Subsystem Block Diagram

Concept A is similar to the Mariner C power system in that it employs a common solar array and battery discharge bus with a series boost regulator to provide regulated 50-VDC output. Shunt voltage regulation is used to limit maximum bus voltage to 51 volts to account for a 1-volt minimum drop across the boost regulator. A simple dissipative series regulator is used to limit battery charging current and terminate charge when maximum voltage is reached in any cell. The battery boost regulator serves to force the solar array to a higher operating voltage in the event that a low battery voltage causes the load current to exceed the array current capability (see Figure 4-56). Since the boost regulator constitutes a constant power load, at lower battery voltages during discharge the load current may reach a level such as  $I_D$ . If the solar array maximum capability upon re-entry into sunlight is as shown, it can be seen that the battery will continue to discharge to share the load current with the array at low battery voltage. Boosting of the battery output is then employed to reverse bias the battery discharge diode and cause the solar array to operate at a higher voltage where it can support the load as well as recharge the battery.

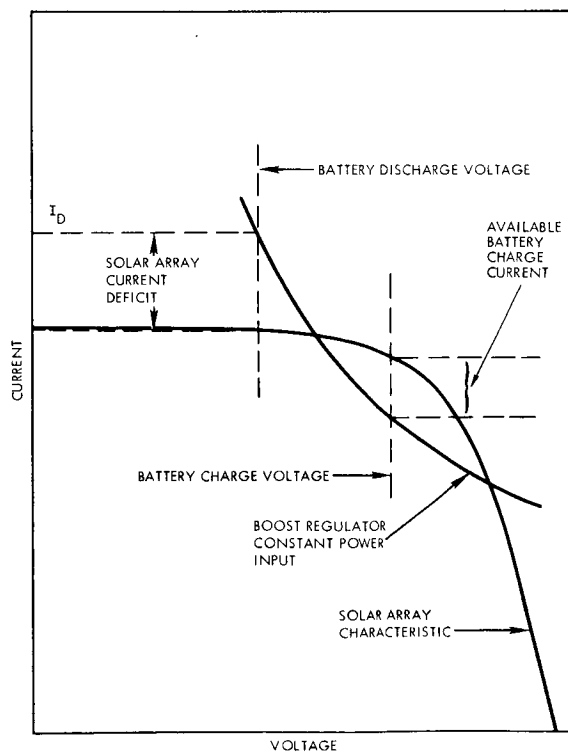


Figure 4-56.  
Comparison of Solar Array Capability with Constant Power Load as Function of Operating Voltage

The battery booster is required only to cause this shift in array operating point and is then disconnected. Designing the solar array to provide sufficient current capability at low voltage to obviate the need for this supplemental battery booster would result in excessively oversizing the array in terms of its maximum power capability at normal voltage.

To provide for maximum power utilization at end of life, the solar array is designed for maximum power output at 51 volts at 1.67 AU. In this case, the boost regulator losses are reduced to that of a single series diode and minimal drive losses and the shunt element dissipation is essentially zero.

Concept B takes advantage of the fact that adequate solar array voltage exists throughout the mission and utilizes a series bucking regulator to provide the regulated 50-VDC bus. This eliminates the need for both boost and shunt regulation of the solar array. A high voltage battery (51 series cells) is used to assure that the bus voltage is maintained during discharge, eliminating the need for boosting the battery output. To charge the battery, however, a boost charge regulator is required. The discharge switch can utilize either an SCR or transistor to assure rapid response to load transients.

At end of life conditions, the solar array operates at 52 volts, which represents its 1.67 AU maximum power point and the series regulator losses consist of the saturated series transistors and maximum drive power. The 70 VDC, upper limit of solar array voltage represents an estimated operating point produced by the series regulator at minimum load and maximum array voltage capability. The relationship of solar array operating point to load voltage and current with a series regulator is illustrated in Figure 4-57 for a typical case.

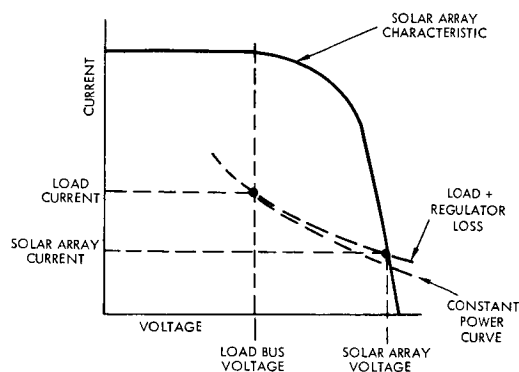


Figure 4-57.

Comparison of Solar Array Operating Point and Load Current and Voltage Using Series (Buck) Regulator

Concept C again utilizes a series bucking regulator but replaces the high voltage battery with a 30-cell battery and discharge boost regulator. The series solar array regulator and battery boost regulators supply the common output bus in a parallel configuration. Battery charge control utilizes a simple dissipative current regulator as in the case of Concept A.

At end of life conditions, the solar array design point and series regulator losses are the same as Concept B.

Concept D controls the 50-volt bus in sunlight by shunt regulation of the array. The dissipative charge regulator is again used to limit battery current. A boost regulator provides compatibility between the reduced battery voltage on discharge and the regulated DC bus. At end of life conditions, the solar array supplies the load at 50 volts without series or shunt regulator losses.

a. Reliability

In comparing the complexity of the four candidate systems, each is seen to include a boost regulator and either a series or shunt bucking regulator.

Comparison of the sequential partial shunt regulator of Concepts A and D with the series bucking regulators of Concepts B and C, shows a higher reliability for the former because of its inherent redundancy. For the recommended case, the shunt elements are divided into 12 sections to achieve compatibility with the 6-panel solar array design. A shorted failure in one shunt section will have no effect until such time as all 12 sections are required to support the load (near end of life). This results in an 8.3 per cent reduction in end of life capability. An open circuit failure in any section will have no effect because under worst conditions of maximum array capability and minimum load, at least two sections will be normally open circuited. As the array output decreases, additional shunt sections will be open circuited. The series regulator, on the other hand, provides no inherent redundancy and either a short or open failure in the power

switching transistor will produce a system failure. No significant differences in complexity of the control loop circuitry for series (buck), boosting or shunt regulators are apparent. In each case, redundant techniques are considered necessary to achieve adequate system reliability.

The remaining major control element in Configurations A, C, and D is the dissipative constant current charge regulator. In Configuration B, a switching element is required for battery discharge. These battery controls are of comparable complexity. Concept A has an added control requirement consisting of the battery booster to remove the system from an undesirable load sharing mode following solar eclipses or maneuvers. The high voltage battery required for Concept B results in a large number of series cells (50) which represents a reliability penalty in comparison to concepts A, C and D, which use 30 cell batteries.

In comparing the four approaches, the selected approach, Concept D offers significant reliability advantages based on over-all complexity, shunt reliability, and the number of series battery cells.

b. Power Utilization

Using a boost regulator in the solar array output in Concept A permits operation at lower solar array voltages near earth with a resultant large excess power capability. For Concepts B, C, and D, the maximum solar array output is limited to the current capability at minimum operating voltage at all times during the mission. With a series regulator, this corresponds to 51 volts based on an assumed minimum 1-volt drop across the saturated regulator and a 50-volt output bus. For the shunt regulated case (D), maximum array current is available at 50 volts with no shunt dissipation. At end of life conditions, the solar array for Concept A operates in the shunt regulated mode as in case D, but must provide rated load current capability at 51 volts to account for an assumed 1-volt drop through the boost regulator.

The minimum solar cell current-voltage characteristics (Figure 4-58) show that the maximum current and voltage compatible with both the 1 and 1.67 AU curves is represented by their point of intersection. Operation at the voltage corresponding to this intercept will result in equal maximum current capability at both 1 and 1.67 AU. As shown, this operating point is within about 2 per cent of the maximum power capability ( $P_{\max}$ ) at 1.67 AU. The minimum load current requirement at 1 AU, however, is 8.5 amperes as opposed to 8 amperes at end of life (including battery charging). It is necessary, therefore, to select a lower operating cell voltage to increase available array current at 1 AU. Because of the steep slope of the I-V curve in this region, a decrease of only 4 millivolts/cell produces a more than adequate 20 per cent increase in cell current. The solar array design is based, therefore, on a cell voltage of 0.44 volt and cell current of 25 milliamperes at the 1.67 AU, end of life point for Concepts B, C, and D. Concept A can be optimized for the maximum power point at end of life, which corresponds to a cell voltage and current of 0.461 volt and 24.5 ma, respectively. The corresponding loss in power capability for Concepts B, C, and D is 2 per cent.

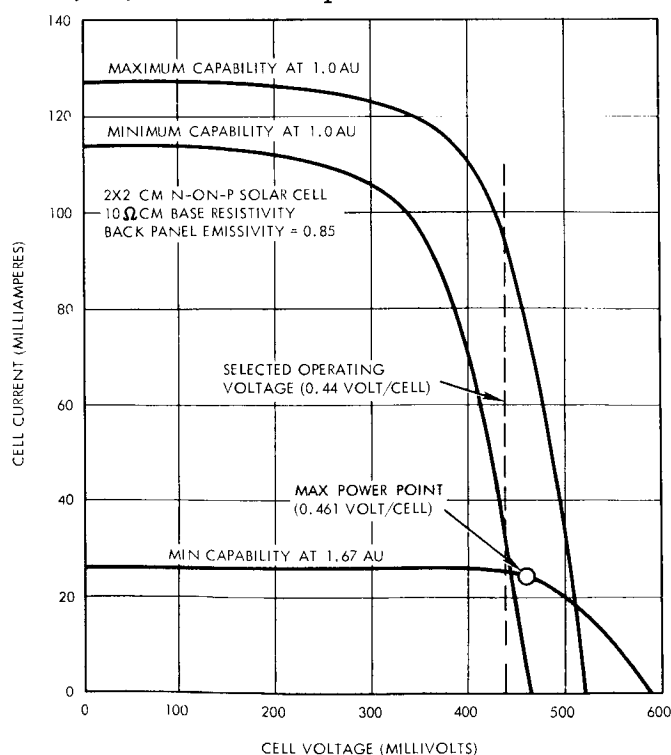


Figure 4-58. Revised S. A. I-V Characteristics

This advantage for Concept A is offset by the series loss in the boost regulator at end-of-life. Assuming a 1-volt drop at 8 amperes, the power loss is 2 per cent of the 400-watt total load requirement. Bypassing the boost regulator with a relay to eliminate this loss is not desirable in view of the added control complexity and resultant slow response to load transients.

Concepts B and C are seriously penalized at end of life by the drive power required to saturate the series regulators. Total series regulator losses in the saturated mode are estimated at 10 per cent of the load power.

Comparing the four concepts, approaches A and D offer distinct advantages over B and C in terms of maximum power utilization and resultant array size. The number of solar cells required for Concept A is 38,988 and 38,976 for Concept D. The 10 per cent increase required for Concepts B and C, based on equivalent power margins at end of life, represents a disadvantage in terms of array weight, although the four configurations are comparable in weight from the point of view of the total subsystem.

c. Compatibility with Spacecraft

Four basic compatibility requirements exist between each component of the power system and the spacecraft. These are the electrical, mechanical, thermal, and magnetic interfaces.

Electrical. The output power characteristics of the four candidate systems are similar; however, concepts A, B, and C permit energizing selected loads from an unregulated DC bus in addition to the regulated DC and AC outputs common to all concepts. This capability permits reducing the electrical rating of the series buck or boost regulators required for these three approaches. Electrical characteristics of the regulated power outputs in each case are similar with response to load changes limited by the series regulator of each. Although Concept D provides improved response characteristics in sunlight because of the shunt regulator, the response during battery discharge is limited by the battery boost regulator. Electromagnetic compatibility will

require similar design implementation of filtering and shielding techniques for the switching regulators and inverters of each system.

Mechanical. Weight estimates of the four candidate systems indicate no significant weight advantage for any one. The major trade-off with respect to mechanical interface considerations among the four candidate systems is that of solar array area. As just discussed the series regulator losses of Concept B and C require an approximate 10 percent increase in array area over that of Concepts A and D. This requires adding solar cells to the bottom surface of the bus. Since radiative cooling from the back surface of this area is not possible, a large number of series cells is required to compensate for a higher operating temperature. This, in turn, results in a requirement for adding more than 10 per cent of the array area to produce the necessary 10 per cent increase in power.

Thermal. Criteria for evaluating the candidate systems with respect to their thermal interface with the spacecraft include considerations of both the total dissipation as a function of range from the sun and the dissipation of each component. In general, minimal heat dissipation at 1 AU is desired and increased dissipation during eclipse in orbit will reduce thermal control penalties associated with maintaining component temperatures above their minimum values. Large component heat dissipation rates penalize the equipment installation and mechanical design with respect to mounting area and heat sink requirements.

In concepts A and D, maximum steady-state shunt dissipation is estimated at 80 and 100 watts, respectively, at 1 AU. This requires additional thermal control louver area to limit maximum equipment temperatures. The maximum shunt dissipation as a function of load reduces with increasing range to a negligible level at 1.67 AU. The increased louver area results in increased heat losses during eclipse but this disadvantage is more than offset by the thermal dissipation of the battery and boost regulator during eclipse. For Concept A this



represents an estimated average dissipation of 105 watts in eclipse. For case D, since the boost regulator handles the total load, an average 140-watt dissipation is present in eclipse.

By comparison, Concepts B and C will significantly reduce power system dissipation at 1 AU because the pulse width modulated series regulators cause the solar array to operate at an inefficient power point when an excess capability exists. Thus the amount of solar energy converted to electrical energy is controlled to match the demand, and losses within the spacecraft are minimized. As before, the battery dissipation during eclipse aids in maintaining equipment temperature limits. The boost regulator losses of Concept C are comparable to those of Concept A. Series regulator losses of Concept B are slightly less because of the higher efficiency of the series regulator.

Based on these considerations, Concepts B and C appear to offer the better thermal characteristics both at 1 AU and in orbit at Mars. The penalties associated with higher shunt regulator dissipation at 1 AU for Concepts A and D, however, represent an estimated increased thermal control weight of less than 2 pounds.

Magnetic Fields. The four concepts appear to be comparable in terms of their magnetic compatibility with the spacecraft. The use of silver-cadmium batteries, relatively high DC voltages, twisted pair wiring and solar panel back wiring techniques together with minimal use of magnetic materials is applicable in each case.

### 3.2.3 Recommended Power Subsystem

In the balance, then, it can be seen that Concept D offers significant reliability advantages over the others, based on over-all complexity, shunt reliability, and the number of battery cells in series. Moreover, Concepts A and D offer advantages over B and C in terms of maximum power utilization and minimum solar array size, and Concept D offers improved response characteristics to load changes in sunlight because of the shunt regulator. Although Concepts B and C offer slightly

better thermal characteristics than A and D, the weight penalty in the additional thermal control louvers required by Concepts A and D amounts to less than 2 pounds. Thus Concept D has been selected as the recommended power system for the Voyager spacecraft.

a. Subsystem Description

A block diagram of the recommended power system for the Voyager mission is shown in Figure 4-59. The system consists of five major functional elements: solar array, solar array shunt voltage limiter, secondary battery, battery regulator and power conditioning inverters. Detailed tradeoffs in each of these areas, discussed in subsequent section, have led to the following decisions. The solar array consists of solar cells installed on six identical panels each containing two parallel connected sections. Each section consists of 116 series and 28 parallel connected 2 x 2 cm 10 ohm-cm silicon solar cells provided with 6-mil fused silica cover slides, making a total of 38,976 solar cells for the array. Suitable tap points are provided to permit partial shunt regulation of the array.

The solar array output is limited to  $50 \text{ VDC} \pm 1 \text{ per cent}$  by shunt regulation of a portion of each series string of solar cell modules. Power dissipation in the shunt elements assembly is minimized by a unique sequential shunt configuration. The shunt elements are controlled from bus voltage sensing and error signal amplifier circuitry located in the power control unit (PCU).

The battery is charged from the 50-volt bus through a simple dissipative current regulator. Charging is terminated by a control signal from individual temperature-compensated cell voltage sensors mounted on the battery cells. When the highest cell voltage decreases below a present level, constant current charging is again initiated. If the solar array does not have sufficient capability to charge the batteries, the PCU voltage sensing and error amplifier circuitry supplies an over-riding control signal to de-energize the charge regulator.

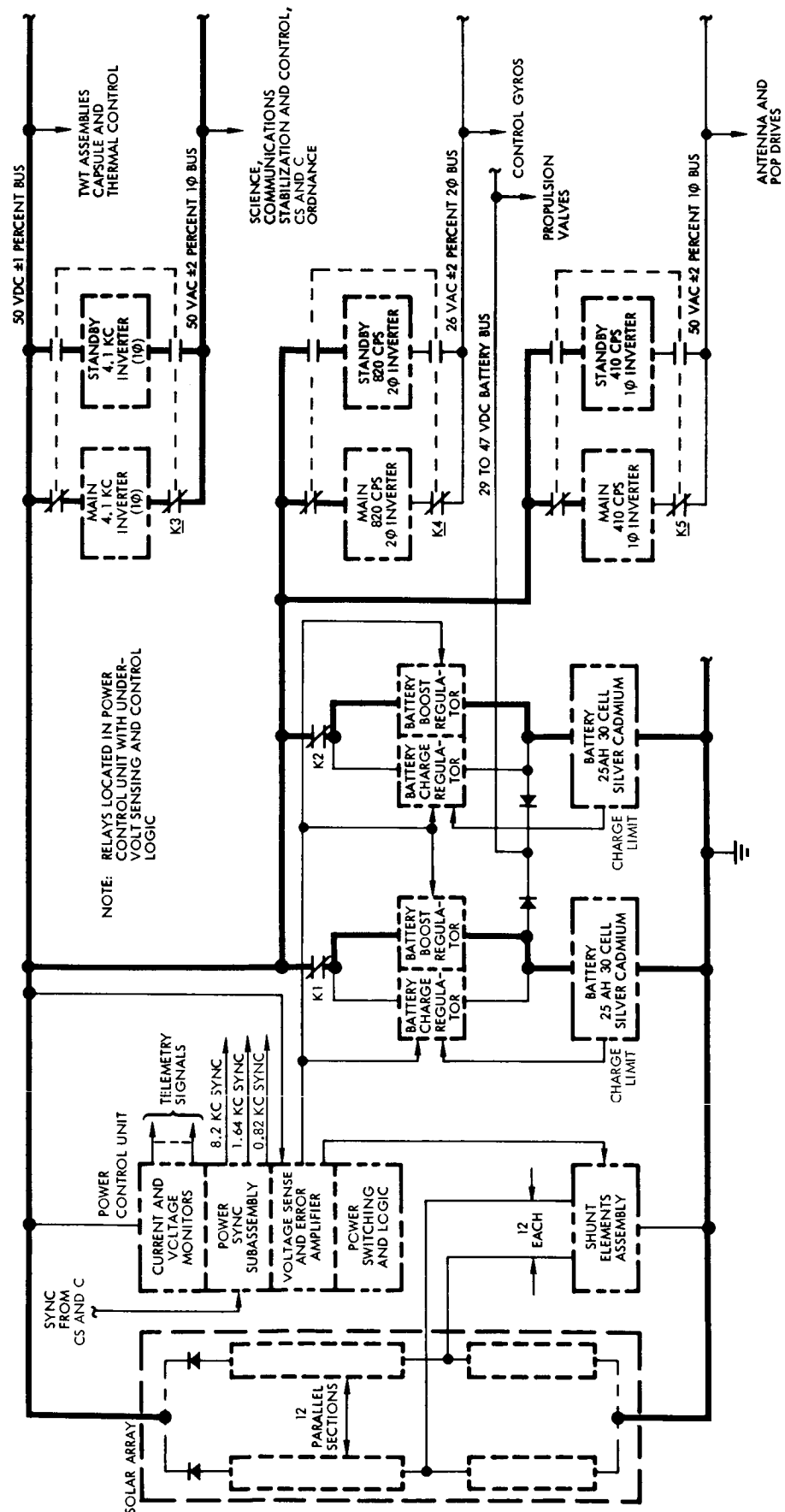


Figure 4-59. Power Subsystem Block Diagram

When the solar array is incapable of supporting the system load, the battery discharges through a boost regulator to maintain the regulated 50-volt bus. A conventional switching type boost regulator is used, controlled by the PCU voltage sensor and error amplifier circuitry.

The two 30-cell, 25-ampere-hour silver-cadmium batteries, each with a charge-discharge regulator, are operated in parallel under normal conditions. In the event of a battery or regulator malfunction, the associated battery and regulator are disconnected by the power switching and logic circuitry in the PCU. Single battery operation is capable of supporting essential spacecraft loads through eclipse and maneuver phases.

The two main outputs from the system are the regulated 50 VDC bus and a 50 VAC  $\pm$  2 per cent, 4.1-kc, single phase, square wave bus.

A simple unregulated inverter is used to supply this AC output. Sequential inverter redundancy is provided by sensing AC bus undervoltage and switching to a standby inverter in the event of inverter failure. This sensing and switching function is performed by the PCU power switching and logic circuitry. The majority of the loads are energized through transformer rectifier (TR) units from the AC bus. These TR units are considered part of the load equipment and may also include supplementary output regulators where required. Additional 410-cps single phase and 820-cps two-phase inverters are provided to supply AC power to the antenna and POP drive motors and to the control gyros, respectively. Sequentially redundant units are provided in the same manner as in the case of the 4.1-kc inverter.

The 20-watt communications transmitters include regulated DC-DC converters to supply the several closely regulated ( $\pm 1/2$  per cent) DC voltages required by the tubes. As a result, these loads are shown to be energized directly from the 50 VDC bus. The use of TR units supplied from the 4.1-kc bus to energize the TWT's is less advantageous in this instance because of the difficulty in providing close regulation of the high level DC voltages required by the tubes.

High current, short duration requirements for propulsion are supplied directly from the battery bus.

A power synchronizing subassembly is provided in the PCU which accepts a sync signal from the CS and C at 4.096 kc and generates suitable sync signals for the boost regulators, inverters, and TWT converters. In the event of loss of input sync, the PCU circuitry will operate from its own oscillator to maintain synchronization of the power equipment. The current and voltage monitors in the PCU provide conditioned analog signals to the spacecraft telemetry system for monitoring power system performance throughout the mission.

b. Reliability and Performance

The selected power system employs redundant circuits and majority voting logic within the PCU control circuits to maximize their reliability. Because of their sequential operation the SEA shunt elements provide inherent redundancy in terms of open circuit failures. Series redundancy of components is employed to protect against shorted failure modes. The remainder of the system provides unit redundancy with automatic switching provisions. In addition, command capability is provided to over-ride each of these switching functions as an additional backup during in-flight operations. A reliability block diagram for the system with unit and system reliability assessments is shown in Figure 4-60.

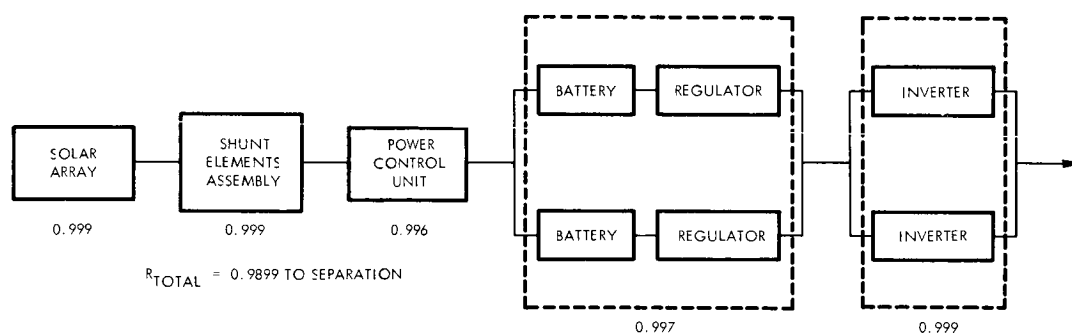


Figure 4-60. Reliability Block Diagram

Figure 4-61 illustrates solar array current margins during the various mission phases. Calculated minimum solar array currents at 51 volts (50 volts at bus) are shown for several solar distances from 1 to 1.67 AU. Estimated average current demands for representative mission phases are also plotted, including periods of battery discharge. The basic current requirements include estimated system losses in power conditioning, regulation and control equipment. In addition to the basic demand, increased current requirements for the reaction control system gas heaters (non-essential load) are shown. As shown, a minimum current margin of 5 per cent is available at 1.67 AU with all essential loads connected.

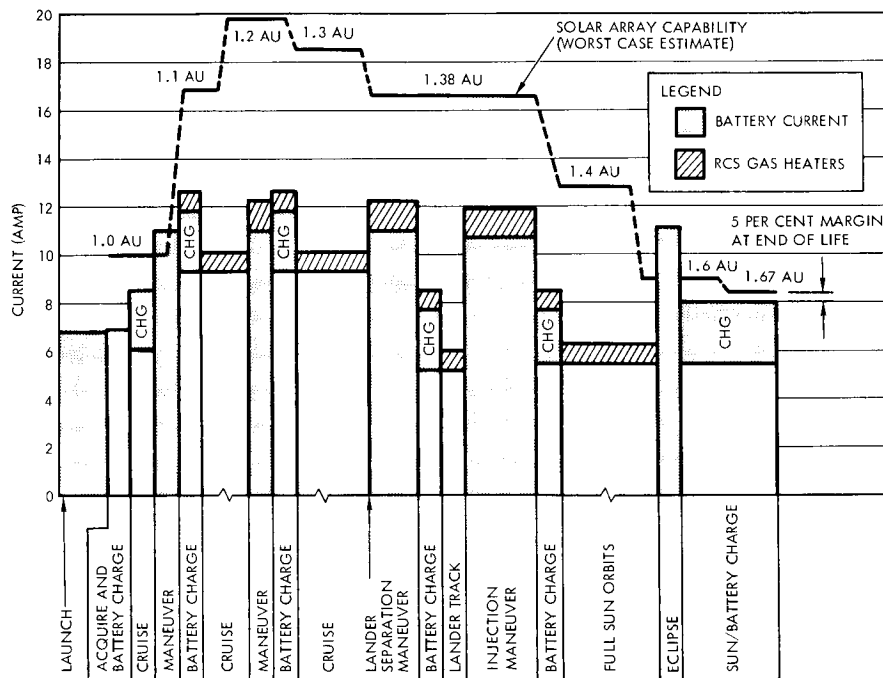


Figure 4-61. Load and Solar Array Current During Voyager Mission

### 3.3 Solar Array

#### 3.3.1 Solar Cell Selection

In establishing the most suitable type of solar cell to be used for the Voyager solar array, the following factors were considered:

- Cell material and type
- Base resistivity versus radiation flux
- Cover glass thickness and material
- Cell area
- Contact type and material
- Cell efficiency
- Glass-to-cell adhesives

From the analysis, the basic solar cell selected is characterized as follows:

- n-on-p silicon solar cell
- 10 ohm-cm nominal base resistivity cell
- 2 x 2 cm area
- 6-mil fused silica cover glass
- Sintered silver titanium contacts on opposite sides of wafer
- Modularized efficiency of 9.5 per cent at 27°C, air mass zero
- 0.440 volt at maximum power, covered, air mass zero illumination
- Sylgard 182 glass-to-cell adhesive

A variety of photovoltaic devices is available for new space-craft power systems. These devices include conventional silicon solar cells (with variations), webbed dendrite cells, gallium arsenide solar cells, and thin films. For the Voyager power systems analysis and

design, the conventional silicon solar cell has been selected on the basis of its availability, proven performance on orbiting spacecraft, lower present-day costs, and substantiated qualification testing covering a variety of environments, including radiation and temperature. Although other photovoltaic devices may prove superior to silicon in the future, insufficient data is available today to permit a thorough power systems analysis and resultant high degree of confidence in final systems performance.

With the silicon solar cell established as the basic solar module building block, it is possible to consider still other alternatives available. These variables include a) cell type: p-on-n or n-on-p, b) base resistivity, c) cell area, d) configuration, and e) efficiency.

a. Cell Type

The radiation environment anticipated in the Voyager mission dictates the selection of a cell type which is resistant to radiation damage. The superiority of n-on-p cells over p-on-n cells in resistance to radiation has been thoroughly documented.\*

In addition, an industry-wide survey indicates that n-on-p cells have been qualified to lower temperature levels in thermal cycling test programs. The choice of n-on-p cells is also desirable because they are readily available in large quantities as compared to p-on-n.

b. Base Resistivity

In Appendix G a tradeoff analysis is presented which substantiates selection of the 10 ohm-centimeter cell over the 1 ohm-cm cell. The analysis was confined to these nominal base resistivity values because of the large amount of data and experience available today. Although cells of other nominal base resistivities have been fabricated, including the high base resistivity aluminum doped cells, insufficient data exists to support their use at this time.

---

\*See, for example, "Handbook of Space Radiation Effects on Solar Cell Power Systems," NASA-SP-3003.



c. Cover Glass Thickness and Material

In considering the degradation because of particle radiation and micrometeorites, analyses were performed for 6, 18, 36, and 54 mil cover glasses to determine the effects on array weight for a specific value of end of life power. It was determined that a 6-mil cover glass using Corning fused silica 7940 provides a minimum array weight. The detailed analysis appears in Appendix G.

Although thinner glass is available, limited experience in fabricating and handling shields thinner than 6-mils argues against their use in that cost and development problems may result.

The material selected for the cover glass was determined by the requirement to minimize radiation damage. Further analysis is required to determine whether the higher thermal coefficient of fused silica compared with microsheet glass can be tolerated in eclipse conditions.

d. Area

In general, the cost per watt (or per unit area) of silicon solar cells decreases as the cell area increases. For example, 2 x 2 cm cells are approximately 25 per cent lower in cost than two 1 x 2 cm solar cells. An additional similar cost reduction is anticipated for the recently introduced 3 x 3 cm cells. The basic cell selected for Voyager is, however, the 2 x 2 cm based upon its cost advantage over 1 x 2 cm cells and the lack of experience, performance data, and technical design information for the larger cells. The 2 x 2 cm cells have been successfully used on the Nimbus A meteorological satellite launched in 1964 and have been adopted for several other space programs.

e. Contact Type and Material

Within the category of configuration, several alternatives are also available. For example, the conventional silicon cell is made with positive and negative contacts on opposite sides of the silicon wafer.

Recently, most of the cell manufacturers have produced limited quantities of wrap-around cells which have both contacts on the non-illuminated side of the cell. The obvious advantage is that virtually 100 per cent of the front face of the cell is available as active area for power conversion. RCA has, under contract to NASA, fabricated limited quantities of these cells, assembled them into modules, and performed thermal cycling tests with excellent results. However, the quantity of practical design and performance data available for wrap-around cells is limited, particularly performance data during low temperature cycling after several hundred cycles. Thus the basis of the Voyager power study is the conventional cell, with approximately 95 per cent active area for power conversion.

N-on-p cells have been fabricated with and without solder coatings on the contacts. The solder, however, is not required for reduction of cell resistance as was the case with contacting methods which cannot take advantage of the high conductivity of silver. The use of sintered silver permits a reduction of cell weight by approximately 20 to 25 per cent because it permits the elimination of solder. Another, more significant advantage of the solderless cells is that degradation by thermal cycling is greater (for identical test units and conditions) for cells with solder, as substantiated by RCA-AED in the Nimbus solar module development program (see Section 3.3.2).

f. Efficiency

The basic n-on-p cell is made in large quantities with air mass zero efficiencies of 10 to 11 per cent at 27°C. Modules fabricated from these cells can be made in large quantities with air mass zero efficiency of 9.5 per cent at 27°C with high production yields and a corresponding minimum cost. The analyses presented here are for a modularized cell with a 9.5 per cent efficiency, i. e., the cell includes all losses because of cover, tabbing, and soldering.

g. Glass-to-Cell Adhesives

Adhesives for bonding cover glass to solar cells are predominately organic, high-polymeric materials. The basic polymer resins are modified by the control of the molecular weight, degree of cross-linking, and the incorporation of additives to improve specific properties. Changes in the chemical balance of the adhesive may lead to drastic changes in the physical properties. In the case of optical adhesives, changes in the refractive index or spectral transmission can considerably affect the solar cell output.

The principal adhesives of interest for space use are epoxides and silicones because of their superior ability to withstand ionizing radiation for long periods of time without structural changes in their optical transmission properties.

Bonded joints present very small adhesive surface area to the vacuum environment. Typical adhesive thickness is  $1 \text{ mil} \pm 0.5 \text{ mil}$ . Selected adhesives have low permeability to gases, low molecular weight fragments, and additives. Outgassing of these volatile materials from the adhesive will be controlled by the diffusion of gases through the polymer matrix to the bond line. The use of a stable adhesive system on the protective cover glasses makes this section of the solar cell module free from vacuum effects.

Photochemical decomposition results in changes in optical properties such as adhesive darkening and increased solar absorptivity. A consequence of this darkening is a general increase in the solar cell operating temperature (lowering the electrical output) due to a reduction in light transmission. By selecting an adhesive which has minimal absorption of ultraviolet photons, and distributing this energy along the polymer chain, the ultraviolet degradation of optical properties can be minimized. Silicones have this property of minimal absorption and energy distribution, and are thus recommended for the Voyager application. Numerical evaluation of the solar cell degrading factor due to UV is given in Section 3.3.3.

Sylgard 182 and RTV-602 are considered as candidate silicone cover glass adhesives for Voyager because of their transparency and resistance to ultraviolet radiation. Of the two adhesives, Sylgard 182 is recommended because of the greater amount of successful experience with this material on space programs at RCA and in other space programs. For example at RCA comparative performance data is available on the following variables on the transmission characteristics of the adhesive when exposed to ultraviolet radiation.

- 1) Degradation between different resin systems
- 2) Degradation within a resin system among batches of resin
- 3) Degradation within a resin system among batches of catalyst
- 4) Degradation within a resin system when ratio of resin to catalyst is varied
- 5) Degradation within a resin system when film thickness of adhesive is varied

Since the expected working temperatures of the solar cell modules will be within the approximate range of from  $65^{\circ}$  to  $-35^{\circ}$ F from launch to time of first eclipse, no degradation of the transmissive properties of the Sylgard 182 adhesive is anticipated from thermal effects. Temperature cycling within the approximate range of  $\pm 120^{\circ}$ F should have no effect on the chemistry of the adhesive as demonstrated by tests at RCA and; hence no changes in the transmissive properties should occur for the adhesive with its associated filter glass.

### 3.3.2 Module Configuration

In determining the optimum module configuration, primary emphasis has been given to achieving the highest possible reliability through the use of proven techniques and materials. The approach adopted was to select module configuration having an extensive background of successful test and qualification data.

The module configurations selected have the following characteristics:

- Submodule consisting of a pair of 2 x 2 cm n-on-p cells
- Ten-cell flat module consisting of five two-cell pairs, (Figures 4-62 and 4-63, modules weighing 4.58 grams).
- Eight-cell flat module consisting of four two-cell pairs, otherwise identical to the 10-cell module; the 8-cell module weighs 3.67 grams.
- Molybdenum tabbing, chosen for its mechanical and electrical characteristics

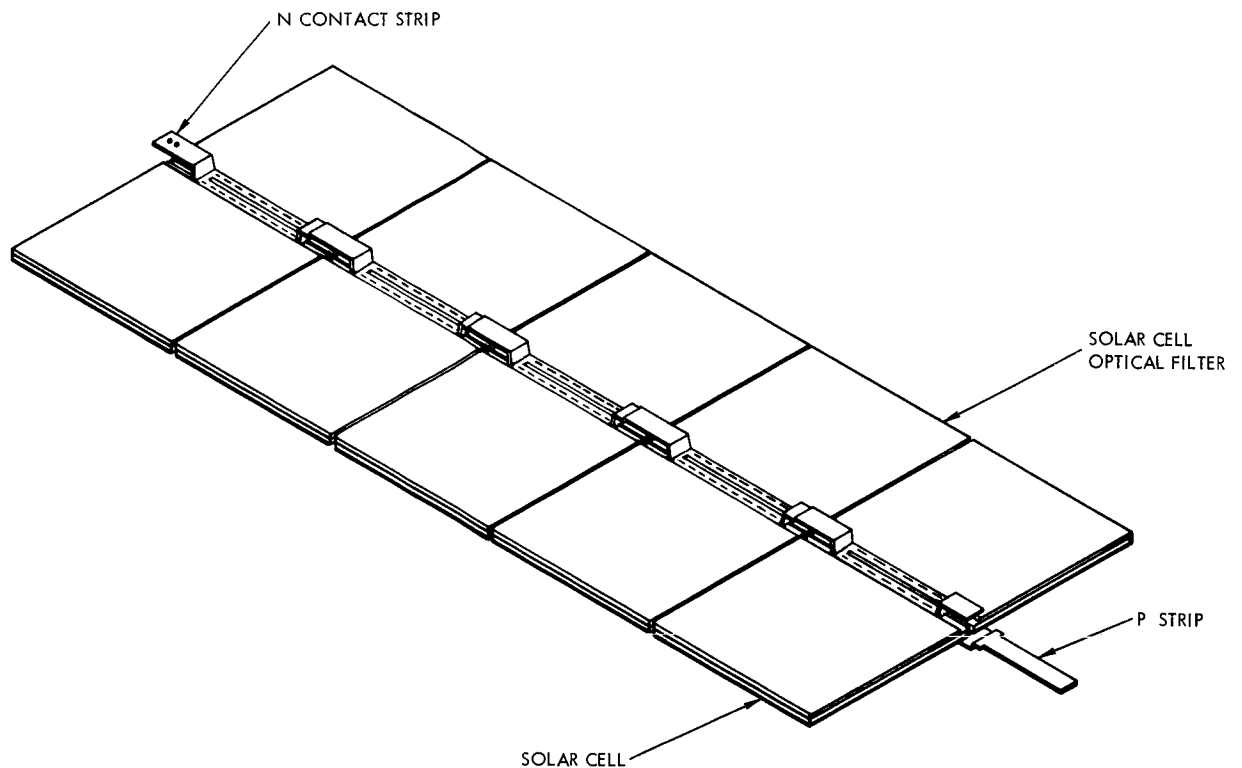


Figure 4-62. 10-Cell Module Assembly

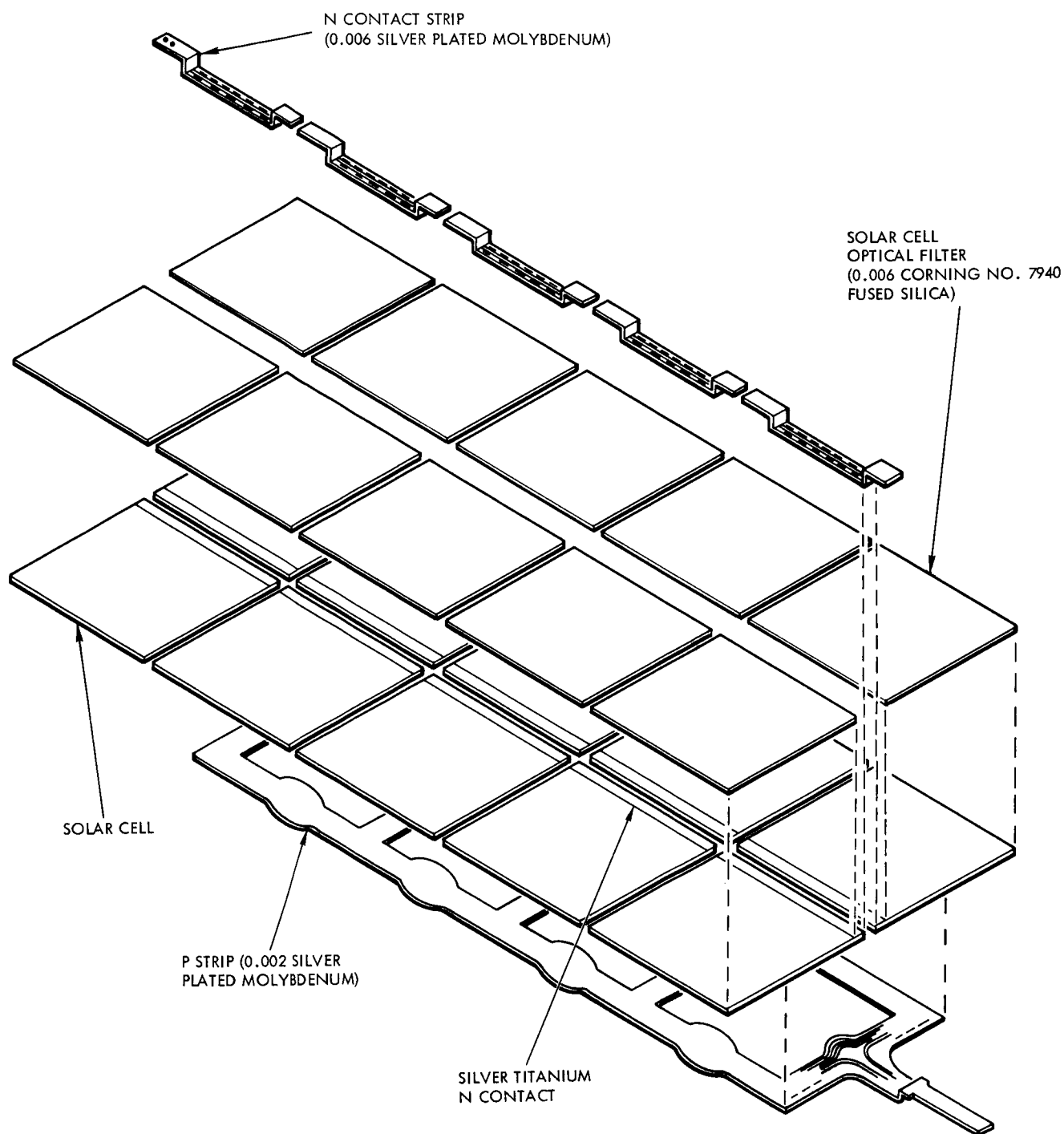


Figure 4-63. 10-Cell Module Assembly Exploded View

a. Possible Configurations

More successful test results have accrued to date for flat modules than for shingles and these results have been for wider temperature extremes and for more thermal cycles than for shingles. Experience has established that temperature extremes and thermal cycling are two of the most difficult factors that a solar array design must overcome in achieving high reliability.

The cell-to-cell solder joints necessitated by shingling cannot be visually inspected adequately since the joint is hidden by the cells. With modules however, cells are fastened together so that the connectors can be readily inspected for proper solder filleting, (see Figure 4-62).

In addition, an analysis of one and two failures on one circuit of an array shows a further advantage of a module over a shingle. For instance, a string of 10 paralleled cell modules is electrically equivalent to a circuit of 10 series strings of shingles since the shingle approach implies series cell-to-cell connections. Should a cell joint open on either a module or a shingle, 10 per cent of the power of that series circuit of the array is lost. However, if a second cell joint opened on the same circuit of the array, the chances of losing another 10 per cent of that circuit are much greater for a shingled array than for a module type of array, because a cell joint failure on any shingle string is catastrophic to that string and there is a high probability that a second cell joint failure will be another string. In the module string, however, the second cell joint failure must be in the same 10-cell module before another 10 per cent is lost. If any other cell joint in any 10-cell module of the circuit opens, no additional ill effects will be observed on the output of that string. In fact, many cell joints can open without the loss of power so long as no two cells open in one module. The chances of this second loss on a shingle array could be reduced by interstring parallel wiring but this could best only approach the redundancy of the module string and would require many more solder joints, extra wire and weight, and would reduce the packing efficiency of the shingle array. Therefore, with a higher confidence level of reliability and the fact that cell joint failures would be less significant, modules were chosen over shingles.

System requirements for a sun-oriented solar cell array to deliver the required raw power at end of life call for a total of 336 2 x 2 cm cells connected in parallel and 116 cells connected in series (see Section 3.3.3 for details). The selected configuration involves a solar cell array composed of six panels. Each panel, therefore, should have the equivalent of 56 single-cell series strings in parallel.

The module configurations selected are the 8 and the 10-cell module. The reasons for this are:

- 1) A combination of 8 and 10-cell modules permits a layout of the equivalent of 56 single-cell strings per panel (four 10-cell module strings, and two 8-cell module strings).
- 2) Based on several cell layout studies, there is no significant increase in the packing factor (ratio of active solar cell area to total area) by using modules of less than 8 or 10 cells (6 or 4).
- 3) There are economic advantages because there are fewer modules (basic elements) in an array using for instance, 10-cell modules as compared to an array using a smaller size module. Moreover, fewer module tests are needed and there are fewer elements to handle on the array level.
- 4) There are fewer n-p solder connections to be made using larger series connected modules.
- 5) Modules of more than 10-cells were not chosen because, packing density generally is decreased when larger modules are used and tooling, test fixtures, and illuminators for 10-cell and smaller modules are more readily available.

b. Specific Design for Voyager

Solar Cell. The electrical characteristics of the solar cell selected for the module are described in detail in Section 3.3.1. The cell is 2 cm x 2 cm in size and nominally 12 mils thick. Its basic material is silicon upon which titanium silver negative and positive contacts and grid lines are sintered.



The negative contact is on the top surface of the cell and is a strip of 0.035 inch nominal width running the length of the cell on one edge. The positive contact is the bottom surface of the cell, this entire surface with the exception of the small band around the edges is kept open to allow for a secure separation of the positive and negative contacts at the edges.

Tab Material and Design. The tab material chosen for this module design is molybdenum. Molybdenum was chosen because its thermal coefficient expansion closely matches that of the silicon cell and because of its low electrical resistivity. A comparison of these properties for various tab materials is given in Table 4-34. It is possible to attain a closer match of the coefficients of expansion by utilizing materials such as the low expansion nickel alloys, but their resistivities are extremely high and they are highly magnetic.

Experience gained from thermal vacuum cycling indicates that the permissible margin of error, with regard to quantity of solder, when using high expansion alloys such as copper and silver, is less than when using molybdenum. A high expansion alloy, such as solder, sandwiched between materials with matched coefficients of thermal expansion (molybdenum and silicon) would develop a lower stress in the silicon than would be developed for materials with mismatched coefficients.

Table 4-34  
Comparison of the Properties of Various Tab Materials

Materials	Coefficient of Thermal Expansion $10^{-6}$ in/in/°C	Electrical Resistivity (Microhm-CM)
Silicon	4.2	5.1
Molybdenum	5.8	2.0
Copper	15.6	81
Low Expansion Nickel Alloys	2.5 - 9.0	49
Kovar	4.5	1.6
Silver	19.6	2.4
Gold	14.2	

The negative tab (n-tab) is 0.006 inch thick and 0.10 inch wide. It bridges the two negative contacts, as shown in Figure 4-63 and makes contact with approximately 60 per cent of the cell contact area. The molybdenum is plated with silver to improve its solderability. Wetting holes are provided in the areas where contact is made to allow inspection of the solder joint.

The positive tab (p-tab) is .002 inch thick and shaped as shown in Figure 4-63. Expansion fingers are provided to reduce the transmission of stress to the cells due to the slight variation in coefficients of linear expansion between the materials. The tab is formed upward, as shown, to overlap the next negative tab to make the series connection. The width of the tab at the series connection point is smaller than the negative tab to allow for any misalignment between modules and to aid in inspection of the solder joint.

The n-tab is intentionally made wider than the n-contact of the cell. By butting the filter platelet against the n-tab, no cell surface remains exposed during assembly, providing protection against low energy proton bombardment and avoiding shunt paths which otherwise might result from micrometeorites.

The mechanical assembly sequence from a single cell to a module is as follows:

- Electrically matched cell pairs are soldered to an n-tab at the n-contact in a fixture using a temperature controlled hot plate and a closely controlled time cycle.
- Cover glass is bonded to each cell and then oven cured.
- Four (or five) two-cell pairs are placed in a fixture with a p-tab, and each cell in turn is soldered to the p-tab using a mechanically held soldering iron.

Solder. The solder chosen for connecting p-and-n-tabs to the solar cells has the following composition: tin, 62 per cent, lead, 36 per cent, and silver, 2 per cent. The purpose of the silver is to reduce migration of the silver from the sintered silver-titanium contacts on the solar cells during the cell contact soldering operation.

c. Development Status and Test Data

The two-cell 2 x 2 cm submodule proposed for Voyager is the basic 2-cell submodule that was used as a building block for the 10 and 6-cell modules used on Nimbus and includes the improvements made to it for the 8 and 6-cell modules for the Lunar Orbiter. The most significant changes from the Lunar Orbiter 2-cell submodules to the proposed Voyager submodule is that the cover platelets have been changed from 6-mil microsheet to 6-mil quartz and the nominal base resistivity of the cell as been changed from 1 ohm-cm to 10 ohm-cm. Both of these changes have been made to increase the radiation resistance of the module. In addition, the plating on the Voyager n-and p-tabs will be silver instead of nickel used on Lunar Orbiter, to comply with magnetic cleanliness requirements.

When thermal caluculations for the Nimbus solar panels predicted a thermal variation of 55 to -80°C during each orbit a program was initiated to develop an array assembly that could withstand repetitious cycling from 65 to -90°C, a temperature range that was considered extreme in 1961. Many module designs were constructed and tested, with combinations of materials and techniques as follows:

- 1) Cells. Plated contacts and sintered contacts, 1 x 2 and 2 x 2 cm.
- 2) Connector Strips. Various materials such as copper, kovar, silver, molybdenum, and beryllium copper; various tempers, thickness, and configurations such as continuous and short sections joined, expanded and flattened, perforated, slip, dimpled and bridged.
- 3) Solder. Various types of solders, temperature range, fluxes, heating times, solder iron tips, and preforms the use of both hand and automated soldering techniques; both localized spot and continuous solder joints.

A total of 22 qualification test boards (Q-boards) were assembled and tested to develop the best design and process.

The outstanding configuration was shown to be a module using 2 x 2 cm cells connected in flat, parallel modules with connecting tabs of expandable copper, the modules being assembled from two-cell

Table 4-35. RCA Thermal Cycle Test Results

Project	Cell Type	Module	Glass and Adhesive	Thermal Test Temperature	Environmental	Total Cycles	No. of Units Tested	Degradation
Relay	N/P RCA sintered contact	Shingle (rigid) with molybdenum P and N tabs	60 mil, 7940 Furane 15E adhesive	50°C max and -70°C min 30 minutes hot-cold-hot	Room atmosphere	250 hot-cold-hot	14	1. After 130 cycles: per cent change in current at 2.30 volts averaged -0.1 per cent with a max of -2.5 per cent. 2. After 250 cycles: per cent change in current at 2.30 volts averaged 2.0 per cent with a max of 3.4 per cent (only one unit was greater than 2.2 per cent.
Tiros	N/P plated contact	Shingle (rigid) with copper P and N tabs	6 mil, 7940 Furane 15E adhesive	80°C max and -30°C min. 20 to 28 minutes hot-cold-hot	Room atmosphere	250 hot-cold-hot	40	After 250 cycles: per cent change in current at 2.30 volts averaged 1.6 per cent. Max. change was 4.6 per cent. 37 units changed by 3.0 per cent or less.
Classified program	N/P RCA sintered contact	Shingle (rigid) with copper P and N tabs bonded to honeycomb substrate and wired into two rows of five cell shingles	6 mil, 7940 and LTV 602 adhesive	50 cycles. 75°C max and -50°C min total time hot-cold-hot, 44 minutes plus; 315 cycles 75°C max and -50°C min total time hot-cold-hot, 9 minutes	Room atmosphere	50 slow cycles plus 315 shock cycles		After 365 total cycles per cent change in current at max power point (11.5 volts for 5 series connected shingles) averaged less than -0.5 per cent for all 10 shingles.
Nimbus	N/P RCA sintered contact	Flat, 10 2x2 cm cells connected with copper on P and N sides. Cells are connected in parallel Modules bonded to substrate	6 mil, 7940 Furane 15E adhesive	-80°C min and 60 to 70°C max 1.5 hours cold-hot-cold time	10 <sup>-5</sup> mm Hg Vibration some humidity and acceleration	1000 800	64 32	Per cent change in current at 0.460 volt averaged under 2.5 per cent with the 3 $\sigma$ limits of -5.0 and +4.0 per cent.
Nimbus (additional tests)	N/P RCA sintered contact	Same as above, but with different connector materials including molybdenum as one type.	6 mil, 7940 Furane 15E adhesive	-80°C min and 60 to 70°C max 1.5 hours cold-hot-cold time	10 <sup>-5</sup> mm Hg	3 Separate tests: 695, 1217, and 919 cycles	Between 20 and 40 modules per substrate	Per cent change in current averaged less than 3 per cent for most module designs tested.
Lunar Orbiter	N/P RCA sintered	Flat six 2x2 cm cells constructed with molybdenum connected in parallel. Modules bonded to substrate.	6 mil, microsheet and Sylgard 182 adhesive and Furane 15E	-120°C and 115°C	10 <sup>-5</sup> mm Hg	600 cycles	12 modules	Per cent change in current at 0.460 volt less than 2.0 per cent for 11 modules. The 12th module was damaged in test.

submodules. Additional tests were then performed on 96 samples of this configuration and were successfully cycled through 1000 thermal oscillations.

The Lunar Orbiter solar panels are expected to cycle between the temperatures of 110 and  $-114^{\circ}\text{C}$  at the rate of once every 3.5 hours; it was decided to qualify the panels for this program over a temperature range of 115 to  $-120^{\circ}\text{C}$  and to test kovar, nickel plated molybdenum, and silver connector strips which have better thermal expansion characteristics relative to the silicon cells than copper connector strips. Solderless backed thin cell modules were tested also because they offer a weight saving. Other module configurations, as well as shingles, were included in the tests.

The solderless backed thin cell modules with nickel-plated molybdenum connector strip using the two-cell submodule building blocks, gave the best results with only 2 per cent degradation in electrical output. Although the proposed Voyager module is expected to be subjected to greater temperature extremes, these tests indicate that the materials selected will be the most reliable in view of the temperature range.

Table 4-35 is a summary of RCA thermal cycle test of results.

d. Modularization Losses

Experimental data based on bare cells must be converted into equivalent performance data for glassed modules. The values for the modularization loss incurred by assembling bare cell into cover glassed modules for Voyager are based on the greatest loss experienced on the Lunar Orbiter program

Standard test conditions, based on past experience and proposed for this program are  $50^{\circ}\text{C}$ ,  $139.6 \text{ mw/cm}^2$  tungsten equivalent intensity, and  $2800^{\circ}\text{K}$  tungsten light temperature. The current at a predetermined cell voltage for bare cells is measured under standard test conditions.

Cells whose current is within one-milliampere interval are matched into a two-cell pair, connected in parallel by an n-strip connector of molybdenum and covered with a 6-mil microsheet cover glass with a blue filter. The adhesive is Sylgard 182. The maximum loss in current at test voltage from the sum of the bare-cell currents is 4 per cent.

e. Electrical Characteristic

Figure 4-64 is the electrical characteristic of the 2 x 2 cm solar cell selected for the mission, at 27°C. It includes all losses accrued in the process of assembling bare cells into glass-covered 10-cell modules, resulting in an effective 9.5 per cent efficiency.

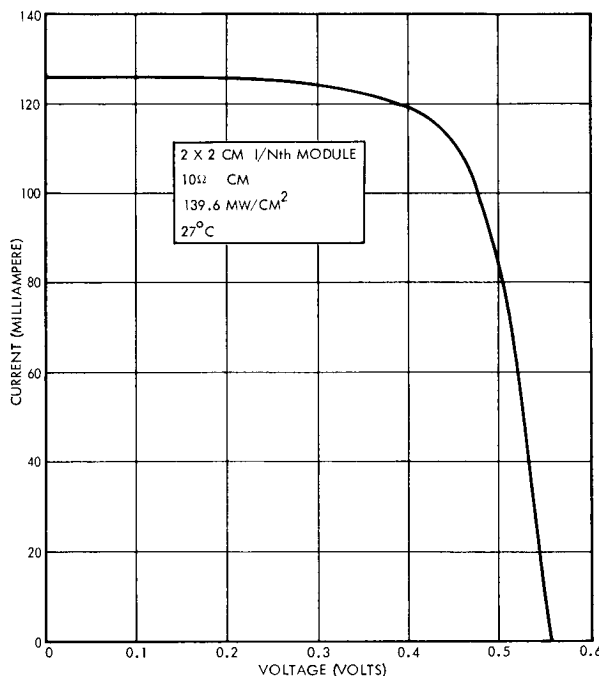


Figure 4-64. Installed Nondegraded Solar Cell Current-Voltage Characteristic

Factors degrading cell performance as a result of environment and array assembly are not included in Figure 4-64. The remaining degrading factors and tolerances are discussed and applied in Section 3.3.3.

f. Module Weight

Average nominal weight of components in the modules proposed for use on Voyager is:

<u>Component</u>	<u>10-Cell Module</u>		<u>8-Cell Module</u>	
	<u>Quantity</u>	<u>Average Total Weight (grams)</u>	<u>Quantity</u>	<u>Average Total Weight (grams)</u>
Solar Cells	10	2.40	8	1.920
Quartz Filters	10	1.484	8	1.187
Filter Adhesive	10	0.033	8	0.026
Molybdenum n Strip	5	0.25	4	0.200
Molybdenum p Strip	1	0.324	1	0.259
Solder Preforms	24	0.090	20	0.072
		<u>4.581 grams</u>		<u>3.664 grams</u>

The average weight on a per square foot basis of the array is detailed below. Maximum weights of components, rather than the averages, were used to obtain loads for the design of the panel structure.

	<u>Average Weight pounds/ft<sup>2</sup></u>
Substrate (19.16 lb. per panel, 31.7 ft <sup>2</sup> )	0.604
Modules (using 4.58 and 3.67 grams per 10 and 8-cell module, respectively)	0.213
Dielectric	0.333
Silicone Primer	0.002
Silicone Adhesive	0.029
Dark Side Thermal Control Coating	0.002
Dark Side Components (wire, terminal boards diodes, diode boards, wire tie downs, encapsulants)	0.090
Wiring on dark side to reduce magnetic effects including wire stakes	0.030
	<u>1.003 lb/ft<sup>2</sup></u>

### 3.3.3 Array Electrical Design

The basic building block of an array is defined as one series string of cell modules; it is the smallest array unit capable of delivering power to load at the proper voltage level throughout the entire mission, despite all the possible environmentally induced variations of the electrical characteristics of that string. Once such a basic unit is defined, to meet the mission power requirements requires selecting the correct number of strings to be paralleled so that the cumulative current output at the required array output voltage amounts to the worst-case power requirement. In determining the number of strings, several design factors must be evaluated, such as the degrading effects of the space environment, variation in solar illumination, and the like.

The output current (short circuit) varies approximately as the cosine of the angle to sun vector. Considerable test data exists on glass covered solar cells (with filters deposited on the glass) demonstrating the angle relationship used in the Voyager power system analysis (see Figure 4-65).

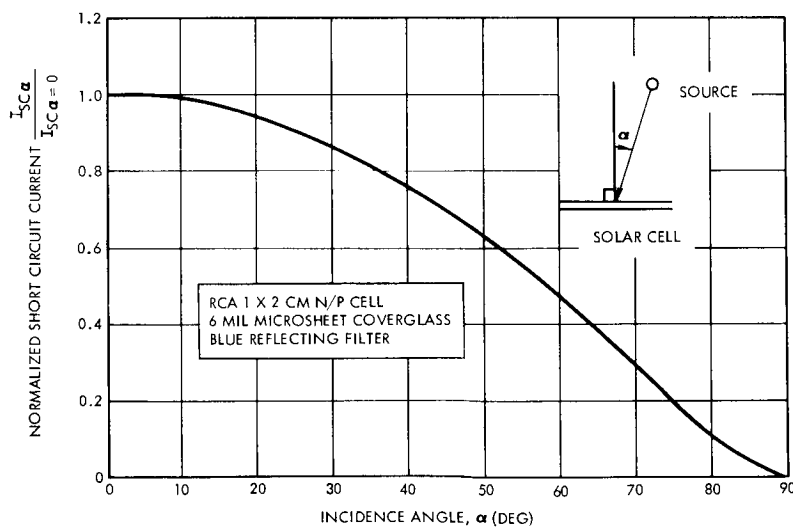


Figure 4-65.  $I_{SC}$  Versus Angle of Incidence



RCA and other experimenters have determined that solar cell, cover glass-to-cell adhesive, and a filter-coated cover glass are affected by ultraviolet irradiation. Test data indicate a 4 to 5 per cent reduction in the air mass zero short circuit current with most of the reduction occurring within the initial 50 hours of exposure. Beyond 50 hours the degradation in short circuit current is gradual, leveling off at about 4.5 per cent maximum after approximately 1 year of continuous exposure.

Tests have been conducted on assemblies of combinations of solar cells of different manufacturers, adhesives including RTV 602, Furane 253, Sylgard 182, 184, XR-6348 and XR-6-3489, cover glass including Corning fused silicon 7940 and Microsheet 0211, and filter coatings on cover glasses for blue reflective coatings. In general the results indicate that the filter, glass, and adhesive each contribute to a reduction in solar cell assembly power output when exposed to ultraviolet but that the silicone based adhesives (all those identified above except Furane 253) are superior in this respect to the epoxy adhesives.

These materials have also been subjected to proton and electron irradiation. The test data show that solar cell assemblies consisting of blue reflective filters on Corning 7940 with a silicone based adhesive for the cover-to-cell adhesive do not degrade up to combined fluxes of  $10^{15}$  electrons per  $\text{cm}^2$  of 1 mev electrons and  $10^{12}$  protons per  $\text{cm}^2$  at 17 mev. At total flux dosages of  $10^{16}$  electrons per  $\text{cm}^2$  (1.5 mev) a small reduction (2-3 per cent) in cover glass transmission has been measured.\* Electron and proton irradiation of microsheet glass indicates a higher susceptibility to transmission reduction than for fused silica 7940 at identical levels.\*\* In addition tests at TRW have shown that the microsheet transmission tends to degrade at lower flux values. In anticipation some degradation at the higher particle flux the combined effect of ultraviolet and particle degradation is estimated as 5 per cent, appearing as a reduction in solar module current.

---

\*"Irradiation of Solar Cell Cover Slides and Adhesives with 1.5 Mev Electrons," Contract AF 04 (657)-987, Lockheed Missile and Space Company.

\*\*Cooley and Janda, Handbook of Space Radiation Effects on Solar Cell Power Systems, NASA, SP-3003.

A value of 2 per cent uncertainty in the solar panel current measurements is included in the design factors, based on an estimate of the errors in the test equipment used for the measurements stemming from nonuniformity of temperature over the panel area, nonuniformity of illumination intensity, and spectral composition of the array of illumination sources. A 2 per cent allowance in the design of the solar cell panels for this current measurement tolerance (or error) will insure that panels when tested under large area illuminators will meet minimum performance specifications.

a. Solar Array Efficiency

Several other factors contribute to the uncertainty in the prediction of solar array output power under air mass zero conditions. These factors include standard cell calibration whereby all measurements of solar cells and panels are referenced to standard cells to calibrate the illumination source or to determine solar intensity in the use of outdoor measurements. Analysis of the methods used to calibrate standard cells and correlation of data from these methods indicates a  $\pm 2$  per cent uncertainty in the air mass zero calibration current of the standard cells. Additional errors result from variations in the values of open circuit voltage and short circuit temperature coefficients from the nominal values assumed, as well as small errors which accumulate in the application of design factors and construction of I-V curves for solar panel design. A 3 per cent total allowance is made in the design of the solar panels for these errors in power prediction.

The short circuit current of a solar cell varies linearly with intensity (for the same relative spectrum) over the ranges of intensity under consideration. As a design factor the short circuit current of the initial or undergraded module is therefore corrected proportionately as the intensity changes from the reference value of  $139.6 \text{ mw/cm}^2$  at 1 AU.

With respect to the degradation to be anticipated from inter-planetary dust particles, experiments have been flown on various spacecraft and measurements have been made of the particle momentum, kinetic energy, and mechanical impact damage, utilizing various sensors and detectors. Data accumulated from numerous experiments has allowed the plotting of particle mass versus influx rate\* and the derivation of equations representing the same data outside of the regions of previous measurements.\*\* Having obtained estimates of the micrometeoroid flux, a common denominator to relate the damage of a glass-covered solar cell to a given flux, mass, diameter, and velocity of micrometeoroids is required and to this end some general guidelines have been derived from experimental data on particle bombardment of solar cells that indicate a need to provide some protection.

In tests\*\*\* involving the sandblasting of Corning fused silica type 7940 covered solar cells with 220 grit silicon carbide, the air mass zero short circuit current degradation ranged from less than 1 per cent at  $10^3$  craters/cm<sup>2</sup> (average crater diameter 30 microns) to a maximum of slightly less than 12 per cent at  $10^6$  craters/cm<sup>2</sup>. Power degradation ranged from 11 per cent at  $10^3$  craters/cm<sup>2</sup> to 60 per cent at  $10^6$  craters/cm<sup>2</sup>. The differences in degradation between the  $I_{sc0}$  (air mass zero short circuit current) and maximum power point current is ascribed to the damage of the cell edges which were hit by the grit particles, causing a significant increase in leakage (shunt path) current. The important fact from these tests is the requirement for protection of the P-on-N junction along cell edges.

---

\*W. M. Alexander, C. W. McCracken, L. Secretan and O. E. Berg, "Review of Direct Measurements of Interplanetary Dust from Satellites and Probes," NASA technical Note D-1669, May 1963

\*\*"Preliminary Voyager 1971 Mission Specification" JPL Document 45, 1 May 1965

\*\*\*B. Ross, "Design Criteria for Satellite Power Supplies Using Radiation Resistant Solar Cells," Hoffman Electronics Corporation, March 1963

The solar cell optical filter substrate dimensions for Voyager are such that the glass-covered substrate will overhang the three edges of the cell (not adjacent to the N strip), providing shielding for the cell edges. The edge of the cell along the N strip is protected by the N strip connector material.

Results of bombarding Corning fused silica type 7940 with glass spheres (2.2 gm/cc, 75 and 35 microns in diameter) were evaluated for over 250 impacts in another test.\* In this test it was shown that thick cover glasses may have a larger crazed area for the same diameter of impacting particle compared to a thinner cover, thus degrading the cell power level to a larger extent. For Voyager, a 6-mil optical filter substrate was selected on the basis of the solar cell radiation damage tradeoff study. The results of micrometeoroid testing provide an additional reason for utilizing a 6-mil thick optical filter substrate rather than a thicker glass.

Based upon the data available, it appears that selection of a thin cover glass and protection of the cell edges by glass overhang will tend to reduce the effects of micrometeoroids. There remains, however, a requirement to provide a design allowance for reduction in solar cell power output due to cratering of the cover glass and erosion of the anti-reflective coatings on the exposed glass surface. The design allowance is estimated as a 5 per cent reduction in current because of micrometeoroid bombardment through the 12-month life of the Voyager spacecraft.

A final design factor is the effective increase in series resistance caused by the resistance of wiring in the solar array and the resistance of soldered connections at wiring junctions and module to module junctions. These produce a voltage loss estimated at 2 per cent of the maximum power voltage.

\*J. A. Fager, "Effects of Hypervelocity Impact on Protected Solar cells," Report GDC-CHD-65-011, General Dynamics/Convair Corporation.

b. Solar Array Design Summary

In summary, the design factors for Voyager solar cell modules are taken as follows:

<u>Current</u>	<u>(per cent)</u>
Angle of incidence (see Figure 4-65)	-
Ultraviolet and particle irradiation	-5
Current measurement tolerance	$\pm 2$
Efficiency prediction uncertainty	$\pm 3$
Solar constant variation	-
Micrometeorite and sputtering	-5
Particle radiation damage to solar cell (see Figure 4-66)	-

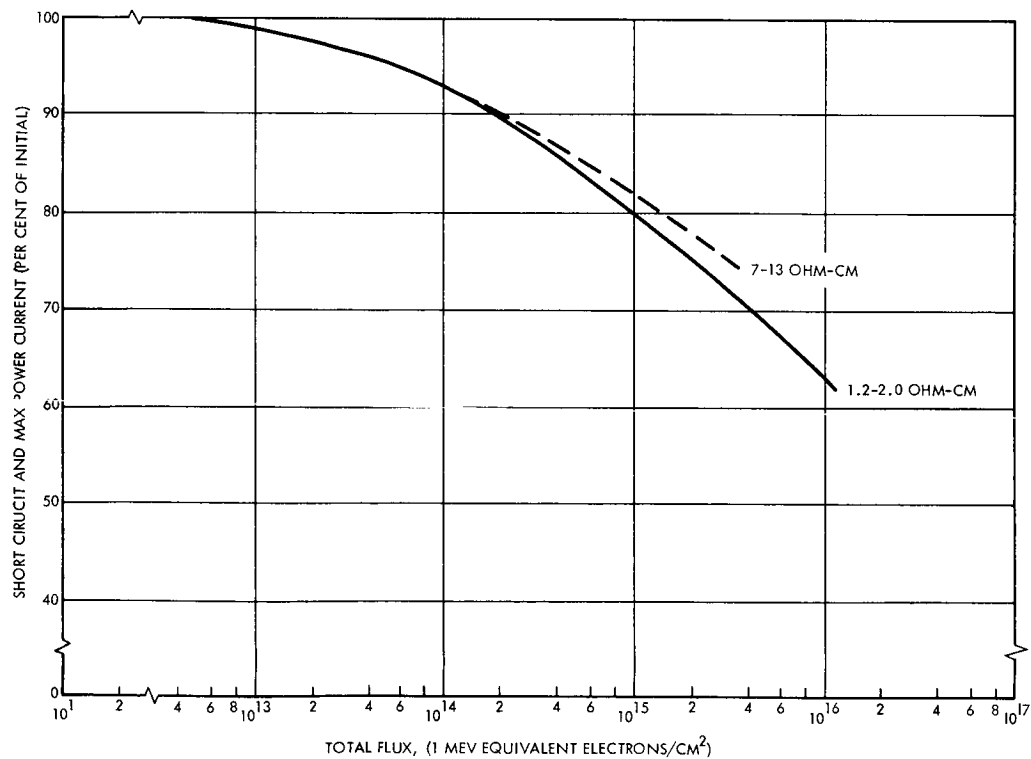


Figure 4-66. Current Degradation Curve AMO Intensity at  $T = 27^\circ\text{C}$

<u>Voltage</u>	<u>(per cent)</u>
Thermal cycling degradation	-2
Wiring loss	-2
Voltage measurement tolerance	$\pm 2$
Particle radiation damage to solar cell (see Figure 4-67)	-

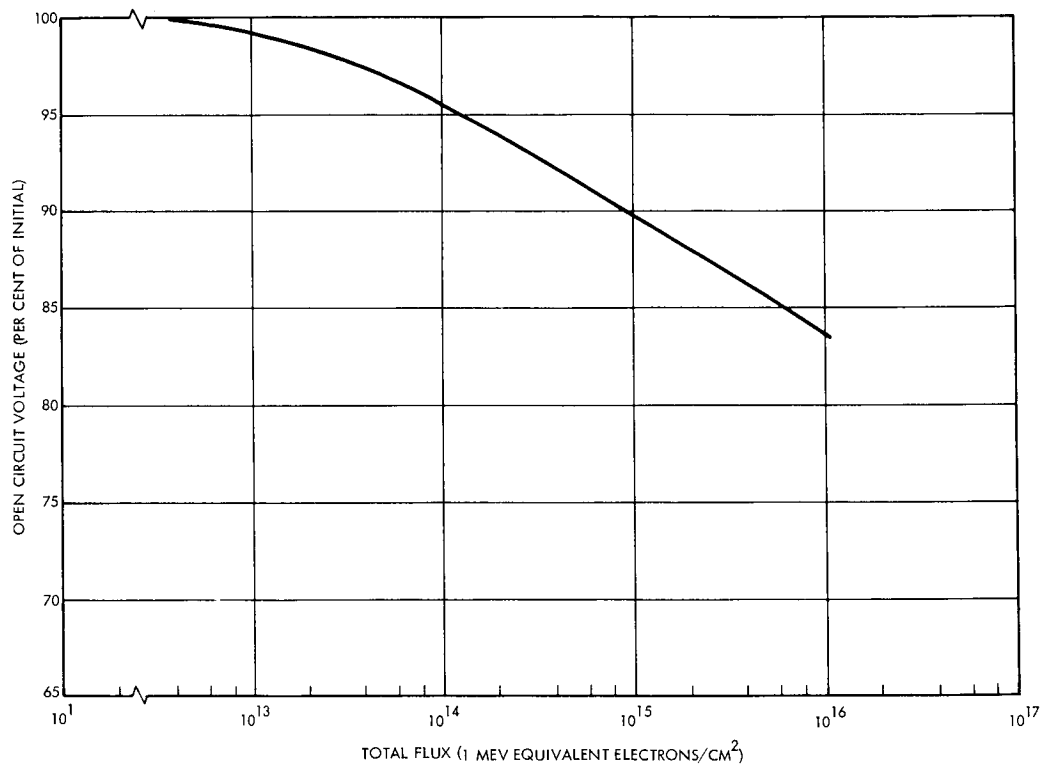


Figure 4-67. Voltage Degradation Curve AMO  
Intensity at  $T = 27^{\circ}\text{C}$

The technique used to construct I-V curves as a function of several variables operating on the Voyager solar array, for the 10-ohm centimeter base resistivity solar cell, incorporates four design parameters, as follows:

- 1) The I-V curve for the 10 ohm-centimeter base resistivity solar cell (Figure 4-64)

- 2) Worst case values of design factors just discussed
- 3) A solar panel back emissivity of 0.85
- 4) A Mars charged particle flux environment equivalent to that of the earth.

Based upon prior experience (Section 3.3.2) an undegraded module (two cells electrically paralleled with interconnecting tabs and cover glassed) will have a beginning-of-life efficiency of 9.5 per cent under air mass zero conditions (F. S. Johnson spectrum). The efficiency is defined for the following conditions:

- 27°C
- $V_{mp} = 0.440$  volt (10 ohm-cm base resistivity cell)
- air mass zero intensity =  $139.6 \text{ mw/cm}^2 = J_N$
- active cell area =  $3.8 \text{ cm}^2$

For this analysis, an equivalent modularized single cell, that is 1/nth of an n-cell module is used. The cell efficiency therefore includes all electrical losses associated with glassing, tabbing, and soldering operations. Figure 4-64 shows the I-V curve for this cell.

The cell parameters which best define the I-V curve are:

- short circuit current,  $I_{sc}$
- current at the maximum power point,  $I_{mp}$
- voltage at the maximum power point,  $V_{mp}$
- open circuit voltage,  $V_{oc}$

The I-V curve is constructed by selection of a measured curve which passes through the worst case values of the above parameters. These parameters are calculated by

$$I_{mp} = \frac{J_N A_s \eta}{V_{mp}}$$

where

$J_N$  is the air mass zero intensity, 139.6 mw/cm<sup>2</sup>

$A_s$  is the active cell area = 3.8 cm<sup>2</sup>

$\eta$  is the cell equivalent efficiency = 9.5 per cent

$V_{mp}$  is defined above = 0.440 volt

$I_{mp} = 114.0$  milliamperes

$V_{oc}$ , determined from electrical measurements on individual 10 ohm-centimeter solar cells, has been found to have a minimum value of 0.560 volt.

Another experimentally derived term is the ratio of  $I_{sc}/I_{mp}$ , which has been determined as a function of temperature. The value of this ratio at 27°C is:

$$D = \frac{I_{sc}}{I_{mp}} = 1.105$$

Using the value of  $I_{mp}$  above

$$I_{sc} = 1.105 (114) = 126 \text{ ma}$$

With the cell parameters established, an I-V curve was fitted through the points as presented in Figure 4-64.

Given the I-V curve for a defined set of conditions, the technique used to translate that curve to a second set of conditions is to calculate the product of the initial  $I_{sc}$  and the product of the current design factors,  $di$ , to obtain the degraded short circuit current.

$$I_{sd} = I_{sc} \times \prod_{n=1}^n di_n$$

$n = I$

The degraded maximum power current,  $I_{mpd}$ , is obtained from

$$I_{mpd} = \frac{I_{sd}}{D}$$



where

$$D = 1.078 \times (T \times 10^{-3})$$

with T in °C

This equation is an experimentally determined relationship over a temperature range of approximately 75 to -30°C.

The degraded maximum power voltage,  $V_{mpd}$ , is related to the  $V_{ocd}$  by.

$$V_{mpd} = V_{ocd} - 0.12 \text{ volt} - \sum_{n=1}^n d v_{mp_n}$$

where the 0.12 volt term is determined experimentally for low radiation fluxes. At high values of radiation flux the equation changes to

$$v_{mpd} = V_{ocd} - 0.11 \text{ volt} - \sum_{n=1}^n d v_{mp_n}$$

where  $d v_{mp}$  is similar to  $d v_{oc}$ .

Module (equivalent cell) degradation factors just discussed as design factors are repeated here to demonstrate the application to I-V curves. They are categorized in a form compatible with the analytical procedure and are identified as constant or variable factors. Constant factors are applied to the initial I-V curve of Figure 4-64 and to all subsequent curves throughout mission life. They are further identified as affecting current or voltage. The current (short current) factors are as follows:

- Ultraviolet radiation damage = 0.95
- Efficiency prediction uncertainty = 0.97
- Current measurement error = 0.98
- Off normal operation for the sun-oriented array (cosine  $10^\circ$ ) = 0.985

For the worst case analysis the minimum values of these factors are selected. The product is  $= (0.95) (0.97) (0.98) (0.985) = 0.89$ . Voltage factors are:

- Wiring losses applied to  $V_{mp} = 0.98$
- Voltage measurement error, applied to  $V_{oc} = 0.98$

Time variable factors are also applied to the I-V curve in Figure 4-64 to obtain I-V curves at discrete points during the mission lifetime. The current (short circuit) factors are as follows:

- a) Solar intensity, calculated using the relationship

$$di_1 = \frac{1}{1 (AU)^2}$$

where AU is the sun-to-spacecraft distance in astronomical units.

- b) Charged particle radiation damage. The value of this design factor,  $di_2$ , is computed using the appropriate value of 1 Mev equivalent electron flux\* encountered up to the specific point during the mission in combination with the current degradation relationship for 1 Mev flux presented in Figure 4-66.
- c) Temperature. The current design factor associated with the illuminated operating temperature of the solar array is calculated for the experimentally determined equation

$$di_3 = 1.0 - B (T-27)$$

where T is the cell temperature in  $^{\circ}C$  and B is -0.05 per cent/ $^{\circ}C$  decrease for up to total equivalent received flux of  $< 10^{14}$  one Mev electrons/cm $^2$  -0.10 per cent/ $^{\circ}C$  decrease for a flux of  $10^{14}$  electrons/cm $^2$  and -0.18 per cent/ $^{\circ}C$  decrease above  $10^{14}$  electrons/cm $^2$ .

- d) Micrometeoroid and sputtering damage. This factor has a value of  $di_4 = 0.95$ . It is assumed for the purpose of these calculations that all damage occurs within 60 days after the start of the cruise phase (AU = 1.1).

The voltage (open circuit) factors are as follows:

- a) The  $V_{oc}$  is affected by all factors affecting the short circuit current. The change in  $V_{oc}$ , that is,  $d v_1$  caused by all current factors (constant and variable) except the radiation damage (treated separately), is computed using the following expression derived from equations which describe solar cell operation

$$d v_1 = \frac{K T}{q} \ln \frac{1}{Y_T}$$

where

$K$  is Boltzman's constant

$T$  is the absolute temperature ( $^{\circ}K$ )

$q$  is the electron charge

and  $Y_T$  is the product of all current factors exclusive of radiation damage

---

\* The method of computing one mev damage equivalent electron flux is described in Section 3.3.1.

- b) Charged particle radiation damage. The value of this degradation factor,  $d v_2$ , is computed for the identical total 1 Mev electron flux used to determine  $d i_2$  above. The curve in Figure 4-67 which relates voltage degradation and flux is used in this case.
- c) Temperature. The voltage design factor associated with the illuminated solar cell operating temperature is calculated using

$$d v_3 = \mu (T(^{\circ}C) - 27)$$

where

$\mu = 0.0022$  volt/ $^{\circ}C$  decrease for 1-ohm centimeter solar cells and 0.0027 volt/ $^{\circ}C$  decrease for 10 ohm-centimeter solar cells.

The only design factor which influences voltage (maximum power),  $V_{mp}$ , that has not been accounted for is the time variable thermal cycling degradation,  $d v = 0.02 V_{mpo}$ . All thermal cycling damage occurs during the period of spacecraft eclipsing in the latter months of orbiting about Mars.

c. Performance Calculations

A sample calculation is presented depicting translation of the initial I-V curve to the end of life (1.67 AU) condition. The curve is based upon these selected array design conditions presented above. Computation of the degraded short circuit current is as follows:

- a) Constant factors = 0.890
- b) Time variable:
  - Solar Intensity  $di_1 = 0.359$  at 1.67 AU for end of mission at 12 months
  - Particle radiation damage  $di_2 = 0.746$  from Figure 4-66 for  $= 3.6 \times 10^{15}$  electrons/cm<sup>2</sup>
  - Temperature  $di_3 = 0.904$  corresponding to  $T = -26^\circ\text{C}$  at 1.67 AU ( $-26^\circ\text{C}$  is the worst case cell temperature (in sunlight) including prediction uncertainties)
  - Micrometeoroid damage  $di_4 = 0.95$

The combined product is 0.205. The degraded short circuit current is calculated to be:

$$I_{sd} = I_{sc} \times \prod_{n=1}^n di_n$$

$$I_{sd} = 126 \times 0.205 = 25.8 \text{ ma.}$$

Computation of degraded maximum power current is as follows:

$$\begin{aligned} I_{mpd} &= \frac{I_{sd}}{D} = \frac{I_{sd}}{1.078 \times T \times 10^{-3}} \\ &= \frac{25.8 \text{ ma}}{1.052} = 24.5 \text{ ma} \end{aligned}$$

Computation of the degraded open circuit voltage is as follows:

a) Constant factors

- Measurement error of 0.98;  $dv = -0.02 V_{oco}$   
 $= -0.02 \times 0.580$   
 $= -0.0112 \text{ volt}$

b) Time variable factors

- Change in  $V_{oc}$  because of change in short circuit current

$$d v_1 = \frac{K T}{q} \ln \frac{1}{\gamma_T}$$

$$\frac{K T}{q} = 0.0216 \text{ at } T = -26^\circ\text{C}$$

and

$$\gamma_T = 0.276$$

(where  $\gamma_T$  is the product of all factors which affect short circuit current except particle radiation damage)

$$d v_1 = -0.028 \text{ volt}$$

- Charged particle radiation damage. The value of  $d v_2$  for the same value  $\phi$  for which  $d i_2$  was computed is  $d v_2 = -(1.0 - 0.865) V_{oco} = -(1.0 - 0.865) 0.560 = -0.0756 \text{ volt}$ . The factor 0.865 is the fraction of  $V_{oc}$  remaining after exposure to a flux of  $\phi$  1-Mev electrons.
- Temperature.  $d v_3$  is computed for 10 ohm-centimeter solar cells

$$d v_3 = 0.1435 \text{ volt at } T = -26^\circ\text{C}$$

The sum total of the constant and variable factors is:

$$- [0.0112 + 0.028 + 0.0756] + 0.1435 = 0.0287 \text{ volt.}$$

The degraded open circuit voltage can then be calculated by

$$V_{ocd} = V_{oco} + \sum_{n=1}^n d v_{ocn}$$

$$= 0.560 + 0.0287 = 0.589 \text{ volt}$$

Computation of the degraded maximum power voltage is as follows:

a) Constant factor wiring loss (0.98)

$$d v = -(1.0 - 0.98) V_{mp} = -0.02 \times 0.440 = -0.088 \text{ volt}$$

b) Variable factor thermal cycling

$$d v = -0.02 V_{mpo} = -0.02 \times 0.440 = -0.088 \text{ volt}$$

c) The degraded maximum power voltage

$$V_{mpd} = V_{ocd} - 0.110 - \sum_{n=1}^n d v_{mpn}$$

$$= 0.5887 - 0.110 - (-0.0880 - 0.0880)$$

$$= 0.461 \text{ volt}$$

The I-V curve is generated by using the values of  $I_{sd}$ ,  $I_{mpd}$ ,  $V_{mpd}$ , and  $V_{ocd}$  calculated above, and a typical I-V curve shape for an irradiated 10-ohm-centimeter solar cell, leading to Figure 4-68 for the end of mission life, i. e., at 1.67 AU. Similarly, Figure 4-69 is a set of curves illustrating the best case from the point of view of the most predicted power. Figure 4-70 is another set of worst case curves, showing a comparison of the cell characteristics at 1.67 AU under three different radiation environment conditions. The various assumptions made in constructing curves in Figures 4-68, 4-69, 4-70 are shown in Tables 4-36, 4-37 and 4-38.

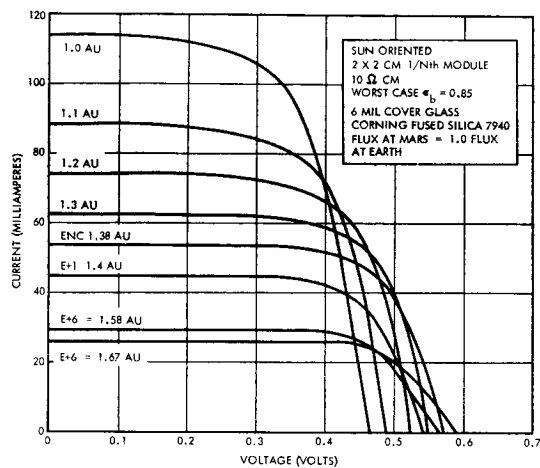


Figure 4-68. Worst Case I-V Curves at Various AU Distances

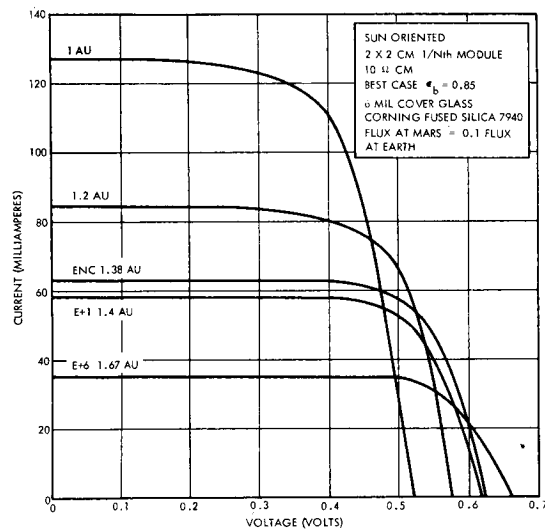


Figure 4-69. Best Case I-V Curves at Various AU Distances

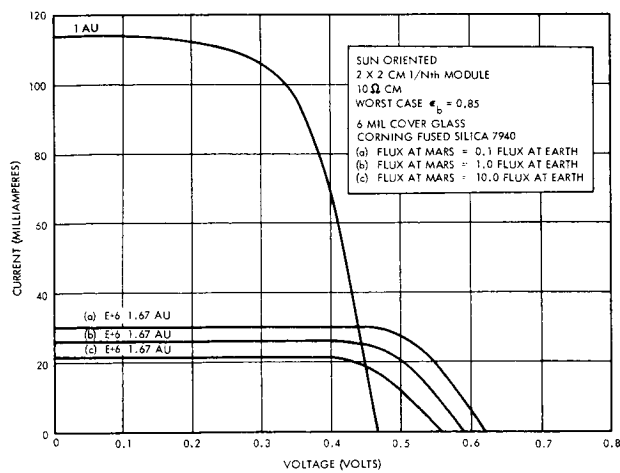


Figure 4-70. Effect of Radiation Flux on I-V Curves at 1.67 AU

Table 4-36. Parameters for Worst Case Curve  
Constructed for Mars Flux Model  $E_o = 1.0$

AU	Equivalent 1 Mev flux (electrons/cm <sup>2</sup> )	Solar Array Operating Temperature (°C)	Point in Mission Life
1.0	0	+ 57	Start (postlaunch)
1.1	$2.90 \times 10^{13}$	+ 42	
1.2	$2.90 \times 10^{13}$	+ 29	
1.3	$2.90 \times 10^{13}$	+ 16	
1.38	$2.90 \times 10^{13}$	+ 7	Encounter
1.40	$0.65 \times 10^{15}$	+ 4	Encounter + 1 month
1.67	$3.6 \times 10^{15}$	- 26	Encounter + 6 months

Table 4-37. Parameters for Best Case Curve  
Construction for Mars Flux Model  $E_o = 10^{-1}$

AU	Equivalent 1 Mev Flux (electrons/cm <sup>2</sup> )	Temperature (°C)
1.0	0	+ 45
1.38	$2.9 \times 10^{13}$	- 3
1.40	$1.12 \times 10^{14}$	- 6
1.67	$4.0 \times 10^{14}$	- 32

Table 4-38. Parameters for Worst Case Curve  
Construction for Mars Flux Model  $E_o = 10^1$

AU	Equivalent 1 Mev Flux (electrons/cm <sup>2</sup> )	Temperature (°C)
1.67	$3.6 \times 10^{16}$	- 26



d. Number of Series Modules ( $N_s$ )

On the basis of the factors and techniques just reviewed it is possible to determine the required number of modules. Figure 4-68 shows the effective degraded cell I-V characteristics reflecting projected worst-case performance for the radiation environment of one-earth equivalent. It shows that the maximum power point of the 1.67 AU (end-of-life) I-V curve is approximately coincident with the point of intersection of that curve with the 1 AU curve, and that no other curve intersect the end-of-life curve at a lower voltage. Thus, if the number of series modules is so chosen that the effective per-cell voltage is the same as or slightly lower than at that intersection point, the following conditions will be satisfied:

- 1) at end of life, cells are operated very nearly at the point of maximum power
- 2) at no time during mission will the array output be lower than at end of life.

To deliver 50 volts array output voltage, and assuming a blocking diode drop of one volt, the number of series modules is selected to be 116, to yield a per-cell effective voltage of

$$\frac{50 + 1}{116} = 0.440 \text{ volt}$$

or slightly lower than the voltage at the intersection of the 1 and 1.67 AU curves, based on the worst-case solar cell characteristics demonstrated in Figure 4-68. Using this figure and the selected per-cell operating voltage, Figure 4-71 is plotted to show variation of the relative output power versus mission life, at both the operating voltage and the instantaneous maximum power point voltage.

The method of selecting  $N_s$  is particularly sensitive to small solar cell voltage variations at the beginning of life. However, cell curves used as the basis for the selection of the operating point reflect the worst-case approach to cell temperature, efficiency distribution, and voltage measurement tolerances, thus assuring that the per-cell

voltage of 0.440 volt at 1 AU will at least meet, but most probably exceed the beginning-of-life cell current requirement of 30 ma implied by Figure 4-68. Any small amount of risk involved appears more than justified to maintain a reasonably simple, reliable, and efficient approach to power subsystem design whereby the array power is delivered directly to various loads at a single, constant voltage level, with no series elements injected to further regulate the d-c voltage output of the array.

The end-of-life cell current will be 25 ma at 0.44 volt.

To determine the largest possible electrical output, the following assumptions concerning degradation factors are made:

- 1) Current and voltage measurement tolerances are applied as numbers greater than unity (i. e., a 2 per cent tolerance becomes a 1.02 factor, instead of 0.98)
- 2) Similar treatment of the efficiency prediction uncertainty is made
- 3) No micrometeorite damage included
- 4) Charged particle radiation environment equivalent to that of one-tenth earth
- 5) Perfect array orientation
- 6) Lowest temperature within the prediction uncertainty band.

The best-case curves are shown in Figure 4-69. Figure 4-72 shows the relative power output variation with mission life for this case.

e. Electrical Output for an Earth-oriented Spacecraft

The plots shown in Figures 4-73 and 4-74 are those of the least output power versus mission time for the earth-oriented case. The same ground rules concerning the charged particle flux and other power-degrading factors were assumed in these plots as for the sun-oriented case. Table 4-39 gives the data for a typical trajectory in 1971.

Comparing Figures 4-71 and 4-74, it is seen that, when in the earth-oriented mode, 20 per cent less power is available at end of the

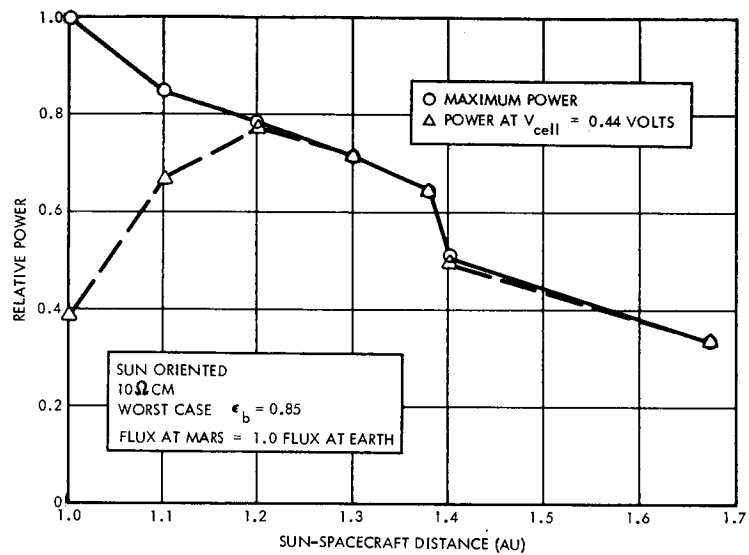


Figure 4-71. Worst Case Relative Power Versus Sun-Spacecraft Distance

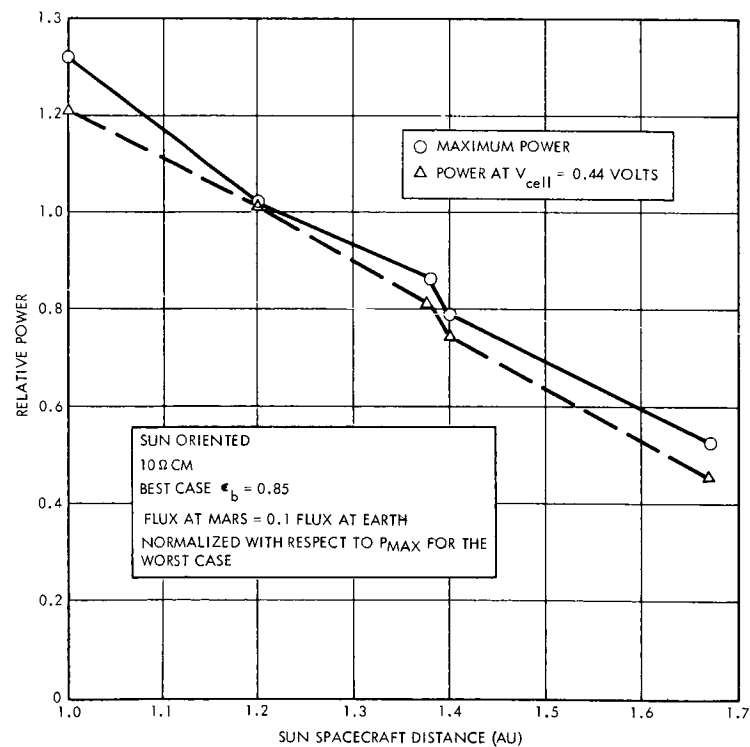


Figure 4-72. Best Case Relative Power Versus Sun-Spacecraft Distance

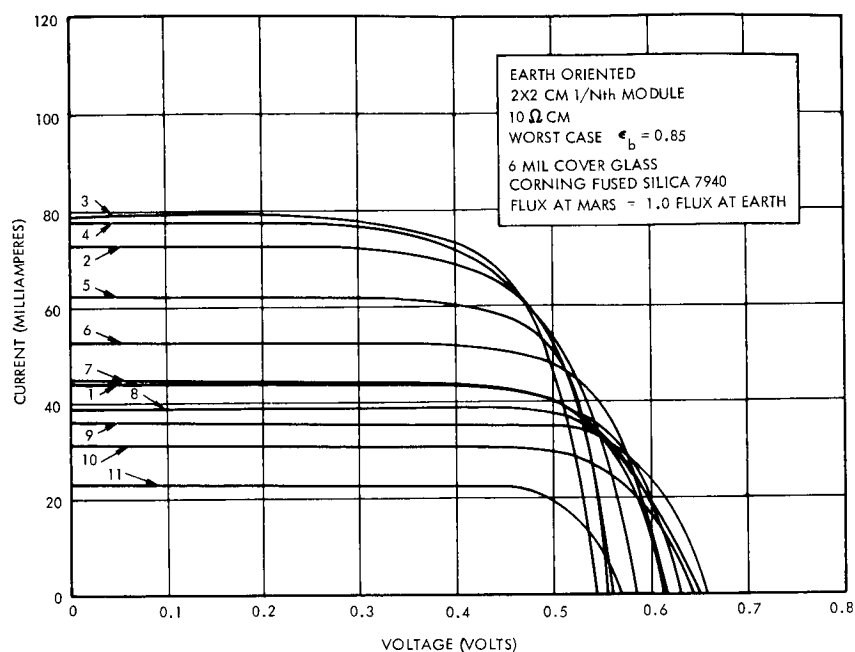


Figure 4-73. Earth Oriented Worst Case I-V Curves

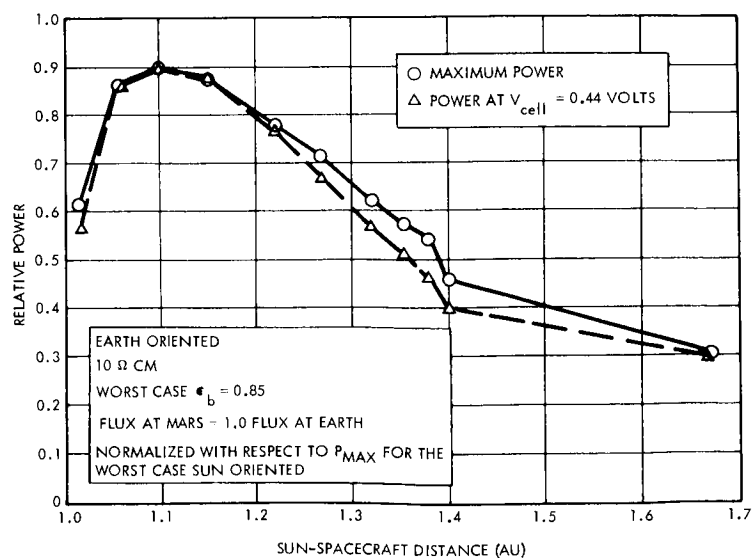


Figure 4-74. Worst Case Relative Power Versus Sun-Spacecraft Distance

first month in orbit (1.4 AU), and 10 per cent less at 1.67 AU, as compared with the sun-oriented case. A case of insufficient power will occur immediately following launch if the earth-oriented mode is employed at that time, because the sun angle is nearly 90 degrees at that time. However, the earth-oriented mode need not be used at that time because the high-gain antenna will not be required.

Table 4-39. Typical Data for Earth-oriented Spacecraft

Curve Number in Figure 4-73	Days After Launch	Average Distance in Astronomical Units	Sun Angle
1	20	1.015	62°
2	40	1.055	37°
3	60	1.100	20°
4	80	1.150	10°
5	100	1.220	22°
6	120	1.270	30°
7	140	1.320	37°
8	160	1.355	42°
9	177	1.380	43°
10	200	1.400	43°
11	360	1.670	24°

f. Array Magnetic Moment

A final factor imposed on the design of the solar array is magnetic cleanliness. The magnetic specification includes evaluation of all magnetic materials as well as field measurements on the solar panels such that the magnetic effect is less than 1 γ at a distance of three times the average dimension of the panel. It further postulates

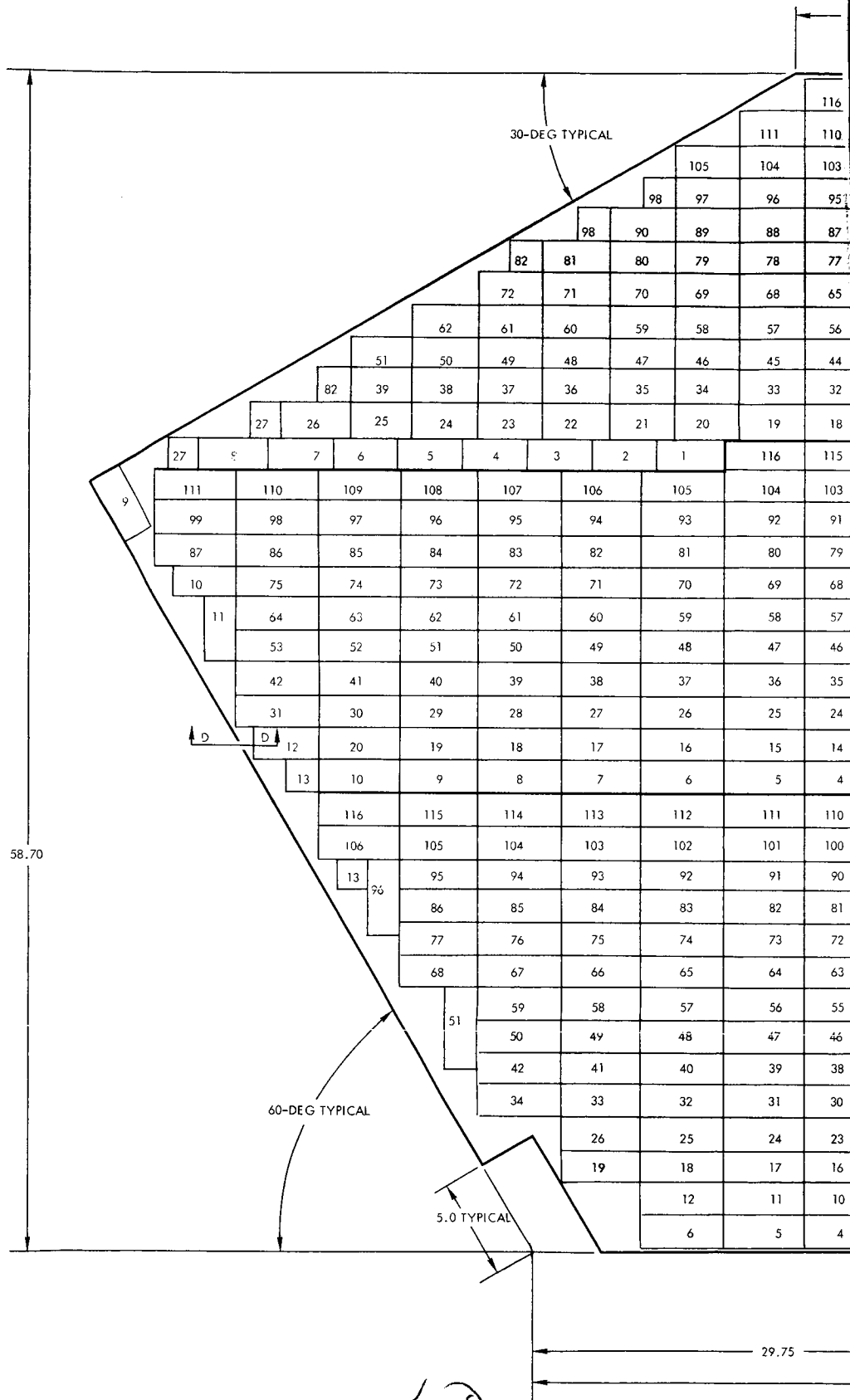
that induced and stray current fields be less than 1  $\gamma$  at 2 feet. Mapping of the magnetic field is to be performed in a field ambient of less than 100  $\gamma$ .

For a preliminary investigation of the magnetic effect of the solar panels, a typical section, 18 x 18 inches in area was checked, in the earth's ambient field, to ascertain the magnitudes of the disturbances. The panel section was typical of the Nimbus construction. Calculations discussed below have been made using a typical per-panel area of 38 ft<sup>2</sup> used as a model. Results quoted apply to the final selected lower area with a degree of conservatism.

The Nimbus type panel showed no more than 2.5  $\gamma$  at a distance of 10 inches from the active surface, and from the edges. When the panel was reversed, the sign of the H vector did not change, indicating thereby that the disturbance is probably one of induction by the earth's field. This test is significant in that the major surface area of the panel did not exhibit a fixed polarization, save at one point near the center, indicative of a local inclusion of magnetic material near this point. In any case, it would appear that the full 38-square-foot panel would show an induced field of 16.9 x 2.5, or 42.3  $\gamma$  at 10 inches. If one assumes a worst case attenuation of the field inversely as the distance cubed, a field strength of 1  $\gamma$  is postulated at 3.3 feet. Tests in a low ambient field are indicated and should be made.

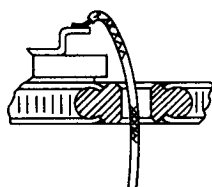
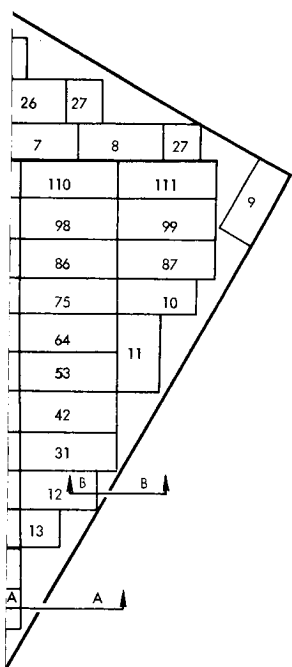
An estimate of the effect of the current loops was made for the proposed solar panels as illustrated in Figures 4-75 and 4-76. In this case the wiring arrangement consist of six series loops, paired symmetrically across the panel centerline, three on each side. Care is taken to null the paired loops in terms of dipole effect. That is, the ampere-turn-meter<sup>2</sup> effect is identical for sign.

For a first approximation, the loops were treated as equivalent point dipoles situated at the center of each loop, and calculated on the basis of enclosed area for one ampere of current. The dipole pairs across the center line were combined into their quadruple equivalent

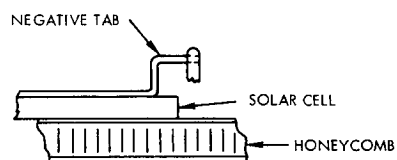






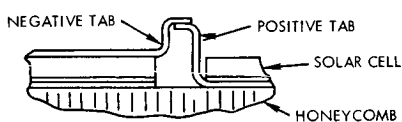


SECTION A-A

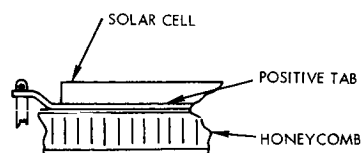


SECTION B-B

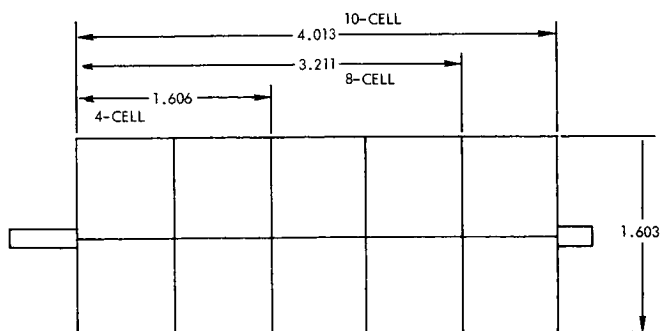
SECTIONS A-A TO D-D NOT TO SCALE



SECTION C-C



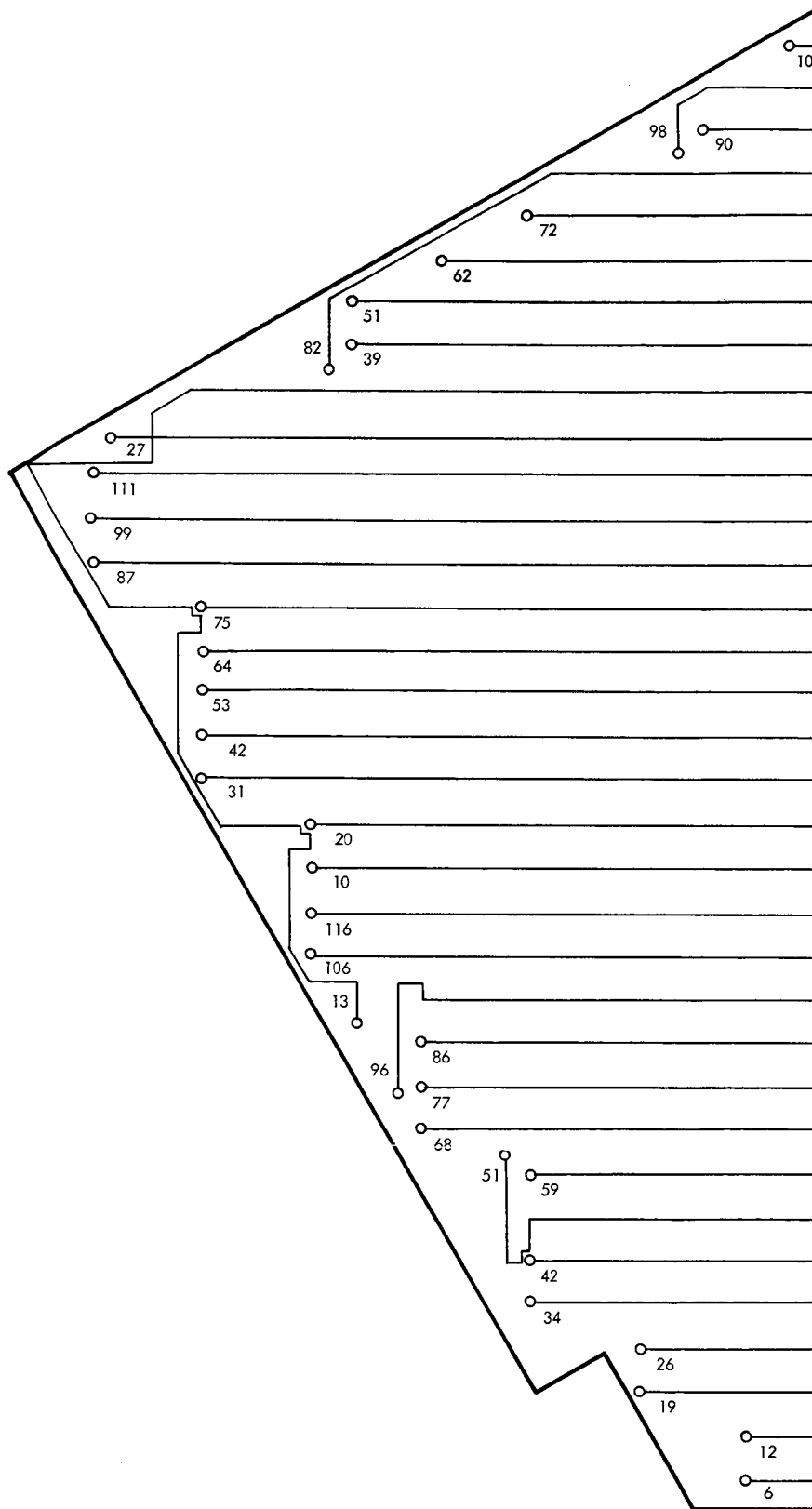
SECTION D-D

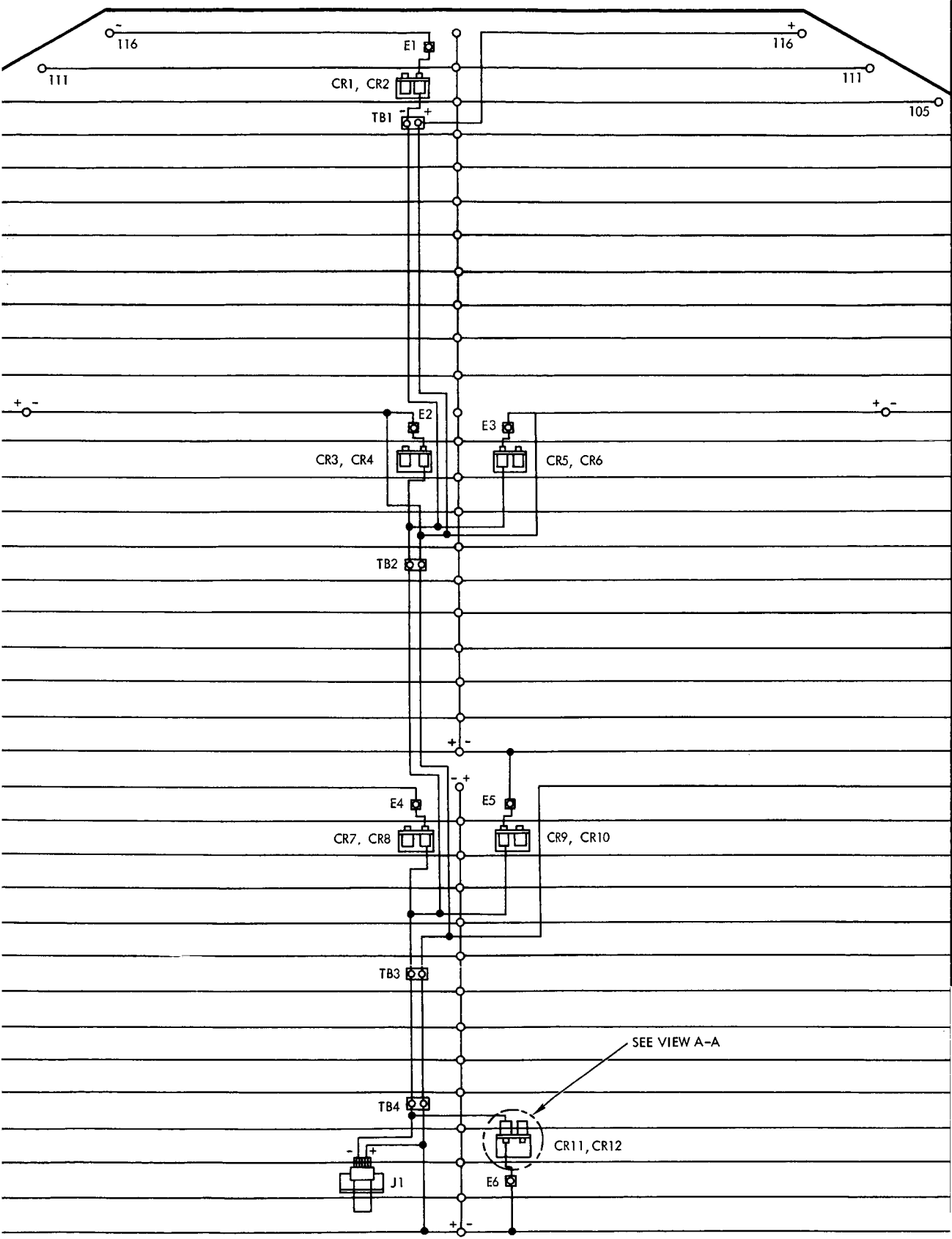


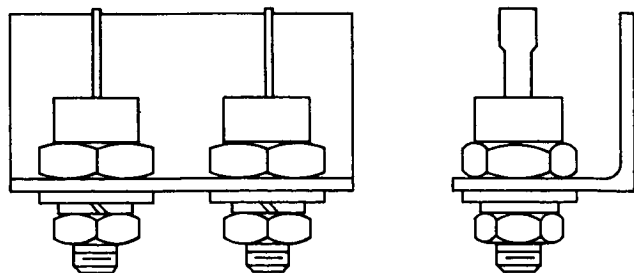
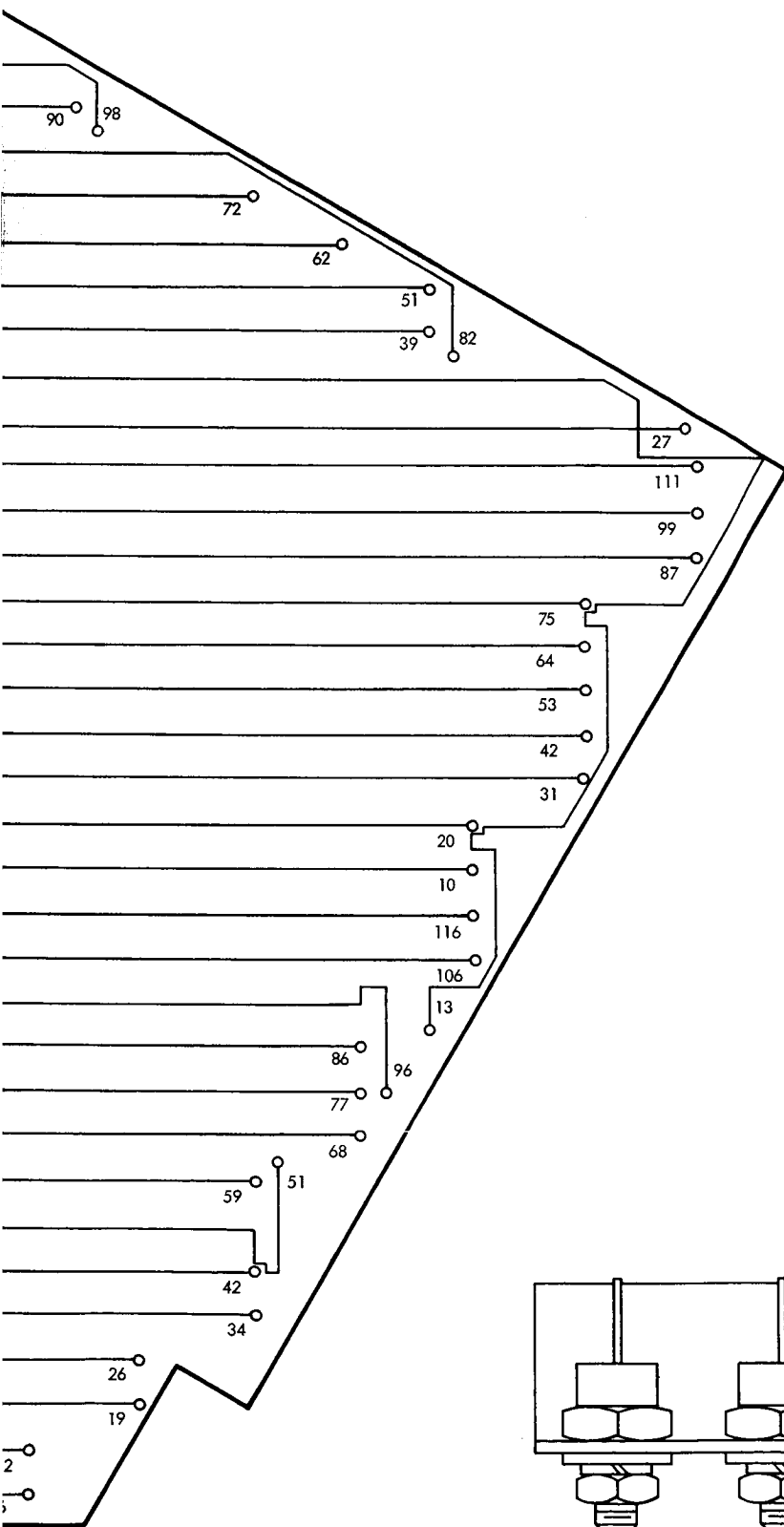
TYPICAL 4, 8, AND 10 CELL MODULE DIMENSIONS

Figure 4-75. Solar Panel Layout (Sun Side)









VIEW A-A  
NOT TO SCALE

Figure 4-76. Solar Panel Layout (Dark Side)

and from this simplification, the far magnetic field was computed. Under these assumptions, the radial field along a perpendicular standing on the center of the panel surface is zero while the tangential field is of the order of 100  $\gamma$  at 100 cm. Along a line inclined 45 degrees to the panel surface, the radial field approximates 150  $\gamma$  at the same distance.

To achieve a field value of less than 1  $\gamma$  at a distance of 2 feet, each string of solar cells is back-wired so that the return path through the wire is separated from the solar cells by the thickness of the panel. In this instance, the panel thickness is taken as 3/8 inch. The field at 2 feet from the panel surface is estimated to have a value of 6  $\gamma$  parallel to the panel, for a current of 1 ampere in the wires.

Further reduction of this field can be obtained by further reducing the enclosed area of the current loops and the current levels in the circuits. In any case, a reduction to a one-gamma field level requires close study, and magnetic measurements of wiring mock-ups simulating the proposed panel design.

### 3.4 Solar Array Controls

Detailed design and analysis of the solar array are given in Section 3.3. Initial investigation of the solar array characteristics developed the current-voltage curve shown in Figure 4-77. Constant voltage operation consistent with these 1 AU and 1.67 AU characteristics must be based on a design point which represents the maximum voltage capability at 1 AU and maximum current capability at 1.67 AU to support a given load requirement.

For this case, an array shunt voltage limiter could provide for constant voltage operation until the array is incapable of supporting the load. The inherent advantage of a shunt regulator in minimizing losses when a marginal solar array capability exists and the relative simplicity of this approach appear to offer strong justification for its use. Both dissipative (proportional) and nondissipative (switching) types can be utilized as well as combinations of these two to utilize desirable features of both.

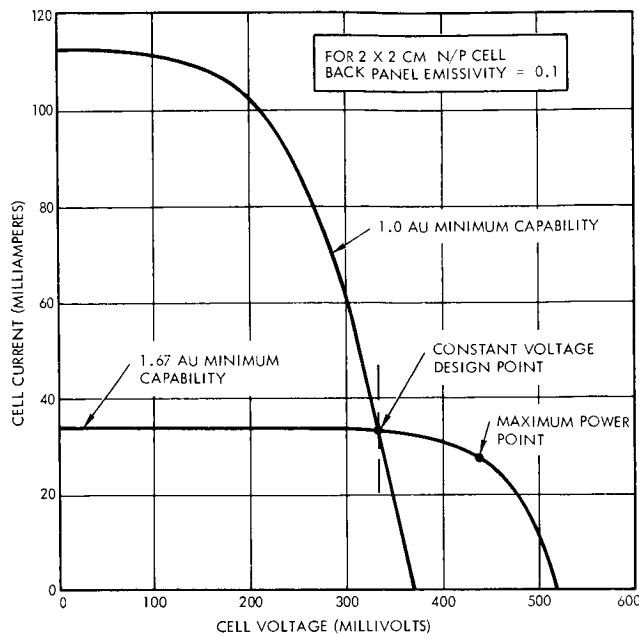


Figure 4-77. Preliminary Solar Cell Current-Voltage Characteristics

The use of zener diodes to limit solar array voltage is considered less desirable than an active regulator for reasons of both reliability and system efficiency. Although simple in concept, the loss in array power, because of single short-circuited zener diode, will result in loss of output regulation and probable complete loss of power of the solar array section controlled by the affected diode. The magnitude of this loss can, of course, be limited by splitting the array into many small sections, each controlled by its own zener shunt. To prevent a single diode short from affecting the remainder of the system, the isolation diodes for that section are located on the output bus side of the zener connection. Open circuit failures will have no effect on the output voltage unless a sufficient number occur to permit the resultant unregulated sections to supply the total load at a higher voltage than desired. In this case, the remaining regulated sections will lose control as their isolating diodes become reverse biased to prevent load current flow. Series or parallel redundancy is not applicable to zener diode shunt limiters because the lowest voltage zener circuit will always control.

The temperature dependence of the zener characteristic is of particular concern for the Voyager application because of the wide temperature ranges of the solar panels during the mission. In addition to panel temperature variations, the variations in zener power dissipation further increase their regulation band. As a result, these voltage variations caused by temperature when combined with the inherent diode impedance and difficulty in achieving closely matched current-voltage characteristics are considered inconsistent with the voltage limiting accuracy necessary to achieve  $\pm 1$  per cent bus regulation and maximum power utilization without additional series regulation such as that employed in the Mariner power system.

Figure 4-78 illustrates a general block diagram of a full dissipative shunt and array operating points for new and degraded conditions. Figure 4-79 indicates power dissipation versus load power for a fixed maximum array capability. The system must be capable of dissipating the total difference power between the array capability and the load

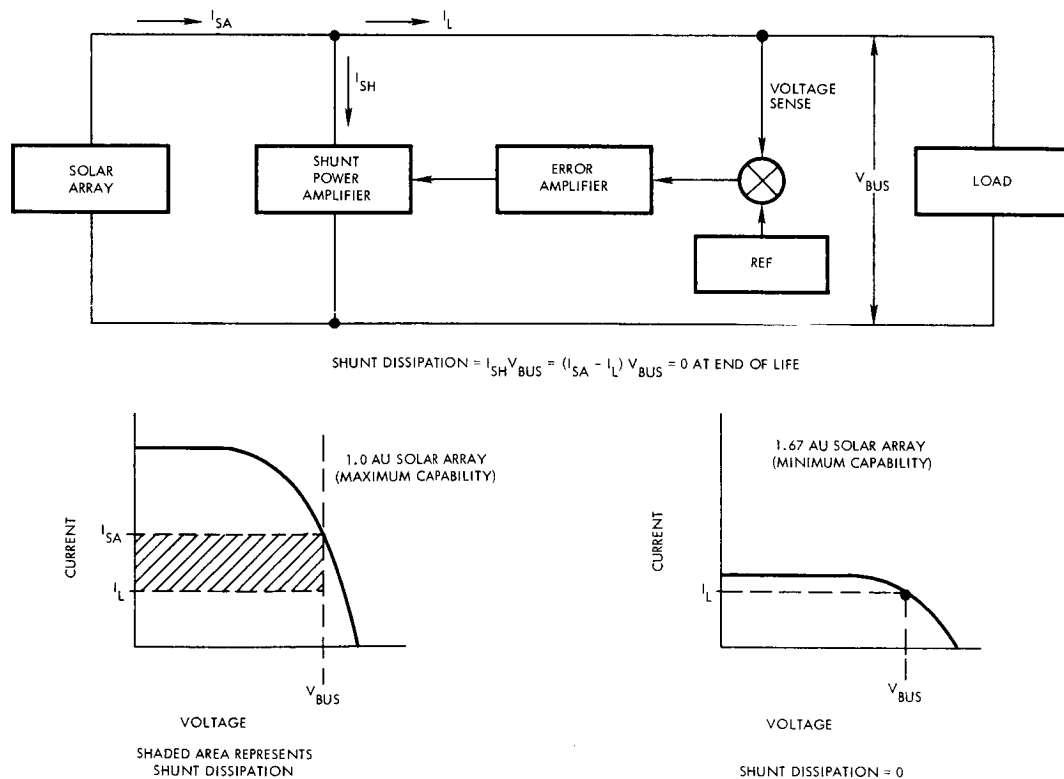


Figure 4-78. Full Dissipative Shunt Regulator

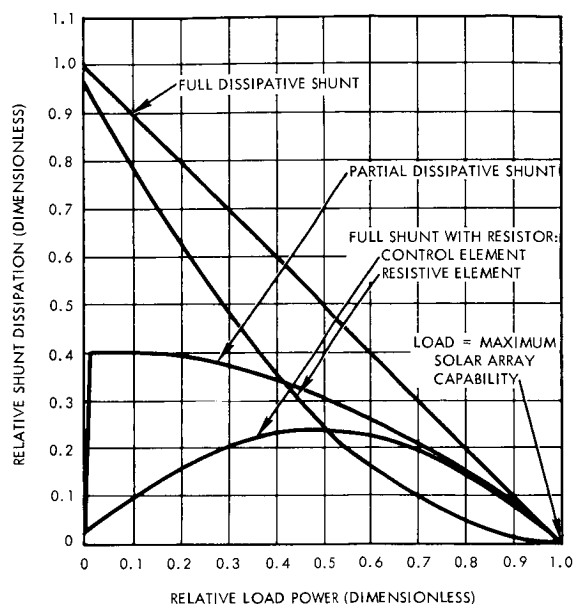


Figure 4-79.  
Comparison of Full and Partial  
Shunts Power Dissipation at 1.0 AU

requirement. The major disadvantage associated with the shunt regulator is that small variations in solar array voltage at 1 AU produce a large increase in current capability at the selected voltage limit and a corresponding excessive amount of power dissipation in the shunt elements. Preliminary calculations have shown the required shunt dissipation to exceed 1 kw if the dissipative elements shunt the full Voyager solar array.

In most spacecraft power system designs, the large dissipation with maximum array capability can be significantly reduced by use of a partial dissipative shunt regulator which taps only a portion of the series connected solar cells as shown in Figure 4-80. For this case, the shunt tap is selected such that with maximum solar array voltage (minimum array temperature) the shunt elements (power transistors) are driven to saturation and the array voltage is equal to the unregulated series cell section voltage at minimum load plus the saturated drop in the shunting transistors. The relationships between shunted section and unregulated section operating conditions are also illustrated in Figure 4-80. Power dissipation versus load is shown in Figure 4-79. TRW has developed dissipative partial shunt limiters of this type which maintain array output voltage within  $\pm 1/2$  per cent. Corresponding bus impedances of less than 1 ohm at frequencies up to 50 kcps have been achieved. For the Voyager application, however, because of the large variation in solar



array capability between 1 and 1.67 AU, use of a conventional partial shunt regulator would still require dissipating more than 500 watts at 1 AU. The penalties imposed on the spacecraft thermal control system by a heat source of this magnitude at 1 AU which decreases to a low value (essentially zero under worst case array degradation) at Mars are sufficiently severe that location of the shunt elements external to the spacecraft is necessary. A convenient location is, of course, on the solar panels themselves. The low panel temperatures experienced in eclipse at Mars, however, require heating of the shunt elements to permit their normal operation upon re-entry into sunlight. This may be done by adding heaters energized from the spacecraft batteries; however, the added battery capability required represents a significant weight penalty. An alternative approach utilizing thermal energy storage to maintain a suitable shunt temperature in eclipse, would also result in a significant weight increase for the Voyager application.

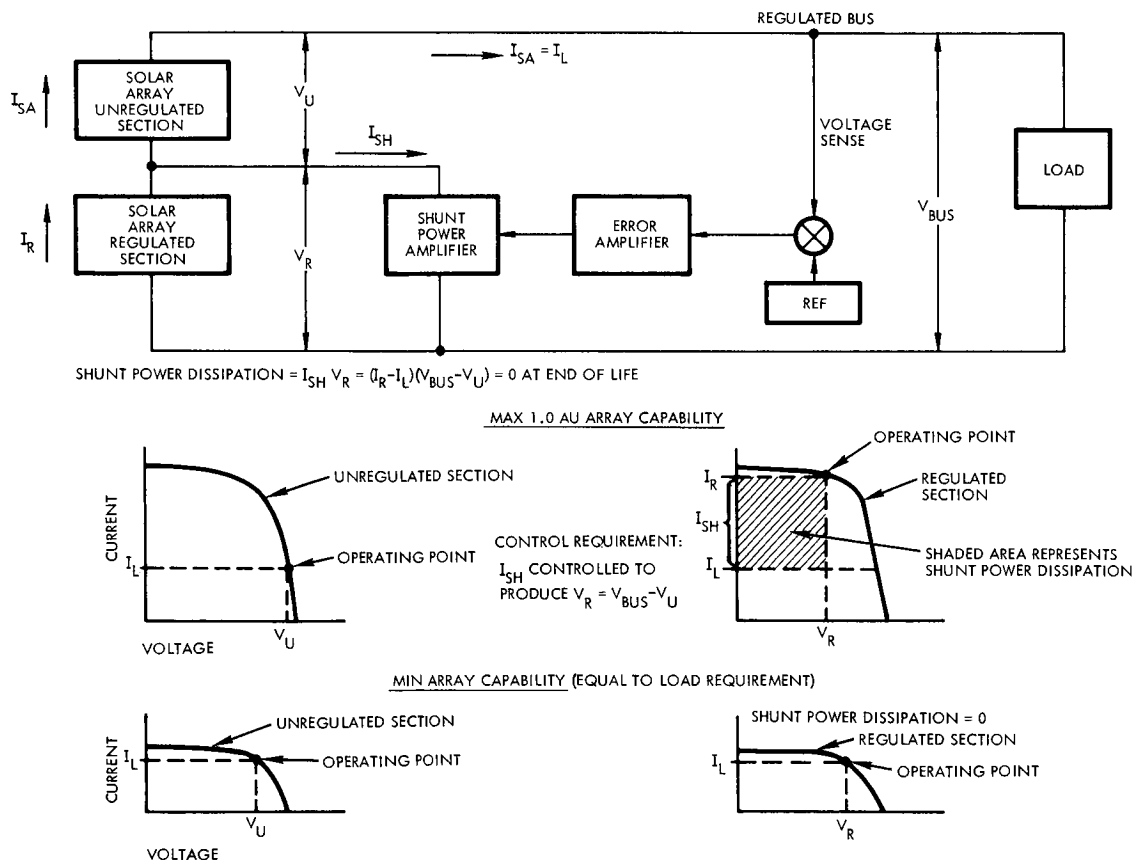


Figure 4-80. Partial Dissipative Shunt Regulator

The possibility of using resistive dissipating elements in lieu of transistors would permit a wider operating temperature range and possibly eliminate the need for heating the elements in eclipse. This approach, however, must still require power transistors to provide proportional control of the shunt elements. An increased tap point (higher voltage) is required for this approach because the shunt elements cannot be saturated at low voltage as in the case of the transistors.

Figure 4-81 indicates a full shunt regulator (100 per cent tap) with resistance in series with the shunt power amplifier. Proper sizing of the resistance value with knowledge of maximum array output and minimum load, allows a reduction by a factor of four in the dissipation of the active power amplifier. These curves are also shown in Figure 4-79. Array operation is identical to that of Figure 4-78.

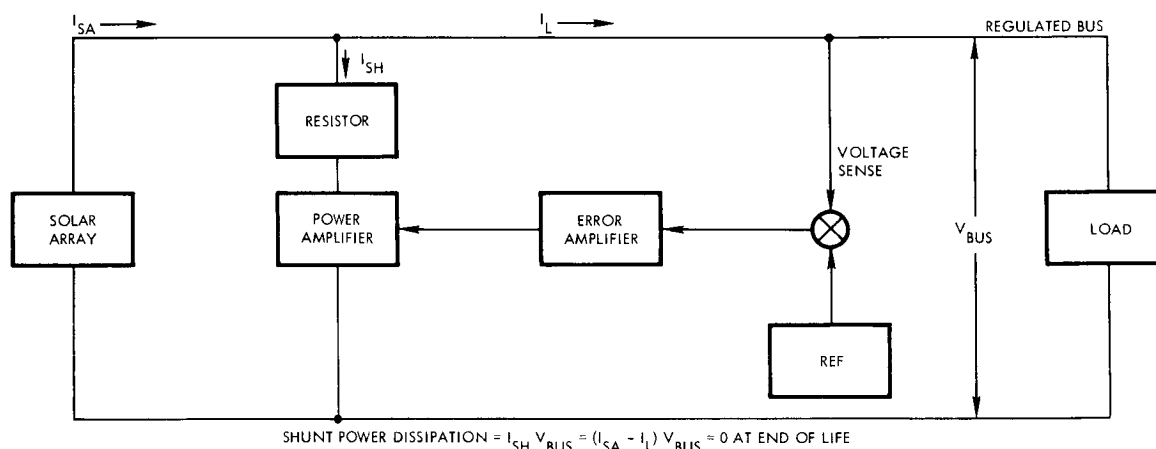


Figure 4-81. Full Shunt Regulator Using Resistive Power Dissipation

Switching pulse width modulated regulators can be usefully employed in full or partial shunt control schemes. Figure 4-82 illustrates a switching partial shunt regulator which, as in common with dissipative partial shunt regulators, acts to maintain a source voltage over a given load and source range with a maximum dissipation of only

a fraction of excess load power capability in the switching element. The advantage of the switching approach is that it allows the shunt power to be dissipated in resistors which can be located on the array. The disadvantages of this approach, in comparison to the dissipative partial shunt, are increased complexity in the control circuits and poorer response due to the filtering requirements.

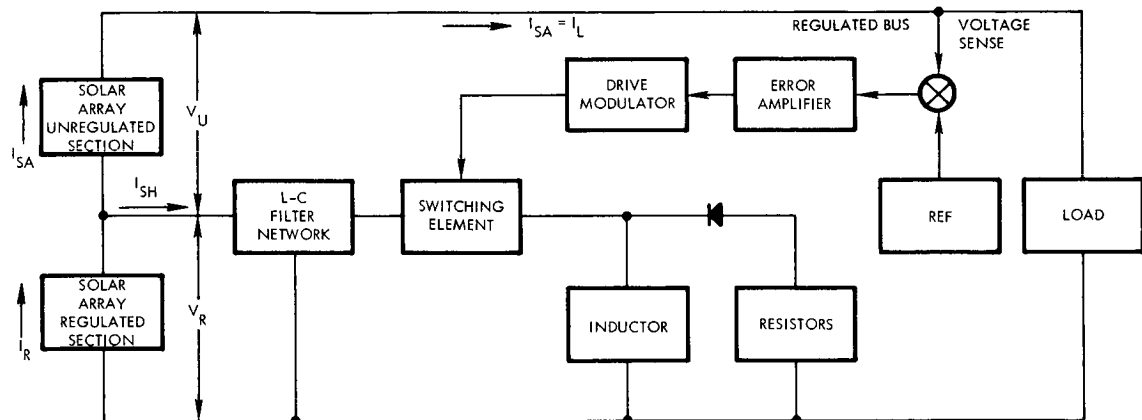


Figure 4-82. Pulse Width Modulated Switching Partial Shunt Regulator

In this scheme, the transistor switch is operated at a rate and duty cycle determined by the control circuitry. When the switch is closed, the inductor charges to a current dependent upon  $V_R$ , the duration of closure and the current existing in the inductor at the time of closure. The diode is reversed biased during this interval. When the switch is opened, the voltage across the inductor reverses and current flows through the resistors. Since current drawn by the switch is pulsed, the smoothing L-C filter is required to average out the current pulses and minimize solar array ripple voltage.

If the array could be operated at a higher voltage at the 1.67 AU condition, it is apparent that increased output power could be derived from the solar array. Conversely, at 1 AU a large excess power capability exists provided the solar array can be operated at a reduced voltage. The apparent incompatibility between these two array

characteristics in terms of maximum power utilization at constant voltage, strongly suggests using a series regulator similar to that discussed in Section 3.7 to boost the 1 AU voltage and permit operation at a bus voltage level consistent with the higher end-of-life voltage at maximum power capability. Since a boost regulator will lose control at high input voltage, an additional voltage limiting array control is necessary to prevent high bus voltage at the low solar array temperatures resulting from loss of array orientation during maneuvers or loss of insolation during orbital eclipses. To satisfy these requirements, both voltage limiting and boost voltage regulation of the solar array are necessary. Both shunt voltage limiting and series boost regulators could be used or these functions could be combined in a buck-boost regulator similar to that illustrated in Figure 4-83.

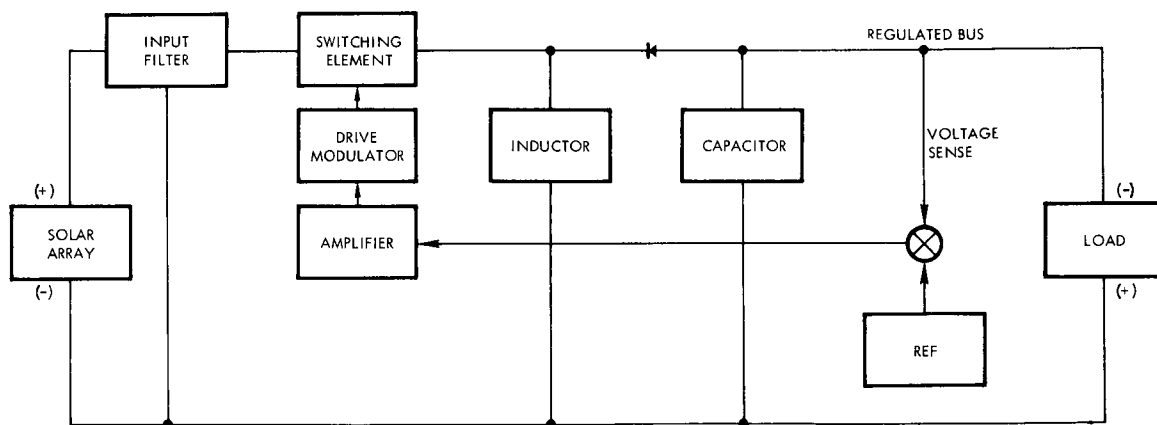


Figure 4-83. Switching Buck-Boost Voltage Regulator

For the dual regulator approach, the shunt voltage limiter can be designed to operate only when excess array capability exists in orbit at the higher array voltage. The magnitude of the required shunt dissipation is drastically reduced as a result of the lower array current capability at Mars. The boost regulator will operate to maintain the bus voltage until such time as the array voltage capability increases to above approximately 52 volts with a given load. This value allows for the

array isolation diode drops and the series diode drop of a boost regulator at high input voltage. At this condition, the losses in the boost regulator are minimal. At lower input voltages (nearer 1 AU), the boost regulator losses are higher; however, the array capability under these conditions is much larger than required.

Referring to Figure 4-83 for the buck-boost regulator, the output voltage is related to the input voltage, by  $t_{on}/t_{off}$ , where  $t_{on}$  and  $t_{off}$  are the power switch on and off times, respectively. At a 50-per cent duty cycle, the voltages are equal ( $t_{on} = t_{off}$ ). With  $t_{on} > t_{off}$ , the circuit boosts and conversely, bucks with  $t_{on} < t_{off}$ . The major disadvantages in this type of regulator when compared to buck only or boost only, switching regulators, are the reversed polarity output (a disadvantage for some applications) and the lower efficiency obtainable over a variable input voltage range. Figure 4-84 shows a typical efficiency versus input voltage characteristic for a 20-watt regulator. Further increase in input voltage beyond 40 VDC results in decreasing efficiency.

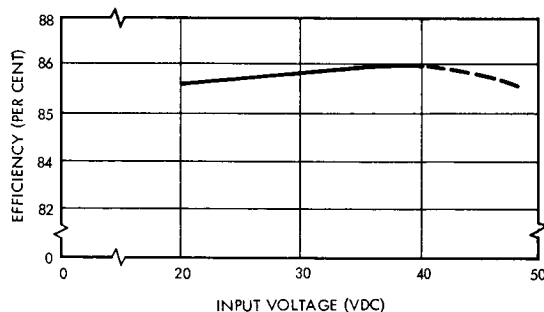


Figure 4-84.  
Buck Boost Regulator Efficiency  
Versus Input Voltage

Further analysis of solar array characteristics using increased back surface emissivity (0.85) has shown the maximum 1-AU voltage at maximum 1.67-AU load current to be much closer to the end-of-life maximum power point. These relationships are shown in Figure 4-85. The higher emissivity will produce lower array temperatures in eclipse; however, this is considered a less serious penalty than the increased system complexity associated with boost voltage regulation of the solar

array. In addition, the higher panel emissivity is required to comply with the maximum  $\alpha/\epsilon$  limit of 0.5 imposed by the mission specification. The shunt regulator alone, as a result, can provide for solar array control throughout the mission with negligible loss of array capability at 1.67 AU. From Figure 4-85 assuming a continuous load requirement of 0.025 ampere, the solar array voltage must be limited to 0.440 volt per series solar cell. The end-of-life maximum power point voltage by comparison is 0.461 volt per cell. The net loss in power capability at 1.67 AU resulting from this approach is approximately 2 per cent.

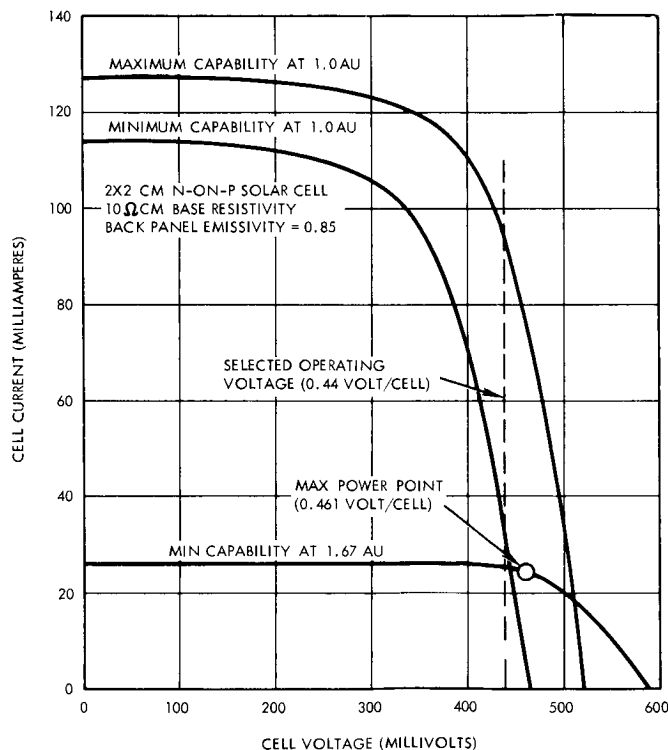


Figure 4-85. Revised Solar Cell Current-Voltage Characteristics

These solar array characteristics also permit consideration of a series bucking voltage regulator in lieu of the shunt voltage limiter. A constant frequency pulse width modulated (PWM) regulator is illustrated in block diagram form in Figure 4-86. The output voltage is related to input voltage by  $t_{on}/T$ , where  $t_{on}$  is the on period of the switch and  $T$  is the drive period. The advantage of this type of control is the high

efficiency obtainable, in comparison with dissipative regulators. Loop stability can be a problem unless the control amplifier time constant is made large, in which case the regulator frequency response suffers when compared to that attainable in dissipative type controls. Peaking of the output impedance over a certain range of frequency, is another characteristic typical of this class of regulator. For larger power requirements and with wide input voltage swings filter requirements may be prohibitive on a size and weight basis. Operation at a higher power switch drive frequency reduces the filter size requirements for a given output ripple but an upper limit of approximately 20 KC in medium power units (30 watts) is imposed before switching losses in state of the art device switching elements become excessive. Figure 4-87 shows a typical efficiency versus input voltage characteristic for this type of regulator. In this plot, the power switch duty cycle is approximately unity at  $E_{in} = 20$  V.

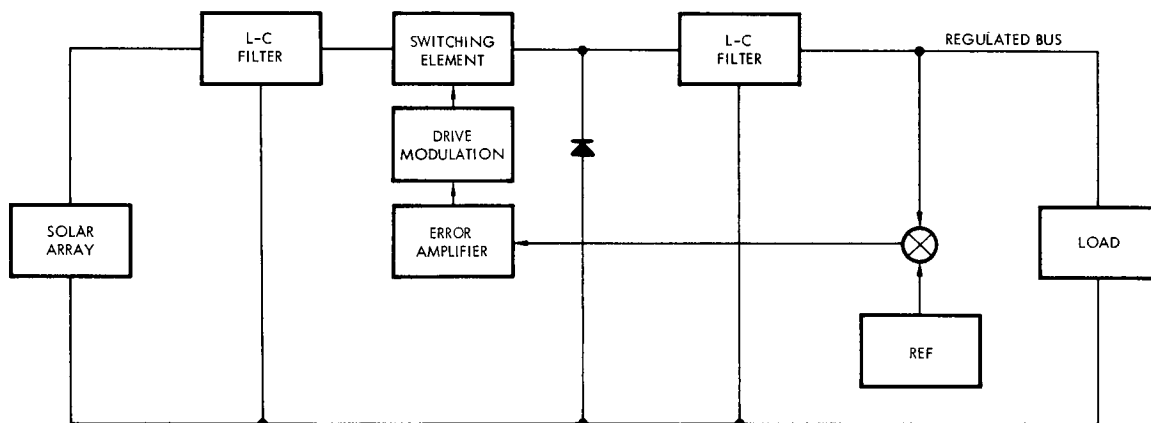


Figure 4-86. Pulse Width Modulated Series (Buck) Regulator

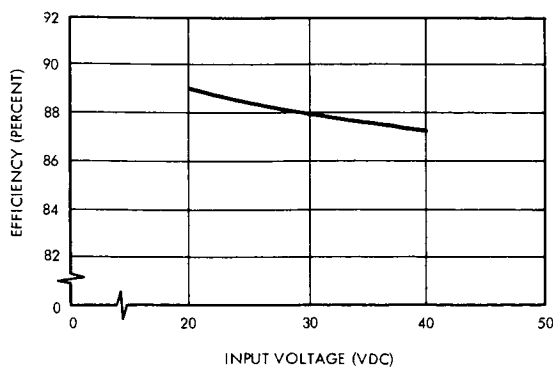


Figure 4-87.  
Typical PWM Series  
Regulator Efficiency  
Versus Input Voltage

The large shunt regulator power dissipation possible at 1 AU with the maximum possible solar array characteristic shown in Figure 4-85 and a dissipative shunt regulator led to additional analysis of design concepts to reduce power dissipation in the shunt elements. It is highly desirable to locate all control elements within the bus. A maximum shunt dissipation of 100 watts was assumed to represent the upper limit compatible with the spacecraft thermal control system.

Switching array sections in response to load requirements offers a basically nondissipative method of array control. Both series and shunt switching regulators are feasible (reference Figure 4-88 and Figure 4-89). The regulator senses bus voltage and switches additional sections of array on (i. e., connected to the bus) when bus voltage decreases below a lower limit, and switches sections off when voltage exceeds an upper limit. Both limits are selected within the bus regulation requirements and could be restricted by maximum allowable bus voltage noise (see Figure 4-90). Limit cycling occurs when the smallest array increment causes a bus voltage variation exceeding the decision

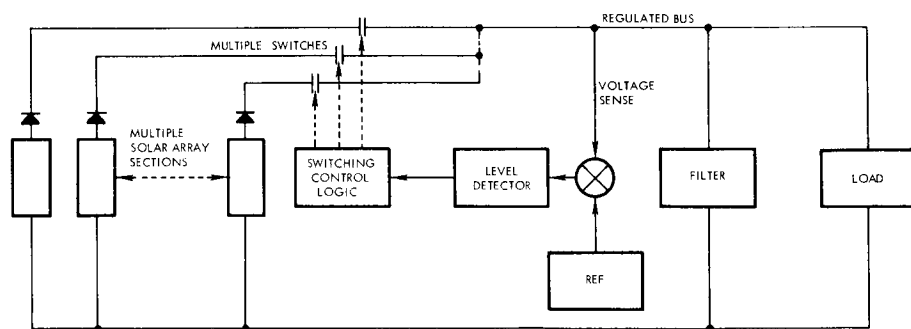


Figure 4-88. Switched Solar Array Scales Regulator

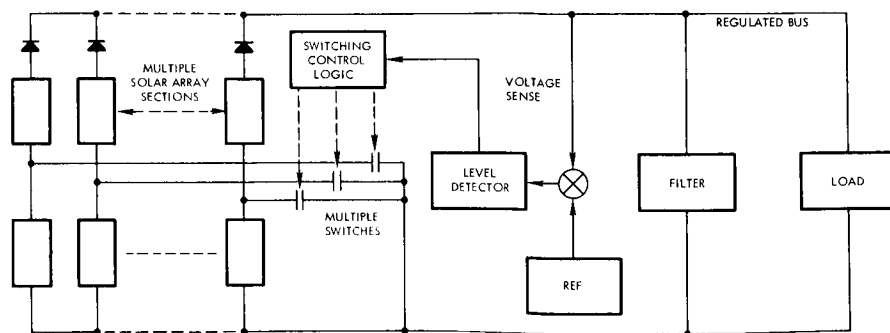


Figure 4-89. Switched Solar Array Shunt Regulator



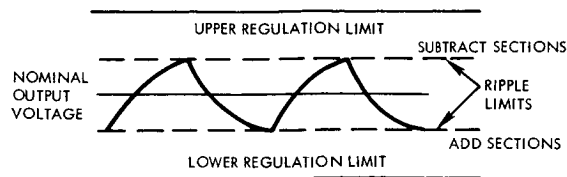


Figure 4-90.  
Switched Solar Array Limits

levels. Limit cycling rate is a function of array increment size ( $\Delta I$ ), and regulation tolerance and inversely related to load bus filter capacity. To gain close control of the array and reduce limit cycling, many array sections are required with resulting complicated controls, large number of switches and attendant wiring problems.

Figure 4-91 shows a block diagram of a combination tapped-array, dissipative shunt control and switched array control. Speed of response to load and solar array variations is greatly improved and limit cycling is eliminated. The shunt controlled array section can be sized to be compatible with the spacecraft thermal capability. The system is still limited in response to large transients and is relatively complex because of the switching control and logic required. Figure 4-92 shows one method of sensing and establishing the decision points for switching array sections on or off. For stability, i. e., no limit cycling, the maximum switched section current must be less than the current change between decision levels.

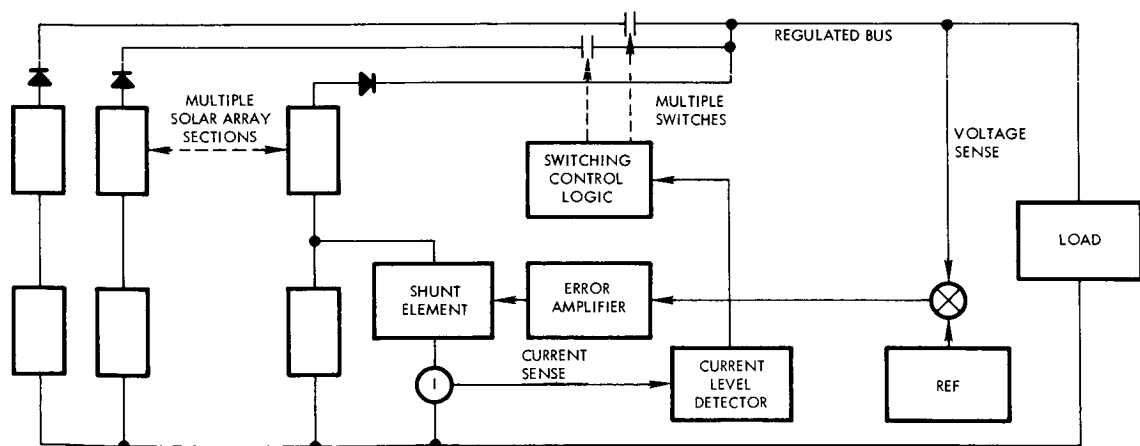


Figure 4-91. Combined Dissipative Shunt and Switched Solar Array Regulator

\*This page contains information proprietary to TRW, Inc. and shall not be reproduced or disclosed to others without the prior written permission of TRW, Inc.

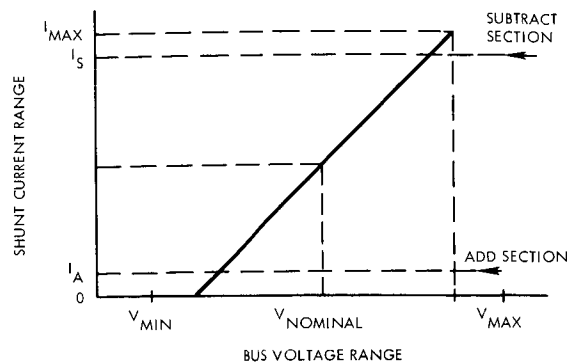


Figure 4-92.

Solar Array Switching  
Control Decision Points  
(Combined Shunt and  
Switched Array)

Figure 4-93 shows a tapped array shunt regulator which performs closely to the shunt plus switched control previously discussed. Each controlled section transconductance is linear between zero and short circuit array current. Combined transconductance of the total regulator is large enough to saturate the total array with the bus voltage error signal within regulation tolerance limits. Each section is controlled at a different effective error signal voltage so that only one power amplifier is linearly conducting at a time. All other sections are either off (non-conducting) or saturated. Base drive current limiters are utilized to limit drive current after each power amplifier saturates. Reduced overall drive power dissipation results from an additional tap, above the power amplifier tap point, which supplies drive current at a voltage significantly less than bus voltage. Array operating points are indicated in Figure 4-94. Section 1 is unregulated supplying load current, Section 2 is proportionately regulated, and Sections 3 through n are saturated to supply no load current. This sequential shunt approach is considered best suited to the Voyager application for shunt voltage limiting of the solar array (see Table 4-40). Comparison of systems using both shunt and series regulation are included in Section 3.2.2.

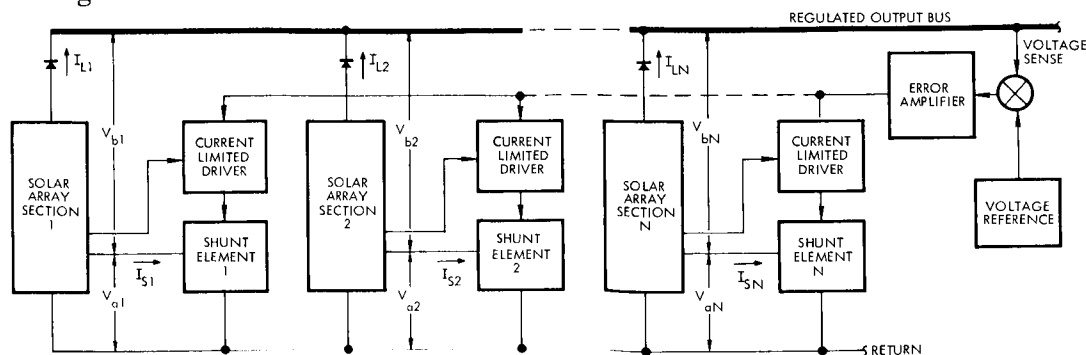


Figure 4-93. Tapped Array Sequential Shunt Regulator

\*This page contains information proprietary to TRW, Inc. and shall not be reproduced or disclosed to others without the prior written permission of TRW, Inc.

Table 4-40. Comparison of Solar Array Control Schemes

Type	Reference/ Figure	Advantages	Disadvantages
Full Shunt Regulators:			
1) Zener Diodes		Simplicity	Poor regulation Poor reliability
2) Power Amplifier	4-78	Close regulation. Can be made highly redundant	Large power dissipation
3) Power Amp and Resistors	4-81	Same as 2) except most dissipation in resistors	Large power dissipation
4) PWM Buck-Boost	4-83	Permits bus voltage selection independent of 1 AU array characteristic - Low dissipation	Reduced response Increased complexity
Partial Shunt Regulators:			
5) Power Amplifier	4-80	Same as 2) with reduced dissipation	Although less than 2) dissipation still large
6) PWM switch and Resistors	4-82	Power dissipation in resistors	Reduced response Increased complexity
Switched Solar Array	4-88 4-89	No shunt dissipation Inherent redundancy in switching elements	Wiring complexity Reduced response
Switched Array and Partial Shunt	4-91	Less dissipation than 5) Can be made highly redundant	Control complexity Reduced response
Sequential Partial Shunt	4-93	Least dissipation of non-switching types. Inherent redundancy	Requires two taps per array section
PWM Series Regulator	4-86	Same as 4)	No protection against overvoltage. Reduced response. Increased losses at end-of-life.

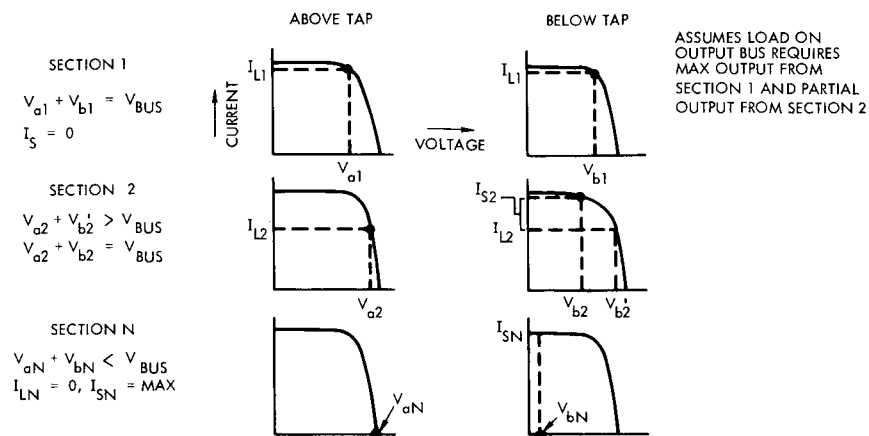


Figure 4-94. Sequential Shunt Regulator Operating Conditions

Based on the sequential shunt regulator concept described above, the maximum possible dissipation in the shunt element assembly for the Voyager system is calculated below:

The maximum possible shunt dissipation occurs under the following conditions at 1 AU:

- a) Maximum solar array capability (see Figure 4-85)
- b) Load requirement just slightly higher than maximum capability of two array sections.

Under these conditions, the third solar array section is just beginning to supply load current. Its shunt element, therefore, is operating at a high current to maintain the required 50-volt output and also, because of the relatively low voltage capability of the array, at a relatively high voltage (18 volts). The remaining nine shunt elements will be maintained in a saturated condition because of the large error signal resulting from the excess array capability at this point. Further load increases will cause the shunt dissipation on the third section to decrease as that section of the array delivers additional load current. The calculated peak power dissipation for the controlling section is 62 watts including shunt driver power losses. The dissipation of each saturated shunt element is 6.5 watts again including drive power losses. This produces a total shunt elements assembly peak dissipation of 121 watts for this

worst-case condition. It should be noted, however, that the probability of achieving this maximum solar array capability and a concurrent worst-case load condition is remote. Any reduction in solar array output or deviation from the worst-case load condition will reduce the shunt dissipation. For thermal analysis, the maximum steady state dissipation is estimated to be 100 watts.

### 3.5 Power Conditioning Equipment

Any design of an electric power system must begin with the characteristics and requirements of the loads which it services. Spacecraft loads generally vary in their voltage and regulation requirements; noise, ripple and transient sensitivity; noise and transient feedback; isolation requirements; and impedance. In addition, some equipment, because of a requirement for high or low voltages, multiple voltage levels, alternating current, or other special needs, must be excluded from any central distribution system.

The Voyager power conditioning equipment must distribute power in the range of 80 to 440 watts, at several closely regulated ( $\pm 2$  to  $\pm 4$  per cent) DC voltage levels (Table 4-33). Tightly regulated ( $\pm 0.5$  per cent) high DC voltage outputs, supplying power in the range of 60 to 70 watts, are required for traveling wave tube operation. Low power (5-50 VA), 400-cps and 800 cps AC power is required for operation of gyros and motor drives. Synchronization of conversion equipment to CS and C signal is a further requirement. Approximately 300 watts of unconditioned DC power is required for thermal control heaters and the flight capsule.

Several schemes exist for delivering power conditioned so as to be compatible with the electrical characteristics of the loads. Overall power system efficiency, weight, reliability, and complexity are influenced by the choice of a particular scheme and its interaction with other power system elements. For the requirement of supplying multiple, regulated DC output voltages from a basic unregulated primary DC power bus, the functions of regulation, inversion, transformation, rectification, and filtering are all required for the over-all power conversion process.

Figure 4-95 shows an inverter-output regulator approach. In this scheme, a driven square wave inverter provides unregulated AC to individual rectifier-filters and output regulators. Regulation can be accomplished with dissipative type regulators, with switch-modulated type regulators, or by controlled rectification techniques, the last indicated in Figure 4-95 for output 3. For the Voyager requirements, this approach has several disadvantages relating to efficiency and/or reliability. The use of dissipative regulators at each output involves considerable power loss, especially with an unregulated input line. This disadvantage must be weighed against the fast regulator loop response possible with dissipative regulators. Regulators employing switch modulation or duty cycle control, although yielding high efficiency in individual output regulators, generally entail greater circuit complexity than is obtained with dissipative regulators. Loop performance also suffers in comparison with dissipative regulators because of the necessity for L-C filtering in the regulator loop.

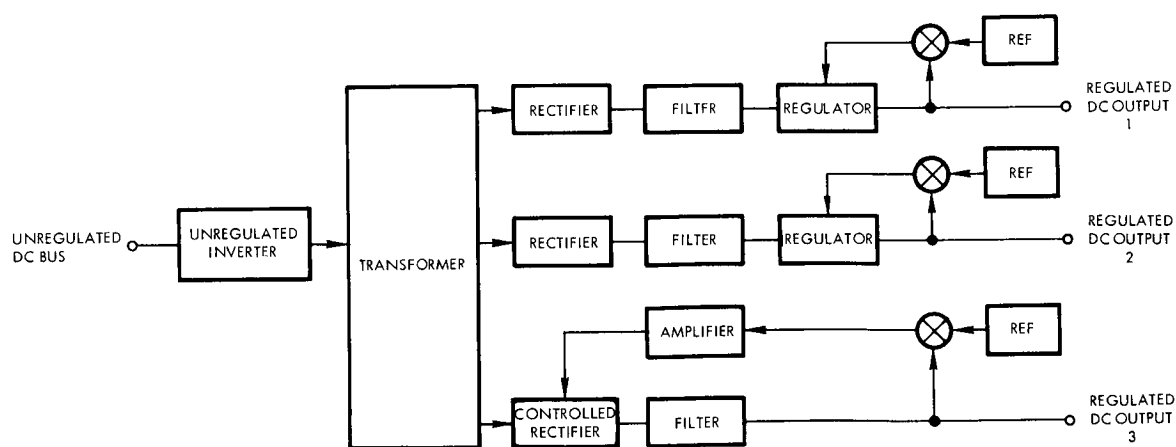


Figure 4-95. Power Conversion System Inverter-Output Regulation

Figure 4-96 shows a DC-to-DC converter scheme where preregulation of the bus voltage is performed before inversion and output rectification. A synchronized or free-running clock oscillator can be utilized to provide drive for the inverter as well as the time base for modulating the input switching regulator. For a multiple output configuration, the sensing or control point can present disadvantages. If the highest rated load voltage is sensed to derive the regulator error signal, the remaining outputs, while regulated against input line variations, will not be compensated for variations in output resulting from changing loads and temperature effects on output rectifier circuitry. An additional problem with the approach of Figure 4-96 is the loop stability compensation required because of the additional filter within the regulating loop. If the sense point is provided at the regulator output, load regulation is not provided at any DC output. A further disadvantage in this scheme, especially at high power levels, is that the preregulator must handle all the input power. Efficiency suffers in that power is lost in effectively two series switching elements, the preregulator transistor switch and inverter switching element. The averaging filter requirements also become severe at higher power levels, with a consequent penalty in size, weight and efficiency.

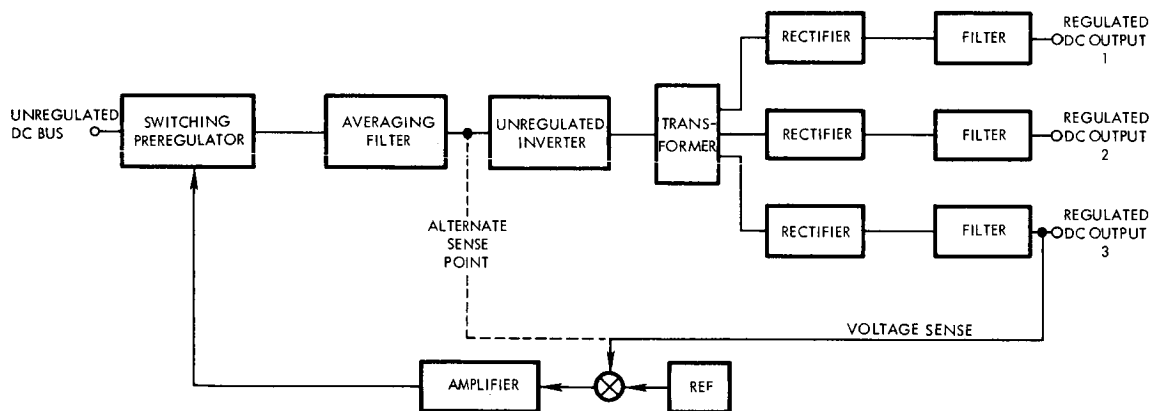


Figure 4-96. Power Conversion System, Preregulation Conversion

Another scheme for multiple-output, DC-to-DC conversion, is shown in Figure 4-97. Regulation is accomplished within the inverter stage by means of pulse-width control of the inverter base drive. This arrangement has higher efficiency than the configuration of Figure 4-96, primarily because the regulator is not an inline function in the power flow path. Other advantages are the relative circuit simplicity and easily controlled loop stability. Loop response, though, again suffers in comparison with dissipative regulators. The same disadvantages, relative to sensing with multiple outputs also apply in this case. Output rectifier filter requirements are increased in comparison to the previous cases because the inverter output is a variable-width chopped square wave. The worst case occurs with a high input line condition and light load.

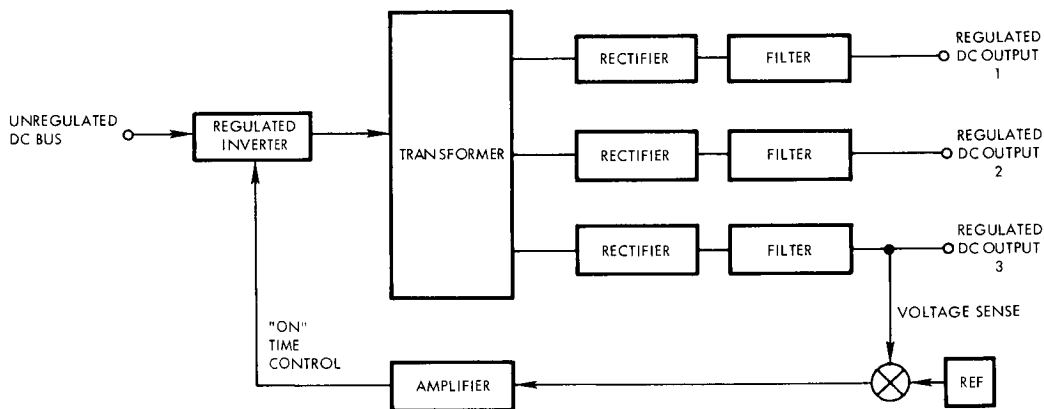


Figure 4-97. Power Conversion System, Combined Inversion and Regulation

A variation to the system configuration of Figure 4-96 is shown in Figure 4-98. In this system, the inverter distributes alternating current power to a number of transformer-rectifier (T/R) units which, in turn, supply the various loads. The units can be installed with the using equipment. Sensing for the switching preregulator is derived at the inverter input. Only those loads requiring regulation greater than provided need have individual output regulators.



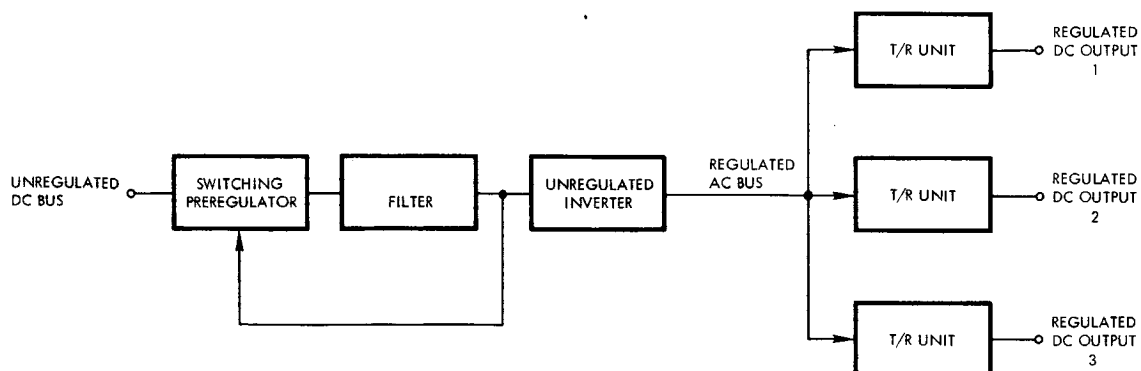


Figure 4-98. Power Conversion System, AC Distribution

The choice of a particular configuration to operate from an unregulated primary power bus depends greatly upon the number of DC outputs, their individual power levels and regulation requirements. If low output voltages are required at significant power levels, the power loss in the output rectifiers alone will result in a severe efficiency penalty and limit the choice of conditioning method to that yielding the least additional loss. Figure 4-99 shows a typical characteristic relating efficiency of transformer-rectifier units to output voltage.

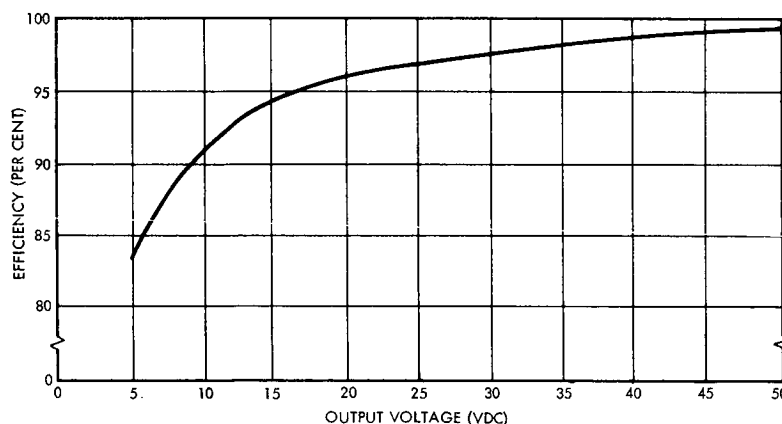


Figure 4-99. Transformer-Rectifier Unit Efficiency Versus Output Voltage

Operation of a power distribution and conditioning system from a regulated primary power yields a system of the simplest and most efficient form. This is the system of Figure 4-100. An unregulated, single-phase inverter, provided with primary power regulated to  $\pm 1$  per cent by the power source controls, distributes square wave AC to multiple transformer-rectifier units supplying individual loads. The AC output variation would be limited to  $\pm 2$  per cent with changing loads

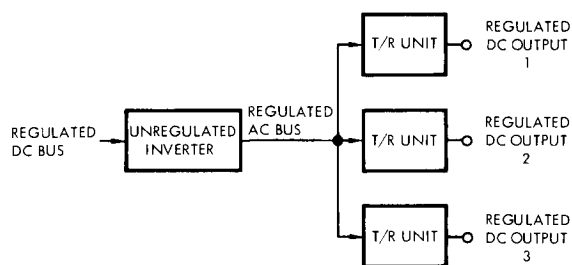


Figure 4-100.  
Selected Power Conversion System

and environment. Regulation of individual DC outputs would probably be in the order of  $\pm 4$  per cent without further compensation. Output regulators would be required for those outputs needing additional regulation. For the specific case of the communications power amplifiers, the high DC voltages required prevent using a T/R unit with output regulators. This load is supplied, therefore, through a separate regulated DC-DC converter directly from the main DC bus. The approach is selected for the Voyager application on the basis of its simplicity, efficiency and the fact that the power system is less dependent on individual load equipment characteristics.

The required  $\pm 1$  per cent main bus voltage regulation required by this approach is provided by the solar array and battery controls. The basic requirement for power source regulation stems from the susceptibility of the battery and electronic parts to damage from overvoltage and from the inefficiencies and increased current handling capability in power conditioning and load equipment which result from low voltage operation. Providing the capability in these regulating functions to maintain close bus regulation does not penalize the system with respect to reliability, efficiency or weight. The selected nominal bus voltage is 50 VDC which represents a reasonable compromise between maximum current handling capability and component voltage ratings.

The electrical, mechanical, and thermal design of power-conditioning equipment for spacecraft power systems involves a compromise among such major requirements as efficiency, input source characteristics, electrical performance (quality of output power), RFI reduction, and physical characteristics (weight, size, etc.). Tradeoff studies of the various types of power conditioning and control circuits were performed to provide a basis for selection of the optimum circuit configurations for Voyager power system requirements.

When evaluating a power conditioning scheme for efficiency, other important parameters such as weight, volume, reliability, frequency, power and voltage levels must be considered. Generally, increased efficiency is obtained at the cost of weight and reliability. Redundant converters, for example, can mean inefficiency since standby losses for the redundant units must be supplied.

The weight-efficiency tradeoff is illustrated in Figure 4-101. Here the weight of a single-phase, unregulated inverter is plotted as a function of unit efficiency. Although Figure 4-101 shows a minimum at an efficiency of 78 per cent, the power source weight penalty associated with low efficiencies for Voyager power levels dictates the choice of a higher efficiency, heavier inverter.

The size, weight, and efficiency of converters or inverters which supply power to spacecraft loads depend, in part, on the magnitude of inverter input voltage and the operating frequency or switching rate of inverters.

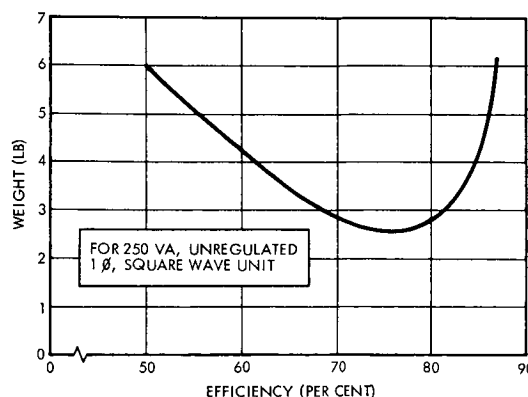


Figure 4-101.  
Typical Single Phase  
Inverter Weight Versus  
Efficiency

In unregulated units, the higher the input source voltage the lower is the current required by inverter transistors and transformers, resulting in lower weight and power dissipation. An input bus voltage of approximately 50 volts yields minimum inversion loss (series drops in the transistor and transformers are less significant) and lower weight (less transformer copper is required) without compromising transistor collector voltage ratings in presently available silicon power units.

Figure 4-102 illustrates the variation of efficiency with input voltage in regulated and unregulated inverters.

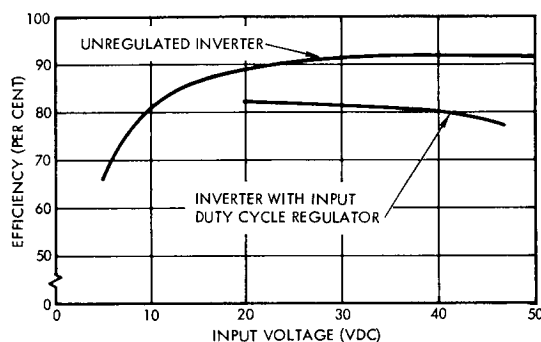


Figure 4-102.  
Inverter Efficiency  
Versus Voltage

For regulated inverters or converters, designed to operate down to a particular input voltage when connected to a variable bus, the efficiency decreases at higher input voltages, depending on the specific circuitry used to provide regulation. For series dissipative-type regulators, efficiency and input voltage are inversely related, however, for inverters or converters utilizing input duty-cycle regulators, the decrease in efficiency with increasing input voltage is not as significant.

Frequency-sensitive components, such as transformers, inductors, and filter capacitors, are made smaller with increased frequency of operation. Figure 4-103 illustrates the reduction in weight of transformers with increase in operating frequency. Losses associated with these components, on the other hand, increase. Also semiconductors used as switching elements become less efficient at higher frequencies. With present power semiconductors, inverters with ratings in the 200-

300 VA range operating at switching frequencies of 4 to 5 kc are available. The variation of efficiency with load for an unregulated, current-drive controlled, 4.1 kc inverter rated at 300 VA, is illustrated in Figure 4-104.

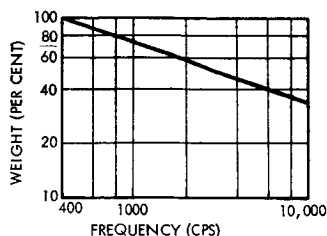


Figure 4-103.  
Relative Weight of Transformers as a Function of Frequency

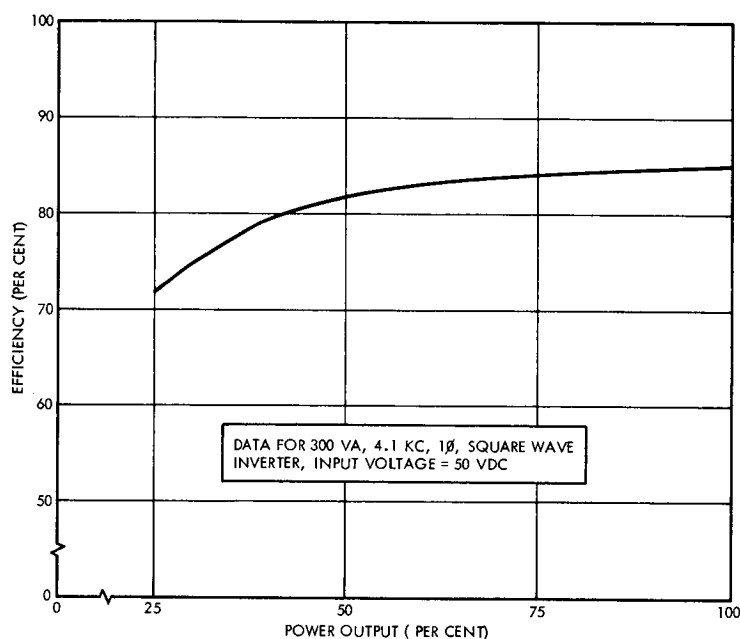


Figure 4-104. Unregulated Inverter Efficiency Versus Power

Figure 4-105 shows parametric data relating power requirements, frequency, weight and volume for unregulated single-phase, square-wave inverters. Weight increase with power rating is primarily a function of increase in inverter transformer size in the higher power ratings, at a given frequency and efficiency.

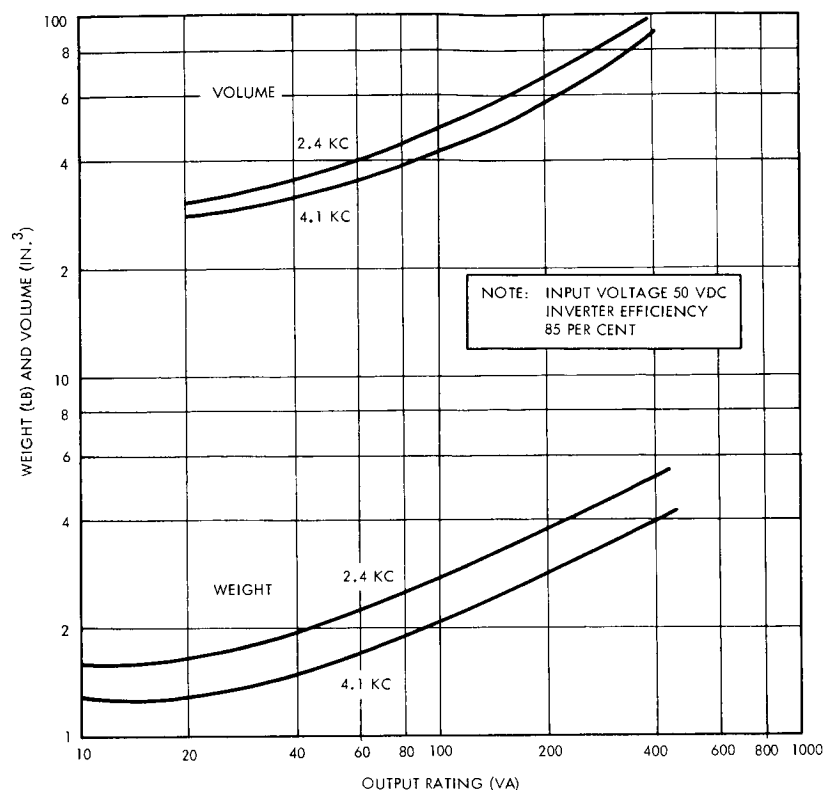


Figure 4-105. Unregulated Shunt Weight and Volume Versus Output Rating

Similar data on regulated DC-to-DC converters is shown in Figure 4-106 and it is indicated that efficiency tends to increase with output power. Figure 4-107 is a block diagram of the particular converter for which the data of Figure 4-106 was developed.

Spacecraft loads requiring low-power AC for gyro and motor drive controls are easily provided by efficient, light-weight square-wave inverters operating from a regulated DC bus. For Voyager, synchronized 400-cps power is required at a low average level (1 VA). A short-run inrush capability must be provided up to a maximum of approximately 50 VA. A single-phase inverter normally synchronized at 410 cps and designed to provide a free-running capability in the event of loss of the synchronization signal will have an efficiency versus load characteristic as depicted in Figure 4-108. This curve applies as well for inverters

that supply 800 cps two-phase power (synchronized to 820 cps). For Voyager, these requirements are approximately 6 VA under steady state conditions with short inrush levels of 27 VA. Conservative figures for weight and volume for the 410 and 820 cps units, respectively, are 3 pounds and 48 cubic inches and 2 pounds and 36 cubic inches. For two-phase motor control (POP and antenna drives), the inverter supplies one-phase and a phase-splitting capacitor is used for the other. An alternate drive scheme utilizes a two-phase oscillator circuit with phase-locking arrangements to eliminate the fixed phase power loss. The disadvantage in this approach is the additional weight that an additional transformer entails.

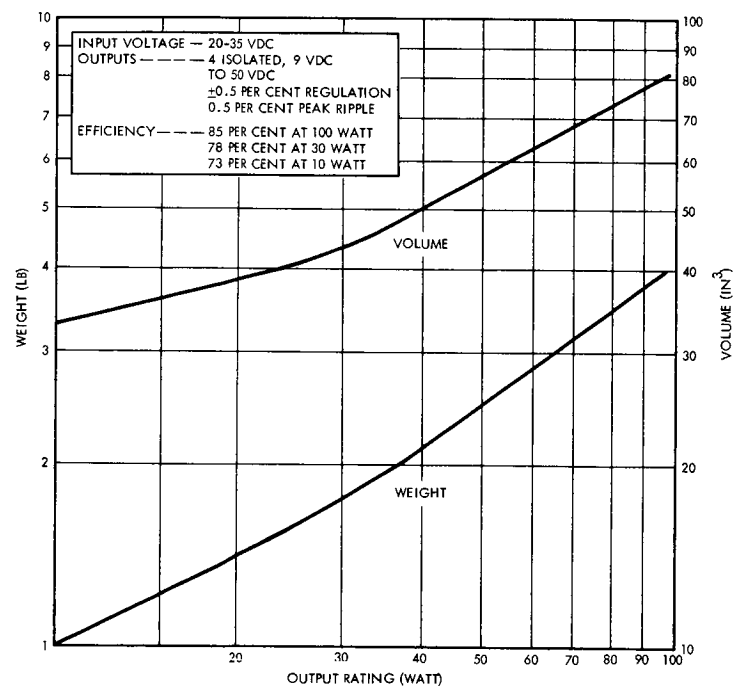


Figure 4-106. Regulated Converter Weight and Volume

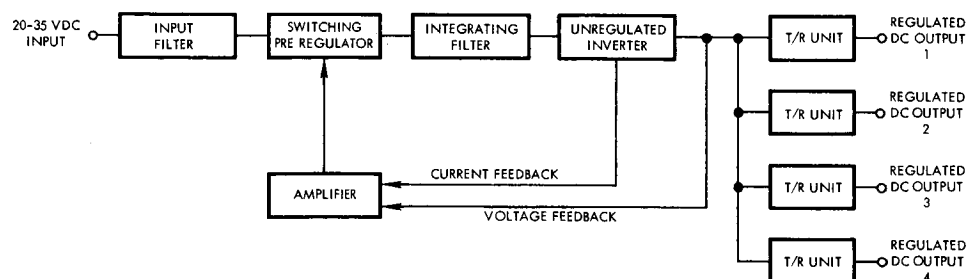


Figure 4-107. Regulated DC-DC Converter

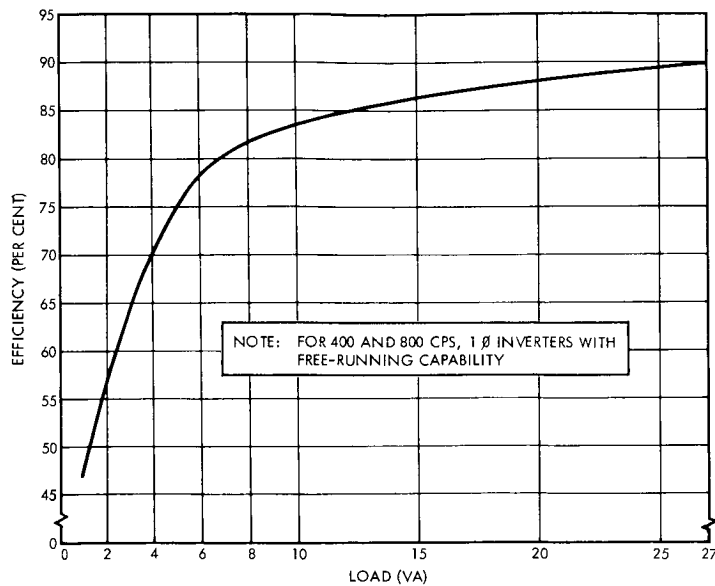


Figure 4-108. Unregulated Inverter Efficiency Versus Load

The tradeoffs leading to the selection of the Voyager power conditioning approach for the multiple DC loads are summarized in Table 4-41. The system provides regulated 50 VDC power for the conditioning inverters, communications power amplifier converters, thermal control heaters, RCS gas heaters and flight capsule. Three unregulated inverters are required to supply regulated ( $\pm 2$  per cent) AC voltages at nominal frequencies of 4.1 kc, 410 cps and 820 cps respectively to the spacecraft loads. The 4.1 kc power is further conditioned by T/R units as necessary within the load equipment to provide the required DC voltages. Each of the inverters provides power to essential loads. Redundant units are employed in each case to assure a high probability of mission success. To minimize system power losses, sequential redundancy is selected in preference to parallel operation of the inverter pairs. Switching from main to standby inverters is provided by redundant sensing and control circuits to maximize the reliability of these automatic functions.



Table 4-41. Comparison of Power Conditioning Approaches

Power Conditioning Approach	Input	Regulation	Output	Conditioning in Load Equipment	Major Advantages	Major Disadvantages
DC - DC Converters	40 VDC +25 per cent	Series input, inv. PWM, and/or output regulator	Multiple +2 per cent DC voltages	Minimal	Permits combining similar requirements to reduce number of converters	Multiple DC feeders. Sensitive to changes in power characteristics of loads
	50 VDC +1 per cent	Output Regulator	Multiple +2 per cent DC voltages	Minimal	Same as above and less complex due to reduced regulation	Same as above
DC - AC Inverters	40 VDC +25 per cent	Series input or inverter PWM	Single +2 per cent voltage	T/R units	Less sensitive to load characteristics Single AC distribution bus	Requires T/R unit for each load
	50 VDC +1 per cent	None	Single +2 per cent AC voltage	T/R units	Same as above and less complex due to elimination of inverter regulation requirements	Same as above
None	40 VDC +25 per cent	None	40 VDC +25 per cent	DC-DC Converters with series, inverter, and/or output regulation	DC-DC Converter, in-DC distribution bus	Least efficient approach. Increased quantity of electronic components and load equipment weight.
	50 VDC +1 per cent	None	50 VDC +1 per cent	DC-DC Converter with minimal output regulation	DC-DC Converter with less complex converters in loads	Low efficiency. Electronic components and weight penalties

### 3.6 Battery

#### a. Silver-Cadmium versus Silver-Zinc Cells

In addition to initial launch to acquisition, midcourse and injection maneuvers, the Voyager battery is required to supply power during eclipses in Mars orbit. For the nominal case of 2000 km periaapsis, 20,000 km apoapsis and 45 degrees orbital inclination to the equator, about 140 orbits will encounter eclipses during six months of orbital operation. The number of eclipsed orbits may vary between 50 to 500 for apoapsis of 10,000 to 30,000 km.

Although nickel-cadmium batteries are well proven for long cycle life in space, they are not acceptable for this application because of their undesirable magnetic properties. The choice of battery type is thus limited to silver-cadmium and silver-zinc.

The cycle life of presently available silver-zinc cells is limited by the irreversibility of the negative electrode and by the tendency of the cell to evolve hydrogen gas from the negative electrode, spontaneously and during charge. Figure 4-109 shows the relationship between estimated cycle life and depth of discharge for both silver-zinc and silver-cadmium cells. At the present time, the data indicate that the maximum useful depth of discharge of sealed silver-zinc cells for cycle life in the range of 100 to 200 cycles is between 20 and 30 per cent, whereas depths of discharge of 80 per cent or more can be obtained using silver-cadmium cells.

Recent work based upon the use of inorganic separators suggests that greatly increased cycle life is achievable with silver-zinc cells. These data are on unsealed cells of simple construction, however, and cannot be considered representative of silver-zinc battery technology for some time.

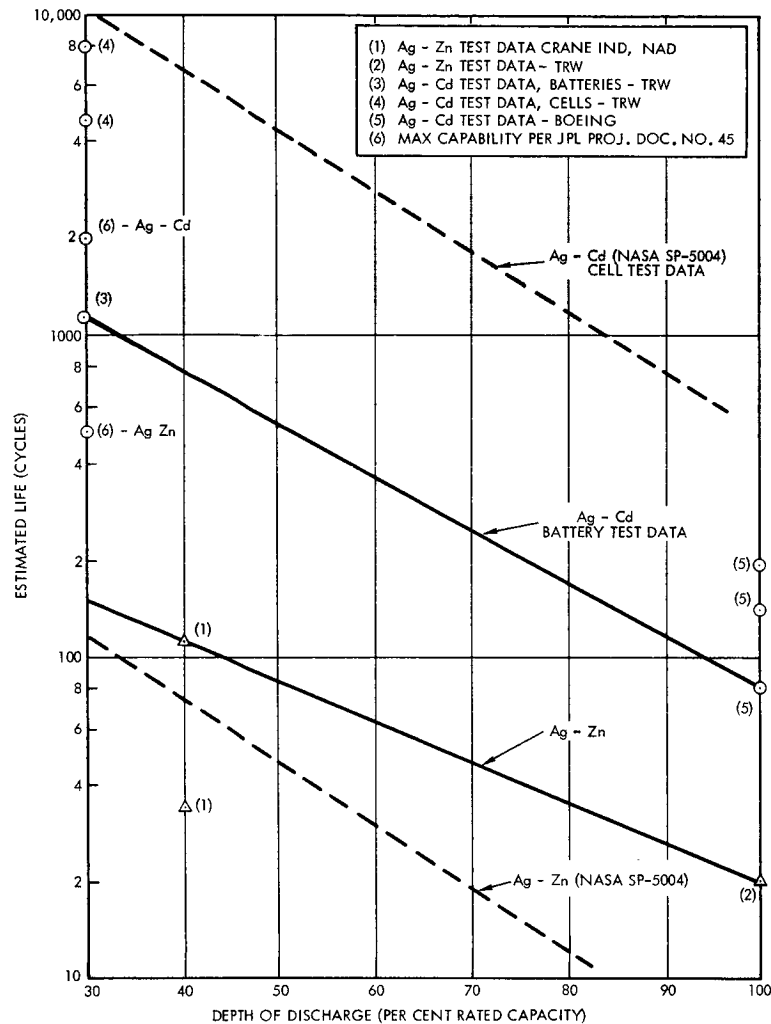


Figure 4-109. Battery Cycle Life Versus Depth of Discharge

Figure 4-110 shows the weights of 1650 watt-hour silver-zinc and silver-cadmium batteries as a function of the number of eclipse cycles required, based upon the useful depth of discharge from Figure 4-109. In all cases, depth of discharge is arbitrarily limited to 90 per cent, regardless of the number of cycles.

Based upon the nominal case, in which approximately 150 total cycles of operation are required, silver-cadmium batteries are the preferred choice using 1965-1966 battery technology. Such a decision is not irrevocable, however, since charge control and power system design will be essentially unaffected by the choice of battery, except in the selection of control parameter settings.

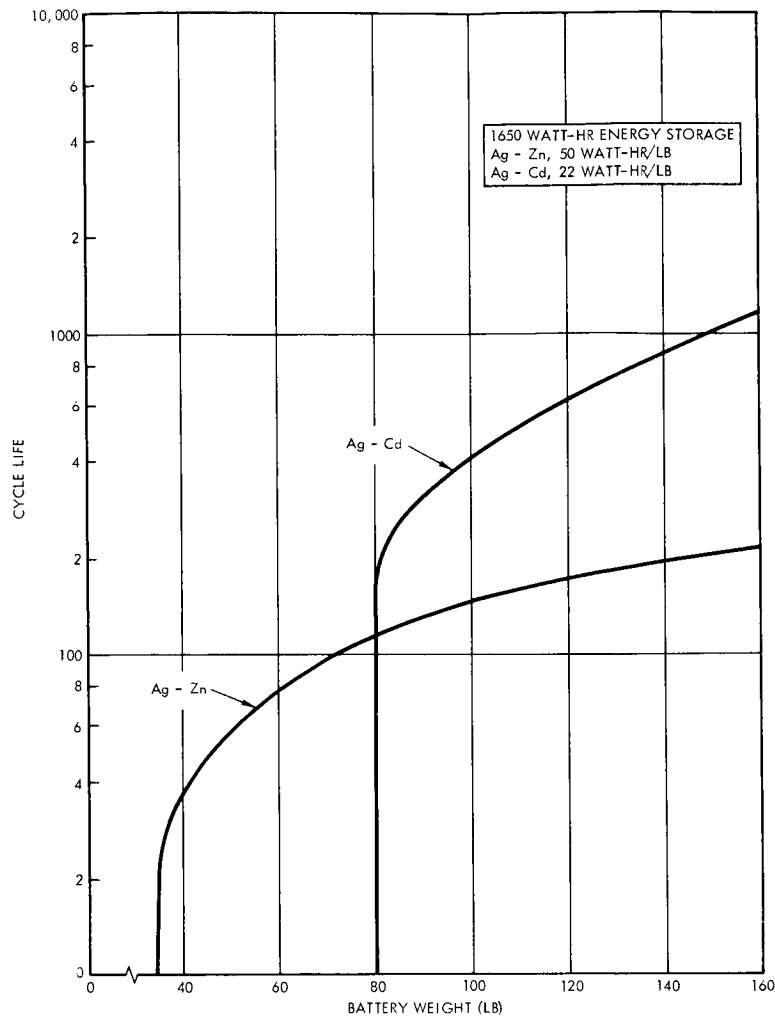


Figure 4-110. Battery Weight as a Function of Cycle Life Required

b. Battery Charge Control Requirements

Many of the difficulties experienced in the design of space power systems with silver-cadmium batteries are created by the problem of reliable battery operation with currently available charge control systems. The most critical properties of the silver-cadmium system which affect charge control methods are illustrated below:

Figure 4-111 shows typical charging curves and the effect of temperature upon cell voltages at constant current. Two features of the curves are significant. The peak voltage which occurs between first and second plateau presents a false indication of full charge if cell voltage is used as an indicator of full charge. This peak varies as a function of current and of temperature (Figure 4-112). Since gas generation tends to occur if charging is continued on beyond the second plateau, it is desirable to terminate the charge at, or near, the beginning of the rise in voltage from the second plateau. This requires compensation for temperature of the limiting voltage at which the charge controller is set. The compensation curve is that shown in Figure 4-113, and is valid only for the C/10 charge rate.

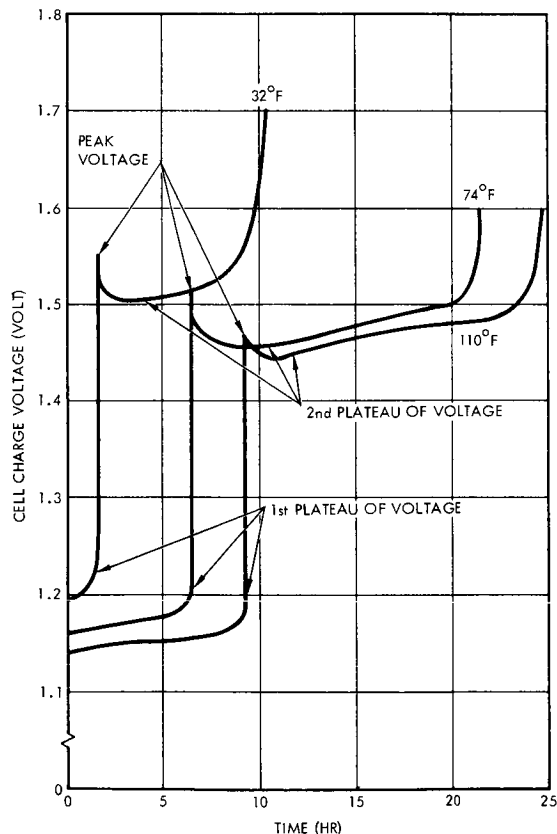


Figure 4-111. Silver-Cadmium Cell Typical Charge Voltage Versus Time as a Function of Cell Temperature

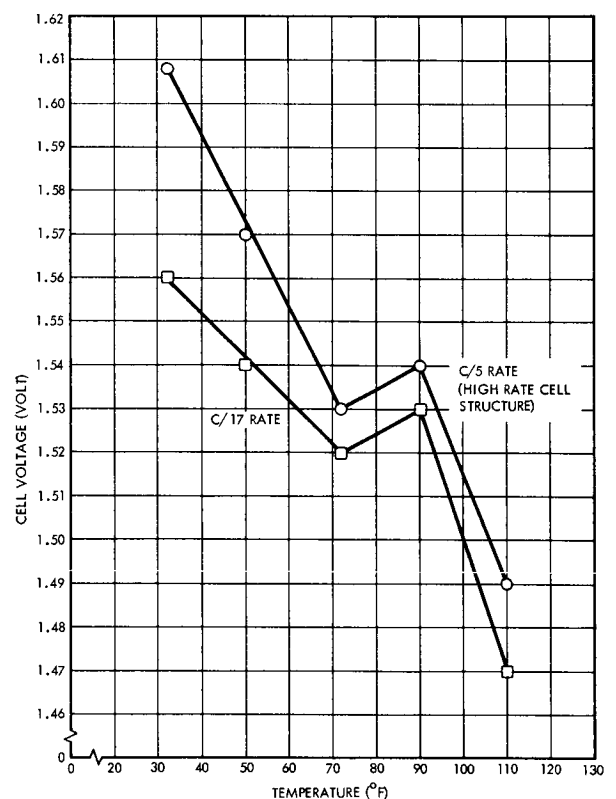


Figure 4-112. Typical Silver Cadmium Cell Data Peak Charge Voltage Versus Temperature

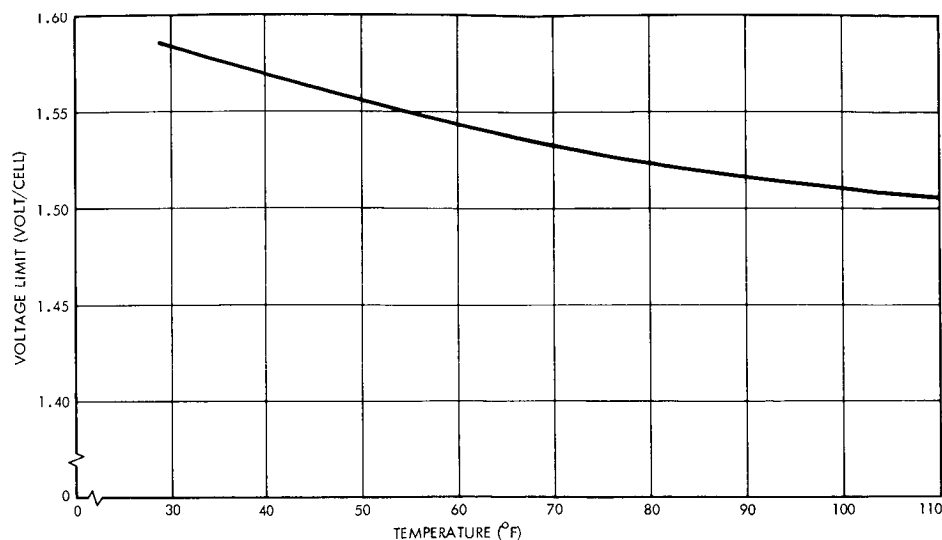


Figure 4-113. Silver-Cadmium Voltage Limit-Temperature Relationship, C/10 Charge Rate

By use of temperature compensation of voltage, it is possible to prevent premature failure of the cells due to overcharging and gas generation. It is clear from Figures 4-114 and 4-115 however, that the performance of the cell suffers greatly at the lower temperature and that it is not possible to achieve full capacity at the low temperatures even with temperature compensation of voltage. Thus, excess capacity must be installed unless battery operation can be maintained within a narrow temperature band between 70 and 100°F.

Pressure measurements made at TRW on silver-cadmium cells show that pressure rise occurs simultaneously with cell voltage rise so that a voltage limiting method can be effectively used to control internal pressure buildup.

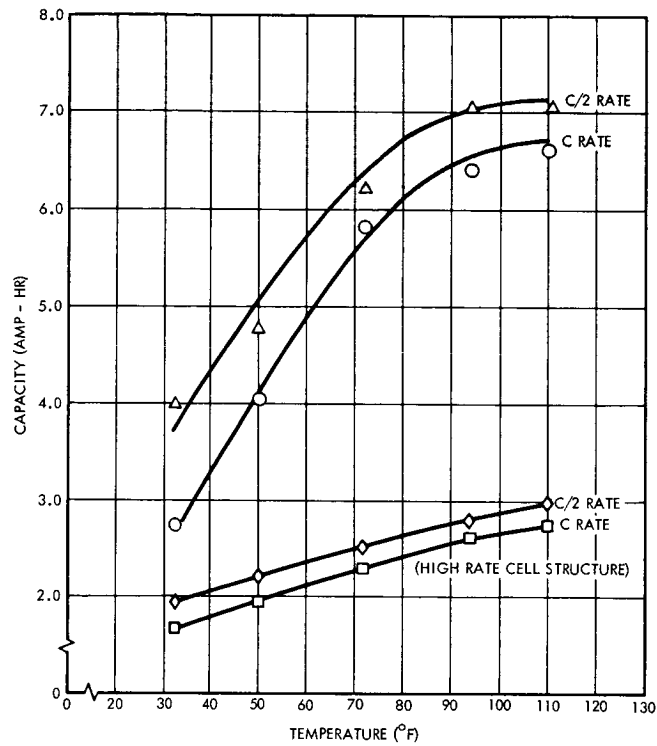


Figure 4-114. Typical Silver-Cadmium Cell Data Capacity Amp-Hr Versus Temperature as a Function of Current

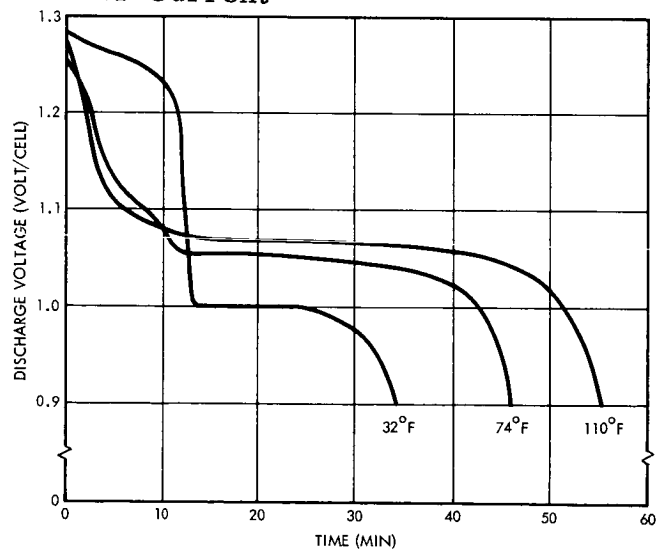


Figure 4-115. Discharge Voltage Versus Time as a Function of Temperature (Constant C Discharge Rate)

A major problem in charge control by measurement of total battery voltages is the tendency of the battery cells to deviate from one another in time of occurrence of the various voltage steps. Deviation increases as the battery ages. This can result in a loss of control and overpressure of one or more cells and premature battery failure. Cell tests have demonstrated the capability for 8000 plus cycles of operation at 30 per cent depth of discharge, whereas battery cycle life has been found to be 800 to 1200 cycles at 30 per cent depth of discharge in a 90-minute orbit. Based on this, the estimated equivalent life, at 95 per cent depth of discharge using cell level controls is approximately 500 cycles, and less than 100 cycles using battery level controls.

The optimum charge control system for silver-cadmium batteries is as follows:

- 1) Charge at constant current or full source output (not in excess of C/5), until the terminal voltage of any cell in the pack reaches a value between 1.50 and 1.60 volts which is a function of current and temperature.
- 2) Terminate charge until the cell voltage falls to a level approximately 100-mv below the charge termination level.
- 3) Resume charge. Cycle between 1 and 2.
- 4) If the battery temperature is above 110°F, do not charge.

The selected charge control system to implement these requirements for Voyager is discussed in Section 3.7.

c. Battery Design

Since loss of power during maneuvers constitutes a mission failure, redundant batteries are necessary for Voyager.

In normal operation, all loads are shared by two silver-cadmium batteries. With a 50-volt bus and a peak charge voltage per cell of 1.6 volts, a 30-cell battery permits use of a simple dissipative current



limiter for charge control. The average discharge voltage per cell is 1.1 volt, and the average discharge voltage for a 30-cell battery is 33 volts. A boosting voltage regulator is therefore required for battery discharge to maintain the 50-volt bus level.

The most critical design requirement is that each of the two batteries must be capable of supplying the essential loads if the other one fails. Examination of the load profile reveals that the maximum eclipse orbit (2.3 hours duration) requires the highest energy storage.

The essential load is 262 watts of battery discharge power, with science and reaction gas heater loads turned off. The discharge energy required is then 601 watt-hours. Allowing a maximum depth of discharge of 95 per cent, the required capacity per battery is therefore 633 watt-hours. The expected minimum Voyager battery temperature is 50°F. From Figure 4-114, a representative loss in capacity is 22 per cent below that of room temperature. The installed battery energy requirement is then  $633/0.78$  or 811 watt-hours. The corresponding capacity at 33 volts is 24.6 ampere-hours. The total installed capacity in the two batteries is therefore 50 ampere-hours, or 1650 watt-hours.

The normal depth of discharge under various battery discharge conditions and maximum load are given in Table 4-42. The depth of discharge numbers are for two batteries.

Table 4-42. Normal Depth of Discharge  
(maximum load)

Phase	Battery Power (watts)	Battery Energy (watt-hour)	Depth of Discharge (per cent)	Approximate No. of Cycles
Launch	225	340	21	1
Midcourse Maneuvers	402	804	49	4
Injection Maneuver	393	786	48	1
Orbital Eclipses	408	940	57	140

The estimated size and weight for each 25 ampere-hour, 30-cell battery are:

Dimensions	- 6 x 4 x 30 inches
Weight	- 40.2 pounds.

d. Conclusions

The basic battery cell selected for Voyager is a 25 ampere-hour sealed silver-cadmium cell. A total of 60 cells are used, divided into two identical batteries of 30 cells each. The total capacity is 50 ampere-hours, or 1650 watt-hours at an average battery discharge voltage of 33 volts. Battery temperature will be maintained between 50 and 90°F.

This battery design satisfies all spacecraft load requirements including:

- Launch to sun acquisition phase
- Midcourse and injection maneuver phases
- Eclipses during Martian orbits
- Various load peaks in excess of solar array capability.

In the event of a battery failure, the remaining unit is capable of supplying essential spacecraft loads.

3.7 Battery Charge-Discharge Control

Implementation of the desired charge-discharge method can be accomplished in several ways depending upon system bus voltage and battery characteristics. A system with regulated bus voltage higher than battery end of charge voltage will require a bucking regulator between bus and battery on charge and a boosting regulator between the battery and bus on discharge. A system with bus voltage lower than battery end of charge voltage will require a boost regulator for charging and a buck or buck-boost regulator for discharge depending upon whether battery end of discharge voltage is higher or lower than bus voltage. Both approaches are considered in the power subsystem comparisons covered in Section 3.2.2.

For either type system, constant current battery charging to an upper voltage limit is desired. Upon reaching this upper voltage limit, which must be compensated for battery temperature, the charge current is to be reduced to zero until the battery voltage decays to a preset lower voltage, at which time the charge current is resumed at a constant rate and the cycle repeats. This operation is depicted in Figure 4-116.

Outputs from a single cell level charge control (Figure 4-117) are utilized to switch the charge regulator on or off. Current feedback is utilized in the charge regulator to limit maximum battery current when charging. An input signal from the solar array regulator controls the charge regulator to assure that the bus voltage regulation and the load requirements are satisfied before battery charging can occur. In effect, this forces load requirements to be supplied before battery charging utilizes any available excess array power. A similar battery control method has been designed, built, and successfully tested at TRW.

An additional signal from the solar array regulator will control the discharge regulator. Derivation of these charge and discharge regulation signals from the solar array regulator allows a single reference and high-gain amplifier to regulate bus voltage both during charge and discharge. This prevents drift of regulation levels which could cause the discharge regulator to turn on while the array is being regulated. The solar array regulator can be made highly redundant through the use of majority voting logic or similar redundancy techniques.

a. Battery Charge Control

Based upon the battery charge control requirements defined in Section 3.6, a study was made of the relative applicability of cell and battery level controls. Table 4-43 shows the results of such a study.

Figure 4-118 is included to help visualize the TRW concept of proper battery control. The diagram is essentially a logic diagram of the desired sequence of charge and discharge. The charge control system recently developed and presently in operation at TRW is capable of accomplishing all of the solid-line functions shown. The new

---

\*This page contains information proprietary to TRW, Inc. and shall not be reproduced or disclosed to others without the prior written permission of TRW, Inc.

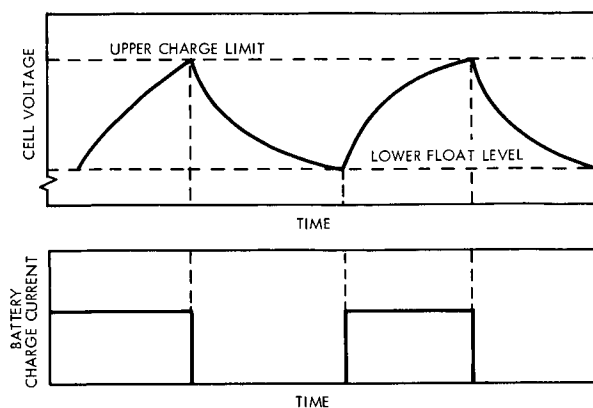


Figure 4-116. Charge Cycling Subsequent to Reaching Upper Voltage Limit

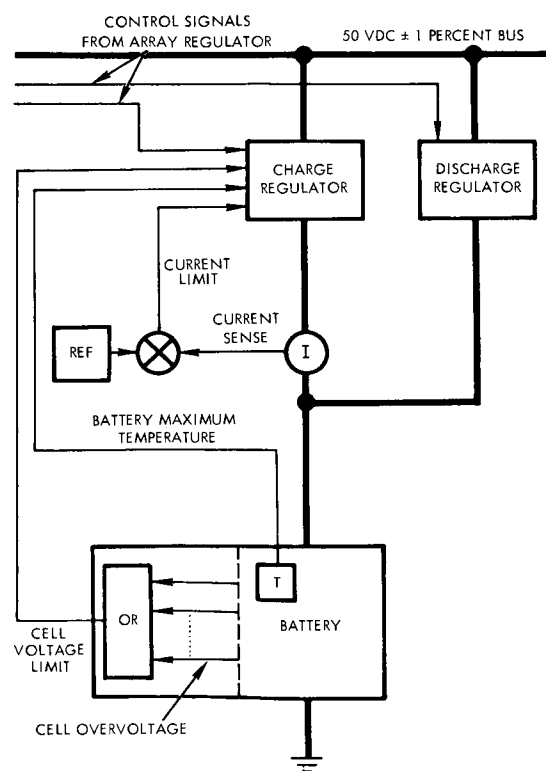


Figure 4-117. Battery Charge-Discharge Control

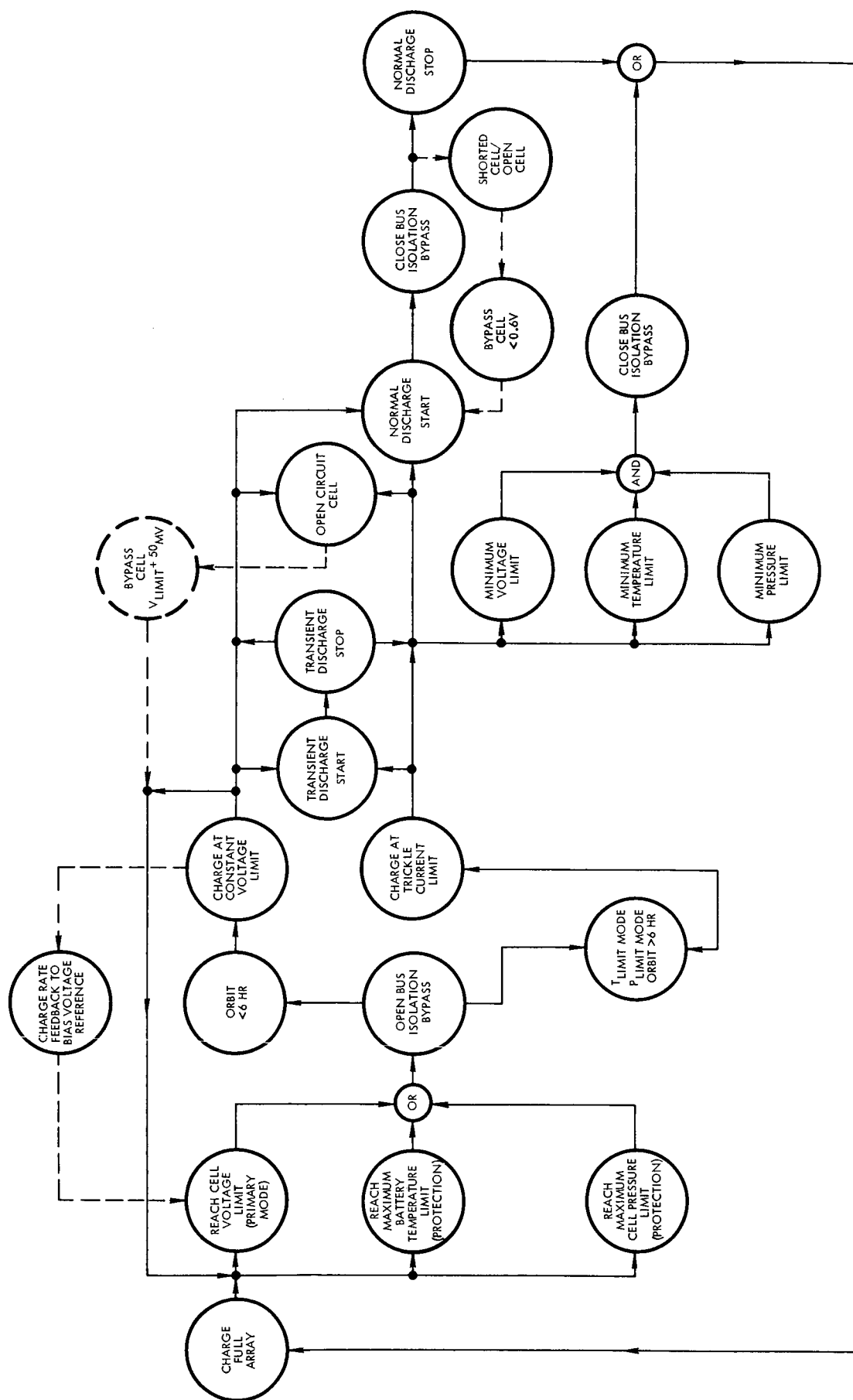


Figure 4-118. Standardized Charge Control Concept Logic Diagram

\*This page contains information proprietary to TRW, Inc. and shall not be reproduced or disclosed to others without the prior written permission of TRW, Inc.

Table 4-43. Comparison of Cell Level and Battery Level Controls

	Cell Level	Battery Level
Expected cycle life at used depth of discharge	* 500 at 95 per cent	* 150 at 84 per cent
Weight differential (due to lower depth of discharge)	--	+4 lb/battery
Cost differential (development)	\$50,000	--
Reliability (see analysis below)	0.999	0.99

\* Maximum eclipse, one battery failed

technology developed consists primarily of the mechanism for controlling and sensing a cell voltage limit which is pre-adjusted to match the voltage versus temperature characteristics of the cell. In addition, it includes charge-rate feedback which adjusts the voltage/temperature characteristics of the cell sensor to compensate for charge-rate, thus making it possible to maximize recharge rates and capacity for short-orbit applications and still protect the cell during long-period non-eclipse seasons which are typically encountered in space. It is anticipated that the stabistor presently being developed would fill the requirements for the dotted-line bypass functions shown in the logic diagram and would act as a primary backup protection of this design. The present development of the charge-rate feedback is directly applicable to silver-cadmium batteries. From the test results gathered under silver-cadmium cell study programs and from the OGO program, it is apparent that the feedback device will be required to operate a silver-cadmium battery properly.

\* This page contains information proprietary to TRW, Inc. and shall not be reproduced or disclosed to others without the prior written permission of TRW, Inc.

In Figure 4-118 the means have been provided to develop a technical concept of charge control for secondary space batteries. Further, TRW has explored the requirements involved for charging batteries in large cell groups over long-life periods without damaging the cells. Typical operation in the past has involved a battery level constant voltage, or modified constant voltage, charge control scheme which operates at the level of the average cell. Typical failures which have been occurring using these charge schemes are low capacity, cell overpressure resulting in battery rupture, and excessive temperature and gassing.

In examining battery operation, it is found that a typical battery cell has four main control variations: 1) voltage, 2) pressure, 3) temperature, and 4) charge rate. A fifth parameter, primarily protective in nature, is to limit the cell minimum voltage to prevent reverse charging for extended periods of time. The system provides a means of controlling these parameters. Control is accomplished with very low power dissipation and with temperature-adjusted voltage control to match the performance characteristics of the cell. The basic concept is to operate the battery in a manner which protects the weakest cell rather than present schemes which operate the battery around a cell-average or attempt to operate the battery as a series of completely independent cell elements. Since the weakest cell ultimately determines the battery capacity and, when not protected adequately, ultimately destroys the battery, a cell-level sensing system is desired. This concept will also protect the battery from overcharge in event of multiple cell shorts as a byproduct. Figure 4-119 is a schematic diagram outlining the system.

These investigations have developed a cell voltage detector, suitable for use on silver-cadmium systems, which contains the temperature-voltage characteristic of the C/10 charge rate. The device weighs 2.2 grams per cell and has a computed reliability in excess of 0.999 for a 30-cell battery

---

\*This page contains information proprietary to TRW, Inc. and shall not be reproduced or disclosed to others without the prior written permission of TRW, Inc.

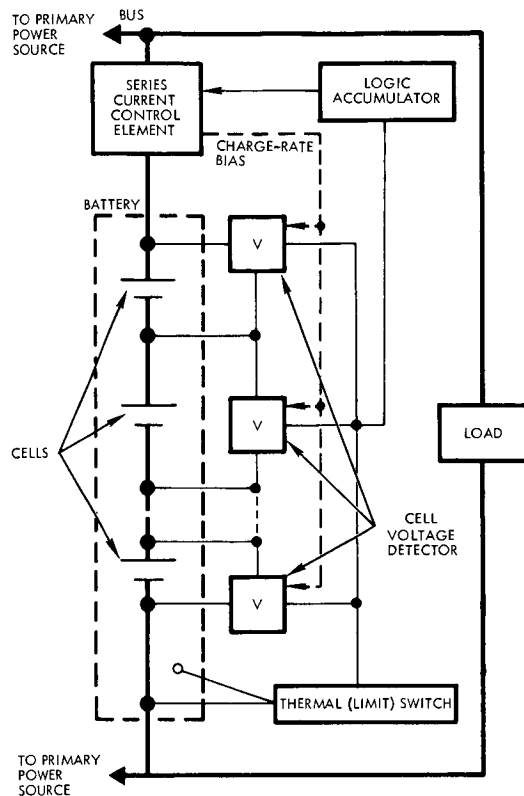


Figure 4-119. Battery with Cell-Level-Sensing Charge Control System Schematic

system. TRW is now in the process of developing the charge-rate adjustment which will shift the voltage level settings, as a function of temperature, along the charge rate. Such correction is very important for the silver-cadmium system. The refinement is now in the advanced design stage and will be breadboarded in the fall of 1965. Preliminary tests have indicated excellent results in cycling cells in this manner.

An additional development which has been undertaken and has been carried through to a working breadboard level is a temperature limit switch with a deadband of less than  $1^{\circ}\text{F}$ . The switch, microminaturized and mounted anywhere within a battery, is an additional fail-safe device required to operate the battery in a space vehicle.

\* This page contains information proprietary to TRW, Inc. and shall not be reproduced or disclosed to others without the prior written permission of TRW, Inc.



The cell level voltage sensors, while undeniably more complex functionally, may be made inherently highly reliable by utilizing more than one sensor output to control the series charging element. Two failure modes are possible, If the sensor fails so as to provide no indication of full charge when the cell is actually fully charged, one half of the sensors must fail in order to reduce the sensitivity of control to that of the battery level control. If the sensor fails so as to give a false indication of full charge, battery charge will terminate. By requiring that three such failures occur before terminating battery charge, the reliability of the system is increased to better than .999, while the sensitivity is maintained at 5 times that of the battery level charge control.

Failure rates are reduced by use of a hybrid integrated circuit on a single clip, with only three terminals, and by use of extremely low power levels.

b. Boost Regulator

A battery control consisting of a variable voltage boost arrangement can be utilized to regulate either battery charging or discharging. Two possible configurations for this type of regulator are illustrated in Figure 4-120 and Figure 4-121. In Figure 4-120 the output of a regulated DC-to-DC converter is added to the battery voltage prior to filtering such that the average output is equal to the desired bus level. In Figure 4-121 a switching shunt-type booster circuit is depicted which achieves the same result. The latter approach is somewhat less complex than that of Figure 4-120. Characteristics relating efficiency, input voltage and power level for the switching boost regulator are shown in Figures 4-122 and 4-123. In Figure 4-122 the efficiency for a 400-watt regulator as function of input voltage is illustrated. Efficiency variation with power level is very small for these boost schemes as most of the losses are directly proportional to output level. Figure 4-123 shows the efficiency variation with load for a typical unit.

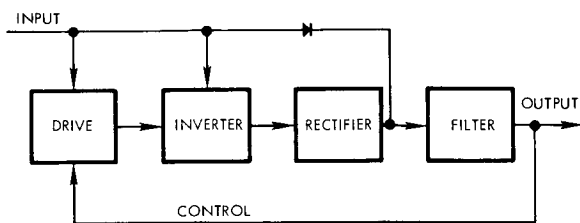


Figure 4-120. Boost Regulator  
DC-DC Converter  
Type

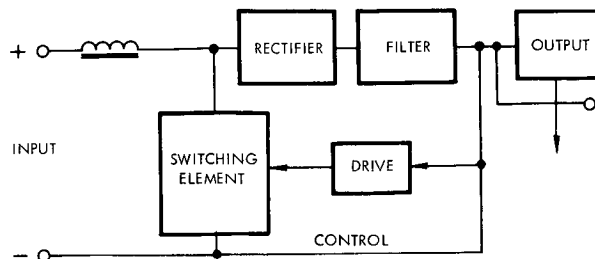


Figure 4-121. Boost Regulator  
Switching Shunt  
Type

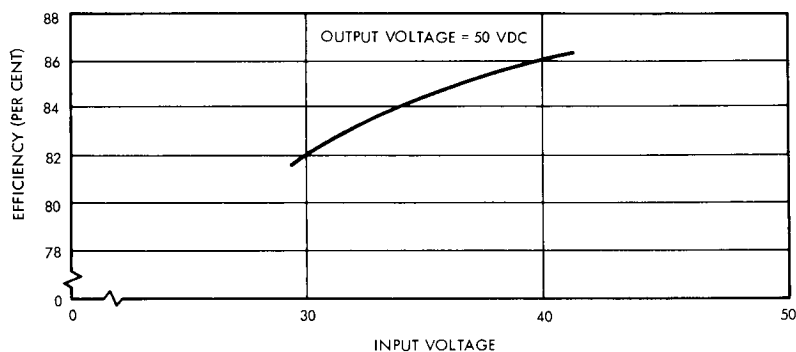


Figure 4-122. Efficiency Versus Input Voltage for  
400-Watt Switching Boost Regulator

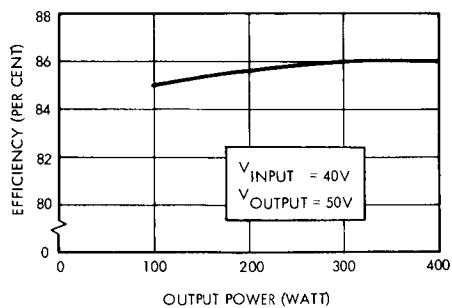


Figure 4-123.  
Efficiency Versus Power  
Level for 50-Volt Switching  
Boost Regulator

## SECTION V. MECHANICAL SUBSYSTEMS TRADEOFFS

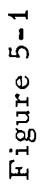
### 1. STRUCTURE

Structural design studies were divided into two interacting phases. The first was to investigate each of the proposed configurations to insure that they satisfied all structural requirements with respect to the selection of materials, the compatibility of the structure with other subsystems, continuity of structure, accessibility, direct load paths, and optimum support paths for large mass items. The second phase consisted of a series of tradeoff studies of individual structural components with respect to strength, dynamics, weights, manufacturing, and cost. The first set of studies is discussed in Sections 1.1 and 1.2. Section 1.3 presents the results of the individual tradeoff studies and recommends design.

#### 1.1 Alternate Structural Configurations

Structural designs were generated for six separate configurations, identified as Configuration A-1, A-2, A-3, B-1, B-2, and C-2. The configurations differ in several major areas, each having a definite effect on the structural design. The Configuration A series represents an evolutionary set based upon the use of a solid propellant engine for main deboost and monopropellant vernier engine for midcourse and orbital trim maneuvers. This series uses a fixed solar array and nominal sun/canopus orientation. The final selected configuration (presented in Volume 2) is A-3. The Configuration B series is similar except that a single bipropellant engine is used for all maneuvers. The Configuration C series represents a significant departure from the Mariner concept. It involves an earth/canopus nominal orientation, a large fixed disk for high data rate communication and deployable solar panels. Like series A, it uses a solid rocket and a monopropellant vernier. The comparison and selection process among these series is discussed in Volume 4.

The liquid propellant subsystem of all configurations is designed on a modular concept so that it can be separated for installation and test. Another basic consideration is the location of equipment within the spacecraft. The dash-1 configurations utilize a separate, cantilevered equipment compartment. All other configurations incorporate the equipment



subsection into the basic load-carrying frame. The final item having a major effect on structural design is the solar array. Three array approaches were studied 1) the array rigidly attached to the spacecraft with integral array and support, 2) rigidly attached supports to which the solar array is attached, and 3) deployable panels mounted at the edge of a fixed antenna (Configuration C only).

The hexagonal arrangement of side panels, as used in Configuration A and C, is preferred over an octagonal arrangement as used in Configuration B because of weight, cost, and greater simplicity. The bipropellant tankage requirements and space availability for Configuration B dictated the octagonal arrangement. There are four propellant tanks, two pressurant tanks and two attitude control gas tanks symmetrically arranged about the spacecraft axis.

#### 1.1.1 Configuration A-1

Configuration A-1 is composed of four major subassemblies: basic bus structure, the solid propellant engine support structure, the bus-to-Centaur interstage structure, and the solar panels. The interstage structure also contains the midcourse monopropellant propulsion system. By this breakdown, the four subassemblies can each proceed independently through assembly, installation, and test; the midcourse propulsion subsystem can be test fired before it is joined to the bus structure subassembly. The general structural arrangement is shown in Figure 5-1. The basic bus structure consists of a hexagonal frame plus an inner 80-inch diameter cylinder. The hexagonal frame is constructed of axial members with frames, top and bottom, made of 7075-T73 angles with tee extrusions of 7075-T73 at the corners. Diagonal struts run from the lower corners at Station 23 to the inner cylinder at Station 59. Top, bottom, and sides have 7075-T6 aluminum honeycomb panels with a 1-inch aluminum truss-grid core and 0.025-inch face sheets. The truss-grid core is used because of its superior meteoroid protection characteristics, as discussed in Section 1 of Appendix C. All panels are bolted to the frame and are removable for access. The outer panels are the mounting surfaces for the electronic subsystems and the thermal control louvers. Semimonocoque skin and stringer construction is used for the inner cylinder. It is made of 7075-T6 skin and hat section stringers. This unit serves as the

load path for all flight capsule, bus, and solid-propellant engine loads. Ring members at the top and bottom provide for attachment of the flight capsule, engine support cone, and the interstage structure.

Support for the solid-propellant engine is provided by a conical structure which is permanently jointed to the cylindrical member of the bus at Station 59. Construction employs 7075-T6 aluminum skin and hat section stringers. The fiber glass attach angle at the lower end of the cone provides for attachment of the motor. Fiber glass is used to reduce heat conduction to the spacecraft. A 1-inch honeycomb panel, 80-inch diameter with a cutout on the centerline for the engine nozzle similar in construction to the bus structure subassembly is located at Station 59 to provide meteoroid protection for the motor and backside of the bus structure subassembly.

A conical interstage module is located between Stations 0 and 23. The module is 120-inch diameter at the aft end to match the Centaur's interstage and tapers to 80-inch diameter where it joins the bus. It consists of 1-inch thick truss-grid honeycomb panels, ring frames top and bottom, and six 7075-T73 stringers which serve as the attach points to the Centaur interstage. A 1-inch truss-grid panel 120 inch in diameter attaches to the ring frame at Station 0. This member provides meteoroid protection and serves as a mounting base for the midcourse propellant engine. Six radial beams also attach to the engine support cone. The propellant, pressurization, and attitude control tanks are supported on a ring frame with a conical flange cradling the tank. Four straps at 90-degree spacing go over the tank and secure it to the frame. The ring frame is attached to the six interstage stringers at Stations 0 and 18 by a tubular truss structure.

All tanks are spherical, fabricated by welding two forged hemispheres. All bosses and lugs are integrally machined into the tank wall. The propellant tanks are made of 6AL-4V titanium heat-treated to 165,000 psi maximum yield strength. The propellant pressurization tanks are made of the same material, annealed.

The solar array, consisting of the basic panel and supporting structure, is a circular disk with a 234-inch OD and circular inner edge that matches the interstage structure. The panel is divided into six equal

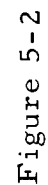
segments. Panels are constructed of 1-inch thick honeycomb panels with a standard aluminum honeycomb core and 0.010-inch 7075-T6 skins. The panels mount to fiber glass attach angles at the interstage joint. The panels attach to six radial aluminum I-beams which mount to the interstage and are supported by aluminum tubular truss members that run from the outer edge of the panels to the six corners of the basic bus at Station 59.

The high gain antenna and planet oriented package are supported by a truss structure with a horizontal member attaching to the solar array and two tubes running from the hinge point to the outer corner of the bus at Station 59.

#### 1.1.2 Configuration B-1

The general arrangement of Configuration B-1 is similar to that of Configuration A-1. It is composed of three subassemblies: 1) the basic bus structure, 2) the propulsion subsystem, and 3) the solar panels. In this configuration, the propulsion subsystem contains the complete bi-propellant subsystem which is used for both midcourse and orbital injection. The general structure arrangement is shown in Figure 5-2.

The bus structure consists of an octagonal equipment bay plus an inner conical structure. The octagonal frame is constructed of axial members with frames at Stations 13 and 50 made from 7075-T73 angle extrusions. The tees at the corners are also made from 7075-T73 extrusions. Tubular struts run from the outboard corners at Station 13 to the conical structure at Station 50. The top, bottom, and outer sides of the bus structure are covered with load-carrying honeycomb panels constructed of 1-inch aluminum truss-grid core with 0.025-inch 7075-T6 aluminum faces. All panels are bolted to the frame and can be removed for access. These panels serve as mounting surfaces for the electronic subassemblies, are part of the thermal control subsystem, and provide meteoroid protection. The conical structure is the main load-carrying member for the bus load, flight capsule, and the propulsion subsystem. It consists of eight main members which are the main load points at both the flight capsule and Centaur interfaces. Ring frames are located at Stations 0 and 59. The cone is a combination of skin and stringer construction in the bus area and honeycomb panels above and below the bus. These panels have the same construction as the bus panels.





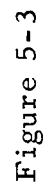
The propellant subsystem structure is in the form of a truncated cone that runs from Station 59 to 9. It is of semimonocoque construction with 7075-T6 skin and stringers. Four large hat section stringers are placed to accept the engine actuation system. At the lower end of the cone, a second smaller cone runs up to Station 23 to provide the mounting surface for the engine support struts. The four propellant tanks mount to the main propulsion cone. Holes are cut in the cone to accept the tanks, and support is provided by a support ring and four tension strap members. The pressurization tanks and attitude control gas tanks mount from support cones on the outside of the propulsion cone and are also retained by straps. A flat cone-shaped honeycomb panel is located between the basic bus frame at Station 0 and the base of the propulsion system support cone to provide a meteoroid protection member across the aft end of the spacecraft. It is a 1-inch thick aluminum honeycomb truss-grid panel.

The solar array consists of the basic panel and supporting structure. The array is a circular disk with a 234-inch OD and a circular inner edge that matches the bus structure. The panel is divided into six equal segments made of 1-inch aluminum honeycomb core and 0.010-inch 7075-T6 skins. The segments mount to the bus with fiber glass angles. Radial support members run from the bus to the outer edge of the array and provide panel mounting along these edges; aluminum tubular members run from the outer edge of the panel at these points to the upper corners of the bus. Additional horizontal support members run from the outer end of one panel support member to the end of the next and support the panel near its outer edge.

The high gain antenna and the POP are supported in the same manner as on Configuration A-1.

#### 1.1.3 Configuration A-2

The major modification between Configurations A-1 and A-2 is the incorporation of the equipment mounting panels as part of the main structure. Configuration A-2 also consists of three major subassemblies: 1) the basic bus structure, including the engine support structure for the solid-propellant motor; 2) the midcourse propellant subassembly; and 3) the solar array. This design allows the same modular assembly and test sequence as the preceding two configurations. The general structural arrangement is shown in Figure 5-3.



The basic bus structure is a hexagonal truncated pyramid. The hexagonal frame is constructed of axial members with frames at Stations 18 and 59 and is made of 7075-T6 channels. Six  $\pi$ -section corner members machined from 7075-T73 run from the lander attach point to the propulsion subassembly joint at Station 18. These members carry all the vertical loads of the bus, propulsion subsystem, and flight capsule. The side panels serve as mounting panels for all electronic subsystems and provide meteoroid protection, a thermal heat sink, and the basic shear path of the structure. The panels are made of 1-inch thick aluminum truss-grid honeycomb core with 7075-T6 aluminum skins. Extruded rails are attached to the backside of the panels to serve as the actual mounting surface for the electronic equipment. All panels are bolted on four sides to the frame with a hinge along the lower edge to facilitate maintenance. The top of the bus is covered with a panel similar to those used on the sides.

The solid propellant motor-support structure is a permanent part of the equipment module. It consists of a motor mount ring at Station 24. Six tubular support members run from the ring to the corners of the bus at Station 59 and carry the boost and thrust loads of the motor. Eighteen horizontal tubes form a truss between the motor mount ring and the frame of the bus at Station 18. They take all side and torsional loads.

The midcourse propulsion subassembly is attached at the Station 18 field joint with six bolts at the six major vertical members. The outer structure of this module is identical to that used in the equipment module. A 120-inch diameter flat circular disk closes off the aft end of the subassembly and provides the meteoroid protection. It is of the same sandwich construction as all other panels. Six radial beams run along the top of this panel to the centerline when they support the midcourse propellant engine-mount structure. The two propellant tanks, the pressurization tank, and the two attitude-control tanks are mounted in conical support rings which are mounted to the structure by a tubular truss which runs to the corner of the module at Stations 0 and 18. Tension straps hold the tank to the support ring. All tanks are made from 6AL-4V titanium forged hemispheres welded together. All bosses and ports are integrally machined into the tank walls. The propellant tanks are of 165,000-psi

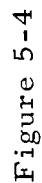
titanium and the pressurization tanks are annealed titanium. The solar array is the same as that used on Configuration A-1, as is the antenna and POP support structure. However, support members for the array run up to the bus at Station 18.

#### 1.1.4 Configuration A-3

Configuration A-3, the selected configuration described in Volume 2, is a refinement of Configuration A-2. Many of the structural concepts and designs are identical. The general structural arrangement is shown in Figure 5-4. The three-module concept of Configuration A-2 is also used on this configuration.

The basic bus structure and geometry are essentially the same as that used in Configuration A-2. The major change is the elimination of the field joint at Station 18 and the incorporation of the midcourse propulsion module with the aft panel at Station 1. The corner members are continuous from Station 0 to 59 and the side panels run from Station 4 to 59. This change, which permits a cleaner bus design, is the result of two other modifications. First, the solar panel, POP, and antenna support structure was revised to accommodate new POP and antenna locations. In so doing, the support struts were carried up to Station 59, which requires a single unit bus module if the array is to be installed before the propulsion module is assembled to the spacecraft. The second change was to mount the propulsion module on the Station 1 panel to allow the single unit bus construction. The top panel of the bus was changed from the honeycomb panel of Configuration A-2 to a lighter beaded single sheet. This was done on the basis that the flight capsule will provide meteoroid protection until separation and that the single skin panel in conjunction with the motor support cone and burned out motor case will provide a Whipple shield meteoroid barrier in Mars orbit.

The solid-propellant motor support structure is a permanent part of the equipment module. It is a semimonocoque truncated cone, of 7075-T6 aluminum skin and hat section stringer design. A fiber glass attach angle is provided at the lower end of the cone for attachment of the motor. Fiber glass is used to reduce heat conduction to the spacecraft during and immediately after solid propellant engine firing. Six of



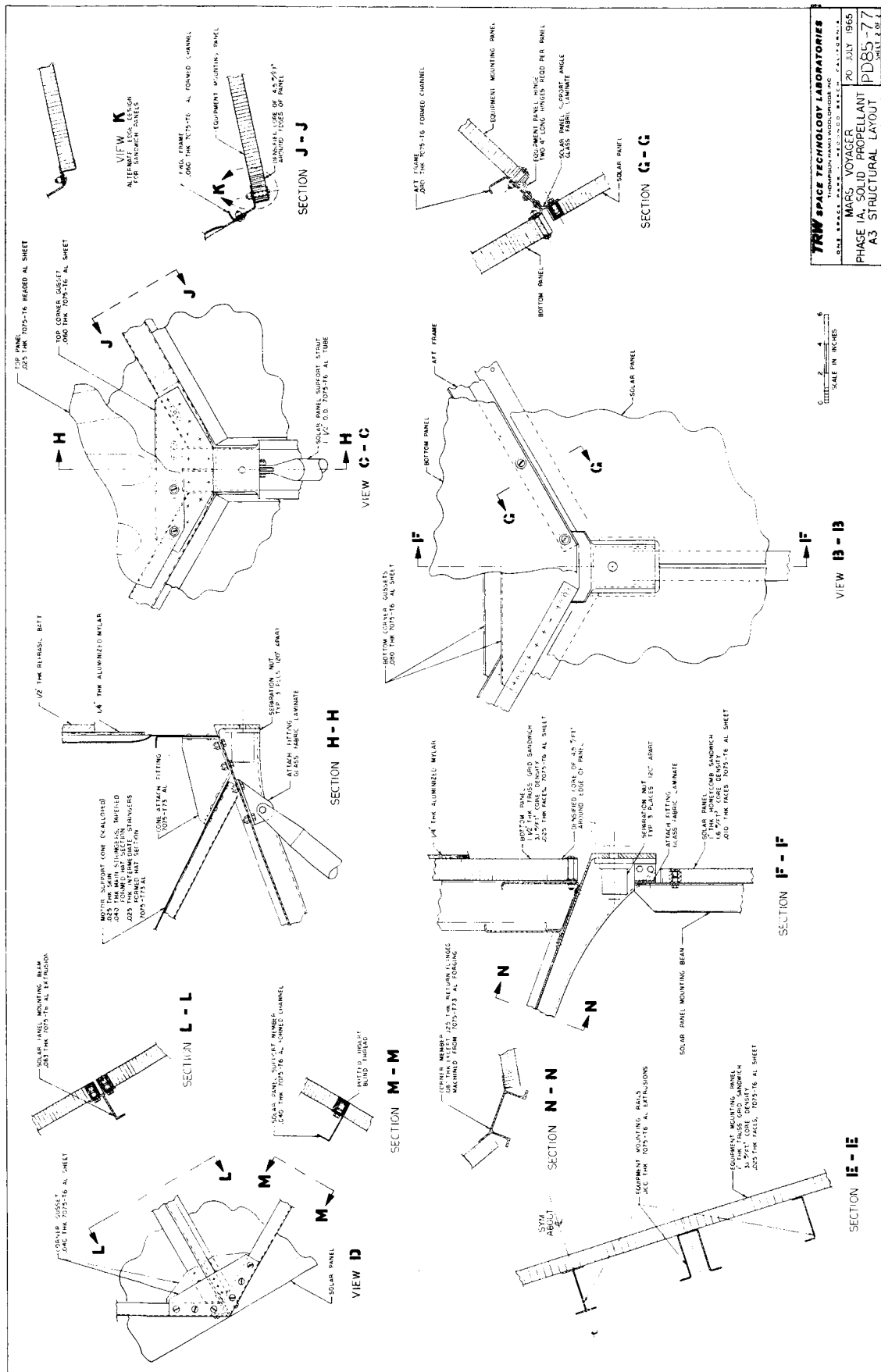


Figure 5-4

stringers will carry the engine loads into the six-corner frame members at Station 58. The design was changed from Configuration A-2 to provide a more uniform support load into the motor case.

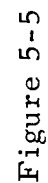
The midcourse propulsion subassembly consists of a horizontal panel at Station 1 and tank support structure. The hexagonal panel is 120 inches across the corners and attaches to the bus lower frame with an interchangeable bolt pattern. Sandwich construction is used for the panel. It has a 1.5-inch thick aluminum truss-grid core with 0.025-inch 7075-T6 skins. The 1.5-inch face spacing provides optimum meteoroid protection versus weight (see Section 1.2.1), and gives added stiffness to the panel. Two combined propellant-pressurization tanks and two attitude-control tanks are mounted to the panel, resting on a horizontal cone-shaped flange on the support frame. Two straps separated by 90 degrees go across the top of the tank and attach to the base of the tank support structure with tensioning devices. The midcourse engine mounts to a support structure located on the centerline of the panel.

The solar array consists of the basic panel and the supporting structure. The array is in the form of a flat panel with a 12-sided outer edge and an inner edge that matches the shape of the basic bus. The panel is divided into six identical units. Construction is identical to Configuration A-2. The panels mount to fiber glass angles on the basic bus. Fiber glass is used to aid thermal control between the panels and the basic bus. Six horizontal radial beams run from the corners of the bus to support the edges of the solar panels. Additional support members run from the end of each beam to the end of each adjacent beam. Vertical loads are carried by tubular struts running from the ends of the horizontal support members to the corners of the bus at Station 59.

The high-gain antenna and POP support will be combined with the solar panel support structure.

#### 1.1.5 Configuration B-2

The major modification between Configurations B-1 and B-2 is the incorporation of the equipment panels as part of the main structure. Configuration B-2 is a three-module design including: 1) the basic bus structure, 2) the propulsion subassembly, and 3) the solar array. The general structural arrangement is shown in Figure 5-5.





The basic bus is an octagonal truncated pyramid. The frame is constructed of axial members with channel frames at Station 0 and 59. Eight  $\pi$  section stringers run down the corners of the bus from Station 59 to 0 and carry all vertical loads of the flight capsule, engine subsystem, and spacecraft equipment. They are machined  $\pi$ -section members of 7075-T73 aluminum and provide the attach points for both the flight capsule and the Centaur. The side panels provide the mounting surface for all the electronic components. They are 1-inch thick honeycomb panels with 0.25-inch 7075-T6 aluminum faces and an aluminum truss-grid core. They are screwed to the frame on all four sides and can be removed for maintenance of the electronic equipment. The top of the bus is also covered with a panel of the same construction as the side panels.

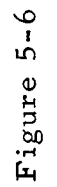
The bipropellant subassembly support structure forms a square truncated pyramid. The corner members are machined stringers with integral end fittings and are made from 7075-T73. These members bolt to four of the eight bus corner members at Station 59. The propellant tanks have four mounting lugs per tank that bolt to these members. Shear panels cover the sides of the support structure above, and below the tanks. The attitude control tanks amount inside the support structure in the corners. Tank construction and material are the same as for the other configurations. A four-bar linkage mounts to the bottom of the pyramid to support the engine at Station 15.

The solar array, antenna support, and POP support are the same as for Configuration A-2.

#### 1.1.6 Configuration C-2

Configuration C-2 is characterized by earth/canopus orientation, a large fixed disk, a small single gimbal auxiliary disk, a deployable solar array, and a single gimbal POP. It is a four-module configuration consisting of the basic bus structure, the propulsion system, a Centaur-to-spacecraft interstage, and deployable solar panels. As with the earlier configurations, it is modularized to enable parallel installation and test operations. The general structural arrangement is shown in Figure 5-6.

The basic module is hexagonal, truncated pyramid that runs from Station 18 to 59. The frame is constructed of axial members with channel



frames at Stations 18 and 59. Six  $\pi$ -section machined corner members run from the flight capsule attach point to the fixed antenna and are made of 7075-T73 material. These members carry all the vertical loads. The side panels serve as mounting panels for all electronic subsystems and provide meteoroid protection, a thermal heat sink, and the basic shear path of the structure. The panels are made of 1-inch thick aluminum truss-grid honeycomb core with 0.025-inch 7075-T6 aluminum face sheets. Extruded I-sections are attached to the back of the panels to serve as the mounting surface for all electronic components. All panels are bolted on all four sides to the bus frame with a hinge along the lower edge to facilitate maintenance. The top of the bus is also covered with a honeycomb panel the same as on the sides. The fixed antenna provides meteoroid protection on the lower face of the bus.

The propulsion subassembly consists of a truncated cone that runs from Station 59 to 22. It is of semimonocoque construction with 7075-T6 skin and stringers. Six main stringers bolt to the bus structure at Station 59. Attachment to the solid motor is through a fiber glass attach angle. The monopropellant and pressurization tanks mount between the cone and the engine bell. A conical support flange mounted to the thrust cone supports the tank. Straps hold the tank to the support cone.

The interstage structure is a semimonocoque truncated cone, running from the Centaur interface to the bus at the antenna surface, with six hard points on both interfaces and stringers running in between. The separation plane is at the aft surface of the antenna. Cutouts are provided to clear the antenna horn A-frame.

Ten deployable rectangular solar panels, approximately 4 x 6 feet are located around the periphery of the fixed antenna. They are made of 1-inch thick aluminum honeycomb with 0.010-inch 7075-T6 faces and a hexcel aluminum core. The support beam runs down the center of the panel and forks into two legs which end at the hinges along the inboard edge of the panel.

## 1. 2 Configuration Evaluation and Conclusions

### 1. 2. 1 Design

Accessibility to the equipment bays is essentially the same for all of the configurations just described, but the area available for mounting equipment varies. Configuration A-3 has the greatest area; the full panel height from Stations 4 to 58 is usable for equipment. The minimum amount of area for equipment mounting is provided by Configuration C-2.

Although Configurations A-1 and B-1 have ample mounting areas, they require a more complex structural arrangement and a heavier configuration than the others since they are successful in achieving efficient multiple-purpose structure members. The equipment-mounting panels of Configurations A-2, A-3, B-2, and C-2 also act as meteoroid protection, heat sinks for the thermal control system, and as shear carrying structure for the vehicle loads.

The B configurations, with their liquid bipropellant subsystem, result in a design with four propellant tanks, two pressurization tanks, and two attitude control tanks. In contrast, the solid-motor configurations have only two propellant and one pressurization tank for the midcourse course correction engine, plus the same two attitude control tanks. In addition, the requirement for a modularized propulsion system with all tanks mounted on the thrust structure results in a tank arrangement that is difficult to support, and it is difficult to minimize tank restraints with this arrangement. The propulsion support method for Configuration A-3 seems to be the simplest, with a conical support for the solid and with the monopropellant tanks all mounted to the horizontal base at Station 1.

When the basic bus structure is evaluated, the criteria used are the achievement of direct load paths and minimum number of units. Configuration A-1 with the separate equipment mounting structure and both the manufacturing joint and break in the direction of the primary load path, appears the least desirable. Configuration B-1 has a single unit basic frame with straight members from the flight capsule to the booster; however, it retains the complexity of the added equipment mounting frame. The simplest frames are those on Configurations B-2 and A-3, where a straight load path exists from flight capsule to booster, with no joints.

Configuration A-2 has the direct load path but has the complexity of an interchangeable joint design at Station 18.

Thus, Configuration A-3, with its direct load paths, single unit frame with multipurpose structure, offers the best over-all structural design.

#### 1.2.2 Strength Analysis

The strength analysis in the Voyager Phase IA study had three goals: 1) to insure structural integrity of all designs, 2) to provide a sound basis for structural weight calculations, and 3) to provide data for the selection of structural component design and materials. The scope and level of detail of the analysis is shown in Appendix C. The techniques used and the assumptions made are either well-established concepts in structural analysis, or conservative in nature. Material properties were obtained mainly from "Metallic Materials and Elements for Flight Vehicle Structure" (MIL-HDBK-5 August 1962, with 1 May 1964 Revision Insert). Where needed information, such as creep data for titanium tankage, was not contained in MIL-HDBK-5, sources such as data published by the Titanium Corporation of America and the Battelle Memorial Institute were used.

The criteria used to analyze all structural concepts were specified in the JPL "Preliminary Voyager 1971 Mission Specification," 1 May 1965. The elements of this specification directly applicable to structure analysis include the two general structure factors of safety: 1) ultimate factor of safety = 1.25 and 2) yield factor of safety = 1.00. Table 5-1 shows the flight loading conditions specified.

Table 5-1. Flight Loading Conditions

Condition	Static		Dynamic		
	Longitudinal	Lateral	Longitudinal	Lateral	Torsion
	G	G	o-peak G	o-peak G	o-peak rad/sec <sup>2</sup>
1	6	1	0.8	0.5	0
2	2	1	1.2	0.75	60
3	1	0	1.6	1.0	60
4	0	0	1.6	0	0

Using these criteria combined in the same manner specified, the major structural members of Voyager Configurations A-1, A-2, A-3, B-1, and B-2 were analyzed. Tables 5-2 through 5-6 list members, their critical load and condition (Table 5-1), and their margins of safety.

Structural members were sized on the basis of the strength analysis in conjunction with meteoroid protection, dynamic analyses, and thermal and packaging requirements. Table 5-7 lists the structural weights computed for each configuration.

### 1. 2. 3 Dynamic Analyses

#### a. Critical Conditions

Critical spacecraft dynamic loading conditions and methods of handling these conditions are discussed in the following paragraphs.

Compression Modes. Gross vehicle and spacecraft longitudinal modes of vibration will be excited by structural/propulsion system interactions at ignition and staging shocks. Spacecraft structure is designed to have natural frequencies above those of the compression modes to preclude excessive spacecraft dynamic loading. The exception is in the case of solar panels. These are designed for allowable deflection, and baseline configuration of the solar panels has been shown to have adequate stiffness to meet these requirements.

Bending Modes. Gross vehicle and spacecraft bending modes of vibration may be excited through coupling with the compression modes or by transient wind loads. Spacecraft structure is designed to have natural frequencies above those of the bending modes to preclude coupling of spacecraft major resonances with those of the launch vehicle.

Broadband Random Noise. Reflected rocket exhaust acoustical noise and max-q turbulent boundary layer pressure fluctuations will cause maximum over-all sound pressure level at the spacecraft of 142 db. The thermal louver, susceptible to acoustic loads because of its large surface area and thin wall blades, is the only critical item on the spacecraft in this respect. During Phase IB, the candidate louvers will be investigated both analytically and by development acoustic tests to insure that acoustically induced failures will not occur.

Table 5-2. Margins of Safety for Configuration A-1\*

Item	Description	Load	Margins of Safety
Solid Motor Thrust Cone	0.032 x 2219 - T62 aluminum monocoque	4970-lb Compression Condition 4 (Table 5-1)	+0.19 (stability)
	0.032 x 6AL-4V titanium annealed monocoque	4970-lb Compression Condition 1	+0.81 (stability)
	16 stringers x 0.020 x 7075-T6 with 0.020 x 7075-T6 skin and a frame at midplane	4970-lb Compression Condition 1	+1.12 (crippling)
Spacecraft Support Cylinder	0.100 x 7075-T6 aluminum monocoque	374-lb/in. Compression Condition 1	+0.18 (stability)
	0.040 x 7075-T6 aluminum stringers at 10.2-in. spacing and 0.032 x 7075-T6 aluminum skin and a frame at midplane	374-lb/in. Compression Condition 1	+0.003 (crippling)
	Honeycomb 1/2-in. - thick x 0.020 x 7075-T6 aluminum faces with core; 6 total panels with 7075-T6 extrusion splice members	374-lb/in. Compression Condition 1	+0.77 (stability)
	Splice member	2525-lb Compression Condition 1	+0.16 (column)
Spacecraft Support Cone	Honeycomb 5/8 in. - thick x 0.025 x 7075-T6 aluminum faces with 3.1 lb/ft <sup>3</sup> aluminum core; 6 total panels	512-lb/in. Compression Condition 1	+0.95 (stability)
Solar Panel Support Strut	1.0 in. OD x 0.025 in. wall 7075-T6 aluminum tube	81-lb Compression Condition 4	+1.04 (column)
Equipment Compartment Support Strut	1.0 in. OD x 0.025 in. wall	762-lb Compression Condition 4	+0.14 (column)

\* See Section 2 of Appendix C.

Table 5-3. Margins of Safety for Configuration A-2\*

Item	Description	Load	Margins of Safety
Solid Motor Support Structure	Six longitudinal load trusses of 1.25-in. OD tubing x 0.028 in. wall x 7075-T6 aluminum alloy, six lateral load trusses of 1.00-in. OD tubing x 0.028-in. wall x 7075-T6	6500 lb Condition 4 (Table 5-1)	0.19 (stability)
	Scalloped cone with 6 full length stringers and 30 partial length stringer and 0.025 x 7075-T6 clad skin	6500 lb Condition 4	0.12 (shear buckling)
Frame Station 59	0.080 x 7075-T6 aluminum extruded angle	3670 lb Condition 1	0.01 (crippling)
Frame Station 18	0.063 x 7075-T6 aluminum extruded channel	2725 lb Condition 4	0.18 (crippling)
Frame Station 0	0.090 x 7075-T6 aluminum extruded channel	6080 lb Condition 3	0.12 (stability)
Axial Load Member	Six column members channel shaped with additional flanges for attaching honeycomb panels	13,850 lb Condition 1	0.01 (stability)
Bus Panels	Honeycomb sandwich, 0.025 faces and 1.0-in. total depth	Sized for meteoroid protection	
Solar Panel Support Struts	7/8-in. OD x 0.028-in. wall x 7075-T6 tubing	203 lb Condition 4	0.40 (stability)

\* See Section 2 of Appendix C.



Table 5-4. Margins of Safety for Configuration A-3

Item	Description	Load	Margins of Safety
Retroengine Support Structure	Scalloped cone with 6 full length stringers and 30 partial length stringers and 0.025 x 7075-T6 clad skin	6500 lb Compression Condition 4	0.12 (shear buckling)
Frame Station 59	0.060 x 7075-T6 aluminum extruded channel	4830 lb Compression Condition 1	0.27 (stability)
Frame Station 0	0.080 x 7075-T6 aluminum formed channel	2810 lb Compression Condition 3	0.02 (stability)
Edge Members	Six column members, channel shaped with return flanges for additional stiffness and for attaching honeycomb panels	13,850 lb Compression Condition 1	0.007 (stability)
Bus Panels	0.025 x 7075-T6 faces with a 1.0 in. total thickness	Sized for meteoroid protection and thermodynamic requirements	
Honeycomb panel bottom	0.025 x 7075-T6 faces with a 1.5 in. total thickness	Sized for meteoroid protection and tank mounting stiffness	
Solar Panel	0.010 x 7075-T6 faces with a 1.0 in. total thickness supported by an 0.040 x 7075-T6 formed channel	Condition 1	0 (bending)

Table 5-5. Margins of Safety for Configuration B-1\*

Item	Description	Load	Margins of Safety
Bus Support Structure	7075-T6 aluminum skin and stringers	477 lb/in. Condition 1 (Table 5-1)	0 (stability)
Propulsion Subassembly Structure	Ring frames 7075-T6 Channels	3450 in. -lb Condition 1	+0.16 (bending)
	Stringers 7075-T6 hats	41,600 in. -lb	0 (bending)
	Engine support cone: 0.025 x 7075-T6 aluminum	820 lb Condition 1	High

\* See Section 2 of Appendix C

Table 5-6. Margins of Safety for Configuration B-2\*

Item	Description	Load	Margins of Safety
Axial Load Member	7075-T6 aluminum struts	8600 lb ultimate Condition 1 (Table 5-1)	0 (stability)
Bus Panels	Honeycomb panels 1-in. thick, 0.025 in. 7075-T6 faces, 3.1 lb/ft <sup>3</sup> core	1490 lb ultimate Condition 1	High
		13,130 lb ultimate Condition 2	+0.46 (shear)
Solar Panel Supports	7075-T6 tubing	90 lb ultimate Condition 1	+0.08 (stability)
Propulsion Subassembly Structure	Vertical I-beams 7075-T6	290 lb Condition 1	0 (bending)
	Upper I-cross beams 7075-T6	1970 lb Condition 1	0 (bending)
	Lower I-cross beams 7075-T6	1970 lb Condition 1	0 (bending)
	Longitudinal struts 7075-T6	1190 lb Condition 1	0 (bending)

\* See Section 2 of Appendix C

Table 5-7. Structure Weights for Alternate Configurations (lbs)

	A-1	B-1	A-2	B-2	C-2	A-3
Structure						
Meteoroid protection panels	439	449	305	319	171	274.8
Frame-work	43	57	82	78	51	76.2
Bus inner structure	70	104	-	-	-	-
Separation provisions	31	31	15	15	15	-**
Equipment mounting provisions	47	47	53	53	53	92.0
Attachments and Miscellaneous (6 per cent)	-	-	27	28	17	26.6
Total =	630	688	482	493	307	469.6
Adapter (Spacecraft-Centaur)	(-)	(-)	(-)	(-)	89	(=)
Miscellaneous Mounts						
High gain antenna	8	8	6.8	6.8	6.8	2.7
Planet oriented package	12	12	8.6	8.6	8.6	3.2
Magnetometer, boom and actuator	-	-	8.5	8.5	8.5	8.5
Low gain antenna	-	-	0.8	0.8	0.8	0.8
External science package	-	-	7.5	7.5	7.5	2.6
Attachments and miscellaneous (6 per cent)	-	-	1.9	1.9	1.9	1.2
Lander receiving antenna						0.6
Standby antenna						1.1
ACS						0.8
Total =	20	20	34.1	34.1	34.1	21.5
Grand Total =	650	708	516.1	527.1	430.1	491.1

\*\* Included in Framework Weight

Shroud Jettison. The longitudinal shroud-splitting detonation and circumferential separation detonation adjacent to the Centaur aft fairing will result in a series of decaying sinusoidal accelerations transmitted through the spacecraft in the radial and longitudinal compression modes. This loading condition could adversely affect certain spacecraft structure, equipment, and mountings. The shock levels and response of the three fore and aft bolts, spacecraft substructure, and equipment can be estimated, but development detonation testing will be required to establish the actual effects on the spacecraft.

Centaur Separation. The Centaur stage is separated from the SIVB stage by circumferential linear shaped charge detonation of the Centaur/SIVB adapter. The event should produce higher shock inputs to the Centaur than shroud jettison. The shock loading will result in decaying sinusoidal accelerations transmitted through the spacecraft in its breathing and compression lower modes. An upper limit to this spacecraft loading, based on the fraction of detonation energy transmitted to the spacecraft as kinetic energy, has been calculated and is shown in Section 2 of Appendix C. To establish actual levels and preclude damage in flight to certain spacecraft equipment, development detonation testing will be required.

Spacecraft Separation. Three release nuts exploded during separation from the Centaur stage and later from the flight capsule will produce shock loads of relatively high amplitude and frequency. However, only structure and equipment adjacent to the release nuts will experience peak loading since relatively little kinetic energy is released to the attachment mountings during detonation. Detonation testing will be required to establish the actual shock levels and their effects on the spacecraft.

Retromotor Ignition. Retrorocket motor ignition will cause a shock to the motor circumferential frame attachments and motor supports. However, this shock should be no more severe to the structure than shroud jettison shocks.

b. Dynamic Models

Dynamic models of the Voyager spacecraft are required to demonstrate spacecraft structural integrity and to define component

vibration environments. Guidance and control of the spacecraft will be dominated by rigid body motions; hence the dynamic model is of secondary importance for this analysis.

Modeling of the spacecraft is separated into two portions: 1) the external appendages such as solar panels, antenna, science payloads, and their support structure, and 2) the basic structure and internal elements. Only the exterior structure has been modeled. Low frequency modes which could couple with the launch vehicle modes involve the external structure, the solar panel, antenna, and science payload support structure. Internal components are not included in the modeling because their natural frequencies will be much higher than those of the appendages and, hence, will be decoupled from the lower-frequency modes.

The exterior structure requires two separate models to describe the conditions of launch and free flight. The basic differences are in the positions of the antenna and science payload during boost phase and free flight and the fact that the spacecraft is fixed to the booster for launch and is free to translate and rotate during free flight. These models are shown in Figures 5-7 and 5-8.

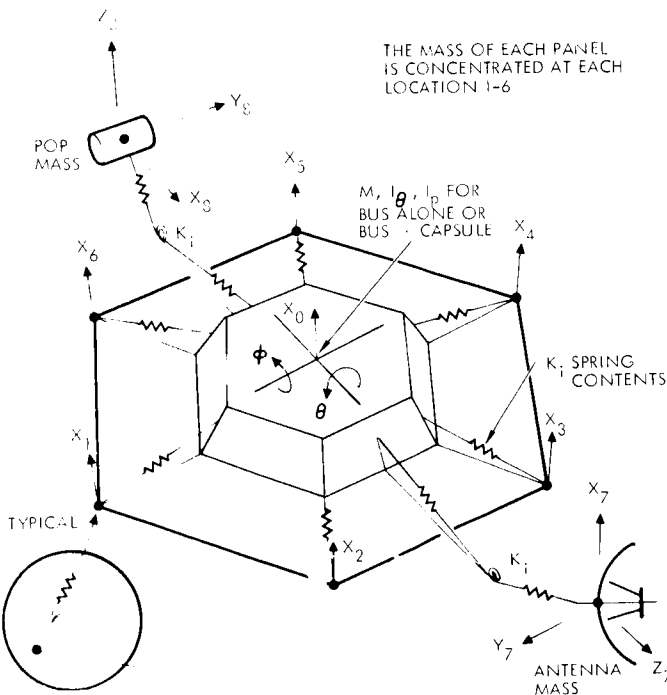


Figure 5-7. Dynamic Model for Free Flight

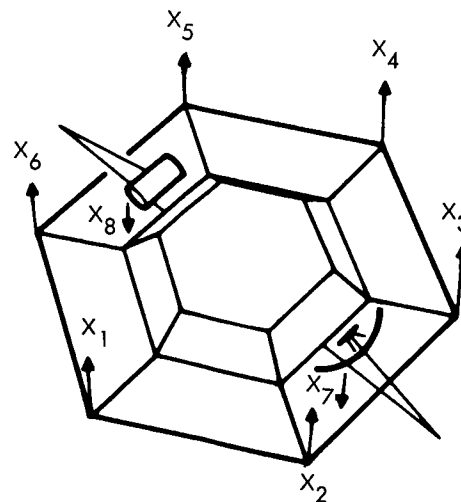


Figure 5-8. Dynamic Model For Launch

The models are put into a mathematical format which includes a mass matrix and stiffness (influence coefficient) matrix. A general form is used so that minor changes in structure can be incorporated and evaluated. A more accurate stiffness matrix will be generated by using the Douglas Redundant Force Program in the final production design analysis. The derivation of the mass and stiffness matrices for the models are shown in Section 2 of Appendix C.

#### 1.2.4 Meteoroid Protection Analysis

Structural resistance to meteoroid penetration was determined using the environment shown in the mission specification and the Summers and Charters penetration equation. Figures 5-9 through 5-11 plot the data for the environments near earth, in transit, and in Mars orbit. The effect of the near-earth environment on structural protection requirements is negligible because the stay-time is short. Transit and Mars orbit environments are critical. Transit time is taken as 177 days, with one-half of this time for particle flux in the vicinity of earth and the other half for the vicinity of Mars. Two Mars-orbit times were considered, 1 month and 6 months. Nominal and extreme environments for both phases were analyzed; their effects on structural requirements are discussed in Section 1 of Appendix C. Figure 5-12 shows the nominal environment structural requirements. The effect of extending the transit time to 250 days is also shown on this figure.

In addition to environment and time, exposed area and a model for predicting penetration are needed to determine structural thicknesses. Two approaches to spacecraft exposed area were investigated: 1) total surface area and 2) effective or equivalent surface area. The total surface area approach uses all the exposed area but does not include the upper portion of the spacecraft for the transit phase of the mission. Adopting the concept of the effective area further reduced this area by the shielding provided by the solar panels and reduced view angle provided by the flight capsule. This added shielding reduced the area 33 per cent during cruise. The area was reduced 9 per cent for Mars orbit since only the solar panels provided shielding and the area of the upper panel is fully effective (exposed). It was found for the transit phase, where the area difference between the two approaches is large that a 7 per cent reduction in structural

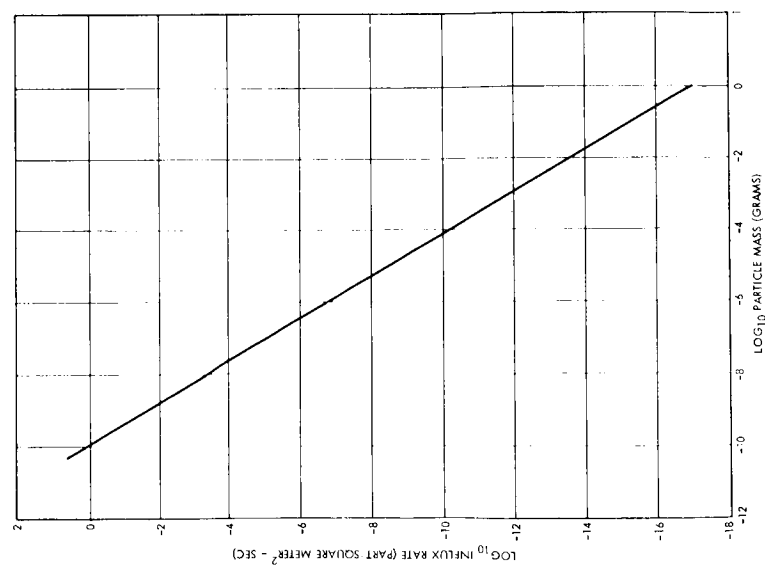


Figure 5-9. Meteoroid Influx Rate Near Earth

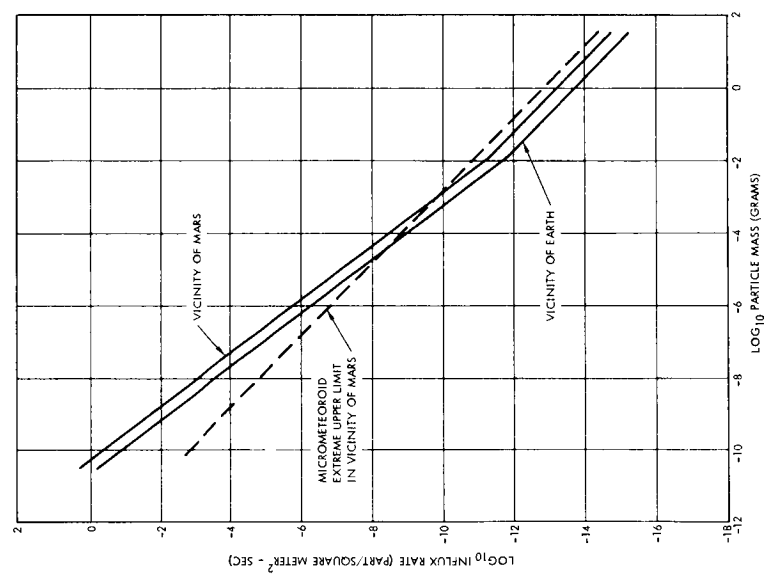


Figure 5-10. Meteoroid Influx Rate Cruise

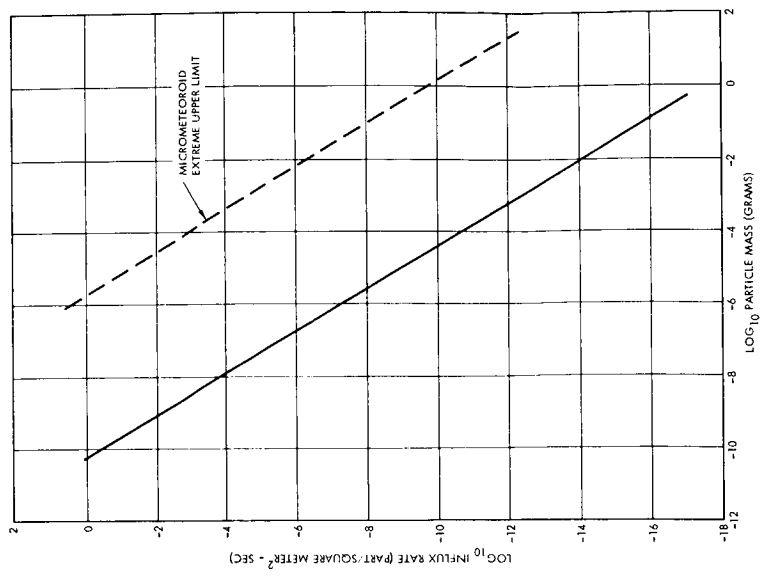


Figure 5-11. Meteoroid Influx Rate Circular Orbit

material is required, a negligible difference in view of the uncertainties in the penetration equations. Figure 5-12 and Table 5-8 show how the three theoretical approaches to penetration affect structural thicknesses. The effective approach and the nominal environment were used to determine the reliability of meteoroid protection. The Summers and Charters penetration equation was selected because of the three equations studied it was the most conservative for the nominal environment.

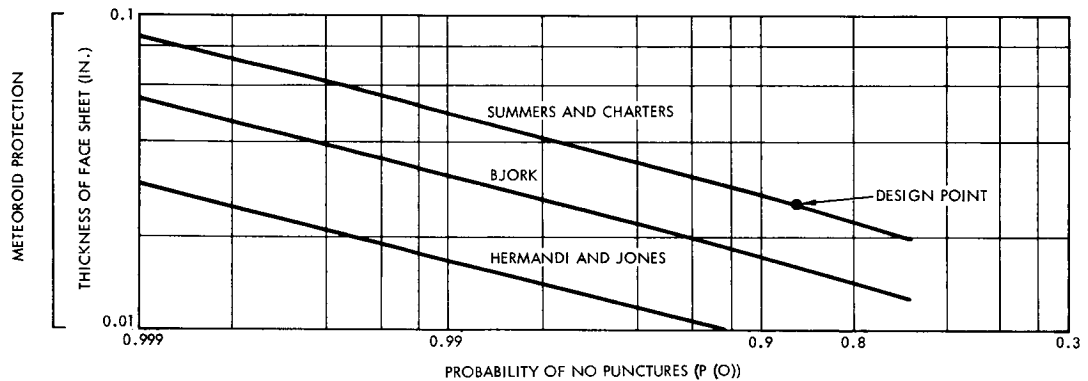


Figure 5-12. Sandwich Face Thickness Versus Probability Of No Puncture

Table 5-8. Penetration Equations\*

Theory	Equation
Summers and Charters	$\frac{p}{d} = 2.28 \left( \frac{\rho_p}{\rho_t} \right)^{2/3} \left( \frac{V}{C_t} \right)^{2/3}$
Bjork	$\frac{p}{d} = 0.88 (\rho_p V)^{1/3} \left( \frac{\rho_p}{\rho_t} \right)^{0.18}$
Herrmann and Jones	$\frac{p}{d} = 0.6 \left( \frac{\rho_p}{\rho_t} \right)^{1/3} \ln \left[ 1 + \left( \frac{\rho_p}{\rho_t} \right)^{2/3} \frac{\rho_t V^2}{0.03922 H_t} \right]$

\*See Section 1 of Appendix C.



Table 5-8. Penetration Equations (continued)

where

---

$p$	=	depth of penetration
$d$	=	particle diameter
$p_p$	=	density of particle
$p_t$	=	density of target
$V$	=	velocity of particle
$C_t$	=	speed of sound of target
$H_t$	=	Brinell hardness

---

The zero penetration probability is 0.868 for a 0.025-inch face thickness. When coupled with the failure mode analysis, it provided a reliability for meteoroid protection in excess of 0.97. Section 1 of Appendix C shows this reliability analysis. Figure 5-12 shows the variation in face thickness as a function of probability of no punctures. If the face thickness increases, the probability of zero puncture is greater. The reliability analysis shows that an increase in face thickness, or probability of no puncture, improves the reliability of the meteoroid shield. For a thickness of 0.030 inch the reliability increases to 0.987.

The increase in structural weight is 29.8 pounds.

#### 1.2.5 Structural Reliability

Structural reliability is considered as a constant for all Voyager configurations and structural component designs except for the reliability associated with meteoroid protection. For all configurations as discussed in Appendix C, a statistical-stress-versus-strength approach was employed based on a 1.25 safety factor and a zero margin of safety for each structural member.

In this preliminary analysis, it was assumed that catastrophic failure of any one structural member produced a catastrophic mission failure and that all structural members had equal reliability. These assumptions allowed calculations of a single member's reliability; raising that value to the 80<sup>th</sup> power, the estimated number of structural members, provided an estimate of the structural subsystem reliability.

In addition to deriving a best estimate for the structural reliability,  $R_s$ , a  $\pm 3\sigma$  confidence interval was obtained to indicate the degree of uncertainty associated with this analysis. The results are  $R_s$  (lower limit) 0.9830,  $R_s$  (best estimate) 0.9973, and  $R_s$  (upper limit) 0.9995. These values apply to all Voyager structural configurations since the structural member count in each configuration does not significantly vary from 80. Since all structural members are designed according to the same general guidelines, the reliability of one structural member design does not change. Material changes do have an effect on component reliability, but their effect is small enough to be neglected in this analysis.

#### 1.2.6 Manufacturing

Of the six Voyager structural configurations reviewed for comparative production complexities, the one presenting the least problems during fabrication, assembly, and production test is Configuration A-3.

The one disadvantage to this concept is that the outer bus structure subassembly is not as inherently rigid as some of the other structures reviewed (Configurations A-1 and B-1). This factor will add to the difficulties encountered, in machining the planes for the interface between the bus and the flight capsule, between the engine thrust cone and the engine, and between the bus and the Centaur adapter. More elaborate fixturing will be required to support the assembly during the interface machining operations. It is possible that special milling equipment will be mounted on the assembly jigs, so that these planes can be machined while the assembly is supported by the assembly tooling.

Configuration A-2 is next in the order of preference, although this concept, like A-3, offers less structural rigidity than some of the other designs. Configuration A-3 is preferred to A-2, since its design eliminates the joint between the two bus subassemblies. This total elimination of one interface actually means one less subassembly to be fabricated and assembled. It also reduces from five to three the number of interface planes which require machining after assembly.

Configuration A-1 has the advantage of more structural rigidity for interface machining. However, the additional box-type structure for instrument and louver panel mounting means more pieces to fabricate and

more assemblies to be made than on either Configuration A-2, A-3, or B-2. The area to be insulated is increased and its application is made more difficult by the added corners and many different surfaces.

Also the contoured honeycomb panels used on the aft structure require more tooling and are more difficult to fabricate and assemble than the flat panels used on Configurations A-2, A-3, and B-2.

Configuration B-1 presents approximately the same advantages and disadvantages as Configuration A-1 except that the disadvantages are more pronounced in that more contoured honeycomb paneling is used: added contoured panels include the aft meteoroid panel and the sections of the bus outer structure forward and aft of the louver panel box-type structure. Additionally, liquid engine as compared with solid motor configurations introduce more complexities in manufacturing, again because more parts are involved. Additional hardware is required to mount the tanks and bottles, more plumbing is required, and additional parts such as actuators and valves must be fabricated, assembled, and tested. The engine section must be sent to a test site for test firing after it is assembled. Time for shipping, cleanup, tools, and shipping fixtures required for transportation to and from the site and time lost from the standard manufacturing flow are considerations.

Configuration B-2 is, again, not as stable for interface machining operations as either Configurations A-1 or B-1. It, too, presents the added complexities for liquid engine concepts that are listed for Configuration B-1.

Configuration C-2 has factors which make its production somewhat more complex than any of the others. Its general arrangement will not permit the midcourse propulsion system to be built up and tested as a unit prior to final assembly. The deployable solar panels add to the overall manufacturing problems for the following reasons:

- a) An additional interchangeable hinge pattern must be controlled on panels and mounting structure.
- b) The panels themselves become more complicated. The hinge mechanism and the strongback beam are additional requirements for these panels.

- c) Flexible connections for attitude control plumbing make this system more difficult to fabricate, assemble, and test.
- d) Actuators are required. These are additional pieces of hardware requiring fabrication, assembly, and production testing.

The fixed antenna adds to the manufacturing problems:

- a) The interface pattern between the top and bottom bus structure subassemblies requires further control. This pattern must be coordinated with and controlled for the antenna manufacturer.
- b) The structures supporting the solar panels, the science payload, and the omni antenna tie onto the fixed antenna. This antenna must be installed before these structures can be located. This factor makes the manufacturing flow dependent upon the timely delivery of this item. Its early installation makes it much more vulnerable to damage during the final assembly procedures, and protective devices must be furnished for its protection.

#### 1.2.7 Relative Costs

Manufacturing comparisons have been made on Configurations A-1, A-2, A-3, B-1, B-2, and C-2. For purposes of comparison, Configuration A-2 is considered as the baseline at 100 per cent cost. All other configurations are related to it.

Configuration A-1 has certain manufacturing advantages which were pointed out in the previous discussion. Cost makes these advantages complex because of added details and complex machining, thus placing Configuration A-1 at about 125 per cent of baseline cost.

Configuration A-3 appears to have manufacturing advantages which will translate into cost advantages in some areas. The elimination of a structural interface between the solid motor section and the midcourse motor section offers attractive savings in both tooling and fabrication requirements. The extent to which these savings will be offset by complexities in the installation and assembly of interior hardware is not precisely known at this time, but a general assessment of Configuration A-3 indicates a probable rating with the Configuration A-2 baseline, 85 per cent of cost.

Configuration B-1 (liquid fueled version), in addition to the manufacturing complexities of A-1, has the costs of the large, thin-wall titanium tanks, their attendant plumbing, servos, manifolding, and supports which give Configuration B-1 a cost rating of approximately 190 per cent of baseline.

Configuration B-2 (also liquid fueled) has less manufacturing complexities than B-1 but has all the costs associated with the liquid fuel tank and attendant plumbing. A survey of costs in this version place it about 180 per cent of baseline.

Configuration C-2, as discussed in the manufacturing comparisons, have numerous manufacturing areas of complexity, such as space constraints, tending to complicate component positioning, support, and insulation. In addition, the requirement that solar panels be deployable complicates this area of cost, so that a comparison to baseline gives us a cost of approximately 175 per cent.

A summary of all the relative costs is shown in Table 5-9.

Table 5-9. Summary of Relative Costs of Various Configurations

Configuration	Relative Cost
A-1	1.25
A-2	1.00
A-3*	0.85
B-1	1.90
B-2	1.80
C-2	1.75

\* Selected configuration

### 1.3 Selection of Structural Component Design

The subassemblies and related components for the basic bus structure, propellant tank support, solid propellant support structure and solar panels are analyzed to provide information used to select the recommended structural designs. Items considered in the analyses are design, strength, and dynamic analysis, micrometeoroid protection, thermal analysis, manufacturing and relative cost.

#### 1.3.1 Basic Bus Structure

Tradeoff studies related to the basic bus design were divided into two categories, one evaluating the frame design and the other concentrating on the external panels.

##### a. Frame

Design. The primary load-carrying members are designed to meet the requirements of compression loading and the attachment of the mounting panels. Other considerations were the attach fitting design at the flight capsule and Centaur interfaces, separation system compatibility, and end frame attachment. Two corner post designs were generated (Figure 5-13).

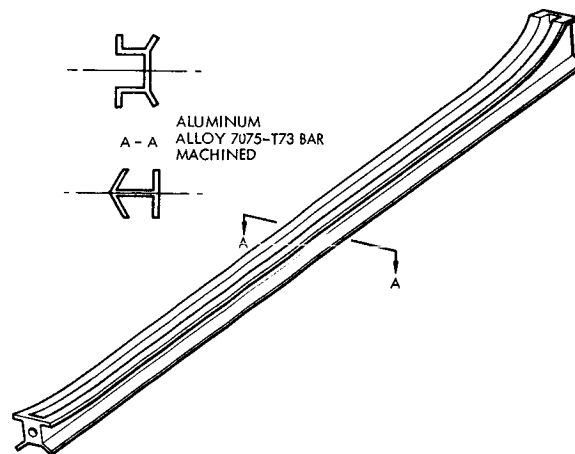


Figure 5-13. Corner Post Design

Although the I-beam offers a somewhat better compression cross-section, the I-beam corner post design is better fitted for the eight-sided configurations than the six-sided ones and the use of single bolt integral end fittings is more difficult with this design. The  $\pi$ -section design can be applied equally well to all configurations and can easily incorporate the

integral end fittings. For these reasons the  $\pi$ -section design (Figure 5-13) is recommended.

Several different materials were evaluated for these members: 7075-T73, 2014-T6, 2024-T4, Lockalloy and beryllium. All designs can be adapted to use any of these materials. The fact that aluminum alloys have been used more widely make them appear the most promising from an over-all design standpoint.

Strength Analysis. Compression is the primary loading condition but tension is also an important condition. The results of the trade-off study, shown in Table 5-10, based on a column strength, indicate that no weight advantage is associated with the aluminum alloys shown. However, the secondary loading condition must be considered. This strut has joints at each end which require integral fittings. These fittings are bolt-attachment points, and the load at its baseplate caused by tension developed during a rebound or high lateral load will be plate bending. To avoid experiment, a material with high allowable tensile stress is desirable. The aluminum alloy 7075-T73 satisfies this condition as well as showing a high resistance to stress corrosion cracking.

Table 5-10. Material Stress and Weight\*

Material	Unit Weight (lb/in)
2014 Aluminum	0.083
2024 Aluminum	0.083
7075 Aluminum	0.083
Lockalloy	0.025
Beryllium	0.025

\* See Section 2 of Appendix C

Dynamic Analysis of Spacecraft Attachment Bolts. The spacecraft attachment bolts connect to integral fittings of the longitudinal frames. The critical flight condition for the aft set of bolts will be detonation shock resulting from Centaur separation from the SIVB stage. Upper limits to forward and aft bolt loadings were calculated (see Section 2, Appendix C), based on distribution through Centaur and spacecraft of the fraction of detonation energy converted to vibration kinetic energy. Allowable bolt loadings were calculated, based on the ultimate tensile strength and strain.

The major assumptions used in the analysis were:

- 1) Kinetic energy resulting from detonation is distributed through a few of the lower modes of vibration.
- 2) Kinetic energy in the compression modes is one half of the kinetic energy in the breathing modes.
- 3) Kinetic energy transfer across a joint is 50%.
- 4) Peak response accelerations attenuate somewhat with distance from the detonation.
- 5) One third of the Centaur propellant acts with the Centaur structure in vibration.
- 6) The payload interstage will deform in bending during breathing modes of vibration, and the spacecraft bolts and shear pins will not experience excessive shear deflections.

Results of the analysis indicate the bolts should transmit the shock loading without bolt failure. Predicted and allowable loadings are shown on Figure 5-14.

Relative Cost. Five materials were considered during the manufacturing investigations. Their relative costs are shown in Table 5-11.

Recommended Design. A  $\pi$  cross-section (Figure 5-13) machined column with integral-end fittings on both ends is recommended



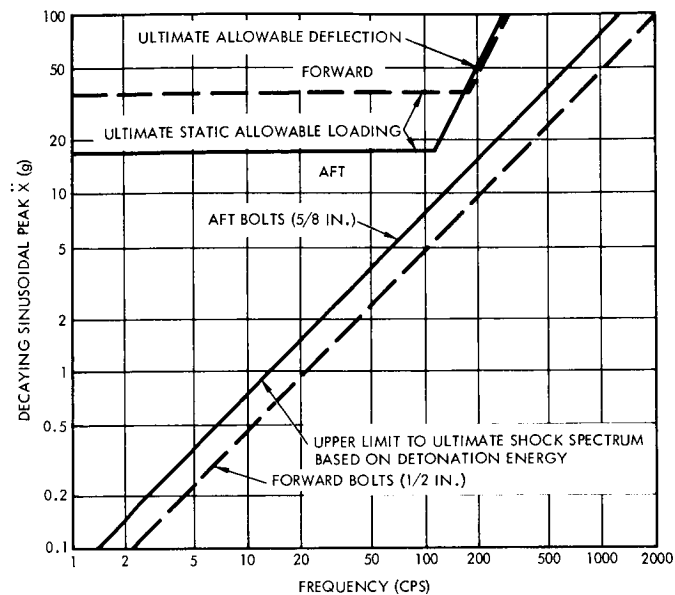


Figure 5-14. Predictable and Allowable Bolt Loading

Table 5-11. Summary of Relative Costs of Various Materials

Materials	Relative Cost
2014	1.00
2024	1.05
7075	1.25
Lockalloy	2.00
Beryllium	2.25

using 7075-T73 for construction. Cross-section was selected because:

- 1) It provides for good panel attachment.
- 2) It constitutes a good compression member.
- 3) It allows for external access to end bolts.

7075 - T73 was selected because:

- 1) It is high-strength and provides resistance to stress.
- 2) Its weight is acceptable.
- 3) Its manufacturing techniques are well established.
- 4) The over-all cost is low compared to beryllium and Lockalloy.
- 5) The T73 heat treat provides better resistance to stress corrosion cracking than T6 heat treat.
- 6) It provides high allowable tensile stress.

b. Equipment Mounting Panels

Design. The equipment mounting panels offer the opportunity to incorporate several functions into one structural member. The panels are the mounting member for electronic subsystems. They are the principal shear carrying members of the spacecraft, provide meteoroid protection, and are an integral part of the bus thermal control system. Additional requirements are the provision for the correct dynamic response for the electronic components, design for ease of electronic component replacement, and the provision for a design capable of flexible mounting locations.

The four most promising designs are shown in Figure 5-15. The first design (a) uses a 1-inch thick aluminum honeycomb panel with a truss-grid core. I, V and extruded members are attached to the inside face and provide the mounting surfaces of the electronic components. The second design (b) uses the same mounting method but replaces the honeycomb panel with a member consisting of two skins,

1 inch apart, jointed by Z-section stiffeners in line with the mounting rails. A single-skin, armor-plate design with mounting rails is shown in (c). The last design (d) uses a honeycomb panel with equipment mounted directly to it by means of inserts epoxied into the panel.

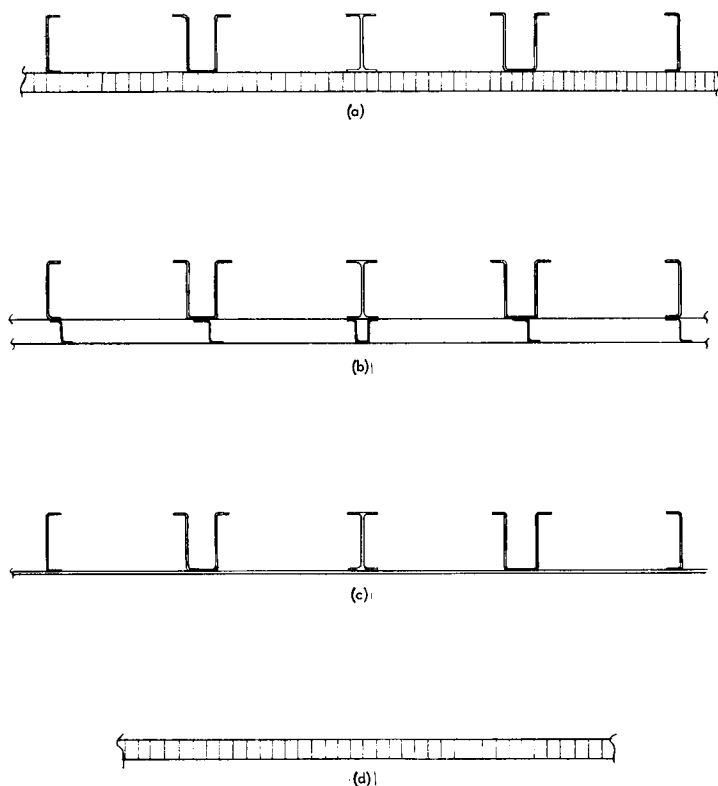


Figure 5-15 Equipment Mounting Panel Design

The following chart indicates an evaluation comparison between the four equipment mounting panel concepts for purpose in aiding in the selection of preferred mounting concepts.

	See Figure 5-15	Thermal Control	Load Carrying Shear Member	Meteoroid Protection	Stiffness	Weight	Flexibility for Equipment Mounting	TOTAL
Honeycomb panel and rail	a	8	10	10	10	6	10	54
Z sandwich panel and rail	b	8	7	8	7	7	10	47
Armor sheet and rail	c	10	9	6	5	4	10	44
Honeycomb panel	d	8	10	10	6	10	8	52

No single design is best for all the varied requirements; however, the one that seems to best satisfy the most design requirements is (a).

Strength Analysis. The equipment-mounting panels were analyzed to establish their shear strength. Figure 5-16 shows the allowable shear stress and the applied stress because of torsion. It is evident

that the strength of these panels is more than adequate, regardless of the face material or core thickness. The selection of the material and core thickness can therefore be based on other considerations.

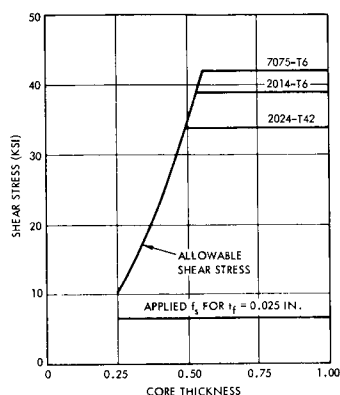


Figure 5-16. Panel Allowable and Applied Stress

The analysis of these panels was based on a sandwich design without equipment mounting rails. It is conservative to apply the conclusions drawn from this analysis to the other designs considered in this tradeoff study. The weight breakdown for all of the designs is shown in Table 5-12.

Dynamic Analysis. The natural frequencies of the candidate panels were calculated to provide stiffness comparisons. A Maximum equipment weight of 130 pounds, uniformly distributed, was assumed for this analysis. For the case of less equipment weight not evenly distributed, this analysis is slightly conservative, that is, calculated frequencies will be lower than actual frequencies. Stiffness in both panel directions was calculated: for design concepts 1 and 5, composite beam stiffness will govern frequencies; for design concepts 2, 3, and 4, plate stiffness will govern frequencies. The frequencies of the five designs are presented in Table 5-13. Panel design concepts 3 and 4 are variations on the basic nonstiffened honeycomb sandwich design. Concept 3 shows the effect of increasing the face thickness to 0.065 inches, and concept 4 shows the change in frequencies because of an

Table 5-12. Equipment Panels Weight Breakdowns

Note: Area = 11.9 ft.<sup>2</sup>/panel (used for weight comparison only)

Configuration/Item	Weight (lb)
<u>Honeycomb Construction (d)</u>	
Faces	8.6
Core	3.1
Bond	1.0
Closing Channels	2.7
Inserts	1.1
Attach and Misc. (6 per cent)	<u>1.0</u>
Total	17.5
<u>Honeycomb and Rails (a)</u>	
Honeycomb Construction	17.5
Rails	11.9
Attach and Misc. (6 per cent)	<u>0.6</u>
Total	30.0
<u>Monocoque Sheet and Rails (c)</u>	
Monocoque Sheet	25.8
Rails	11.9
Attach and Misc. (6 per cent)	<u>2.2</u>
Total	39.9
<u>Space Sandwich and Rails (b)</u>	
Faces	8.6
Main E Sections	2.2
Secondary E Sections	1.4
Rails	11.9
Inserts	
Closing Channels	3.0
Attach and Misc. (6 per cent)	<u>1.5</u>
Total	28.6

increased core thickness from 1 to 2 inches and face thickness increased to 0.055 inch. On a stiffness basis the design concepts 4 and 5 are adequate, since DAC and TRW experience indicates electronic equipment panels with natural frequencies above 50 cps are satisfactory.

Table 5-13. Summary of Dynamic Analysis\*

Panel Design Concept	Frequency (cps)		
	1st Mode	2nd Mode	3rd Mode
1. Plate and rails	58	232	521
2. Basic sandwich	43	96	121
3. Sandwich with 0.065-in. faces	46	101	127
4. Sandwich with 0.055-in. faces but 2-in. core	84	187	235
5. Basic sandwich with rails (1-in. core)	145	284	360

\* See Section 2 of Appendix C

Meteoroid Analysis. Tradeoff studies were conducted to determine how material and core thickness affect the meteoroid protection qualities of spacecraft structure. Figure 5-17 shows the relative weights of beryllium, magnesium, aluminum, titanium, and stainless steel to provide equivalent material resistance to penetration. The Charter and Summers penetration equation was used to obtain the values with speed of sound and density of the target materials as variables in the analysis. Considering aluminum as the base for this evaluation, beryllium shows a 51.5 per cent reduction in weight and magnesium, a 12.7 per cent reduction. The two materials studied, heavier than aluminum are titanium (19 per cent) and stainless steel (40 per cent). Penetration

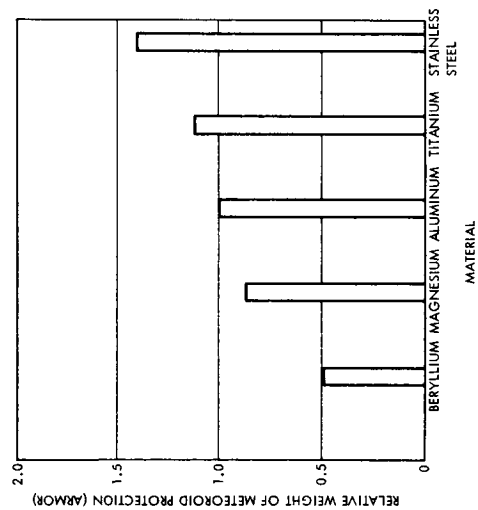


Figure 5-17. Material Comparison for Meteoroid Protection

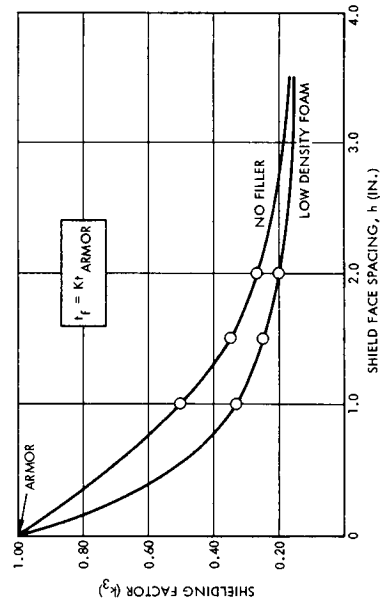


Figure 5-18. Meteoroid Shielding Factor

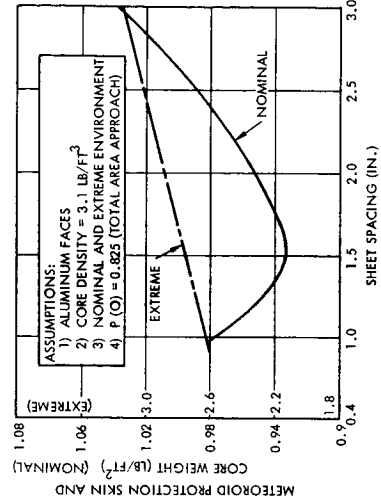


Figure 5-19. Optimum Sheet Spacing for Meteoroid Protection



experiments have shown that aluminum is superior on a weight basis to beryllium-copper, molybdenum, tantalum, Rene 41 and other materials. \*

Designs that incorporate spaced-sheet provide a large increase in stopping power over armor-plate or single-sheet designs. Figure 5-18 shows this effect. \*\* Using this data and the nominal meteoroid environment, an optimum sheet spacing was obtained. When the extreme environment was considered, an optimum thickness did not show up. Figure 5-19 shows the results of this optimization study for both environments based on the same criteria of zero penetration and aluminum faces for the Whipple shield.

Thermodynamic Analysis. As discussed in Section 1.1, all structural designs sought the multiple use of structure. Thus equipment mounting panels, which are used as thermal radiators, had to satisfy requirements for meteoroid protection, minimum weight, and stiffness. A solid sheet is optimum for thermal requirements, but sandwich construction shows definite advantages in all other areas. A thermodynamic analysis was made to determine the effect of sandwich construction on the base plate temperature of the electronic equipment boxes. Results of this analysis are given in Section V.2 (Temperature Control).

Manufacturing. The four proposed designs were compared for manufacturing complexity. The design using a single skin and rails involved much less effort than any of the others because of simpler manufacturing operations; moreover, its assembly requires no special tooling. The double skin with Z- and J-section stiffeners design was preferred next. Access for bucking rivets can be obtained by peeling back the outer sheet during assembly, and using blind rivets to close off the panel. The truss-core sandwich designs were the least desirable. In addition to the more complex processing and handling operations, the possibility of damaging the buried threaded inserts is a greater risk than in the first designs where the nutplates are completely accessible for replacement.

---

\* Astronautics and Aeronautics, June 1963

\*\* V. C. Frost, Aerospace Report TOR-269 (4560-40)-Z

Relative Cost. Heavy gage panels with rails, Z-extrusion panels stiffened internally with extruded mounting rails, flat honeycomb panels with inserts for mounts, and flat honeycomb panels with extruded mounting rails were evaluated. Their relative costs are shown in Table 5-14.

Table 5-14. Relative Costs of Various Designs

Configuration	Relative Cost
Heavy Gauge Panels	1.00
Z-Extrusion Panels	1.20
Flat Honeycomb Panels	1.30
Flat Honeycomb Panel with Extruded Mounting Rails	1.40

Recommended Design. The recommended design is a 1-inch thick honeycomb panel with equipment mounting rails as shown in Figure 5-15 (see section VI for additional factors pertaining to the selection). The skin is 0.025 7075-T6 with a 3.1 lb/cu ft aluminum truss grid core. The mounting rails are 7075-T6 extrusions. The reasons for this selection are:

- 1) 1-inch core was selected as a compromise between meteoroid and thermal requirements.
- 2) Truss grid core was selected because it provides adequate strength, is a good energy absorber for meteoroids and the conductivity of the core is acceptable.
- 3) The design provides high frequency response.
- 4) High frequency response was considered more important than minimum weight.
- 5) 7075 material was selected for its thermal conductivity properties, ease of manufacture, low cost, and good meteoroid protection efficiency.
- 6) It provides high shear carrying capability.

a. Top and Bottom Panels

Design. Fewer requirements exist for the top and bottom panels than for the side panels. Their principal functions are to provide meteoroid protection and act as the end shear members. In addition the bottom panel helps support the midcourse propulsion system. These designs are proposed for the top and bottom panels (see Figure 5-20). A standard 1-inch thick truss grid honeycomb panel is shown in Figure 5-20(a). The second design (b) uses two skins spaced apart by Z-section stringers approximately 7 inches on center. The last design is a beaded single skin configuration (c).

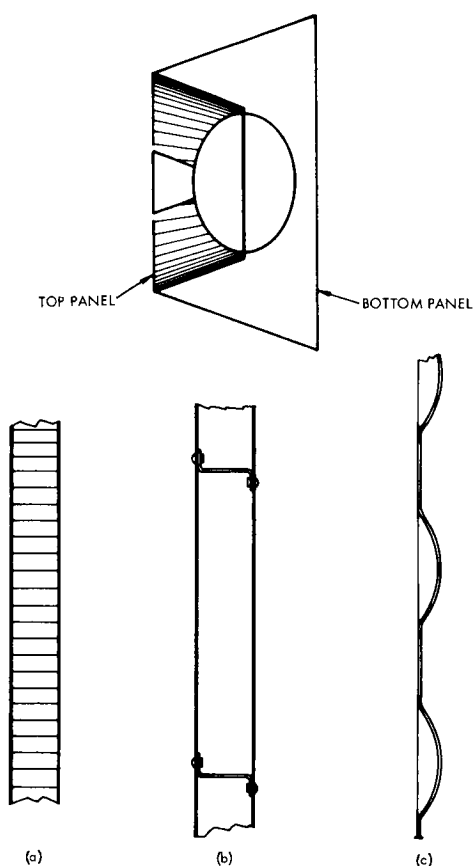


Figure 5-20. Designs for Top and Bottom Panels

The solid propellant motor is protected from meteoroids by the flight capsule and its sterilization container until just before orbital injection firing, after which it does not require protection. In fact, after burn-out the motor case along with the thrust cone provides a second meteoroid barrier for the basic bus. This fact allows the single-skin design

shown in Figure 5-20(c) for working with the second barrier, since it is an efficient Whipple shield. The aft panel requires a two-skin design for meteoroid protection requirements. The weight breakdown for the top panel designs considered is shown in Table 5-15.

Meteoroid Protection. The meteoroid protection requirements for the panel at Stations 1 and 59 (top and bottom of the spacecraft) are the same as those of the equipment mounting panels; however, there are significant differences in total requirements. The top and bottom panels do not have the thermal or vibration restraints to contend with, and the top panel is completely shielded during transit from earth to Mars. Since the exposure time and surface associated with this panel is small, it can be a beaded single skin. For the selected configuration, a semimonocoque thrust cone used in the solid engine support would in effect act as a second sheet. This combination of two sheets, with a large standoff, would provide superior meteoroid shielding for equipment. The bottom panel is exposed during the entire mission. Since the thermal restraint of high conductivity does not apply to the bottom panel, however, the core thickness can be increased from the 1-inch selected for the equipment panels. As shown on Figure 5-19 the optimum thickness is approximately 1.5 inches. An increase in panel stiffness also is achieved.

Manufacturing. Top panels under consideration are 2 facing-sheets separated by Z-section spacers, flat facing-sheets reinforced by beaded panels, and thruss-grid aluminum honeycomb panels.

The construction method involving the least manufacturing effort is the second item, the beaded-panel reinforced structure. Simple fabrication requirements and the ability to assemble the panels without tooling contribute to this preference. The second choice is the two facing-sheets separated by Z-section spacers. Again the fabrication requirements are unsophisticated, and a simple fixture can fulfill the assembly needs. The last choice is the truss-cone sandwich. The more complex

Table 5-15. Bus Top Panel Structure Weight Breakdowns

Note: Area = 31.4 sq ft

Configuration/Item	Weight (lb)
<u>Honeycomb Construction</u>	
Faces	22.7
Core	8.1
Bond	2.5
Closing Channels	3.0
Attach and Misc. (6 per cent)	<u>2.2</u>
Total	38.5
<u>Space Sandwich Construction</u>	
Faces	22.7
Stringers	3.8
Mid-Frame	0.7
Closing Channels	4.6
Attach and Misc. (6 per cent)	<u>1.9</u>
Total	33.7
<u>Beaded Sheet Construction</u>	
Top Panel	9.1
Inner Ring	0.2
Inner Sheet	4.0
Additional Frame Weight	4.8
Attach and Misc. (6 per cent)	<u>1.1</u>
Total	19.2

assembly procedure, the handling and processing, and the additional time required to layup and bond the assembly make this configuration the least attractive of the three.

Relative Cost. The relative costs of the panels considered are shown in Table 5-16.

Table 5-16. Summary of Relative Costs  
of Top and Bottom Panels

Configuration	Relative Cost
Beaded Panel	1.00
Compound Panel	1.20
Honeycomb Panel	1.35

Recommended Design. For the top panel a single skin beaded panel of 7075-T6 aluminum as shown in Figure 5-20(c) was selected because:

- 1) Lightest design
- 2) Provides adequate meteoroid protection
- 3) Best from a fabrication standpoint
- 4) Low cost design
- 5) Provides adequate shear strength.

For the bottom panel, the 1.5-inch thick honeycomb panel as shown in Figure 5-20(a) was selected with skins of 0.025 7075-T6 aluminum with a 3.1 lb/cu ft truss-grid aluminum core because:

- 1) 1.5-inch core was selected as optimum for meteoroid protection and provides increased bending strength for monopropellant system support.
- 2) Provides a universal mounting surface.

### 1.3.2 Propellant Tank Support Structure

#### a. Design

The principal design considerations in the tank support methods are tank restraint, stress concentrations, and weight. A method must be used that does not impose additional loads from deflection of the supporting structure and does not impart a localized load to the tanks. The two designs presented in Figure 5-21 satisfy these requirements. The design in (a) consists of a conical support flange on a horizontally mounted support structure. Two tension straps at 90 degrees to each other go over the top of the tank where they are joined and down to the base where they attach with tensioning straps. This design is the general method that has been successfully used by Douglas on all Saturn IV boosters for small tank mounting. The second design (b) has a horizontal support flange at the maximum tank diameter. An integral flange on the tank sets down on this support flange. The tank bolts down to the flange. Slotted holes in the flange and spacers to prevent high torquing of the tank to the support allow for fuel tank expansion

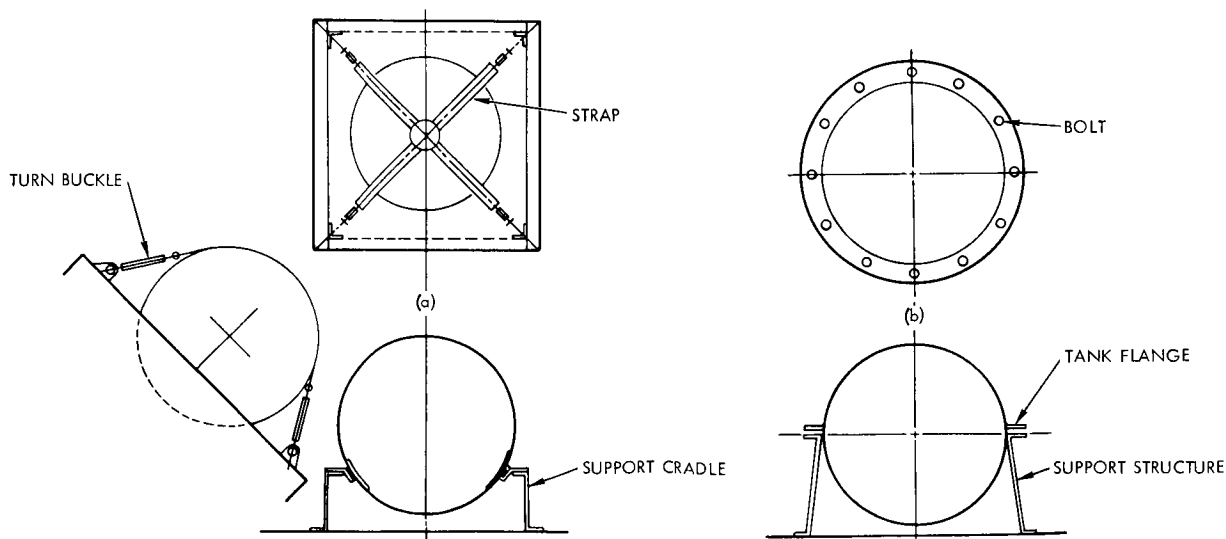


Figure 5-21. Typical Tank Attachment and Support Structure

b. Strength Analysis

The most efficient shape for the tanks is spherical but this shape presents a problem in attachment to the spacecraft structure. Two major methods of mounting are proposed: one is a strapping of the tanks to a base, the other is to have an integral hemispherical ring on the tank to mount a base.

The strapped mounting consists of resting the tank on a base support with four pretensioned straps retaining it. An analysis was made of the monopropellant tanks with 1.25-inch wide by 0.030-inch thick straps pretensioned to 20,000 psi. The attitude of the tank was chosen to impart the highest inertial load to the system (see Section 2 of Appendix C). The major contributors to the strap load were the pretensioning and the bottle pressurization. An increase in general thickness occurs at the base edge on the tank and at the hub for the strap intersection.

The integral hemispherical ring consists of a flange for mounting the tank to a backup structure. An analysis was made of the monopropellant tanks with an 0.050-inch-thick ring. It was concluded that the greatest contributor to the stress level was the discontinuity caused by the hemispherical ring. An increase in thickness is required in the tank wall in this area. Table 5-17 shows weight breakdowns.

c. Manufacturing

A restraining method which cradles the tank in a formed support by straps has been compared to a method which utilizes a sheet metal cylinder with a flange at one end and four lugs at the other for ease of manufacturing. The flange bolts to a ring, which is integral with the tank at the tank equator, and the lugs are for bolts which secure the assembly to the bus structure.

The formed support and retaining straps involve somewhat less manufacturing effort than that involved in the second method of securing the tank. The addition of the integral ring to the tank creates



Table 5-17. Tank Support Structure Weight Breakdown

Configuration/Item	Weight (lb)
<u>Cradle Support</u>	
Cradle Side	2.14
Cradle Top	2.33
Collar	0.70
Frames	0.25
Tank Pad	0.18
Harness	0.40
End Fittings	0.40
Attach and Misc.	0.38
Total	6.78
<u>Flange Support</u>	
Support Structure	3.15
Tank Flange	0.75
Tank Pad	0.51
Attach and Misc.	0.26
Total	4.67

additional effort in the manufacture of the tank itself. The fabrication of the remainder of the items would involve substantially equal effort for either configuration.

d. Relative Cost

A manufacturing investigation of the two proposed propellant tank-support methods indicated both systems about equal from a cost standpoint.

e. Recommended Design

The recommended design is the cradle-supported tank with straps. However, only two design concepts were analyzed in this study; other designs should be investigated to ensure that the best approach is selected. Since the results of the analyses show only small differences, the cradle-and strap arrangement was selected because this concept is a flight-test proven design.

### 1. 3. 3 Solid Propellant Support Structure

#### a. Design

The main design consideration for the solid-propellant support structure was to provide uniform support for the motor case. Thermal isolation of the structure, weight and rigid compression structure were also considered. Three designs were evaluated. The first design consists of a semimonocoque truncated cone with 7075-T73 skin and hat-section stringers. Six of the hats transfer all loads from the cone to the six main load-carrying members of the bus. A fiber glass attach-angle mounts to the motor and provides insulation during and after firing as shown in Figure 5-22(a). A second design is similar, differing only in that it uses a monocoque skin design reinforced in the six bus attach points.

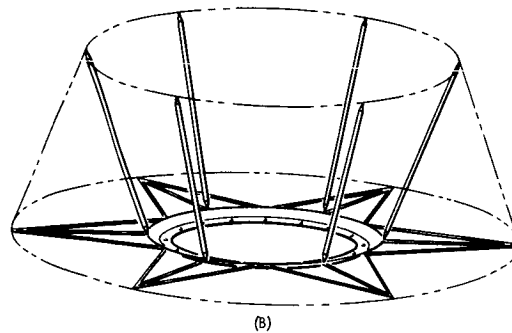
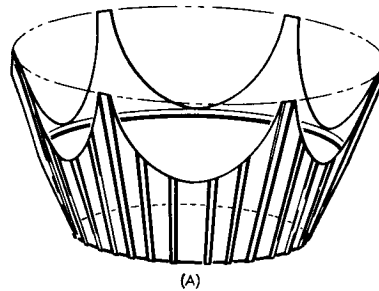


Figure 5-22. Solid Motor Support Structure

The last design uses a tubular truss with six tubes running radially up from an engine attach ring to the bus load points at Station 59. Eighteen horizontal tubes carry side and torsional loads to the bus structure as shown in (b).

b. Analysis

The solid retroengine motor case is an oblate spheroid with a mounting ring at the midplane of its motor case. This ring provides the mounting provision for the engine. Three supporting systems were analyzed: a truss work, a cone of skin and stringers, and a monocoque cone. Although the truss system is the lightest, it introduces concentrated loads at the engine case. It is sized by both the maximum longitudinal load condition and by the rebound load condition (see Section 2 of Appendix C). The skin-and-stringer cone is scalloped at its attachment to the spacecraft structure introducing hard points and a shear in the skin. This shear load sizes the skin and the hard point load sizes the hard point stringers. The critical load condition is the rebound.

The monocoque cone is sized for over-all buckling stability coming from the rebound condition. It is the heaviest of the three systems studied. None of the systems were sized by engine peak thrust, but local attachments will be. Table 5-18 shows the weight breakdowns of this structure.

c. Dynamic Load Conditions at Retrothrust

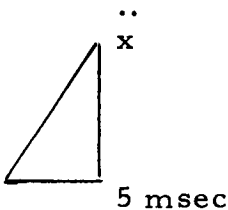
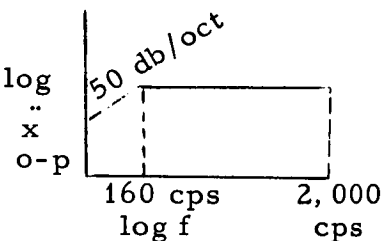
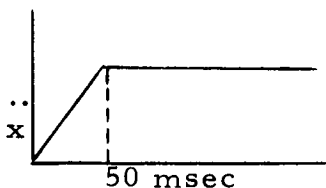
Shock and vibration loadings at the retrothrust motor supports are based on an analysis of Goddard Space Flight Center Report No. 631-141 to obtain estimates of sea level vibration and ratios of vacuum to sea level vibration. Results indicate some reduction of ignition shock and an order of magnitude reduction in steady random mechanical vibration for vacuum (versus sea-level) firing. Based upon experience with other motors, and a weight ratio procedure from NASA TND-1836, predicted vibration and shock levels were obtained for the solid and bipropellant configurations.

Table 5-18. Solid Motor Support Structure  
Weight Breakdowns

Configuration/Item	Weight (lb)
<u>Thrust Cone-Scalloped Skin and Stringer</u>	
Intermediate Frame	1.19
Lower Frame	1.93
Main Support Strut	2.16
Intermediate Stringers	1.95
End Fittings	1.86
Lower Skin	6.60
Upper Skin	2.63
Side Truss	6.71
Attach and Misc. (6 per cent)	1.50
Total	26.53
<u>Thrust Cone-Monocoque</u>	
Skin	30.8
Doublers	1.8
End Fittings	1.9
Lower Frame	1.9
Side Truss	6.7
Attach and Misc. (6 per cent)	2.6
Total	45.7
<u>Truss Support</u>	
Longitudinal Load Members	4.25
Lateral Load Members	3.64
End Fittings	4.43
Motor Attach Ring	8.04
End Lateral Ring (Main Structure) Gussets	1.10
Mid Lateral Ring (Main Structure) Gussets	0.38
Attach and Misc. (6 per cent)	1.31
Total	23.15

The bipropellant levels are less reliable in this analysis since most of the available data was for solid propellant motors. Predicted dynamic loads at the motor supports are presented in Table 5-19.

Table 5-19. Predicted Dynamic Loads for Retrothrust Motors

Dynamic Load	Direction	Solid	Bipropellant
Equivalent Shock: 	Longitudinal Lateral	4.0 g 1.9 g	7.9 g 3.8 g
Vibration: 	Longitudinal Lateral  Duration	0.4 g 0.2 g  95 sec	0.5 g 0.3 g  830 sec
Thrust: 	Longitudinal Nominal  Longitudinal Maximum (3σ and Temperature Factors)	8,000 lb  8,800 lb	1,000 lb  1,000 lb

#### d. Manufacturing

For motor thrust-cone fabrication, the configurations compared for manufacturing effort are a sheet metal thrust-cone structure and a concept consisting of a set of strut members supporting an engine-mount ring.

In terms of manufacturing effort alone, the strut members and ring are more desirable. However, the mount ring supports a fiber glass heat block which is machined after assembly. This machining consists of facing the matching interface plane for the solid engine case. It is felt that the additional rigidity of the metal conical structure will better assure the integrity of this critical interface plane.

e. Relative Cost

The manufacturing cost evaluation of the two proposed solid propellant motor support designs slightly favors the tubular truss design.

f. Recommended Design

The selected design is a semimonocoque truncated cone as shown in Figure 5-22(a). The skin and all stringers are 7075-T6 aluminum. This was selected because:

- 1) It provides uniform support for the solid motor case.
- 2) It provides an efficient and rigid compression member.
- 3) It provides lightest design in combination with single skin top meteoroid panel.
- 4) It provides the second sheet of the two-sheet top panel meteoroid protection.
- 5) It is more compatible with configuration A-3.

1.3.4 Solar Panels

a. Design

Deflection and weight governed the solar panel structure design. The final tradeoff studies were based upon three different configurations. The cross-sections of each design are shown in Figure 5-23.

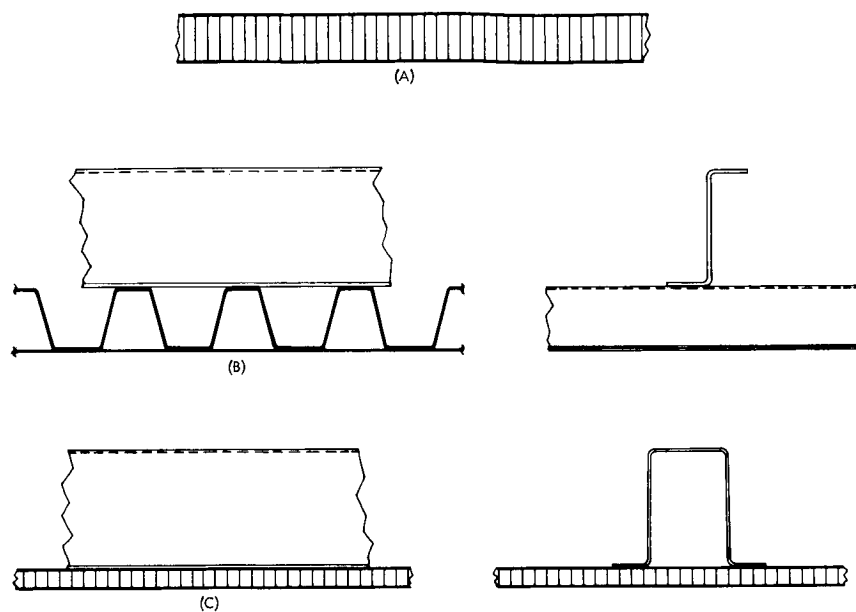


Figure 5-23. Solar Panel Cross Section Design

The honeycomb panel design (a) has a 1-inch-thick standard aluminum hex cell core with 0.010-inch 7075-T6 face sheets. All support is provided at the edge of the panels. Outer support on A3 is a transverse beam inside the edge.

The second design (b) consists of a flat 0.010-inch aluminum skin bonded to a corrugated sheet of 0.008 inch aluminum. The square corrugations, 1-3/8-inch high, run outward at right angles to the bus side. Two channel supports run parallel to the bus sides at the third points of the panel and end on the main panel support members.

The third design (c) consists of a 3/8-inch-thick aluminum honeycomb panel with 0.005-inch aluminum faces. Tapered hat sections with a maximum height of 3 inches will span the panel with two running parallel to the outer edge and the third running radially at the mid point of the panel.

#### b. Strength Analysis

Deflection of the solar panel was calculated for a static load produced by a maximum axial acceleration condition. This analysis

shows the effect of weight and designs on panel deflection. Figure 5-24 presents the results. Using the parameters of panel weight in lb/sq ft and panel deflection, the two structural designs of Figure 5-23(a) and (b) were analyzed. Panel weight in this analysis includes structure, solar cells, and electrical connectors. For both designs, the maximum deflection occurs at the outer edge and midpoint of the panel.

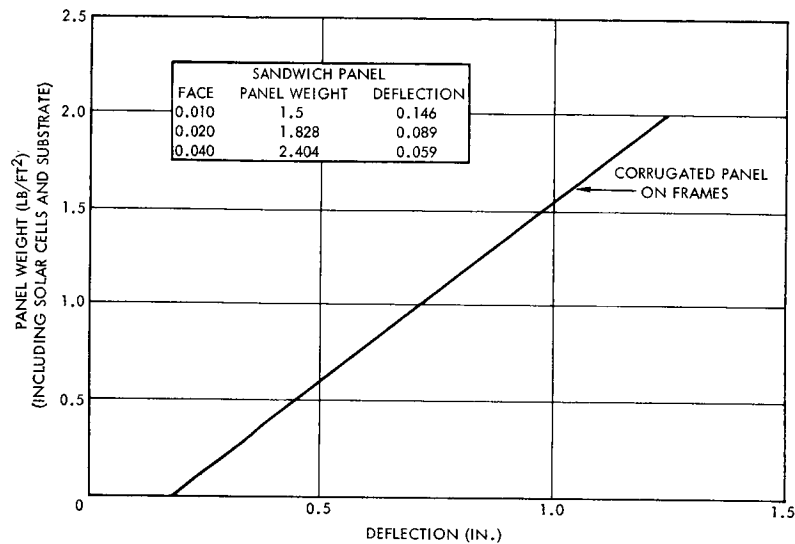


Figure 5-24. Solar Panel Deflection

Figure 5-25 pertains to the sandwich design. The moment of inertia used in this analysis was kept constant. Any changes in face thickness or core thickness could, with the use of this chart, be related to weight. In this case only structural weight is considered. The jump in the total weight curve is due to the adhesive weight change. For face thickness of 0.010 or less an adhesive weight of 0.040 lb/ft<sup>2</sup> is used but above 0.010 a weight of 0.080 is used.

Figure 5-25 shows the weight of the recommended design. Its weight is slightly higher than shown on the parameter curve because detail design included additional members and the weight estimate provided for attachments and contingencies. Table 5-20 shows the weight breakdown of three designs.



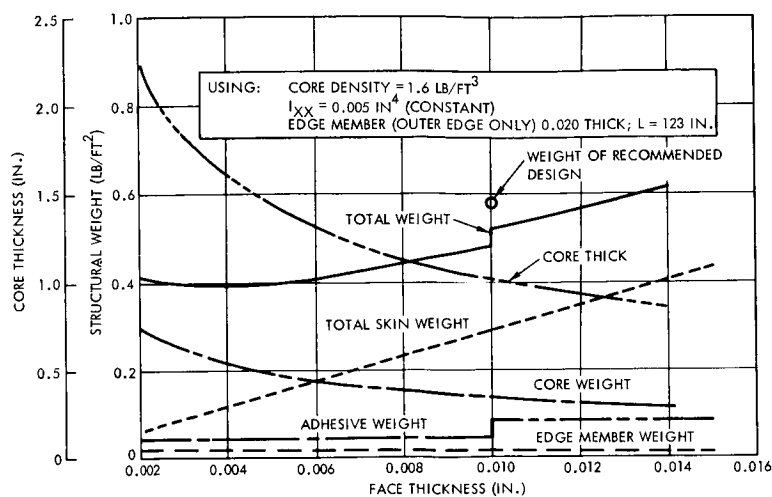


Figure 5-25. Solar Panel Design Study

Table 5-20. Solar Panel Structure-Typical Section for an Area of 42 ft<sup>2</sup> Weight Breakdowns

Configuration/Item	Weight (lb)
<u>Honeycomb Construction (1.6 lb/ft core)</u>	
Skin	12.1
Core	5.6
Bond	1.7
Closing Channels	2.3
Z-Stiffeners	1.4
Attach and Misc. (6 per cent)	1.4
Total	24.5
<u>Corrugation Construction</u>	
Corrugation and Skin	15.5
Outer Beam	4.2
Inner Beam	1.5
Doublers	0.5
Closing Members	0.7
Attach and Misc. (6 per cent)	1.3
Total	23.7
<u>Honeycomb with Stiffeners</u>	
Bond (Honeycomb)	1.8
Skin	6.2
Core	3.2
Stiffeners	9.3
Bond (Stiffeners)	0.8
Gussets and Hardware, etc.	1.6
Z-Stiffener	1.4
Total	24.3

### c. Dynamic Analysis

Solar Panel A. A modal-response analysis of the PD85-70 configuration was performed to determine deflections of the sandwich construction solar panel design shown in Figure 5-23(a). Deflection of this panel is critical because it must not violate the dynamic deflection envelope provided for the spacecraft. Due to location of the solar panel,

a 1-inch dynamic deflection will reach the dynamic envelope. The major assumptions used in the analysis were:

- 1) Input to the panel is 1.6 g limit-load superimposed on a 1 g static load.
- 2) Response is 10 times input, at resonance ( $Q=10$ ) due to coupling with the gross vehicle compression mode.
- 3) A rectangular panel (of area equal to actual panel area) with three sides simply supported, and one side free, is equivalent to the actual panel.
- 4) The panel modes are uncoupled and each one may be treated as a linear quasi-single-degree-of-freedom system.
- 5) Conservatively, the modal deflections may be added linearly to obtain total deflection.

Frequencies for a four-sided, simply-supported plate were transformed on the basis of static deflection, to the assumed edge conditions. Then a correction was made for the honeycomb construction weight and stiffness. Finally, the solar cell weight was accounted for.

The resultant maximum, under ultimate-load deflection is predicted to be 1.33 inch for PD85-70. The supporting beam and strut were found to have negligible deflection (beam frequency = 245 cps). Predicted solar panel maximum limit-load deflection and frequency for each mode are presented in Table 5-21. Mode shapes used in the analysis are shown in Figure 5-26.

Table 5-21. Solar Panel Frequencies

Mode	Deflection (inch)	Frequency (cps)
1. 1	0.89	19
2. 1	0.26	35
3. 1	0.086	61
1. 2	0.086	61

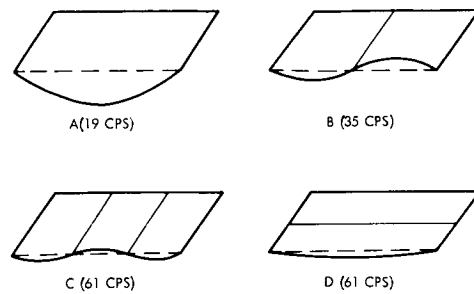


Figure 5-26. Mode Shapes Used for Dynamic Analysis of Solar Panels

The final configuration has less solar panel area and greater stiffness and will have a maximum deflection under ultimate load of less than 1 inch.

Solar Panel B. The maximum deflection of this design concept shown on Figure 5-23(c) is predicted to be 1.9 inches. This occurs at the midpoint of the stiffener's largest span. The loading used in the analysis was 1 g static, plus 1.6 g dynamic, with a response 14 times input at resonance, ( $Q=14$ ). The value of  $Q=14$  was obtained from Lunar Orbiter and Nimbus data. Therefore the total acceleration of this structure is  $\ddot{x} = 1 + 14 (1.6) = 23.4$  g.

d. Manufacturing

The solar panel designs under consideration are: 1) supporting panels comprising standard hexagonal cone bonded to two aluminum facing sheets, Figure 5-23(a), 2) a bonded assembly consisting of 0.008-inch-thick aluminum hat sections bonded to an 0.010-inch aluminum facing sheet, reinforced by two Z-section beams, Figure 5-23 (b), and 3) 3/8-inch-aluminum honeycomb panels with 0.005-inch aluminum facing sheets, reinforced by four aluminum U-section beams, Figure 5-23(c).

Of the first and third configurations, the first is preferred by Manufacturing. The third configuration involves the same effort as the first plus the fabrication and installation of the U-section beams. The

second and third configurations would involve substantially equal manufacturing effort. Current investigation indicates very similar costs in all three configurations.

f. Recommended Design

The selected configuration is a 1-inch-thick honeycomb panel with 0.010-inch 7075-T6 aluminum skins and an aluminum hexagon cell core as shown in Figure 5-23(a). The reasons for this selection are:

- 1) Best dynamic characteristics
- 2) Simplest design
- 3) Lightweight design
- 4) Highest level of manufacturing experience
- 5) Versatility of external attachments
- 6) Good thermal characteristics (uniform temperature distribution in eclipse)

## 2. THERMAL CONTROL SUBSYSTEM

The thermal control subsystem design studies have centered principally on the Mariner concept of an insulated compartment with internally generated heat radiated to space through individually actuated louvers. The heat-generating equipment is mounted to the internal surfaces of the honeycomb side panels through which heat is conducted and then radiated through the louver system to space. The system is summarized in Section 2.8.

The over-all heat balance, discussed in Section 2.1, is the basic tool utilized to determine requirements on the thermal control equipment. This is an energy management technique by means of which radiating area requirements are determined and on the basis of which it was determined that a completely passive design is not feasible and that the performance of a louver system such as these on Mariner and OGO is adequate.

Section 2.2 presents the representative performance of the subsystem based upon a simplified computer model of the spacecraft. The tradeoff studies are also discussed which determined the effect of allowable variations in power density on operating temperatures as a function of the number of louvers and honeycomb face sheet thickness. This study was extended to determine the packaging constraints on high power density equipment such as the traveling wave tubes.

Although the final over-all heat balance shows adequate performance of the louver systems, alternate louver systems (Section 2.3) were investigated as a possible augmented system permitting a lower heat loss when closed and actuation over a narrower temperature range.

The insulation and heat conduction analyses are presented in Section 2.4. These analyses are utilized in the over-all heat balance to determine the insulation requirements on structural attachments between the main compartment and the external structures, principally the solar array.

Tradeoff analyses on the solar array substrate weight and backside emissivity are discussed in Section 2.5 to show the requirements for survival in long Martian solar eclipses. Although a low emissivity array backside violates the specification of an array  $\alpha/\epsilon$  less than 0.5, the minimum weight design for eclipse durations greater than 70 minutes requires the lowest available backside emissivity.

Analyses of the effects of plume heating are presented in Section 2.6, determining the convective heating rates of the liquid engines and both convective and radiative heating rates for the solid engine.

Thermal control considerations for externally mounted equipment such as the POP, externally mounted sensors, and gimbals are analyzed in Section 2.7 to determine thermal design requirements such as heater power to maintain proper temperatures.

The thermal control subsystems for the three spacecraft configurations (see Volume 4) are similar. All external surfaces other than the louvered areas are covered with 20 layers of 1/4-mil aluminized Mylar sandwiched between two layers of 3-mil Mylar for handling ease. The Mylar side of the outer layer faces space to protect the insulation when irradiated by the sun. The inner layer is clear Mylar for electrical insulation. The engines are insulated with blankets of alternating layers of aluminum foil and fiberglass paper such as Linde SI-62 to protect the components from engine case radiation during firing and to limit heat loss from the main compartment after firing. In Configuration A a bifilar wound heater on the motor case and a Mylar insulation blanket covering the nozzle exit plane (destroyed at ignition) are required to maintain adequate propellant grain temperatures during transit. A 1/2-inch thick layer of Refrasil batt, such as used on Vela, is required to protect the upper surface of the spacecraft from the radiation of the aluminum oxide particle plume. The radiating areas under the louver system are coated with white potassium-zirconium silicate paint having a solar absorptivity of 0.2 after 100 hours of normal ultraviolet

exposure (initially 0.17)\* and a total hemispherical emissivity of 0.85. The internal surfaces within the main compartment are coated with high emissivity finishes such as black Cat-a-lac epoxy resin paint ( $\epsilon \pm 0.86$ ) or anodized ( $\epsilon$  varies between 0.76 and 0.83 depending upon treatment) to promote internal heat transfer.

## 2.1 Over-all Heat Balance

The concept of an over-all heat balance is an energy-management approach to determine, for the insulated, louvered concept, that the total energy balance in the main compartment remains within limits controllable by the louver system and that margins are available to compensate for heat leaks to assure that the spacecraft average temperature remains within the operating range of the louvers. The average spacecraft temperature limits are taken as 40 to 85°F which are consistent with the constraints imposed by individual component temperature requirements (see VS-3-111 in Volume 2) generally 30 to 110°F but with batteries 50 to 90°F and propulsion tankage 40 to 90°F.

### 2.1.1 Hot Condition (Near-Earth Cruise Mode)

The hot conditions are as follows:

<u>Loads in the Main Compartment</u>	<u>Watts</u>
Electrical power subsystem (100-watt solar array shunt dissipation)	137
Communication subsystem (less 20 watts RF)	78.4
Stabilization and control	13.7
Command and sequencing	8.5
Science	<u>55.5</u>
Total dissipated (p)	293.1

---

\* Completion of Test Program: Vacuum and Ultra-Violet Degradation of STL Manufactured Potassium Silicate - Zirconium Silicate Thermal Coating MT-6-2, TRW Document 63-9723.3-187.

<u>Heat Fluxes in Main Compartment</u>	<u>Watts</u>
Solar array attachment fittings	14
Solar array struts	-15
Attitude control lines	1
Aft insulation	2
Forward insulation (assumed zero with capsule on)	<u>0</u>
Net heat flux (q net)	2

The amount of louver area required is determined from the overall heat balance:

$$A_L E_L + (A_S - A_L) q_i = p + q_{\text{net}} + \alpha_L F_{L-SA} \epsilon_{SA} E_{SA} A_L$$

where  $A_L$  and  $A_S$  are the louvered and total areas of the trapezoidal sides,  $q_i$  is the heat loss from the insulation on the side areas (0.125 watt/ft<sup>2</sup> as predicted by the analysis of Section 2.4\* for 20 layers of aluminized Mylar),  $E_L$  and  $E_{SA}$  are the emissive powers of a fully opened louver system (30 watts/ft<sup>2</sup> at 85°F) and the solar array (57 watts/ft<sup>2</sup>), and the product  $\alpha_L F_{L-SA} \epsilon_{SA}$  is the effective absorptivity of the louver system to emitted solar array radiation. From the above the required louvered area is calculated to be 12 ft<sup>2</sup>. For added margin and transients this is increased by 10 per cent to 13.2 ft<sup>2</sup>.

### 2.1.2 Cold Condition

The worst case cold conditions steady state may be either prior to capsule separation where the power supply shunt dissipation is down to 25 watts (Table 5-22) or in a full sun orbit at 1.67 AU without the capsule but with power dissipations higher because of the orbital mode of operations (Table 5-23). The eclipses are not expected to present a worst case because the increased internal dissipations due to the

\* This value is based upon vendor and Douglas Aircraft calorimeter tests. The effective conductance across the insulation is approximately  $2.9 \times 10^{-3}$  BTU/hr ft<sup>2</sup>°F. Tests on insulated packages at TRW indicate a conductance of  $5 \times 10^{-3}$ . To be conservative the low conductance value is used in the hot case and the higher value is the cold case.



battery charge and recharge cycle will compensate for added heat loss through solar array attachments. Also in this transient condition the energy stored as sensible heat in the on-board equipment is available to maintain adequate temperatures compared to a steady state condition where only the dissipated power is available to compensate for heat losses through complex heat paths (heat leak) that have established a true steady-state condition due to the long duration of the flight.

Table 5-22. Worst Case Cold Conditions  
Down to 25-Watt Shunt Dissipation

Encounter (Precapsule separation)

<u>Loads in the Main Compartment</u>	<u>Watts</u>
Electrical power subsystem (25 watts shunt dissipation)	62
Communications subsystem (less 20 watts RF no bulk storage operations)	76.8
Stabilization and Control (cruise mode)	13.7
Command and sequencing (cruise mode)	8.5
Science (cruise mode)	<u>55.5</u>
Total dissipated power	216.5

Heat Fluxes in Main Compartment

Heat loss through closed louvers (effective emissivity 0.1, panel temperature 40°F)	41.5
Heat loss through solar array attachment fittings	10
Heat loss through solar array struts	15
Heat loss through aft insulation, 67 ft <sup>2</sup> (solar constant 57.2 watts/ft <sup>2</sup> , conductivity degraded 25 per cent, nominally 0.076 watts/ft <sup>2</sup> )	6.5
Heat loss through side panel insulation 111.3 ft <sup>2</sup> (conductivity degraded 25 per cent, nominally 0.45 watt/ft <sup>2</sup> )	65.5
Heat loss through Canopus sensor and earth detector openings (two 5 x 5 in. and one 4 x 4 in. openings)	14.3
Heat loss from attitude control lines	<u>4</u>
Total Heat Loss	156.8
Margin for heat leak (above insulation uncertainty) and for maintaining higher spacecraft temperatures	59.7

Table 5-23. Worst Case Cold Conditions in Full Sun  
at 1.67 AU

1.67 AU (Capsule Off, Orbital Mode)

<u>Loads in the Main Compartment</u>	<u>Watts</u>
Electrical power subsystem (shunt dissipation assumed zero)	65
Communication subsystem (less 20 watts RF bulk storage on)	98.4
Stabilization and control (orbital mode)	19.7
Command and sequencing (orbital mode)	12.0
Science (some science loads turned off)	<u>63.0</u>
Total power dissipated	258.1
<u>Heat Fluxes in Main Compartment</u>	
Heat loss through closed louvers	41.5
Heat loss through solar array attachment fittings	14
Heat loss through solar array struts	15
Heat loss through aft insulation 67 ft <sup>2</sup> (solar constant 46.7 watts/ft <sup>2</sup> , 25 per cent degradation)	8.6
Heat loss through side insulation (same as encounter)	65.5
Heat loss through forward insulation 26 ft <sup>2</sup> (25 per cent degraded, nominally 0.45 watt/ft <sup>2</sup> )	12.2
Heat loss through Canopus and earth sensors (same as encounter)	14.3
Heat loss through attitude control lines	4
Heat loss through spacecraft lander interface fitting	3
Heat loss through expended rocket case	<u>12</u>
Total heat loss	190.1
Margin for heat leak (above degraded insulation) and for maintaining higher spacecraft temperatures	68

As seen in both postulated cold cases, an energy margin of 27 and 26 per cent of dissipated power exists at encounter and 1.67 AU respectively, to compensate for heat leaks that cannot be either analyzed or established fully during limited duration space simulation tests.

### 2.1.3 Over-all Heat Balance with a 40-Watt Output TWT

One of the alternate designs considered included a 40-watt traveling wave tube. Since this tube would not be used until after encounter the extra dissipation need not be included in the hot condition for louver area sizing. Thus the worst cases in the over-all heat balance and the total louvered area remain the same. Considering failure mode where the 20-watt tube fails early in life, the one-watt transmitter radiating through the high gain antenna can provide communication at 128 bps at encounter when the 40-watt tube will be activated. (See Volume 2, VS-4-310, paragraph 5.2.) However, as discussed in Section 2.2, local problems are encountered in distributing the heat from a 40 watt TWT.

### 2.1.4 Conclusions

A fully passive system sized to accommodate the hot condition would have a heat loss of 220 watts from the radiating areas alone at a temperature of 40°F. With the other heat losses given in Table 5-22 the total heat loss would be 335.3 watts compared to 216.5 watts dissipated. Thus, even if the impractical case of assuming that all other heat losses through attachments and insulation could be absolutely minimized, a passive system would have no margin. Conversely, sizing the radiators passively for the cold condition would cause high spacecraft temperatures near Earth. Therefore, an active louver system is required in general. The active control is even more beneficial considering local changes in power dissipation on the electrical power panel. There are no differences between the 20 and 40 watt versions considering required louver area. Thus, a 40-watt configuration does not affect the thermal control design on an over-all basis.

The margin assumed in sizing the louver system is 10 per cent, based upon a fully opened louver system which absorbs 8 watts per square foot from the solar array. As will be seen in the following section the actual panel temperatures are less than 70°F rather than the assumed 85°F, indicating an effective margin greater than 10 per cent. The margin in the cold case is approximately 26 per cent above internally dissipated power. The conservative assumptions on insulation conductances

( $2.9 \times 10^{-3}$  Btu/hr-ft<sup>2</sup>-°F in the hot condition compared to  $5 \times 10^{-3}$  in the cold condition) also adds effective margin.

Other conclusions that can be drawn from the results of the over-all heat balance are that a 20-layer blanket of 1/4 mil aluminized Mylar such as NRC-2 is adequate and that a louver system of the Mariner - OGO type is adequate from the standpoint of heat loss in a closed position.

## 2.2 Spacecraft Thermal Model and Mounting Surface Analysis

### 2.2.1 Spacecraft Thermal Model

A thermal computer model of the spacecraft was established to determine a representative performance to evaluate the effects of the constraint that all parts of any one subsystem are mounted on a single panel and to investigate the best distribution of panels about the spacecraft. The lumped node technique of analysis was utilized. A schematic of the model is presented in Figure 5-27. The TRW Thermal Analyzer Program (TAP) was utilized for solution of the resultant network. TAP is an n-dimensional, asymmetric, finite difference program run on the IBM 7094.

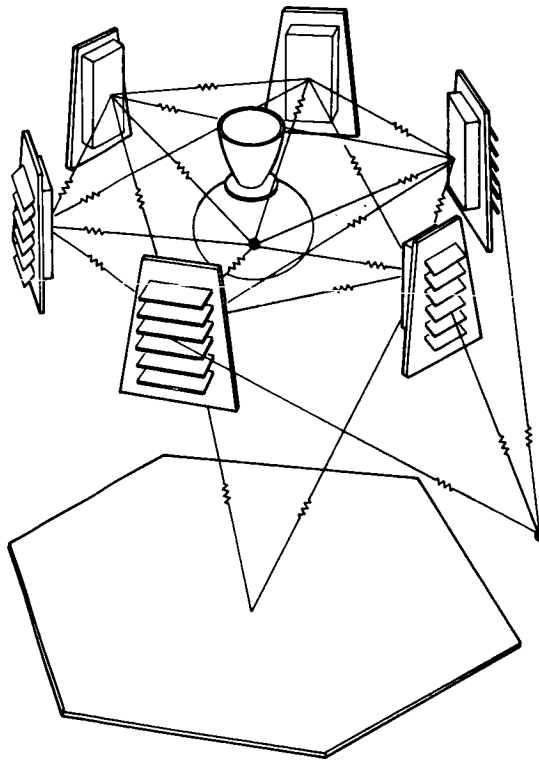


Figure 5-27. Schematic of Spacecraft Thermal Model

The model consists of 20 nodes, one each for the six side panels, top and bottom panels, one each for the eight insulation panels, one node representing the lumped internal equipment, one node for the solid engine, one node for the solar array, and one for space ( $-460^{\circ}\text{F}$ ). The power dissipating equipment was lumped with the side panels. The effect of louver opening was included by varying emissivity on the radiating areas with the radiator temperature according to the louver opening curve as shown on Figure 5-28. The absorptivity of the louvers to

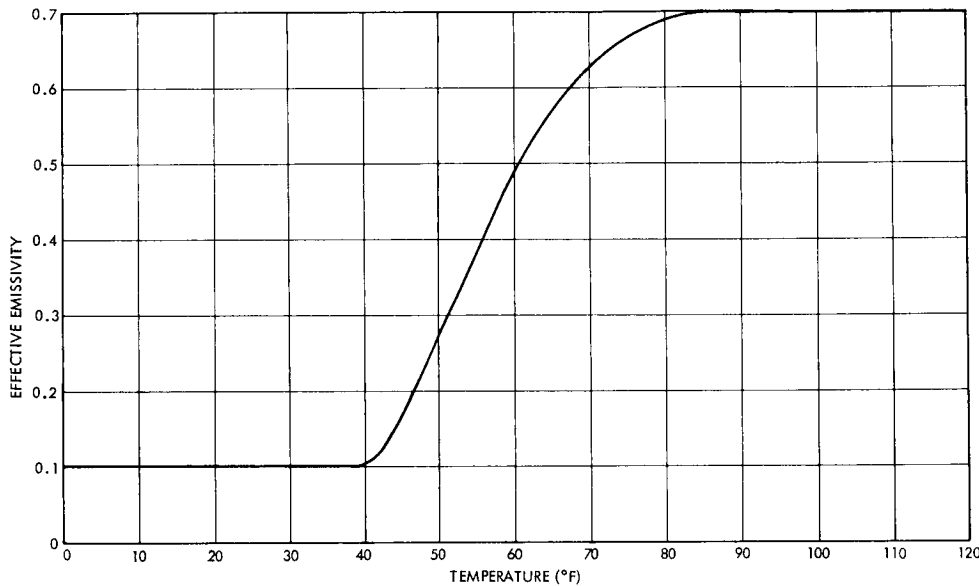


Figure 5-28. Effective Emissivity of a Louvered Panel Radiating to Space

solar-array emitted radiation was programmed by varying the emissivity of the radiation resistor coupling the array and the louvers according to the data derived in Section 2.3.

Steady state cases were run for conditions at 1, 1.38, and 1.67 AU. Initial temperatures were obtained from this data to run non-nominal orientations at 1 and 1.38 AU to obtain data on the allowable duration of maneuvers. The solar vector was assumed normal to the communication equipment panel. With the 1.67 AU steady state data, runs were made for a 2.3-hour eclipse. The assumptions regarding power profiles during these conditions are presented in Table 5-24. These representative cases are for the alternate 40-watt output version, which is a worst case. The data for the selected 20 watt version and selected inboard profile are presented in Volume 2, VS-4-510.

Table 5-24. Power Profiles of Equipment Panels

<u>Communications Panel</u>	<u>Notes</u>
1 AU, 138.4 watts	Worst case assuming a 40-watt transmitter on
1.38 AU, 138.4 watts	Worst case for non-nominal orientation, 40-watt transmitter
<u>Power Panel</u>	
1 AU, 137 watts	Worst case assuming array tolerances cause 100 watt shunt dissipation
1.38 AU, 62 watts	Cruise mode converter dissipation, 25-watt shunt dissipation
1.67 AU, 87 watts (in sun)	Orbital mode converter dissipation, no shunt dissipation
1.67 AU, 197 watts (eclipse)	Battery and boost regulator increases dissipation
<u>Stabilization and Control and Command Sequencing Panel</u>	
1 AU, 22.2 watts	Cruise mode
1.38 AU, 31.7 watts	Maneuver mode
1.67 AU, 31.7 watts	Orbital mode
<u>Bus Experiments Panel</u>	
1 AU, 55.5 watts	POP remote hardware off all DAE on
1.38 AU, 55.5 watts	Same
1.67 AU, 63 watts	POP remote hardware portion of orbit

The inboard profiles examined are presented in Figures 5-29 and 5-30, the indicated size of the louvered area on each panel based on the power dissipation on each panel.

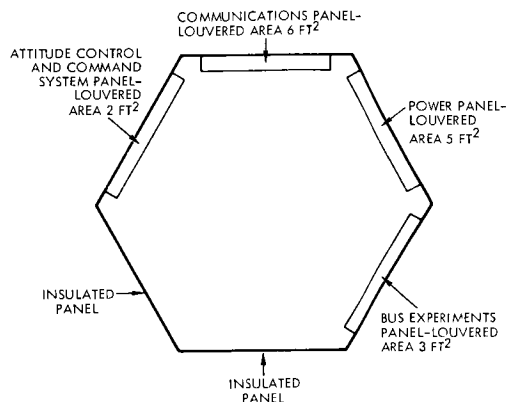


Figure 5-29. Configuration I Inboard Profile

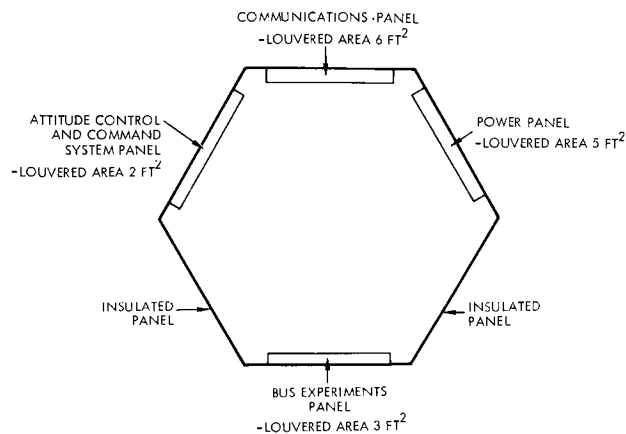


Figure 5-30. Configuration II Inboard Profile

The computed results are presented in Table 5-25. As seen, the temperature variation is quite small because of the individual sizing of louver area to the appropriate panel and because of the large internal radiation coupling; no conduction between panels was assumed except to the solar array. In addition, the variation in panel temperatures is small comparing the two inboard profiles. Since the Configuration I profile is more convenient for spacecraft weight balancing, it was chosen for further analyses.

The assumption of coupling the panels by radiation to a central node representing all internal equipment was examined by halving the configuration factor from the panels to the central node from 0.44 to 0.22. The results, in Table 5-26, show that the decreased internal coupling affects average temperatures by at most  $2^{\circ}\text{F}$ , indicating that the louvers are regulating most of the heat flow.

Figure 5-31 shows the performance when the solar vector is normal to the communications equipment panel, a condition which may exist during the early midcourse maneuvers. A 40-watt transmitter was assumed for this calculation, to provide a worst case. The communications panel average temperature rises from  $64^{\circ}$  to  $86^{\circ}\text{F}$ , reaching essentially steady state in 50 minutes. On the average, this temperature

Table 5-25. Average Equipment Panel Temperatures

Configuration 1, Steady-State Temperatures

Range from sun (AU)	1	1.38	1.67
Communications panel (°F)	64	58	54
Power panel (°F)	67	51	54
Bus experiments panel (°F)	59	53	54
CS and C panel (°F)	56	51	50

Configuration 2, Steady-State Temperatures

Range from sun (AU)	1	1.38	1.67
Communications panel (°F)	63	59	55
Power panel (°F)	66	52	55
Bus experiments panel (°F)	59	55	55
CS and C panel (°F)	56	53	52

Table 5-26. Average Steady-State Equipment Panel Temperatures

Full Internal Coupling

Range from sun (AU)	1	1.38	1.67
Communications panel (°F)	64	58	54
Power panel (°F)	66	51	54
Bus experiments panel (°F)	60	53	54
CS and C panel (°F)	57	51	50

50 Per Cent Reduced Internal Coupling

Range from sun (AU)	1	1.38	1.67
Communications panel (°F)	64	59	54
Power panel	67	51	54
Bus experiments panel (°F)	59	53	54
CS and C panel (°F)	55	50	50

2.2.2 Mounting Surface Analysis

A tradeoff study was performed to determine the combined effects of constraining the power distribution, the number of louvers, and the



rise does not present a problem, although a problem may exist in the vicinity of the transmitter which detailed analysis may show necessitates local increased honeycomb face sheet thickness.

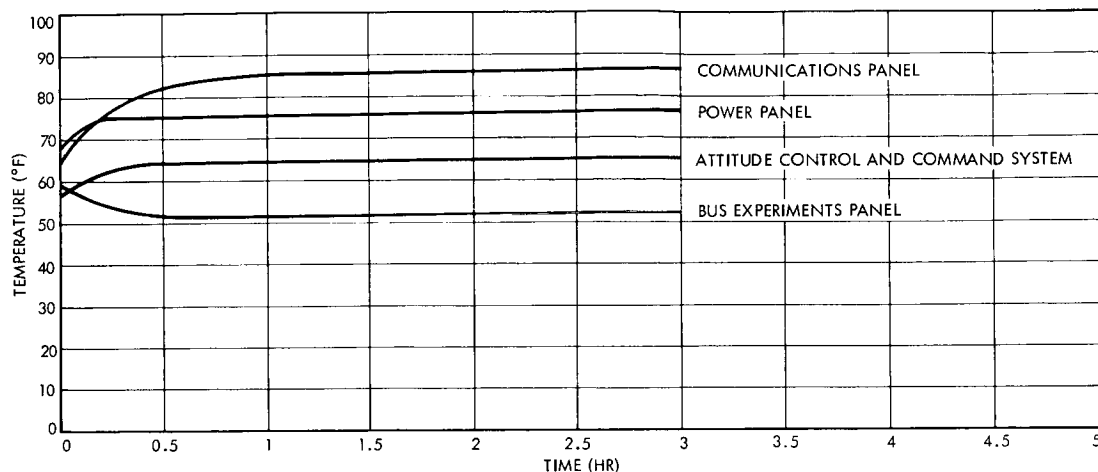


Figure 5-31. Temperature Histories of Equipment Panels at 1 AU with Sun Normal to the Communications Panel. (For conservation all thermal capacities are taken at half actual values.)

The same orientation was run at 1.38 AU considering the long term orientation for deboost (Figure 5-32). The average communications panel temperature rose to only 71°F with the 40-watt transmitter on because of the decreased solar constant. Compared to the previous case approximately 15°F margin exists even for a 3-hour (practically equilibrium) condition.

A 2.3-hour eclipse was simulated (Figure 5-33) utilizing initial temperatures for the 1.67 AU condition. All average temperatures remained above 40°F, with the power panel decreasing the least because of the larger dissipation in the batteries and boost regulator.

The simplified computer model has shown adequate performance throughout the mission. Although many of the details of the actual construction have been omitted, in Section 2.1, margins in the worst cases were determined and found to be adequate. In addition, the following analysis examines the effect of power distribution on an individual equipment panel on the temperature gradients.

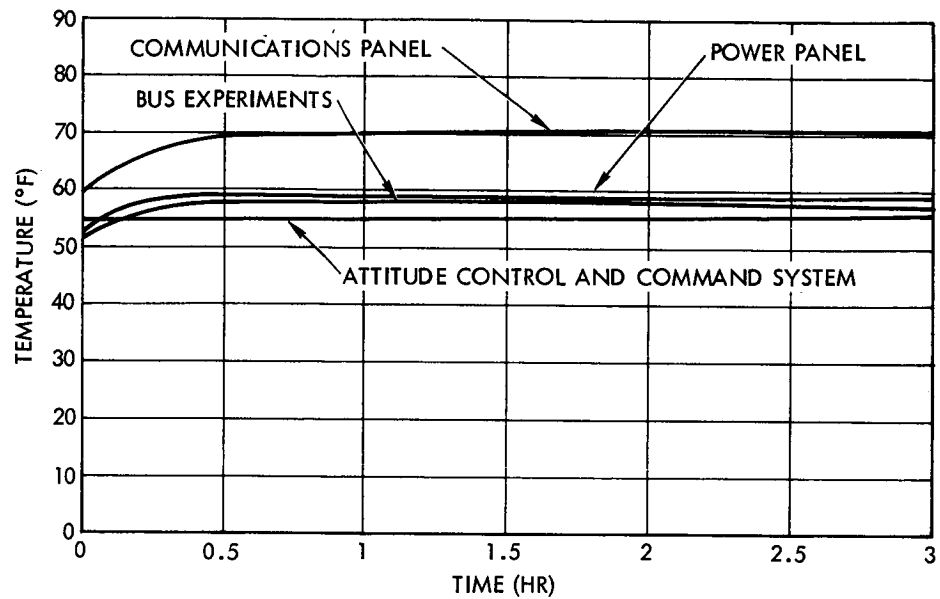


Figure 5-32. Temperature Histories of Equipment Panels at 1.38 AU with the Sun Normal to the Communications Panel and the Deboost Engine Firing. Half Thermal Thrust

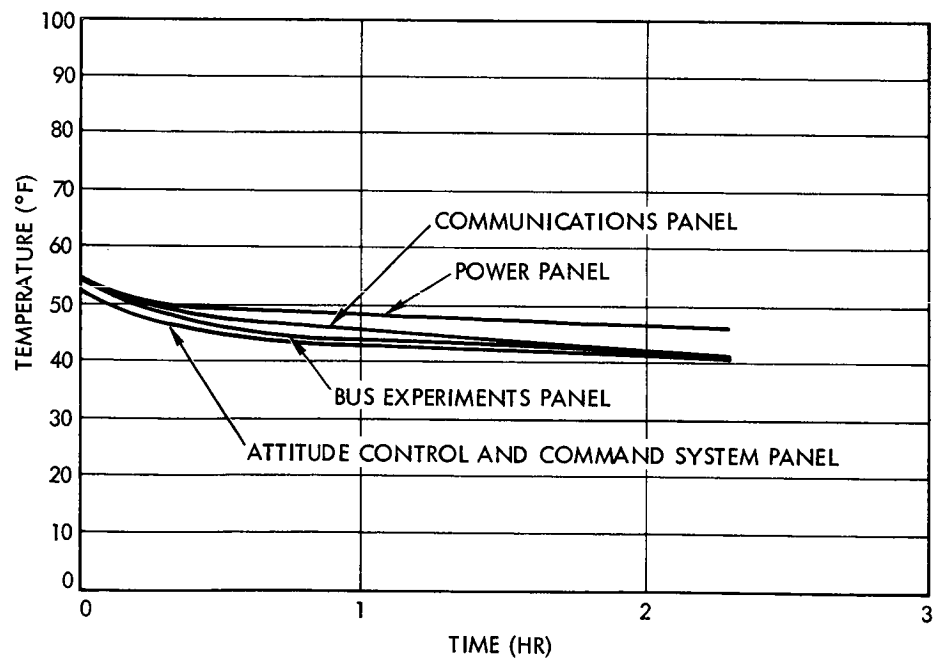


Figure 5-33. Temperature Histories of Equipment Panels During Eclipse at 1.67 AU. Half Thermal Capacities

face sheet thickness of the honeycomb panels on temperature gradients within a panel. The general layout of power on the panel conformed to the four abreast standardized packaging technique proposed. A nominal power density of  $0.2 \text{ watt/in}^2$  was chosen and the tolerance about this was varied for  $\pm 0.2$ ,  $\pm 0.1$ ,  $\pm 0.05 \text{ watt/in}^2$ . Face sheet thicknesses considered were 0.01, 0.025, and 0.05 inch. To determine the gradients only, the conductance across the core was neglected such that the mounting surface was equivalent to a solid plate twice the thickness of the honeycomb face sheet thickness. The power distributions are shown in Figure 5-34 and the louver configurations are shown in Figure 5-35. The louver effective emissivity as a function of temperature is presented in Figure 5-36.

The TRW thermal analyzer program was utilized for a steady state solution of the network. The temperature maps resulting from the analysis are presented in Appendix D. The curves summarizing the data are shown in Figure 5-37 for the 12-louver configuration and in Figure 5-38 for the 24-louver configuration. As seen, the 24-louver configuration decreased gradients in the panel by approximately 40, 20, and  $10^\circ\text{F}$ , for the 25-mil face sheets for power density variations of  $\pm 0.2$ ,  $\pm 0.1$ , and  $\pm 0.05 \text{ watt/in}^2$ , respectively. Since sizable gains in temperature uniformity are realized with a two-abreast louver configuration this approach appears to be the best for the Voyager application.

The effect of face sheet thickness is as follows for the 24-louver configuration:

- 1) For the  $\pm 0.2\text{-watt/in}^2$  constraint, a  $20^\circ\text{F}$  gain in uniformity can be obtained by increasing face sheet thickness from 25 to 50 mils.
- 2) For  $\pm 0.1$  and  $\pm 0.05 \text{ watt/in}^2$  the gain is  $10^\circ\text{F}$  and  $4^\circ\text{F}$  respectively, and is not considered significant for the weight penalty.

For 25-mil face sheets a gain of  $30^\circ\text{F}$  is achieved by increasing the constraint from  $\pm 0.2$  to  $\pm 0.1 \text{ watt/in}^2$  and a gain of approximately  $15^\circ\text{F}$  from  $\pm 0.1$  to  $\pm 0.05 \text{ watt/in}^2$ . The relatively large gain in temperature uniformity by limiting power density in general to  $0.3 \text{ watt/in}^2$  constitutes a genuine gain in reliability and electronic performance that

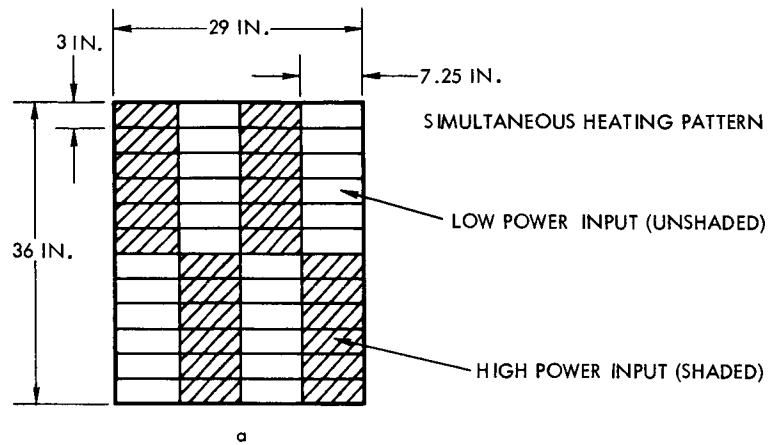


Figure 5-34. Power Distribution for the Panel Gradient Study

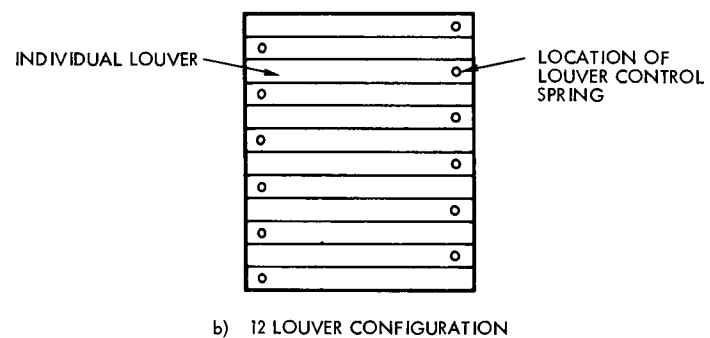
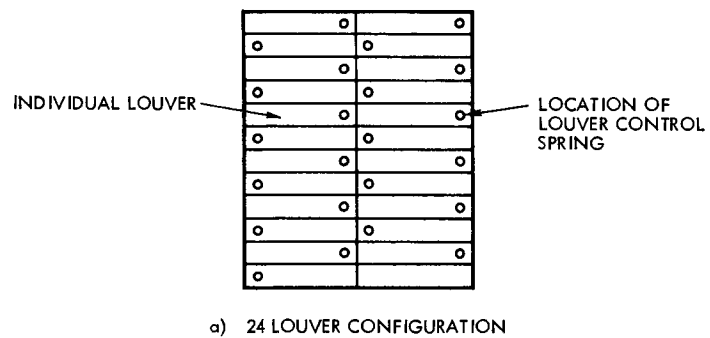


Figure 5-35. Louver Configuration

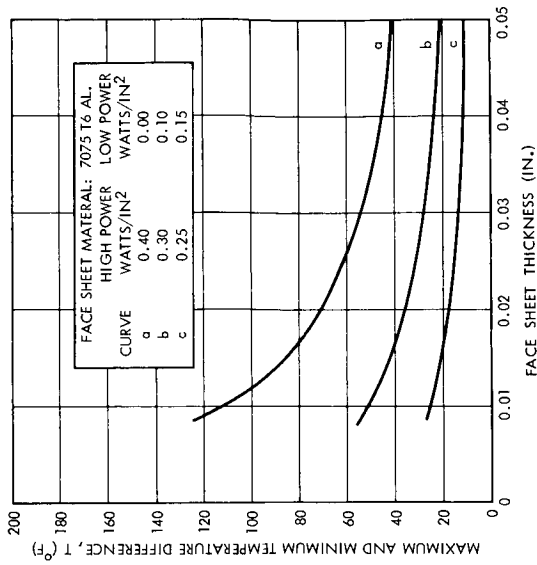


Figure 5-38. 24-Louver Configuration

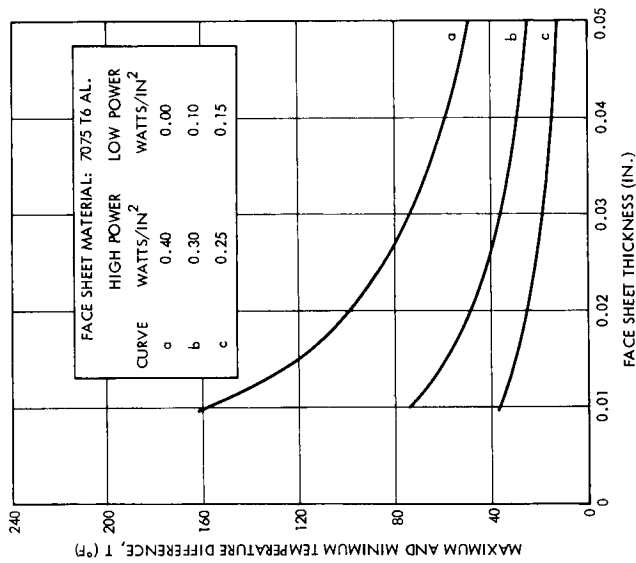


Figure 5-37. 12-Louver Configuration

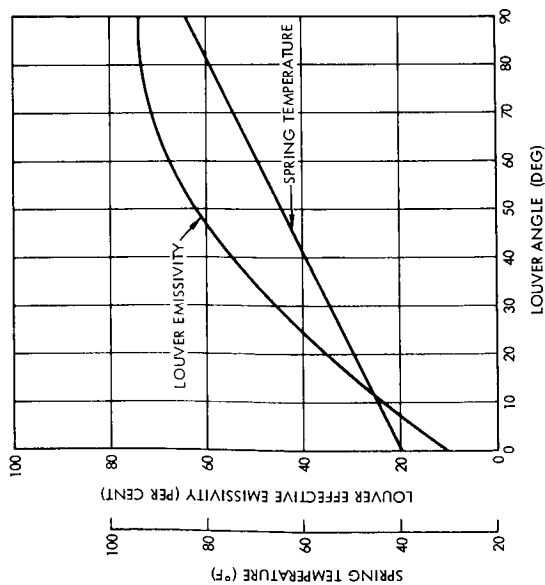


Figure 5-36. Power Data

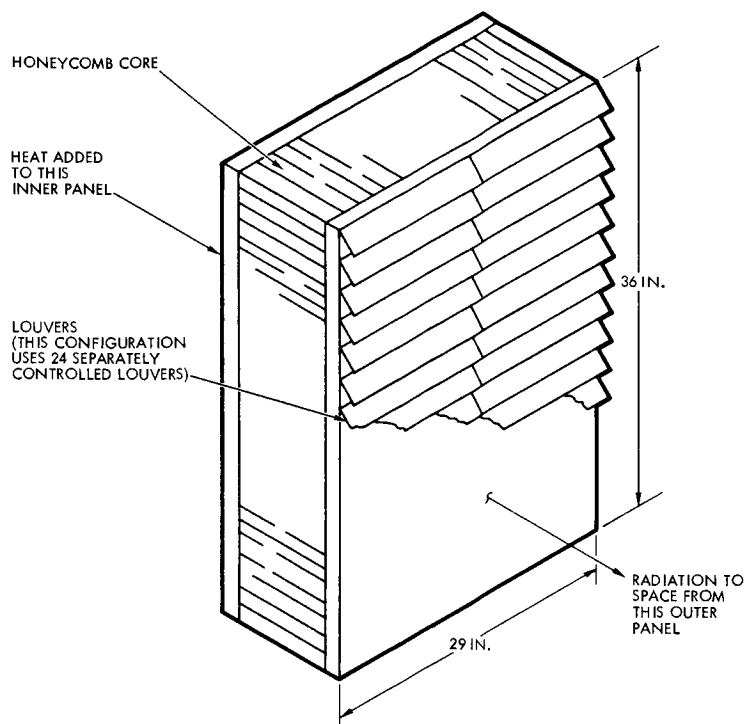


Figure 5-39. Honeycomb Panel Configuration

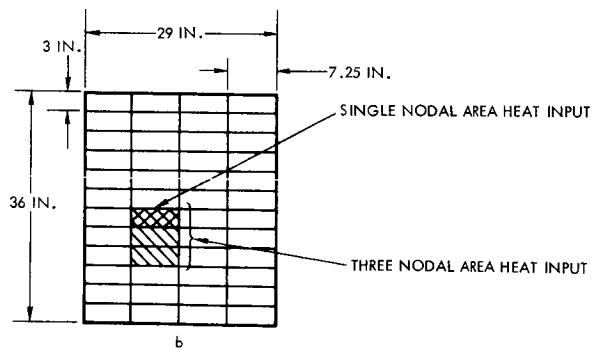


Figure 5-40. Power Input Fabrication

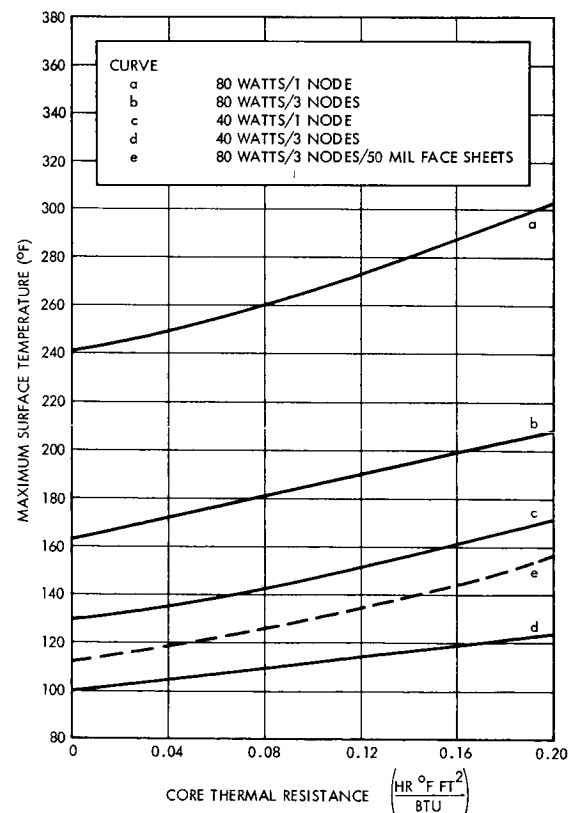


Figure 5-41. 24 Louvers for 29 x 36 Inch Panel

is desirable but difficult to evaluate. Experience with OGO temperature control has shown that a loose constraint of 0.2 to 0.3 watt/in<sup>2</sup> provides a workable design. Based upon the OGO experience and the tradeoff analysis showing a  $\pm 15^{\circ}\text{F}$  variation about the mean panel temperature, the Voyager packaging should probably be constrained, in general, to 0.3 watt/in<sup>2</sup> with 25-mil honeycomb face sheet thicknesses.

The above power density constraint inflicts severe penalties in the case of traveling wave tubes, however, and for this one case must be relaxed. The foregoing study was extended to incorporate a high power source, the effect of the honeycomb core, and the effect of the component baseplate area (Figure 5-39). The parameters examined were a 40 or an 80 watt power load distributed over one node (21.75 in<sup>2</sup>) or three nodes (65.25 in<sup>2</sup>) for core conductances of 5 and 15 Btu/hr-ft<sup>2</sup>- $^{\circ}\text{F}$ . The former conductance is an estimated value for the truss grid and the latter is a typical value for honeycomb such as used on Pioneer. The placement of the concentrated source is shown in Figure 5-40. Another 40 watts of power was uniformly distributed on the panel. The face sheets were assumed to be 25 mils thick for the honeycomb runs, while the effects of 50-mil face sheets were examined for infinite core conductance and the results extrapolated. The results of the analyses are presented in Figure 5-41. The selected 20-watt output traveling wave tube dissipates approximately 47 watts with a maximum allowable baseplate temperature of 185 $^{\circ}\text{F}$ .

An RTV-11 silicone rubber filler is required to decrease the temperature drop between the baseplate and the honeycomb face sheet. Tests conducted at TRW show a conductance of 50 Btu/hr-ft<sup>2</sup>- $^{\circ}\text{F}$  for this type of filler and baseplate dimension.\* The temperature drop is then 7 $^{\circ}\text{F}$  and the maximum allowable face sheet temperature is 178 $^{\circ}\text{F}$ . Extrapolating from Figure 5-41, the trussgrid core (thermal resistance of 0.2 hr-ft<sup>2</sup>- $^{\circ}\text{F}$ ) with the 25-mil face sheets provides a maximum face sheet temperature of 132 $^{\circ}\text{F}$  for a 47 watt concentrated source if the baseplate couples to three nodes. Thus with the selected configurations there exists 46 $^{\circ}\text{F}$  of margin. Since the two tubes are never on simultaneously both could be mounted to the same baseplate for weight savings.

---

\*"Bi-Monthly Progress Report No. 4, Prediction of Space Vehicle Performance," TRW Report 4182-6004-SU-000, 1 March 1965.

On the other hand it is undesirable to have the TWT's sharing the same louvers so that a single louver failure does not overstress both tubes.

The alternative 40 watt output traveling wave tube dissipates approximately 91 watts with the same maximum allowable baseplate temperature of 185°F. Again, a large baseplate is needed to meet the requirement. If the baseplate radiates internally to an environment at 85°F with an emissivity of 0.85, the power dissipated through the honeycomb is 76 watts. An RTV-11 silicone rubber filler limits the temperature drop through the honeycomb to 11°F and the maximum allowable face sheet temperature is 164°F. From Figure 5-41 the trussgrid core (thermal resistance of  $0.2 \frac{\text{hr-ft}^2}{\text{Btu}} - ^\circ\text{F}$ ) with 50-mil face sheets provides a maximum face sheet temperature of 158°F for an 80-watt concentrated source. This combination will be acceptable for temperature control of the 76-watt dissipation of the traveling wave tube, producing an estimated face sheet temperature of 142°F based on an extrapolation between the 40 and 80 watt cases. A temperature map of the case of an 80-watt dissipation in three nodes with 25-mil face sheets is presented in Figure 5-42. The map shows that only the locally surrounding nodes are effective in distributing the power dissipation such that an optimum solution (minimum weight) would be a locally thickened face sheet and a detailed tradeoff on baseplate area.

TWO EACH 0.025 IN. FACE SHEETS-7075 T6 AL.  
HONEYCOMB CORE CONDUCTANCE = 15.0 BTU/HR°F FT<sup>2</sup>  
NO. OF LOUVERS = 24  
AVERAGE TEMPERATURE OF NODE, °F      NODE NO.

45.3	1	47.1	2	46.3	3	43.9	4
46.0	5	48.6	6	46.5	7	43.3	8
47.1	9	51.7	10	48.1	11	43.1	12
49.7	13	59.9	14	49.9	15	42.0	16
53.4	17	72.5	18	55.0	19	42.5	20
60.7	21	101.7	22	59.9	23	41.0	24
68.1	25	162.9	26	69.6	27	43.3	28
71.7	29	179.8	30	70.8	31	41.8	32
68.7	33	163.7	34	69.9	35	42.9	36
61.8	37	103.4	38	60.4	39	40.0	40
55.6	41	76.1	42	56.0	43	40.7	44
53.4	45	66.0	46	51.3	47	38.6	48

POWER SOURCE AREA →

Figure 5-42. Temperature Map for 80-Watt Dissipation



### 2.3 Louver Design

The louver system used on Mariner, OGO, and Pioneer has been selected for Voyager, but louver systems with a smaller temperature differential between the closed and open positions and with lower louver heat leak when closed are possible. Such improved performance would lead to reduced temperature limits with a corresponding (although difficult to evaluate) improvement in reliability. It would also allow a wider variation of dissipated power and a reduced sensitivity to component locations. Both features are desirable for growth potential and flexibility.

Achieving such higher performance may require a louver blade of lower conductivity, a decreased gap between closed louver blades and at end fittings. Since decreasing the gaps between blades and end fittings requires a more forcible closure and spring actuated end inserts, an actuator more powerful than a bimetal spring is required, such as a piston driven by a wax which changes volume at the melting point. This type of actuator is also capable of narrow open-to-close temperature limits.

More torque and narrower temperature ranges can be achieved in the bimetal actuators at the expense of weight. However, experience on Pioneer has shown that manufacturing techniques with nonmagnetic bimetal springs currently limit the closed to open range to 45°F. The OGO bimetal spring has a 30°F range, but is highly magnetic (2000  $\gamma$  at 6 inches, demagnetized to 42  $\gamma$ , compared to Pioneer, which is less than 3  $\gamma$  at 3 inches).

Additional actuator mechanisms which were examined include rack and pinion drives and cable-pulleys. Also briefly examined were such devices as wax- or gas-filled bellows actuators, variations on bimetal actuation, and bourdon tubes (see Appendix D).

Other types of active systems such as rotating masks to expose high and low emissivity areas and circulating fluids have not been considered due to the greater simplicity and efficiency afforded by louvers.

### 2.3.1 Thermal Performance

A study was performed on the effect of the louver blade conductivity and gap fraction (that fraction of the radiator area not covered by louvers due to end clearance or imperfect closure) on the effective emissivity of the radiator. The assumptions and program solution are presented in Appendix D. The results are presented in Figure 5-43 and show that the dominant factor is the gap fraction. The effective emissivity of the Mariner-OGO type louver system when it is closed is approximately 0.1. To gain significantly in insulating performance from these flight-tested systems would require a more forcible closure and spring-actuated end fittings which, in turn, would require a more powerful actuator. With such an improved louver system the gap fraction is estimated to be 0.02, with an effective emissivity of 0.041. If such a high performance system were required, the louver material would remain the easily fabricated hollow aluminum blade but the actuation technique and blade end design would become more complex.

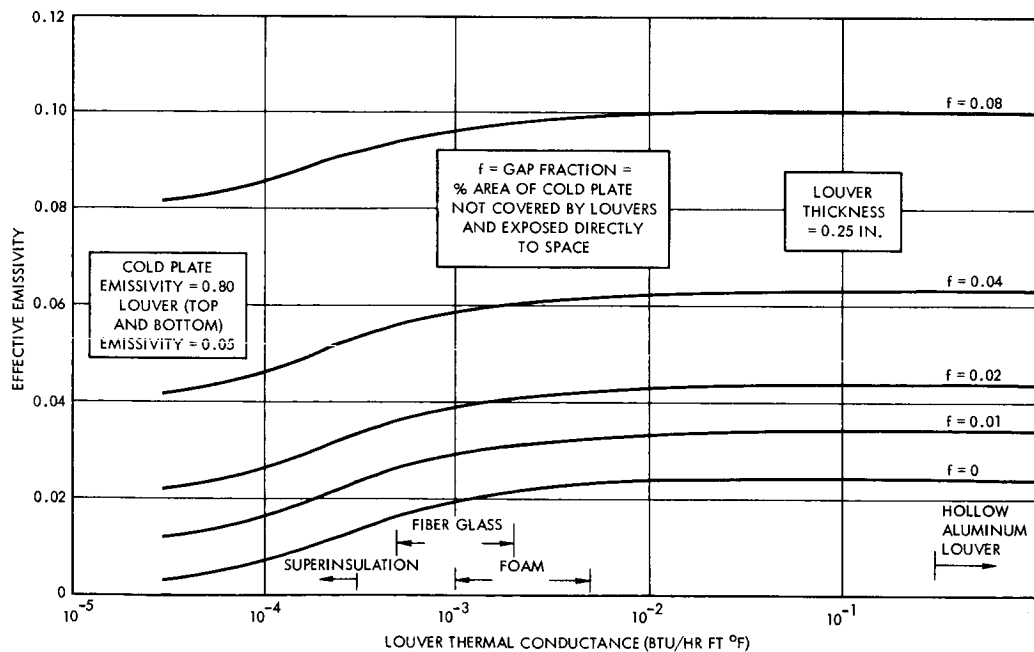


Figure 5-43. Louver Performance (fully closed position with diffused or specularly reflecting louver surfaces)

Equations for the effective emissivity in the fully open condition are developed in Appendix D. Parametric curves for the assumption of a diffusely infrared reflecting louver are presented in Figure 5-44 and for the specular assumption in Figure 5-45. With a mounting surface emissivity of 0.85 the effective emissivity for the diffuse case is approximately 0.63 and with specular surfaces approximately 0.83 with a louver emissivity of 0.05 or a 30 per cent increase. Since the bare aluminum surfaces of Mariner-OGO type of blades are specular, the larger effective emissivity is used. Notable is the weak effect of the louver emissivity on the effective emissivity with the specular blades. Since the absolute tolerance on the value of emissivity is approximately  $\pm 0.02$  the actual value of the emissivity, while unknown by a large percentage, will have a small effect on performance ( $\pm 0.01$  accuracy on the effective emissivity).

### 2.3.2 Environmental Inputs

As part of the external environment, the solar array will cause added heating of the louver-covered radiator. Since the louver blades are specular reflectors there is a portion of the array, for a particular louver angle, for which incident energy will be reflected to space. Hence, the heat absorbed by the radiator which is emitted by array can be expressed as

$$q = \epsilon_A E_A \alpha_{BP} F(\theta)$$

where

$q$  = Absorbed heat flux (Btu/hr-ft<sup>2</sup>)

$\epsilon_A$  = Infrared hemispherical emittance of solar array back side (dimensionless)

$E_A$  = Black body emissive power of array (Btu/hr-ft<sup>2</sup>)

$\alpha_{BP}$  = Infrared absorptivity of radiator (dimensionless)

$F(\theta)$  = Effective shape factor of array as viewed by louver system, a function of louver angle and position of louver with respect to array (dimensionless)

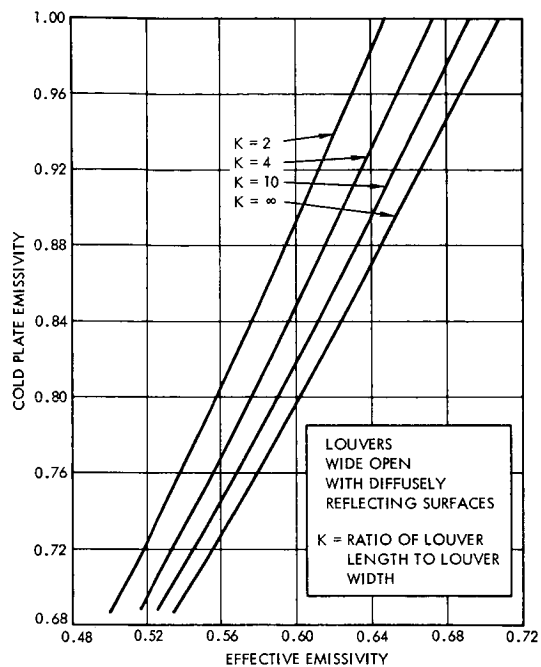


Figure 5-44. Cold Plate Effective Emissivity as a Function of Cold Plate Emissivity and the Ratio of Louver Length to Louver Width

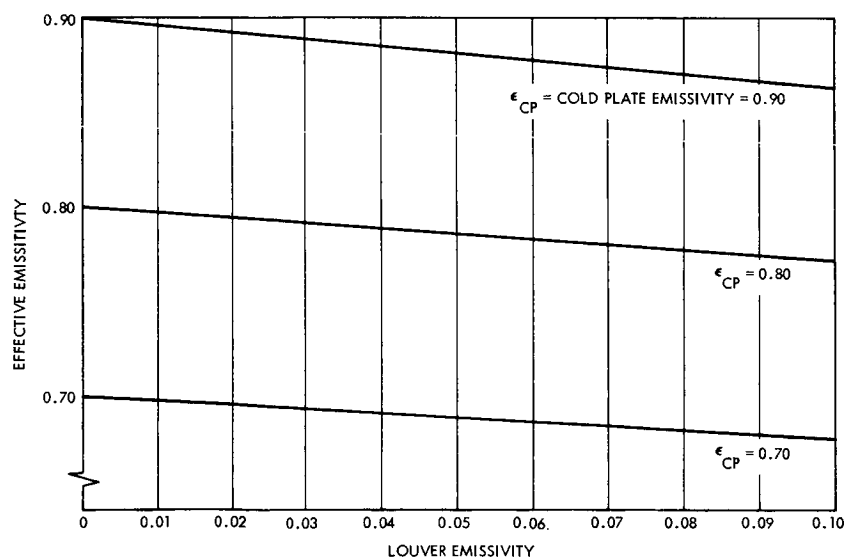


Figure 5-45. Louver Performance (Louvers wide open with specularly reflecting surfaces)

The effective shape factor,  $F(\theta)$ , is evaluated by considering that array radiation originating between  $X = 0$  and the line of intersection of the louver blade surface normal is reflected entirely to space (see Figure 5-46).

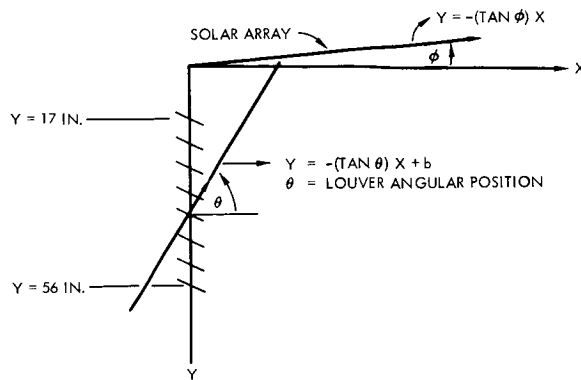


Figure 5-46. Reflection of Array Radiation

The intersection of the line representing the array and the line coincident with the surface normal of a louver is given by

$$-(\tan \phi) X = -(\tan \theta) X + b$$

or

$$X = \frac{b}{\tan \theta - \tan \phi}$$

The array varies from  $X = 0$  to  $X = 65$  inches and  $\phi = 17$  degrees. The louver system varies from  $Y = 17$  to  $Y = 56$  inches. Thus

$$17 \leq b \leq 56 \text{ inches}$$

The portion of the array contributing to heating of the louver system is given by

$$65 - X = 65 - \frac{b}{\tan \theta - \tan \phi}$$

which must be greater than zero and less than 65 inches.

The TRW Shape Factor No. 1 computer program was used to evaluate shape factors from the louver blades to the portions of the array

contributing to heating of the radiator, the results of which are presented in Figure 5-47. The effective shape factor is present in Figure 5-48. The analysis is preliminary; a more detailed analysis is planned for Phase IB comparable to Becker's.\*

The absorptivity of the louver system to solar radiation was taken from OGO data\*\* as 0.25 with the louvers fully opened and the solar vector normal to the mounting surface. Radiation to the louvers from the capsule was neglected because of the shading of the capsule by the solar array and the small amount of heat dissipated in the capsule. Considering the canister surface to have the lowest emissivity available (0.03), for a capsule area of  $325 \text{ ft}^2$  the canister temperature is  $-10^\circ\text{F}$ . The emitted energy is then only  $0.6 \text{ watt/ft}^2$  and the configuration factor from the louvered face to the capsule is approximately 0.25 such that the heat input to the louvers is  $0.15 \text{ watt/ft}^2$ . During non-nominal orientations the bottom of the canister could present a problem area in absorbing and re-emitting solar energy or in reflecting solar energy into the louver systems. From the spacecraft side of the interface the canister bottom should be an insulated surface having a high solar absorptivity.

### 2.3.3 Actuation Mechanisms and Louver Construction

Several actuators and actuation mechanisms were examined. Presented in this section are the three most promising designs (other designs appear in Appendix D). Two different actuators were studied, a bimetal spiral and a thermal actuator utilizing volumetric change of a wax about the melting point (called a thermal actuator). Since the thermal actuator can develop a powerful stroke, it is utilized for an augmented, high performance design. Because of its flight proven performance, the bimetal is used in our selected design.

---

\* Raymond Becker, "Analysis of Solar Panel Effects on Louver Performance," Technical Report No. 32-687, Jet Propulsion Laboratory, 1 June 1965.

\*\* "Thermal Control Systems," OGO Engineering Data Book, 2311-0010-OU-000, 3 June 1965.

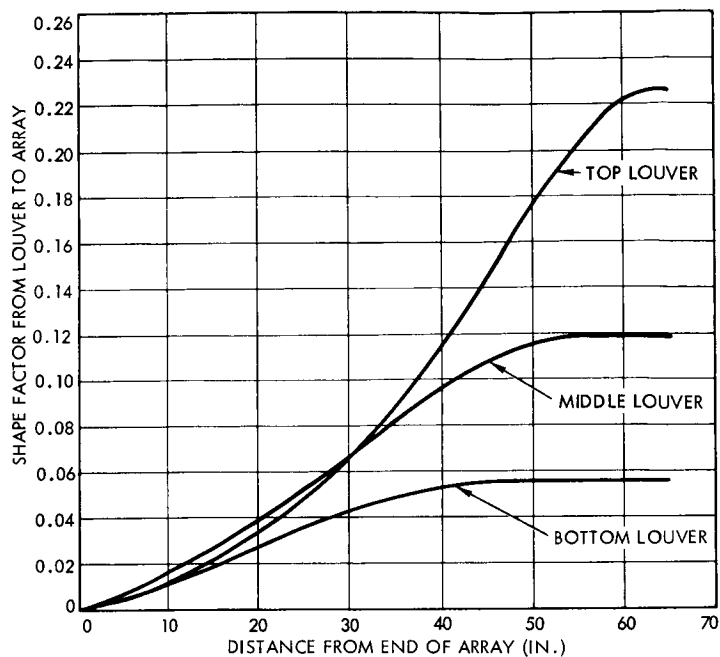


Figure 5-47. Black Body Shape Factor of Array as Viewed by Louvers

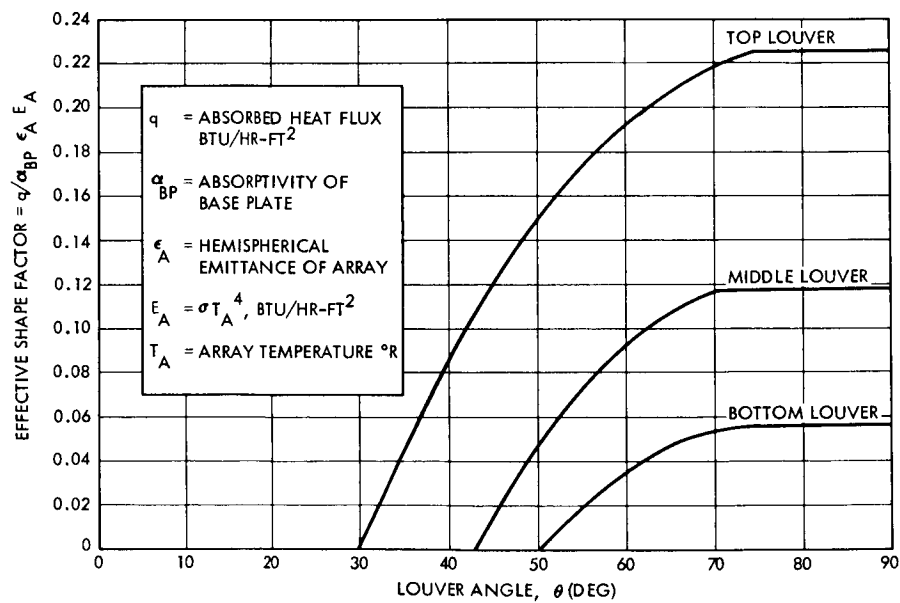


Figure 5-48. Heat Input to Louver System from Solar Array

a. Selected Louver System

A cross-section of the Mariner-OGO type of louver system is presented in Figure 5-49. It is proposed to replace the bi-metal with the Pioneer type bimetal (40 to 85°F closed to open) for magnetic cleanliness, providing a field of less than 3 γ at 3 inches. The Pioneer bimetal is manufactured in a proprietary process by the W. M. Chase Co. of Detroit, designated alloy No. S992. The bearings are sintered silver impregnated with molybdenum disulfide to avoid cold welding and stiction. The louvers are formed of 3-mil aluminum halves spot welded together with the ends of the louver blades having phenolic inserts to insulate the louver from the actuator. This type of louver construction is a relatively simple manufacturing task. The bimetal is covered by a multi-layer insulated housing to closely couple the bimetal to the mounting surface through radiation.

b. Augmented Louver System

An augmented system utilizing the thermal actuator is shown in Figure 5-50. This actuator utilizes a special wax and bronze mixture which is highly sensitive to temperature changes. The expanding material forces a moulded synthetic rubber plug into a reduced diameter in the plunger guide, which multiplies the plunger movement by an extruding action.

The plug and diaphragm are nonhygroscopic and are insensitive to barometric pressure and extreme temperature environment. In operation, the piston moves smoothly throughout its full stroke and does not chatter with rapid temperature fluctuations.

The actuator plunger terminates in a rack gear which drives a pinion gear on the louver shaft. A teflon bearing block mounted on the louver inner frame acts as a guide for the rack and pinion assembly, and provides a position adjustment for louver travel limits. The base of the actuator is inserted into the cold plate for improved heat transfer. An overshoot spring is provided to prevent assembly damage in case of an over temperature condition. The spring backup plate attached to the actuator body allows for adjustment of the



# EVALUATION OF THERMAL ACTUATORS

1.	WEIGHT . . . . . (9)	0.038 LB
2.	COST . . . . .	9
3.	RELIABILITY . . . . .	0.9995
4.	ADJUSTMENT . . . . .	10
5.	MANUFACTURING . . . . .	6
6.	SIMPLICITY . . . . .	6
7.	HEAT TRANSFER ABILITY . . . . .	5
8.	TORQUE LEVEL . . . . .	3
9.	FAIL SAFE . . . . .	5
10.	GAP FRACTION . . . . .	5
11.	RESEARCH AND DEVELOPMENT . . . . .	10
12.	AVAILABILITY . . . . .	9
13.	MAGNETIC LEVEL . . . . .	9

TOTAL . . . 86

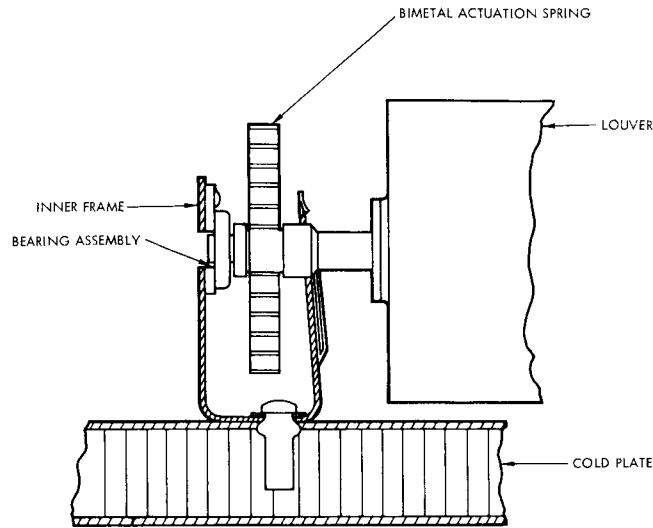


Figure 5-49. Spiral Bimetal Actuation

# EVALUATION OF THERMAL ACTUATORS

1.	WEIGHT . . . . . (6)	0.0883 LB
2.	COST . . . . .	7
3.	RELIABILITY . . . . .	0.9996
4.	ADJUSTMENT . . . . .	7
5.	MANUFACTURING . . . . .	4
6.	SIMPLICITY . . . . .	6
7.	HEAT TRANSFER ABILITY . . . . .	8
8.	TORQUE LEVEL . . . . .	10
9.	FAIL SAFE . . . . .	9
10.	GAP FRACTION . . . . .	10
11.	RESEARCH AND DEVELOPMENT . . . . .	6
12.	AVAILABILITY . . . . .	6
13.	MAGNETIC LEVEL . . . . .	9

TOTAL . . . 88

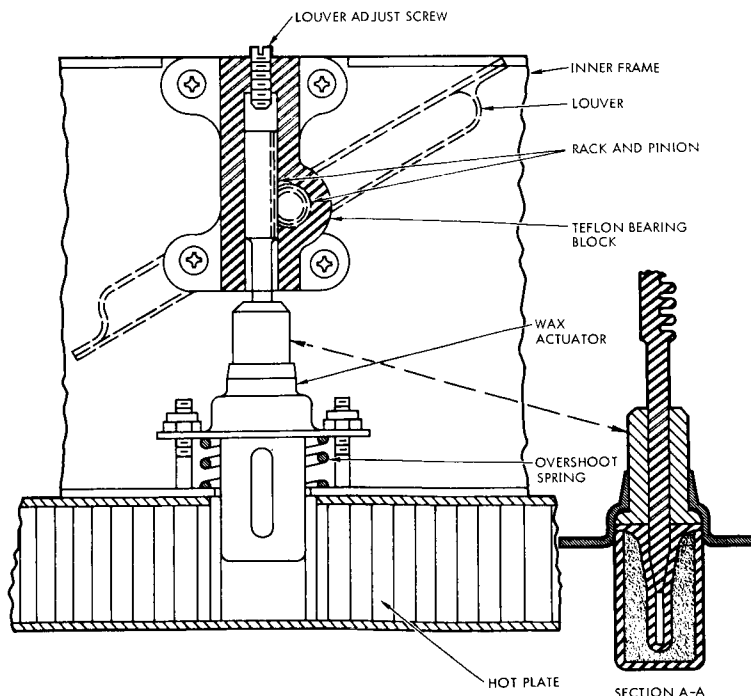


Figure 5-50. Wax-Filled Thermal Actuator Rack and Pinion

louver open position. The thermal actuator develops sufficient force to provide a minimum gap closure between louvers and to drive a sliding fixture at the louver ends to minimize the end gap, a feature which cannot be achieved by the bimetal.

The louver proper (Figure 5-51) is made of two 3-mil aluminum halves spot welded at the edges to form a hollow louver. To minimize end-gap fraction, teflon plugs are made to slide inside the louvers. These plugs are lightly spring-loaded from inside the louver to press the plugs against the louver frame, thus providing a zero-gap sliding member. A thin shaft runs the full length of the louver. Ends of this shaft are larger in diameter to provide for bearings and support. The small diameter, center section of the shaft acts as a torsional return spring for the actuator and a fail-safe closure device in the event of actuator failure.

This system provides sufficient power to eliminate gap fraction and its operating characteristic provides full louver travel over a small temperature differential.

Figure 5-52 describes a similar system except that the rack and pinion drive is replaced with a flexible drive cable. This feature gives more flexibility in mechanical alignment. In all other respects, it is the same as Figure 5-50.

#### c. Evaluation

Each system was evaluated on the basis of terms appearing in the tables accompanying Figures 5-49, 5-50, and 5-52. While weight and reliability are assigned actual numbers, the other factors are assigned weighting numbers up to 10 (the best). The overall evaluation shows the three systems practically equivalent. The simpler system of an Mariner-OGO type blade with the Pioneer bimetal is chosen because it has been developed and flown, the reliability has been determined from OGO test data rather than handbook failure rates, and the overall heat balance and representative performance temperatures have not necessitated a higher performance system. Presented in Figure 5-53 is a photograph of a Mariner-OGO type louver system with the bimetal insulation housings removed on one end.

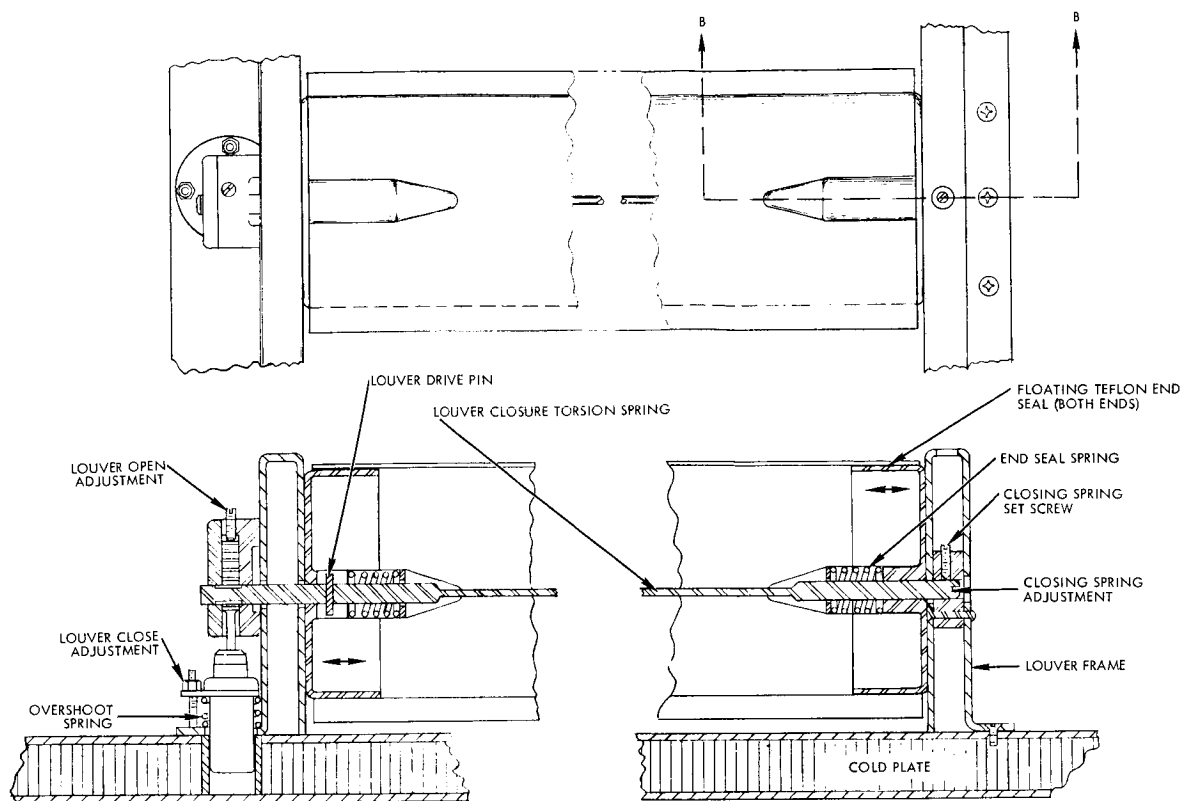


Figure 5-51. Augmented Louver Blade Design

EVALUATION OF THERMAL ACTUATORS		
1. WEIGHT . . . . .	(6)	0.1083 LB
2. COST . . . . .	7	
3. RELIABILITY . . . . .		
4. ADJUSTMENT . . . . .	6	
5. MANUFACTURING . . . . .	4	
6. SIMPLICITY . . . . .	5	
7. HEAT TRANSFER ABILITY . . . . .	8	
8. TORQUE LEVEL . . . . .	10	
9. FAIL SAVE . . . . .	9	
10. GAP FRACTION . . . . .	10	
11. RESEARCH AND DEVELOPMENT . . . . .	6	
12. AVAILABILITY . . . . .	6	
13. MAGNETIC LEVEL . . . . .	9	
TOTAL . . . . .		86

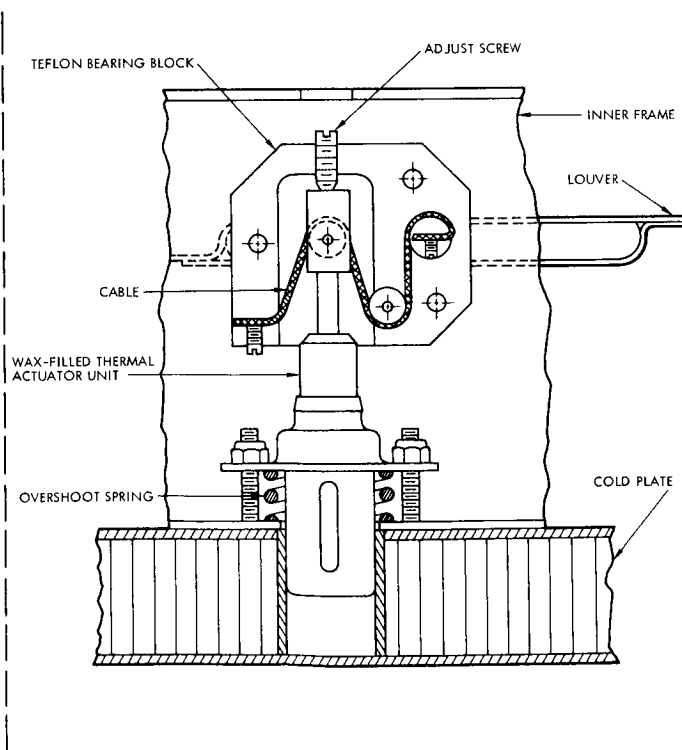


Figure 5-52. Wax-Filled Thermal Actuator Cable and Pulley Drive

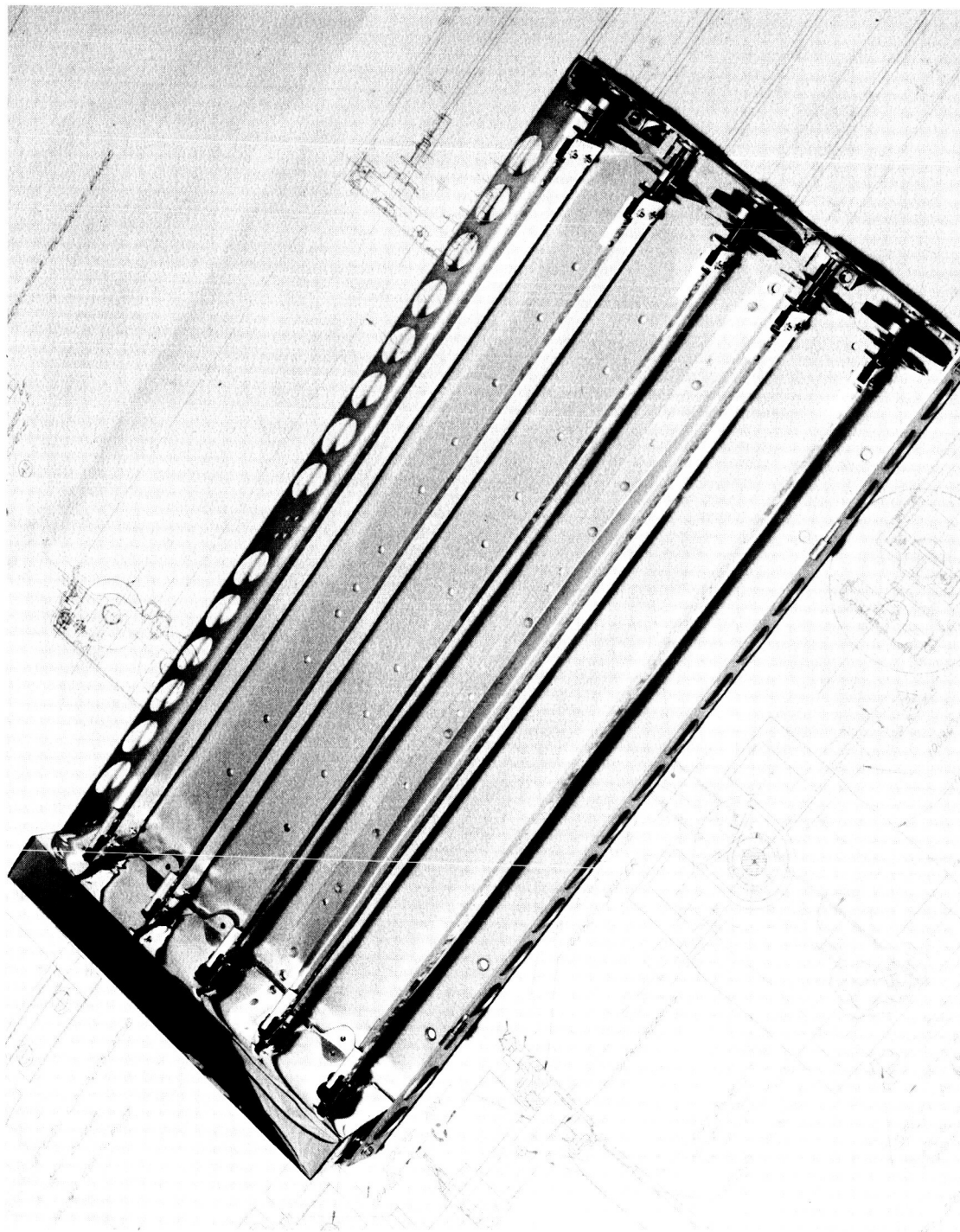


Figure 5-53. Test Model of Mariner - OGO Type Louver System

## 2.4 Insulation

From both a thermodynamics and weight standpoint the ideal type of insulation is multilayer high-performance insulation such as NRC-2 consisting of crinkled 1/4-mil aluminized Mylar layers. Foam insulations were briefly examined and rejected both on weight and insulative deficiencies.

Aluminized Mylar insulation degrades in performance with temperatures over 300°F. By having the Mylar side of the outer 3-mil layer facing space, the absorptivity is 0.24 (undegraded)\* and the emissivity is 0.78 so that normal solar radiation will not cause excessive temperatures.

Results of a parametric analysis detailed in Appendix D are presented in Figures 5-54 through 5-57. Each figure presents the heat flow through a square foot of insulation as a function of insulation thickness and spacecraft interior temperature for a specified value of the solar constant. Tables 5-27 and 5-28 present the heat flux out through 1/4-mil aluminized Mylar insulation with 20, 30, and 40 sheets of insulation as a function of the amount of solar heating. This data was taken from Figures 5-54 through 5-57 and is applicable to insulation with an exterior surface finish of  $\alpha = 0.24$  and  $\epsilon = 0.78$ . Negative values indicate the heat flow is into the spacecraft.

To attach the insulation so that it has a high thermal performance but is still easily removable, the approach on OGO and Pioneer employs Velcro tape and ultrasonic welding. The edges of the insulation blanket are spot welded ultrasonically to fasten the blanket into one piece. The tape is applied to the edges of the blanket and the blanket outline on the spacecraft skin by activating the tape adhesive with methyl-ethyl ketone. The blanket or assembly is then attached to the mating tape by applying pressure along the edges. Figure 5-58 illustrates this technique.

---

\*Preliminary test shows degradation of  $\alpha$  to 0.32 after 1000 hours of UV exposure, "Ultraviolet of 3M No. 850 Mylar tape (OGO), Gold and Silver," TRW document 65-9723.3-72, 16 February 1965.

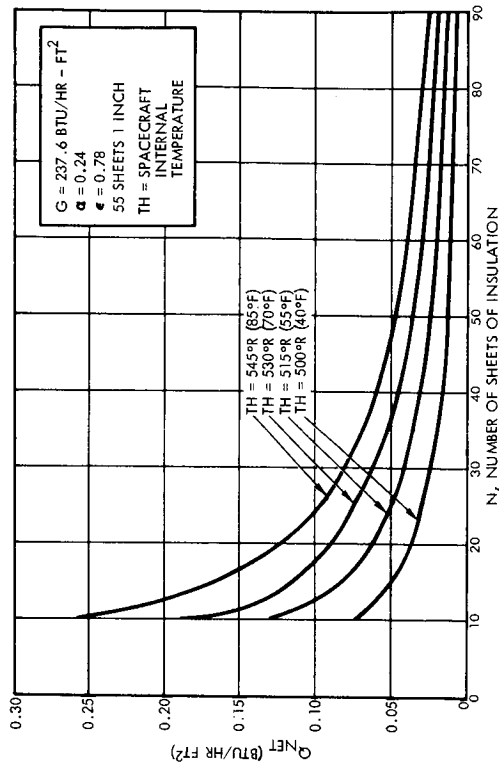


Figure 5-54. Heat Flux as a Function of Insulation Thickness

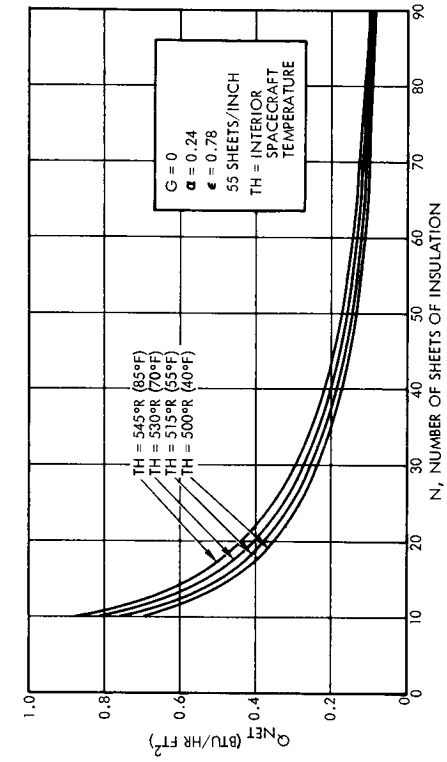


Figure 5-55. Heat Flux as a Function of Insulation Thickness

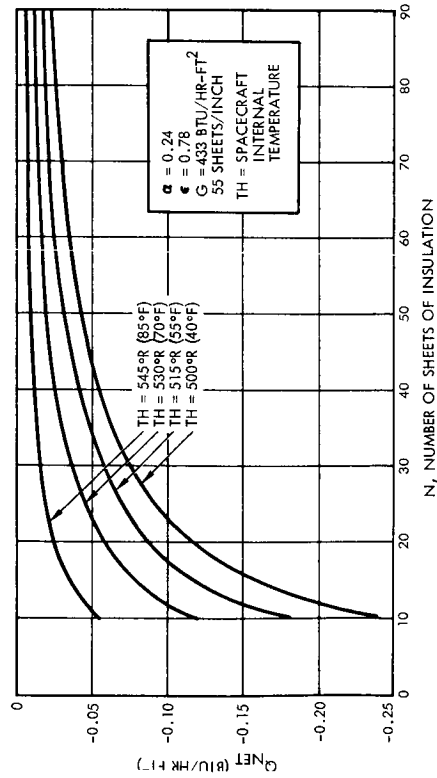


Figure 5-56. Heat Flux as a Function of Insulation Thickness

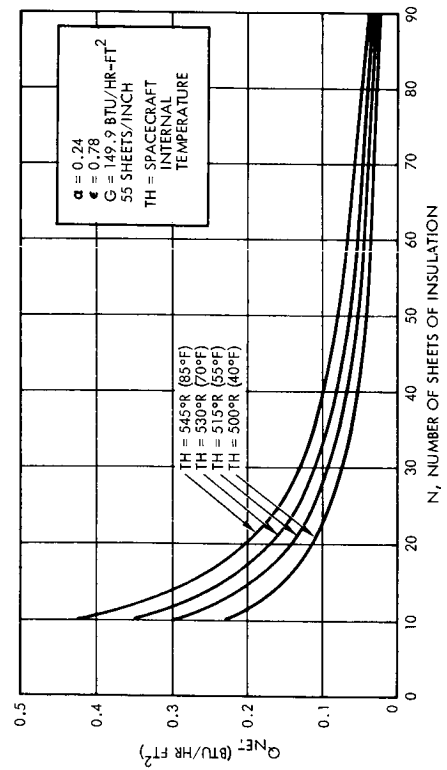


Figure 5-57. Heat Flux as a Function of Insulation Thickness

Table 5-27. Heat Flux Out Through 1/4-Mil  
Aluminized Mylar Insulation for  
Spacecraft Interior Temperature =  
40°F, Heat Flux Rates in Watts/Ft<sup>2</sup>

Solar Heating Rates (watts)	Number of Sheets of Insulation		
	20	30	40
127	-0.033	-0.022	-0.016
70	0.010	0.007	0.005
44	0.032	0.021	0.016
0	0.101	0.067	0.051

Table 5-28. Heat Flux Out Through 1/4-Mil  
Aluminized Mylar Insulation for  
Spacecraft Interior Temperature =  
85°F, Heat Flux in Watts/Ft<sup>2</sup>

Solar Heating Rates (watts)	Number of Sheets of Insulation		
	20	30	40
127	-0.008	-0.005	-0.004
70	0.036	0.023	0.018
44	0.058	0.038	0.028
0	0.126	0.084	0.063

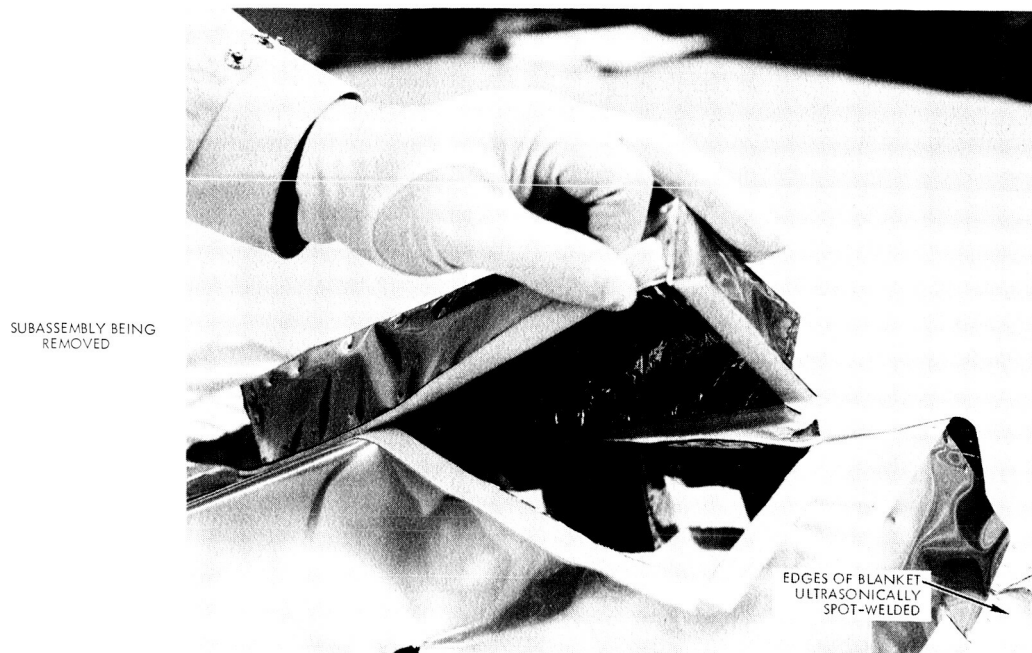
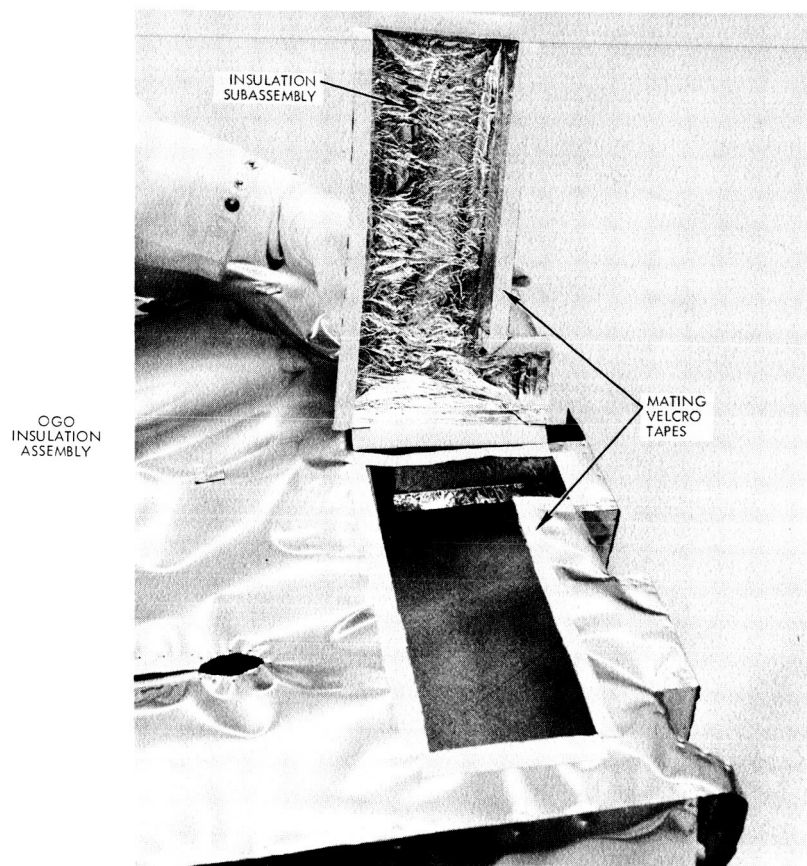


Figure 5-58. Use of Velcro and Tapes and Ultrasonic Spot Welding for Insulation Attachment on OGO



Another technique, which has performed successfully in tests at DAC, is to button the insulation in place. One end of a thread is bonded to the vehicle skin, the other end fastened to the button. Slits, for button holes, are made in the insulation using a hot cutter to avoid tearing. Both approaches, shown in Figure 5-58 and 5-59 allow repeated removal and replacement of the insulation without degrading its thermal performance.

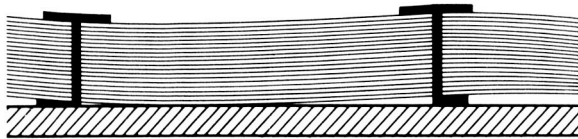


Figure 5-59. Button Insulation Attachment

An important problem in the evaluation of insulation effectiveness is the effect of heat shorts, i.e., areas which allow large amounts of heat to flow through them. In the case of the Voyager spacecraft, any part on the exterior which is structurally attached to the interior is a potential heat short. Typical examples are the solar array attach ring and supporting struts, the spacecraft-lander attach area, attitude control lines, and mapping package support.

Particular care was used in the analysis of the heat short between the solar array and the spacecraft, as it is potentially the largest or most critical short. Results were obtained for the solar array sun oriented both near Mars and near earth and at the end of Martian eclipse (2.3 hours duration). Near earth, with an  $85^{\circ}\text{F}$  internal spacecraft temperature, approximately 14 watts of heat flows into the spacecraft. Near Mars, and assuming a  $40^{\circ}\text{F}$  internal temperature, the heat flow amounts to 14 watts out of the spacecraft. At the end of Martian eclipse the heat flow out of the spacecraft is 60 watts.

The struts which attach the outer perimeter of the solar array to the spacecraft are also heat shorts. The analysis shows that at this short the heat flow can be maintained at 14 watts or less leaving the spacecraft, at the end of Martian eclipse.

The spacecraft-lander attach area was also analyzed. As long as the spacecraft and lander are attached, the heat flow through this area is negligible. After the lander has separated, however, the exposed attach points or ring can radiate heat to space. If the temperature of the exposed area is 40°F and its emissivity 0.80, the heat leak out of the spacecraft is 22 watts. With a low-emissivity finish on this area, for example, an emissivity of 0.1, the heat leak is reduced to 3 watts.

The attitude control lines extending from the spacecraft in the area of the solar array allow about 5 watts of heat to leak out during Martian eclipses; the loss is 1 watt when the spacecraft is in the sun near Mars. A heat gain of 1 watt exists when the spacecraft is in the sun near the earth.

Table 5-29 lists the value of the heat flow through the analyzed shorts at various times. Negative values indicated that the heat flow is into the spacecraft.

Table 5-29. Heat Flow Through Heat Shorts

Heat Short (watts)	In Sunlight Near Earth	In Sunlight Near Mars	End of Martian Eclipse
Solar Array Attach Ring	-14	14	60
Solar Array Attach Struts	14	14	14
Spacecraft-Lander Attach Area	0	3	3
Attitude Control Lines	-1	1	5
Totals	-1	32	82

## 2.5 Solar Array

The thermal analysis for the solar array is based on the following equations. For the steady state conditions existing in the sun, the temperature can be determined from

$$\sigma T^4 = \frac{(\alpha - \eta)}{(\epsilon_F + \epsilon_B)} \frac{G}{D^2} \cos \theta$$

Transient temperatures during eclipses were determined from

$$\frac{1}{\sigma T_F^3} - \frac{1}{\sigma T_i^3} = \frac{3t(\epsilon_F + \epsilon_B)}{w C_P}$$

where

$C_P$  = average specific heat

$D$  = distance in astronomical units from the sun

$G$  = solar constant at earth (433 Btu/hr-ft<sup>2</sup>)

$T$  = steady state temperature

$T_F$  = temperature at end of eclipse

$T_i$  = temperature at start of eclipse

$t$  = time

$w$  = weight per unit area

$\alpha$  = solar absorptivity

$\epsilon_F$  = emissivity of front face (solar cell cover glass)

$\epsilon_B$  = emissivity of back face of array

$\sigma$  = Stefan-Boltzmann constant

$\theta$  = angle between the sun vector and the solar array

$\eta$  = array efficiency (array power =  $\eta G$ )

Mars- or earth-emitted radiation and albedo were not included in the temperature prediction shown in this analysis. For the Mars orbits considered, the distance from the planet to the spacecraft is great enough to make the effect of these heat inputs negligible. The earth inputs were neglected as a rapidly decreasing transient.

Except for the analysis of the in-sun steady state temperatures for an earth-oriented spacecraft, the angle between the sun vector and the normal to the solar panel was taken as zero. Efficiencies of the solar array varied from 7 to 10 per cent.

Figures 5-60\* and 5-61 indicate the temperature range for the panel with back face emissivities of the nominal 0.85 and the minimum allowable emissivity of 0.7 to remain within the  $\alpha/\epsilon$  constraint of less than 0.5. Variations in temperatures because of tolerances on measured values of absorptivity to emissivity are shown on this figure. At 1.38 AU, the release of the landing capsule results in the back of the solar array having a larger view factor to space and therefore lower temperatures. This can be noted on Figures 5-60 and 5-61 by the abrupt change of temperatures at 1.38 AU. The blockage because of the landing capsule is included in the calculation by modifying the above equations as follows:

$$\sigma T^4 = \frac{(\alpha + \eta)}{(\epsilon_F + \epsilon_B)} \frac{G}{D^2} \cos \theta$$

where

$$\epsilon'_B = (1 - F_{AC} F_{CA}) \epsilon_B$$

$F_{AC}$  = geometric view factor from solar array to landing capsule

$F_{CA}$  = geometric view factor from landing capsule to solar array

Tolerances of  $\pm 0.02$  (measurement accuracy) were used for the anticipated values of absorptivity and emissivity. The view factors from the back of the solar array to the landing capsule and from the landing capsule to the back of the array were estimated at 0.54 and 0.39

---

\* Figures 5-60 through 5-73 are shown following the solar array discussions. (Section 2.5)

respectively. When the landing capsule is ejected, the view factor from the array to space was estimated at 0.97. A tolerance of 15 per cent was taken on the view factors for calculating the temperatures shown in Figures 5-60 and 5-61.

The equation for  $\epsilon'_B$  assumes that the capsule surface is adiabatic and a diffuse radiator. The radiation from the back of the solar panel to the landing capsule is assumed to be reflected back to the panel once. For a high emissivity on the back surface of the array, the assumption of a single reflection results in a negligible error, since only a small portion of the energy remains for rereflections and approximately 75 per cent of those are lost to space.

The tolerance analyses were performed to permit array power output evaluation under worst cases caused by shifts in I-V curves due to temperature variation.

After Mars encounter, the Voyager spacecraft can be eclipsed from the sun for a nominal time of 2.3 hours (see Volume 4, Section III. 5. 4). For lightweight arrays, temperatures below  $-160^{\circ}\text{C}$  could occur. The parameters which must be considered in determining the best design for the array are:

- a) Minimum allowable panel temperatures
- b) Weight per unit area
- c) Power per pound of heat sink substrate
- d) The emissivity of the back face
- e) The effect of eclipse time on minimum array temperatures.

If array temperature at the end of eclipse must remain above that achieved with maximum emissivity coatings and a structurally adequate substrate, a tradeoff can be performed between decreasing emissivity of the back face of the solar panel and increasing the weight of the panel. A decrease in the emissivity increases the equilibrium temperature of the panel in sunlight, resulting in less power per unit area, has the

advantage of increasing the time constant of the solar panel. An increase in the time constant in turn decreases the requirement of added weight per unit area for increased thermal capacity.

Figure 5-62 indicates the wide range in the steady state temperature of the solar panel at 1.65 AU which can be achieved if the back face emissivity of the panel is varied. A comparison of transit temperatures for low and high emissivities is shown in Figure 5-63. The calculations for this figure assumed that the view factor from the back of the panel to space is unobstructed. It is worthy to note that near earth array temperatures with the low emissivity backface may be above  $100^{\circ}\text{C}$ .

Figure 5-64 shows the array temperature as a function of eclipse time for the extremes of emissivity, with weight per square foot as a parameter. The present qualification limits of  $-120^{\circ}\text{C}$  on the lunar orbiter solar array and  $-140^{\circ}\text{C}$  on OGO are noted. With the Voyager reference design,  $-140^{\circ}\text{C}$  would be reached after 70 minutes of eclipse. Figures 5-65 through 5-68 are plots showing the required specific weight as a function of eclipse duration with allowable minimum temperature and backside emissivity as a parameter. The corresponding array output when illuminated is also noted. Presented in Figure 5-69 are the combined effects of in-sun temperature on array output per unit area and minimum allowable eclipse temperature on the power per unit weight. This shows no optimum point in the emissivity-weight tradeoff: the minimum weight design (highest power per unit weight) is at the highest achievable in-sun temperature and the lowest achievable minimum temperature in eclipse assuming no area limitations.

Use of beryllium substrates such as on OGO to obtain a higher thermal capacity for equivalent weight has been examined; the results are presented in Figure 5-70. Because of the strong dependency of the specific heat on temperature (Figure 5-71) and the low initial temperature at Mars, aluminum substrates are equivalent or superior to beryllium.

During retropropulsion, the back of the array is exposed to radiation from the particle plume of the engine. The heat flux impinging

on the array is calculated in Section 2.6 as  $3300 \text{ Btu/hr-ft}^2$ . The effect on array temperature has been calculated and may be seen in Figure 5-72, for three array backside coatings: black Cat-a-lac paint having an absorptivity of 0.95 to the solar and plume spectra, and an infrared emissivity of 0.86, potassium-zirconium silicate paint having an absorptivity to the solar spectrum of 0.2, an absorptivity to the plume spectrum of 0.33, and an infrared emissivity of 0.85, and a bare metal surface having an estimated absorptivity to the plume of 0.15 and an infrared emissivity of 0.1. The initial temperature was determined for the sun vector normal to the solar array with the highest flux expected at encounter ( $67 \text{ watts/ft}^2$ ). Under these conditions the white coating is the design selection to avoid high temperature problems.

Array temperatures for the earth-oriented configuration C for a nominal history of sun-spacecraft-earth angle are shown in Figure 5-73. The initial low temperatures are not realistic because spacecraft orientation would be constrained to that where the solar array would shadow the louver system.

## 2.6 Rocket Engine Heating

The effects of the propulsion systems upon the spacecraft thermal requirements have been assessed in view both of the heat from the exhaust plume and the conducted heat from the engine. The analytical techniques are described in Appendix D.

### 2.6.1 Plume Heating

Heat transfer to the spacecraft from the exhaust plumes by radiation and convection from the plume of the solid motor and by convection from the plume of the liquid bipropellant engine were considered. The radiation heat transfer rates to two regions of the spacecraft were calculated: the aft end of the spacecraft lying in the exit plane of the solid motor and the aft face of the solar array. Spacecraft configurations A-1 and A-2 were analyzed.

The maximum heating rate for the aft end of the bus does not vary between the two configurations. The calculated incident rate is

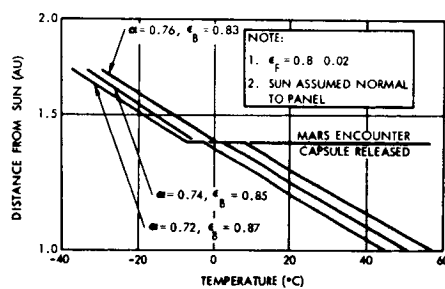


Figure 5-60.

Solar Panel Temperatures Including Tolerance  $\epsilon_B = 0.85$

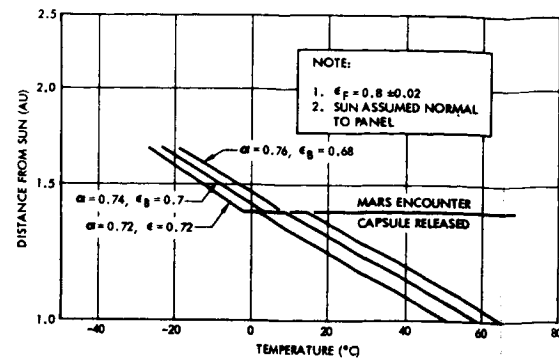


Figure 5-61

Solar Panel Temperatures Including Tolerances  $\epsilon_B = 0.7$

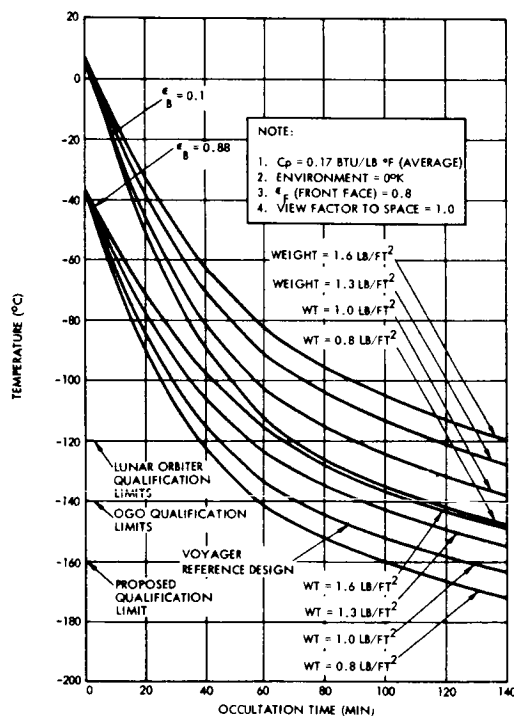


Figure 5-64

Solar Panel Temperature During Occultation

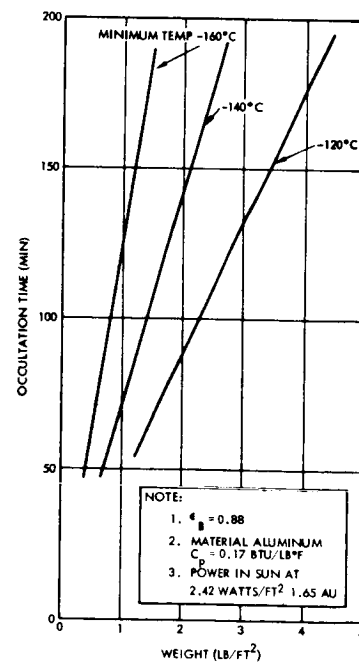


Figure 5-65

Solar Array Temperature During Eclipse

113①



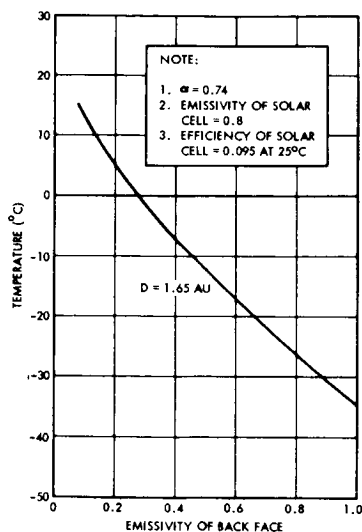


Figure 5-62

Equilibrium Temperature of Solar Array 1.65 AU

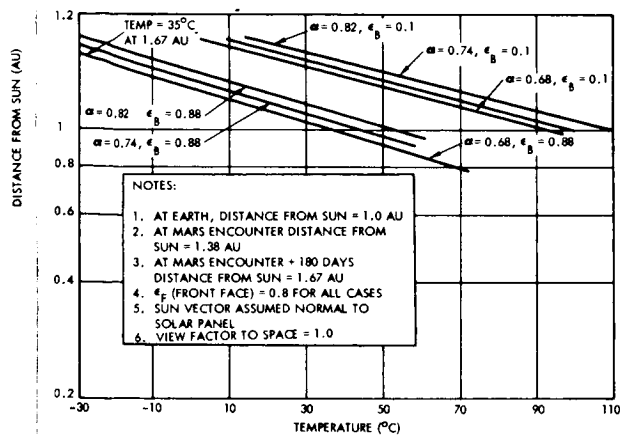


Figure 5-63

Solar Panel Equilibrium Temperature

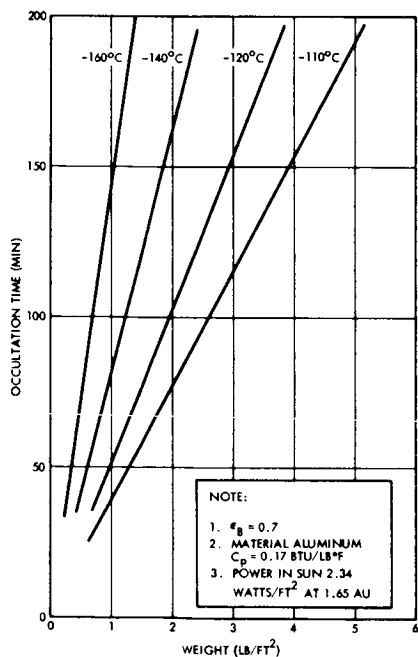


Figure 5-66

Transient Panel Temperatures During Eclipse (View 1)

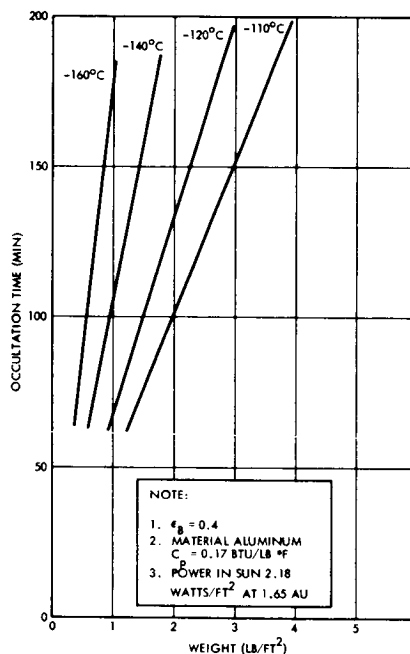


Figure 5-67

Transient Panel Temperatures During Eclipse (View 2)

2

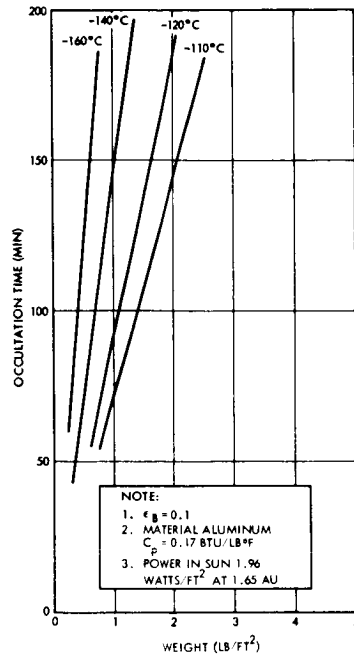


Figure 5-68  
Transient Panel Temperatures During  
Eclipse (View 3)

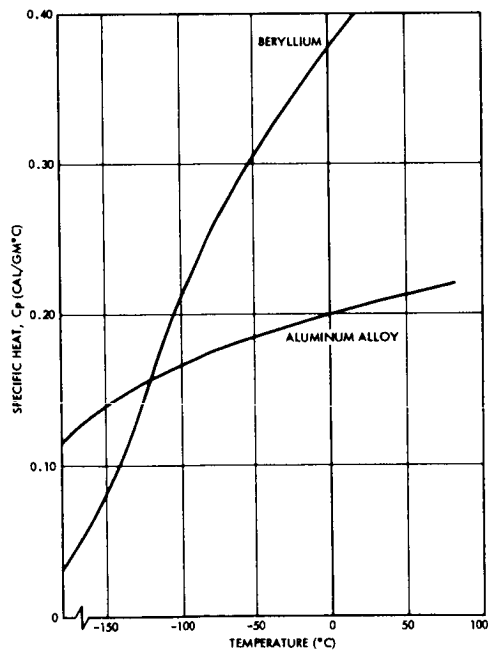


Figure 5-71  
Specific Heat Versus Temperature

115 ①

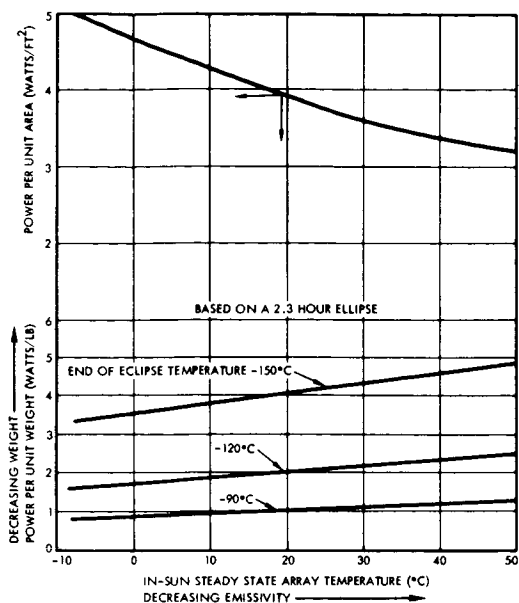


Figure 5-69  
Array Power at 1.38 AU

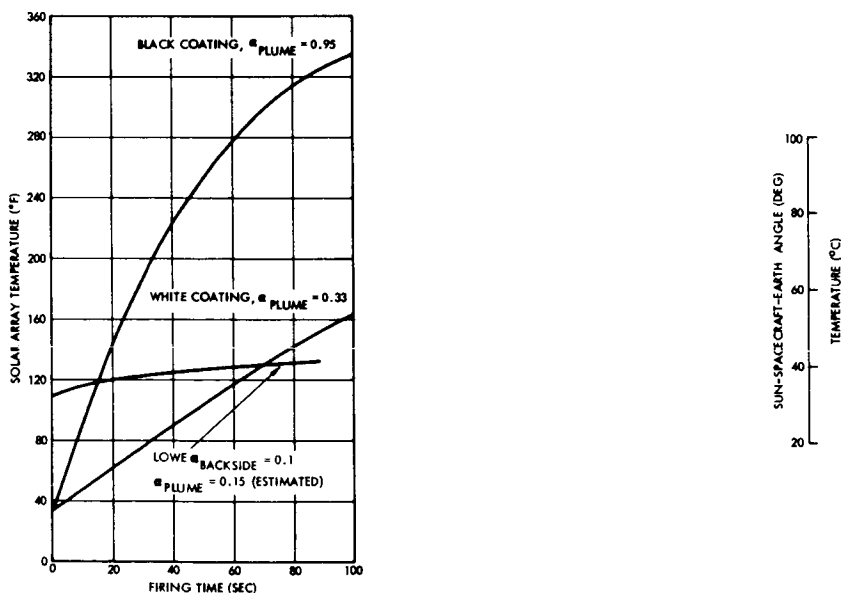


Figure 5-72

Solar Array Temperature Rise Due  
to Radiant Heating from the Solid  
Rocket Particle Plume

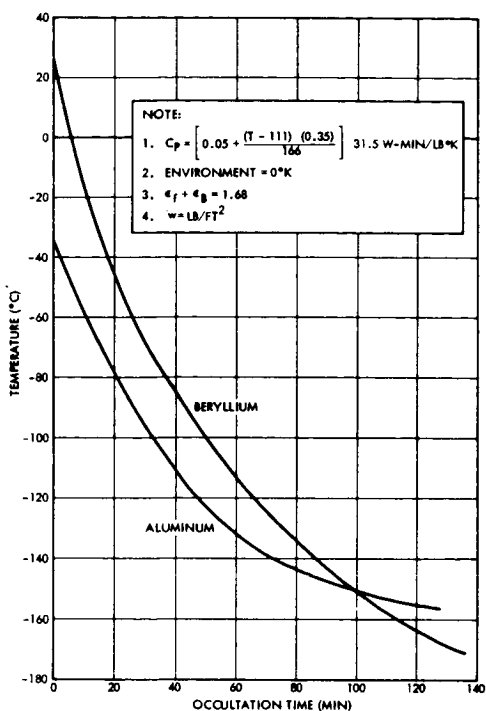


Figure 5-70

## Solar Panel Temperatures - Transient

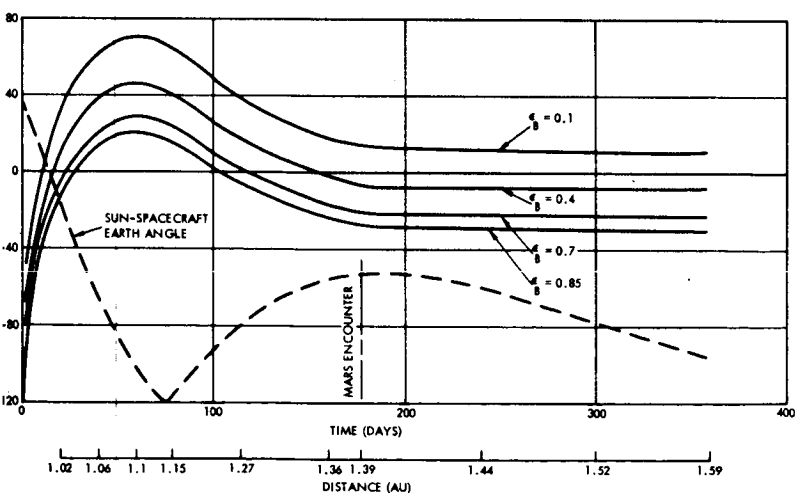


Figure 5-73

## Solar Panel Temperature - Voyager Earth-Oriented Array



13.5 Btu/ft<sup>2</sup>/sec. In applying this rate to an analysis of insulation and structure, it is multiplied by the surface absorptivity. A simple seven-node model of the Refrasil batt was established to determine the heat soak into the aft surface. The batt thermal properties are:

Conductivity in vacuum	0.04 Btu/hr-ft <sup>2</sup> -°F/inch
Thermal capacity	0.2 Btu/lb-°F
Density	3.16 lb/ft <sup>3</sup>
Emissivity	0.85

The heating rate was reduced by the absorptivity of the batt to plume radiation (0.17) and applied to the insulation for 90 seconds. The back surface temperature history is presented in Figure 5-74. As seen, the temperature rise is less than 30°F and does not present a problem.

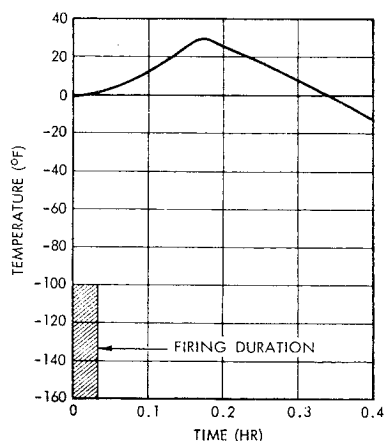


Figure 5-74  
Refrasil Batt Interval  
Surface Temperature  
History Due to Plume  
Radiation Heating

The heating incident upon the aft end of the solar array varies between the two configurations because of the difference in shading by the spacecraft. The calculated incident heat flux for configuration A-2 is considerably greater than for configuration A-1, 0.92 Btu/ft<sup>2</sup>/sec for A-2 and 0.6 Btu/ft<sup>2</sup>/sec for A-1. The effect on the solar array was presented in Section 2.5.

The exhaust plume of the solid propellant motor is shown to expand forward of the nozzle exit plane and would therefore impinge upon

portions of the spacecraft structure. Figure 5-75 shows lines of constant properties and the plume boundary, for the motor being studied. Data from this figure were used to predict the convective heat transfer rate to the spacecraft structure. This data was generated by Aerojet-General Corporation.

From the properties along the  $M=20$  line, the stagnation heating was calculated to be  $0.023 \text{ Btu/ft}^2/\text{sec}$  ( $83 \text{ Btu/hr-ft}^2$ ). This predicted heating rate is so much lower than the radiation heating rate that it can be neglected. Even by itself, the convective heating rate is below a level of concern.

Exhaust plume characteristics for the liquid bipropellant engine are illustrated in Figure 5-76.

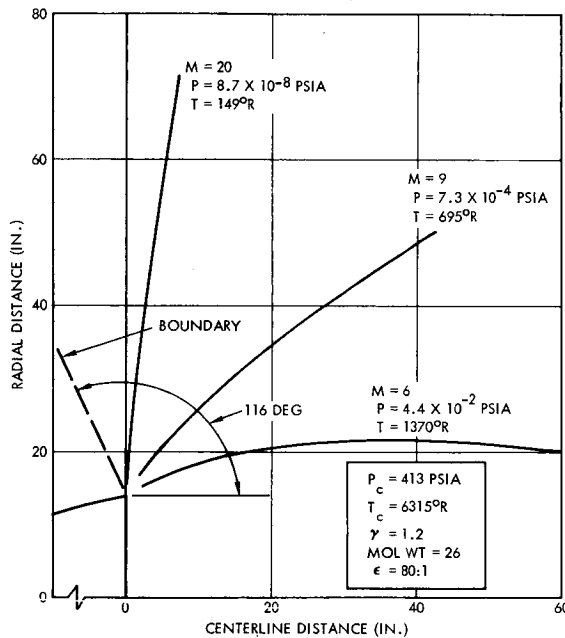


Figure 5-75. Solid Motor Plume Characteristics

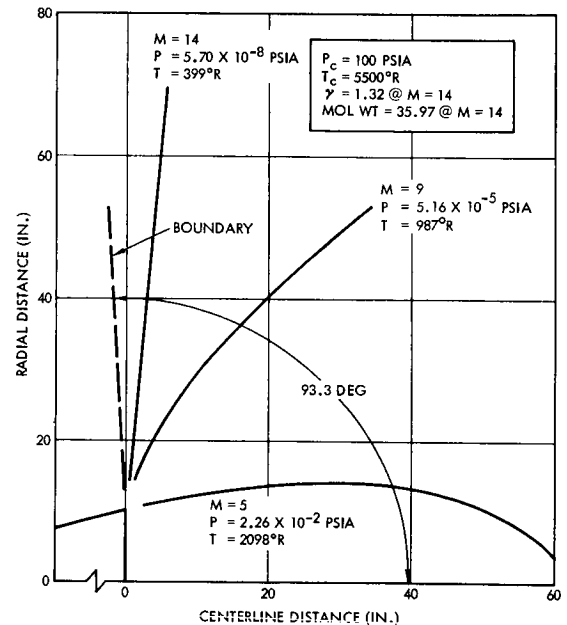


Figure 5-76. Bipropellant Engine Plume Characteristics

A convective-heat transfer analysis was performed in the same manner as for the solid motor plume. From the properties along the  $M=14$  line, a stagnation heating rate of  $0.016 \text{ Btu/ft}^2/\text{sec}$  ( $57.5 \text{ Btu/hr-ft}^2$ ) was calculated. A heating rate of this magnitude does not require alteration of the thermal protection requirements.

### 2.6.2 Heat Transfer Between the Solid Motor and Spacecraft

The solid motor must be thermally isolated from the spacecraft for two reasons: the motor becomes a source of heat immediately after firing, and later, after it has cooled, it becomes a path for heat loss to space.

Radiation isolation is achieved by covering the motor with a blanket of multilayer insulation such as Linde SI-62. Conduction isolation is obtained by placing a high thermal resistance pad between the motor and its support structure. A phenolic-fiberglass gasket, with a difference in the inner and outer radii of 0.1 inch, placed between the motor and thrust structure, gives a contact area of 15 square inches and meets the structural requirements. The heat loss from the spacecraft through the expended motor as a function of gasket thickness is presented in Figure 5-77. It is assumed that the motor radiates to space through the nozzle exit with an emissivity of unity. As shown in Figure 5-77, thicknesses greater than 0.5 inch offer little improvement. A one-half inch thick gasket permits a heat loss of 12 watts which is acceptable.

The one-half inch thick gasket limits the peak heat transfer rate from the hot motor into the spacecraft to 13.6 watts, assuming a spacecraft temperature of  $85^{\circ}\text{F}$  and a maximum motor case temperature of  $275^{\circ}\text{F}^*$ . Experience from the Vela program has shown that a peak motor case temperature of  $600^{\circ}\text{F}$  can occur. This would result in a peak heat transfer rate of 36 watts. Even the higher value of heat flux is acceptable, being well within the heat rejection capability of louver system.

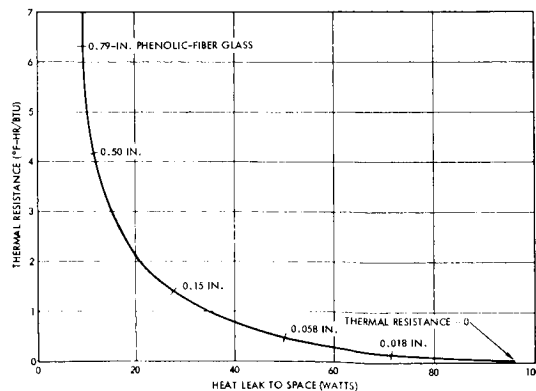


Figure 5-77. Solid Motor Insulation Requirement

\*Data obtained from Aerojet-General Proposal.

## 2.7 External Equipment

Externally-mounted equipment will require a thermal design which is independent of the main compartment. The thermal designs are based upon minimizing thermal coupling between the equipment and their support structure, as well as minimizing the effects of the varying external radiant environment. Thermal isolation is accomplished through the use of low-conductance mounts (stacked washers, phenolic blocks, etc.), multilayer radiation insulation, and where possible minimizing radiator view angles of the spacecraft and the sun. Thermostatically controlled heaters will be used to prevent excessively low temperatures, and the radiators, if required, are passive or actively controlled through the use of thermal louvers. All heaters are bi-filar wound such that the magnetic fields cancel.

### 2.7.1 Planet Oriented Package (POP)

The POP will house a variety of experiments, television systems, ultraviolet and infrared spectrometers, radiometers, and Mars-scanning radiometers. Of these experiments, the TV optical systems place the greatest demands upon the thermal design in that they require a nearly uniform temperature environment to maintain optical resolution and pointing accuracy. A Mars-scanning radiometer also requires a fairly uniform temperature environment since it also has an image forming optical system. The remaining experiments have temperature level but not temperature gradient requirements.

Several POP configurations and locations have been examined. The same basic concepts have been employed for each:

- a) Insulate the entire package with multilayer aluminized Mylar except for viewing ports and radiators.
- b) Provide low conductance mounts.
- c) If required, use a passively controlled or louver-covered radiator, depending upon the orientation of the package with respect to the sun.
- d) Use local electrical heaters and thermostats to minimize temperature gradients in the region of the fine resolution TV camera lens systems and for the Mars scanning radiometer.



- e) Use thermal shutters, if required, over the TV lens aperture to reduce heat leaks. The shutter, an insulated door, is open during picture taking modes, estimated to be less than 15 minutes per orbit. The rotating light filter for the TV optical system could be used to reduce heat leaks, instead of a separate shutter, by having a portion of the filter opaque to thermal radiation. The sequencer could be programmed to rotate the opaque portion of the filter over the lens aperture after every picture taking sequence.
- f) Place thermal doors over experiment apertures, similar to those proposed for the TV system, to reduce heat leaks.

If local areas within POP require lower temperatures than their surroundings, this could be achieved by insulating the area from the package and providing a view to space. Figure 5-78 presents for a hypothetical cylindrical volume the temperatures which could be achieved by isolating the volume and giving it a view of space, with heat leaks into the volume from a 60°F environment.

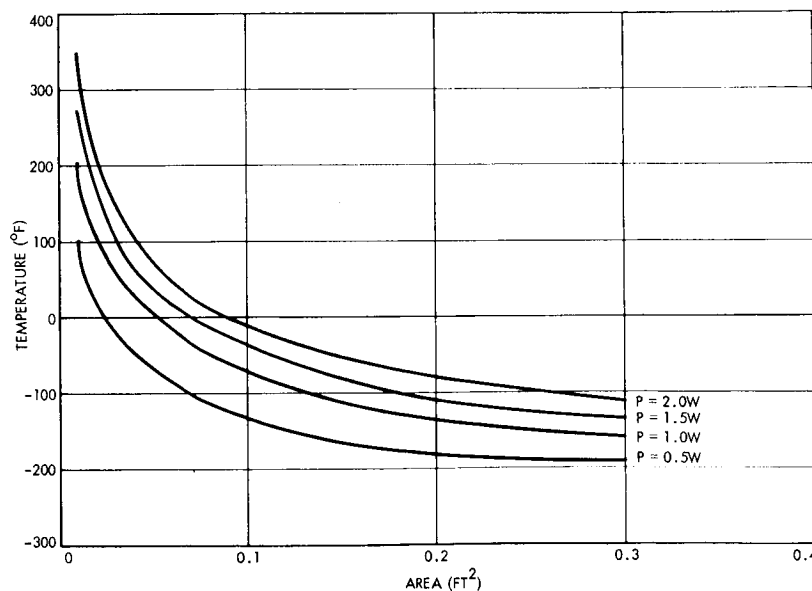


Figure 5-78. Local Temperature of a Cylindrical Volume, 2 Inches High by 2 Inches in Diameter, as a Function of View Area to Space

One of the locations investigated for the POP was that of placing a two-axis gimbal on the end of the array with the POP extended on an arm (Figure 5-79a). The postulated experiment opening requirements were a total of 1/2-square foot. The thermal design requirements for either an active or passive system were examined.

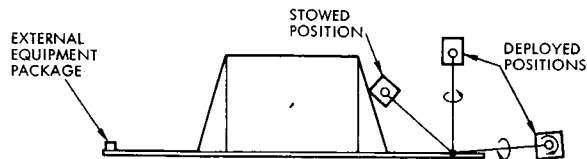


Figure 5-79a. Preliminary POP Configuration

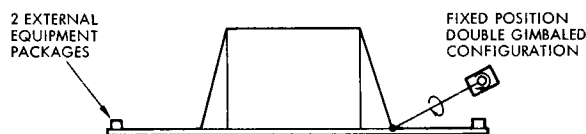


Figure 5-79b. Selected POP Configuration

First, for the passive configuration, consider the hot case where the experiments are looking at the sun through the Martian atmosphere. If no active thermal shutters are used, the experiment openings (assumed thermally black) absorb 33.5 watts; with the 9-watt nominal power dissipation, one square foot of radiating area (coated with potassium-zirconium silicate paint) is required to maintain a package temperature of  $100^{\circ}\text{F}$ . The radiating areas are located on the oriented face because it is the least exposed to the sun in nominal (Mars-oriented) operation. In the cold condition the package is assumed shaded from the sun, receiving negligible heat from the array and spacecraft, and all sensors are turned off. Again, with no active shutters, 33 watts of heater power is required to maintain a package temperature of  $0^{\circ}\text{F}$ .

An active system utilizing louvers under the same conditions requires 2.4 square feet of louvered area to maintain an upper temperature limit of  $85^{\circ}\text{F}$  and 20 watts of heater power to maintain  $40^{\circ}\text{F}$  in the cold case. The operating temperature requirements of the sensors (see VS-3-111 in Volume 2) are zero to  $140^{\circ}\text{F}$ . A passive design is thus adequate at the expense of 13 watts of heater power.

In the selected POP configuration (Figure 5-79a) the POP is partially shaded from the sun, and the TV apertures are never required to look at the sun. During transit the package position is such that none of the experiment apertures receive solar radiation. The selected configuration

has an increased aperture area of one square foot. In the hot condition the aperture area alone is sufficient to reject the dissipated power and absorbed solar energy at 85°F; therefore no additional radiating area is required. In the cold condition, when all sensors are off, 25 watts of heater power is required to maintain a package temperature of 0°F.

### 2.7.2 External Experiment Packages

The external experiment packages will house various sensors and detectors such as meteoroid sensors and plasma detectors. These experiments are low-powered, on the order of 3 watts total power dissipation, and can thus be completely insulated except for experiment apertures. Heater power will be used to make up for heat leaks and heat losses out of experiment apertures. Where possible, windows which are opaque to thermal radiation but transparent to the frequencies of interest will be placed over the detector apertures. Bare metal windows which view the sun will have sufficient conduction coupling to their housing to prevent excessively high temperatures. The packages are insulated from the 4- and 8-inch diameter plasma detector plates since the temperature limits of the plates are those of the metallic plate material.

The experiments are conceived as housed within one package on the edge of the solar array, as shown in Figure 5-79a. Approximately 1/4 square foot of black openings is required by the sensors, which would radiate 8 watts at an average temperature of 40°F. For a nominal dissipation of 2.5 watts, approximately 7.5 watts of heater power are required.

If the experiments were housed within two packages on the edge of the solar array as shown in Figure 5-79b, 1.5 watts of additional power (totaling 9 watts) are needed because of the increase in heat leaks caused by increasing mounting area and the surface area to be insulated.

### 2.7.3 Gimbals

Antenna and POP gimbals must be maintained within a 20 to 120°F temperature. The gimbal systems, discussed in Section II, are essentially electrically passive and must rely on heater power to maintain

acceptable temperature limits. The gimbal mechanisms, motors and bearing, are insulated with low conductivity mounts to reduce heat leaks; cable leads are also insulated. The thermal capacity of the gimbal systems is used to absorb drive motor power dissipation during their brief periods of operation.

The antenna gimbal systems, consisting of a primary and secondary gimbal motor and bearing, each require approximately 2 watts of heater power; the main bearing require approximately 1 watt of power.

The 6-foot antenna gimbal system requires approximately 6 watts of power; the 3-foot antenna requires approximately 4 watts of power in order to maintain acceptable temperatures.

The total heater power requirement for all gimbals is estimated to be 15 watts.

#### 2.7.4 Antennas

The antenna surfaces facing the sun are painted black to eliminate the problem of focusing the sun's rays on the antenna feed. The aft surface is painted white to reduce solid rocket plume heating.

The near-earth antenna and feed temperature was evaluated to be  $143^{\circ}\text{F}$ ; the Martian orbit minimum and maximum temperatures were evaluated to be  $54$  and  $-350^{\circ}\text{F}$ , respectively. The antenna dish is expected to rise to  $354^{\circ}\text{F}$  because of solid rocket plume heating. The antenna feed is isolated from the antenna by a phenolic insert as shown in Figure 5-80 and the leads insulated to insure that the upper temperature limit of  $200^{\circ}\text{F}$  on the feed is not exceeded during rocket firing.

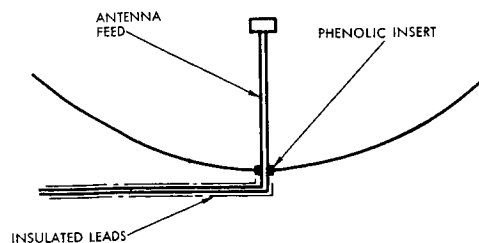


Figure 5-80. Antenna Feed Insulation Concept

#### 2.7.5 Magnetometer

The magnetometer, located on a boom, is insulated from the sun

with multilayer insulation (Figure 5-81) with a radiator facing outboard and never seeing the sun except possibly during midcourse orientations and deboost maneuvers. The radiator is painted white to reduce solar heating during maneuvers and plume heating from the solid engine. Electric heaters are used to insure that the power rejected by the radiator is greater than heat leaks. This is of concern for a low continuous power dissipating magnetometer where power dissipation is the same order of magnitude as heat leaks, since heat leaks are difficult to predict and cannot be controlled. Heater power requirements are such that heat leaks will be less than 20 per cent of the total power to be dissipated by the radiator. Heat leaks have been estimated to be approximately one watt for the magnetometer; thus the total power rejected by the radiator is 5 watts, requiring a radiator area of approximately 25 square inches and leading to an average temperature variation of 20 to 70°F. The average maximum radiator temperature during orientation maneuvers near earth is 140°F. The temperature rise of the radiator during deboost is slight, on the order of 10°F, since the radiator faces away from the major portion of the plume.

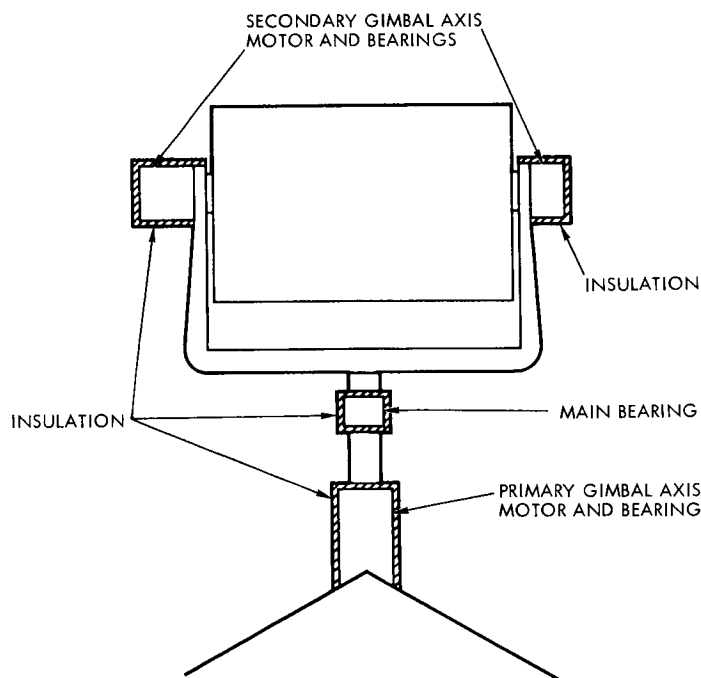


Figure 5-81. POP Gimbal System

## 2.8 Summary of the Selected System

Thermal control features of the selected design are shown in Figure 5-82.

### 2.8.1 Louver System

Although the alternate louver and actuator designs show potential performance improvement over the selected design, the performance analysis and over-all heat balance has shown that the already developed and flight tested Mariner-OGO type of louver and actuator is adequate and reliable. In addition, improvements in magnetic cleanliness are possible with the Pioneer-type bimetal, at some small sacrifice in actuation range. The selected design is then a Mariner-OGO type louver blade actuated by a Pioneer-type bimetal. Some performance gains may be realized with the selected system through careful design and improved fabrication techniques to achieve very small gap fractions. The louver system has been sized for a margin of 10 per cent in the hot condition; however, the performance curves show average temperatures less than  $70^{\circ}\text{F}$  compared to the sizing at  $85^{\circ}\text{F}$  indicating a margin of 17.8 per cent on excess radiating capability.

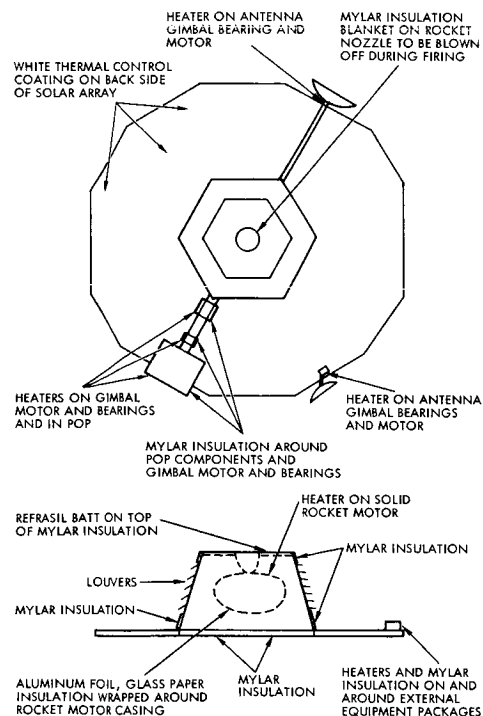


Figure 5-82. Thermal Control Features of the Selected Voyager Configuration

### 2.8.2 Insulation

The over-all heat balance shows 26 per cent margin of internally dissipated power above that lost through closed louvers, insulation, and identifiable heat shorts with 20 layers of aluminized Mylar. Although adequate, additional margin may be realized by allocating weight reserves for more insulation. The Velcro attachments have been proven on OGO and Pioneer and are chosen for the Voyager application.

### 2.8.3 Power Density Constraints

The tradeoff study on power distribution along with experience on OGO has shown that a loose constraint of 0 to 0.2 and occasionally as high as 0.3 watts/in<sup>2</sup> of baseplate will provide adequate temperature control for most electronics, perhaps 30 to 100°F. Use of a 20 watt TWT transmitter poses no special problems. If a 40 watt TWT transmitter is used, it would be necessary to enlarge baseplates and thicken face sheets to provide adequate control, the upper limit on local high power sources being approximately 1.4 watts/in<sup>2</sup> with an attendant operating temperature of 185°F.

### 2.8.4 Rocket Engine Heating

It has been determined that gaseous heating from the engine plume presents no thermal problem for the selected design. However, the solid particle plume of the selected configuration constrains the back surface of the solar array to be a white coating, presents a problem in thermally insulating the antenna feeds from the dish, requires Refrasil batt insulation on the top surface, and may require the use on external packages of insulation with a higher allowable temperature.

### 2.8.5 Externally-Mounted Components

The externally-mounted experiments require insulation and heater power to maintain adequate temperatures but the approach is straightforward. Gimbals present a problem area in requiring an operating temperature above 20°F while exposed to space and attached to the solar array. Thermostatically-controlled heaters, multilayer insulation, and low conductivity attachments offer a solution. However, an accurate sizing of the power needs requires the detailed thermal analysis and design effort planned for Phase 1B.

### 3. SEPARATION SYSTEMS

Means for separating the spacecraft from the booster and the capsule cover base from the spacecraft have been studied in detail. Although no specific designs for separation of the capsule cover or separation of the capsule from its cover were developed, the implications of these operations on the spacecraft design were considered, particularly the requirements imposed by on-pad operations with the over-all spacecraft enclosed in the launch fairing. The considerations leading to selection of the final concepts are described in the following paragraphs.

#### 3.1 Spacecraft-Booster Separation

It has been assumed that spacecraft-booster separation will rely on retrorockets on the Centaur stage and that these rockets are under the control of the Centaur programmer; thus no means are incorporated in the booster-spacecraft separation studies here for providing any differential velocity. It is further assumed that the signal to initiate separation will be from the Centaur stage. Additional ground rules for design are that no wiring for separation should cross the separation interface, and wire cutters will not be required. The heavier parts of the separation assemblies will remain with the booster, and non-magnetic material should be used where possible. Preliminary analysis of the worst case of static and dynamic loads indicates that three bolts will carry the tension loads. The temperature range over which the stage separation system must operate is  $-100$  to  $+165^{\circ}\text{F}$ .

In configurations in which the separation nuts remain with the launch vehicle, standard gas-sealing capture nuts can be used, and no special provision need be made to prevent outgassing.

##### 3.1.1 Mechanisms Considered

Four separation concepts were studied for possible use in separating the Voyager planetary vehicle from the Centaur stage.

The first concept considered for stage separation consisted of an interface with a release device located at each of six hard points of the spacecraft structure. However, since stress analysis



showed that adequate margins could be obtained with three attach points and since the additional mechanisms would be in line with respect to reliability, this approach was not selected. Consideration was given to ways of minimizing the number of in-line operations requiring actuation.

A second arrangement which reflects the information gained from the stress analysis performed on the first arrangement contains three bolts and three separation nuts and three shear pins (Figure 5-83). This arrangement provides an improved reliability due to the use of fewer release mechanisms; it is also lighter in weight. A release system of this type will impart little shock into the system. The simultaneity of release of the bolts is in the order of 2 msec; thus the attitude of the vehicle will not be significantly perturbed.

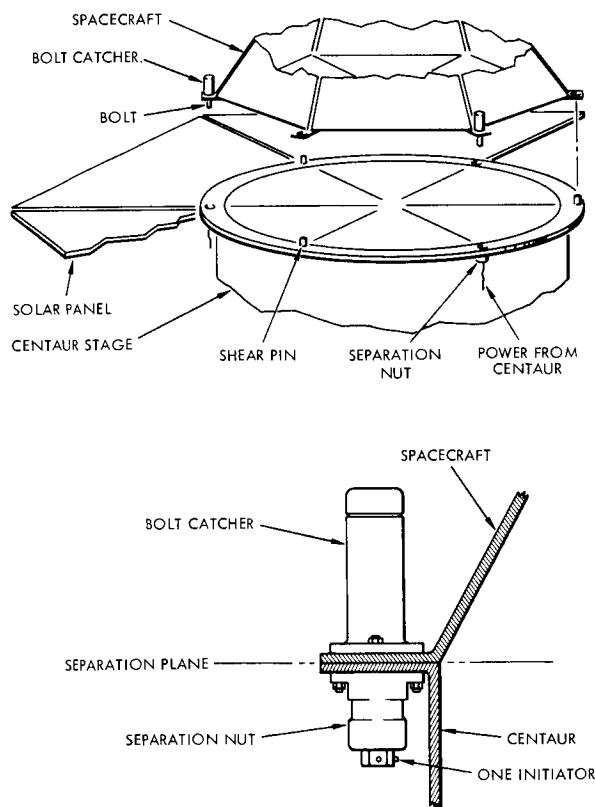


Figure 5-83. Separation Joint Assemblies

A third arrangement (Figure 5-84) consisted of a continuous cable connection between the two stages. In theory the reliability of this approach is high, especially if two cable cutters are used. The concept was discarded, however, for the following reasons:

- a) The weight would be greater than that of separation nuts.
- b) There would be loose pieces of cable which could spring back and damage the solar panels.
- c) Because of uneven drag from the cable, attitude tip-off rates would be higher than with other approaches.

A fourth arrangement studied consisted of a Marman V-clamp which would hold a flange on the spacecraft to a flange on the launch vehicle (Figure 5-85). This is a good system which has been successfully used on small-diameter missile and payload release systems. Redundant bolt cutters or releases perform the release function. On a joint as large in diameter as that of the Centaur-spacecraft (120 inches), and with tension loads as high as those calculated for the Voyager system, the V-clamp system looks less attractive for the following reasons:

- a) Several turnbuckle tighteners would be required to equalize the clamping loads against the sliding friction loads.
- b) A flange would be required on the spacecraft side of the joint, in place of bolt tabs at the load-carrying points.
- c) The loose parts of the V-clamp would require flexible retaining connectors to keep them with the launch vehicle.

The four types of separation systems were evaluated in terms of seven factors: weight, simplicity, availability, shock, outgassing, safety, and reliability. It was found that in all of these respects, except shock, the concept illustrated in Figure 5-83 was equal or superior to the other three. Although the V-clamp and the cable concepts appear to be slightly less shock-inducing in the separation event, their margin is quite small and the shock resulting from the three bolts and shear pins is well within acceptable tolerances. Moreover, the Figure 5-83 concept is the simplest and lightest in weight and appears to offer the most reliable separation. It was therefore selected as the preferred design.

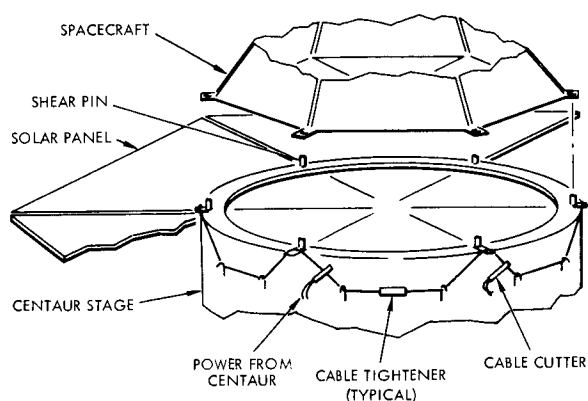


Figure 5-84. Separation Joint Assembly Showing Cable Connection

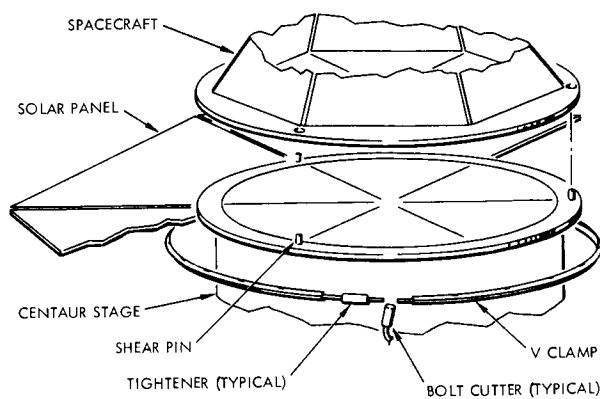


Figure 5-85. Separation Joint Assembly Showing V-Clamp Connection

### 3.1.2 Weight-Reliability Tradeoff

Methods of improving reliability by the use of redundant elements were considered. The results of this evaluation are as follows:

	<u>Reliability Estimate</u>	<u>Weight</u>
3-nuts, 3-dual bridge cartridges	0.99852	2.2
3-nuts, 6-dual bridge cartridges	0.9998	2.3
above + 3-pin pullers and 6 cartridges	0.9999	5.7

The selected approach uses three nuts with six dual bridge cartridges, with a reliability estimate of 0.9998.

### 3.2 Capsule Cover Base Jettison System

After the capsule cover has been opened and the lander separated, the cover base will be left with the spacecraft. On the spacecraft configuration where a solid-propellant retrorocket is used, the cover must be removed and jettisoned prior to motor ignition. A separation system for performing this function would be similar to that considered for spacecraft separation, with the additional requirement of providing force to move the cover away from the spacecraft. The study presented here is without the benefit of any information on the capsule release mechanism. Close cooperation and a good interchange of data will be necessary between the capsule contractor and the spacecraft contractor before the design can be finalized.

An arrangement (Figure 5-86) whereby three hard points take all shear and three hard points take all tension from the capsule was selected in this study. Preliminary analyses indicate that three 1/2-inch studs would hold the lander in position during launch and flight. These same three studs are released to jettison the portion of the capsule cover remaining after lander separation. This mechanization does not intrude into the capsule attachment point adaptors as shown in Figure 4 of the JPL Preliminary Voyager 1971 Mission Specification. A preliminary calculation to substantiate the practicability of a spring deployment system is shown in Section 2 of Appendix C.

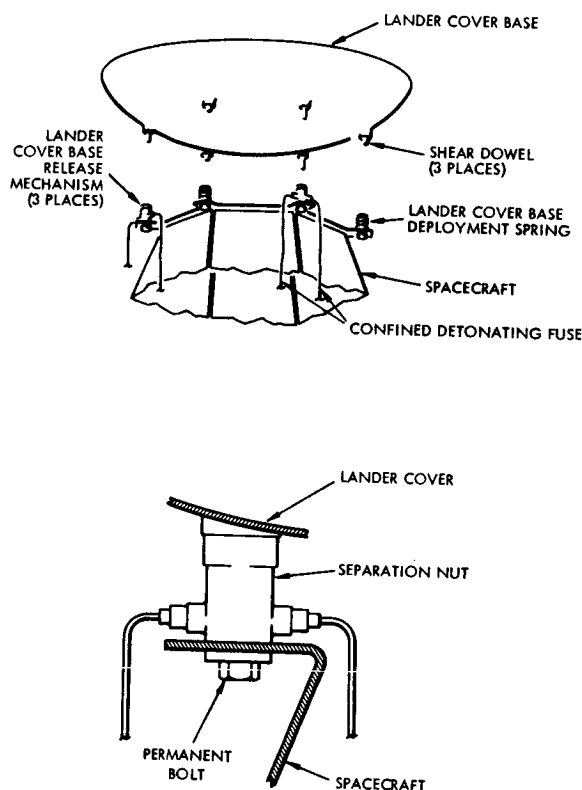


Figure 5-86. Lander Cover Base Release Mechanism

A design constraint is that requirement for installing all ordnance in the spacecraft before it is placed in position on the Centaur stage. Arming of the ordnance, that is the installation of the electro-explosive initiator, should be done as late as possible in the countdown.

A method of accomplishing these two requirements would be the installation of release nuts, with nonelectric pressure cartridges to actuate the release nuts. Attached to each of the nonelectric pressure cartridges would be two tube-enclosed confined detonating fuzes (CDF). The other ends of the confined detonating fuzes would be attached to an arming block located for convenient access on the bottom of the spacecraft. CDF has been used with great success on Thor and Zeus programs. However, the flight times of these missiles have been short compared to Voyager, and tests of CDF under hard vacuum conditions have demonstrated that the material loses weight. The design presented here anticipates enclosing each CDF lead in a sealed metal tube, which performs the function of protecting the CDF from the hard vacuum and also acts as a pressure seal for the actuators after firing.

The comparison of separation approaches in Section 3.3.1 is also applicable to the lander cover base separation. Reliability and weight tradeoff for this system lead to the same dual bridge configuration, with a reliability estimate of 0.9998.

#### 4. PYROTECHNICS

##### 4.1 Requirements and Design Criteria

In addition to mission specification requirements, the following criteria were used in evaluating candidate pyrotechnic devices and selecting the devices recommended for the Voyager spacecraft:

- a) Efficient, reliable performance of the required functions.
- b) Static and dynamic analyses of devices that induce low shock are preferred.
- c) The mission temperature range of +165 to -300°F. All devices will not be subjected to the entire range.
- d) Nonventing, and nonrupturing devices providing positive gas containment to preclude surface deterioration.
- e) Reliability evaluation of the electroexplosive devices based on test data and accumulated history. Pyrotechnic devices (hardware) will be evaluated with greater emphasis on the basic design because less history exists. The selected items will all receive reliability evaluation tests in the exact configurations selected.
- f) RF analysis made to assure that the 1 amp/lw no-fire standard initiator with twisted shielded firing circuit survives the RF environment specified. In the event that the RF environment is increased beyond the survival capability of the 1 amp/lw squib equipped with completely shielded firing circuit, filters have been designed and can be installed ahead of the squibs.
- g) Capability of electrical circuitry to:
  - Short initiator circuits to protect electro explosive devices (EED)
  - Switch initiator circuits from shunt position to fire position
  - Provide 5 amps of current for 50 msec to each bridgewire, and at no time exceed 22 amps on any one bridgewire.
- h) Minimize total number of items used on the Voyager program. Qualification costs, lot acceptance, and development testing will probably exceed the cost of

of the parts. Consideration must be given to maintaining a balance between total cost and value.

- i) Simple design for reliability and lower cost of manufacturing, handling, and personnel training.
- j) Amount of damage that an explosive part is capable of inflicting and the relative sensitivity of the explosives used in the device.

The Apollo standard initiator is a device that meets the requirement of the Voyager mission specification. There are presently two sources for the device.

#### 4.2 Pyrotechnic Devices

The types of EED-actuated pyrotechnic devices considered for use in the Voyager spacecraft include the following:

- Explosive bolts
- Separation nuts
- Flexible linear shaped charge
- Mild detonating fuse
- Primacord
- Pin pullers
- Reefing line cutters

##### 4.2.1 Explosive Bolts

Explosive bolts can perform the primary function of spacecraft separation. They have the advantage of being lightweight, have a good accumulation of performance data behind them, and their availability is good. They are simple devices and are easy to install and arm (Figure 5-87).

Disadvantages of explosive bolts are their larger-than-standard diameters, fragments, and vented gas. In addition, EED redundancy is usually attained by using the stud form and placing an EED in

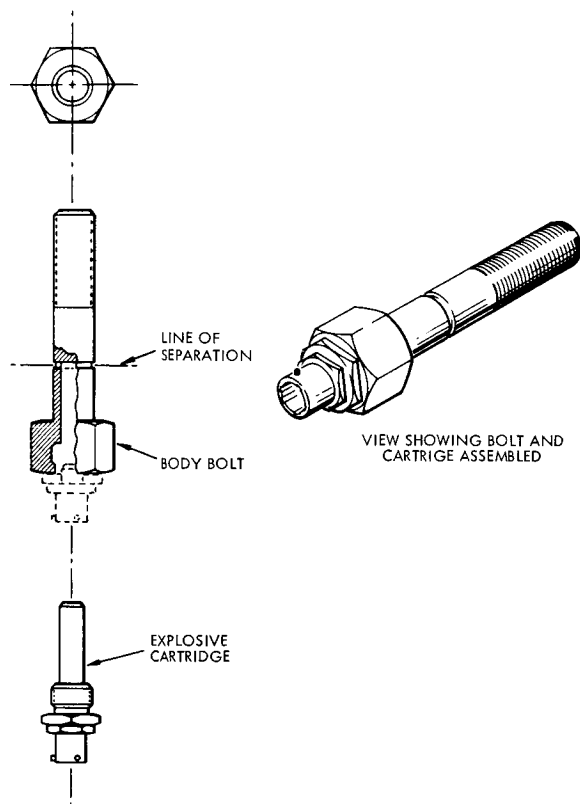


Figure 5-87. Typical Explosive Bolt

each end.\* Force-of-breaking drives the single-ended bolts forward, necessitating the use of a bolt catcher.

#### 4.2.2 Separation Nuts

Separation nuts with captive, removable flange bases (see Figure 5-88) were considered for performing the stage release function. Advantages of these devices are: 1) the retention of all fragments and gases within the case, 2) the use of less explosive and a slower explosive, and 3) less shock introduced into the system than introduced by explosive bolts or a flexible shaped charge.

---

\* A notable exception to most of the disadvantages is the Space Ordnance Systems, Inc. pressure bolt; however, the number of sizes available and the history on these items is limited.



Separation nuts can be obtained with or without a bolt-ejection feature. Dual EED cartridges, for redundancy, can be installed on the same side of the separation joint. Good history exists for separation nuts and may be reconditioned and reused. Disadvantages of separation nuts are: 1) heavier than explosive bolts, 2) not as simple in construction or installation, 3) limited as to sources of supply of qualified items, and 4) need of bolt catchers if bolt ejectors are used.

#### 4.2.3 Collet Release

A collet release has been investigated as a stage separation release mechanism.\* (See Figure 5-89) This device uses a fuse wire to hold the collet in a locked position. Advantages of the collet release are: 1) elimination of all explosives, 2) induction of less shock than release nuts, 3) installation of dual fuse wires for redundancy, and 4) installation can be made from one side of the separation plane.

The disadvantages of the collet release method are: 1) the complexity of the device and the close tolerances needed in the construction of the device, 2) increase in weight over explosive bolts or release nuts, 3) meager history of these units (they have never been used for stage separation), and 4) the electric power required to operate the fuses is two to three times that of the EED.

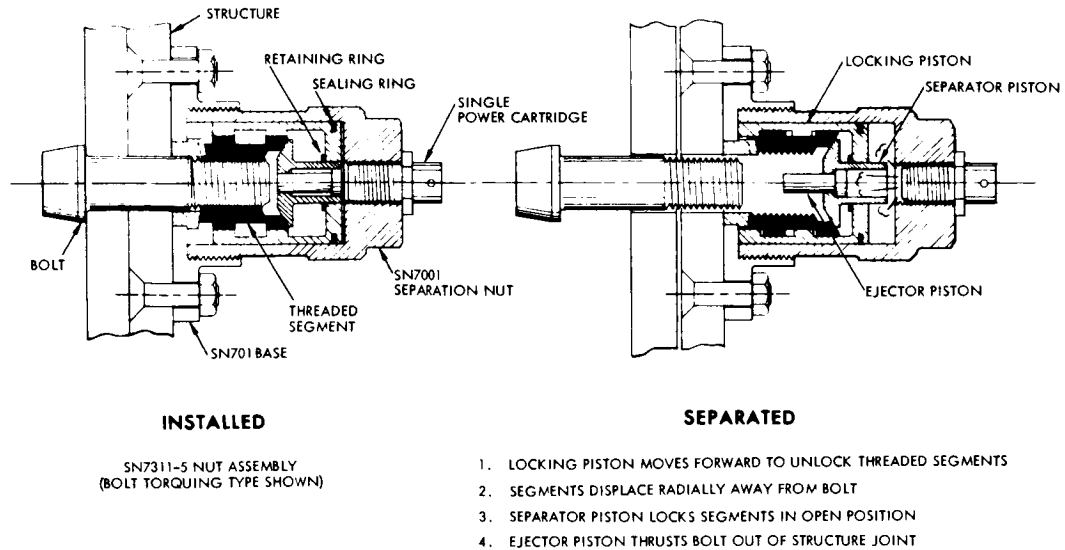
#### 4.2.4 Pin Pullers (and Reefing Line Cutters)

Pin pullers (Figure 5-90) were considered for stage separation. The advantages of pin pullers are the same as those indicated in Paragraph 4.2.2 for release nuts.

The greatest disadvantage of pin pullers is their weight, which is, with the required brackets and turnbuckle, greater than that of explosive bolts or release nuts. Another drawback in the application under consideration is the dependence on proper torquing of turnbuckles to provide identical shear preloads to pin pullers. Not providing this

---

\*Grey and Huleguard, Inc., Subsidiary of Mertronics Corp.



### DESIGN FEATURES

1. GAS RETAINING
2. LOW REACTION FORCE TRANSMITTED TO STRUCTURE
3. ULTRA FAST RELEASE TIME DUE TO MINIMUM MOMENT OF PARTS 1.6 MILLISECONDS HAS BEEN OBTAINED
4. POSITIVE BOLT EJECTION
5. NO FRAGMENTATION. ALL PARTS ARE RETAINED AND LOCKED IN PLACE

### OPTIONAL INSTALLATION METHODS - USING BASIC NON-CAPTIVE SEPARATION NUT

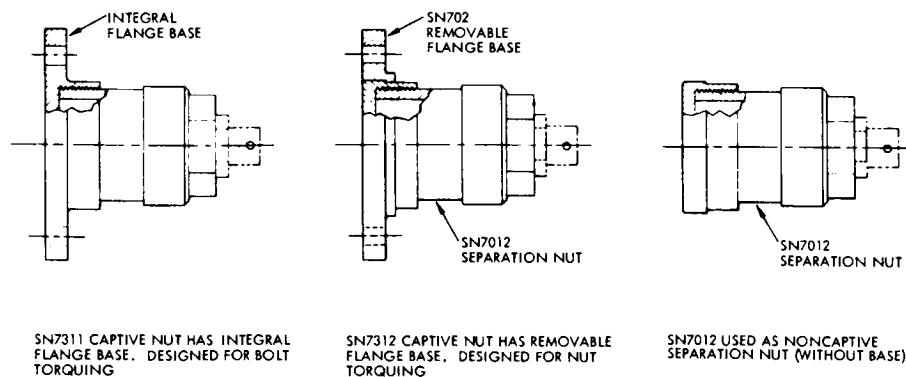
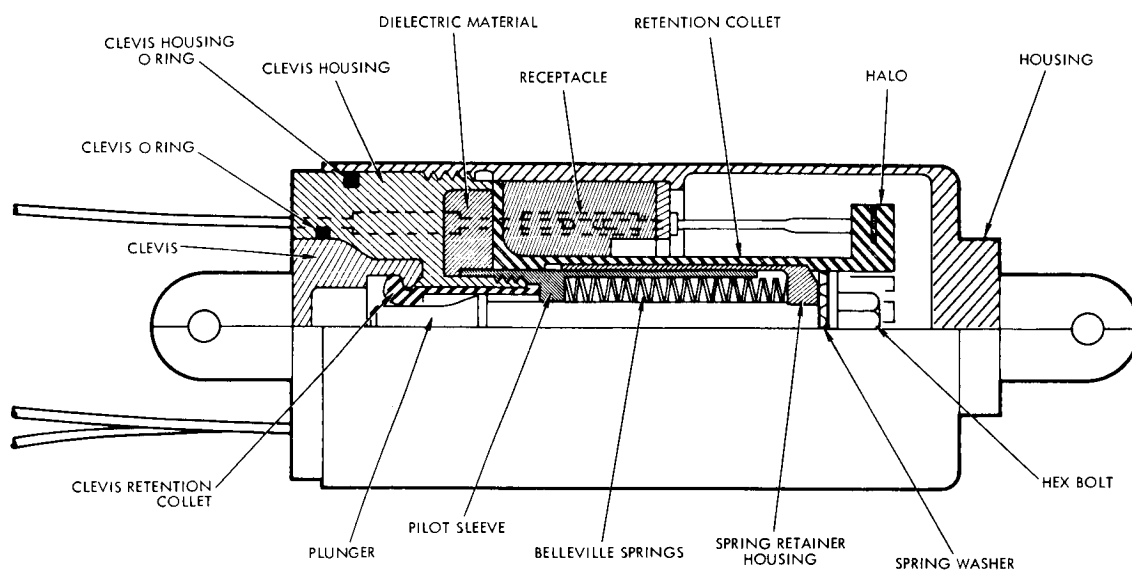
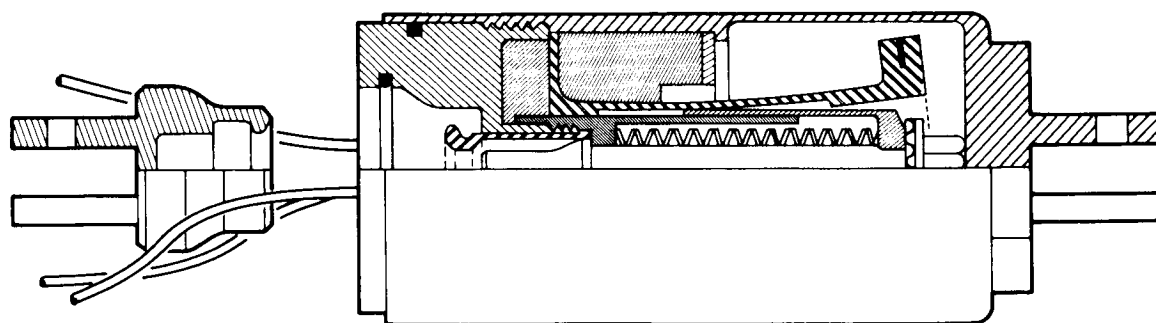


Figure 5-88. Separation Nut



681 ARMED

WITH THE ACTUATOR IN AN ARMED CONDITION, THE 681 BECOMES A SOLID MECHANICAL LINK. IT WILL BE NOTED THAT THE ACTUATOR PLUNGER MAINTAINS A POSITIVE MECHANICAL LOCK BETWEEN THE CLEVIS RELEASE COLLET AND THE CLEVIS



681 SEPARATED

AN ELECTRICAL CURRENT IS PASSED THROUGH THE HALO ELEMENTS, THE HALO CEASES ITS KEEPER FUNCTION AND ALLOWS THE SPRING LOADED ACTUATOR PLUNGER TO BE WITHDRAWN FROM THE CLEVIS RETENTION COLLET. THIS CAUSES THE TENSION LOADED CLEVIS TO COLLAPSE THE RELEASE COLLET (AIDED BY A MECHANICAL PRESSURE ANGLE) AND BE DRAWN FREE FROM THE HOUSING

Figure 5-89. Collet Release

uniform loading could cause hang-up on one puller pin.

#### 4.2.5 Flexible Linear Shaped Charge

Flexible linear shaped charges (FLSC) (Figure 5-91) have been used for stage separation on other programs, and Douglas has done considerable testing of this material. The advantages of FLSC lie in the simplicity of the explosive system and, in some cases, ease of installation and low weight.

Disadvantages of FLSC in the Voyager application are: 1) the shock imparted into the structure and thus into the instruments, 2) the production of shrapnel, and 3) the emission of gases. Moreover, if the side away from the jet is protected from blast effect, the weight of an FLSC system will be greater than any other system considered.

All of the foregoing assumes cutting a continuous thin-walled cylinder. If three tension-straps were used instead of a complete cylinder, the advantages and disadvantages of the FLSC would then be approximately equal to those of explosive bolts (Paragraph 4.2.1).

#### 4.2.6 Summary and Selection Criteria

A summary and comparative evaluation of the pyrotechnic selection criteria are indicated in Table 5-30.

Table 5-30. Evaluation of Selected Pyrotechnic Criteria

	<u>Weight</u>	<u>Simpli- city</u>	<u>Avail- ability</u>	<u>Shock</u>	<u>Gas Pro- duction</u>	<u>Reli- ability</u>	<u>Safety</u>	<u>Total</u>
Bolts	10	9	10	2	7	8	7	53
Nuts	9	8	9	9	9	9	9	62
Collet	6	6	5	10	10	9	10	56
*Pin Puller	8	8	10	9	9	9	9	62
FLSC	10	10	10	1	6	10	2	49

\* and Reefing Line Cutters

Note: Rank 1 to 10 in order of preference.

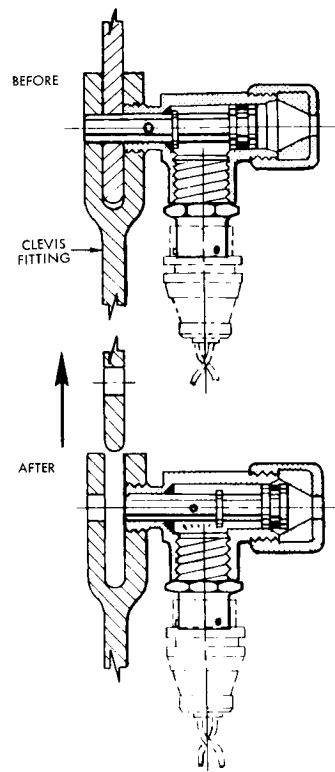


Figure 5-90. Typical Pin Puller

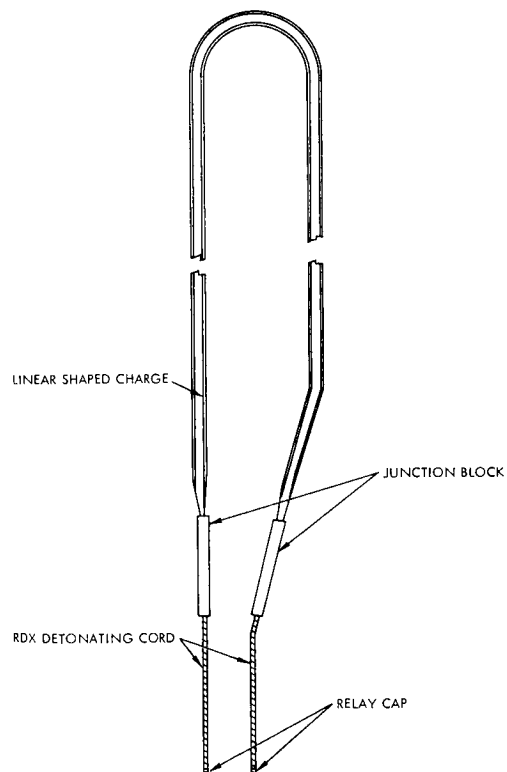


Figure 5-91. Flexible Linear Shaped Charge

Separation nuts rank among the highest in the comparative evaluation and have been selected for use in stage separation. Pin pullers and reefing line cutters are also recommended for specific applications. Items which produce high shock are not recommended.

#### 4.3 Spacecraft Destruct Systems

In view of the Voyager spacecraft design, the launch vehicle provisions, and the requirements imposed by AFMTC 80-7, the Voyager spacecraft should not require a separate destruct system. AFMTC 80-7 states that each missile must have two separate flight termination systems. The Voyager launch vehicle has three separate destruct systems: Stage IB, Stage 4B, and Centaur (two systems, in the case of the Atlas-Centaur 1969 configuration). The AFMTC regulation states in the discussion of ballistic missiles that the redundant destruct systems must be in the last powered stage of the missile. If Voyager is treated as a ballistic missile, the last powered stage would be the Centaur. The engine in the flight spacecraft is a retrorocket which points in the opposite direction from the three boost stages. The retrorocket requires the following sequence of events to become significantly propulsive:

- Separation from Centaur
- Jettison of spacecraft capsule container
- Motor ignition signals

Because of the problems of insuring against inadvertent operation of a destruct system during Mars transit and because of its implications on Mars contamination, it is highly desirable to omit the destruct system. TRW Inc. has successfully justified not including a destruct system in other orbiting vehicles which contain solid propellant engines and feels that a waiver should be attainable for Voyager. However, in the event that a waiver cannot be obtained, design studies have been made to select a technique for the spacecraft. These studies are summarized in the paragraphs which follow.

##### 4.3.1 Destruct System Concepts

Four destruct system concepts are as follows:

- a) Shaped-charge explosives contained in the Centaur inter-stage and initiated by Centaur destruct explosives train to rupture the retrorocket case.
- b) Explosives contained in the spacecraft and initiated by the Centaur electrical destruct signal. The explosives are designed to rupture the retrorocket case and also to puncture all high pressure gas storage tanks.
- c) Explosives contained in the spacecraft and initiated by the Centaur electrical destruct signal to rupture retrorocket motor case only.
- d) Explosives and command destruct receivers are installed in the spacecraft to rupture the retrorocket case.

#### 4.3.2 Comparative Evaluation

In the discussion which follows, these four concepts are ranked in order of preference in regard to their possible effect on the following:

##### a) Mission Weight and Reliability

Concept a) - Since all weight is added to Centaur stage instead of Spacecraft, this is an advantage for the spacecraft.

Concepts b) and c) leave explosives in spacecraft during entire mission and add weight to spacecraft.

Concept b) is heavier and more complex than Concept c). It is not believed to be necessary to destroy all high pressure bottles if the rocket is made nonpropulsive.

Concept d) has the greatest complexity, added weight, and modes of inadvertent destruct actuation.

##### b) Range Safety

Concept d) will destroy the spacecraft as long as it is within range of the destruct transmitter.

Concepts b) and c) would not operate if the Centaur had separated from the spacecraft unless a "booby trap" type firing device was included in the spacecraft. This device would fire on separation unless disarmed by another system prior to the separation command.

Concept a) would not be effective in case of premature Centaur separation unless such a booby trap device was built into the Centaur.

c) Avoidance of Mars Contamination

Concept a) would contaminate Mars only if fired after Centaur second burn and before Centaur trajectory deflection is accomplished after Spacecraft separation. This hazard is already present in Centaur destruct system.

For Concepts b) and c) inadvertent firing of destruct by micrometeoroid collision, solar heating, or heat from retrorocket (during Mars injection burning) could put parts of unsterilized Spacecraft into Mars collision course.

Concept d) has all of the disadvantages of Concepts and with the additional hazard of inadvertent firing by spurious destruct signals.

4.3.3 Brief Description of Destruct System Design

If required, two safe and arm devices (S and A) capable of arming, firing, or disarming on command could be installed in the Spacecraft. In addition, the S and A should provide a readout of their condition; that is, armed or disarmed. Each S and A should be provided with two firing circuits and two explosive trains (paths). Two sources of power should be provided. In the safe position the EED leads must be shorted. Attached to the output of each S and A would be a totally enclosed explosive harness so arranged that the output of any one of four trains would initiate the harness. The harness would lead to shaped-charge components placed adjacent to the motor or four large pressure vessels (Configuration B only). Each shaped charge will be capable of producing a jet which would penetrate the motor or tank at which it is directed. It is anticipated that all other range safety gear will be in the Centaur stage, and will be unnecessary after spacecraft separation.

Explosives are initiated by heat and shock. Therefore, exposed explosives could be initiated by micrometeoroids. All explosives planned for use in the Voyager spacecraft will be enclosed in a metal envelope, and most of the explosives will be protected by the spacecraft bus. Those parts not inside the buss will have additional insulation protection to cut down on heat flow and to protect the explosives from micrometeoroids.

The total cross-section of explosive items is an extremely small percentage of the total cross-section of the spacecraft.



Micrometeoroids travel at high velocities, but protection can be provided by providing a covering which will break them up and dissipate their energy.

#### 4.4 Safe and Arm Provisions

The S and A could be located in the bottom plane of the spacecraft for easy access. Plug-in units are planned to permit the destruct charge to be installed on the ground without the initiators. A plug-in simulator could be inserted to permit safety system checkout, and arming could be done late in the countdown.

## 5. DEPLOYMENT MECHANISMS

### 5.1 Magnetometer Sensor Deployment

One of the magnetometer sensors is required to be deployed at least 30 feet from the spacecraft center - 20 feet from the edge of the solar array. Also, as indicated in VS-4-572 (Volume 2), the sensor axes are required to be predictable within 3 degrees. The sensor weighs 1.6 pounds and is 6 in. long by 3 in. diameter. Ten to 12 lead wires are required to be deployed with the sensor.

The major problems considered in the design and selection of a suitable system are as follows:

- a) Storing a deployable boom of the required length within the spacecraft envelope.
- b) Deployment of lead wires with the sensor.
- c) Design of a boom which can withstand or avoid the solid motor g-loads during retrothrust.
- d) Maintaining the required sensor orientation with consideration given to bending of the boom during cruise by solar heating and uneven temperature distribution.
- e) Design to withstand launch and mission environment.
- f) Design to meet spacecraft nonmagnetic requirement.

Solution of the orientation problem for each configuration is based on: 1) a thorough analysis to determine the maximum temperature differential expected and maximum deflection expected on a particular design, 2) optimization of the design to minimize deflection, and 3) mounting of the sensor on the boom at a predetermined bias to assure that its orientation does not exceed requirements.

#### 5.1.1 Mechanizations Considered

##### a. STEM System (Storable Tubular Extendable Member)

The STEM system is manufactured by the DeHavilland Aircraft Company of Canada and has been used successfully on other space systems (Gemini, Mercury, and Agena). The design for Voyager is

shown in Figure 5-92. When stored, the size of the required STEM unit is approximately 18 x 6 x 7 inches. The boom is a tubular element which consists of several layers of various lengths formed out of strip metal. The element is stored in a strained flattened condition by winding it onto a drum. As the circular element is retracted, it is smoothly transformed into the flattened condition by passing it through a guiding element. The boom is extended or retracted by rotating the drum in the appropriate direction, using an electric motor. The motor power requirements are approximately 5 watts to extend and 50 watts to retract. The lead wires to the sensor are deployed through the tube as an integral part of the STEM unit.

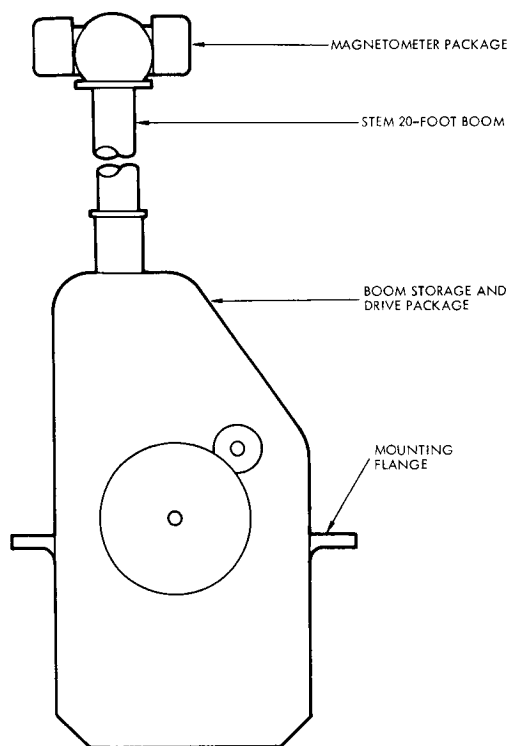


Figure 5-92. De Havilland STEM-type Boom

The STEM unit would be mounted on the edge of the solar array (Figure 5-93). At the start of cruise, a command is given to extend the boom. Just before retrothrust, the boom is retracted to avoid deflections resulting from the g loads. By controlling the time during which power is applied to the drive motor, the length of the boom can be selected.

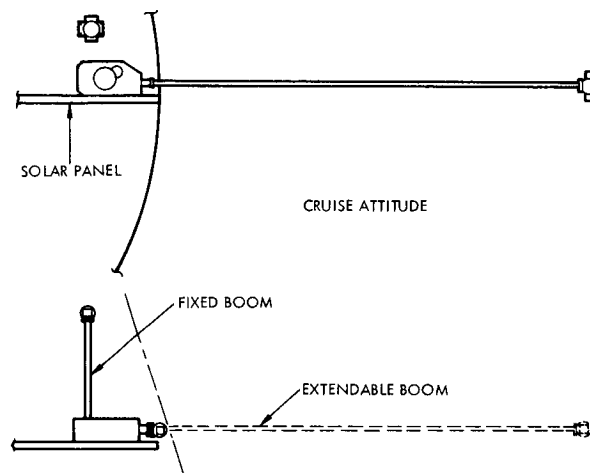


Figure 5-93. STEM Boom With Fixed Backup Boom

After extension, the a STEM unit will experience bending caused by thermal gradients between its sunlit and dark sides. The gradients and therefore the deflections are reduced by using a silver coating on the tube. The deflection at 1 AU is about  $2 \times 10^{-4} L^2$  ft, where  $L$  is the boom length in feet. Thus a 20 foot boom will deflect up to 0.08 feet or an angle of about 0.3 degrees, which is well within the goal of 3 degrees. The maximum angle uncertainty caused by the deployment mechanism is 0.6 degrees. Without the silver coating the thermal deflection will be an order of magnitude larger. Discussions with DeHavilland indicated that the booms can support the magnetometer weights under an acceleration exceeding 4.5 g.

b. Nonretractable Folding Boom

The folding boom, illustrated in Figure 5-94, is an alternate method considered for deploying the magnetometer sensor. The system consists of a tension spring and segment actuator and locking mechanism at each joint similar to the improved OGO configuration. Both sections of the boom are of beryllium-copper tube. The release system is a nylon cord and a pyrotechnic cable cutter programmed to fire when release is desired. The sensor lead wires are inside the tube with care taken at the joints to assure that the wires are not damaged during actuation. Such a boom is not retractable and thus must be strong enough to withstand the retrothrust g load, with a significant weight penalty.

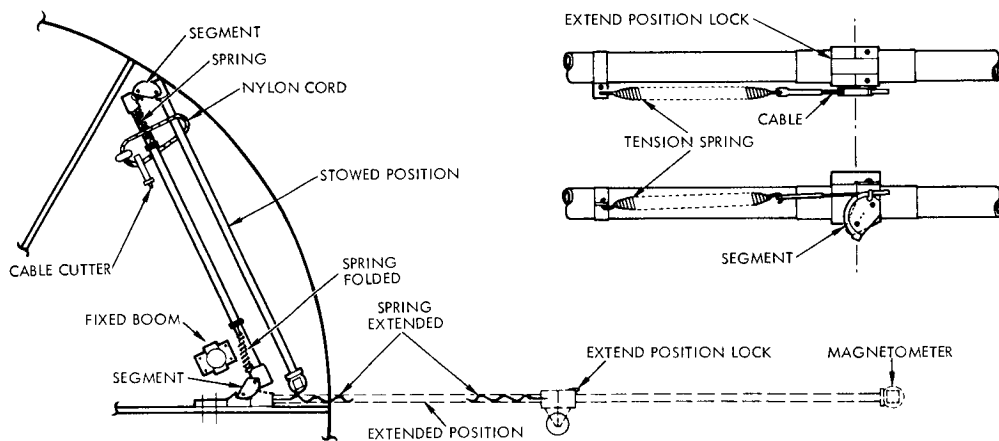


Figure 5-94. Nonretractable Boom

c. Retractable Folding Boom

A retractable folding boom can be employed in a configuration similar to the nonretractable folding boom. In this case the boom is lighter since it need not withstand the retrothrust g loads. An electric motor is used to retract the boom using a drum-wound cable attached

to the boom. The pyrotechnic release system used in the nonretractable folding boom would not be required. Figure 5-95 shows the arrangement.

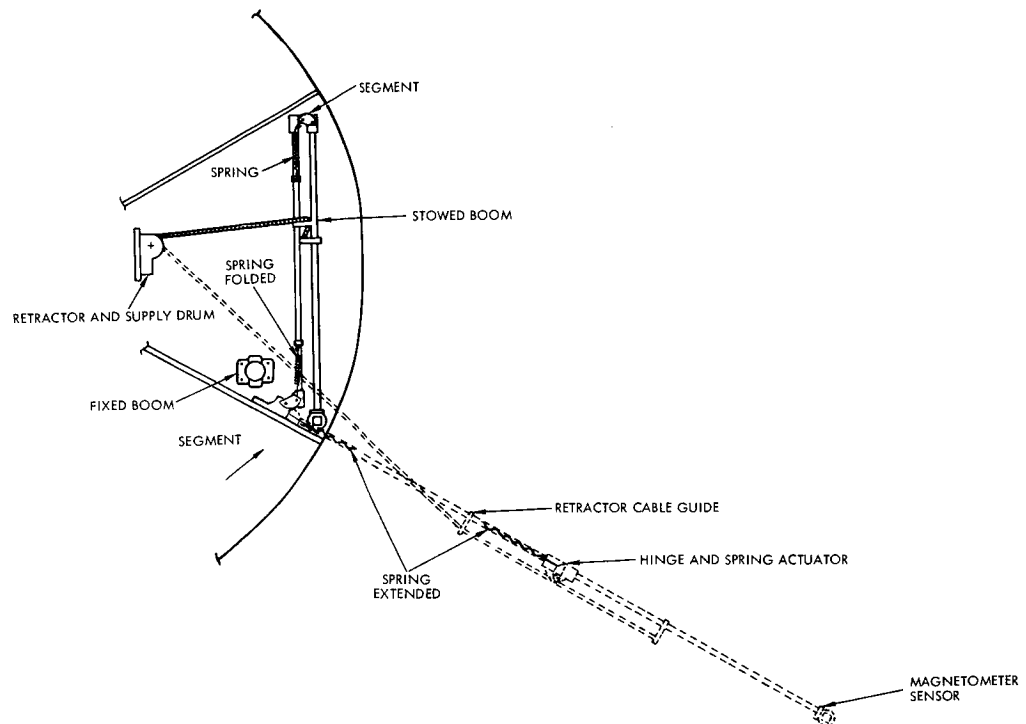


Figure 5-95. Retractable Boom

d. Expendable Folding Boom and Fixed Backup Sensor

To eliminate the need for retracting the lightweight folding boom, a second sensor can be permanently mounted on the spacecraft for use after retrothrust in Mars orbit. Thrusters are programmed to fire the expendable boom assembly off the spacecraft prior to the

retro-thrust maneuver. A pyrotechnic cable cutter severs the wires to the boom. Figure 5-96 shows the design arrangement.

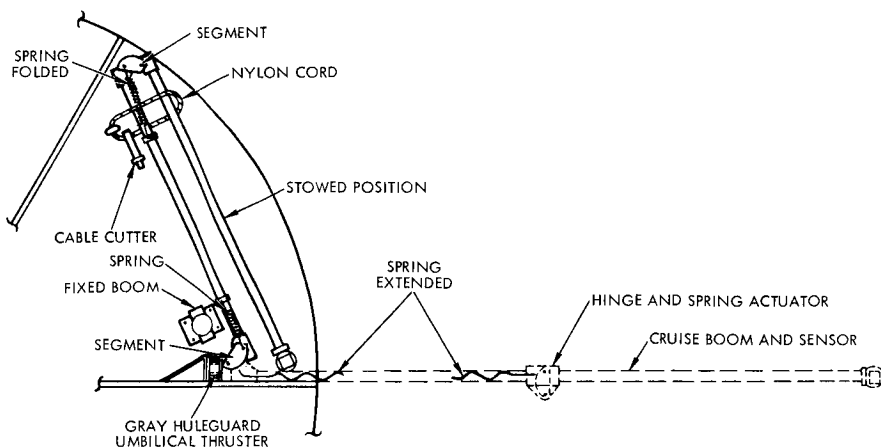


Figure 5-96. Nonretractable, Expendable Folding Boom

The thruster system could be of the pyrotechnic type or a nonexplosive "Gray-Huleguard (G-H) umbilical thruster joint" whereby actuation is made by a spring held in position by a wire which melts upon application of power. The G-H unit incorporates an umbilical disconnect for the sensor wires, eliminating the requirement for a cable cutter.

#### 5.1.2 Configuration Evaluation

Each of the configurations just discussed has been evaluated on the basis of several tradeoff factors, with the results presented in Table 5-31. As a result of this comparison, the STEM unit plus a sensor fixed at the edge of the solar array are used in the selected spacecraft design.

#### 5.1.3 Material Considerations for Selected Designs

Development work by the DeHavilland Aircraft Co., of Canada has indicated that the optimum boom material is beryllium-copper because of thermal expansion, elasticity, strength, and magnetic considerations.

Table 5-31. Evaluation of Magnetometer Sensor Deployment Subsystems

Item	Design				Nonretractable Folding Boom	Retractable Folding Boom	Nonretractable Expendable Folding Boom
	STEM	STEM Plus Fixed Boom	Nonretractable Folding Boom	Retractable Folding Boom			
1. Weight	8 (9.4 lb)	7 (10.0 lb)	0 (13.5 lb)	3 (12.0 lb)	10 (8.5 lb)		
2. Cost	10	9	8	5	7		
3. Reliability	8	10	6	9	7	7	
4. Calibration	10	10	8	7	7		
5. Repeatability	10	7	8	8	8		
6. Simplicity	7	7	10	8	9		
7. Deployment Power	7	8	10	6	8		
8. Heat Bending	8	10	8	8	8		
9. G Loading	10	10	10	10	10		
10. Development Required	10	10	9	7	8		
11. Availability	10	9	7	3	5		
12. History of Usage	9	9	8	5	8		
13. Magnetic Level	<u>9</u>	<u>9</u>	<u>9</u>	<u>7</u>	<u>8</u>		
Total	116	115	101	86	113		



The STEM boom is capable of withstanding retrothrust and could remain extended. The second sensor mounted on a fixed boom will be used in Mars orbit. The STEM system has been qualified for other space programs but not for as long as 9 months. Development testing is continuing on the STEM system for other applications.

Plating the element surface with material such as silver will reduce the absorptivity while increasing element thermal conductivity. This results in reduction of boom bending due to solar heating.

Use of magnetic materials is to be minimized to comply with spacecraft specifications.

## 5.2 Solar Panel Release and Deployment System

The investigation of solar panel release mechanisms applies only to Spacecraft C. This configuration has 10 solar panels whose dimensions are approximately 4 ft x 6 ft. The panels are hinged on the 4-foot side. When stowed, the major axis of the panels would be approximately parallel to the roll axis of the spacecraft. The panels are required for deployment into a plane perpendicular to the roll axis of the spacecraft. Deployment is to take place upon initial insertion of the spacecraft into the earth-to-Mars cruise trajectory. A suitable system for accomplishing all the requirements of deployment would have the following elements:

- a) A release device which holds the panels rigidly in the stowed position and releases them upon command.
- b) An actuator device which supplies torque to move each panel from the stowed to the deployed position.
- c) A damper device which limits the actuation rate and prevents damage when the panels reach the stops.
- d) A locking device to hold the panels in the deployed position.

### 5.2.1 Deployment Configurations Studied

#### a. Fixed Support, Pin Puller, Hinge Spring and Damper

The design configuration is shown in Figure 5-97. The release device is a pyrotechnic pin puller mounted on each solar panel. Upon command, the pin puller releases the joint between the solar panel and a support which is fixed to the structure. Torque is supplied to the panel by two hinge springs. Rate damping is provided by a linear piston, hydraulic-type damper. The panels are locked into the extended position by a hinge lock.

#### b. Fixed Support, Pin Puller and Linear Actuator-Damper-Lock Assembly

The design configuration shown on Figure 5-98 makes use of a release and hinge similar to the configuration described above. The actuator, damper, and lock are combined into one assembly. The lock is a piston ring which expands into a step when in the extended position.

#### c. Nylon Cord and Bolt-Cutter Release, and Linear Actuator

The configuration shown on Figure 5-99 uses a release system consisting of 1) a panel release latch which is pivoted on a fixed support, 2) a detent on each panel to which the latch catches, 3) two nylon cords which hold the latch in the panel-stowed position, and 4) two pyrotechnic bolt cutters which cut the nylon cords and release all of the panels simultaneously.

#### d. Nylon Cord and Bolt-Cutter Release, and Hinge Spring Actuator

A fourth configuration makes use of a release system the same as that discussed in c, above, together with hinge springs and hydraulic damper that are the same as in a, above.

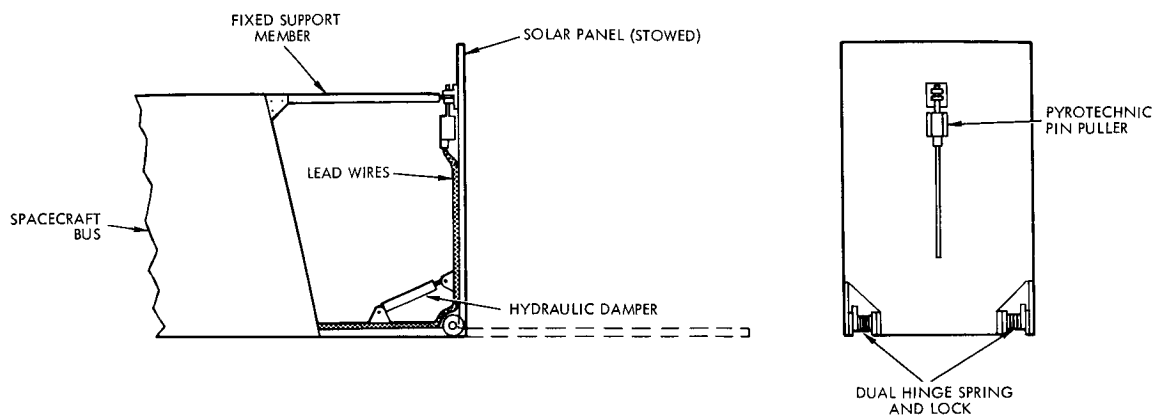


Figure 5-97. Pin Puller and Spring Hinge System

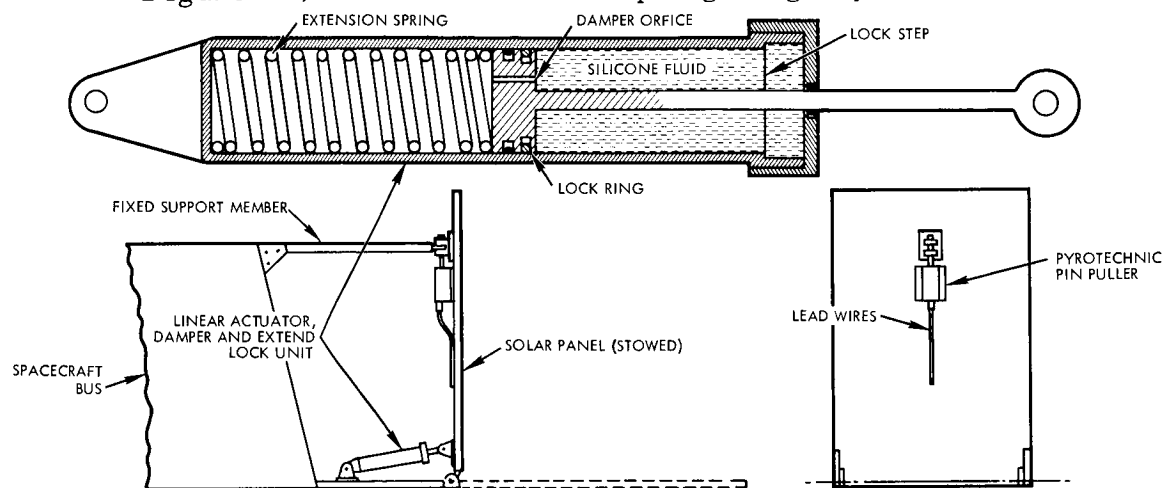


Figure 5-98. Spring Actuator and Pin Puller

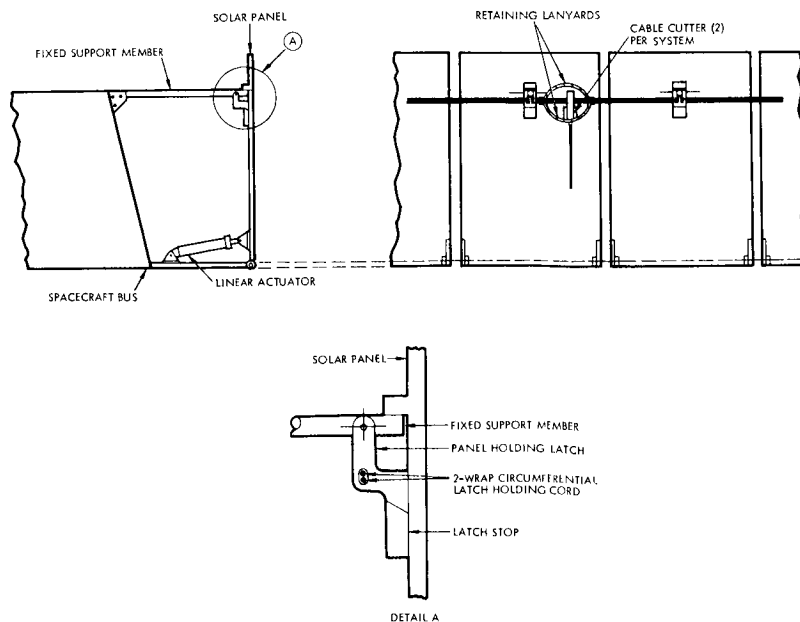


Figure 5-99. Cable Cutter System

e. Pin Puller and Latch Release, and Linear Actuator

The configuration shown on Figure 5-100 has a release system consisting of a mechanism which pulls a latch out of a swiveled catch attached to a fixed support member. The mechanism is actuated by a pyrotechnic pin puller. The stroke of the latch and the rotation of the catch makes it possible for all the solar panels to be released when the mechanism on every other panel is actuated. The actuator damper lock assembly is the same as described in b, above.

5.2.2 Configuration Evaluation

Each of the five configurations has been evaluated on the basis of several tradeoff factors. The results are given in Table 5-32. As a result, the design shown on Figure 5-99 has been selected.

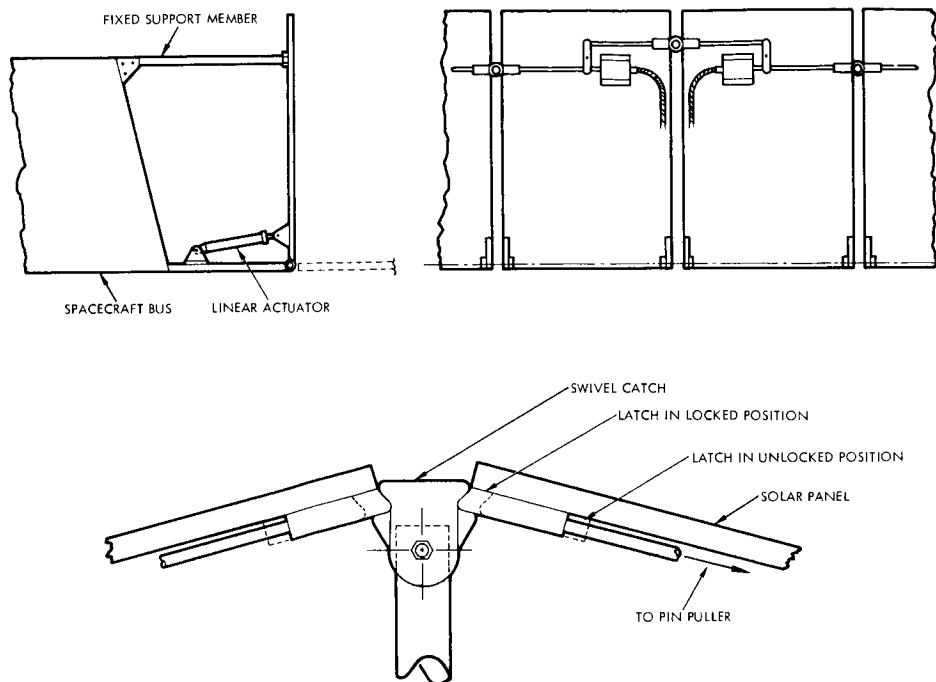


Figure 5-100. Pin Puller and Swivel Catch

Table 5-32. Evaluation of Solar Panel Deployment Subsystems

Item	Design			
	Pin Puller and Hinge Spring	Pin Puller and Linear Actuator	Cable Cutter and Linear Actuator	Pin Puller and Linear Actuator
1. Weight	8 (12.54 lb)	9 (11.13 lb)	10 (9.79 lb)	8 (12.84 lb)
2. Cost	10	9	8	8
3. Reliability	7 (0.99324)	6 (0.99314)	8 (0.99757)	9 (0.99804)
4. Simplicity	9	9	9	8
5. External Power Required	6	6	10	7
6. Development Required	8	8	8	7
7. Availability	9	9	9	9
8. History of Usage	10	9	10	8
9. Fail Safe	5	5	5	8
Total	72	70	77	72

## VI. ELECTRONICS PACKAGING AND ELECTRICAL DISTRIBUTION

### 1. ELECTRONICS EQUIPMENT PACKAGING

Except for sensors and science equipment which require mounting at particular places on the spacecraft structure, all electronic assemblies will be mounted on temperature-controlled panels (Figure 6-1). These panels will form the exterior surface of the spacecraft, act as heat sinks, and provide micrometeorite protection for the electronics. Thermal louvers on the space-facing sides of the panels provide thermal control. At present only four of the six bus faces are required to mount the electronics.

The electronics packaging studies have involved consideration of heat sink, thermal, and stress properties, methods of mounting equipment to potential heat sink materials, arrangement of boxes and cable assemblies, and study of internal packing approaches for electronics assemblies. Structural and material considerations leading to the design selection of the heat sink are described in Section V of this volume.

#### 1.1 Design Objectives and Constraints

Objectives and constraints covering the disciplines of equipment integration, electrical distribution, and electronic packaging are discussed below, grouped according to considerations affecting system design, electrical performance, and general packaging.

The equipment design and integration objectives are to achieve an arrangement compatible with the spacecraft system regarding:

- Efficient utilization of equipment space and mounting area in a manner which lends itself to effective control of vehicle center-of-mass.

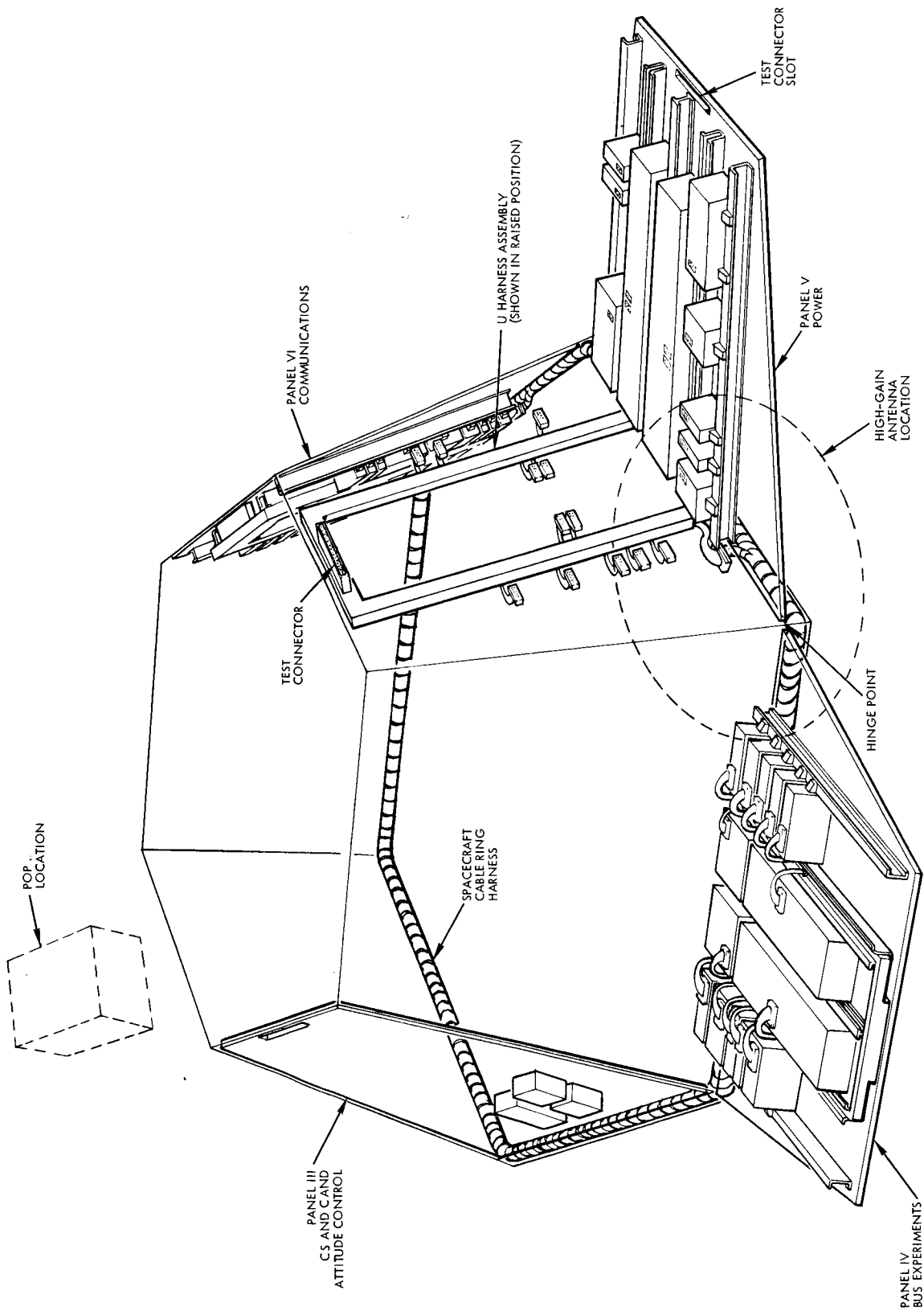


Figure 6-1. Electronic Equipment Subsystem Panel Installation Accessibility Concept



- Flexibility of equipment installation to facilitate temperature control and to obtain uniform power distribution.
- Allowance for testing complete panels with electronics prior to installation on the spacecraft.
- Capability for testing panel-mounted items without removal from the spacecraft.
- High panel structural rigidity consistent with low weight, with electronics assemblies contributing to over-all stiffness.
- Adequacy of micrometeorite protection.
- Cable routing and shielding for minimum losses and interference.

The objectives relating to electrical performance are to provide a package design which is compatible with functional requirements of:

- RF and EM interference shielding.
- Signal isolation.
- Minimization of circuit losses and capacitance effects.

A third objective is to develop a package design which is compatible with general packaging technique requirements regarding:

- Standardization of package size, method of construction, and method of installation.
- Standardization in the use of parts, materials, and process techniques.
- Selection, use, and control of parts, materials, and processes with a proven history of performance.
- Flexibility of design accommodating growth and varying packaging techniques (i.e., cordwood modules, board-mounted components, I. C. on multilayer boards, RF construction).

- Thermal design which minimizes the temperature difference between components and the mounting panel.
- Structural design for best vibration protection of components and internal wiring.
- Efficient utilization of material for minimum weight.
- Accessibility for installation and checkout.
- Easy producibility and minimum cost.

## 1.2 Alternate Approaches and Selection

### 1.2.1 Cable Routing and Attachment

The three most promising cable routing approaches of those considered are shown in Figure 6-2. Their advantages and disadvantages are listed in Table 6-1.

- a) Approach 1. This approach has panel-mounted assemblies connected by a U-shaped assembly harness. Both legs of the U connect to the system ring harness (at the aft or wide end of the bus) through a hard mounted connector. The system ring harness interconnects all assembly harnesses. A service loop is added to the assembly harness to facilitate hinging of the panels for equipment access.
- b) Approach 2. This approach is the same as Approach 1 except that the ring harness is located at the forward instead of the aft end of the bus.
- c) Approach 3. This approach has assemblies connected on each panel by two assembly harnesses which extend between a forward and an aft ring harness. The assembly harnesses connect on each end through a service loop to a hard-mounted connector on the trough of the ring harness. The service loop at the forward end of the panel must permit manual access to the connectors.

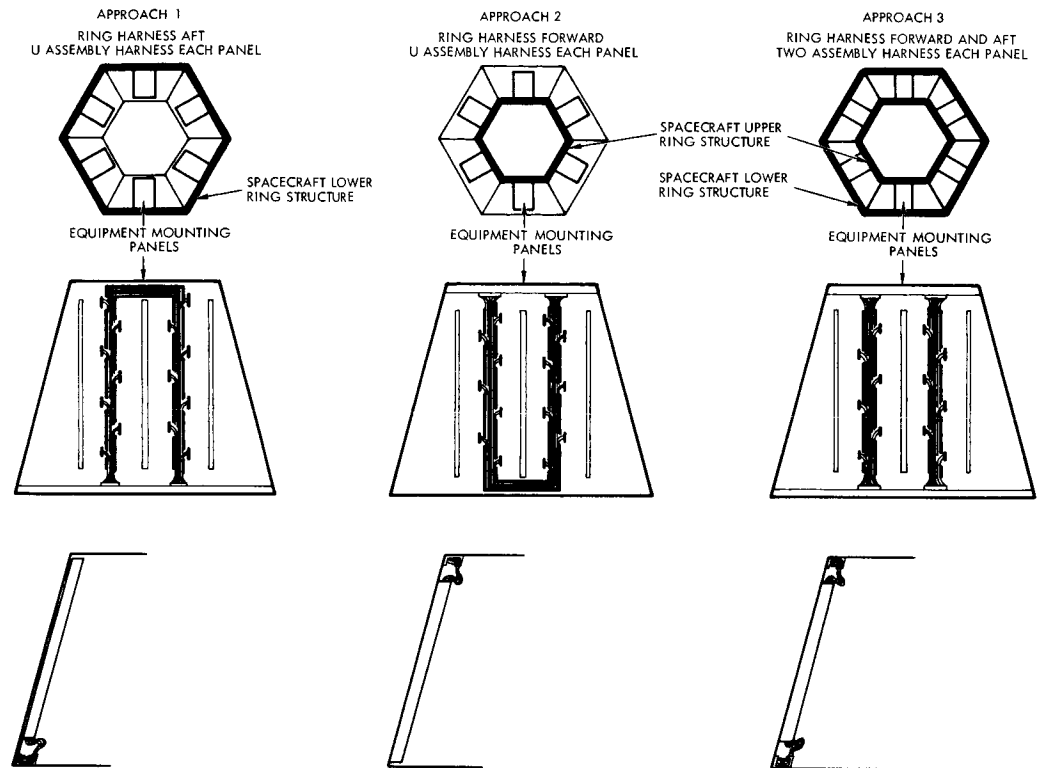


Figure 6-2. Cable Routing and Attachment Tradeoff Considerations

The distinguishing features of a hard-chassis assembly harness are that the harness and connectors are housed and supported in an individual chassis. Subassemblies equipped with mating connector halves make connections when they are inserted into their mounting positions. Tradeoff considerations for two assembly harness design approaches, labeled A and B, are listed in Table 6-2.

- a) Approach A. This approach has the assembly harness and associated plug-in connectors installed in a chassis which is integrated into the spacecraft system as a rigid physical item. Equipment assemblies mate with their appropriate connectors when they are inserted into their mounting position.
- b) Approach B. This approach provides for an assembly harness which is installed and rigidly supported within troughs which are integral to the spacecraft structure. Cable loops and connectors issue out of the trough at places as appropriate to make connection with equipment assemblies.

Table 6-1. Cable Routing Approach Tradeoff Considerations

<u>Approach 1</u>	<u>Approach 2</u>	<u>Approach 3</u>
<u>Advantages</u>	<u>Advantages</u>	<u>Advantages</u>
<ul style="list-style-type: none"> <li>• Electrical checkout can be performed with panels open and without auxiliary cables</li> <li>• Panels hinged at aft edge provide good access to equipment</li> <li>• Short cable runs to POP and solar panels</li> <li>• Short coaxial cables to antennas</li> </ul>	<ul style="list-style-type: none"> <li>• Smaller harness ring diameter requires less cable length</li> <li>• Electrical checkout can be performed with panels open without auxiliary cables</li> </ul>	<ul style="list-style-type: none"> <li>• Best possibility for short cable lengths for all equipment connections</li> <li>• Largest capacity for increases and changes</li> <li>• Best opportunity for alternate cable routes for signal separation</li> </ul>
<u>Disadvantages</u>	<u>Disadvantages</u>	<u>Disadvantages</u>
<ul style="list-style-type: none"> <li>• Large harness ring diameter requires more cable length than Approach 2</li> <li>• Less flexibility for alternate routing than Approach 3</li> </ul>	<ul style="list-style-type: none"> <li>• Long cable runs to POP and solar panels</li> <li>• Long coaxial cable to antennas</li> <li>• Panel hinged at forward edge may not be convenient for equipment installation</li> </ul>	<ul style="list-style-type: none"> <li>• To allow opening of panel, connection to one ring harness requires hard mounted connectors or large cable loops</li> <li>• Electrical checkout with open panels requires auxiliary cables</li> </ul>

a. Method of Attachment

The method of support and attachment of the cables and harnesses is the same for all three configurations. The ring harness lies in and is rigidly secured to a trough which goes around the inside of the bus. The aft trough is nested into the corner formed by the side panels and the aft end of the bus, while the forward trough is similarly positioned at the forward end. Connections to the ring harness are made through plug-in connections which are hard mounted to the trough. The assembly harness mounts into two channels which traverse the length of each panel.

b. Shielding and Grounding

Shielded or twisted wires are used to satisfy electrical and magnetic field requirements.

c. Configuration Selection

The only advantage Approach 2 has over Approach 1 is the smaller ring diameter. This does not offset the longer cable run that would be required for items mounted on the solar panel. Approach 1 is also a more natural arrangement to allow opening the panels for equipment test or removal. Approach 1 is therefore preferred over Approach 2.

Approach 3 has a larger capacity and better flexibility than Approach 1 at the expense of more cabling and more complicated panel access. Since it is not clear that the capacity of Approach 3 is required, and since Approach 1 can, if necessary, grow into Approach 3, Approach 1 is preferred.

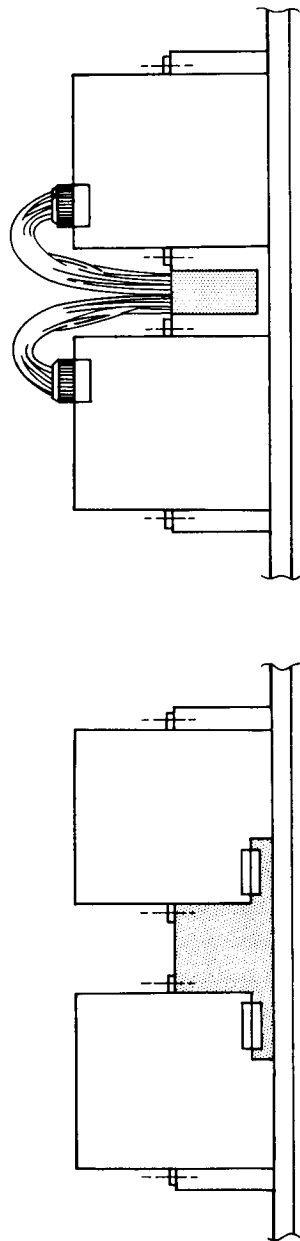
In the selection of an assembly harness design, Approach B is preferred over Approach A for reason of better design flexibility and minimum dimensional tolerance problems.

1.2.2 Equipment Panels and Equipment Mounting

The three most promising approaches to equipment mounting that were considered are shown in Figure 6-3 and tradeoff factors are listed in Table 6-3.

- a) Approach 1. A honeycomb or truss-grid panel with five rows of rails attached to inserts in the panel. Equipment

Table 6-2. Two-Assembly Harness Design Tradeoff Considerations



#### Approach 1

Schematic representation of hard-chassis assembly harness with hard-mounted connectors

#### Advantages

- Rigid support for all cables

#### Disadvantages

- Little flexibility for changes
- High tolerance problem
- Need for insertion and extraction aids to prevent damage to connectors
- To remove harness, all subassemblies may have to be removed

#### Approach 2

Hard-chassis assembly harness with cable loops to connectors

#### Advantages

- Good design flexibility
- Easy access to connectors
- Harness can be removed without removing subassemblies

#### Disadvantages

- Cable loops may require additional support

is mounted to the panel by bolting to the rails in such a manner that the base of the boxes will be pressed against the panel.

- b) Approach 2. A truss-grid panel to which equipment is mounted directly by use of inserts imbedded in the mounting plate.
- c) Approach 3. A solid plate with five rows of rails attached to one surface. Equipment is mounted to the plate by bolting to the rails.

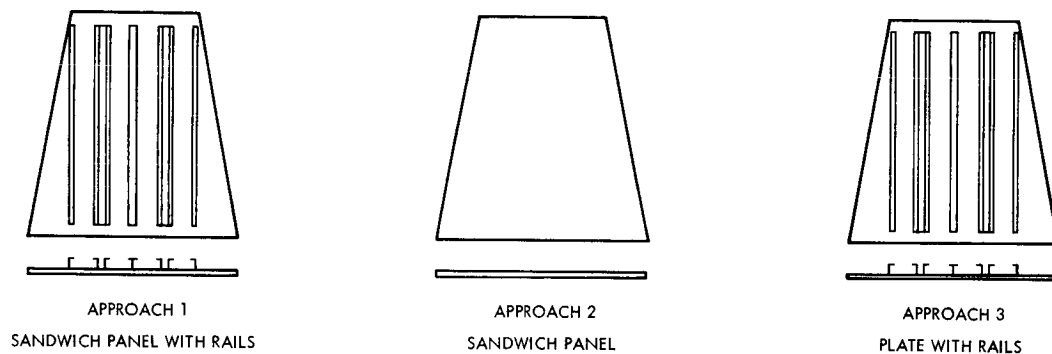


Figure 6-3. Equipment Mounting Tradeoff Considerations

In most cases a thermal filler, such as RTV-11, will be required to provide good conduction to the heat sink.

a. Structural Rigidity Requirements

For failure modes arising out of relative motion, such as between components and chassis, the stress induced is proportional to the relative motion which, in turn, varies inversely with the square of the frequency. Since the fatigue life increases exponentially as stress decreases, and the stress decreases exponentially with increase to frequency, much fatigue life is bought with a small increase in frequency. Typically, a 75 per cent increase in frequency produces two orders of magnitude increase in fatigue life.

Since rigidity is bought at the expense of weight the question arises as to the proper amount of rigidity. There is no simple answer to this question. Experience on other programs has shown that failures because of excessive flexing of leads or pulling on connecting joints can generally be controlled by a) avoiding bridging of wires between

Table 6-3. Equipment Mounting Tradeoff Considerations

<u>Approach 1</u>		<u>Approach 2</u>		<u>Approach 3</u>	
<u>Advantages</u>		<u>Advantages</u>		<u>Advantages</u>	
<ul style="list-style-type: none"> <li>• Sandwich panel has best weight efficiency for micrometeorite protection</li> <li>• Rails contribute to panel rigidity</li> <li>• Rails provide good equipment mounting points, particularly for high slender assemblies</li> <li>• Rails provide flexibility to modifications, since rails can be replaced without requiring changes to the insert in the sandwich panel</li> <li>• With rails, less than half the number of inserts are required in the sandwich panel</li> <li>• Rail mounting permits equipment to contribute to panel rigidity</li> </ul>		<ul style="list-style-type: none"> <li>• Sandwich panel has best weight efficiency for micrometeorite protection</li> <li>• For equal weight with Approach 1 approximately the same rigidity is achieved; however, thermal resistance is increased</li> <li>• Mounting equipment directly to panel provides better thermal conduction to panel</li> <li>• Simpler fabrication</li> <li>• Greater flexibility in selection of mounting locations, providing inserts can be readily installed</li> </ul>		<ul style="list-style-type: none"> <li>• Plate provides best thermal conduction for spreading of heat</li> <li>• Rail advantageous same as for Approach 1</li> </ul>	
<u>Disadvantages</u>		<u>Disadvantages</u>		<u>Disadvantages</u>	
<ul style="list-style-type: none"> <li>• Poorer thermal contact between equipment base and panel</li> </ul>		<ul style="list-style-type: none"> <li>• Equipment mounted to panel is dead weight, since it cannot contribute to the rigidity of the panel</li> <li>• Support of tall, slender equipment chassis inadequate</li> </ul>		<ul style="list-style-type: none"> <li>• Less micrometeorite protection</li> <li>• Lowest natural frequency for equal weight</li> </ul>	



potentially resonating structural members; b) properly securing wires and leads to prevent pulling on connection joints, and c) avoiding low-frequency, high-displacement resonances.

It has been found that for an equipment chassis with a considerable amount of wiring which is susceptible to flexing and pulling, a minimum resonance frequency of 300 to 400 cps eliminates virtually all displacement failures without incurring a severe weight penalty. Experience has also shown that the assembly and system connection cables can easily sustain much larger deflections than the internal wiring of an assembly. Typically, minimum primary resonances of the order of 100 cps for the equipment and cable support structure have proven satisfactory for limiting deflection.

From the standpoint of vibration transmission to the equipment, it is desirable to avoid cascading of resonances. Therefore, a design goal calling for a minimum primary resonance frequency of 100 cps for the equipment panel and 400 cps for the assemblies has been used.

For the three panel design concepts under consideration, the weights and natural frequencies are compared in Section V-1 of this volume. Some of these considerations are summarized in Table 6-4. These data show that mounting components directly to the panel is the lightest approach but it also has the lowest natural frequency. When the panel is stiffened to achieve a frequency comparable with the panel with rails, its weight is also comparable. Also shown is the normalized life fatigue factor for the various panels compared with the panel-mounted approach.

b. Integrated Structural Design

An integrated structural design allows subassemblies to contribute to the strength and rigidity of the assembly which, in turn, contributes to the strength and rigidity of the spacecraft structure. The design concepts which utilize rails (Approaches 1 and 3) lend themselves to this integrated structural design. With this approach the installed equipment forms a beam in the direction across the rails. (See Figure 6-4) This beam has the ability to take tension, compression,

Table 6-4. Mounting Panel Tradeoffs

Panel and Mounting Configuration	Panel Weight Including Attachments (lb.)	Lowest Mode Frequency (cps)	Double Amplitude Deflection (in.) (1)	Fatigue Life Factor (2)
0.15-inch solid cold plate and rails	56.4	58	0.24	50
1-inch honeycomb with epoxied inserts (0.025-inch face sheets)	23.1	43	0.43	1
2-inch honeycomb with 0.065-inch face sheets	43.5	46	0.37	1.33
2-inch honeycomb with 0.055-inch face sheets	45.6	84	0.12	>1600
1-inch honeycomb with rails (0.025-inch face sheets)	41.5	145	0.036	>>1600

(1) Based on 40 g shock response.

(2) Relative to life at lowest frequency.

and shear forces, thereby increasing the natural frequency by increasing the rigidity of the panel in a direction across the rails.

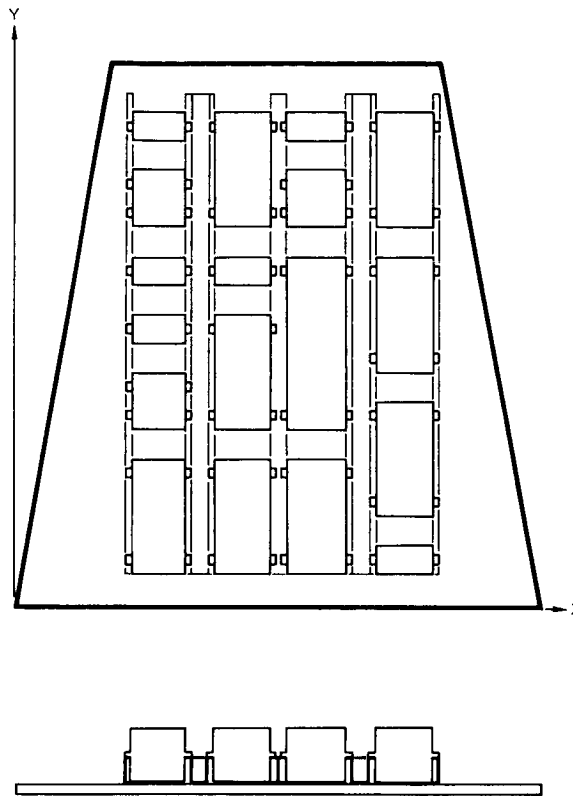


Figure 6-4. Typical Arrangement of Equipment Mounted to Panel

c. Selection of Preferred Approach

The solid equipment panel (Approach 3) was discarded because of the relatively poor protection it provides against micrometeorites and because of its low natural frequency. Approaches 1 and 2, for the same stiffness, are comparable on a weight basis. Approach 1 was selected because of the discipline it introduces into box and circuit board standardization, its flexibility, its suitable thermal conductivity, and its provision of an integrated structural design.

1.2.3 Equipment Size Standardization

Selection of a standard equipment size is influenced largely by the requirements of packaging and the efficient utilization of available

equipment space. A variety of equipment sizes were considered, of which three logical selections are shown in Figure 6-5 and compared in Table 6-5. The 6-inch width permits mounting of four rows of equipment on each panel, with sufficient spacing for rails and cable routing. The 7.25-inch width allows for three rows of equipment instead of four, or for four rows if the rows do not extend the full length of the panel. The height of the equipment is limited in some regions near the engine to 6 inches. Both the 6 x 6-inch and the 5 x 7.25-inch are compatible for most of the packaging; however, there are some requirements (batteries and possibly tape recorders) for a two-row width. For the 6 x 6-inch standard, the two-row width is 13.5 inches, while for the 5 x 7.25-inch standard, the two-row width is 16.0 inches. Approach 1, using a 6-inch width and variable thickness, was selected for the reasons given in Table 6-5.

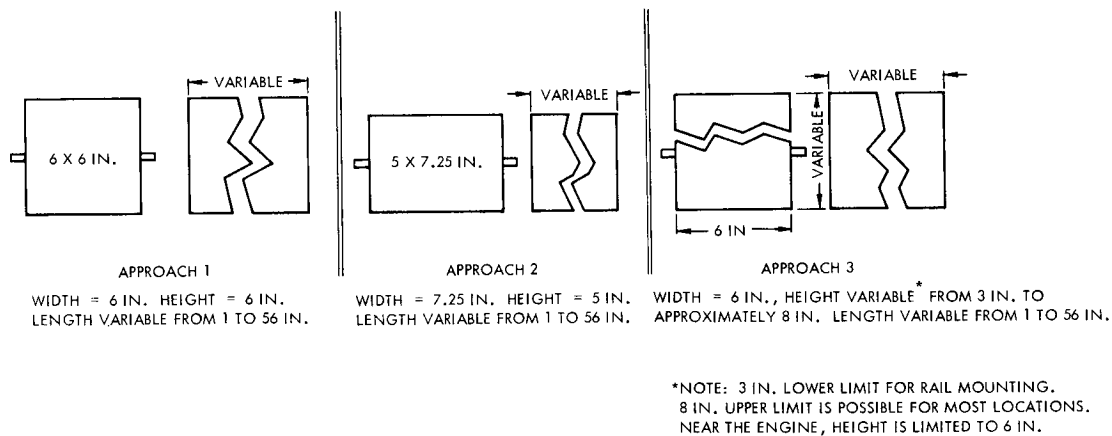


Figure 6-5. Equipment Size Standardization

#### 1.2.4 Electronic Packaging Techniques

Electronic packaging techniques cover many different methods and processes which go into the productizing of equipment. Some lend themselves readily to generalized tradeoff considerations, while others can be evaluated only in terms of specific functional circuit requirements. Examples of the latter are selection of an interconnection matrix, selection of the method of joining leads to terminals, and selection of modules versus board mounted components.

Table 6-5. Equipment Size Standardization Tradeoff Considerations

<u>Approach 1</u>		<u>Approach 2</u>		<u>Approach 3</u>	
<u>Advantages</u>		<u>Advantages</u>		<u>Advantages</u>	
<ul style="list-style-type: none"> <li>• Tallest standard within closest restriction affords best space utilization without mounting restriction based on height</li> <li>• Width standard compatible with panel size for good utilization of mounting area</li> </ul>		<ul style="list-style-type: none"> <li>• Approximately 20 per cent larger base area with same cross-sectional area as Approach 1; hence, better thermally for high power density equipment</li> </ul>		<ul style="list-style-type: none"> <li>• Greatest degree of packaging flexibility</li> <li>• Permits decreasing height and increasing base area for high power density equipment</li> </ul>	
<u>Disadvantages</u>		<u>Disadvantages</u>		<u>Disadvantages</u>	
<ul style="list-style-type: none"> <li>• Less flexibility to achieve efficient packaging</li> <li>• More restrictive thermal design than Approach 3</li> </ul>		<ul style="list-style-type: none"> <li>• Width standard limits equipment mounting to three rows if the full length of the panel is used, which means less efficient utilization of mounting space</li> </ul>		<ul style="list-style-type: none"> <li>• More different parts for fabrication</li> </ul>	

a. Assembly Chassis Designs

The design concept of the chassis strongly influences the method of interconnection. Three design approaches, which are shown in Figure 6-6 and compared in Table 6-6 are representative of three widely different assembly concepts.

- 1) Approach 1. In this design an assembly is housed in a single chassis. Subassemblies may consist of individual or pairs of circuit board cards.
- 2) Approach 2. A number of subassembly chassis are mechanically strapped together to form one assembly. Subassembly interconnection can be internal, as illustrated in Figure 6-7, or can be with external plugin connectors and jumper cables.
- 3) Approach 3. A number of individual subassembly chassis which are not mechanically tied together and which depend entirely on external plug-in connection.

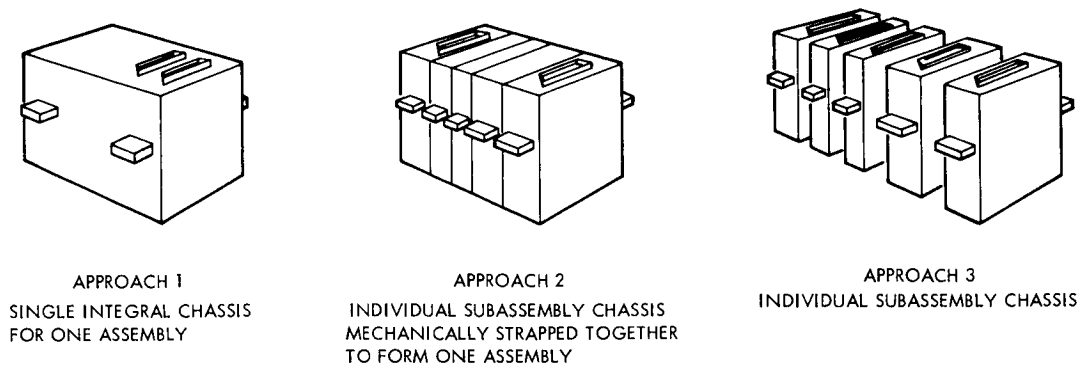


Figure 6-6. Packaging Technique I  
Tradeoff Consideration

b. Subassembly Chassis Design

Even within a single concept the design of a subassembly chassis may take a number of variations, depending on specific packaging requirements. Two configurations, shown in Figure 6-8, and compared in Table 6-7, are representative of the packaging philosophy used on two different programs. To facilitate tradeoff considerations between the two,

Table 6-6. Packaging Technique I Tradeoff Considerations

<u>Approach 1</u>		<u>Approach 2</u>		<u>Approach 3</u>	
<u>Advantages</u>		<u>Advantages</u>		<u>Advantages</u>	
<ul style="list-style-type: none"> <li>• Fewer number of separate parts</li> <li>• Large chassis promotes good spreading of heat</li> <li>• Compatible with all internal interconnection techniques</li> </ul>		<ul style="list-style-type: none"> <li>• Good flexibility for changes</li> <li>• Good access for servicing</li> <li>• Compatible with most internal interconnection techniques</li> <li>• Chassis amenable to standardization</li> <li>• Thermal conduction between chassis improves temperature for high power density sub-assemblies</li> </ul>		<ul style="list-style-type: none"> <li>• Good flexibility for changes</li> <li>• Very good access for servicing</li> <li>• Chassis amenable to standardization</li> </ul>	
<u>Disadvantages</u>		<u>Disadvantages</u>		<u>Disadvantages</u>	
<ul style="list-style-type: none"> <li>• Limited flexibility for changes</li> <li>• Generally restricted access for servicing</li> <li>• Chassis not very amenable to standardization</li> </ul>		<ul style="list-style-type: none"> <li>• Access to a subassembly requires removal of entire assembly from the spacecraft</li> </ul>		<ul style="list-style-type: none"> <li>• Requires external connectors and cables for subassembly interconnection</li> <li>• Practically no thermal conduction between chassis; thus each chassis must reject its own heat</li> </ul>	

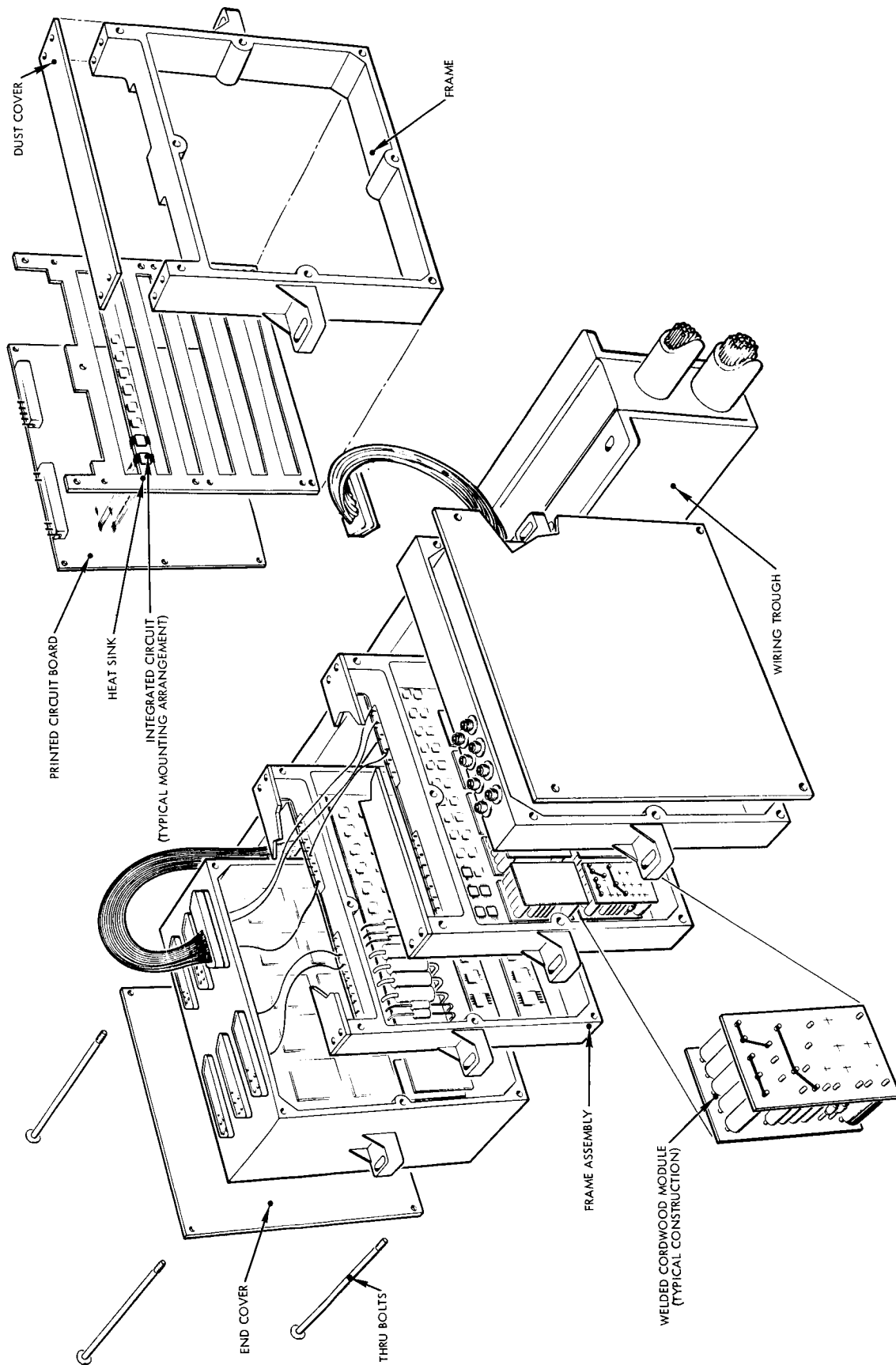


Figure 6-7. Perspective of Generalized Packaging Technique



both are shown in their board mounted component configurations.

- 1) Approach 1. Subassembly chassis consists of a frame and center web. A circuit board is bonded to each side of the web.
- 2) Approach 2. Subassembly chassis consists of a frame and a separate heat sink. The board is constructed so that only terminals are exposed on the top surface. When the board is bonded to the heat sink, cut-outs in the heat sink leave the terminals exposed. The component bodies are bonded to the heat sink, while the leads are bonded to the terminals. Through bolts clamp the heat sinks to the frames. (See Figures 6-7 and 6-9).

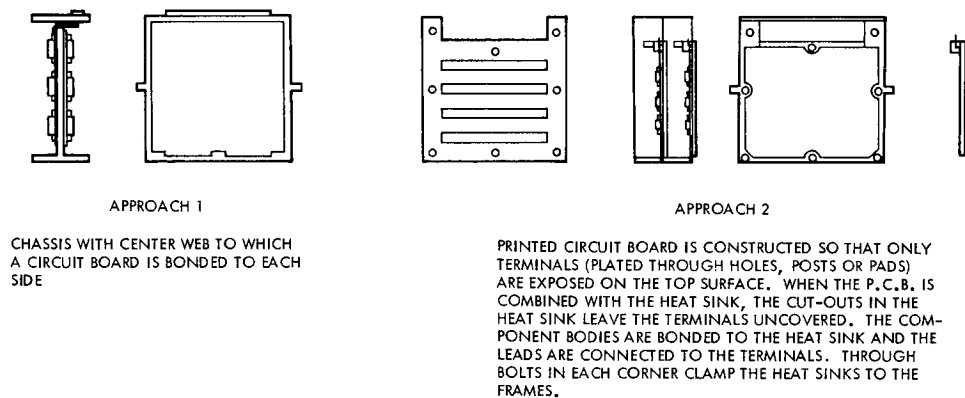


Figure 6-8. Packaging Technique II Tradeoff Considerations

The construction of the equipment chassis permits selection of a number of materials and fabrication processes. There are three distinct approaches which are employed frequently in chassis construction. Tradeoff considerations for these are listed in Table 6-8.

- 1) Approach A. Casting approach using thin-wall, light-weight alloys, such as aluminum A356-QQ-A-601 Comp. 3, aluminum C612-QQ-A-371 Comp. Z, or magnesium AZ 91C-QQ-M-56. The fabrication process includes investment, semipermanent, and permanent costing techniques.

Table 6-7. Packaging Technique II Tradeoff Considerations

Approach 1

Advantages

- Simple one-unit construction
- Provisions for good tie-down of chassis base
- Amenable to good standardization

Disadvantages

- Heat must be conducted through circuit board before reaching chassis
- Very difficult to make repairs

Approach 2

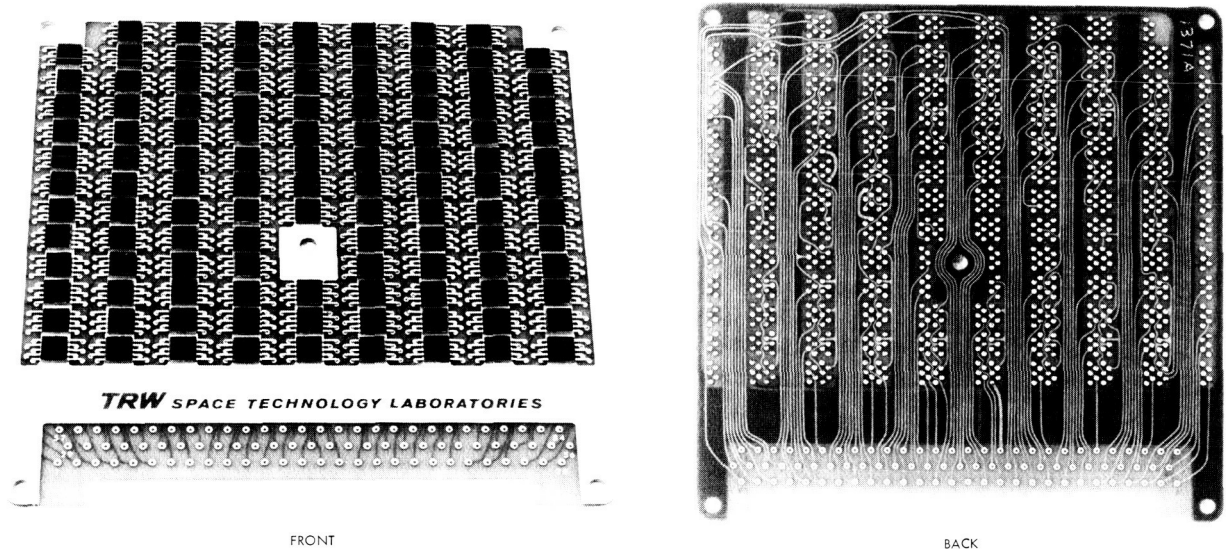
Advantages

- Good thermal conduction from component to chassis
- Good accessibility to components and circuit board for repairs
- Amenable to good standardization
- Permits use of several internal subassembly-to-subassembly interconnection techniques

Disadvantages

- More parts required
- Tie-down of chassis can be added, but would complicate sandwich panel construction, due to the many inserts required

- 2) Approach B. Machining approach using generally milling operations to cut the chassis out of a solid block. Common materials, such as aluminum 6061-T6 and 2024-T3, are used for this purpose.
- 3) Approach C. Build-up approach using generally standard sheet, roll, or extruded stock which are joined together as required to form the chassis. Joining processes may consist of dip-brazing, welding, and diffusion bonding.



MULTILAYER CIRCUIT BOARD WITH HEAT SINK ATTACHED. TUBE GRADED CIRCUIT FLAT PACKS ARE SHOWN MOUNTED TO THE HEAT SINK. THIS BOARD DESIGN IS USED ON ANOTHER PROGRAM AND IS USED HERE TO ILLUSTRATE THIS CONCEPT

Figure 6-9. Packaging Technique

c. Selection of Preferred Approaches

For the assembly packaging no single approach is preferred but rather a preferred approach to each type of circuit. For boxes with a large number of digital circuits, Approach 1, Figure 6-6 is preferred. In this case an interconnection matrix is almost a necessity. Proper registration of cards with respect to the matrix requires close tolerance control which cannot be achieved with a segmented box approach. For battery packs the same approach is preferred since the best design is a single container sized to the total battery cell array.

For analog and RF circuits Approach 2, Figure 6-6 and 6-8 is preferred because compartmentalized construction and shielding is easier to achieve. Subassembly chassis that are mechanically tied

Table 6-8. Equipment Chassis Design Materials and Processes Tradeoff Considerations

<u>Approach 1</u>	<u>Approach 2</u>	<u>Approach 3</u>
Cast Chassis	Machined Chassis	Build-Up Chassis
<u>Advantages</u>	<u>Advantages</u>	<u>Advantages</u>
<ul style="list-style-type: none"> <li>• Minimum cost for large quantities. For average complexity break point would be at 5 units</li> <li>• Ease for accommodating intricate shapes</li> <li>• Minimum handling for finishing</li> </ul>	<ul style="list-style-type: none"> <li>• High design flexibility for changes</li> <li>• Minimum physical distortion</li> <li>• Best ability to provide close dimensional control</li> <li>• No restriction in use of different alloys</li> <li>• Best suited for prototype quantity fabrication</li> </ul>	<ul style="list-style-type: none"> <li>• Inexpensive for most designs</li> <li>• Minimum schedule lead time for fabrication</li> </ul>
<u>Disadvantages</u>	<u>Disadvantages</u>	<u>Disadvantages</u>
<ul style="list-style-type: none"> <li>• High first article cost for tooling</li> <li>• Limitation to specific castable materials</li> <li>• Reduced mechanical properties; usually 30 per cent reduction in strength</li> <li>• Low design flexibility for changes</li> <li>• Long schedule lead time required</li> </ul>	<ul style="list-style-type: none"> <li>• High cost for large quantities</li> <li>• Large quantities require automated production equipment</li> </ul>	<ul style="list-style-type: none"> <li>• Most joining methods result in distortion problems</li> <li>• Restricted to material possessing proper chemistry, i.e., for dip-brazing, welding</li> <li>• Joints have reduced mechanical properties</li> <li>• Limited in accommodating complex shapes</li> </ul>

together have the advantage over Approach 3 by providing a single physical item for checkout and test. Approach 2 has also a thermal advantage over Approach 3, since heat from a hot chassis has a better chance to be distributed. Exploded views of typical assemblies are shown in Figure 6-7. The selected approach for both digital and analog or RF circuits is shown.

No single material and process approach is preferred at this time. A selection will be made as specific design considerations are generated. Table 6-8 lists the factors which generally determine such a selection.

## 2. ELECTRICAL DISTRIBUTION EQUIPMENT

The electrical distribution equipment consists of the following components: 1) all interconnect cabling throughout the spacecraft, 2) the necessary junction boxes for multiple distribution of electrical functions and a producible cabling configuration, 3) power switching circuits, 4) circuit protective devices, and 5) the circuitry for the control and initiation of pyrotechnic devices.

### 2.1 Interconnect Cabling

It is not anticipated that any new cabling materials, i.e., wire, insulation and connectors, will appear prior to July 1966 which will produce significant advantages, from the standpoint of weight, reliability or ease of manufacture, over those available at the present time. Materials are presently available which meet the Voyager requirement in the areas of outgassing and nonmagnetic properties. The use of crimp-type connectors has been examined and will be pursued further. These have the advantage of easing cable manufacture and eliminating some of the quality control problems attendant to the inspection of soldered connections. Flat ribbon wire has been examined and may be applicable in limited areas. This wire has decided disadvantages where twisting, shielding or both are required to control magnetic fields and to prevent electromagnetic interference. An additional disadvantage is that no acceptable connector has been developed for flat ribbon wire.

The cabling implementation must be compatible with the over-all packaging philosophy and techniques discussed in Section I.

### 2.2 Power Switching Circuitry

It is necessary at specific points in the spacecraft to switch electric power loads which are normally beyond the capability of the circuitry contained in the on-board signal generation equipment and the circuitry containing the outputs of the ground command receiving and processing functions. These requirements normally consist of switching power to equipment which are not required to operate continuously or to switch between redundant equipments.

In the majority of past and current TRW spacecraft programs, electromechanical relays have been used with success for the switching of primary and secondary electrical power as well as low level signal switching. Relays have a disadvantage, however, insofar as Voyager is concerned, in that they are magnetic components. The OGO spacecraft, in which relays are used extensively, has imposed upon it rather stringent magnetics requirements, but the requirements are imposed at the magnetometer, located at the tip of a 20-foot boom. In contrast, the magnetics requirements imposed by the Voyager specification are placed upon the individual spacecraft assemblies.

The Pioneer program also has stringent magnetics requirements, though again the requirements were imposed at the magnetometer location at the tip of a 6-foot boom. In this case, electromechanical relays were almost totally eliminated from the spacecraft, the exception being that relays are used for switching currents to pyrotechnic devices. The Pioneer solution consists of power control to using assemblies by the switching on and off of the drive signal to power conditioning circuits in DC-DC power converters. Since the Voyager distributed power is intended to be AC and each power consumer will provide or be provided a conditioning power supply it appears probable that the technique used on the Pioneer can be applied to Voyager. Further study of this technique and its applicability will be made in Phase IB of the Voyager program.

The difficulty in meeting the Voyager requirements does not, however, totally eliminate the use of relays. Shielding and magnetic field compensation techniques have been developed and are in use on Pioneer and other spacecrafts. These techniques, however, suffer the disadvantage of added weight.

### 2.3 Circuit Protective Devices

It is probable that the Voyager spacecraft will require devices to protect the power subsystem from catastrophic overloads. Devices are available, such as the microelectron fuse, which provide non-resettable protection. These have been successfully used on the OGO,

Vela and Pioneer programs. It is desirable that resettable protection be available and the applicability of all potential devices should be reviewed and compared with other techniques of overload protection.

The capability for handling marginal circuit overloads (non-catastrophic) by detection and applying corrective action by ground command is now available in all spacecraft subsystems.



## 2.4 Pyrotechnic Control

### 2.4.1 Solid-State Firing Circuits

Solid-state circuits (silicon-controlled rectifiers, transistors, diodes, etc.) have many definite advantages over conventional firing circuitry. Designed properly, current and transient control can be obtained to a very close tolerance. Switching time, if an important factor, can be made extremely rapid, and switch and contact losses are eliminated. The entire circuit can be made very small, lightweight, vibration and shockproof (when immersed in epoxy), and highly reliable. Printed circuits can be used for nominal current values; and if the circuit is mounted on boards or in cans, troubleshooting and replacement can be made simple. The entire circuit can be removed and tested; and if found to be defective, it can be replaced by a new circuit (as in computers - plug-in type). With present-day devices, circuits can be designed to accommodate fairly large currents, although care should be taken so that transient currents do not far exceed current ratings.

There are problem areas that must be considered for design. Solid-state devices are very sensitive to temperature, particularly high temperature resulting either from excess current or environmental temperatures. Effects of pressure are generally not very important to the functioning of the circuits, although this should not be overlooked. If cryogenic temperatures are a design factor, tests should be conducted at these temperatures to determine characteristics. High temperature effects are very important, and performance characteristics are greatly affected by temperature. If the device experiences heat (from any source) for a given length of time, thermal runaway can occur and destroy the device, or possibly cause the circuit to switch.

The circuitry must be tested and analyzed in very environmental condition it will experience.

#### 2.4.2 RF Environment

The maximum power density to which the vehicle will be exposed in the frequency range of 150 kc/sec to 10 Gc/sec is 36 dbm/m<sup>2</sup> or 4 watt per sq m.

All EED have 1-amp, 1-watt, 5-minute no-fire at DC: each of the two bridge circuits is capable of surviving the application of 1 amp DC and can dissipate 1 watt of power for 5 minutes.

The entire firing circuit, including the EED bridge, is shielded continuously with no gaps or discontinuities. The shield is capable of reducing ambient electromagnetic power densities by a factor of 10,000 and of reducing the maximum electromagnetic environment of the circuit to a level of  $4 \times 10^{-4}$  W g/m<sup>2</sup>. The EED and associated firing circuit shield meet the Eastern Test Range requirements of "General Range Safety Plan," AFMTCP 80-2, Vol. I.

To create a safety hazard, the firing circuit would have to create an antenna with a coupling factor of 2500. If a 20 db safety factor for dudding protection is required, a maximum coupling factor of 25 would be permissible. Shielded circuits normally have coupling factors much less than one.

The proposed design, the Apollo standard initiator, will not fire when subjected to discharge from a 500 pico-farad capacitor charged to 25,000 watts. This initiata is safe in the presence of the stated RF power densities.

## VII. PROPULSION SUBSYSTEM

The selection of the type of propulsion subsystem represents one of the main decision points in this study, not so much because the two types differ significantly in performance and reliability, but because the propulsion type has a strong influence on the over-all spacecraft configuration.

The basic alternatives considered for the spacecraft propulsion subsystem were: 1) a combination system in which a monopropellant hydrazine propulsion subsystem is used to provide impulse for midcourse velocity corrections and orbit trim maneuvers and a solid propellant motor is used to provide impulse for the retro maneuver, and 2) a single-engine storable liquid bipropellant system in which impulse for both the midcourse correction and the retro maneuver is provided by a single engine. More elaborate propulsion approaches such as multiple monopropellant or a side firing engine were eliminated in early over-all vehicle configuration studies. (See Volume 4.)

The propulsion subsystem study involved several phases. The first compared various design solutions within the basic alternatives to define representative baseline subsystem for each alternative. Next weight-reliability tradeoffs were performed to determine the reliability potential and the appropriate levels of redundancy within the subsystem. In parallel, this data was incorporated at the system level to define the A, B and C series of configurations discussed in Volume 4. At this point, the system selection of Configuration A was made, the configuration that uses the monopropellant vernier together with a solid propellant retro-motor. The final phase refined the selected design. In particular, the monopropellant midcourse propulsion subsystem was significantly simplified at the expense of only a modest weight penalty.

This section discusses the various design solutions and problem areas for both of the two basic alternatives and derives two representative designs. The comparison of these systems in terms of vehicle performance and vehicle interactions is covered in Volume 4. As indicated

in that volume, it became evident, early in the study, that both alternatives met the minimum requirements of the Voyager mission specification and that the differential between the relative merits of the alternatives in comparable features, such as retro  $\Delta V$  capability or predicted reliability, would be inadequate to justify selection of either alternative on such grounds alone.

In view of the fact that both choices are essentially equivalent insofar as ultimate performance is concerned, the major factors which precipitated the choice for Configuration A were:

- a) The relative high density and compact nature of the combination system resulted in significantly greater flexibility, applicable not only to currently planned missions and in the adaptability to the 1969 mission, but also to future missions in which the mission's scientific objectives may require new or additional equipment.
- b) The status of propulsion technology is well established for all elements of the combination system. No fundamental problem areas requiring extensive development testing for reliability verification are anticipated, a conclusion that cannot be applied to the single-engine bipropellant system. Although the feasibility of the bipropellant system is sufficiently well established to qualify for consideration under the general guidelines, several components including the main engine will require relatively lengthy development programs to verify the design and ensure that the reliability potential has been achieved.
- c) The bipropellant engine, as configured, does not have orbit trim capability because of the limited positive displacement approach. If trim capability is provided, the engine is no longer comparable in performance with the solid system.
- d) The selected system has a small (40 to 50 pound) performance advantage and a slightly better reliability.

## 1. PROPULSION SUBSYSTEM REQUIREMENTS

The propulsion subsystem requirements can be classified into three general categories:

- o Mandatory requirements to satisfy the mission specification and mission guidelines

- o Desirable requirements to refine the capability of the spacecraft or to compensate for potential malfunctions of other spacecraft subsystems
- o Requirements generated by consideration of interactions with other spacecraft subsystems.

This section restates the requirements, discusses the areas where exceptions to the requirements were considered, and presents considerations which resulted from interaction with other spacecraft subsystems.

### 1.1 Mandatory Requirements

The mandatory requirements given in the mission specifications and mission guidelines include performance specifications, operational limitations, and restrictions on the types of hardware to be evaluated. In general, these requirements were assumed to be inviolate at the subsystem level. Consequently, potentially higher performance alternatives such as the use of a combination system with a solid-propellant retro-motor and a bipropellant midcourse correction system, which essentially meets all other fundamental constraints, were not considered to be within the ground rules of the study. However, at the component level there were a few specific instances, such as the requirement for positive expulsion propellant tanks, where a close interpretation of the specification appeared to be an unreasonable constraint. In these instances several alternates were evaluated during the study.

The requirements which were assumed to be mandatory are as follows:

#### a) Configuration Options:

- 1) A monopropellant hydrazine midcourse velocity correction subsystem and a solid-propellant retro-propulsion motor
- 2) A single-engine, earth-storable liquid bipropellant, pressure fed propulsion subsystem.

#### b) Performance Requirements:

- 1) Capability of providing a minimum velocity correction of 75 m/sec for midcourse for 1) above and 50 m/sec for 2) above (if propellants for midcourse are available from the main propulsion tank)

- 2) Capability of adding a velocity increment at least as small as 1 m/sec with a maximum allowable error of 0.1 m/sec.
  - 3) Capability of providing three start-stop cycles plus one backup cycle for midcourse maneuvers
  - 4) Capability of sufficient  $\Delta V$  retrothrust to inject the planetary vehicle into orbit about Mars.
- c) Structural Requirements:
- 1) Hazardous vessels designed with a 2.2-safety factor
  - 2) Pressure vessels mounted to avoid restraints which could induce high stress concentrations
  - 3) Minimum wall thickness to diameter ratio of tanks not smaller than 1/1000
  - 4) Vessels pressurized in the vicinity of personnel fabricated of Ti-6Al-4V titanium in the annealed condition
  - 5) Pressure vessels not pressurized in the vicinity of personnel fabricated of Ti-6Al-4V titanium heat treated to 165,000 psi maximum yield strength.
- d) Operational Requirements:
- 1) Propellant on-stand loading not permissible during 1971 launch operation

## 1.2 Desirable Requirements

In addition to the mandatory requirements, the mission specifications and mission guidelines referred to several performance characteristics as desirable or highly desirable and in general dictated that the basic design philosophy should be simple and conservative. Requirements which fall in this category as follows:

- a) Minimum  $\Delta V$  increment should be 0.1 m/sec with a  $3\sigma$  error of 0.01 m/sec
- b) Capability for one orbit trim maneuver of about 50 m/sec (highly desirable)
- c) Capability for two or more orbit trim maneuvers with up to 100 m/sec total  $\Delta V$  velocity capability
- d) Nonmagnetic materials used wherever possible

- e) Confined to a single assembly for ease of handling, check-out, and qualification testing.

### 1.3 Requirements Resulting from Spacecraft Interactions

The principal areas of interaction between propulsion and other vehicle subsystems are in considerations of structure, stabilization and control, and thermal control. However, significant interactions also occur between propulsion and the power, CS and C, and the electrical distribution subsystems. In addition to the on-board interactions, the propulsion system interacts significantly with OSE and launch operations. The major interactions encountered during this study are as follows:

- a) Structure. The two basic propulsion alternates are the major variables in the spacecraft structural design. Other propulsion subsystem requirements such as the desire for modular construction or potential contamination and heat transfer from exhaust plumes were determining factors in prescribing the relative location of components such as solar panels and the rocket motor nozzle.
- b) Stabilization and Control. The best approach to stabilization and control of the spacecraft during retromotor firing is obviously dependent on the basic propulsion alternate. However, even after the basic alternate of the solid motor was selected, several different approaches to thrust vector control were found to be suitable. The use of liquid injection, a gimbaled nozzle, and a separate solid gas generator system, and other approaches were evaluated in terms of propulsion and S and C interactions.
- c) Thermal Control. The thermal control interface requires that the propulsion subsystem be maintained within prescribed limits and other spacecraft subsystems be protected against heat produced by the propulsion subsystem.
- d) Power. Power requirements vary significantly between basic alternates and even between potential components such as control valves.
- e) Electrical Distribution and CS and C. Alternate component types and system arrangements resulted in significant variations in requirements imposed on the electrical distribution and the CS and C.

## 2. SOLID PROPELLANT INJECTION MOTOR

A survey was made to see if any existing solid-propellant rockets or minor modifications thereof could meet the mission requirements. No

suitable candidates were found. A preliminary specification outlining the requirements for the motor was then prepared. (A copy of this specification is included as Section 2.5.) This specification was submitted to the following manufacturers: Hercules Powder Company, Thiokol Chemical Corporation, Aerojet-General Corporation, Lockheed Propulsion Company, Atlantic Research Corporation, and United Technology Center. These companies were invited to submit their recommended design solutions for the solid propellant motor as well as backup technical information to support the feasibility of the proposed approach. Thiokol and Atlantic Research declined to submit information at this time, because of the pressure of work in process. The remainder submitted technical discussions of a proposed approach. From the technical information thus obtained, it was apparent that a motor capable of meeting all the requirements of the mission could be procured using proven propellants, case and nozzle design, and thrust vector control. In addition, significant improvement in the over-all motor performance could be obtained, at somewhat higher risk, by using higher energy propellants than those in current operational use.

Brief descriptions of each of the motor designs submitted by the different vendors are given in Section 2.6. A tabular comparison of their important design parameters is presented in Table 7-1. Based on this information, the best features of the various designs were integrated into the composite design shown in Figure 7-1. The following sections describe the solid propellant motor which TRW proposes for the Voyager mission and presents the rationale for design selection in those areas where multiple choices were available.

## 2.1 Component Selection

Since it appeared that all of the proposed motors satisfactorily met all performance requirements, it was necessary to develop rationale for design selection in each of the several components. These choices are discussed in the following paragraphs.



Table 7-1. Comparison of Vendor Solid Propellant Designs

Manufacturer	Hercules			Lockheed Propulsion			United Technology		Aerojet
Motor Variant	No. 1			No. 2			No. 1	No. 2	
Performance Parameters	Double Base 10% Be			Double Base 15.5% Al			PBAA 16% Al		PBAA 15% Al
Propellant Composition									
Standard Specific Impulse Isp <sub>0</sub> 1000 (sec)	268			260			250		253
Vacuum Specific Impulse (sec)*	303			304			286		293
Total Motor Weight (lb)**	3,020			2,980			3,280		3,060
Mass Fraction (Propellant/Total)	0.89			0.88			0.91		0.89
Mass Fraction (Expended/Total)	0.92			0.91			0.93		0.92
Maximum Thrust (lb)	15,000			15,800			14,000		12,000
Maximum Chamber Pressure (psia)	540			1,230			1,010		690
Expansion Ratio	32			81			30		60
Burn Time (sec)	77			94			103		95
Design Features									
Envelope Dimensions (in.)	48 dia. x 56 long***			48 dia. x 56 long***			47 dia. x 54 long		53 dia. x 52 long
Case Material	Fiber Glass			Fiber Glass			Fiber Glass		Fiber Glass
Throat Material	Graphite			Pyrolytic Graphite			Graphite		Tungsten
Nozzle Extension	Ablative			Ablative			Ablative		Ablative
Igniter	Single			Dual Pyrogen			Single Pyrogen		Single Alcojet
TVC Method	LITVC			Gimballed Nozzle			LITVC		Auxiliary Thrusters

\* Based on expended weight

\*\* Based on imparting a  $\Delta V$  of 7000 ft/sec to a 2300 pound payload

\*\*\* Includes 6 inch diameter x 4 inch length relief for mounting of monopropellant system

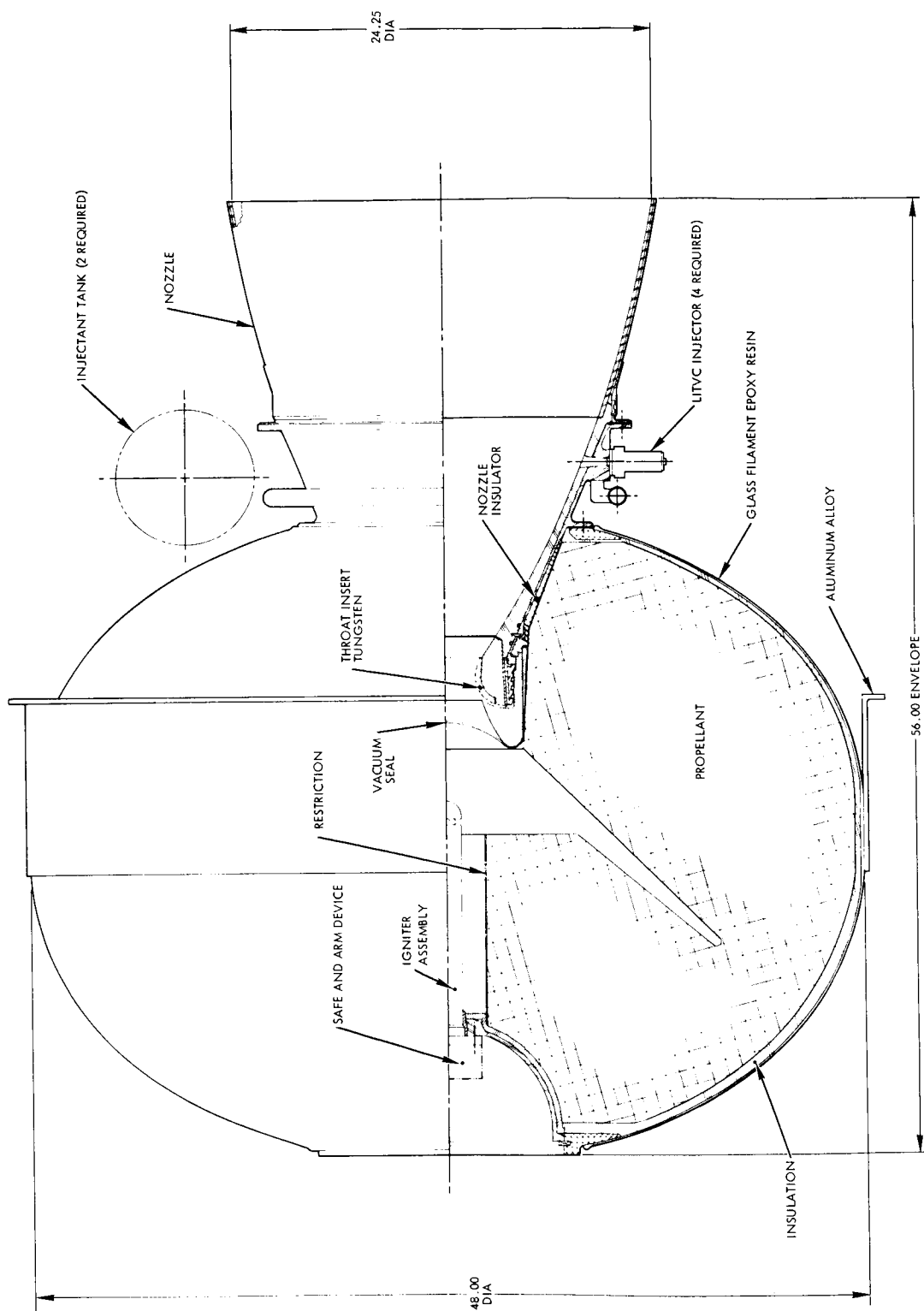


Figure 7-1. Solid Propellant Injection Motor

### 2.1.1 Propellants and Performance

A parametric indication of the impulse requirements is shown in Figure 7-2 where the required specific impulse is given as a function of the retro  $\Delta V$ . Both the specific impulse and mass fraction parameters are defined in terms of the weight expended during firing rather than the more conventional basis of the propellant mass. This convention will be followed throughout this section. The range of velocity increments shown corresponds to  $\Delta V$ 's between 3.7 and 4.5 km/sec for entries into the nominal 2000 x 20,000 km orbit. The two sets of payload curves shown correspond to the nominal 2000-pound payload plus the required monopropellant system (75 m/sec for a 7800-pound spacecraft) either full of propellant (upper set) or with the propellant completely expended (lower set). The nominal design point for the solid has been set at  $\Delta V = 7000$  ft/sec with a zero midcourse (full monopropellant tanks). From the information presented in Table 7-1, it appears that an effective engine mass fraction of 0.92 will be relatively easy to obtain in this application. The required specific impulse is then determined from Figure 7-2 as 291 seconds. (This procedure is justified because the mass ratio is the less sensitive variable and because Table 7-1 is based on fairly detailed designs. The mass ratio selection is more fully justified in the following sections.)

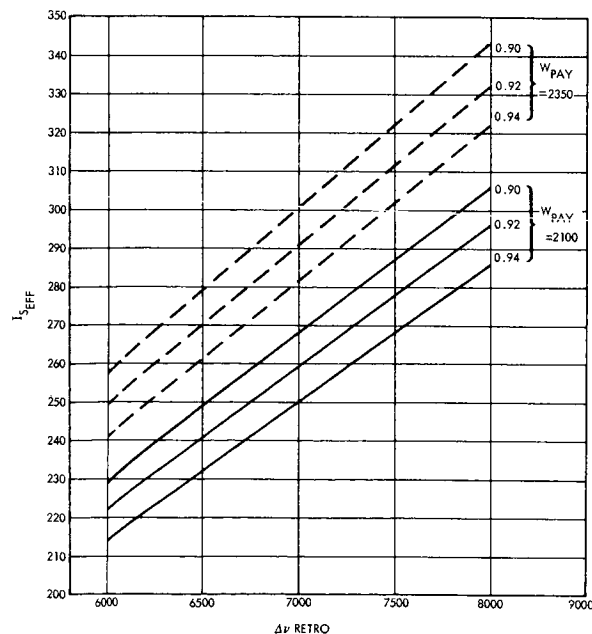


Figure 7-2. Parametric Indication of the Impulse Requirements

Information presented by the vendors and gained from past experience of TRW with various ballistic missile and space programs was used in evaluating proposed propellants. The propellants considered for this application can be classified in the three categories discussed in the following paragraphs.

a. Rubber-Base Propellants

The rubber-base propellants are characterized by the encapsulation of a high percentage of solids (ammonium perchlorate and 15 to 25 per cent aluminum powder) in a rubber binder which provides structural integrity of the propellant and acts as the fuel. Polyurethane and polybutadiene are two common types of rubbers used in these propellants. The polybutadienes, in general, maintain structural integrity with a high percentage of solids and thus have a higher performance. Comparative performance characteristics of polybutadiene propellants are shown in Figure 7-3. This figure shows  $I_{sp}$  versus expansion ratio. A quantitative version of this figure has not been included because of its security classification. Curves are presented for a propellant loaded with approximately 84 per cent solids and one loaded with 88 per cent solids. The former is typical of the state of the art of approximately 2 to 2-1/2 years ago (i.e., Minuteman Wings I and II, Stages I and II; Polaris A2, Stage I; Scout, Stages I and II; and Surveyor). The 88 per cent loaded solid is typical of the more advanced polybutadiene propellants which are presently operational in vehicles such as Stages I and II of the Wing VI Minuteman. In Figure 7-3, the points shown correspond to inflight specific impulse measurements on qualified stages. The specific impulse of the propulsion companies' proposals is shown for comparison. It is apparent that all of the proposed PBAA performance figures are well within current state of the art. The characteristics of these propellants are:

- Highly reproducible
- Safe to manufacture and handle-Class 2 Army Ordnance classification. (Nondetonable)

- Member of well-characterized family of propellants
- Relatively inexpensive.

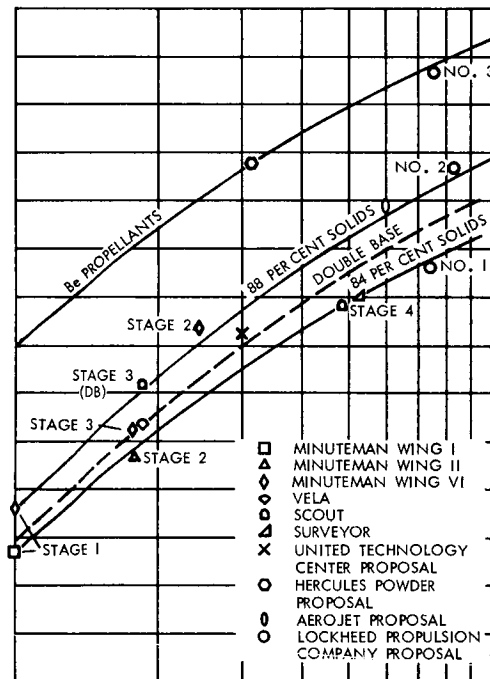


Figure 7-3. Comparative Performance Characteristics of Polybutadiene Propellant

b. Double Base Propellants

Double-base propellants are characterized by the use of nitro compounds (usually nitrocellulose and nitroglycerine) as plasticizers to form a structural material. In general, they yield a higher performance and better mechanical properties than rubber-base propellants for an equivalent solid loading. However, they have an appreciably higher flame temperature for a given specific impulse and typically higher burning rates. A typical curve for a common double-base propellant series is shown in Figure 7-3. Recently, further advanced double-base propellants have been developed for use on Polaris A-III. However, because of their extremely high flame temperature, development of a nozzle capable of withstanding a firing time of approximately 100 seconds could be a serious problem.

c. Beryllium Propellants

By substitution of beryllium for the aluminum in either rubber-base or double-base propellants, it is possible to achieve appreciably higher performance. Typical performance is shown in the upper curve in Figure 7-3. The development status of these propellants is less extensive than that of the aluminized propellants, since the majority of the tests with beryllium propellants have been with small charges (40 pounds or less); only a few large charges (up to 1000 pounds in total weight) have been tested. A small mass ratio penalty is incurred with these propellants since they have approximately 5 per cent lower bulk density. In addition, the toxic products of combustion present a potential test firing hazard. Thus, while the beryllium propellants represent appreciable growth potential for the solid propellant motor, it does not seem justifiable at this time to utilize them for this application.

#### d. Propellant Selection

Figure 7-3 shows that the required performance can be provided by the high-solids-ratio aluminized rubber-base propellants provided that the expansion ratio is above 35. Because this propellant is in widespread usage and considerable design information is available, a minimum development program is to be expected. Hence, the rubberized aluminum propellant was felt to be the lowest risk solution to the problem and was selected. Since the burning time for the Voyager motor is considerably greater than for a typical missile application, it is expected that the effective specific impulse may be lowered somewhat by the proportionately greater insulation required. Thus it appears prudent to select a target expansion ratio in the range of 45 to 50.

##### 2.1.2 Grain Design

The selected geometry was dictated by the envelope constraints of 48 inches diameter x 52 inches long (or 56 inches long with a 6 inches diameter x 4 inches long relief in the head end). In particular, the efficient Aerojet design could not be accommodated within this envelope. The required internal volume is provided by a short cylindrical section with elliptical ends. The desired expansion ratio of 45 to 50 requires that a submerged nozzle be used. The resultant grain geometry is shown in Figure 7-1. The slot geometry has not been optimized but is an adaptation of the Aerojet design. It is believed that the internal burning surface geometry will be a routine development task.

##### 2.1.3 Case

The manufacturers considered maraging steel, titanium, and filament wound fiberglass as possible candidates for the case material. Each manufacturer recommended fiberglass because of its weight advantage and highly developed fabrication technology. The advantage for a motor of this size is significant; the indicated 50 pound differential corresponds to a one point mass ratio improvement. By comparison, the titanium alternative would be a more difficult fabrication problem with

higher unit costs. The steel alternative showed a weight substantially higher than the titanium. A preliminary weight computation showed that the combination of the most conservative case and nozzle designs yielded a system mass greater than would be allowable. The decision to use fiberglass was made because this material in conjunction with a conservative nozzle design would yield higher reliability and lower developmental risk within the allowable weight bounds. The concomitant problem thereby created was one of vacuum-soak degradation effects on the composite glass epoxy material. This problem is discussed in Section 2.3.

#### 2.1.4 Insulation

A fairly large divergence appeared between the various proposals in the insulation weight allowance. An order of magnitude analysis by TRW of the submissions resulted in the conclusion that they ranged from extremely optimistic to reasonable. The Aerojet proposal was judged best in this respect and was therefore used as a basis for estimation of the proposed motor requirements. The proposed insulation would be of the silica-rubber type which is widely used in operational missiles.

#### 2.1.5 Nozzle

It was initially felt that the relatively long burning time of the Voyager retro combined with the desire to minimize the thrust vector shift during burning would dictate the use of a hard throat insert. The vendors' proposals did not totally agree with this premise and considerable divergence was evident in their selection of throat materials. Possibilities included graphite, pyrolytic graphite washers, and tungsten. The pyrolytic washer option was eliminated on the basis that no known flight experience has been obtained with this design. Despite the weight penalty associated with the tungsten option, it was still felt that the tungsten design would have a better chance of proving satisfactory for Voyager. Since a sufficient weight allowance was available (see above discussion, paragraph 2.4), the tungsten alternative was adopted.



The nozzle-throat design shown in Figure 7-1 is essentially a duplicate of the one proposed by Aerojet, which in turn grew out of AGC's experience in the design and development of the Minuteman Wing VI second-stage nozzle. In this design, the tungsten throat is supported by molybdenum, titanium, and steel supporting members with molded graphite phenolic in the entrance section. The nozzle is submerged at the 15:1 exit-area-ratio point.

While initial considerations of the exit cone design had included both ablative and radiative cooling, the "buried" location of the motor within the spacecraft dictated use of the lower-wall-temperature ablatives to limit heat input during retromotor firing. Although the radiative cone would be approximately 25 pounds lighter than the ablative version, it is probable that most of this advantage would be absorbed in protecting the spacecraft from the additional heat input. The resulting design would certainly be more complex and less rigid. (Note: The wall temperature requirement was issued to the vendors subsequent to preparation of the preliminary requirements given in Section 2.5.)

Silica-phenolic should be satisfactory for the exit cone liner material in view of the low heat rates expected in this area, while structural support might be either fiberglass or, as Aerojet suggested, a material which provided sufficient strength and gave better insulation such as tape wrapped silica-phenolic. The exit geometry shown in Figure 7-1 is designed according to the Rao criterion and has a length equal to 82 per cent of a 17 degree half-angle conical nozzle. Optimization calculations will have to be made to find the contour which maximizes the thrust coefficient in the available length.

It should be noted that the 3 g limitation placed on the solid propellant contractors (which ultimately determined the burn time) is not an absolute upper limit. The limiting component (structurally) is the antenna drive mechanism which can be designed for an acceleration slightly in excess of 4 g's without entailing undue size or weight. Hence

an alternate solution is available should nozzle life become a critical development problem.

#### 2.1.6 Thrust Vector Control

As shown in Table 7-1, a considerable divergence appeared in the vendors' recommended systems for pitch/yaw control of the thrust vector during burning. However, in reaching these recommendations, remarkable unanimity was evident on one basic premise: "Of the TVC systems considered, secondary liquid injection has had the most development and is therefore best understood." This was postulated because some manufacturers considered only the LITVC while others used it as a baseline of comparison in evaluating other proposed candidates. TRW's experience corroborates this judgment. While the swivel-nozzle concept proposed by Lockheed appears attractive because of its low weight (100 pounds lighter not including actuator), it is still in the early development phases and cannot be considered a well understood design. Also, the relatively short axial separation between the predicted spacecraft center of gravity and the throat would require fairly large gimbal angles (approximately 5 to 7 degrees) which may present serious developmental problems. Aerojet's alternative of a solid gas generator hot-gas system appeared promising and resulted in a substantial weight saving (50 pounds). Since a similar system is in use for roll control on Minuteman, Wing VI Stage 2, development problems with this system should not be serious. However, vehicle integration studies showed that impingement from the forward-facing-pair of nozzles would create a fairly severe thermal protection problem on the solar panels (see Volume 4). For these reasons, the secondary injection thrust vector control system was chosen for use on Voyager. This choice must be regarded as the most conservative of the several available, due primarily to the extensive experience which has been gained with this system which, in addition to Minuteman, includes use on Titan IIIC solids and Polaris A3 Stage 2.

The proposed system consists of the injectant supply system and four injector nozzles located at 90-degree intervals on the exit cone. Choosing freon over  $N_2O_4$  as an injectant is again the more conservative choice. Most of the development work done to date has employed these injectants. The freon injectant is housed in two spherical containers and is expelled by gas evolved by a solid gas generator pressurization source. Butyl bladders are used for positive expulsion in the freon tanks. The flow control valves are the continuous-flow proportional type shown schematically in Figure 7-4 resulting in the entire injectant being expended during burning. The solid gas generator is similar to one which is operational on Minuteman and is, therefore, not anticipated to be a development problem.

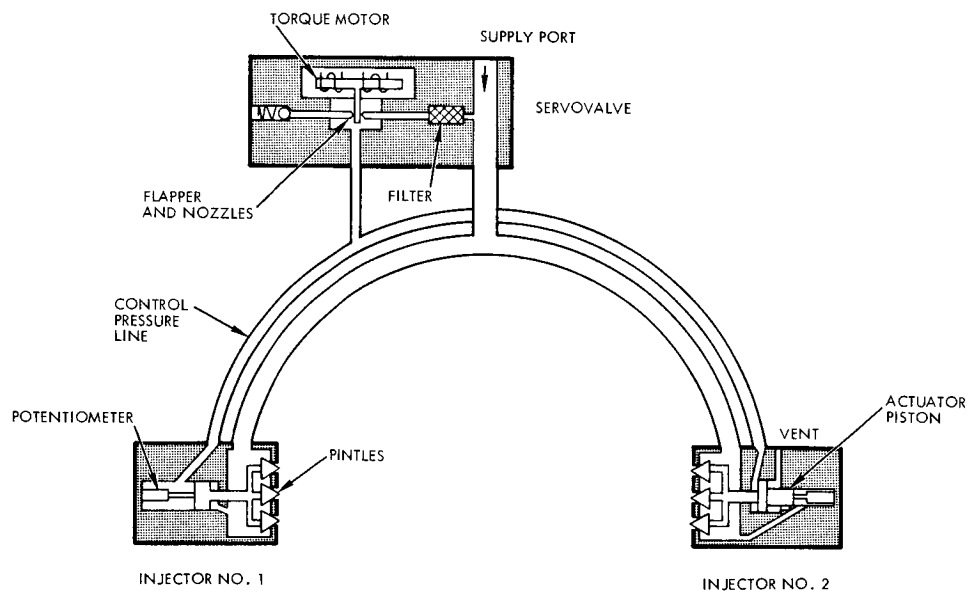


Figure 7-4. Servoinjector Schematic (One Axis)

Based on scaling from other engines the predicted roll disturbance torque produced by the solid engine is expected to be less than 3 ft-lb. This level can be accommodated using the cold gas attitude control system, but it will require higher thrust than is used for the cruise mode. Thrusts of about 1 pound appear suitable. The exact value of roll torque required will be reevaluated when engine characteristics are better known. If considerably larger thrusts are required,

pressurizing gases from the solid engine TVC system can be used in the same manner as the cold gas.

## 2.2 Weight and Performance

Table 7-2 contains a summary of performance and design parameters of the selected retromotor. The variables of primary importance are the effective specific impulse and the effective mass ratio. Justification of the listed specific impulse has been presented in Section 2.1.1. It will be noted that the effective mass ratio is somewhat lower than the targeted value. Since this is a function of the weight of the inert parts only, a detailed examination of these weights is indicated.

Table 7-3 contains weight breakdowns for the TRW selected configuration compared with the vendors' proposals. Such a comparison is of particular interest since the 0.92 target had been selected on the basis of the latter information. It may be noted that the TRW total inert weight is 65 to 100 pounds greater than those of the vendors. Of this difference 25 pounds result from the 6-per cent contingency, which was not a requirement on the vendors. This factor alone represents nearly a 1-point decrease in the mass ratio. The remaining portion of the difference can be accounted for by comparison of the individual component weights. For example, Aerojet's component weights are quite similar to TRW's except for the case mass. This deviation was not unexpected, since the AGC proposal was based on a more efficient shape. Minor differences were also noted in the TVC mass (as noted previously, AGC's auxiliary thruster system should be somewhat more efficient) and in the nozzle mass which is at least partially due to TRW's lower expansion ratio (50 versus 60). All of the remaining proposals made use of graphite throat inserts, which at least partially accounts for the lighter nozzle weights quoted. The Hercules proposal is probably too optimistic in the case, insulation, and nozzle weights. Since the weights given in Table 7-3 were not explicitly quoted by Hercules but obtained by extrapolation from a heavyweight breakdown, it is difficult to make a more definite

Table 7-2. Performance Parameters of Selected Retromotor Design

Performance:

Standard specific impulse $I_{sp1000}^o$ (sec)	249
Effective vacuum specific impulse (sec)	293
Mass fraction (propellant/total)	0.87
Mass fraction (expended/total)	0.90
Maximum thrust (lb)	15,000
Average thrust (lb)	8500
Maximum chamber pressure (psia)	700
Expansion ratio	50
Burn time (sec)	90-100

Propellant Properties:

Density (lb/in <sup>3</sup> )	0.064
Burning rate (in/sec)	0.21-0.25

Table 7-3. Weight Breakdown and Comparison with Vendor Proposals

Motor	TRW Selected Design	Aerojet Proposal	Hercules Proposal	UTC Proposal (No. 1)	Lockheed Pro- posal (No. 1)
Propellant Weight (Ref.) (lb)	2750	2714	2691	2975	2873
Inert Weight (lb)					
Case	110	80	66	151	101
Insulation*	90 } (70)	89 } (74)	20 } (60)	30	96 } (77)
Nozzle	90	96	78	25	118
Igniter	5	3	4	11	12
TVC	90 (35)	77 (27)	160 (30)	90 (63)	***
Contingency**	25				
Total	410	345	328	307	327

\* The amount shown in parenthesis is the portion lost during firing.

\*\* A Contingency of 6 percent of the inert weight is included according to an assumed ground rule.

\*\*\* TVC is provided by a swivelable nozzle. The actuators required are included under the nozzle weight.

statement as to which items might be suspect. The Hercules TVC weight is more conservative than TRW's since the former was based on providing an effective deflection of 4 degrees throughout burning while the latter was sized for 2 degrees steady-state deflection with a 4 degrees transient maximum. UTC's insulation weight is so low as to be suspect, while their low nozzle weight is at least partially due to the short 30:1 nozzle to which they were limited. Lockheed's weights compare with TRW's; the main difference is the gimballed nozzle, unique to their proposal.

Since the TRW weights were obtained independently, it can be concluded that the weight budget for the selected configuration can be achieved with a high degree of confidence.

The velocity capability of the selected motor is shown in Figure 7-5 for various values of the required midcourse velocity increment. Curves are shown for the retromotor only, the retro plus orbit trim, and the total of the three maneuvers. The effect of the lowered effective mass fraction is seen in this figure since the desired 7000 ft/sec retro capability is not achievable if the sum of the midcourse corrections is less than 15 m/sec. Since this is roughly the same magnitude as the  $1\sigma$  value for the midcourse corrections, it is likely that such a trim would be required if the trajectory selection requires the full 7000 ft/sec retro velocity increment. Figure 7-5 shows that the orbit trim  $\Delta V$  capability varies between 235 m/sec for a zero midcourse to zero for a maximum midcourse.

If the length restrictions were relaxed, a higher expansion ratio could be used and the performance of the selected motor thereby improved. If it is desired to use the increased capability to increase the payload, the tradeoff coefficient is approximately 2 pounds of payload per inch. If the increased performance is used to increase the velocity increment, the tradeoff coefficient is 9 ft/sec per inch. Both of these coefficients include the additional weight of the nozzle extension.

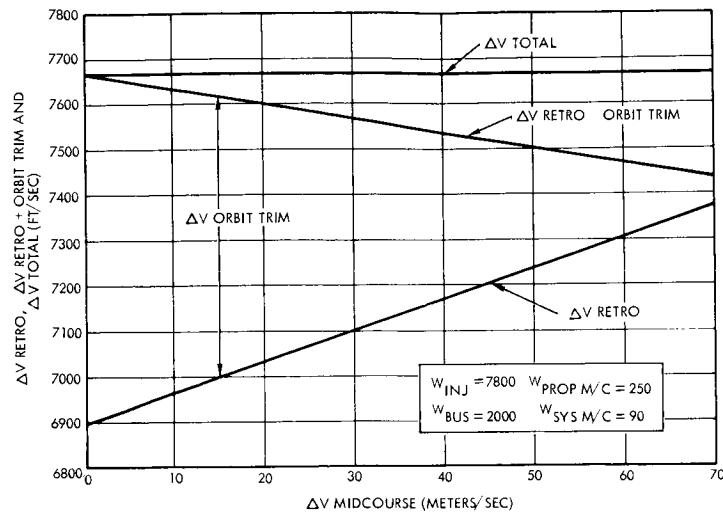


Figure 7-5. Velocity Increment Capabilities of Selected Design

### 2.3 Problem Areas

This section discusses several problem areas which may have potentially serious implications on the development of the Voyager retropropulsion system. Further detailed analyses of these problems will be required early in the development program.

#### 2.3.1 Storage in Space Environment

The following discussion of the motor's space environment storage capability is presented essentially as it was submitted by Aerojet-General.

The flight of the Voyager vehicle from launch to ignition of the retropropulsion system will constitute a 6 to 9-month storage period in space. The potential hazards known to exist in space include ionizing radiation of all types, hard vacuum, micrometeorites, and solar thermal radiation. The first two of these hazards are discussed in some detail below. For the latter two, it is sufficient to note that the retromotor is surrounded by other vehicle structure in the Voyager vehicle. As a result, the motor is shielded from the intense thermal radiation and from micrometeorites. Design of the spacecraft side



panel is based on providing a high degree of protection against micro-meteorites. Furthermore, the structure of a solid rocket motor is less susceptible to damage from micrometeorite impact than many other components of the spacecraft.

a. Radiation

The principal sources of ionizing radiation which the Voyager will encounter in space include primary cosmic rays, solar flares, Van Allen belt and a possible similar radiation belt around Mars. The expected radiation dosage for the various motor components is under investigation. For example, in Reference 7-1 it is conservatively estimated that maximum exposure dose to the liner or grain of a solid rocket motor for a 1 year exposure in the most severe Van Allen region would be of the order of  $1 \times 10^6$  rad. This estimate is based on an order-of-magnitude analysis of the flux in the Van Allen belts, and on the assumption that the motor has a metal case which will shield the interior from low energy particles. (Because of their higher energy, particles of proton radiation are the most important source of damage.) The glass case used on the Voyager motor would also provide an effective radiation shield for the grain (Reference 7-2). However, the retromotor is entirely surrounded with metal structure in the spacecraft which provides a further radiation shield for the motor. Since the Voyager flight is less than a year (6 to 9 months) during which the residence time in the Van Allen region (1400 to 12,000 mile altitude) would be approximately 15 minutes; and since the doses due to solar flare particles, the solar wind, solar electromagnetic radiation, and cosmic rays are small (References 7-1, 7-2) (radiation from solar flares is estimated at less than 10 per cent of the Van Allen dose rates); the estimated  $10^6$  radian dose for the Voyager should be conservative.

A considerable number of tests have been performed at Wright Air Development Division to determine the threshold of degradation caused by gamma radiation of commercially available structural

plastic materials (Reference 7-3). The effects of gamma radiation and elevated temperature simultaneously on glass-reinforced plastic laminates were also investigated. In general, the mechanical and electrical properties of reinforced plastic laminates of various resin types were not adversely affected by gamma radiation of a maximum dosage of  $7.8 \times 10^8$  rad. This dosage is far more severe than would be encountered in many years of exposure to Van Allen radiation.

Two series of experiments were conducted at Jet Propulsion Laboratory (Reference 7-2) and Battelle Memorial Institute (Reference 7-1) to determine the effects of radiation on propellants with various types of binder systems. The results are summarized on Figure 7-6 through 7-10. These data show that all of the propellants tested were able to absorb a dose of  $10^6$  rad with negligible change in mechanical or ballistic properties.

While these data combined with the previous estimates of radiation dosages are a strong indication that a radiation problem does not exist, this problem cannot be neglected in future work. It will be necessary to understand fully the radiation problem so that a confident prediction of radiation absorption effects in the retromotor can be made. With these results as a background, testing must be performed on the specific materials selected for the retromotor design to determine the effect of this radiation on the potential failure modes in the motor. Only in this way can the requisite high motor reliability be assured.

b. Hard Vacuum

In space between earth and Mars the ambient pressure is estimated to be approximately  $10^{-8}$  torr. Under these conditions, volatile materials will evaporate from the surface and escape. The rate of evaporation (Reference 7-4) is dependent on the equation

$$G = KPA \left( \frac{M}{T} \right)^{1/2},$$

where  $G$  = Weight loss per unit time

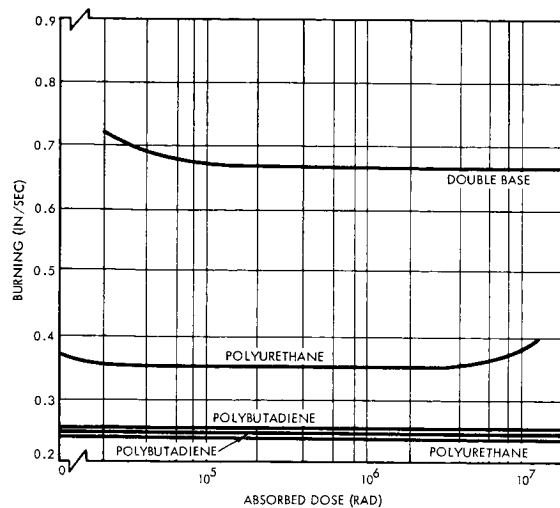


Figure 7-6. Propellant Burning Rate Versus Absorbed Radiation

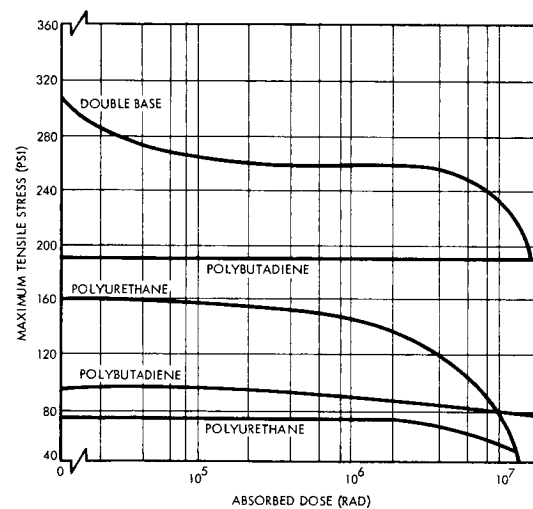


Figure 7-7. Maximum Tensile Strength Versus Absorbed Radiation

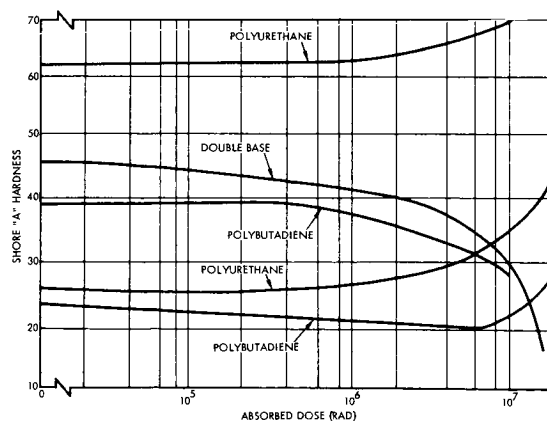


Figure 7-8. Per Cent of Strain Versus Absorbed Radiation

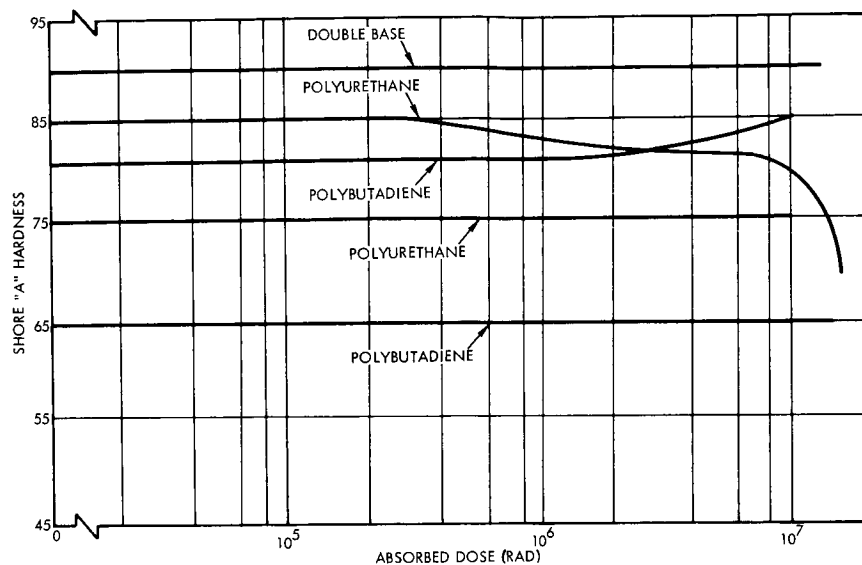


Figure 7-9. Shore "A" Hardness Versus Absorbed Radiation

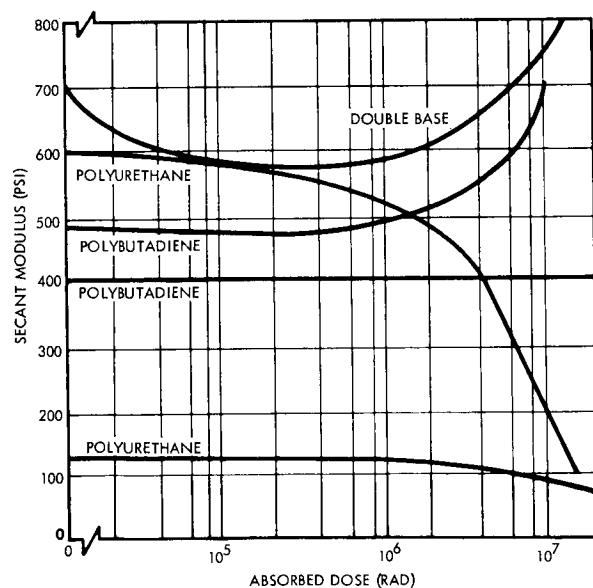


Figure 7-10. Secant Modulus Versus Absorbed Radiation

K = Dimensionless constant (see Reference 7-1 and 7-5)

P = Vapor pressure of the specie evaporating

A = Characteristic area

M = Molecular weight

T = Temperature of the specie evaporating.

This equation indicates that to minimize G it is necessary to avoid the use of materials with high vapor pressures. However, this equation also indicates that the weight loss can be reduced by minimizing the area.

The area term in the above equation depends on the physical conditions. For a body in a vacuum, A is the surface area of the body. If the body is inside a container and the container has a small opening in relation to the mean free path of the molecules within the container, A is the area of the opening if the container is submerged in the vacuum. This would be the case for a rocket and A would be the throat area. Inside the container the molecules emitted from the surface accumulate until an equilibrium number are present. At this condition, some molecules are emitted from the surface and at the same time other molecules are striking and condensing. Occasionally a molecule will escape out of the opening in accordance with the above equation. The only weight loss is caused by those escaping molecules.

If the throat can be sealed, the weight loss can be made negligible. The pressure inside the motor will then be the vapor pressure of the evaporating species. In a solid rocket the vapor pressure should be relatively low, and normal sealing techniques should yield escape areas which essentially eliminate weight loss from the inside of the motor.

The external surface of the fiberglass case, while partially shielded by the structure, will have to be capable of prolonged exposure

to hard vacuum. An indication of the ability of this material to withstand hard vacuum is contained in Reference 7-5. Specimens were exposed to a radiant energy flux concentrated in the range from 2500 to 5800 angstroms but equivalent in amount to the solar constant temperatures of 300°F and reduced to pressures of  $10^{-6}$  to  $10^{-7}$  torr. It was observed that no significant degradation occurred in 500 hours of exposure. When exposed to vacuum and a temperature of 300°F, a polyester laminate lost approximately 2 per cent in weight and 20 per cent in strength. However, the epoxy and phenolic laminates lost only 0.5 and 1 per cent in weight, respectively, and experienced no loss in strength. It is concluded (Reference 7-5) that the extent of degradation in epoxy and phenolic laminates is a function of temperature rather than high vacuum or combined high vacuum and temperature. Certainly, further work is indicated.

### 2.3.2 Nozzle Development

As has been stated previously, development of a nozzle capable of withstanding the 100 sec burn time with low throat erosion may turn out to be a problem. No engines of comparable size and performance have been developed to date with as long a burn time. (In the large solids such as the Titan III booster which have comparable burning times, the change in the throat area is not a problem since the erosion rate is not critical in nozzles of this size.) Although the tungsten throat is expected to greatly decrease the potential problem, special attention will be required to provide sufficient support for the insert. The regressive pressure characteristic will help here since the pressure and heat-rate loads will drop as the firing time increases. Also, the thermal environment of the proposed motor should not cause surface melting of the tungsten material. It is concluded that development of this component is only a slight extension of the current state of the art which should be accomplishable by development of current techniques rather than innovation.

## 2.4 Reliability

The following analysis of the reliability of a solid retromotor for Voyager was extracted from the technical backup material prepared by Aerojet-General. While it cannot be considered to be a definite treatise, it is a reasonably cogent approach to this difficult problem.

For reliability estimating purposes, the successful performance of a solid rocket motor may be represented as the successful functioning of a small number of independent components. To be considered successful, a component must maintain structural integrity prior to and during the firing and must not interact in an untoward manner with other components. Further, certain prime components (igniter, propellant, and TVC) must deliver the required ballistic performance. Using the simple product rule, a preliminary estimate of motor reliability for a new design can be calculated as the product of these individual component reliabilities.

The best estimate for these component reliabilities for this program can be obtained by examining the record for similar components developed in previous programs and evaluating the results in terms of the conditions that will be applicable during the development of the proposed retromotor.

Table 7-4 depicts the historical pattern of failure rate reduction experienced for the same basic types of components to be used in the retromotor. Note that the four sections of the nozzle (entrance, throat, exit, and extension) are considered as separate components since they are made of different materials and are exposed to different loads and environments.

In calculating the failure rate for a typical component, each basically different configuration evolved during a given program was considered to represent a new learning series and the occurrence of failures was classed in accordance with the number of tests of that configuration. In applying the data to a new program, it must therefore

be assumed that a certain number of early development tests will be required before the final configuration is evolved.

To obtain an over-all picture of the trend in failure rate reduction, the data for all components was pooled and the average rate calculated for increments of five tests. The results are shown in Figure 7-11.

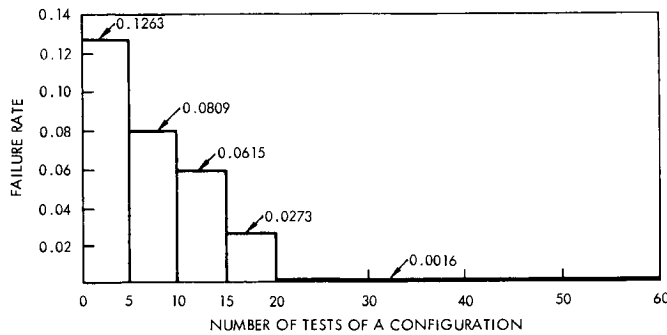


Figure 7-11. Results of Failure Rate Tests

As can be seen, the failure rates are reduced steadily in successive increments. Most of this reduction results by resolving design problems and eliminating or controlling unanticipated failure modes. After the 20th test of a configuration, failures rarely occur. In Table 7-5 both the total firings for configurations tested more than 20 times and the number of post-20th test failures are shown. A statistical test indicated that none of the observed failure rates, save that of the case, differed significantly from each other or from zero. Further analysis indicates that the seven failures occurring in the 4169 post-20 tests were primarily of two types. One type resulted from schedule pressures on certain programs which forced the use, in static development tests, of obsolete configurations which had experienced previous failures and whose replacements were not yet available. These failures typically occur in the 20th to 40th test of a configuration. Significantly, no such failures occurred in flight tests or in motors delivered to the customer. The second type of failure appears to be more random in nature. This type of failure can be caused by a rare combination of forces or conditions or a random undetected process error.

Because the development and delivery schedule for the retromotor



Table 7-4. Failure Rate Reduction History for Components  
Similar to Voyager Design

<u>Component</u>	<u>1 to 10 Tests</u>	<u>11 to 20 Tests</u>	<u>Over 20 Tests</u>
Case	0.06122	0.03703	0.01449
Insulation	0.03415	0.00990	0.00245
Propellant	0.00000	0.00000	0.00000
Igniter	0.00000	0.00000	0.00411
Auxiliary TVC	0.26000	0.03226	0.00000
Nozzle Entrance	0.10126	0.00000	0.00000
Nozzle Throat	0.23626	0.12281	0.00255
Nozzle Exit	0.09396	0.04545	0.00000
Nozzle Extension	0.00000	0.00000	0.00000

Table 7-5. Failure Rates After the 20th Test

<u>Component</u>	<u>Tests</u>	<u>Total Tests For Configu- rations Tested More Than 20 Times</u>	<u>Failures After 20th Test</u>	<u>Post-20th Test Observed Failure Rate</u>	<u>Post-20th Test Observed Reliability</u>
Case	153	87	1	0.01149	0.98851
Insulation	596	409	1	0.00245	0.99755
Propellant Grain	90	45	0	0.00000	1.00000
Igniter	311	243	1	0.00411	0.99589
Auxiliary TVC	114	31	0	0.00000	1.00000
Nozzle Entrance	593	464	0	0.00000	1.00000
Nozzle Throat	2162	1872	4	0.00255	0.99745
Nozzle Exit	1200	1005	0	0.00000	1.00000
Nozzle Extension	42	13	0		
Total	5263	4169	7		

does not contain the schedule pressure that caused the failures in the case and insulation components, it is reasonable to exclude these malfunctions in calculating the estimated failure rate for Voyager components. It is further proposed that the remainder of the test and failure experience be pooled to obtain the best estimate for Voyager component failure rates for the following reasons:

- The remaining failures occur randomly and stem from causes that are random in nature
- There is no significant difference in the observed failure rates, once the early development failures are excluded
- It appears that these random design and process error type of failures could occur on any component.

The resulting pooled component failure rate of five failures per 4169 tests can be viewed as measure of the likelihood of encountering a random design or process error failure on a developed component, as evidenced by historical data.

Although the five failures per 4169 tests appears to be an accurate estimate of the historical failure rate for configurations tested over 20 times it does not completely reflect the type of reliability and quality control program proposed for the retromotor program. To provide added assurance that the system reliability goal for the retromotor of 0.99 is met, certain additional reliability activities will be undertaken to reduce the probability of encountering the types of design or process error that produced the five failures. It is estimated that these activities should reduce the probability of design failures by 50 per cent and the probability of process error failures by 90 per cent. Table 7-6 presents an evaluation of these failures. The resulting residual failure rate of 0.000312, based on a total 1.3 failures per 4169 tests is therefore used for retromotor component reliability.

The 0.000312-failure rate is equivalent to a component reliability of 0.999688. Raising this to the 9th power (for the nine components

shown in Table 7-4) yields a predicted reliability of 0.99719, compared to the goal of 0.99. Even though the environmental conditions will be more severe for Voyager than most of the programs used in the historical data, the integrated test program will provide ample opportunity for early detection of induced failure modes such as vacuum-aging. It is expected that the learning rate evidenced in past programs will be equaled or exceeded on the Voyager retromotor program.

Table 7-6. Evaluation of Historical Failures

<u>Component</u>	<u>No. of Failures</u>	<u>Cause of Failure</u>	<u>Probability of Occurrence in Voyager Motor (%)</u>	<u>Evaluated Residual Number of Failures</u>
Igniter	1	Design	50	0.5
Nozzle Throat	1	Design	50	0.5
Nozzle Throat	3	Process Control (Inadequate NDT Criteria)	10	0.3
				<hr/> 1.3

## 2.5 Preliminary Design Requirements

A preliminary design specification was prepared for the six contractors to obtain preliminary design information. This section presents the unabridged specification. Section 2.6 summarizes the design solutions which were submitted in response to these requirements.

# PRELIMINARY DESIGN REQUIREMENTS

## VOYAGER RETRO ROCKET

### 1.0 SCOPE

This document outlines design requirements for a solid propellant rocket motor to be used to retro the Voyager spacecraft from a fly-by trajectory into Mars orbit. Since the TRW study is at present only conceptual, the requirements presented are intended only as guides to preliminary design and are not firm; exceptions are permitted if it can be shown that corresponding benefits accrue.

### 2.0 DESIGN REQUIREMENTS

#### 2.1 Ballistic Performance (Vacuum Conditions)

2.1.1 Velocity imparted to a 2300 lb payload shall be 7000 ft/sec with a standard deviation less than 0.25 per cent over the range of environments in paragraph 2.6.

2.1.2 Thrust level to limit axial acceleration with 2300 lb payload to 3 g (2.5 g preferred).

2.2.2 Diameter not to exceed 48 inches exclusive of attachments.

2.2.3 Over-all length not to exceed 52 inches, except that the length may be increased up to an additional 4 inches if a well of comparable length is provided in the forward end.

2.2.4 Motor to be symmetrical about thrust axis. A single fixed nozzle is considered desirable.

2.2.5 Motor design is to be compatible with provision of attachment surfaces capable of transmitting specified loads and permitting alignment to precision required. Location is not identifiable at this time.

#### 2.3 Mechanical Alignment and Thrust Vector Control

2.3.1 Loaded motor center of gravity radial offset from the motor axis is not to exceed .05 inch.

2.3.2 The thrust vector control device must be capable of generating upon command any desired thrust deflection up to 4 degrees and a total control impulse of up to 1 per cent of axial total impulse. Roll control is not required. Frequency response shall be 5 cps minimum.

2.3.3 With the TVC system nulled, the nozzle axis must be parallel to the motor axis within .001 radian and coincident within .010 inch laterally. The thrust axis is assumed to be coincident with the nozzle axis when no defection is commanded.

2.3.4 Nozzle erosion is to be sufficiently uniform to insure:

2.3.4.1 Compliance with ballistic performance tolerances;

2.3.4.2 Lateral shift in centroid of nozzle throat (post burn) not to exceed .02 inch.

## 2.4 Igniter

2.4.1 Redundant squibs and firing circuit wiring are mandatory; redundant igniter charges are optional.

2.4.2 An electromechanical S and A device shall provide electrical safety between the power supply and the squibs and interpose a mechanical barrier between the squibs and subsequent pyrotechnic train until such time as the ability to achieve actuation (arming) is desired.

2.4.3 The igniter charge shall be a separable subassembly.

2.4.4 Access for manual safing and visual status readout of the S and A will be provided.

2.4.5 The igniter must be capable of firing if only one of the redundant squibs in the S and A fires.

## 2.5 Nozzle Seal

A nozzle seal shall be provided to insure against loss of propellant volatiles and to promote ignition.

2.5.1 The nozzle seal must maintain at least 5 psia internal pressure after 9 months assuming 1 atmosphere at launch.

2.5.2 The nozzle seal shall provide thermal insulation at least equal to the case insulation in the motor aft end.

2.6 Environmental Constraints

The motor must perform within requirements of paragraph 2.1 when exposed to any combination of the following environments.

2.6.1 Acceptable firing temperature limits are 40°F to 90°F. Reliable performance within specification over broader limits is desirable.

2.6.2 Flight acceleration.

2.6.2.1 Prior to ignition, nozzle end is forward.

2.6.2.1.1 Up to 12 g axial.

2.6.2.1.2 Up to 3 g lateral.

2.6.2.2 During burning.

2.6.2.2.1 Up to 3 g axial.

2.6.3 Flight vibration, any axis.

2.6.3.1 Sinusoidal

<u>Frequency, cps</u>	<u>RMS g level</u>
10 - 100	3.5
100 - 300	5.0
300 - 2000	7.5

2.6.3.2 Gaussian Random

<u>Frequency, cps</u>	<u>Level <math>g^2</math>/cps</u>
20 - 300	0.04
300 - 2000	0.12

2.6.4 Vacuum exposure for 9 months.

2.6.5 Magazine storage up to 2 years in any attitude, and at any temperature between 30°F and 100°F.

2.7 Safety Considerations

2.7.1 Propellants containing beryllium are acceptable.

2.7.2 Motor including igniter and S and A to be capable of 20 foot drop onto steel-faced reinforced concrete without ignition or explosion and must be safe to dispose of.

2.7.3 Electrical safety. An electromechanical S and A device is required for primary ignition safety.

2.7.4 Structural safety factor. Motor pressure vessel stress at mean + 3 sigma maximum temperature reached during firing.

2.8 Design manufacture, and inspection should be consistent with a reliability goal of 0.99.

## 2.6 Contractors' Design Solutions

This section summarizes the design solutions submitted by United Technology Center, Aerojet-General Corporation, Lockheed Propulsion Company, and Hercules Powder Company in response to the requirements given in Section 2.5.

### 2.6.1 United Technology Center (UTC)

UTC proposed two designs which differed mainly in choice of case material. The propellant is a state-of-the-art formulation (polybutadiene-acrylic acid-acrylonitrile/ammonium perchlorate/aluminum) developed for use in the Titan III-C booster, which differs from that motor's current propellants only by a burning rate additive. The burning rate is 0.21 in/sec with rate exponent  $n = 0.24$  and temperature sensitivity coefficient,  $\pi_r$ , of 0.11 per cent/ $^{\circ}\text{F}$ . Density is 0.064 lbm/in<sup>3</sup> and the pressure sensitivity coefficient,  $\pi_k$ , is 0.15 per cent/ $^{\circ}\text{F}$ .

The grain is a case bonded conocyl design with a circular port resulting in a regressive thrust-time curve to limit the maximum acceleration to approximately 3 g's. The two case options have slightly different geometrical configurations to minimize case weight. The fiberglass case, which UTC selected for prime emphasis, has a cylindrical section with optimumly-contoured elliptical ends. This configuration is shown in Figure 7-12. The steel case was nearly spherical, resulting in a 1 inch greater diameter. The nozzle consisted of a submerged graphite throat with an ablative nozzle extension. The length restriction limits the expansion ratio to 30 with a 20 degree half-angle conical nozzle. A forward-mounted pyrogen igniter is employed. Internal insulation is provided by General Tire and Rubbers' V-3050 insulation.

A secondary injection liquid freon TVC system is utilized. The pintle-modulated injector valves are scaled-down versions of the Titan booster design which are actuated by an off-the-shelf torque motor. The injectant is stored in a bladder inside the motor, eliminating an external propellant tank container and pressurization source. This



concept has been demonstrated by subscale firings at UTC and shows an ultimate performance advantage of nearly 40 pounds over the conventional methods.

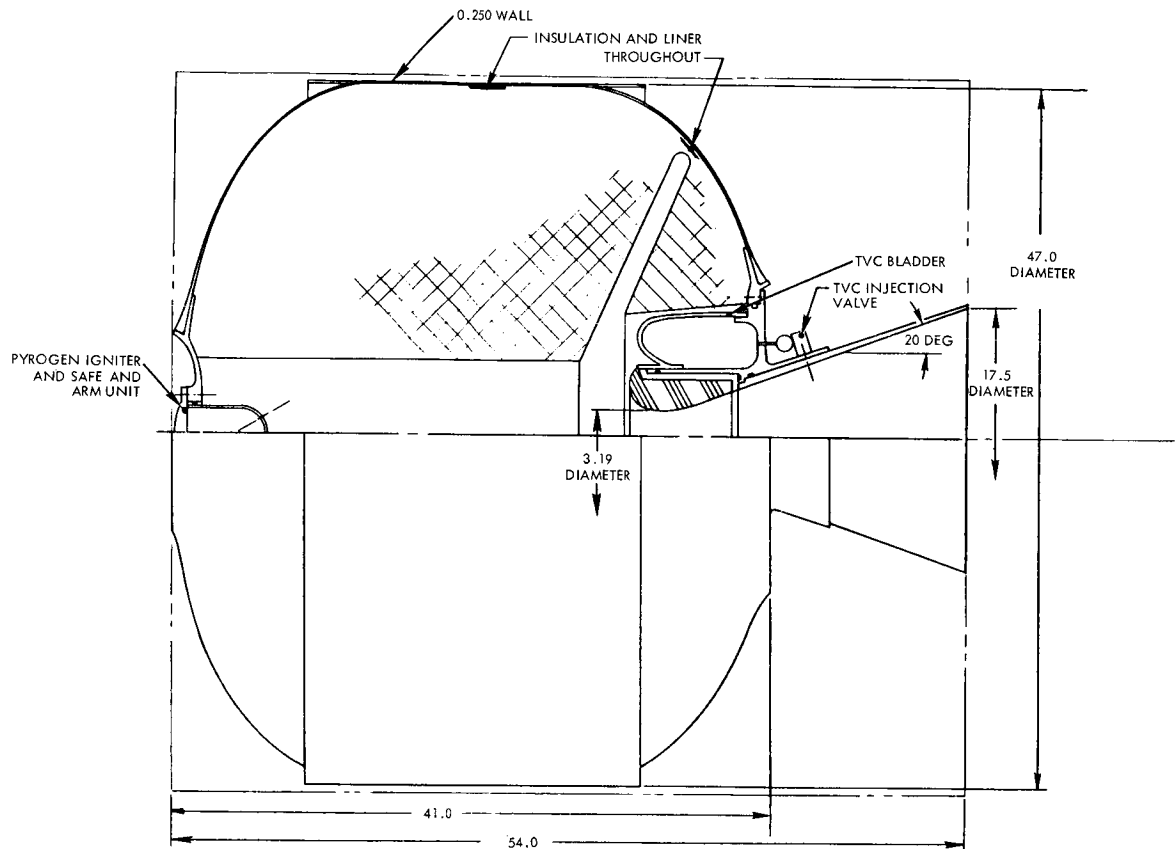


Figure 7-12. United Technology Center Design

#### 2.6.2 Lockheed Propulsion Company (LPC)

LPC proposed three possible motor configurations which differ primarily in the choice of propellant. The three candidate propellants were: 1) a conventional rubber-based propellant containing 18 per cent Al (carboxy-terminated polybutadiene/ammonium perchlorate/aluminum), 2) a modified double-based propellant containing 16 per cent aluminum and a solid oxidizer, and 3) a high-performance version of No. 2 containing 10 per cent Be instead of the aluminum. Propellant No. 1 is Class 2 (nondetonable) while No. 2 and No. 3 are Class 9.

Several alternate grain designs were evaluated prior to selection of the proposed grain which is a casebonded, modified end burner with slots in the aft end to give the required regressive characteristics. The maximum acceleration for the propellant No. 1 was approximately 2.8 g while the double base propellants result in a maximum 3.0 g because of differences in the burning rate.

Three materials (maraging steel, titanium, and fiberglass) were initially considered as case material candidates. A preliminary comparison showed that fiberglass was the lightest by 34 to 44 per cent. Based on the limited environmental interaction data available, it was concluded that the required storage in space would not present a structural problem for the fiberglass material. This material is, therefore, proposed in the baseline design. The nozzle is a contoured, partially submerged design which possesses the same efficiency as a 20 degree conical nozzle. The expansion ratio was in the range of 75 to 81. The throat is a composite design with pyrolytic graphite washers to reduce erosion. The nozzle is completely ablative, using graphite and silica phenolics. Dual pyrogen igniters are mounted in an aft location. Insulation is Buna "N" for the rubber based propellant and butyl rubber for the double base options. The configuration is shown in Figure 7-13.

A swivel nozzle TVC concept was selected at the conclusion of a preliminary comparison which also included a secondary injection liquid TVC system. The selected "Lockseal" design is a toroidal structure of alternating rubber and steel spherical rings in which angular motion is accommodated by shear in the rubber. This is a Lockheed proprietary design which is currently being developed under Air Force sponsorship.



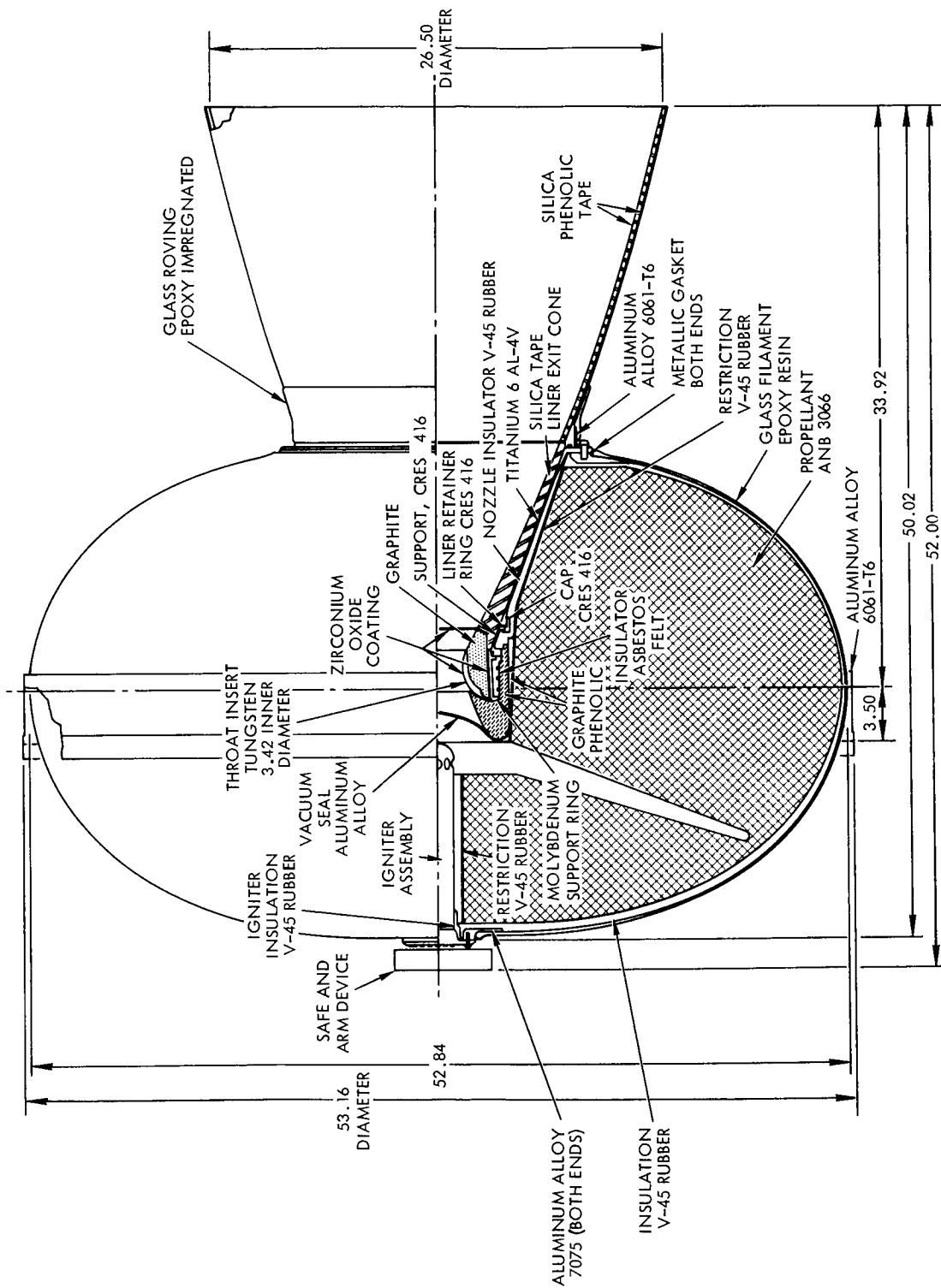


Figure 7-14. Aerojet-General Corporation Design

section. An alclojet igniter is used located in the motor head-end. The insulation is General Tire Company's V-45 silica rubber which is extensively used in Minuteman and Polaris.

Three TVC systems were initially considered: liquid secondary injection, translatable nozzle, and a solid gas generator auxiliary thruster. AGC chose the latter system on the basis that it was the most reliable and least costly. A system of this type is employed for roll control on one model of Minuteman. This system showed a weight advantage of 43 pounds over the secondary injection system but was 30 pounds heavier than the translatable nozzle.

#### 2.6.4 Hercules Powder Company

Hercules limited their consideration to propellants which contain beryllium. This resulted in a conclusion that the requirements could be met by one of several propellants which are now in early development. Use of one of the better characterized Be propellants was prohibited by the burning rate requirement ( $r \leq 0.3$  in/sec). A slotted tube grain design is used and the resultant maximum acceleration is 3 g. A layout of the proposed configuration is shown in Figure 7-15.

The case material is fiberglass and EP-87 insulation is used. A submerged nozzle is used which employs a graphite throat and uses silicatape phenolic and carbon-tape phenolic in the entrance and exit section. The nozzle is conical with 23 degree divergence half angle allowing an expansion ratio of 32. TVC is provided by a secondary injection of liquid freon.

### 3. MIDCOURSE PROPULSION SUBSYSTEM

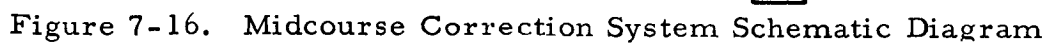
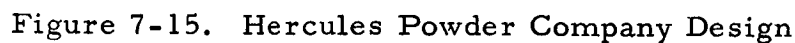
The midcourse propulsion subsystem (MPS) study began as a comparison between various schematic arrangements of pressurization control schemes. The object was to trade off reliability against weight to determine an optimum configuration. However, it became obvious that this analytical technique was unsatisfactory because the reliability estimates of nearly all of the various redundant arrangements approached

unity (on paper) and the weight differences were relatively insignificant.

The selected system, shown schematically in Figure 7-16, is thus justified more on engineering judgement and some experimental tests than on the analytic optimization. The system is characterized by a combined gas storage and propellant tank which is operated in a blowdown mode, a single monopropellant engine, and explosive-actuated flow control valves with a backup solenoid valve. The weight penalty associated with this system, as compared to the conventional regulated pressure systems, was originally estimated to be 18 pounds. This penalty is believed to be overly conservative in consideration of tests performed during the study to verify performance of a monopropellant engine when operated in the blowdown mode. These tests, summarized in Figure 7-17, show that the engine, nominally designed for 50-pound thrust, will operate smoothly and at essentially constant performance over a thrust range of 25 to 75 pounds (down to a chamber pressure of 80 psia). Hence the pressurant weights assumed in the study could probably be reduced by 25 per cent. Based on this evidence and the advantages of the selected system in terms of ultimate reliability, design simplicity, and minimum spacecraft interactions, the blowdown system was judged to be superior to any of the other schemes.

### 3.1 Thrust Chamber Design

The thrust chamber design proposed for the MPS, shown in Figure 7-18, is an adaptation of the 50-pound thrust Ranger engine, the major difference being the use of a spontaneous catalyst in place of the H-7 catalyst. This modification permits multiple starts without the complication of multiple  $N_2O_4$  start cartridges. Another modification includes the control valve arrangement which provides for potentially unlimited starts through the use of a solenoid backup valve. TRW Systems fabricated a prototype motor (Figure 7-19) during the study period to verify performance and ability to function in the proposed blowdown mode. The test results, as previously shown, were successful.



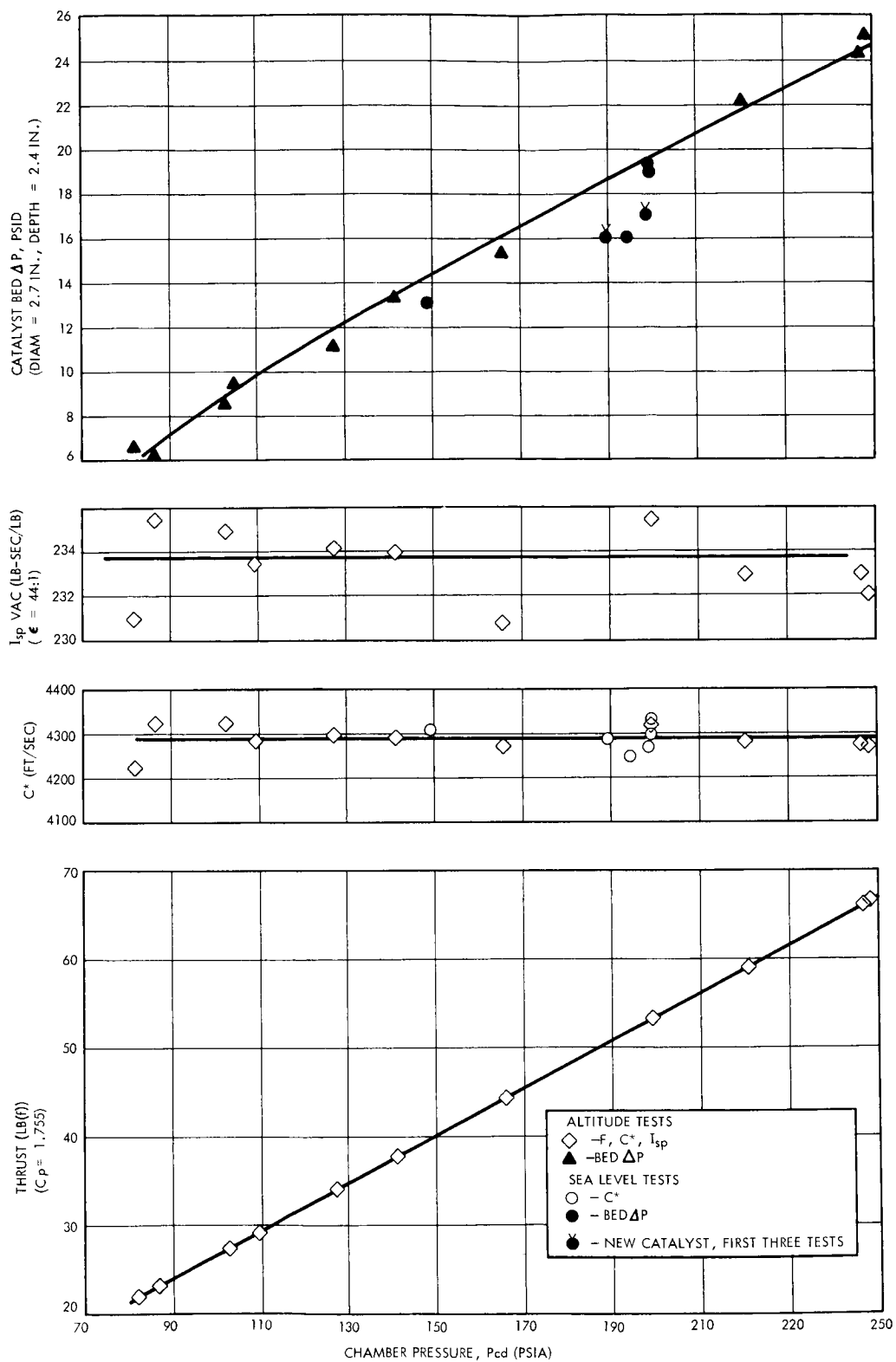


Figure 7-17. Voyager Midcourse Propulsion System  
50 Lb (f) Monopropellant Hydrazine --  
Preliminary Test Data



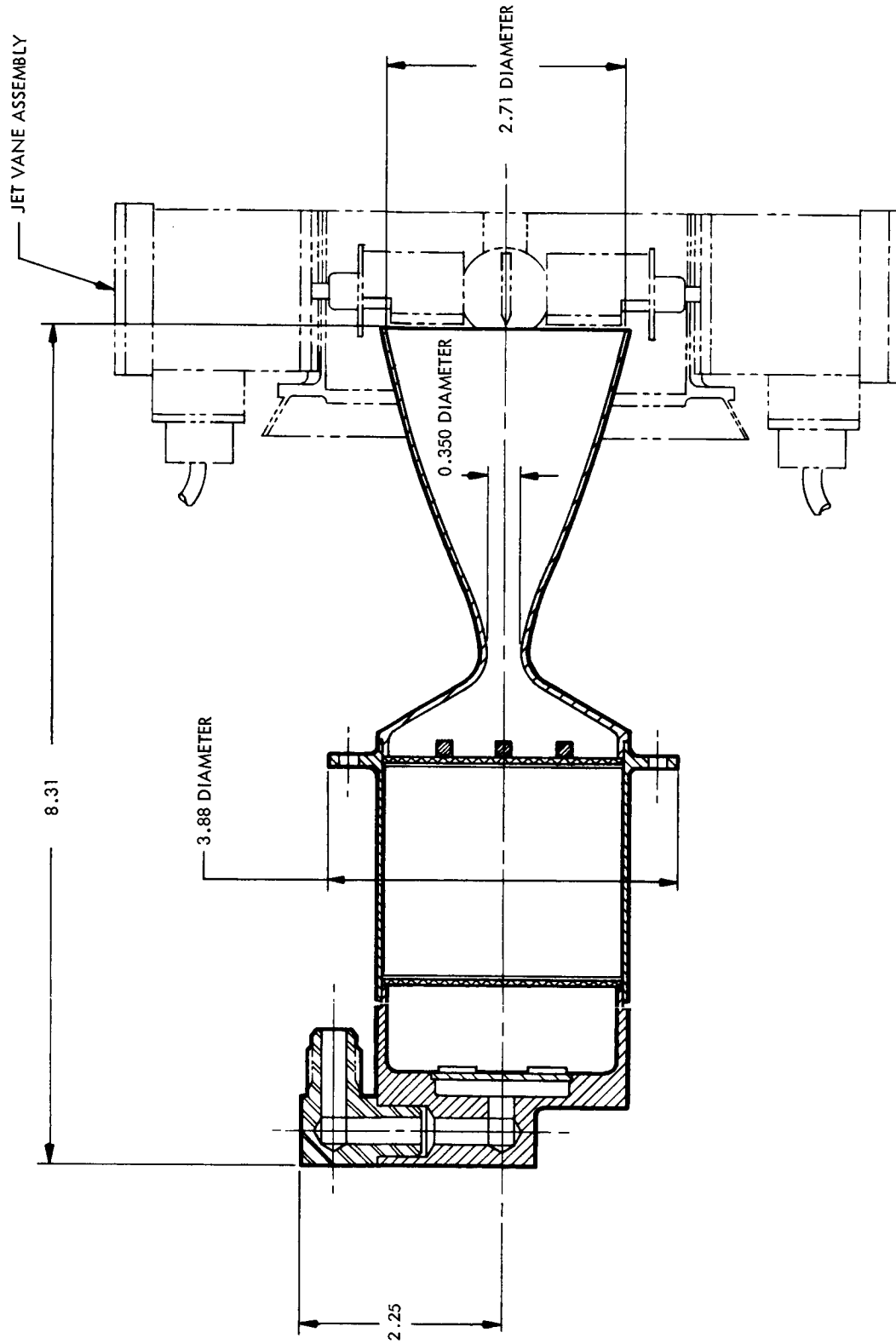


Figure 7-18. Midcourse Voyager

### 3.1.1 Thrust Level Selection

The governing restraint on the thrust level for the midcourse maneuver is the minimum  $\Delta V$  requirement. The minimum increment objective of 0.1 m/second can readily be achieved for thrust levels of the order of 50 to 100 pounds. Since lower thrust levels would result in unnecessarily long burning times with little weight savings or effective improvement in accuracy and the 50-pound thrust engine has proven to be successful in both the Ranger and Mariner applications, this value was chosen for the Voyager mission.

### 3.1.2 Thrust Chamber Configuration

The multiple start requirement entails the most significant change to adapt the Ranger thrust chamber to Voyager. Of the two approaches immediately available, the substitution of a spontaneous catalyst or the use of multiple start slugs, the former is preferable. Multiple start slugs were successfully employed on the Able-4 and -5 monopropellant hydrazine propulsion system (18-pounds thrust) built by STL in 1959, (Reference 7-6). This system was built before the successful development of a spontaneous hydrazine catalyst and incorporated complications and subsequent reliability penalties not necessary within the present state of the art.

Two spontaneous catalysts (Shell 405 and STL 1404-21) which are capable of reliably igniting hydrazine and meeting the Voyager mission requirements are now available. Although modification to the Ranger bed configuration will be necessary because of the difference in shape, porosity, and activity between spontaneous catalysts and H-7, they can be accomplished without major alteration of the head-end or nozzle. The head-end would be modified to eliminate the  $N_2O_4$  injection port and the nozzle would remain unchanged.

However, two basic considerations in the use of spontaneous catalyst must be noted. First this type of catalyst is inherently weaker than the H-7 type because of the structure of the catalyst support

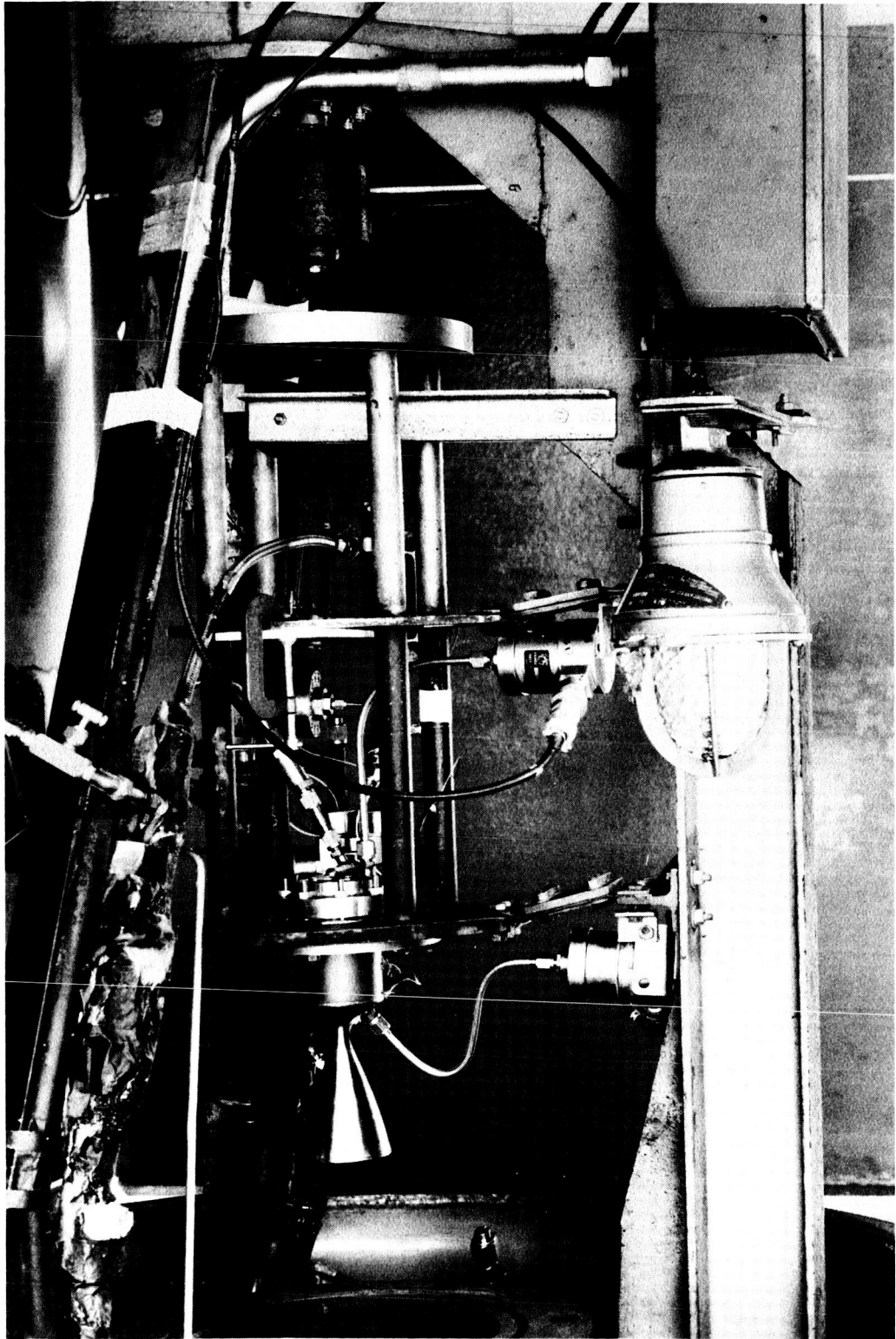


Figure 7-19. Prototype Motor

material. The crush strength of Shell 405 is about half that of H-7, and the catalyst bed design and qualification must be guided by this fact. Second, no spontaneous catalyst system has been qualified under space vacuum. While it is unlikely that any serious deterioration of the catalyst would ensue, an experimental evaluation of the effect of prolonged exposure of the catalyst to high vacuum should be undertaken as soon as possible.

### 3.2 Monopropellant Feed System

The blowdown feed system selected for the midcourse propulsion subsystem, illustrated in Figure 7-18, is similar in concept to the Able-4 and -5 monopropellant hydrazine pressurization and feed systems built at TRW in 1959. The feed system contains no electrical controls, regulators, or other functional components. The fill and vent valves are manually operated and can be capped and permanently sealed after the system has been loaded and pressurized. The system was selected over the more conventional regulated pressure systems although the regulated systems are approximately 18 pounds lighter and can be made sufficiently reliable by various redundant arrangements of components.

Some justification for the blowdown system can be made on the basis of fewer components and spacecraft interactions in terms of electrical circuitry and CS and C inputs. However, the primary attraction is the inherent simplicity of the concept.

A discussion of alternate systems evaluated and eventually rejected is presented in Appendix J.

#### 3.2.1 Operation

The system characteristically operates with decaying thrust as the pressurization gas expands and propellant inlet pressure decreases. Hence, burning time required to produce a velocity correction is dependent on the initial conditions in the tanks. If an accelerometer were used to measure the velocity increment, this would be inconse-

quential but the accelerometer is not required since the system can be calibrated so that the burn time to produce a prescribed velocity increment can be predicted to within the required tolerance. This mode of operation requires that expended propellants be accounted for and that either pressure or temperature of the tanks be monitored. A third option is using the accelerometer as an override to terminate thrust if the velocity increment is attained in less than the predicted time. It was tentatively decided not to use the accelerometer. However, this decision should be reevaluated in the light of the empirical characterization of the entire subsystem.

### 3.2.2 Pressurization Gas

Helium was selected as the pressurant instead of  $N_2$  because of a weight saving of approximately 10 pounds. A discussion of the concomitant leakage problem associated with He is given in Appendix J. In brief, the discussion concludes that even in a bipropellant system, for leakage rates as determined by conventional techniques, the leakage would be an insignificant amount, of the order of  $6 \times 10^{-4}$  lb/yr. The leakage of helium across the bladder into the hydrazine will eventually result in saturating the hydrazine. This will produce a small predictable throttling of the engine which could be accounted for in the programmed commands.

The potential problem associated with helium coming out of solution to form a bubble on the wrong side of the bladder, because of the reduction in tank pressure during a firing has been shown not to be serious. In recent tests conducted at TRW where helium gas was mixed with hydrazine, as a means of throttling the propellant flow, no ill effects on combustion stability or efficiency were detected. Hence it is clear that the bubble, if trapped in a high velocity region such as the feed line, would pass through the injector with negligible effect. If trapped in the tank, the bubble would simply float to the top.

### 3.2.3 Expulsion Device

The rubber bladder design, successfully used on Mariner, was selected without considering alternate designs. It is interesting to note that, whereas selection of the expulsion device for the monopropellant system is straightforward, the same problem for the oxidizer in the bipropellant system is considered difficult.

### 3.2.4 Selection of System Design Pressure

An optimization technique for a blowdown system tank design is given in the JPL memo\*. A simplified but similar analysis given in Appendix J was conducted during the study. The analysis showed that the optimum tank pressure is of the order of 600 psia, a pressure that was thus tentatively selected and used for weight purposes. However, the analysis was based on a conservative estimate of a practical lower limit for chamber pressure. Tests conducted during the study showed the feasibility of operating the engine at pressures as low as 80 to 100 psia. Hence, the optimum pressure and ultimately system weight would be reduced. The exact extent and actual optimum conditions can best be determined empirically.

## 4. BIPROPELLANT PROPULSION SYSTEM

### 4.1 Voyager Bipropellant Engine Design

As discussed in the Introduction, the bipropellant engine constituted a fundamental part of one of the alternate configurations studied for Voyager, the Configuration B defined in detail in Volume 4. The preferred configuration adopted instead a solid propellant retropropulsion engine in conjunction with a monopropellant midcourse engine. Configuration B, however, called for the bipropellant engine to perform both of these roles. Since these dual functions are optimally provided by engines of widely different thrust levels, the design making use of a single engine must be based on a compromise between the conflicting requirements.

---

\* D. H. Lee, J. S. Martinez, A. F. Grant, Jr., "A Monopropellant-Hydrazine Thrust Unit for Velocity Control of Extraterrestrial Vehicles," JPL Memorandum No. 20-161, 3 February 1958 (C)

Ignoring state-of-the-art considerations of bipropellant engines, the total system performance and impulse accuracy design criteria dictate a thrust level in the general range of 600 to 800 pounds. Unfortunately, the resultant burning times during the retromaneuver, 1200 to 1400 seconds, are pushing the technology of nonregeneratively cooled high performance bipropellant engines. Hence, a more conservative thrust level of 1000 pounds, consistent with chamber life currently being demonstrated on the LEM DE was selected. Similarly, a 100-psia chamber pressure was selected because of current ablative chamber experience rather than system optimization analysis. The engine configuration used as a base point to compare the system potential between the bipropellant single-engine propulsion subsystem and the combination of monopropellant for midcourse and solid propellant for retropropulsion is shown in Figure 7-20. The engine is characterized by a single element coaxial injector; an all ablative lined chamber, throat, and nozzle divergent section; and a quad redundant bipropellant valve.

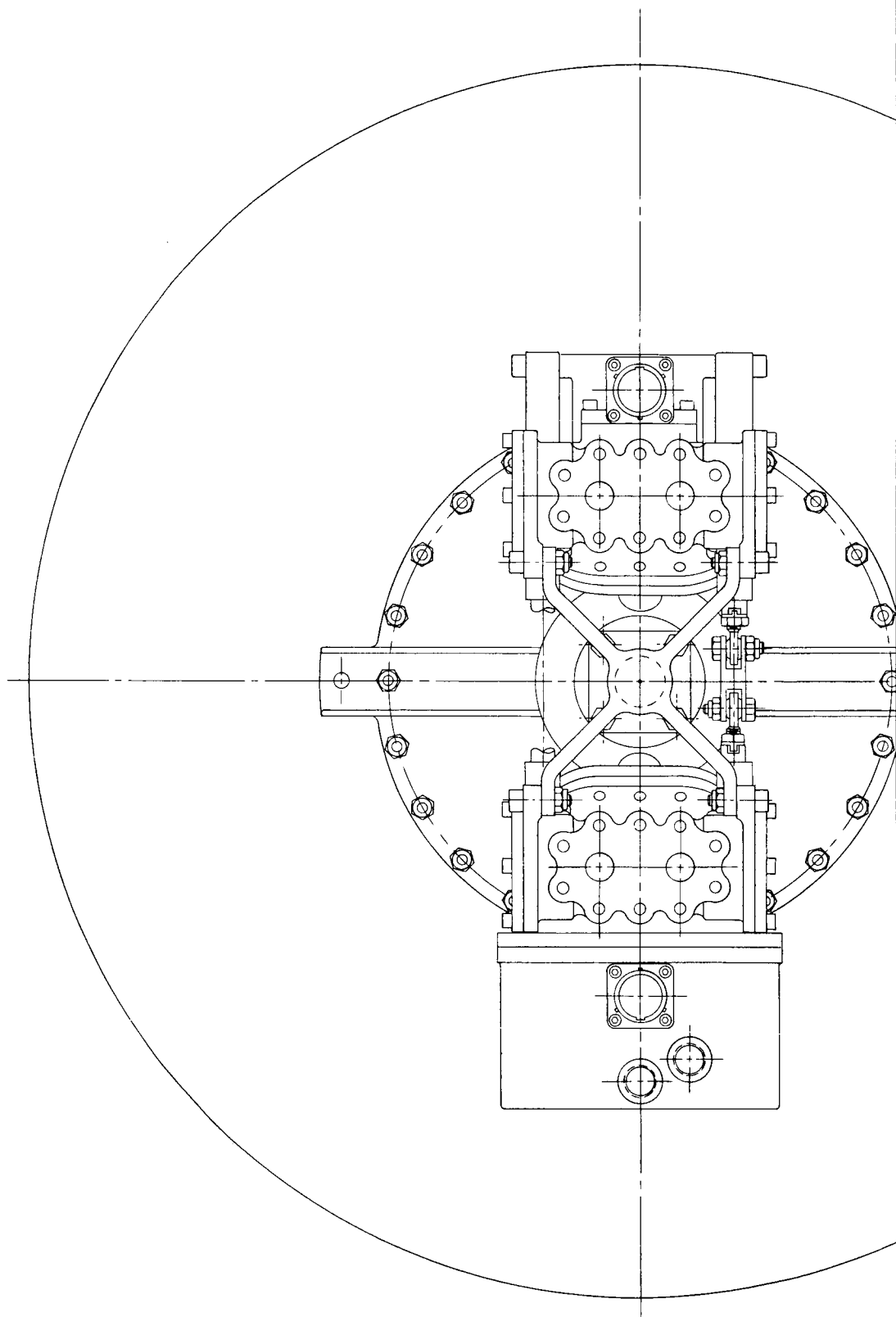
#### 4.1.1 Performance Characteristics

To provide a realistic basis for comparison, an attempt was made to configure both the solid-propellant retromotor and the bipropellant engine to similar degrees of design conservatism. Hence the nominal performance figures in Table 7-7 are considered to be realistic targets within the confines of Voyager schedules and not the ultimate performance potential of the engine.

#### 4.1.2 Engine Design

The major alternatives in the design of the engine include operating parameters, propellants and mixture ratio, and engine component design details. The major considerations which dictated the design solution are as follows:

- Selection of the operating parameters, thrust, and chamber pressure was based on a compromise between optimum system performance and current chamber technology



55①



MX2625 SIL

8

OXID.  
INLET

FUEL  
INLET

5-5-6

SILICA PHENOLIC

MX2600 SILICA PHENOLIC  
HELICAL TAPE WRAP

MX2646 SILICA PHENOLIC  
60° ORIENTED

30

10.05

7.92  
DIA.

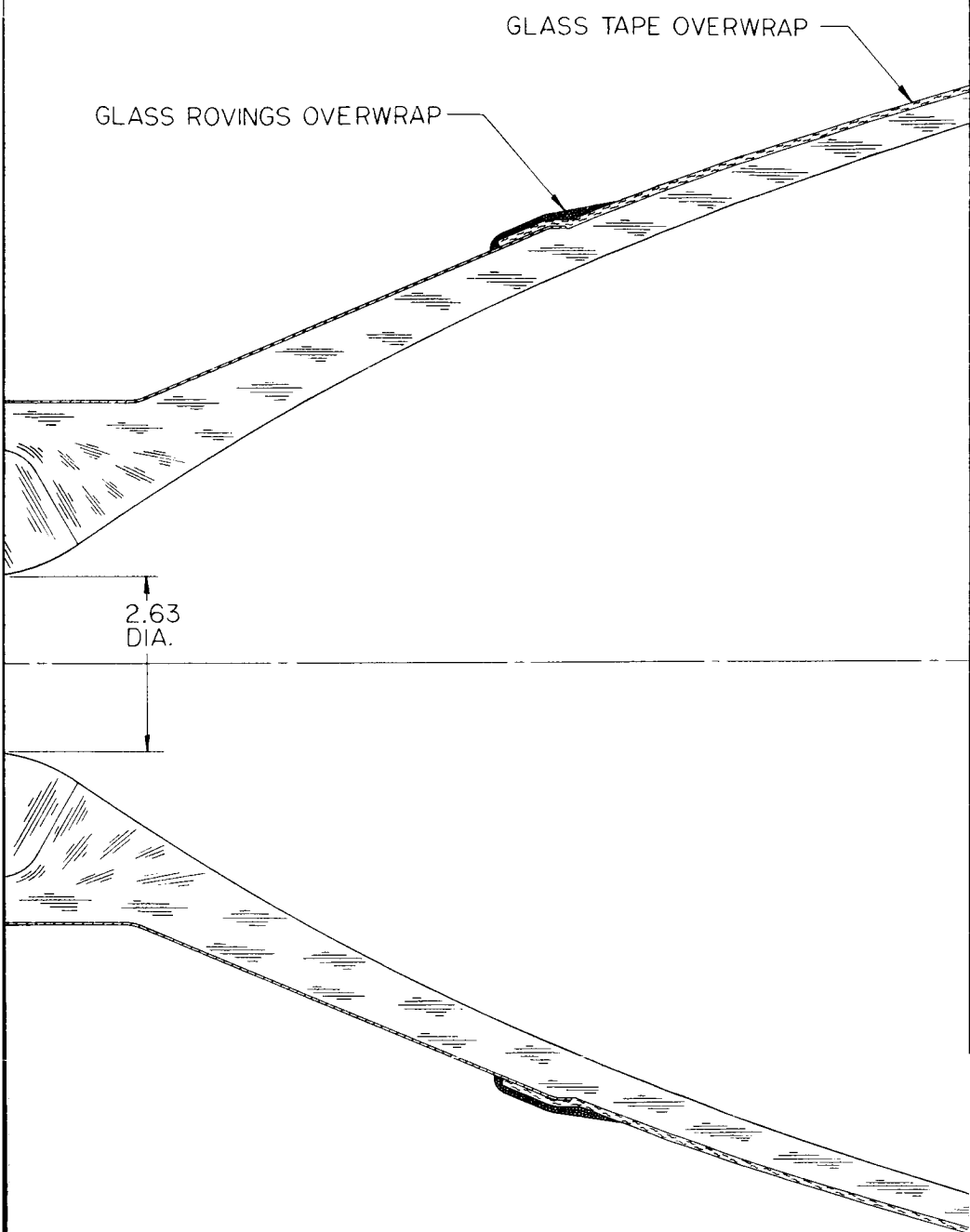
5.26  
DIA.

TITANIUM PRESSURE CASE

17-4 PH STAINLESS  
STEEL INJECTOR

5-5-3

42.43



SS (4)

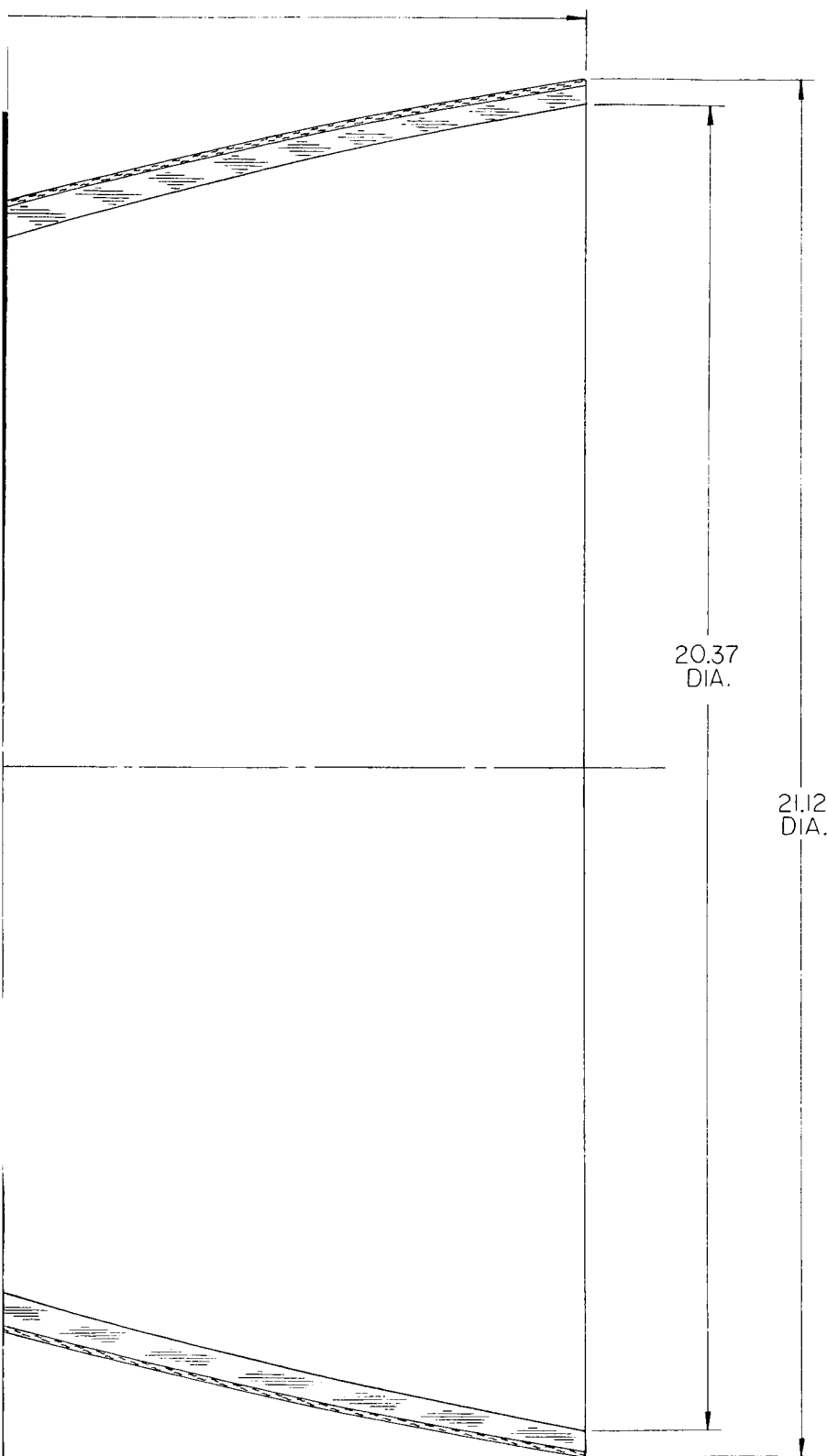


Figure 7-20. Voyager 1000-Lb Propellant

Table 7-7. Engine Performance Parameters

	<u>Units</u>	<u>Max Thrust</u>
Thrust, F (nominal)	lb	1000
Chamber pressure, $P_c$ (nominal)	psia	100
Mixture ratio (nominal)		1.65
Nozzle expansion area ratio		60
Characteristic velocity, $C^*$ (nominal)	ft/sec	5530
(percentage of kinetic recombination $C^*$ )		98
Thrust coefficient, $C_F$ (nominal) at $t_o$		1.786
(percentage of theoretical kinetic recombination flow)		95.6
Specific Impulse, $I_{sp_i}$ (nominal) (based on kinetic flow)	lb-sec/lb	307.0
Fuel inlet pressure, $P_f$ (nominal)	psia	195
Oxidizer inlet pressure, $P_{ox}$ (nominal)	psia	195
Throat diameter	in.	2.67
Exit diameter	in.	20.9
Chamber diameter (I. D.)	in.	5.34
Contraction ratio $(D_c/D_t)^2$		4.0
Engine weight	lb	95.0
Burn time (maximum)	sec	850
Ablative wall thickness	in.	1.30

- Selection of the propellants and mixture ratio was primarily based on empirical experience obtained at TRW Systems on current engine development programs
- Selection of engine component design details was also based on empirical experience obtained at TRW Systems in current engine development programs.

a. Propellant Selection

Because the propellant storage compartment will be maintained above 40°F for reasons independent of the propulsion system, MON as the oxidizer was eliminated and  $N_2O_4$  was selected. The selection of the fuel is not as obvious, however.

In its engine development programs TRW Systems has acquired extensive experience with  $N_2H_4$ , 50/50 UDMH/hydrazine, and MMH. Based on this experience it appears that the criteria for selecting the fuel are the relative compatibility of the propellants with thrust chamber materials, the relative combustion stability and performance under off-design operating conditions, the relative ease of achieving a high percentage of the theoretic available energy, and existence of a developed, high performance, chamber compatible injector.

Chamber Material Compatibility. The ability to operate non-regeneratively cooled combustion chambers with the candidate propellant combinations has been demonstrated in engines currently in advanced phases of development. However, the development difficulties encountered, the performance degradation required, the effects of non-optimum injection conditions, and reproducibility (hence reliability) vary significantly between the candidate fuels. For example, the first firings at TRW Systems with  $N_2O_4 + N_2H_4$  in an ablative chamber (at performance levels in excess of 97 per cent theoretical C\*) showed essentially no erosion and low uniform char rates. These tests were conducted with a coaxial injector tuned to maximum performance (in a water-cooled chamber) with no consideration given to radial distribution of the combustion gases. Subsequent tests verified the relative ease

of achieving thrust chamber compatibility with this combination. In comparison, chamber compatibility (in terms of throat erosion) during the LEM DE development program (the LEM DE uses  $N_2O_4$  + 50/50 UDMH/hydrazine) was a major problem area. The solution to this problem was a fairly delicate adjustment of the injection velocities which provided a low-temperature, fuel-rich zone at the chamber wall. Other engines which use 50/50 UDMH hydrazine, such as the LEM ascent engine and the radiation cooled Apollo reaction control engines, achieve a similar low-temperature, fuel-rich zone at the chamber wall by injecting fuel around the periphery of the injector. It is difficult to assess the minimum performance penalty associated with these techniques. However, it is clearly in the range of 1 to 2 per cent for ablative type chambers and even higher for radiation type chambers.

Considering the similarity between 50/50 UDMH hydrazine and MMH, it might be concluded that ablative chamber compatibility with MMH would be similarly difficult. However, empirically, at least with the coaxial injectors, it has been observed that erosion in chambers burning  $N_2O_4$  + MMH has not been a serious problem. Identical injectors run with MMH +  $N_2O_4$  and with 50/50 UDMH/hydrazine show nearly an order of magnitude difference in erosion rates. Streak tests with relatively soft ablative throats on the Surveyor and C-1 engines (which use MMH +  $N_2O_4$ ) invariably show negative throat area change after typical 200-second injector acceptance tests. With "hard throats" 90-10 tantalum-tungsten, firing times in excess of 3600 seconds have been demonstrated.

Hence, in the area of thrust chamber material compatibility both  $N_2H_4$  and MMH show clear superiority over 50/50 UDMH/hydrazine.

Combustion Stability and Performance Under Off-Design Conditions. The relationship between propellants, injector design, and combustion stability is not well understood; and the problem has, historically, been solved by empirical techniques. The coaxial injectors used on TRW engines have demonstrated dynamic stability with all three candidate propellant combinations. (Artificially induced pressure

transients in excess of 200 per cent nominal chamber pressure damp out within 20 to 40 milliseconds.) Hence, a dynamically stable injector can be developed for any of the fuels, and the probability of a destructive instability occurring in a qualified engine is remote. However, considerable evidence shows that the general level of combustion roughness and the frequency of random pressure spikes can be attributed to the fuel.

TRW's experience with all three propellant combinations indicates that smooth, stable, high-performance combustion can be achieved for any reasonable set of design operating conditions. However, the sensitivities of the various propellant combinations to off-nominal operating conditions are significantly different. This fact, which has been observed in thousands of development test firings, favors the selection of MMH. On the LEM descent engine performance has been evaluated over a wide range of injector configurations and operating conditions. It has been observed that relatively small changes in seemingly unimportant parameters produce significant changes in performance and chamber compatibility. On the Surveyor vernier engine and the C-1 engine (which use MMH), the converse appears to be true: performance is practically insensitive to wide variations in mixture ratio, propellant temperatures, and injection pressures.

TRW's experience with neat  $N_2H_4$  is not as extensive as with the other propellants. During early development tests of a 500-pound thrust coaxial injector, stable high performance combustion was readily demonstrated. However, no attempt was made to characterize the injector over a range of off-design conditions. Hence, TRW's experience is not sufficient to verify or reject  $N_2H_4$  on this basis. General experience throughout the industry, however, indicates that  $N_2H_4$  is inherently more difficult to combust smoothly than even 50/50 UDMH/hydrazine, as evidenced in fact by the existence of the 50/50 UDMH/hydrazine blend.

Hence, on the basis of the empirical experience, insofar as



stability and performance at off-nominal conditions, MMH appears to be superior to both 50/50 UDMH/hydrazine and  $N_2H_4$ .

Ease of Achieving High Performance. The task of achieving high performance in a nonregeneratively cooled rocket engine is complicated by the fact that the injector must not only achieve efficient mixing of the propellants, but must also provide a fuel-rich, low-temperature region at the chamber wall. The difficulty has been alleviated with all three candidate fuels by several different thrust level coaxial injectors. However, the injector development has proven to be significantly less difficult with MMH than with 50/50 UDMH/hydrazine.

b. Engine Component Design

The thrust chamber, the injector, and the flow control valves were evaluated to determine the best design approach and to examine potential problem areas which could delay or extend the development time. The evaluation indicated that a bipropellant engine for the Voyager mission would extend the state-of-the-art valve design, but that the injector and thrust chamber would not present fundamental development problems. The reasons for selecting the single element coaxial injector, the all-ablative lined chamber, and the quad valves are discussed in the following paragraphs.

Injector Design. The injector for a long-burning, high-performance engine with a nonregeneratively cooled thrust chamber must not only produce high combustion efficiency but must also have a uniform circumferential combustion pattern and produce a fuel-rich, low-temperature zone at the chamber wall. The coaxial tube injector chosen for the Voyager bipropellant engine is similar to that used on the TRW C-1, SVE, MIRA 500, and LEM descent engine. Combustion efficiencies in excess of 98 per cent of theoretical kinetic  $C^*$  have been demonstrated in all of these engines, and chamber compatibility in terms of char and erosion rates in excess of that required for the Voyager engine has been demonstrated.

In the coaxial injector the oxidizer is injected axially as a hollow cylinder which arrives at the impingement zone with a uniform circumferential velocity profile prior to atomizing. The fuel is injected radially with sufficient velocity to penetrate the cylindrical oxidizer sheet so that no preferential separation of oxidizer and fuel can occur. Throughout the resultant expanding propellant spray the liquid phase reactions generate gas and vapor which atomize and distribute the remaining liquid oxidizer and fuel uniformly in all directions, thereby producing high combustion efficiency.

The over-all symmetry of the mixture ratio distribution characteristics of the coaxial tube injector is significant, because of its favorable effect on combustion efficiency and the fact that it provides the necessary uniform circumferential heat load to the chamber walls and nozzle throat. In practice, a wide range of velocity ratios which will produce high performance was found. This range includes velocity ratios which permit the establishment of a radial mixture ratio gradient, resulting in the formation of a low-temperature, fuel-rich zone adjacent to the chamber wall and nozzle throat. When operated in this manner, it is possible, with the coaxial injector, to obtain long life and high performance with thrust chambers made of state-of-the-art materials.

Combustion Chamber Design. The proposed combustion chamber and nozzle assembly consists of an ablative lined chamber, throat, and nozzle divergent section encased in a titanium pressure case. The ablative liner is 60 degrees oriented phenolic refracil ablative composite, tape wrapped with a 0 degree oriented phenolic refracil. The liner is contained in a titanium pressure case. Similar designs have been successfully used on the LEM descent engine, C-1, and SVE engines.

The experience of TRW during the LEM descent engine, C-1, and SVE development programs has shown that the key to developing a successful combustion chamber is the integration of a satisfactory chamber design with an injector producing a mild thermochemical

environment. The proposed injector configuration (fuel centered coaxial) has demonstrated on the SVE and C-1 engines both high performance ( $>96$  per cent  $C^*$ ) and a favorable thermochemical wall environment. Based on both transient and steady-state temperature measurements made during the SVE and C-1 development programs, the boundary layer temperature of the gas stream at the chamber throat is between 2300 and 2800<sup>0</sup>F. At this temperature the refrasil reinforcement is quite strong and will maintain the integrity of the throat. Linear erosion rates of less than  $10^{-4}$  in/sec on all ablative throats have been consistently demonstrated with this configuration. For a 750-second firing this would result in an area increase of less than 6 per cent.

The effect of the long soak in the space vacuum on the ablative composite used for the combustion chamber represents a major unknown area in the development of the Voyager engine. Among the problems associated with the effect of the deep vacuum on the ablative combustion chamber are:

- a) Loss of resin from the ablative composite, reducing the efficiency of the cooling
- b) The possibility of appreciable loss from the silica matrix due to volatilization immediately after engine shutdown
- c) The possibility, as experienced on a number of engines, of foaming of the silica portion of the composite to partially plug the nozzle.

It is possible that these problems could lead to expensive development program even if the problems proved not to be detrements and many engines would have to be fired in high vacuum to demonstrate satisfactory solution. An alternate approach to eliminate questions of the effect of the loss of resin material from the ablative composite is to design the thrust chamber to provide satisfactory life when operating on a completely charred (hence no volatile resin) matrix. For the long-duration firing associated with the Voyager mission, the increase in weight resulting from this conservatism is calculated to be quite small

(about 4 pounds). Thus, the development emphasis can be shifted from an extensive evaluation of combustion chamber(s) in high vacuum to sea level tests on fully precharred matrices. This mode was proved feasible in tests in which ablative chamber life in excess of 3600 seconds were demonstrated.

Reducing the loss of silica material immediately after engine firing could be accomplished by satisfactory film cooling of the engine to maintain the hottest portion of the combustion chamber below 3000°F under all conditions. As previously discussed, the injector configuration selected should result in a maximum chamber wall temperature below 2800°F. Negligible volatilization rate would be expected at these temperatures. The low maximum surface temperature also serves to prevent foaming from becoming a major problem. At temperatures below 3000°F, the viscosity of the silica is high enough to preclude foaming as a significant factor.

Flow Control Valves. The Voyager mission places unusual requirements on the engine flow control valves. An evaluation of alternate design approaches has been made leading to a tentative selection, but it is clear that further analysis is required before a final design commitment could be made.

The requirements for the shutoff valve are:

- a) Nine months' storage in space with minimum of five operations
- b) Maximum leakage in vacuum of 1 cc/day
- c) Maximum power consumption of 50 watts during operation
- d) Reproducible closing time to  $\pm 2$  ms
- e) Maximum pressure drop of 10 psi at rated flow.

To increase the potential reliability, the following additional design constraints have been imposed on the valve:

- a) Use of bellows for all dynamic seals

- b) Mechanical or hydraulic linkage of the oxidizer and fuel pintles to ensure simultaneous operation
- c) Use of high hydraulic closing forces to ensure rapid closing and high unit loading of the seal.

The major problem areas in selecting a valve are those associated with the effects of the long storage in the space environment. Although many sealing techniques are available in the existing valve technology, all techniques are modifications of either the soft seat deformed to provide a tight seal or two high-precision hard surfaces in intimate contact. The space environment presents problems for both of these design concepts. The soft seal generally incorporates an elastomeric or plastic material such as Teflon, and the effect of exposure of Teflon to the combination radiation and high vacuum of space is still uncertain. Present indications are that less than 10 per cent (Reference 7-7) of the Teflon will be vaporized on exposure to the space environment for one year, but these results cannot be applied simply to the Voyager requirements since the effects on the Teflon while it is in contact with the actual propellant have not been examined. It is shown in Reference 7-6 that the presence of oxygen (and hence probably nitrogen dioxide) accelerates the effect of radiation upon Teflon.

The second problem is associated with the use of hard metal-to-metal seats. Under high vacuum and high loads, a tendency toward cold welding of even relatively dissimilar metal surfaces has been experienced. It is possible to impregnate the surfaces of the hard metals with relatively low strength or low friction materials such as Teflon, gold, or silver, but it has not been demonstrated that these types of surfaces would effectively reseal after continual operation. Hence, it is felt that this component will require improvement beyond the state of the art and would thus constitute a development risk.

Four basic types of flow control valves are available for the Voyager application, poppet, ball, slide, and explosive, each of which presents both advantages and disadvantages.

Poppet Valves. Poppet valves are, in general, the simplest approach to a valve design. Since the poppet can be completely supported by bellows, cold welding and high wear can be avoided. Both hard and soft seat designs are available and the state of technology is quite high. Disadvantages are the difficulties of mechanically linking the oxidizer and fuel pintles without having interpropellant seals and the relatively high pressure drop associated with this type of design. It would be expected that for a given pressure drop, a poppet valve might weigh approximately twice as much as either a ball valve or a slide valve. Another problem associated with the poppet valve is presented in the high force levels required for effective sealing, making it difficult to operate such a valve without either hydraulic or pneumatic piloting.

Ball Valves. Ball valves can employ either soft metals or plastic seats. Because of the relatively large surface area associated with ball valves, leakage tends to be a problem. In addition, the rotary action requires joints, pinions, or gears to translate linear into rotary motion. However, ball valves permit a relatively light weight for a given pressure drop. They are presently used by TRW on the LEM design with success.

Slide Valves. The slide or plug valve represents a compromise between poppet and ball. The slide valve has a relatively high sealing area and requires high forces in order to seal. In general, slide valves are designed with metal-to-metal seats, which would tend to cold welding. Slide valves lend themselves well to mechanically linking oxidizer and fuel pintles and have excellent sealing qualities. Because of the relatively tight clearance, they are not susceptible to contamination, the closing action being self cleaning.

Explosive Valves. Explosive valves avoid all of the problems associated with cold welding and effective resealing, but a severe weight penalty would accompany their use and the electrical interface would have to be more complex by an order of magnitude. They were

therefore not considered competitive with the other three approaches.

For the purposes of the initial design, a quad redundant arrangement of ball valves similar to those in use on the LEM descent engine has been selected. This design has the advantage of several years of development history and has been thoroughly debugged. With the exception of the long-term vacuum storage it has demonstrated performance very close to the Voyager requirements.

#### 4.2 Bipropellant Feed System

The feed system design task involved selecting an optimum configuration from the many possible combinations of feed system components. The technique used in the study was first to configure a baseline design, i. e., the simplest design providing high reliability without redundancy. The design was then perturbed with various component changes, alternate arrangements of components and addition of redundancy to improve reliability. The modifications were then compared on the basis of reliability improvement versus weight increase. Weights of major elements were based on detailed analysis of actual layouts; weights of components were based on existing similar hardware. Reliability of components was based, in general, on historical data.

As was expected, reliability improvements with redundancy were less spectacular than for other subsystems, largely due to the already high intrinsic reliability of the baseline system. Details of this process are given in Appendix J and the system application and summary results are discussed in Volume 4.

a. The selected design is shown schematically in Figure 7-21. The system includes a helium pressurization supply tank; quad redundant solenoid valves to isolate the high pressure gas; a pneumatic and electric regulator (a solenoid valve controlled by pressure switches) in series; bladder type positive expulsion fuel tanks; positive ullage displacement steel bellows in the oxidizer tanks; and associated hand valves for fill, vent, and drain. The weight is summarized in Table 7-9.

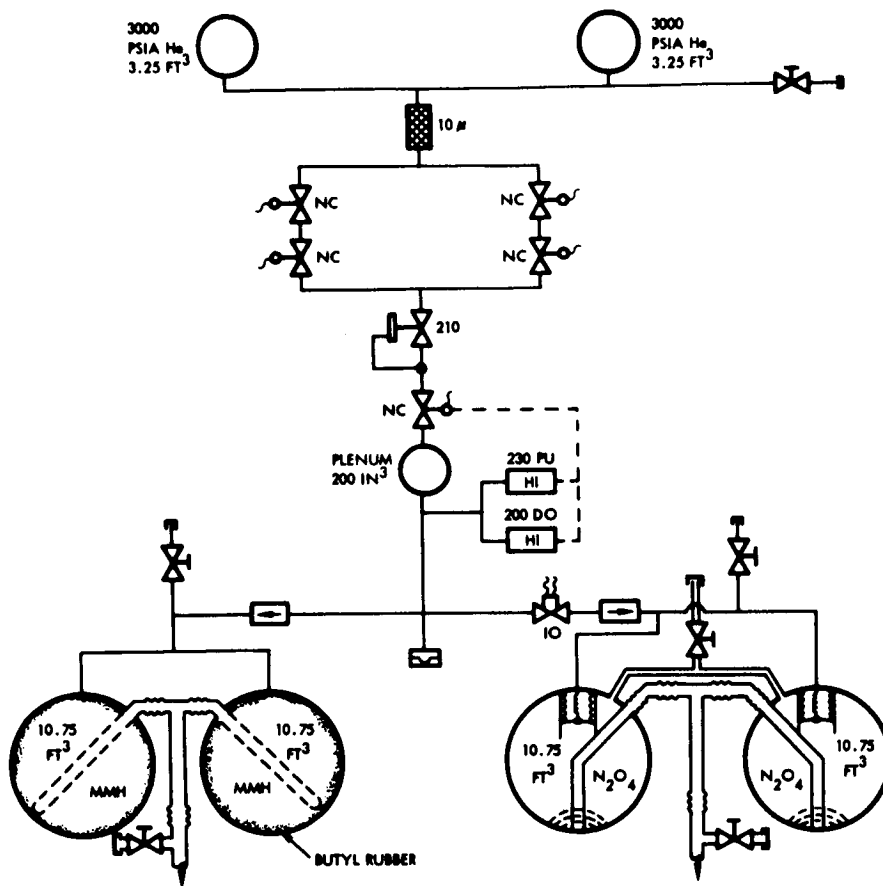


Figure 7-21. Bipropellant Augmented Configuration

#### 4.2.1 Component Selection and Arrangement

As can be seen from Table 7-8, of the 491 pounds inert weight only 19.5 pounds (approximately 4 per cent) are for valves, regulators, and other control devices. Hence, perturbations to the design which substitute various types of components and component arrangements have little effect on the total system weight and hence, system performance. As can be seen by the reliability data presented in Appendix J, arranging the control devices in any of several different redundant schemes results in reliabilities in excess of 0.999. Component arrangements with predicted reliabilities in excess of 0.999 do not really help



the system since the weaker links in the system simply become the dominant failure modes. Hence the component arrangement selected which illustrates two of the more common redundant approaches is really one of several possible representative designs.

#### 4.2.2 Gas Pressurant and Storage Tanks

As configured in the selected system, the pressurant and storage tanks constitute about one third of the total feed system weight. The choice of He instead of  $N_2$ , as used on Mariner, was dictated by a weight saving of the order of 20 to 40 pounds (depending on various other design assumptions). The higher leakage potential of He was not considered to be a significant problem, particularly since it is planned to use welded connections and stringent leak check procedures during final system checkout. (The predicted leakage rates are discussed in Appendix J.)

The gas storage bottles were designed per the specification requirements for hazardous vessels. Consideration was given to the potential weight savings, about 15 to 20 pounds, which could be achieved if the storage bottles were designed for remote pressurization during launch operations. The disadvantage of this approach is that it requires an umbilical connection to the spacecraft, and precludes a final leak check of the system. It was decided that this approach is the type of contingency one would like to save for growth potential and that the 15 to 20 pounds weight savings were insufficient justification for violating the specification requirement.

A second approach considered was the use of a solid-propellant gas generator to reheat the gas and supplement the He during the retro firing. This alternate results in a weight saving of about 62 pounds. It was rejected primarily for reliability considerations; however, if the system proved to be marginal in performance, a solid-propellant gas generator would need to be reconsidered as a real possibility.

Table 7-8. Component Weight List Single  
Engine Bipropellant Supply  
Augmented Configuration Less  
Engine and Engine Valves

Item	Weight (lb)	
Pressurization Subsystem		158
Tanks (2)	142.6	
Controls	13.7	
Fill and Dump Hand Valve	0.4	
Filter (2)	0.8	
Solenoid Valves (5)	5.5	
Pressure Regulator	2.5	
Pressure Switches (2)	0.4	
Plenum Chamber	2.0	
Burst Disc	0.2	
Check Valves (2)	0.8	
Squib Valve	0.3	
Vent and Relief Hand Valve and Cap	0.8	
Lines	1.0	
Fittings and Clips	0.5	
Propellant Subsystem		166
Tanks (2)	115.6	
Controls	5.8	
Fill and Drain Hand Valve and Cap	4.8	
Recirculation Valve	1.0	
Lines	4.9	
Flex Lines	2.5	
Fittings and Clips	1.2	
Positive Expulsion	36.0	
N <sub>2</sub> O <sub>4</sub> Tanks	23.2	
MMH Tanks	12.8	
Engine Plate Actuation Structure		8
Thermal Control		9
Insulation - Engine Envelope	6.6	
Heaters and Thermostats	2.0	
Propulsion Module Structure		150
Dry Propulsion Structure		491
Pressurant		10
Unusable Propellants		60
Usable Propellants		<u>2,840</u>
TOTAL		3,401

#### 4.2.3 Propellant Tank and Expulsion Devices

The propellant tank configuration of four spherical tanks symmetrically located about the roll axis is dictated as much by the over-all spacecraft geometry as by weight considerations. The propellant expulsion devices, particularly in the oxidizer tank, are the least understood portion of the feed system design. The choice of a small cylindrical steel bellows tank submerged in the main oxidizer tank as shown in Figure 7-22 derives from data indicating that Teflon bladders, reversing metal diaphragms, Teflon-metal laminates as bladders, and fine mesh or twilled fabrics for propellant orientation lack operational flexibility (inability to recycle), have not been demonstrated in flight type design, or would present difficulty in establishing confidence of adequate reliability. Steel bellows were thus considered to be the conservative approach. However, the steel bellows in titanium tanks with full positive expulsion capability were found to involve an additional weight of about 120 pounds.

The bellows tank in the selected design is sized so that extended it will displace a volume equivalent to the oxidizer expended during 75 m/sec of midcourse correction plus sufficient volume to ensure ignition during the retro maneuver. During the retrofiring the propellants are oriented by the engine gravity field; when the bellows reaches the fully extended position the plug is released from the diaphragm by steel cable.

This system by itself preempts the orbit trim capability of the bipropellant system. However, orbit trim capability may possibly be regained by the use of tightly woven screens at the tank exit. Whereas this method of orientation was not considered adequately demonstrated for propellant orientation during the 6-to 9-month flight, there appears to be a high probability of successful propellant containment for a shorter period following injection into the Martian orbit. Since loss of the orbit trim capability would not represent a mission failure, this scheme appeared to be the best compromise of the available choices. For the fuel tank, where material compatibility is not as severe a problem, Teflon or Teflon-metal laminates or perhaps rubber bladders appear to be feasible and are chosen because they are the lowest weight solution.

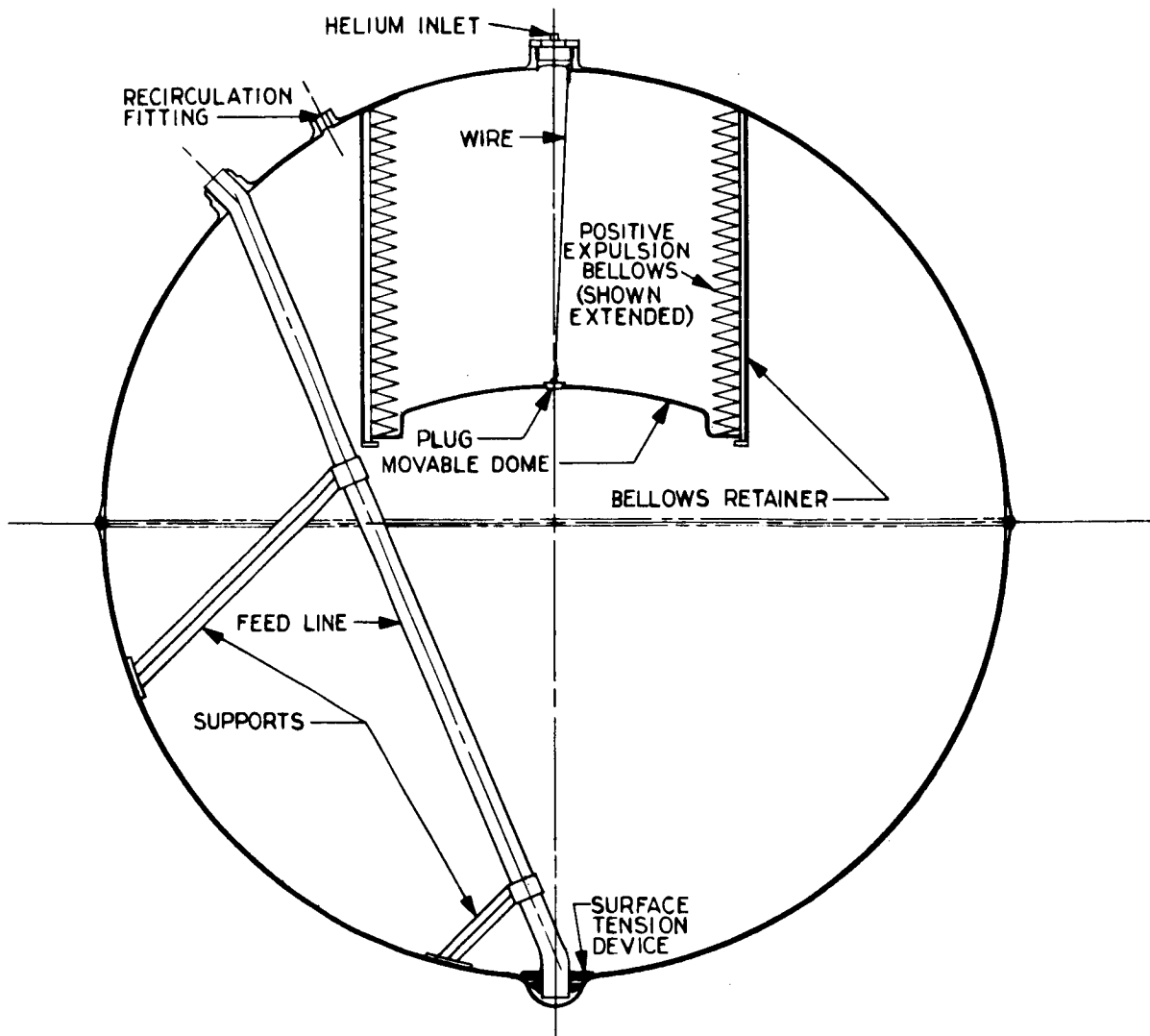


Figure 7-22.  $N_2O_4$  Tank Cross-Section

## 5. REFERENCES

- 7-1. J. M. Allel, et al, Battelle Memorial Institute, "Evaluation of Solid Propellants and Solid Propellant Systems for Space Application," Interim Report, Contract NAS 8-1683, 15 April 1963.
- 7-2. R. E. Gardner, "Effects of Ionizing Radiation on Solid Rocket Motor Components," ARS Journal, Vol. 32, Page 1050, 1962.

- 7-3. Richard L. Keller, "Effects of Nuclear Radiation on Structural Plastics," report to the 14th Annual Meeting of the Reinforced Plastics Division of the Society of the Plastics Industry, February 1959.
- 7-4. S. Dushman, Scientific Foundations of Vacuum Technique, Library of Congress No. 61-17361, 2nd Ed., p. 18, Wiley and Son, New York, 1962.
- 7-5. Norman E. Wahl, and Roy R. Lapp, "The Effects of High Vacuum and Ultraviolet Radiation on Plastic Materials," Cornell Aeronautical Laboratory, Inc., WADD Technical Report 60-125, February 1960.
- 7-6. R. L. Larson, et. al., "A Monopropellant Space Vehicle Propulsion System," TRW Paper No. 2217-61.
- 7-7. Jaffe, "Effect of Space Environment upon Plastics and Elastomers," CEP, Volume 59, Number 40, 1963.

AUG 12 1965

SIGNIFICANT ERRATA. TRW Systems, Phase 1A  
Study Report, Voyager Spacecraft  
August 11, 1965

Volume 1. Summary

Substitute new p. 79 attached.

Volume 2. 1971 Voyager Spacecraft

- p. 10. Item h) "necessary landed operations" should read "necessary lander operations."
- p. 143. Section 3.4.1.a. second line should read "threshold of 0.25 gamma"
- p. 282. Lines 3 and 4. Delete "or incorrect spacecraft address"
- p. 284. Figure 5. Change "128 Word DRO Core Memory" to "256 Word DRO Core Memory"
- p. 327. Denominator of second term on right hand side of equation should read

$$\left( \frac{1}{\epsilon_1} + \frac{1}{\epsilon_2} - 1 \right) (N - 1)$$

- p. 351. Figure 1, Section F-F. "separation nut" should read "bolt catcher"

Volume 3. Voyager Program Plan

Substitute new p. 12 attached.

- p. 13. Figure 2-3. PTM Assemblies in item 7 move 1.5 months to right
- p. 16. Figure 2-6. First milestone date should be September 1, 1969, instead of mid-January 1970, and all subsequent dates should be correspondingly adjusted 4.5 months earlier.
- p. 20. Table 2-2. Third item in 1969 column should read "coincident with completion of proof test model assemblies. Fifth item in this column change "2 weeks" to "3.5 months." Fourth item in 1971 column, change "4 months" to "5 months."

- ~~p. 67.~~ Figure 5-2. Under Intersystem Interface Specification add a block entitled "Spacecraft to OSE Interface Specification"
- ~~p. 120.~~ Last line of paragraph c should read "shown in Table 5-2."
- ~~p. 126.~~ Figure 5-13. Year should be 1966 instead of 1965.
- ~~p. 153.~~ Figure 5-18. Ignore all numbers associated with lines in figure.
- ~~p. 167.~~ Figure 5-21. In line 20 change "design revisions" to "design reviews"
- ~~p. 254.~~ Second paragraph, third line, "The capability of the transmitter to select" should read "The capability of the transmitter selector to select."
- ~~p. 258.~~ Section heading n should read Experiment Data Handling
- ~~p. 604.~~ Section 3.2.1 beginning of second paragraph should read "The hydrazine fuel ..."

#### Volume 4. Alternate Designs: Systems Considerations

- ~~p. 103.~~ Figure 3-19. Caption should read "Radial Center of Mass..."
- ~~p. 151.~~ Last paragraph, second line, "For the baseline, the reliability..." should read "The reliability ..."
- ~~p. 158.~~ 8th line, replace "0.06 pound/watt" by "0.6 pound/watt"
- ~~p. 215.~~ Figure 3-50. Dot in ellipse at right should be 0.
- ~~p. 230.~~ Section 5.3.2, second paragraph, 7th line, should read "Figure 3-52."
- ~~p. 239.~~ Second line, "with a variable V" should read "with a variable  $\Delta V$ "
- ~~p. 247.~~ First line, "3250 km/sec" should read "3.250 km/sec"
- ~~p. 261.~~ Figure 3-64. Interchange coordinates, clock angle and cone angle
- ~~p. 293.~~ Figure 3-81. An arrow should connect "Low-gain spacecraft antenna" and the dashed line at  $73 \times 10^6$  km

#### Volume 4. Alternate Designs: Systems Considerations Appendix

- ~~p. 6.~~ Figure A-2. The shaded portion under the lower curve should extend to the right only as far as 325 lb.

- p. 9. Table A-1, part (1). In last column heading change " $W_3$ " to " $W_1$ ". In part (4) last column heading change " $W_3$ " to " $W_4$ "
- p. 22. Second line below tabulation, replace " $575 \times 35$ " by " $570 \times 35$ "
- p. 29. Tabulation at bottom of page, change "18" to "30" and "400" to "240"
- p. 207. Numerator of equation for  $\lambda$  best at bottom of page should read "0.0201," and numerator of equation for  $\lambda$  worst should read "9.21"
- p. 209. Table 5B, fifth line. Delete " $\times 10^{-}$ ". Also p. 213, Table 7A, seventh line, and p. 232, Table 3B, fifth line.
- p. 217. Top portion of Table 9B should be labeled "primary mode" instead of "other modes"
- p. 220. In equations following words "clearly" and "thus" insert ">" before second summation.

#### Volume 3. Alternate Designs: Subsystem Considerations

- p. 3-15 Fifth line, "... is extended, spacecraft" should read "... is extended, two spacecraft"
- p. 3-38 Last line, change " $= \frac{32}{4500} = M$ " to " $= \left( \frac{32}{4500} \right) (M)$ "
- p. 3-51 Two equations at bottom of page should read
 
$$D = 4\pi A / \lambda^2$$

$$A = \frac{D\lambda^2}{4\pi} = \frac{1000\lambda^2}{4\pi}$$
- p. 3-67 Third line, last parenthesis " $\left( \frac{\pi}{2} + \phi \right) - "$ "
- p. 3-82 6th line should read "50 degrees" instead of "50-140 degrees," and seventh line should read "140 degrees" instead of "50-140 degrees"
- p. 3-111 Last line, change "50 Mc" to "1 Mc"
- p. 3-137 Item g) for "... followed by 5 frames of real time" substitute "... followed by 11 frames of low rate science data and 5 frames of real time"



pp. 3-150 and 3-151 are interchanged.

p. 3-156 Last line, should read "gates, a 7 bit"

p. 5-21 Second paragraph, third line, for "others since they are" substitute "others which are"

p. 5-33 Bjork equations should identify 0.18 as an exponent, and the exponent for  $(\rho_p/\rho_t)$  in the Hermann and Jones equation should be  $2/3$  in both cases.

p. 5-33 Figure 5-12 should be replaced with Figure C-7 of Appendix C.

p. 5-40 Three lines above Table 5-10 substitute "permanent set" for "experiment"

Volume 5. Alternate Designs: Subsystem Considerations. Appendix I

p. C-11 Bottom of page, for " $r^{2/3}$ " substitute " $(V/C)^{2/3} r$ "

p. C-4 The title of Figure C-2 should read "Figure C-2. Meteoroid Influx Rate Circular Orbit Mars", and the title of Figure C-3 should read "Figure C-3. Meteoroid Influx Rate Cruise"

p. C-5 At bottom of page, add the following: "\*Within 50,000 km of Mars"

p. C-6 Line 13 should read: "... of low density ( $\rho_p < 2.4 \text{ gm/cm}^3$ )..."

p. C-6 Figure C-4. The ordinate "2" should read "100"

pp. C-17 C-21 The figures C-6 and C-7 on pages C-17 and C-21 should be reversed.

p. C-28 The title of Figure C-8 should read "Meteoroid Shield Test Specimen"

p. C-29 The title of Figure C-9 should read "Cutaway of Meteoroid Shield Test Specimen"

p. C-34 In Section 1.8 the first sentence should be replaced by the following two sentences: "Preceding sections of this appendix contain derivations of the probability of penetrations of the spacecraft outer skin by meteoroids. It is clear that to design an outer skin of sufficient thickness to reduce the probability of no penetrations to a low level, such as 0.05 to 0.01, would be prohibitive in terms of the weight required."

- p. C-35 In the first equation, the expression " $(t \text{ in } m^2)$ " in two places should read " $(t \text{ in } cm)$ " and " $A$ " in two places should read " $(A \text{ in } m^2)$ "
- p. C-38 In Table C-2, all values in inches should be in centimeters. A zero should be inserted immediately following the decimal point, for example:  $(0.020\text{-inch}) = 0.05080$ ,  $(0.020\text{-inch}) = 0.06096$ ,  $(0.020\text{-inch}) = 0.04064$ , etc.
- p. C-40 In Section 1.8.7 Computation of  $R_i$ 's, the sixth line should read "... than  $10^6$  are neglected"
- p. C-45 In listing under "Values of  $t$  Used for Extreme Environment Analysis," under Inch, the first number should read 0.020 instead of 0.202
- p. C-52 In 1.10 NOMENCLATURE, " $K_2$ " should be defined as " $K^{-2/3} (4 \pm 2)$ " and " $B$ " should be
- $$\frac{1000 \rho_t V^2}{9.806 H_t}$$
- pp. C-150 and C-151 should be reversed.
- p. C-208 Along the ordinate in the graph, " $\text{Stress} \times 10^{-3}$ " should read " $\text{Stress} \times 10^{-2}$ "

Volume 5. Alternate Designs: Subsystem Considerations. Appendix II

- p. F-23 Lines 7 and 10 change all subscript  $\tau$  to  $T$
- p. F-24 Line 14, change " $ME_1$ " to " $mE_1$ "
- p. F-29 Figure F-9 title should be "Reflection Phase Angle  $\phi$  (deg)" and Figure F-10 title should be "Reflection Magnitude  $R$ "
- p. F-30 Last line, change "0.27" to "0.175"
- p. F-31 Lines 14 and 15, change "14,700 ft/sec to 460 ft/sec" to "14,700 ft/sec minus 460 ft/sec" and "14,700 ft/sec to 10,000 ft/sec" to "14,700 ft/sec minus 10,000 ft/sec"
- p. F-32 Last line in item 4), change "27 per cent" to "17.5 per cent"
- p. F-35 Table F-4, under Assumed Parameter for item 2 insert " $\pm 2 \times 10^{-5}$ ", for item 3 insert " $\pm 3 \times 10^{-5}$ ", and for item 4 insert " $\pm 2 \times 10^{-5}$ "

- p. F-53 Item d. Noise Figure, change "4 db" to "3.5 db"; Gain, change "20 db" to "10 db", last line change "10 db" to "4 db"
- p. F-58 Figure F-21. Change 102 kc to 112 kc.
- p. F-59 Line 22, change to " $M_1 = 21.5$  deg or 0.375 radians (rms, peak)"
- p. F-60 Line 2, change to
- $$M_2 = \sqrt{(1.1)^2 - (0.375)^2}$$
- p. F-60 Line 3, change to " $M_2 = 1.03$  radians (rms) or 1.46 radians (peak)"
- p. G-3 Paragraph 1.4, second line, change "from  $E_M = 10^1 E_0$  to  $10^4 E_0$  ..." to read "from  $E_M = 10^{-1} E_0$  to  $10^4 E_0$  ..."

#### Volume 6. Operational Support Equipment

- p. 25 Figure 6. Caption should be "Typical Grounding Scheme"
- ~~p. 33~~ Section 1.3.3, change opening of first sentence to read "Launch pad equipment consists of the ground power and RF consoles and the test flight program power and control equipment ..."
- p. G-31 Figure 1. Lines enclosing Data Format Generator should be solid.
- p. G-102 Last line substitute "4500" for "45"
- p. G-113 In Section 4.4.2, change "25 per cent" to "250 per cent"
- p. G-184 Section 4.5, substitute "6.5 feet" for "six feet"
- p. G-311 Fifth line, change "30 per cent" to "20 per cent"
- p. G-398 Section 4.2 should begin with "The hoist beam is ..."
- p. G-419 Second line "4 optical alignment targets" instead of 8. Same correction top of p. G-421.
- p. G-423 Section 4.9.2, substitute "20 per cent" for "50 per cent"

Volume 7. 1969 Flight Test Spacecraft and OSE

- p. 90      First line should read "Launch pad equipment consists of the ground power and RF consoles and ..."
- p. 107     Last line, change Volume 5 to Volume 6.